Experimental alteration of diet-related dental wear and isotope proxies in teeth - implications for fossil food web reconstruction of Permo-Carboniferous vertebrates

Dissertation zur Erlangung des Grades eines `Doktor rerum naturalium (Dr. rer. nat.)' der Fachbereiche:

- 08 - Physik, Mathematik und Informatik
- 09 - Chemie, Pharmazie und Geowissenschaften,
- 10 – Biologie,
- Universitätsmedizin

der Johannes Gutenberg-Universität"

vorgelegt von

Katrin Weber

geb. 18.04.1991

in Mainz

Max Planck Graduate Center mit der Johannes Gutenberg-Universität Mainz

Angefertigt am Institut für Geowissenschaften

Mainz, 30.11.2020

Dekan:

1. Gutachter:

2. Gutachter:

Tag der mündlichen Prüfung: 8.04.2021

Eidesstattliche Erklärung

I hereby declare that I wrote the dissertation submitted without any unauthorized external assistance and used only sources acknowledged in the work. All textual passages which are appropriated verbatim or paraphrased from published and unpublished texts as well as all information obtained from oral sources are duly indicated and listed in accordance with bibliographical rules. In carrying out this research, I complied with the rules of standard scientific practice as formulated in the statutes of Johannes Gutenberg-University Mainz to insure standard scientific practice.

……

Katrin Weber

Mainz, 30.11.2020

Zusammenfassung

Der Fokus der vorliegenden Dissertation liegt auf der Untersuchung von post-mortem Diagenese und deren Auswirkungen auf die chemische Zusammensetzung von Zahngewebe und auf die mikroskopische Textur der Zahnschmelzoberfläche, um unter anderem die treibenden Mechanismen hinter Diagenese zu verstehen. Der erste Teil dieser Arbeit beschäftigt sich mit der mechanischen und chemischen Widerstandsfähigkeit von mikroskopischen Oberflächentexturen (dental microwear texture, DMT) und nicht-traditioneller stabiler Isotope gegen verschiedene post-mortem Alterationsszenarien. Diese wurden in unterschiedlichen Experimenten simuliert. DMT und nicht-traditionelle stabile Isotope wurden jeweils vor und nach den einzelnen Experimenten gemessen, um Abnutzungsspuren auf der Schmelzoberfläche und Veränderungen der chemischen Isotopenzusammensetzung im Zahngewebe zu charakterisieren. Im zweiten Teil der Dissertation wurden sowohl DMT als auch nicht-traditionelle stabile Isotope in permokarbonischen Tetrapoden gemessen, um Ernährungspräferenzen und die Besetzung unterschiedlicher Nischen in den frühesten terrestrischen Nahrungsnetzen zu rekonstruieren.

DMT Analysen und nicht-traditionelle Isotopensysteme werden zunehmend auf eine Vielzahl von taxonomischen Gruppen, wie Reptilien (einschließlich Dinosaurier) und Fische, sowie in modernen und fossilen Ökosystemen angewandt, um Nahrungskategorien und Positionen in den jeweiligen Nahrungsnetzen zu bestimmen. Allerdings können diese sogenannten Proxies besonders im Fossilbericht durch post-mortem Alteration beeinflusst werden. Zahnschmelz ist, im Gegensatz zu anderen phosphatischen Hartgeweben wie Dentin und Knochen, hoch mineralisiert und daher weniger anfällig für Diagenese. Allerdings kann auch fossiler Zahnschmelz diagenetisch überprägt sein. Um die Auswirkungen von mechanischer Alteration auf DMT durch fluvialen Transport von Fossilien, sowie Erosion der Zahnschmelzoberfläche durch äolischen Sedimenttransport oder die Verdauung von verschluckten Zähnen zu bewerten, wurden Tumblingexperimente, sowie ein Sandstrahl- und ein Magensäureexperiment mit verschiedenen Wirbeltierarten unter Verwendung verschiedener Sedimentkorngrößen und Säurebedingungen durchgeführt. Diese experimentell erzeugten Datensätze wurden mit einem Referenzdatensatz schlecht erhaltener Zahnoberflächen ergänzt, die beispielweise bei Ausgrabungen, Präparation und Probennahme entstanden sind. Die Datensätze wurden mit standardisierten Texturparametern analysiert. Die Ergebnisse zeigen, dass sich die Parameterwerte von post-mortem DMT kaum von nahrungsbezogenen DMT Werten unterscheiden. Daher ist es notwendig, dass erfahrene Anwender der Methodik post-mortem Texturen identifizieren und bewerten können bevor potentiell alterierte Schmelzoberflächen in einen Datensatz aufgenommen werden. Neben Diagenese können aber auch ein reduziertes Kauverhalten oder kontinuierlicher Zahnwechsel Einfluss auf DMT haben. Einige Arten mit wenig

ausgeprägtem Kauverhalten und lebenslangem Zahnwechsel, wie Schuppenechsen (Reptilien), zeigen ernährungsspezifische mikroskopische Schmelzoberflächentexturen (DMT), während Ergebnisse in der vorliegenden Dissertation zeigen, dass einige rezente Hai-Arten keine ernährungsspezifischen Texturen ausbilden. Bei Haien scheint der Zahn-Nahrungskontakt auf Grund von stark reduziertem Kauverhalten oder sehr schnellem Zahnwechsel, oder einer Kombination aus beidem, zu gering zu sein, um ernährungsbedingte Abnutzungsspuren zu erzeugen.

Zusätzlich wurde ein *in-vitro* Alterationsexperiment durchgeführt, um das Verständnis der Auswirkungen von Diagenese auf die isotopenchemische Zusammensetzung von Zahngewebe, Schmelz und Dentin, zu verbessern. Dabei wurden Elefantenzahnwürfel für unterschiedliche Laufzeiten und Temperaturen in einer isotopenangereicherten, wässrigen Lösung eingelegt. Auf der Grundlage der Veränderungen in der Kristallstruktur und in den Isotopenverhältnissen der Zahngewebe wurden Lösungs- und Ausfällungsprozesse als Reaktionsmechanismen identifiziert. Darüber hinaus konnte gezeigt werden, dass Zahnschmelz sehr resistent gegen Alteration der chemischen Isotopenzusammensetzung der getesteten Isotope ist, während Dentin anfälliger für diagenetische Veränderungen ist.

Im zweiten Teil dieser Dissertation wurden DMT Analysen und nicht-traditionelle stabile Isotopensysteme ($\delta^{44/42}$Ca und $\delta^{88/86}$Sr) in ausgestorbenen permokarbonischen Tetrapoden gemessen, um frühe pflanzen- und fleischfressende Arten in fossilen Ökosystemen verschiedener Lokalitäten in den USA, Südafrika und Deutschland zu identifizieren. Als Ergänzung zu dem fossilen Isotopendatensatz wurden zusätzlich $\delta^{44/42}$Ca und $\delta^{88/86}$Sr in rezenten Schuppenechsen unterschiedlicher Ernährungskategorien gemessen. Die $\delta^{44/42}$Ca Werte zeigen einen Unterschied zwischen fleisch- und pflanzenfressenden Arten sowohl bei rezenten Schuppenechsen als auch bei ausgestorbenen permokarbonischen Tetrapoden, wobei Fleischfresser niedrigere Werte haben als Pflanzenfresser. Insekten- und eierfressende Schuppenechsen haben die höchsten $\delta^{44/42}$Ca Werte. Es ist kein systematischer Unterschied zwischen Knochen- und Zahnproben in rezenten Schuppenechsen feststellbar, in fossilen, ausgestorbenen Tetrapoden zeigen die Zahnschmelzproben allerdings weniger negative $\delta^{44/42}$Ca Werte als fossilen Knochenproben. Mit dem vorliegenden Datensatz kann nicht geklärt werden, ob diese Unterschiede durch diagenetische Überprägung oder durch Unterschiede in den physiologischen Fraktionierungsprozessen verschiedener Tierarten verursacht wird. Generell zeigen die $\delta^{44/42}$Ca Werte der Tiere aus dem oberen Perm einen ausgeprägteren Unterschied zwischen den Trophiestufen im Vergleich zu Arten aus dem unteren Perm. Dieser Unterschied wird möglicherweise verursacht durch Unterschiede in der Ernährung oder in physiologischen Fraktionierungsprozessen, besonders zwischen Pflanzenfressern aus dem unterem und oberem Perm. Die $\delta^{88/86}$Sr Werte zeigen, ähnlich wie $\delta^{44/42}$Ca, ebenfalls starke Unterschiede zwischen verschiedenen Ernährungskategorien in rezenten Schuppenechsen.

In permokarbonischen Fossilien ist die ante-mortem Sr Zusammensetzung allerdings deutlich durch Diagenese überprägt, was zu positiven $\delta^{88/86}$Sr Werten führt. Des Weiteren zeigen DMT Daten von fossilen permokarbonischen Tetrapoden keine Unterschiede zwischen Fleischfressern und Pflanzenfressern während sich die Insektenfresser signifikant von beiden unterschieden. Interessanterweise wurden Unterschiede innerhalb der pflanzen- und auch der fleischfressenden Ernährungskategorien festgestellt, was darauf hindeutet, dass die Tiere sich von Nahrung mit unterschiedlichen Materialeigenschaften (z. B. unterschiedliche Arten oder unterschiedliche Teile) ernährt haben und/oder unterschiedliche ausgeprägte Kauverhalten hatten, was zu signifikanten Unterschieden in den Abnutzungsspuren der Schmelzoberfläche führt.

Die Kombination von DMT Analysen und $\delta^{44/42}$Ca in einer Hauptkomponentenanalyse zeigt signifikante Unterschiede zwischen verschiedenen fleisch-, pflanzen- und mutmaßlich allesfressenden Arten aus dem späten Karbon, unterem und oberem Perm. Daraus kann geschlussfolgert werden, dass diese Arten artspezifische ökologische Nischen in spätkarbonischen und permischen Ökosystemen besetzten. Allerdings werden mehr Fauna- und Floraproben aus den jeweiligen Ökosystemen benötigt, um die $\delta^{44/42}$Ca Werte der Primärproduzenten, also der Pflanzen, zu bestimmen und die Unterschiede der $\delta^{44/42}$Ca Werte in den Pflanzenfressern besser interpretieren zu können. Die Ergebnisse der vorliegenden Dissertation zeigen, dass die Kombination von DMT Analysen und stabilen Ca Isotopen das Potenzial zu einer, im Vergleich mit einem Einzel-Proxy-Ansatz, präziseren Rekonstruktion von Nischenbesetzung und Trophieebenen in fossilen Ökosystemen hat.

Abstract

The main focus of this thesis was to determine whether dental microwear texture (DMT) and non-traditional stable isotopes are overprinted by diagenetic influences to provide a more thorough understanding of mechanisms behind, and effect of, post-mortem alteration in dental tissues. First, the teeth of several extant species were subjected to different experimental conditions intended to simulate diagenetic alteration. DMT and non-traditional stable isotopes were measured both before and after each experiment, to characterize dental wear features and *in-vivo* chemical composition as a result of simulated diagenetic alteration. Second, both dental microwear texture analyses (DMTA) and non-traditional stable isotopes were applied to fossil Permo-Carboniferous non-mammalian tetrapods to reconstruct dietary preferences and niche partitioning in the earliest terrestrial food webs.

In general, DMTA and non-traditional isotope systems are increasingly being applied to a great variety of taxonomic groups, such as Reptilia (including dinosaurs) and fish, as well as in modern and fossil ecosystems, to determine feeding categories and positions in trophic webs. In the fossil record, DMTA, as well as non-traditional stable isotopes might be biased by mechanical or chemical post-mortem alteration. Although, fossil tooth enamel is highly mineralized, and thus less prone to mechanical and chemical alteration compared to other hard tissues such as dentin and bone, it can still be diagenetically overprinted. To evaluate the impact of post-mortem fluvial transport, aeolian sediment transport or digestion of teeth on the dental surface, a tumbling, a sandblasting and an acid etching experiment were performed with different vertebrate species using various sediment grain size fractions and acidity conditions. These experimentally produced datasets were compared to a reference dataset of badly preserved dental surfaces resulting from sample excavation and preparation (e.g. adhesive varnish, bubbles in the mould). Using standardized parameters for dental wear (i.e. ISO surface and SSFA), the results of these analyses demonstrate that many post-mortem dental surface alterations are difficult to distinguish from diet-related ante-mortem wear features using DMT parameters alone. Instead, it is necessary for an observer to identify post-mortem features, and to evaluate the degree of alteration before samples are included in a dataset. In addition to diagenesis, limited oral processing behaviour or variable tooth replacement rates can also bias DMTA. For example, while some suborders with reduced mastication and tooth replacement, such as extant lepidosaurs (Reptilia), show diet-related ante-mortem wear features, the results presented in this thesis indicate that extant shark species are not good candidates for diet reconstruction using dental microwear texture. In sharks, it seems that either tooth-to-food contact is too reduced, tooth replacement rate is too fast, or a combination of both factors prevent diet-related dental wear from forming.

To increase our understanding chemical alteration on dental tissue, i.e. dentin and enamel, an *in-vitro* alteration experiment with cubes cut from an elephant tooth were placed in

aqueous isotope-enriched tracer solution at different temperatures and for different durations. Based on changes in the isotope ratios and Raman spectra of experimentally altered dental cubes, dissolution and re-precipitation was identified as the alteration mechanism. Furthermore, it was demonstrated that tooth enamel is highly resistant to chemical alteration of isotopic composition (at least for the isotopes tested in this study), while dentin is more prone to diagenetic alteration.

Finally, DMTA and non-traditional stable isotopes ($\delta^{44/42}$Ca and $\delta^{88/86}$Sr) have been applied to extinct non-mammalian tetrapods, to identify early herbivorous and faunivorous taxa in fossil ecosystems from different Permo-Carboniferous localities in the U.S.A., South Africa, and Germany. For the stable isotopes, extant lepidosaurs with distinct feeding strategies were measured to establish a modern comparative dataset. $\delta^{44/42}$Ca showed a separation of carnivorous and herbivorous taxa in both extant lepidosaurs and extinct non-mammalian tetrapods, with carnivores being more negative than herbivores. Insectivorous and ovivorous extant lepidosaurs yielded the least negative $\delta^{44/42}$Ca values of the measured samples. In general, no systematic offset between lepidosaur bones and teeth were detected, while in fossil non-mammalian tetrapods bones displayed less negative $\delta^{44/42}$Ca values than tooth enamel. So far it is not clear if this offset is caused by diagenesis or by physiological fractionation processes. $\delta^{44/42}$Ca values of upper Permian specimens show a more pronounced trophic spacing compared to lower Permian species, possibly caused by differences in diet or in physiological fractionation processes. $\delta^{88/86}$Sr showed distinct trophic spacing in extant lepidosaurs, similar to that observed for stable Ca. However in fossil specimens, Sr is clearly diagentically overprinted, resulting in positive $\delta^{88/86}$Sr values. In fossil tetrapods, DMTA revealed no differences between carnivores and herbivores, while insectivores differed significantly from both. Interestingly, differences were detected between taxa in both herbivorous and carnivorous feeding groups, suggesting that the mechanical properties of a food (e.g. type and part) and/or different oral processing behaviours, can introduce significant variation in dental wear signals, even within a feeding category.

Principal component analyses of combined DMTA and $\delta^{44/42}$Ca revealed distinct differences between carnivorous, herbivorous and presumed omnivorous taxa. Therefore, it is assumed that these taxa occupied species-specific niches in Late Carboniferous and Permian ecosystems. However, more faunal and floral samples from the respective ecosystems are needed to reconstruct $\delta^{44/42}$Ca values of the primary producers, i.e. plants, and to better understand the differences in $\delta^{44/42}$Ca values in herbivores. Nevertheless, the combination of DMTA and stable Ca data presented in this thesis illustrate the significant potential of this toolkit for more precise reconstruction of niche partitioning in fossil ecosystems when compared to a single proxy approach.

Acknowledgement

Table of Contents

Commonly used abbreviations

Ma: million years

DMTA: dental microwear texture analysis

3DST: 3D surface texture

SSFA: scale-sensitive fractal analysis

REE: rare earth element

EPMA: electron microprobe analysis

ICP-MS: inductively coupled plasma mass spectrometry

LA: laser ablation

MC-ICP-MS: multi-collector inductively coupled plasma mass spectrometry

NIST: National Institute for technology

RM: reference material

SD: standard deviation

TLE: trophic level effect

List of Figures

List of Tables

Chapter 1 Introduction

Diet connects animals and their environment and plays a major role for the evolution of the vertebrate terrestrial life. The ability of utilizing new food resources, such as cellulose-rich plant matter, and therefore new ecological niches is the key for a successful colonisation of new habitats and leads to a diversification of vertebrates over time (Price et al., 2012). During the mid-Ordovician (~ 467 Ma), colonization of land by the first plants began and spread rapidly earthwide during the early Silurian (~ 443 Ma; Strother et al., 1996; Tomescu, 2006; Steemans et al., 2009; Rubinstein et al., 2010, 2019). Almost 24 million years later, during the Lower Devonian period (around 419 Ma), the first land vertebrate fauna appeared, while the earliest tetrapods evolved from lobe-finned fishes (Payne et al., 2009; Dahl et al., 2010; Servais et al., 2010; George and Blieck, 2011). Through the first few millions of years of evolution and radiation of vertebrate terrestrial life, those animals were not able to access the available cellulose-rich plant matter. During the Lower Pennsylvanian, around 100 million years later, the first fully terrestrial amniotes, including sauropsid and synapsid clade, appeared (about 315 Ma; Sahney et al., 2010). The first terrestrial food webs were less complex than today with a lack of herbivorous vertebrate taxa. Herbivory, however, is a fundamental innovation for the development of a trophic structure in terrestrial ecosystems as we know them today, with a high number of herbivores feeding on primary producers and a lower number of carnivores feeding on herbivores (e.g. Olsen, 1966; DiMichele et al., 1992; Sues, 2000; Pearson et al., 2013; Reisz and Fröbisch, 2014). High-fibre herbivory evolved almost 100 million years after the first terrestrial tetrapods appeared, in the Late Carboniferous, near the Permo-Carboniferous boundary (~ 298.9 Ma, Reisz, 1997; Sues and Reisz, 1998).

Herbivory includes a great diversity of different more specialized feeding strategies, such as frugivory, algaevory or folivory and evolved independently multiple times in both major monophyletic groups of amniota, Sauropsida and Synapsida (Reisz and Sues, 2000; Reisz and Fröbisch 2014). Synapsids are of particular interest for understanding the evolution of extant communities, since mammals evolved within this clade (Reisz and Sues, 2000). During the Palaeozoic non-mammalian synapsids dominated the terrestrial fauna with a great diversity, while sauropsids (including extant reptiles and dinosaurs) were less divers and less widely distributed (Kissel and Reisz, 2004, Reisz and Fröbisch, 2014). Synapsids were able to occupy different ecological niches and developed a great variety of feeding strategies within one single clade, including large herbivorous taxa such as Edaphosauridae (e.g. Spindler et al., 2020) and Caseidae (Reisz and Fröbisch, 2014), piscivorous taxa like *Ophiacodon* (Romer and Price, 1940; Reisz, 1986), or smaller faunivores as well as large apex predators such as *Dimetrodon* (e.g. Brink and Reisz, 2014). Also, their dentition underwent a functional diversification including the development of dental occlusion, which ultimately led to the oral processing of food, i.e. chewing (Sues and Reisz, 1998; LeBlanc et al., 2018). An improved

understanding of synapsid diet preferences and feeding behaviour, especially the evolution of herbivorous feeding strategies, will help to better constrain their radiation and survival across the largest extinction event in Earth history at the Permian-Triassic boundary (Erwin, 1990, 2015; Sahney and Benton, 2008).

Dietary reconstruction of extinct synapsids can be difficult and is mostly based on tooth shape analyses or morphological features of the cranial and postcranial skeleton (e.g. Modesto, 1995; Maddin et al., 2008; Brink and Reisz, 2014). Direct evidence of diet, such as gastrointestinal contents or coprolites (e.g. Karlsruhe and Sues, 1993; Kowalewski and Kelley, 2002), however, are rarely preserved in the fossil record. An unexplored dietary proxy for synapsids is dental microwear texture analysis (DMTA), which provides information about mechanical food properties of the last meals (Winkler et al., 2020a). DMTA has already successfully been used to differentiate between various dietary groups in mammalian, as well as in non-mammalian taxa (i.e., grazer and browser: Schulz et al., 2010; Fraser and Theodor, 2011; Calandra and Merceron, 2016; faunivores: DeSantis et al. 2012, 2015, 2017; Stynder et al., 2019; reptiles: Bestwick et al, 2019; Winkler et al., 2019a; mammal-like reptiles: Kalthoff et al., 2019; fish: Purnell et al., 2016, aquatic mammals: Purnell et al., 2017; Bethune et al., 2019). However, since DMTA is a mechanical proxy it might be biased by diagenetic alteration and dental surfaces should therefore be evaluated carefully prior to analysis (Böhm et al., 2019). Chemical proxies, such as traditional and non-traditional stable isotopes, however, are increasingly used to reconstruct diet, trophic level, and predator-prey relationships of vertebrates (e.g. Skulan et al., 1997; Kohn and Cerling, 2002; Knudson et al., 2010; Newsome et al., 2010; Schoeninger, 2012; Jaouen et al., 2013; Martin et al., 2014, 2017a; Tacail et al., 2020). Nitrogen isotopes ($\delta^{15}N$) of bone collagen and more recently tooth enamel are an established trophic level proxy (e.g. DeNiro and Epstein, 1981; Leichliter et al., under review), as well as stable carbon isotopes ($\delta^{13}C$, e.g. DeNiro and Epstein, 1978). Non-traditional stable isotopes, such as Ca, Sr, Mg, and Zn are stored in the bioapatite of bone and tooth material, and elemental ratios of Sr/Ca or Ba/Ca are used as proxies for trophic level and diet reconstruction in both terrestrial and marine food webs (e.g. Burton et al., 1999; Blum et al., 2000; Balter, 2004; Martin et al., 2014, 2015a). The major element Ca, as well as the trace elements Zn, Mg and Sr are successfully used as dietary and trophic level proxies ($\delta^{44/40}Ca$ or $\delta^{44/42}Ca$: Skulan et al., 1997; Clementz et al., 2003; Heuser et al., 2011; Melin et al., 2014; Tacail et al., 2020; $\delta^{66/64}Zn$: Jaouen et al., 2013, 2016a, b, 2020; Bourgon et al., 2020; $\delta^{26/24}Mg$: Martin et al., 2014, 2015b; $\delta^{88/86}Sr$: Knudson et al., 2010; Lewis et al., 2017). In general, bone (collagen and the mineral phase) and tooth dentin are prone to diagenesis due to their high organic content. Therefore, their trace and main element composition can be altered due to post-mortem diagenesis (Tütken and Vennemann, 2011; Kohn et al., 2013). Tooth enamel, however, is highly mineralized and consists almost exclusively of hydroxylapatite, therefore

pristine trace element ratios and major element isotope compositions may be preserved over millions of years (Kohn et al, 1999; Sponheimer and Lee-Thorp, 2006). This is especially true for Ca, which is the major component of bones and teeth (~ 380 mg/g) and is therefore much more resistant against post-mortem alteration than other elements that occur in lower concentrations (Heuser et al., 2011). The combination of non-traditional stable isotope systems with dental microwear texture analysis could provide important new insights into fossil trophic systems, and serve as a new toolset for sophisticated dietary reconstruction of extinct taxa based on both chemical and mechanical proxies.

1.1. Definition of goals

The focus of this thesis was to determine the resistance of DMTA and non-traditional stable isotopes against diagenesis in an effort to provide a better understanding of alteration of dental wear features and *in-vivo* chemical composition in dental tissues. Diagenetic alteration experiments, including tumbling in sediment suspension, sandblasting and acid etching, will be used to obtain qualitative and quantitative data regarding the influence of mechanical and chemical alteration to DMTA. An in-vitro alteration experiment using isotopically enriched tracer solution will provide information on the mechanisms behind post-mortem changes in isotope composition (traditional and non-traditional) of dental tissue (dentin and enamel), as well as qualitative and quantitative statements on differences in the vulnerability of dental tissues and different isotope systems to diagenetic alteration.

The ultimate goal of this thesis was the combination of DMTA and Ca and Sr stable isotopes to reconstruct long-term (evolutionary) and short-term (ontogenetic) dietary preferences and feeding categories in Permo-Carboniferous non-mammalian tetrapods. Stable isotopes should distinguish between different trophic levels (herbivorous and faunivorous taxa), while DMTA should distinguish between hard- and soft-object feeders within specific trophic levels and ecological niches.

1.2. Structure of this thesis

The initial requirement for using this combined tool set for diet reconstruction was validating the stability of the different dietary proxies over prolonged time spans and for different diagenetic alteration scenarios. The first part of the following thesis therefore focuses on four experimental studies, each designed to address a specific diagenetic scenario, exploring its application to new taxa, as well as testing the stability of different isotopes systems under experimental diagenesis conditions. The resistance of diet specific dental microwear textures against diagenetic alteration, fluvial transport in particular (**Manuscript I, Chapter 3**), is tested in a tumbling experiment, using teeth from two large and one small mammal. The zebra (*Equus* sp.) was chosen as a grazing and the row deer (*Capreolus capreolus*) as a

browsing taxon, as well as one small mammal (*Otomy* sp., African vlei rat) as comparison. Teeth were tumbled in a sediment-water suspension with three different sand grain size fractions (51 – 513 µm) for up to 336 hrs (equivalent to ~ 366 km). Their surface texture was measured both before and after the experiment to quantify the impact of mechanical abrasion on the dental surface due to fluvial transport. In a second study (**Manuscript II, Chapter 4**) further tumbling experiments with one shark (*Carcharhinus plumbeus*, sandbar shark) and one crocodile species (*Crocodylus niloticus*, Nile crocodile), as well as a larger gravel grain size fraction, a sandblasting and an acid etching experiment were conducted. For the sandblasting experiment, polished dental surfaces were sandblasted with loess (Ø 36.86 µm) and quartz fine sand (Ø 166.01 µm) to simulate mechanical abrasion due to aeolian sediment transport. The acid etching experiment was conducted to simulate chemical erosion during digestion in a predator stomach, using teeth from the African vlei rat, the sandbar shark and the Nile crocodile. In addition to the experimental post-mortem dental surfaces, a first catalogue of badly preserved and taphonomically altered dental enamel surfaces was compiled (**Manuscript III, Chapter 5**), i.e. a set of bad surfaces resulting from excavation or preparation blunders. In a novel approach, such altered surfaces were not only visually identified by an observer, but also by using a set of standardised DMTA parameters employed for dietary reconstruction. Additionally, the application of DMTA for further non-mammalian taxa, in this case sharks, was explored (**Manuscript IV, Chapter 6**). Therefore, dental surfaces of 24 different extant as well as 12 extinct shark species were analysed to test whether ante-mortem wear is related to ingested diet or habitat preferences and resistant to post-mortem alteration processes.

Apart from DMTA, the evaluation of geochemical diagenetic stability was also tested by an in-vitro alteration experiment. Dental material from an African elephant (*Loxodonta africana*) was cut into cubes of enamel and dentin (about 3.3 mm mean edge length) and immersed in an isotopic tracer solution at different durations up to 3 months and two different temperatures (30 and 90 °C). The tracer solution was isotopically enriched in ^{25}Mg, ^{44}Ca, ^{67}Zn and ^{86}Sr to assess the diagenetic stability of Ca and Sr isotopes as well as Mg and Zn as additional potential dietary proxies in dental enamel (**Manuscript V, Chapter 7**). Changes in element concentrations, isotope ratios and crystal structure were quantified using LA-(MC-)ICP-MS, EMPA and Raman spectroscopy.

In the second part of this doctoral thesis, the application of the new combined tool set for diet reconstruction is explored to connect different methods of dietary reconstruction. DMTA as well as Ca and Sr isotopes were measured for a great variety of Permo-Carboniferous non-mammalian tetrapods from localities in South Africa, Germany and the U.S.A. (**Chapter 8**). As a comprehensive dataset for Ca and Sr in fossil specimens, a set of extant lepidosaurs

(Sauropsida, Reptilia) were measured as well. These measurements present the first preliminary DMTA and stable isotope datasets for fossil non-mammalian tetrapods.

Chapter 2 Theoretical background

To understand how diet influences vertebrate hard tissues, i.e. bones and teeth, including dental wear and chemical composition, knowledge about their formation is necessary. The following paragraphs provide an overview of the different aspects of tooth and bone formation and discuss the analytical methods commonly used for diet reconstruction. Due to the proposed application to past food webs, information about Late Carboniferous, Permian and Lower Triassic sites and tetrapods will also be provided.

2.1 Skeletal tissue

Vertebrates differ from invertebrates in that they possess endoskeletons, i.e. skeletal hard tissues within their bodies, in which the essential Ca and P are stored. Due to the higher fossilisation potential of hard tissues in comparison to soft tissues, the evolution of biomineralization of hard tissues resulted in an increasing number of body fossils, i.e. fossil bones and teeth, at the beginning of the Phanerozoic (~ 541 Ma) (Lowenstam, 1980; Lowenstam and Margulis, 1980; Lowenstam and Weiner, 1983, Cook and Shergold, 1984; Murdock and Donoghue, 2011). The increased preservation of hard tissues through time provides more opportunities to reconstruct the ecology of extinct organisms.

2.1.1 Bones

In the early ontogenetic stage of vertebrate life, bone material is formed by the osteoid (unmineralized, organic basic substance of bone tissue), into which hydroxylapatite ($Ca_{10}(PO_4)_6(OH)_2$, Berkovitz and Shellis, 2016) is incorporated and subsequently mineralised (Boskey and Posner, 1977; Lowenstam and Weiner, 1989; Olszta et al., 2007). This primary mineralised bone is remodelled constantly during the lifetime of a vertebrate by dissolution and precipitation processes. During the ontogeny, this remodelling leads to significant structural and chemical changes of bone tissue composition and bone density. The degree of mineralisation increases, while the collagen content and water content decreases (Posner, 1969; Lowenstam and Weiner, 1989; Dorozhkin and Epple, 2002; Olszta et al., 2007). Young secondary bone has a high porosity and consist of ~ 650 mg/g mineral phase, ~ 250 mg/g organic matrix, mostly collagen and 100 mg/g water (Lowenstam and Weiner, 1989; Dorozhkin and Epple, 2002; Currey, 2003; Olszta et al., 2007). Different types of bones, as well as different parts of the same bone show different remodelling speeds leading to time averaged

values in the chemical composition of bulk bone samples. Therefore, these bulk samples reflect the last years of vertebrate's life, depending on the turnover rate and the animal's longevity (e.g. Burkhardt et al., 1984; Agerbaek et al., 1991; Eriksen, 1986, 2010; Hill, 1998).

2.1.2 Teeth

In mammals, teeth are formed over a relatively short span of time, ranging from months up to two years early in an animal's life and are not remodelled afterwards (Hillson, 2005). During ontogeny, different teeth within the jaw are formed at different ontogenetic ages. While some teeth are formed prenatally, others begin to form after birth. This timing of formation is species-specific (e.g. Hillson, 2005; Jernvall and Thesleff, 2012; Koch et al., 2017; Kreiborg and Jensen, 2018). In general, mammalian tooth mineralisation starts during early ontogeny, although there are some dental tissues (e.g. rodent incisors or tusks) which are ever-growing. In contrast to monophyodont (without tooth replacement) and diphyodont (deciduous and permanent teeth) mammals (**Fig. 2.1A**), teeth are continuously replaced throughout life (polyphyodonty) in some fish, reptile or amphibian species (**Fig. 2.1A**). In these animals teeth do not reflect only the early ontogenetic life stages of an animal (e.g. Berkovitz and Shellis, 2016; Kreiborg and Jensen, 2018).

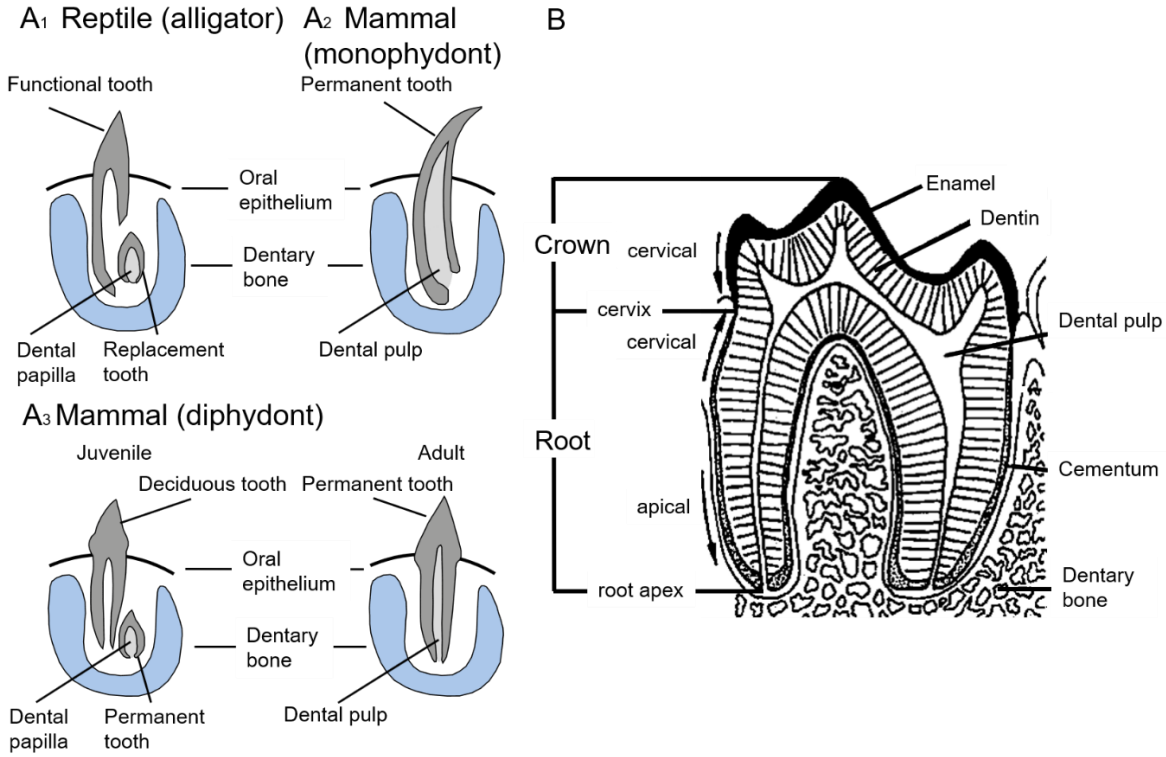

Figure 2.1. Schematic sketch illustrating tooth formation. A_1 Functional and replacement tooth in alligator (Reptilia), A_2 Permanent tooth in a monophyodont mammal, A_3 Deciduous (juvenile) and permanent (adult) tooth in diphyodont mammals. B Illustration of tooth structure with enamel covering the dentin at the crown, modified from Berkovitz and Shellis (2016, 2018).

The mature teeth of most vertebrates consist of three different types of hard tissue: tooth enamel or enameloid, dentin and tooth cementum (**Fig. 2.1B**). Enamel formation is separated into general two phases, (pre-)secretion and mineralisation). First, an organic matrix is produced by formative cells (secretion) and second the matrix mineralizes due to the deposition of calcium phosphate (apatite mineralisation, for more details see Berkovitz and Shellis, 2016). The enamel is the outermost functional part of a tooth and covers the dentin at the crown. The root of a tooth consists of dentin and is covered with a thin layer of tooth cementum, which attaches the tooth to the jawbone (Hillson, 2005; Berkovitz and Shellis, 2016, 2018). The cementum has the highest organic content (around 230 mg/g) and is not often included in isotope studies on dental material (Hillson, 2005; Goldberg and Smith, 2004; Ungar, 2010). Dentin is more resistant against diagenetic alteration due to its higher hydroxylapatite content (around 700 mg/g; Ungar, 2010). It is also more resistant than bone, since it is more compact with a different and randomized crystal structure (Hillson, 2005). Nonetheless, dentin still has a relatively high organic content (collagen ~ 200 mg/g) and is penetrated by dental canaliculi, which make it porous and susceptible to diagenetic alteration (Kohn et al., 1999; Heuser et al., 2011). The hard tissue most resistant against diagenetic alteration is tooth enamel/enameloid. Enamel has a higher density and crystallinity, as well as a lower porosity and organic content than both dentin and bone. It's hydroxylapatite content is ~ 970 mg/g, while the remaining fraction is composed of water and organics (amelogenin and phosphoprotein, ~ 9 mg/g, Hillson, 2005; Maas and Dumont, 1999; Ungar, 2010). Tooth enameloid covers the tooth dentin of all sharks and most bony fish and consists, in contrast to tooth enamel, exclusively of fluorapatite ($Ca_5(PO_4)_3F$, Suga et al., 1991; Berkovitz and Shellis, 2016). Tooth enamel/enameloid and dentin are continuously deposited in increments during tooth formation, reflecting the isotopic composition of the body fluid of the associated time span of formation. The isotopic time period over which dietary and environmental information are recorded in enamel differs between species, however, it represents a time series for the duration of enamel formation (Balasse, 2002; Hoppe et al., 2004).

2.2 Bone and tooth chemistry

Skeletal and dental tissue is formed and remodelled (bones) chemically is influenced by the chemical composition of body fluid, namely blood, of an animal (Bryant and Froelich, 1995; Martin et al., 2017a). The chemical composition of body fluid is determined by the chemical composition of ingested food and drinking water and the fractionation of different isotopes during metabolism and tissue formation (Bryant and Froelich, 1995). Therefore, skeletal and dental tissue can be used to reconstruct modern and fossil ecosystems and environments (e.g. Trueman and Tuross, 2002; Ambrose and Krigbaum, 2003, Sponheimer

and Lee-Thorp, 2003; Bedaso et al., 2013), as well as trophic ecology (for a review see Martin et al., 2017a) during a specific period of an animal's life (e.g. Hoppe et al., 2004). Depending on an individual's age and life expectancy, bones reflect the last year(s) of life as a result of bone remodelling (e.g. Eriksen, 2010). Teeth reflect different time spans, depending on species, time of tooth formation and rate of tooth replacement (e.g. Hillson, 2005).

In the following section, a brief overview of different isotope systems and their use for palaeoenvironmental, palaeoecological or palaeobiological studies is provided. In general, both organic and inorganic matter of the skeletal and dental tissues can be used in geochemistry, however reconstructions based on the organic matter in skeletal tissues, namely collagen, are limited since collagen is prone to diagenetic alteration and therefore only rarely preserved in fossil bones and teeth (e.g. Jones et al., 2001; Avci et al., 2005; Schweitzer et al., 2005; Lee et al., 2017). Carbon, nitrogen and sulphur isotopes in collagen can be used for diet and trophic reconstruction in extant and extinct food webs ($\delta^{13}C$: e.g. DeNiro and Epstein, 1978; Vogel, 1978; Zanden and Rasmussen, 2001; van der Merwe et al., 2008; Lee-Thorp et al., 2010; Schoeninger, 2012; $\delta^{15}N$; e.g. DeNiro and Epstein, 1981; Ambrose, 1986, 1990; Zanden and Rasmussen, 2001; Jürgensen et al., 2017; Leichliter et al., under review (in tooth enamel); $\delta^{34}S$: e.g. Hesslein et al., 1991; Richards et al., 2001; Goedert et al., 2016; Rand and Nehlich, 2018), dating (^{14}C: e.g. Bronk, 2008; Harvey et al., 2016) and provenance reconstruction ($\delta^{34}S$; e.g. Trust and Fry, 1992; Connolly et al., 2004; Doubleday et al., 2018). The inorganic matrix of skeletal and dental tissue is more resistant to diagenetic alteration (Wang and Cerling, 1994; Hedges, 2002) and records major as well as trace elements in the hydroxylapatite ($Ca_{10}(PO_4)_6(OH)_2$). The main components of hydroxylapatite are calcium (Ca), phosphorous (P), oxygen (O) and hydrogen (H) (**Fig. 2.2**). All elements can be substituted ante- and post-mortem by different trace and major elements (**Fig. 2.2**).

Calcium can be substituted by trace elements, such as strontium (Sr), zinc (Zn), magnesium (Mg) and rare earth elements (REEs) (Kohn et al., 1999). Stable isotopes of Ca ($\delta^{44/42}Ca$, $\delta^{44/40}Ca$), magnesium ($\delta^{26/24}Mg$), zinc ($\delta^{66/64)}Zn$, strontium ($\delta^{88/86}Sr$), as well as element-to-calcium ratios provide information about diet and trophic position in extant or extinct food webs (e.g. Sillen and Lee-Thorp, 1994; Skulan et al., 1997; Balter et al., 2002; Clementz et al., 2003; Sponheimer et al., 2005; Knudson et al., 2010; Heuser et al., 2011; Jaouen et al., 2013, 2016a, b, 2020; Melin et al., 2014; Martin et al., 2014, 2015a, b; Lewis et al., 2017). CO_3 can be substituted ante-mortem for the PO_4 group (~ 90 %) as well as for the OH group in hydroxylapatite **(Fig. 2.2**), and thus can also be used for diet reconstruction ($\delta^{13}C$: e.g. DeNiro and Epstein, 1978; Lee-Thorp et al., 2010; Schoeninger, 2012) or dating (^{14}C: e.g. Bronk, 2008; Harvey et al., 2016). Oxygen stored in the hydroxylapatite (PO_4, CO_3, OH) is mainly used for climate reconstruction ($\delta^{18}O_{PO4}$: e.g. Longinelli, 1984; Koch et al., 1989; Fricke and O'Neil,

1996; Amiot et al., 2011) and reconstruction of body temperature ($\delta^{18}O_{CO3}$: e.g. Amiot et al., 2006; Bernard et al., 2010; clumped isotopes: Eagle et al., 2010, 2011).

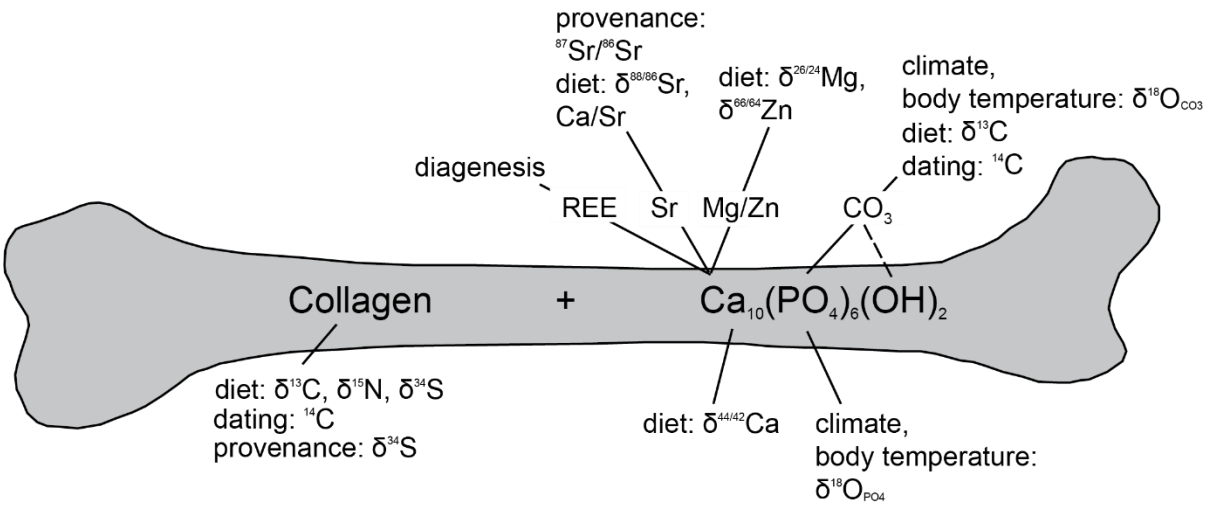

Figure 2.2. Schematic sketch illustrating which isotopes occur in collagen and hydroxylapatite in bone and their methodological applications, modified from Tütken (2003).

Radiogenic Sr ($^{87}Sr/^{86}Sr$) is used for reconstructing migration and provenance (e.g. Bentley, 2006; Fischer et al., 2013; Martin et al., 2016). Rare earth elements (REEs) are typically incorporated into skeletal and dental tissue only in minor sub ng/g quantities while the animal is alive, and start to accumulate in significant amounts only after the death of an animal. and are thus mainly used as a proxy for diagenetic alteration (e.g. Kohn et al., 1999; Tütken et al., 2008; Reynard and Balter, 2014). In addition, Uranium (U) can substitute Ca in hydroxylapatite and is sometimes used for dating of fossil skeletal and dental material, using combined ($^{234}U/^{238}U$) and ($^{230}Th/^{238}U$) activity ratios (e.g. Reynard and Balter, 2014). However, bones and teeth are usually not a closed system for U and Th, hampering the successful application of U-series disequilibrium dating (e.g. Bourdon et al., 2003).

2.2.1 Calcium and Strontium isotopes

Calcium is an essential element and exclusively incorporated into the organism from ingesta and drinking water. There are six stable, naturally occurring Ca isotopes (^{40}Ca, ^{42}Ca, ^{43}Ca, ^{44}Ca, ^{46}Ca, ^{48}Ca). During incorporation from the ingesta into the body, a strong fractionation against the heavier ^{44}Ca occurs with preferred incorporation of the light ^{42}Ca. This leads to a decreasing $^{44}Ca/^{42}Ca$ ratio in the bone/tooth compared to the diet (expressed as $\delta^{44/42}Ca$ value in permil (‰)), with a systematic offset between diet and bone of about -0.57 ± 0.10 ‰, i.e. bone being isotopically lighter than diet (Skulan and DePaolo, 1999; Chu et al.,

2006; Hirata et al., 2008; Tacail et al., 2014). When moving up the trophic food chain the less heavy ^{44}Ca is available and therefore the $\delta^{44/42}Ca$ of bioavailable Ca is decreasing with increasing trophic level of a vertebrate (marine ecosystems: Clementz et al., 2003; Martin et al., 2015a, 2017b, terrestrial ecosystems: e.g. Heuser et al., 2011; Melin et al., 2014; Martin et al., 2017a, 2018; Hassler et al., 2018). In general, herbivorous taxa have lower $\delta^{44/42}Ca$ values than their plant diet, and faunivores have lower $\delta^{44/42}Ca$ values than their meat diet, if they ingest also more than 1-2 % of bone, which is Ca-rich and^{44}Ca-depleted (**Fig. 2.3A**, Heuser et al., 2011; Martin et al., 2018). Using this systematic fractionation, or trophic level effect (TLE) along the food chain, it is possible to identify apex predators with high bone ingestion rates as well as herbivores in fossil food webs. Importantly, unlike other trace elements, the original Ca isotope composition of skeletal and dental tissue should have a long-term preservation potential, since the concentration of Ca in diagenetic fluids is negligible compared to the concentration of Ca in hydroxylapatite (Martin et al., 2017a). Therefore, Ca should be a reliable proxy for diet reconstruction in deep time (Heuser et al., 2011; for a detailed review on Ca isotopes in vertebrate palaeontology see Tacail et al.,2020).

Another promising, but largely underexplored, isotope system for diet reconstruction is stable Sr. Preliminary studies suggest that this isotope might be useful as a complementary trophic level proxy to stable Ca. Strontium is incorporated into tissues via food and drinking water. This element substitutes for Ca in hydroxylapatite (Martin et al., 2017a) and has four naturally occurring isotopes (^{84}Sr, ^{86}Sr, ^{87}Sr, ^{88}Sr). One of these isotopes, ^{87}Sr is radiogenic (the daughter isotope of ^{87}Rb), and is a commonly used proxy for determining provenance and migration patterns in archaeology (for review see Bentley, 2006) and palaeontology (e.g. Hoppe et al., 2003; Kocsis et al., 2009; Martin et al., 2016; Terrill et al., 2020). The radiogenic Sr signatures ($^{87}Sr/^{86}Sr$) of the bedrock which underlies the areas in which the animals spent their lives varies with age and bedrock composition. This composition is recorded, without measurable biological fractionation in animals' biological tissues and thus can be used as a geological fingerprint. Although less commonly reported, stable Sr isotopes ($\delta^{88/86}Sr$), can be measured in the same samples and serve as a dietary proxy. Similar to Ca, fractionation takes place during biological processes, resulting in the preferred incorporation of the lighter ^{86}Sr over the heavier ^{88}Sr, in turn resulting in decreasing $\delta^{88/86}Sr$ values along the food chain (**Fig. 2.3A).** Therefore, by measuring Sr in archaeological human populations it is possible to evaluate differences in paleodiet ($\delta^{88/86}Sr$) together with paleomobility ($^{87}Sr/^{86}Sr$) from the same specimens (Knudson et al., 2010). However, Sr is a trace element and occurs in lower abundance in bioapatite compared to Ca, so Sr is more prone to post-mortem alteration (Kohn et al., 1999; Hoppe et al., 2003), thus limiting the application of stable Sr in fossil material. Various rock types display characteristic Sr isotope composition with positive $\delta^{88/86}Sr$ values while humans and animals typically yield negative therefore $\delta^{88/86}Sr$ values (Hajj et al., 2017;

and references therein). Therefore, such non-depleted $\delta^{88/86}Sr$ values in fossil vertebrates would imply a diagenetic alteration of ante-mortem Sr composition (Neymark et al., 2014).

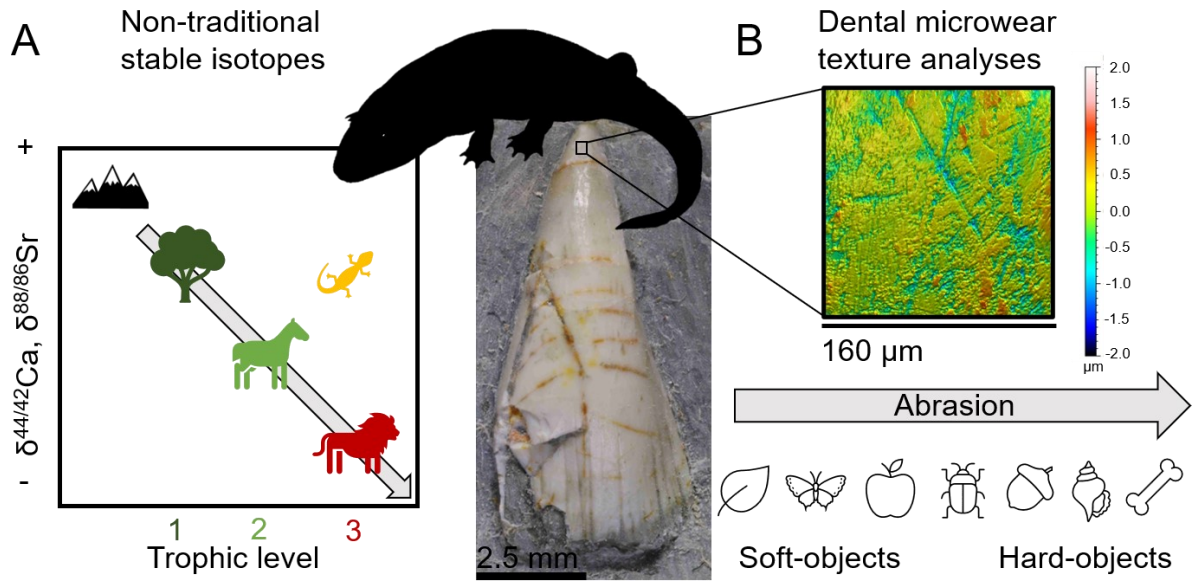

Figure 2.3. Illustration of non-traditional stable isotopes and DMTA as dietary proxies. A. the trophic level effect (TLE) in Ca and Sr isotopes and B. effects of soft- and hard-objects on abrasion of dental surface in dental microwear texture analysis (DMTA) together with an exemplary tooth of a lower Permian eryopid (amphibious Temnospondyli).

2.3 Dental microwear texture analyses

The masticatory apparatus, including teeth, is the link between ingested diet and the organism itself. For endothermic animals such as mammals, all the energy needed to sustain their high metabolic rate comes from their ingested diet, therefore, it is necessary to extract nutrients from the food as efficiently as possible (Clissold, 2007). The teeth, together with the muscles, mechanically reduce food to small pieces prior to swallowing. During this mastication process both the food and also the teeth themselves are mechanically damaged. Tooth-to-tooth contact (attrition) and tooth-to-food/ tooth-to-particle contact (abrasion), fracture and abrade enamel material on the dental surface and lead to material loss and the formation of distinct wear features at the µm-scale (Dahlberg and Kinzey, 1962). Dental wear analysis is typically performed on tooth enamel at a variety of spatial scales (mesowear: e.g. Green and Croft, 2018; Ackermans, 2020; microwear: e.g. Gordon, 1988; Ungar et al., 2003; dental microwear texture analysis: e.g. Calandra and Merceron, 2016). Tooth enamel is preferred over dentin because enamel covers the whole occlusal surface it is functionally more important during the mastication process in mammals (Hillson, 2005). Furthermore, according to its higher crystallinity (Hillson, 2005), enamel is harder than dentin and therefore mechanically

more resistant to diagenetic alteration. However, dental microwear has also been successfully applied on e.g., orthodentin of Xenarthra (Green and Resar, 2012; Resar et al., 2013) and different dinosaur species (Williams et al., 2008; Kubo and Kubo, 2014; Varriale, 2016).

One of the first studies connecting dental wear features to abrasion was performed by Baker et al. (1959). They found dental wear features on sheep's teeth to be caused by abrasion with opal-phytoliths of fodder plants, as well as potentially by opal-phytoliths and other minerals from the soil. Subsequent microwear studies were performed using a scanning electron microscope (SEM, e.g. Walker et al., 1978; Ungar, 1995), which is very time consuming. In general, 2D microwear is based on the quantity of pits and scratches, categorized depending on their length-width ratio, scored by an observer (Gordon, 1988). The technique was further developed and improved by methodological changes that employ low-magnification stereomicroscopy (Solounias and Semprebon, 2002) including the analysis of a standard enamel surface area (of 0.09 mm²), the establishment of size-based categories for wear features and the use of image analysis software (Merceron et al., 2004, 2005). In general, using classical 2D microwear, it is possible to statistically distinguish between the diets of different herbivorous ungulates, by counting the number of scratches (more grass consumption) versus pits (more browse diet, e.g. Semprebon et al., 2004a, b; Merceron et al., 2006, 2010; Ungar et al., 2007; Calandra et al., 2008; Solounias et al., 2010). However, 2D microwear is strongly limited by observer bias, because the method is based on visually counting single wear features, and is difficult to reliably reproduce by different observers (Grine et al., 2002). See Ungar et al., 2003 for a review of dental microwear studies.

Dental microwear texture analysis (DMTA) has several advantages compared to classical 2D microwear analysis. However, since DMTA is one of the main analytical methods used in this thesis and extensively described in the following chapters, it will only be briefly discussed at this point. In this method, the 3D topography of dental surface is quantified using confocal microscopy and wear features are automatically characterised using length-scale and area-scale fractal parameters (SSFA, e.g. Ungar et al., 2003, 2012; Scott et al., 2006; Scott, 2012) and standardised surface texture roughness (ISO 25178) and flatness (ISO 12781), motif, furrow and direction parameters (3DST, e.g. Schulz et al., 2010, 2013a, b; Purnell and Darras, 2016; Kubo et al., 2017; Purnell et al., 2017; Winkler et al. 2019b). This standardised method avoids observer-induced bias and errors, and improves comparability across different users and laboratories. Originally, DMTA was developed for extant and extinct terrestrial mammals (e.g. Ungar et al. 2003, 2007, 2008, 2020; Scott et al., 2005; Merceron et al., 2007; Merceron and Madelaine, 2008; Scott et al., 2009; Schulz et al., 2010; Calandra et al., 2012; Purnell et al., 2013; Schulz et al., 2013b; Winkler et al., 2013, 2016; Kubo et al., 2017; Schulz-Kornas et al., 2019), as a short-term proxy, reflecting the last consumed meals. The temporal scale on which diet specific microwear texture is formed and overwritten (turnover) differs

between species and depends on factors including food properties, environment and oral processing (Teaford and Glander, 1991, 1996). In rats, for example the turnover rate of microwear features is about 28-35 days (Winkler et al., 2020a) while in vervet monkeys it is about 1–2 weeks (Teaford and Oyen, 1989).

Different soft- or hard-object feeding strategies are characterized by specific wear features, which allow the assignation of individuals to specific feeding categories (**Fig. 2.3B**, e.g. Scott et al., 2005; Merceron et al., 2007; Schulz et al., 2010; Winkler et al., 2013). However, unlike mammals, other clades of animals such as fish, ancient non-mammalian synapsids or reptiles (including dinosaurs), food items are not processed by thorough mastication, and tooth-to-food contact is therefore short. Recent studies, however, have successfully applied DMTA to many extant and extinct vertebrate taxa other than mammals (reptiles: Bestwick et al., 2019, 2020; Winkler et al., 2019a; mammal-like reptiles: Kalthoff et al., 2019; fish: Purnell et al., 2016), and have demonstrated that even reduced tooth-to food contact produce diet related wear features.

2.4 Diagenetic alteration of bones and teeth

After the death of an organism, all physiological processes stop and tissue decay processes begin directly post-mortem. From a carcass to burial to subsequent decay, an organism undergoes various taphonomic processes, including disarticulation, transport or weathering (**Fig. 2.4**, for an overview see Müller, 1992; Denys, 2002). After burial, microbial activity, pH, temperature, water and soil compositions all influence the fossilization process. Only a small fraction of vertebrate remains actually fossilize (Müller, 1992). After the decay of soft tissues, chemical and/or mechanical alteration of the hard tissues begins. The diagenesis of skeletal and dental tissues is an active and large area of research. The summary provided here is not meant to be exhaustive, but rather focuses on certain key diagenetic processes which are weathering, abrasion, transport, recrystallisation and mineralisation.

The chemical alteration of skeletal and dental tissue can be rather complex so only the main points are presented in the following paragraph. Bone diagenesis can be separated into two phases, early and late diagenesis (Pfretzschner, 1998, 2000, 2001, 2004). During early diagenesis, the organic matter, namely collagen, is degraded and removed and consequently the porosity of hard tissue and the crystallinity of the hydroxylapatite changes (Pfretzschner, 1998, 2004; Hedges, 2002). In general, there are two types of collagen degradation during early diagenesis; microbial and chemical decay, which can occur simultaneously (Collins et al., 1995, 2000, 2002; Nielsen-Marsh et al., 2000; Carter et al., 2007; Turner-Walker, 2012).

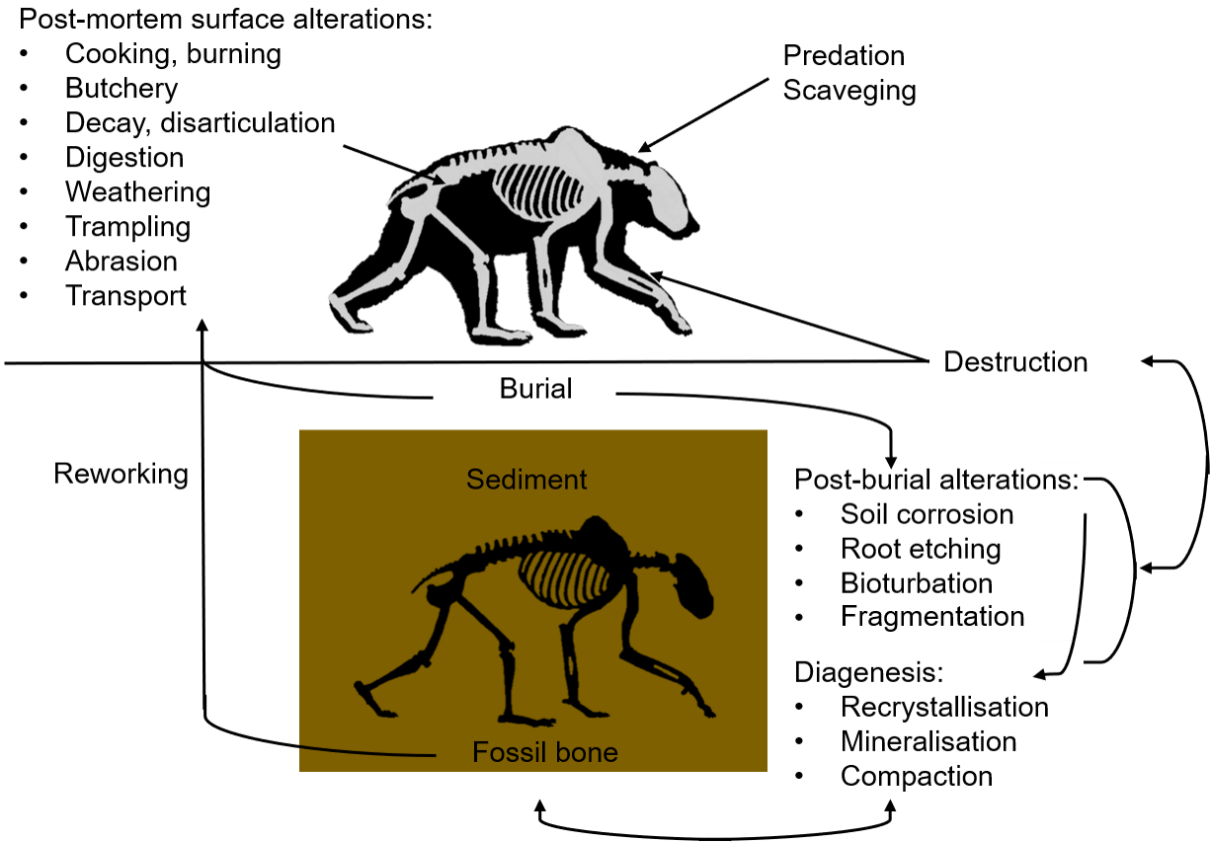

Figure 2.4. Schematic illustration of pre-burial and post-burial post-mortem alteration processes (modified from Deny, 2002).

Microbial decay occurs for around 500 years (Hedges, 2002) during which time the bioapatite is dissolved by acidic metabolites secreted by the microbes in order for the microbes to reach the collagen (Child, 1995). This bioerosion leads to characteristic “tunnels” that partly destroy the bone and tooth histology and increase the porosity of the tissue (e.g. Hackett, 1981; Hedges et al., 1995; Jackes et al., 2001; Cobaugh et al., 2015). Additionally, after dissolution and resorption of the original apatite and collagen, the microbes secrete a more highly mineralised apatite, which is deposited in the bioerosion tunnels (Hackett, 1981; Jackes et al., 2001). The much slower inorganic chemical decay breaks the peptide bonds of the collagen by hydrolysis and transforms it into a gel (Collins et al., 1995; Nielsen-Marsh et al., 2000). Due to possible storage of water molecules into protein chains, the collagen expands and swells, leading to volume changes in the bone and formation of diagenetically induced micro-fissures. These fissures produce pathways for diagenetic fluids to enter, leading to faster collagen decay and ion uptake and exchange (Pfretzschner, 2000). The chemical decay of collagen is very sensitive to temperature, resulting in different preservation potential and reaction speeds in different climate zones, soils and burial depths (Hedges, 2002). Both types of collagen reduction further enable a secondary filling of the pore space and rapid

recrystallization of the biogenic hydroxylapatite. According to thermodynamic instability and high absorption potential in aqueous solution, a potential isotope and ion exchange of the hydroxylapatite with the surrounding fluid and sediment takes place during this recrystallization (Berna et al., 2004; Kohn, 2008; Trueman et al., 2008). After the recrystallization new, thermodynamically stable crystals are formed (Berna et al., 2004). During this process, foreign ions (e.g. F^-, Fe^{2+}, Mn^{2+}, Sr^{2+}, REEs, UO_2^{2+}) can be substituted at different positions in the hydroxylapatite and can be incorporated into the apatite crystal lattice (Kohn et al., 1999; Nielsen-Marsh and Hedges, 2000; Keenan, 2016; Keenan and Engel, 2017). In this case, diagenetic alteration of the original element and isotope composition of the hydroxylapatite takes place (for overview see Tütken and Vennemann, 2011; Martin et al., 2017a). In general, recrystallisation of bone apatite is estimated to happen relatively quickly (around 30 ka years, Kohn, 2008), though it is important to note here that diagenesis is strongly depend on the surround physio-chemical milieu and not directly on fossilization time (Hedges, 2002; Keenan, 2016; Keenan and Engel, 2017). During the early stage of diagenesis, the skeletal and dental tissue is in active isotope and ion exchange with the surrounding environment (Trueman et al., 2008), though it may retain its structural and chemical composition after recrystallisation is completed (late diagenesis, Hedges, 2002)

Post-mortem mechanical alteration of skeletal and dental tissue can potentially bias morphological and textural analyses of original shapes and surfaces. These types of alteration can happen directly after death due to decomposition, disarticulation, predation by scavengers, abrasion and erosion due to fluvial transport or reworking after burial and weathering processes or digestion (**Fig. 2.4**, Müller, 1992). All these processes can damage and break hard tissues into small pieces, making morphological identification of fossil bone and tooth material very difficult (Lyman and Lyman, 1994). They can also lead to abrasion of ante-mortem enamel structure on the macro- to micrometer scale, hindering dental surface texture analyses (e.g. Teaford, 1988; King et al., 1999; Martínez and Pérez-Pérez 2004; Calandra and Merceron, 2016, Böhm et al., 2019). In general, post-mortem mechanical alteration strongly depends on the surrounding environmental conditions before burial, but also on re-working processes after burial (Müller, 1992).

2.5 The Permian terrestrial ecosystem

The Permian (298.9 to 251.9 Ma) followed the Carboniferous around 300 Ma ago. The landmass of Gondwana drifted northwards, and the collision with Laurentia lead to the Variscian orogeny event resulting in the formation of a large mountain range along the equator. The southern Gondwana landmass was covered by a thick layer of ice during the Upper Carboniferous, which disappeared during the lower Permian as it drifted northwards. During

the lower Permian, all major landmasses were agglomerated into the single supercontinent Pangaea (Johnson, 1981; Blakey, 2003; Benton and Pfretzschner, 2007). This supercontinent facilitated the development of a megamonsoon climate system, including a hot, dry climate zone in the mid latitudes and cool to cold temperatures in the polar regions (Tabor and Poulsen, 2008, Tabor et al., 2017). This climate system led to major changes in the flora, generally containing ferns, seed ferns such as *Glossopteris*, cycadales, early conifers (e.g. *Ullmannia*) and first-time ginkgo plants (Rothe, 2000), and was followed by a major vertebrates faunal turnover during the Permian, i.e. a transition from synapsid-dominated to therapsid-dominated ecosystems (Olson, 1962; Lucas, 2006; Benton and Pfretzschner, 2007; Brocklehurst et al., 2013; Olroyed and Sidor; 2017). The During the Permian, non-mammalian tetrapods occupied all kinds of ecological niches and evolved a great variety of feeding strategies (Olson, 1962; Olson, 1966; Kemp, 2006; Sahney and Benton, 2008; Ruta et al., 2011; Benton, 2012; Benson and Upchurch, 2013; Brocklehurst et al., 2013; Brocklehurst and Fröbisch, 2017). The Permian faunal turnover and diversification is particularly unique because it was during this period that the first terrestrial herbivorous taxa evolved and began to radiate. The increasing abundance and diversity of herbivores led to the development of the complex terrestrial food webs that characterize present day ecosystems (**Fig. 2.5**; Pearson et al., 2013). With the evolution of high-fibre herbivory, terrestrial vertebrates became primary consumers, feeding mostly on leaves, stems, roots, and rhizomes of Permian flora (Sues and Reisz, 1998; Reisz and Sues, 2000).

The first evidence for terrestrial vertebrate herbivory appears in the fossil record near the Permo-Carboniferous boundary (Sues and Reisz, 1998). During the lower Permian two clades of early synapsids, caseids and edaphosaurs, evolved herbivorous taxa, (Sues and Reisz, 1998; Reisz and Sues, 2000). Herbivory evolved more than one time during synapsid evolution with different feedings strategies and oral processing mechanisms. Caseids, for example, only rarely orally processed their ingesta, i.e. no chewing occurred, and therefore their teeth have no occlusal surfaces (Maddin et al., 2008; Reisz and Fröbisch, 2014) while edaphosaurs, had teeth which were used for crushing food (Modesto, 1995).

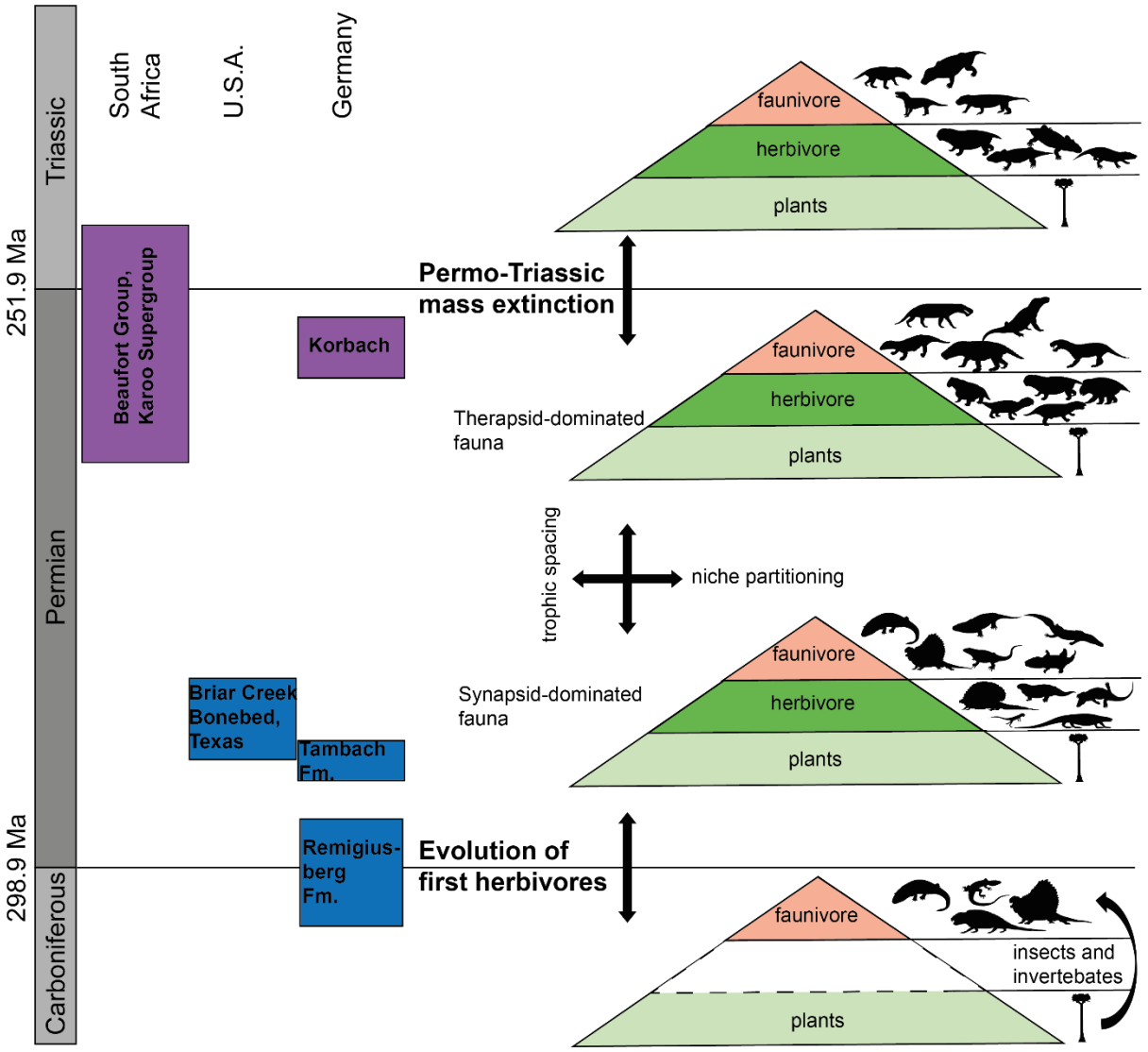

Figure 2.5. Stratigraphic ranges of Late Carboniferous, Permian and Lower Triassic with key fossil localities/food webs in South Africa (Beauford Supergroup, Karoo Basin), U.S.A. (Briar Creek Bonebed, Texas) and Germany (Korbach fissure filling; Tambach Fm., Bromacker Quarry; Remigiusberg Fm., Saar-Nahe Basin) within each period indicated on the left side of the figure. On the right, theoretical trophic pyramids illustrating faunal evolution over the course of the Permian. Note that non-mammalian tetrapod icons are not scaled to their relative sizes.

In general, besides dental adaptations, herbivory requires numerous morphological and physiological adaptations to extract and process the difficult-to-digest nutrients in a plant diet (Sues and Reisz, 1998; Reisz and Sues, 2000). Herbivorous taxa evolved longer and bulkier digestive tracts capable of facilitating fermentation by necessary gut endosymbionts for the digestion of plants. This adaptation resulted in the elongation and enlargement of the whole thorax in herbivore species (Sues and Reisz, 1998; Reisz and Sues, 2000; O'Grady et al., 2005), as can be seen in caseids (Reisz and Fröbisch, 2014). Additionally, the evolution of

herbivory was accompanied by a dramatic increase in body size, a phenomenon not observed to the same extent in sympatric carnivorous taxa (Reisz and Fröbisch, 2014). Herbivory also evolved independently several times in diadectids (Diadectomorpha); consequently the first true herbivores already lived during the Upper Pennsylvanian (Late Carboniferous, Kissel and Lehman, 2002), in captorhinids (Dodick and Modesto, 1995) and probably also in bolosaurids, as suggested from their dental morphology (Reisz et al., 2007; Berman et al., 2000a). This evolution is assumed to have occurred over a longer period of time during the Late Carboniferous and lower Permian (Pearson et al., 2013). The diversity of herbivorous taxa increases during the lower and middle Permian and was disrupted by a smaller extinction event (known as Olson's gap) at the end of the middle Permian (Lucas and Heckert, 2001; Lucas, 2005; Fröbisch, 2008; Lucas, 2009; Pearson et al., 2013). The Olson gap marks the time of faunal transition from a synapsid-dominated to a therapsid-dominated fauna, with richer and more complex faunal communities afterwards (Benton, 2012).

2.5.1 The terrestrial Permian life

In the following, a very brief overview of vertebrate taxa relevant to this study is given. Vertebrates have a worldwide distribution with Tetrapoda, which means "four feet", as the largest group. Tetrapods originated during the Middle Devonian and inhabit all major habitats in the modern time (Clack, 2012). Most are terrestrial, but several have secondarily returned to the aquatic environment such as various salamanders, frogs, turtles, sea snakes, pinnipeds (seals and walruses), and whales. Some tetrapods are capable of flight (birds and bats), while others like flying squirrels and flying dragons (Clack, 2012), glide. The two tetrapod groups of relevance for this study are the Diadectomorpha and Amniota clade, which existed during the Late Carboniferous and Permian.

2.5.1.1 Diadectomorpha

The Diadectomorpha is a sister-clade of the Amniota clade, containing semi-aquatic and terrestrial vertebrates living during the Late Carboniferous and the Permian (Laurin and Reisz, 1995, 1997, 1999; Lee and Spencer, 1997). One representative of the clade is *Diadectes*, known from the U.S.A. as well as from Germany (Berman et al., 1998). A massive animal, with short legs and a compact body. *Diadectes* belongs to the first herbivorous terrestrial vertebrates. It had short, pin-like teeth in the front and broad cheek teeth in the back of his mouth (Sues and Reisz, 1998). Another representative of this clade is *Orobates* (**Fig. 2.6A**), which was found in the lower Permian locality of Bromacker, Germany. This taxon

was also herbivorous and fed on high fibre plants (for detailed information see Berman et al., 2004).

2.5.1.2 Amniota

Currently the earliest record of amniotes comes from a Middle Pennsylvanian locality in Nova Scotia (Carroll, 1964). These fossils indicate that amniotes first diverged into two lineages, one lineage (Synapsida) resulted in mammals, including all extinct mammalian ancestors, while the other lineage (Sauropsida) includes all living sauropsids (including birds, lizards and snakes, crocodiles, and turtles) and their extinct relatives (Laurin and Reisz, 1995).

Sauropsida

The majority of taxa included in the second part of this thesis are non-mammalian synapsids, therefore, only two relevant groups of the Sauropsida clade are described in the following section. This includes the very small group of Bolosauridae (Parareptilia) with taxa from the lower Permian Bromacker Quarry Germany (Berman et al., 2000a), Texas (Cope, 1878), Fort Sill Oklahoma (Reisz et al., 2002) or the middle Permian of Russia (Reisz et al., 2007) and China (Müller et al., 2008). One representative of this group is the ~25 cm long, bipedal *Eudibamus cursoris*, the first evidence for biped tetrapods (Berman et al., 2000a). *Eudibamus* had dome-shaped teeth with occlusal surfaces, i.e. the teeth of lower and upper jaw came into contact during food processing suggesting that the animals fed on plant matter (Reisz, 2006). Recent studies suggest that bolosaurids replaced anterior and posterior teeth in a single wave which occurred from the front to the back of the dental arcade (Styder et al., 2020). The Bolosauridae went extinct at the end of the Permian (Benton and Pfretzschner, 2007). Another group of Sauropsida are the Pareiasauridae (Parareptilia), which were large amniotes, restricted to the upper Permian, mostly found in South Africa (e.g. Owen, 1876; Haughton and Boonstra, 1929), Germany (Tsuji, 2011) and Russia (Hartmann-Weinberg, 1930; Bulanov and Yashina, 2005; Tsuji, 2011). Most representatives of this group were quite large, with body size ranging from 2 to 3 meters, and massive bodies with short legs. The leaf-shaped dentition of Pareiasauridae suggests an herbivorous diet of relatively soft plant matter (**Fig. 2.6B**, Lee, 1997; Benton and Pfretzschner, 2007; Van den Brandt et al., 2020).

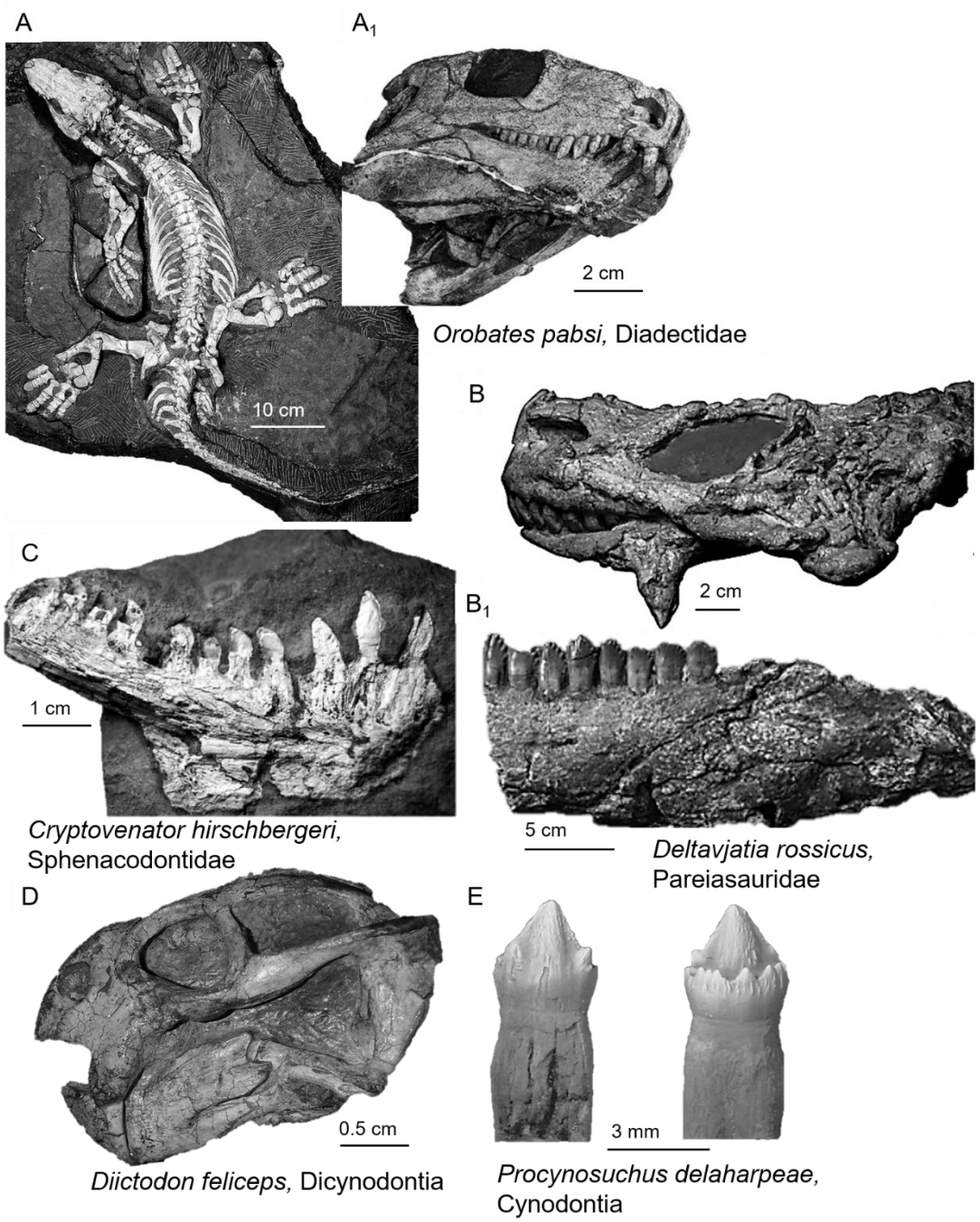

Figure 2.6. Examples of fossil Permian tetrapods. A. Complete skeleton of *Orobates pabsti* (MNG 10181), A_1 Crania of *Orobates pabsti* (MNG 8980), both specimens from the Tambach Fm. (Berman et al., 2004). B. Crania of (KPM 232) and B_1 lower jaw (PIN 2212/6) of *Deltavjatia rossicus*, both from the Kotel'nich locality (Tsuji, 2013), C. Lower jaw of *Cryptovenator hirschbergeri* (LFN-PW 2008/5599-LS) from the Remigiusberg Fm., D. skull of *Diictodon feliceps* (USNM 22949, right lateral view, Kammerer et al., 2020, DOI:10.7717/peerj.9925/fig-2), E. labial and lingual view of isolated lower postcanine tooth of *Procynosuchus delaharpeae* (NMT RB3) from Tanzania (Weide et al., 2009).

Synapsida

The oldest known synapsid fossils come from Late Carboniferous deposits in North America and Czechia (Reisz, 1972; Mann et al., 2019; Maddin et al., 2020). Synapsids radiated quickly and became the most taxonomically diverse, widespread, and common amniotes in the late Palaeozoic and early Mesozoic (Benton and Pfretzschner, 2007). The family of Varanopidae (for a review of the phylogeny of Varanopidae see Spindler et al., 2018) for example, lived in North America (Campione and Reisz, 2010) and Germany (Berman et al., 2014) during the lower Permian until the upper Permian in South Africa (Modesto et al., 2001) and Russia (Anderson and Reisz, 2004). Based on the body plan of these animals, it is assumed that they were small, active and fast small carnivores or insectivores (Reisz, 1986; Benton and Pfretzschner, 2007; Shelton, 2015). Two further groups of synapsids from the lower Permian evolved a body plan with large sails on their back formed by elongated neural spines extending from the vertebrae and probably covered with skin that possibly served as display (Mazierski and Reisz, 2011; Shelton, 2015) and for thermoregulation (Bennett, 1996). The first group is the medium to large sized carnivore Sphenacodontidae (**Fig. 2.6C**, Reisz, 1986), which lived during the Late Carboniferous and early to middle Permian (although not all members of this clade evolved sails (Berman et al. 2001; Benton and Pfretzschner, 2007; Fröbisch et al. 2011)). One representative of this group is the genus *Dimetrodon*, represented by at least 14 species (Brink, 2015; Brink et al., 2015). This taxon is found, for example in Texas and Oklahoma (Brink et al., 2019), as well as in Germany (Berman et al., 2001). The herbivorous Edaphosauridae are another synapsid group with a huge sail on their back and are found from the Late Carboniferous until the lower Permian (Spindler et al., 2020). Edaphosauridae had very small skulls with pin-like and large palatine teeth for crushing plant matter (Modesto, 1995). However, the earliest Edaphosauridae from the Late Carboniferous, *Ianthasaurus hardestii*, potentially fed more on insects than on plants (Reisz and Berman, 1986; Spindler, 2015). Representatives of Edaphosauridae can be found, inter alia, in the U.S.A. (e.g. Reisz and Berman 1986; Benson 2012) and also in Germany (Remigiusberg near Kusel, Rhineland-Palatinate; Spindler et al., 2020).

Within the clade of Synapsida, the clade of Therapsida (including mammals and most of their upper Permian and more recent relatives) evolved during the lower Permian from the Sphenacodontia (Laurin and Reisz, 1990, 1996; Amson and Laurin, 2011; Benton, 2012). One group within the Therapsida are the Dinocephalia, which are known from the upper Permian mostly from Russia and South Africa (Simon et al., 2010). This group contains carnivorous, as well as herbivorous and omnivorous taxa, which makes fragments of unidentified dinocephalians difficult to use in studies dealing with trophic level effects (Boonstra, 1969; Benton and Pfretzschner, 2007; Nicolas and Rubidge, 2010).

An important, exclusively herbivorous group are the Dicynodontia, with so far around 70 described species from the middle Permian to Lower Triassic (King, 1990; Angielczyk, 2001, Benton and Pfretzschner, 2007). They were the dominant herbivores in a typical upper Permian fauna assemblage (Benton, 1983; Edler, 2000). Dicynodontian taxa differ significantly in body size, varying from very small up to hippo-sized species, such as *Lisowicia bojani* (Sulej and Niedźwiedzki, 2019), but all had a barrel-shaped body and a particularly interesting chewing apparatus and dentition (**Fig. 2.6D**, e.g. Benton and Pfretzschner, 2007). For dicynodontian species like *Pristerodon*, a complex jaw movement and chewing process is evident (Crompton and Hotton, 1967), teeth of some other Dicynodontia show traces of abrasion due to chewing movement and the tusks of some species show grinding or grubbing marks (Hotton, 1986). These marks, however, probably originate from digging through the ground in search of roots, ferns or other plants near the ground and not from chewing or the oral processing of food (e.g. King et al., 1989; Edler, 2000; Benton and Pfretzschner, 2007; Jasinoski et al., 2009; Cox and Angielczyk, 2015). Dicynodontia almost went extinct at the end of the Permian (King, 1990; Benton and Pfretzschner, 2007; Racki and Lucas, 2020). The dominant faunivorous group within the Therapsida clade during the upper Permian, were the Gorgonopsia, a relatively large group, known from Russia, China and Africa (Sigigneau-Russell and Sun, 1981; Maisch, 2002; Kammerer, 2015; Kammerer et al., 2015; Kammerer and Masyutin, 2018). Gorgonopsia vaguely resemble sabre-toothed tigers with very prominent canine teeth, suitable for slicing large pieces of flesh from the carcasses of prey (Kemp, 1969). They probably specialised in hunting Dinocephalia and Dicynodontia, as gorgonopsians went extinct along with these taxa at the end of the Permian (Botha and Smith, 2006; Benton and Pfretzschner, 2007). A group of faunivorous Therapsida that survived the end Permian extinction event are the Therocephalia, which consist of small insectivorous as well as larger carnivorous species (Rubidge and Sidor, 2001; Benoit et al., 2016; Huttenlocker and Sidor, 2016). During the Lower Triassic this group also evolved some herbivorous species (Benton and Pfretzschner, 2007; Brocklehurst, 2019).

Finally, a group that originated in the upper Permian radiated very successfully during the Triassic (including basal mammals) are the Cynodontia (for detailed information see Kammerer, 2016). In cynodonts tooth replacement similar to that of extant reptiles is evident (Botha et al., 2005). Species like *Procynosuchus*, known from the upper Permian of South Africa, Tanzania and Germany, were dog-sized animals that evidence mammalian-like characteristics (e.g. Sues and Munk, 1996; Abdala and Allinson, 2005; Weide et al., 2009). The dentition of *Procynosuchus* together with its small size suggest a predominantly insectivorous diet (**Fig. 2.6E**, Benton and Pfretzschner, 2007).

2.5.2 Permian tetrapod fossil localities

The following section will give a brief overview and very short description of the geological setting of lower and upper Permian localities important for this thesis (**Fig. 2.5 and 2.7**).

Late Carboniferous and lower Permian tetrapod fossil sites

Remigiusberg Formation, Saar-Nahe Basin, Germany

The Saar-Nahe Basin in SW-Germany is an intra-mountainous basin within the Variscan mountains and contains a several km thick succession of terrestrial and fluvio-lacustrine Late Carboniferous and lower Permian sediments of the Rotliegend Group (**Fig. 2.7A**, Schindler, 2007; Uhl and Jasper, 2016). The Remigiusberg Formation, is part of the lower Rotliegend deposits and its base is formed by an around 50 m thick subvolcanic kuselite intrusion from the Early Permian. The Remigiusberg Formation itself consists of an around 30 m thick fluvio-lacustrine succession of reddish-brown to grey-green clay-, silt- and sandstone and carbonate layers from sediments of a long-lasting shallow freshwater lake, Lake Theisbergstegen (Boy and Schindler, 2000; Voigt et al., 2014). The Saar-Nahe Basin has yielded a largest number of vertebrate fossils from the Late Carboniferous and lower Permian in Europe (Boy, 2007). Among the fossils from many different lake deposits, such as the Remigiusberg Fm., are exquisitely preserved aquatic taxa, such as xenacanthiformes (cartilaginous fishes), palaeonisciformes (ray-finned fishes), lepospondyls (Reptiliomorpha), branchiosaurids (Amphibamiformes) and Stereospondylomorpha (Temnospondyli) (e.g. Boy and Schindler, 2000, 2012; Boy, 2003; Witzmann, 2013; Voigt et al., 2014) and a great diversity of terrestrial tetrapod tracks (Fichter 1983; Schindler, 2007; Voigt, 2007; Boy and Schindler, 2012). The tracks provide evidence for the likely presence of diadectids, parareptiles, diapsids, and synapsids in the Saar-Nahe Basin. However, during the first 165 years of mining and excavation not a single terrestrial tetrapod fossil apart from the abundant aquatic amphibians was found in the Remigiusberg Formation. The first amniote body fossil from the latest Carboniferous of the Saar−Nahe Basin referred to Sphenacodontidae, *Cryptovenator hirschbergeri*., a relatively small animal with ~ 100 cm body length, representing to oldest amniote fossil of Germany (**Fig. 2.6C**, Fröbisch et al., 2011). In the following recent years, an increasing number of fossils of some of the oldest European terrestrial vertebrates were found, revealing a rich species diversity of aquatic, semi-aquatic and terrestrial animals. The species found in the Remigiusberg Formation include among *Cryptovenator*, the dvinosaurian temnospondyl *Trypanognathus remigiusbergensis*, Eryopidae (*Eryopide* indet.), Edaphosauridae (*Remigiomontanus robustus*), different Diadectomorphs and small diapsid

skeletons (**Fig. 2.8A**, e.g. Boy and Schindler, 2000; Schindler, 2007, Witzman, 2013; Voigt et al., 2014, 2019; Witzmann and Voigt, 2015; Schoch and Voigt, 2019; Spindler et al., 2019).

Bromacker Quarry, Germany

A second lower Permian locality from the lowermost unit of the Upper Rotliegend Group is the Bromacker Quarry, located in the Tambach Formation in Thuringia (**Fig. 2.7B**). The site covers ~ 500 m² and the fossil bearing layer is an approx. 1 m thick succession of mudstone within the Tambach Sandstone (for detailed information see Eberth et al., 2000; Berman et al., 2000b). The Bromacker locality represents sediments deposited in an internally drained upland locality in the lower Permian with a lack of fully aquatic taxa, such as fish and certain aquatic anamniotes. In contrast to Bromacker, most other lower Permian vertebrate fossil assemblages are described from low-land localities with extensive coastal or alluvial plains (**Fig. 2.8A**, Eberth et al 2000; Martens et al., 2005b). In general, the fossils from the Bromacker Quarry are well-preserved, which indicates a relatively short exposure of carcasses and limited reworking, maybe during sheetflood events, prior to final burial (Eberth et al., 2000). The fossil flora and fauna are relatively low in diversity compared to other lower Permian terrestrial assemblages, probably as a result from the small size of the quarry, only around 12 taxa were found at the quarry so far (e.g., Berman et al., 2000b, 2001, 2004, 2011, 2014, 2020; Eberth et al., 2000; Martens et al., 2005b; Müller et al., 2006; Anderson et al., 2008; Henrici et al., 2011; Wings and Eckert, 2018). However, the most abundant tetrapods in this ecosystem were herbivorous diadectids, with *Diadectes absitus* and *Orobates pabsti* (**Fig. 2.6A**, Berman et al., 2004). In general, the locality shows a high abundance of herbivorous species besides diadectids, such as the bolosaurid parareptile *Eudibamis cursoris* (Berman et al., 2000a) and four skeletons of *Martensius bromackerensis* (Caseidae; Berman et al., 2020). Another highly abundant taxon at Bromacker is the carnivorous *Seymouria sanjuanensis* (Seymouridae), including the famous “Tambach Lovers”, a pair of completely articulated skeletons fossilized near each other (Eberth et al., 2000; Berman et al., 2000b). Apart from *Seymouria*, carnivorous taxa are underrepresented with only *Dimetrodon teutonis* (Sphenacodontidae) and *Tambacarnifex ungifalcatus* (Varanopidae) (Berman et al., 2001, 2014).

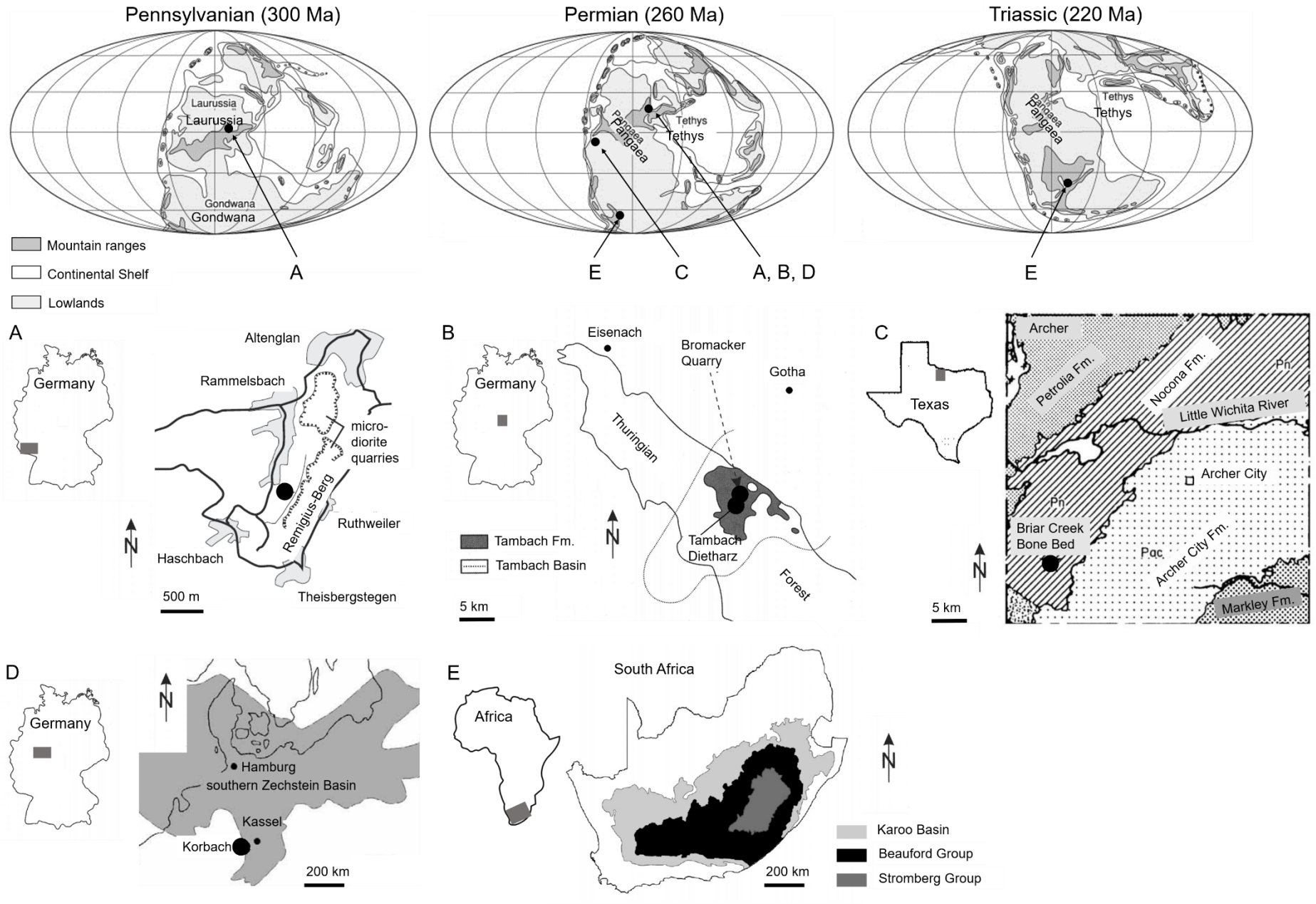
Pennsylvanian (300 Ma)
Permian (260 Ma)
Triassic (220 Ma)
Laurussia
Gondwana
Pangaea
Tethys
Mountain ranges
Continental Shelf
Lowlands
A
E
C
A, B, D
E
A
Germany
Altenglan
Rammelsbach
micro-
diorite
quarries
Remigius-Berg
Ruthweiler
Haschbach
Theisbergstegen
500 m
B
Germany
Eisenach
Bromacker
Quarry
Gotha
Thuringian
Forest
Tambach Fm.
Tambach Basin
Tambach
Dietharz
5 km
C
Texas
Archer
Petrolia Fm.
Nocona Fm.
Pn.
Little Wichita River
Archer City
Pn.
Briar Creek
Bone Bed
Pac.
Archer City Fm.
Markley Fm.
5 km
D
Germany
Hamburg
southern Zechstein Basin
Kassel
Korbach
200 km
E
Africa
South Africa
Karoo Basin
Beauford Group
Stromberg Group
200 km

Figure 2.7. Map of the key fossil localities. Palaeogeographical maps of the Late Carboniferous (Pennsylvanian), the Permian and the Triassic with the important tetrapod fossil localities marked with black dots (modified from Lucas, 2005). A. Late Carboniferous and lower Permian Remigiusberg Fm. in the Saar-Nahe Basin, south-western Germany (modified from Fröbisch et al., 2011); B. Lower Permian Bromacker Quarry in the Tambach Fm., central Germany (modified from Henrici et al.,2011); C. Lower Permian Briar Creek Bonebed (BCBB) in the Nocona Fm., north Texas, U.S.A. (modified from Labandeira and Allen, 2007; Shelton, 2015); D. Upper Permian Korbach fissure filling in the Zechstein Basin, west Germany (modified from Sues and Munk, 1996); E. Upper Permian Beauford Group, South Afrika (modified from Botha and Smith, 2007; Hancox et al., 2013).

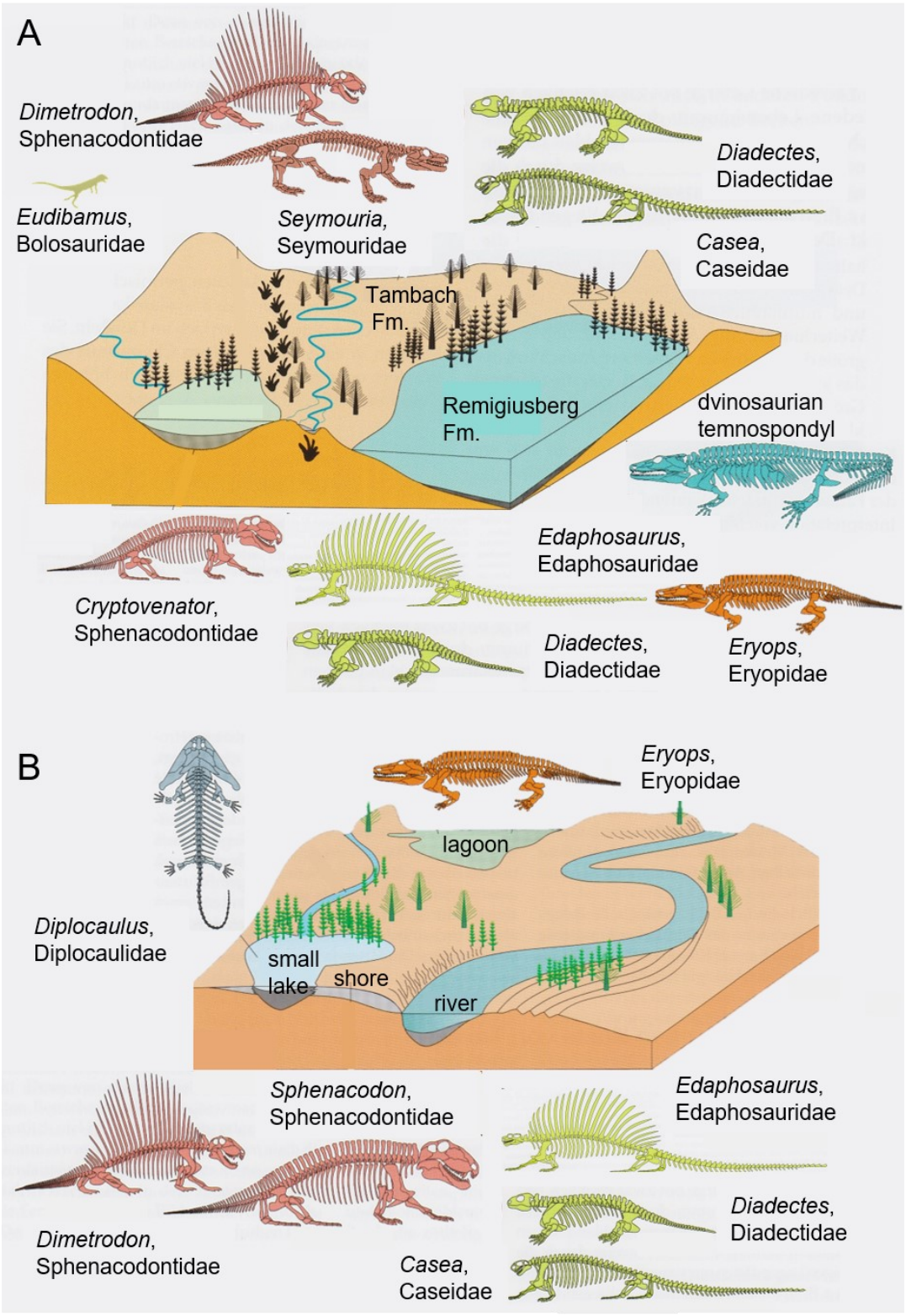

Figure 2.8. Lower Permian terrestrial ecosystems of A. Tambach and Remigiusberg Fm., Germany and B. Texas, U.S.A.. Red colour indicates carnivores, yellow-green and green indicate herbivores, orange colour shows carnivorous Eryopidae (Temnospondyli), light blue indicates unspecified dvinosaurian Temnospondyli and dark blue indicates lepospondyl amphibians. Footprints in A show ichnofossils found in lower Permian localities in Germany (modified from Rothe, 2000).

Briar Creek Bonebed, Texas, U.S.A.

The lower Permian material from Texas, U.S.A., is mostly concentrated in and around the Archer County area (**Fig. 2.7C**, Konietzko-Meier et al. 2016). Lower Permian terrestrial and aquatic vertebrates have been collected from the Texas redbeds for over a century (e.g. Case, 1915; Sander, 1987, 1989; Shelton et al., 2013, Shelton, 2015) and the Briar Creek Bonebed (BCBB) had were been discovered in 1912 by E.C. Case (Case, 1915). The BCBB is an about 30 cm thick grey mudstone and contains disarticulated vertebrate skeletons of variable preservation, e.g. ironstone covering some fragments (Konietzko-Meier et al., 2016). The crushed bone and tooth fragments possibly indicate scavenging, however, the fragments do not show signs of abrasion due to water transport (Shelton, 2015). It was originally hypothesized by Case (1915), that the BCBB is a fossil swamp or lake system which conserved vertebrate remains in a manner similar to a macerating tank. However, it has also been hypothesized that the bone bed is a fossil meandering river system which formed a lake or swamp similar to what is hypothesized for the Geraldine Bonebed (Archer County, Texas, Sander, 1989; Konietzko-Meier et al., 2016). A diverse fossil faunal assemblage is found in the bonebeds of Texas including *Eryops* (Eryopidae), *Diadectes* (Diadectidae), and the synapsids *Edaphosaurus* (Edaphosauridae) and *Dimetrodon limbatus* (Sphenacodontidae), as well as the freshwater shark *Orthocanthus* (**Fig. 2.8B**, e.g. Shelton, 2013, 2015).

Upper Permian tetrapod fossil sites

Korbach fissure-filling, Germany

This upper Permian terrestrial tetrapod fossil assemblage from a karst fissure-filling in marine limestone sediments of the early Zechstein near Korbach (Northern Hesse, Germany) is located at the edge of the Rhenish Slate Mountains (**Fig. 2.7D**, Kulick, 1997). The Korbach fissure-filling was first discovered by J. Kulick in 1964 and classified as upper Permian fossil assemblage much later (Kulick and Paul, 1987). The Korbach fissure presumably resulted from a combination of tectonic activity and karstification, whereby the karstification started along smaller fissures and quickly deepened into the surrounding carbonate rock (Zeeh et al., 2000; Becker, 2002; Zeeh and Becker, 2005). The sediments in the fissure consist of a siliciclastic and a carbonate component, whereby the clastic component consists of quartzitic silt and fine sand and an illite matrix from the eastern edge of the Variscan mountains. The carbonate component (calcite and dolomite) consists of a transported carbonate and diagenetically formed fine matrix and poikilitic calcite crystals from the surrounding (Bökenschmidt, 2006). The sediment and the vertebrate remains therein were most likely washed into the fissure in a constant sediment water suspension, as a mudflow over the coastal area of the Zechstein Sea (Bökenschmidt, 2006). The disarticulated bone fragments are mostly preserved as

hydroxylapatite (Bökenschmidt et al., 1999) and show no signs of longer transport (Sues et al., 1996). Regarding the preservation of the fossil material, it is assumed that the animals died, decayed and disarticulated for different durations before the skeletal remains were washed into the fissure and reworked (Bökenschmidt, 2006). The Permian faunal assemblage is comparable to those from South Africa and Russia of similar age, with most of the taxa being restricted to the upper Permian, while some survived into the Triassic (Bökenschmidt, 2006). Fragments of upper Permian terrestrial vertebrates are found in the fissure-filling, comprise taxa such as *Procynosuchus* sp. (Therapsida, Procynosuchidae), a small faunivore/ insectivore animal (e.g. **Fig. 2.6E**, 2.9, Sues and Munk, 1996), *Protorosaurus* (Protosauridae) and *Parasaurus* (Pareiasauroidea, Captorhinida) (Sues and Boy, 1988; Sues and Munk, 1996). No evidence for aquatic taxa, such as temnospondyls or fishes are found (Sues and Munk, 1996); even the more recent discovery of a new Chroniosuchia taxon, *Hassiacoscutum munki*, is suggested to have been a primarily terrestrial vertebrate (Witzman et al., 2019). The upper Permian vertebrate fossils of the Korbach fissure filling have the same age as fossils from the upper Permian Kupferschiefer, such as *Protorosaurus*. It can be assumed that the fissure filling might be a tertiary fossil deposit with fossils from the Kupferschiefer washed into the fissure (Bökenschmidt, 2006).

Karoo Supergroup, South Africa

The deposits of the Karoo Supergroup cover large geographic areas of south-central Africa represented a time interval from the Late Carboniferous until the Lower Jurassic (**Fig. 2.7E**, for review see Hancox and Rubidge, 2001; Catuneanu et al., 2005; Nicolas, 2007). The Supergroup includes different lithostratigraphic units, for this thesis, the Beauford Group is the most important one, since this unit contains fossil tetrapod assemblages from the middle Permian until the Lower Jurassic, however, the absolute age is not well constrained (Rubidge, 1995; Hancox and Rubidge, 1996). In general, the Beauford Group is divided into eight biozones: *Eodicynodon*, *Tapinocephalus*, *Pristerognathus*, *Tropidostoma*, *Cistecephalus*, *Dicynodon*, *Lystrosaurus* and *Cynognathus* assemblage zones (Rubidge, 1995; Hancox and Rubidge, 1997). The Beauford Group is located in South Africa and consists of a ~ 3000 m thick sedimentary succession of sedimentary sandstones and mudrocks. The sandstones are deposits in fossil channels, while the mudrocks are deposits of overbank settings (Hancox and Rubidge, 2001).

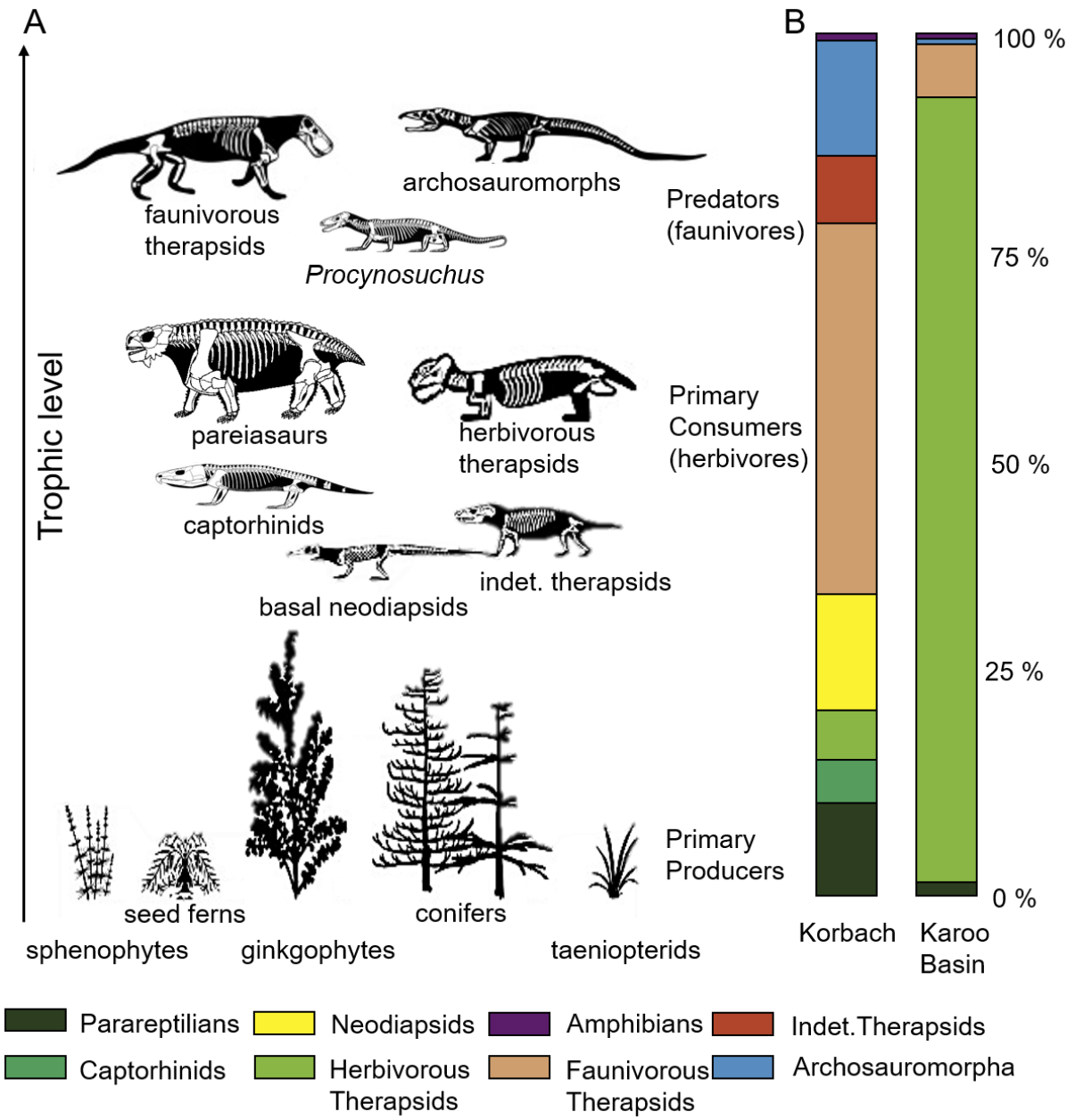

Figure 2.9. Exemplary upper Permian terrestrial trophic levels with primary producers, small and large primary consumers (herbivores) and small and large (apex-) predators (faunivores) (A). B. showing composition of faunal assemblage of the Korbach fissure filling and Karoo Basin, South Africa (modified from Bernardi et al., 2017, Fröbisch et al., 2018, Fröbisch pers. comm.)

The fossil vertebrate fauna of the Beauford Group is very diverse and large, however, generally different taxa are found in great diversity and abundance in the different assemblage zones. The following paragraph only gives a brief overview over abundant taxa, without mentioning referring assemblage zones, for more detailed information see Nicolas and Rubidge (2010). A large diversity of freshwater fish, including sharks and lungfishes, were

found, hinting at an aquatic freshwater palaeoenvironment (Rubidge, 2005). Furthermore, a very diverse temnospondyl amphibian fauna, represented in different numbers in the different assemblage zones (Shishkin and Rubidge, 2000; Damiani and Rubidge, 2003) was found. The Amniota clade, taxa such as *Pareiasaurus* (Pareiasauridae), *Tapinocephalus atherstonei* (Therapsida, Dinocephalia), *Jonkeria boonstrai* (Therapsida, Dinocephalia), *Pristerognathus* (Therapsida, Therocephalia), *Diictodon* (Therapsida, Dicynodontia), numerus Gorgonopsidae (e.g. *Dinogorgon*, *Rubidgea*), *Lystrosaurus* (Therapsida, Dicynodontia), *Cynognathus* (Therapsida, Cynodontia) are among the most abundant species and partly eponymous for the different assemblage zones. Apart from that, many other taxa within the Pareiasauridae, Dinocephalia, Therocephalia, Dicynodontia, Gorgonopsidae and Cynodontia are found in the Beauford Group. The Beauford Group is rich in fossils, however, low in diversity, with a high percentage of herbivorous species (varying between different assemblage zones), and a low percentage of carnivorous and omnivorous taxa (**Fig. 2.9**, Nicolas and Rubidge, 2010, Bernardi et al., 2017)

2.5.3 The end of the Permian ecosystem

The end of the Permian which coincides with the end of the Palaeozoic Era (~ 252 Ma) was marked with the most disastrous mass extinction event in earth history, with a loss of 50-75% of terrestrial and ~80-96 % of aquatic families (Benton and Twitchett, 2003; Sahney and Benton, 2005; Benton and Pfretzschner, 2007). The most plausible reason for the mass extinction event is a combination of massive volcanic events (e.g. Siberian trap basalts), global warming, and ocean anoxia due to methane hydrates and acidification (Benton and Twitchett, 2003; Algeo and Twitchett, 2010; Algeo et al., 2011; Clarkson et al., 2013; Burgess and Bowring, 2015; Garbelli et al., 2016, 2017; Polozov et al., 2016; Black et al., 2018). Over a time of approx. 500.000 years during the upper Permian, massive eruptions of Siberian basalt lava occurred covering an area of around 2 million km³ (Campbell et al., 1992; Benton and Pfretzschner, 2007; Reichow et al, 2005, 2009; Saunders and Reichow, 2009). The eruption would have led to an enrichment of volcanic gases in the atmosphere, such as CO_2 and SO_2, followed by massive reduction of O content and changes in the global temperature (Saunders and Reichow, 2009). The resulting greenhouse effect in the atmosphere and the ocean would have killed terrestrial and aquatic flora, resulting in an increasing erosion of the ground and increasing organic input into the oceans. This would be followed by an increasing temperature and could have led to a release of methane, trapped as frozen methane hydrate in the continental shelf (Benton and Twitchett, 2003; Brand et al., 2016). This would have led to a further increase of the greenhouse effect and a further increasing temperature. The end-Permian mass extinction seems to have been rather a gradual process over a short time span

of around 500.000 years than a long-lasting event (Smith and Wang, 2001; Burgess et al., 2014; Shen et al., 2018). The faunal turnover across the Permo-Triassic boundary suggested by fossils in continental sediments from the Karroo Basin, South Africa, show a gradual disappearing of tetrapod fauna over a very short time span of perhaps about 50000 years (Smith and Ward, 2001). Due to the extinction event, the number and diversity of tetrapod families dropped rapidly, however, in order to refill the free ecological niches, a fast increase of diversity appears until the late Lower Triassic (Olenekian). However, during the Triassic, the taxonomic diversification rate dropped, with only one new additional family every 25 Ma (Sahney and Benton, 2014). Additionally, the end-Permian mass extinction is followed by a "Lilliput effect" (Urbanek 1993), where only a few large species and many small species survived (Sahney and Benton, 2014). One of the survivors of the extinction event was probably *Lystrosaurus*, which radiated quickly over the whole world and contributed almost 95 % of the vertebrate fauna afterwards (Benton and Pfretzschner, 2007). Also, the newly formed ecosystem was affected by the extinction event, the number of herbivores and predators decreased, while the number of piscivorous taxa increased, however, this went stepwise back toward a pre-extinction state with more predators and herbivores, than piscivorous and insectivorous taxa during the Triassic (Sahney and Benton, 2014). For detailed review on the effect of the end-Permian mass extinction and the faunal recovery during the Triassic see Sahney and Benton (2014).

Chapter 3 Manuscript I: Post-mortem alteration of diet-related enamel surface textures through artificial biostratinomy: a tumbling experiment using mammal teeth

Post-mortem alteration of diet-related enamel surface textures through artificial biostratinomy: a tumbling experiment using mammal teeth

Böhm, Katrin[1]; Winkler, Daniela E.[1]; Kaiser, Thomas M.[2]; Tütken, Thomas[1]

[1]Applied and Analytical Palaeontology, Institute of Geosciences, Johannes Gutenberg University, J.-J.-Becher-Weg 21, 55128 Mainz, Germany,

[2]Center of Natural History (CeNak), University of Hamburg, Germany

This manuscript is published in a similar version in *Palaeogeography, Palaeoclimatology, Palaeoecology 518 (2019) 215–231.*

3.1 Abstract

In the fossil record, teeth are often all that remains of a fossil organism. Dental microwear texture analysis (DMTA) is a common proxy for diet using dental wear features at the µm-scale, enabling comparative and quantitative assessments of various feeding traits in extant and extinct species. In extinct species, original diet-related dental wear features may be overprinted by post-mortem alteration including fluvial transport. Here we experimentally investigate the effects of mechanical alteration on diet-related 3D enamel surface texture (3DST) patterns of different mammal teeth. Post canine teeth of *Equus* sp., *Capreolus capreolus* and *Otomys* sp. are tumbled in sediment-water suspensions using three different grain size fractions of sand. The 3DST of the enamel surfaces are measured prior to and after each tumbling interval and characterised using ISO normed surface texture and SSFA parameters. In all species, we find several parameters to be almost unaffected by tumbling (stable parameters), while other parameters show inconsistent-directional shifts (unstable parameters). For *Otomys*, all three sediment grain size fractions result in abrasion of peaks and a reduction of overall surface roughness. For *Equus*, tumbling results in visible abrasive changes in the original wear patterns and the introduction of new wear features. *Capreolus capreolus* shows high variability in surface texture patterns prior to and after the experiment, hence we see ambiguous trends for changes in parameter values. However, even after 336 hrs of tumbling the browsing *C. capreolus* can still be distinguished from the grazing *Equus* sp.

Thus, biostratinomy may potentially modify diet-related 3DST causing non-systematic bias via mechanical abrasion, which is related to sediment grain size, duration of transport and geometry of teeth. However, the original diet-related 3DST is still preserved and a more prominent characteristic in DMT than the experimentally induced diagenetic alteration.

3.2 Introduction

Dental microwear texture analysis (DMTA) is a powerful proxy for oral behaviour, reflecting the mechanical properties of ingesta consumed during the last few days or weeks, and for tooth function in general. The tribosystem of occluding teeth is largely controlled by abrasion and attrition as a cause of material loss (Dahlberg and Kinzey, 1962). Patterns of wear features at µm-scales (roughness texture) can be related to feeding traits, enabling quantitative and comparative assessments of diet/ingesta related traits such as soft- or hard-object feeding among extant and fossil vertebrates (Solounias et al., 1988; Scott et al., 2005; Merceron et al., 2007; Semprebon and Rivals, 2007; Schulz et al., 2010; Winkler et al., 2013). Baker et al. (1959) were among the first link microscopic wear features on teeth with abrasives ingested in the diet. In their study of sheep teeth, they concluded that internal abrasives, such as phytoliths, where hard enough to scratch enamel and thus indicate diet. Since then, many

studies of tooth wear analyses at different spatial scales (mesowear, microwear, dental microwear texture analysis) for a large variety of vertebrates (mostly mammals) have been performed, and characteristic wear patterns related to their assumed natural diets have been described (Fortelius and Solounias, 2000; Schulz et al., 2010; Fraser and Theodor, 2011; DeSantis et al., 2013; Purnell et al., 2013; Calandra and Merceron, 2016).

In the fossil record, teeth are often the only preserved parts of animals and are therefore a crucial source of information about the feeding behaviour of extinct taxa. Dietary reconstructions based on the wear features of fossil occlusal tooth surfaces can easily be biased post-mortem due to mechanical and/or chemical modification (King et al., 1999; Dauphin et al., 2018). Therefore, reconstructions should be restricted to areas of a tooth which are relatively unaltered by post-mortem processes. This makes distinguishing between ante- and post-mortem surface alterations a crucial issue for reliable palaeodietary reconstructions based on 3DST (Calandra and Merceron, 2016).

There are two primary sources of post-mortem mechanical surface alteration on teeth (Teaford, 1988):

I. Material loss occurring after death or before/during the burial of an animals remains.

II. Material loss caused by excavation and preparation during/after the collection of a fossil.

Both sources of mechanical surface alteration can have an impact on ante-mortem occlusal wear features and possibly alter or obscure those wear features. Most post-mortem wear features are distinctively different in their size, shape or orientation (Teaford, 1988). In addition to mechanical alteration, chemical alteration may modify ante-mortem wear features, e.g. by acid attack in the stomach of a predator (e.g. Dauphin et al., 2003; 2018) or by dissolution processes in the soil/sediment environment. Overall, there is a substantial lack of experimental data on the effect of biostratinomy on mammalian teeth. Gordon (1983; 1984) tumbled extracted human molars and premolars with four different types of sediment, ranging from volcanic ash to “pea” gravel (~4-8 mm), in aqueous and non-aqueous environments for different time intervals (unspecified). Gordon found significant changes to the ante-mortem dental wear after 5 hours and determined that alteration of the microwear pattern correlated positively with sediment grain size. However, tumbling seemed to abrade the identifiable microwear rather than add or produce new wear features (Gordon, 1984). Similarly, King et al. (1999) tumbled three human lower molar teeth from the late Neolithic with three different grain size fractions of sediment and water for 2-512 hours and found evidence for changes in dental

microwear only with the smallest grain size fraction. Coarse sand (500-1000 µm) produced no change in dental microwear and quartz pebbles (2000-11000 µm) also resulted in little surface damage on the tooth. However, a noticeable abrasive effect was observed for the grain size fraction between 250 to 500 µm, which completely removed the original microwear features. Both studies showed a polishing effect on the dental surface rather than formation of new wear features comparable in morphology with those of the ante-mortem wear (Gordon, 1984; King et al., 1999). Nevertheless, taphonomically altered dental wear patterns could still be easily identified and distinguished from diet-related wear patterns (Teaford, 1988; King et al., 1999). For example, Martinez and Perez-Perez (2004) tested whether taphonomic and non-taphonomic wear features were clearly distinguishable on the buccal enamel surfaces of fossil hominin teeth from Olduvai and Laetoli (Martinez and Perez-Perez, 2004). In this sample, they found evidence for both chemical and mechanical alteration, as well as for well-preserved dental surface areas with no obvious post-mortem material loss, enabling the identification of taphonomically altered teeth. The combination of mechanical and chemical post-mortem wear has often drastically reduced sample sizes of analyses of fossil material (e.g., Ungar et al., 2008), however, this may not always be necessary.

All experimental studies conducted thus far are qualitative and have only been performed on human teeth. Although there are numerous studies connecting dental wear in other mammalian taxa with ingesta properties (e.g. Mainland, 2003a, b), there is as of yet no experimental approach to assess the influence of post-mortem abrasion on non-human teeth. Here we present the first experiment to quantitatively test the effect of biostratinomy on DMTA in three different herbivorous mammalian species.

We employ an experimental setup with three different sediment grain size fractions (fine to middle sand, 63-500 µm) and different tumbling time periods (from 0.5-336 hours). Dental surface texture measurements of the same areas on wear facets were performed on teeth of three herbivorous (grazer and browser) mammals (*Otomys* sp., *Capreolus capreolus* and *Equus* sp.) before and after each tumbling interval, using a high-resolution disc-scanning confocal 3D-surface measuring system µsurf Custom. To quantify dental wear and detect potential alteration by the selected sediments during the experiments two DMTA methods were employed: scale-sensitive fractal analysis (SSFA) and, what we refer to as 3D surface texture analysis (3DST). Both approaches employ optical profilometry to obtain 3D representations of the enamel surface at submicron resolution and evaluate the overall distribution and three-dimensional geometry of topographic features. In SSFA, surface features are characterised using length-scale and area-scale fractal analyses, describing complexity and anisotropy of the surface (e.g. Ungar et al., 2003; 2012; Scott et al., 2006; Scott, 2012). In 3DST, standardised roughness (ISO 25178) and flatness (ISO 12781) parameters plus additional motif, furrow, and direction parameters are employed to characterise wear features (Schulz et

al., 2013a; 2013b; Purnell and Darras, 2016; Kubo et al., 2017; Purnell et al., 2017). A major focus of diet reconstruction via dental wear has been on the browser-grazer dichotomy in the artiodactyla and perissodactyla (e.g. Rensberger, 1973; Fortelius and Solounias, 2000; Damuth and Janis, 2011; Fraser and Theodor, 2011; Schulz et al., 2013a). The browser-grazer dichotomy is well reflected at the different scales of dental wear evaluation (i.e. mesowear, microwear, and dental microwear texture analysis). Browsers are characterised by less abraded tooth wear, which is reflected in a mesowear profile with sharp cusps (Fortelius and Solounias, 2000; Kaiser et al., 2000). The surface is dominated by high complexity and low anisotropy values (SSFA, Scott, 2012; Ungar et al., 2012) and an overall smooth surfaces with low microscopic peaks (3DST, Schulz et al., 2013a, b) and pits (microwear, Walker et al., 1978). In contrast, grazers show mesowear dominated by rounded or blunt cusps and dominated by scratches (microwear, Walker et al., 1978), with an overall greater surface roughness, higher and more frequent peaks and deeper dales but a generally less variable pattern (3DST, Schulz et al., 2013a, b) and high anisotropy/low complexity values (SSFA, Scott, 2012; Ungar et al., 2012).

The aim of this study is to test whether diet-related 3DST (i.e. browser-grazer differences) are resistant against mechanical alteration during sediment transport under a post-mortem abrasive regime. If biostratinomical changes on the wear facets of teeth occur, are they recognizable as post-mortem wear or do they show patterns comparable to ante-mortem wear? We therefore tested if the 3DST of teeth from a grazer (*Equus* sp.) and browsers (*Capreolus capreolus*) could still be assigned to the correct dietary category after tumbling intervals of up to 336 hrs. In other words, could the surface texture parameters normally found to distinguish between these two dietary categories still distinguish between browsers and grazers despite mechanical abrasion meant to mimic sediment transport? We expect that different surface texture parameters will be affected differently by our experimental setup. We anticipate that parameters which describe extremes of the surface (e.g. maximum height) will be more prone to alteration by abrasion compared to parameters describe mean roughness of the surface. Thus, we intend to identify parameters that show the potential to bias dietary interpretations. Our goal is further to test the hypothesis that sediment grain size has an impact on dental microwear texture, but that tooth geometry does as well. Additionally, we analysed the altered parameters after the experiment to test the hypothesis if extreme outliers in parameter values can be used as indicators of taphonomic alteration.

3.3 Material and Methods

Cheek teeth from three different extant small and large mammal taxa were used to investigate the physical effects of post-mortem abrasive action on 3DST patterns on chewing

facets. Due to the potentially destructive nature of the experiment, dental material with low scientific value (e.g. no precise locality data) was used. This resulted in a variable sample composition including both molars and premolars and, due to unequal preservation, different enamel facets (**Fig.3.1**). Such a sample composition is thus more representative of the type of mixed tooth assemblage often recovered in the fossil record.

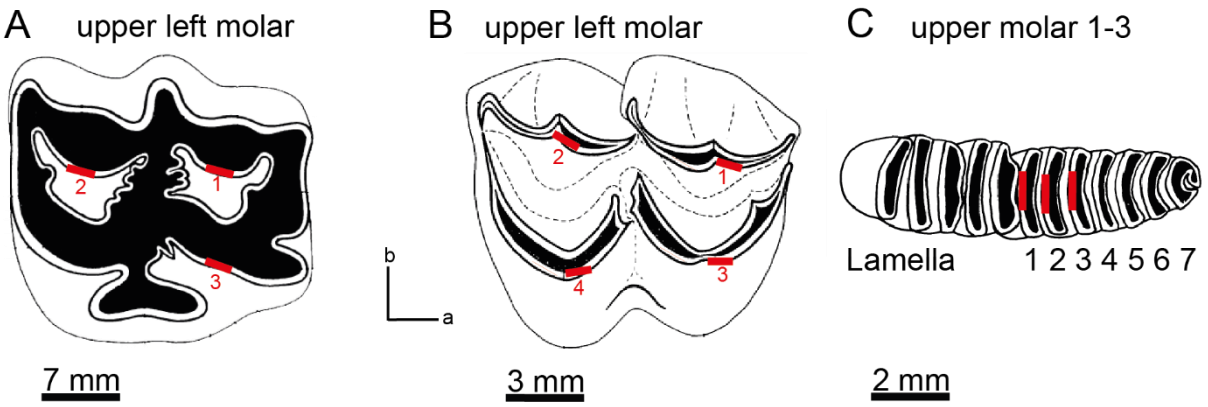

Figure 3.1. Schematic representation of the tumbled specimens. A. Upper left molar of *Equus* sp. with the three possible facets (red bars). B. Upper left molar of *Capreolus capreolus* with the four possible facets (red bars). C. Upper molar 1-3 of *Otomys* sp. with the possible lamellae on the third molar (red bars). Occlusal tooth views modified after Thenius (1989).

Nine teeth of each taxon were used: molars and premolars belonging to *Equus* sp. (Zebra), *Otomys* sp. (African vlei rat or groove-toothed rat) and *Capreolus capreolus* (roe deer) (**Table 3.1**). The samples represent wild species from landscape and museum collections, with no obvious sign of post-mortem dental alteration. The zebra teeth have a mean occlusal width of 2-3 cm, the roe deer 1.5-2 cm and the *Otomys* teeth are the smallest with ~ 2-4 mm in length (**Fig. 3.1**). Zebra and roe deer samples have the same prismatic structure in mature enamel, with horizontally arranged multiserial Hunter-Schreger bands (Hillson, 2005). Rodent molar teeth have enamel with a more irregular and less sharply defined structure on the occlusal surface (Hillson, 2005). All specimens were tumbled in sediment-water suspensions containing siliciclastic sediment particles of three different grain sizes (63-125 µm, 125-250 µm and 250-500 µm) using commercially available tumbling machines. For each grain size fraction, three teeth of each species (one per barrel) were tumbled for eight different time intervals of 0.5, 1, 2, 4, 8, 12, 16 and 336 hours (**Table 3.1**). At each 3DST measurement, the tumbling interval was interrupted and continued after the measurement.

Table 3.1. Tumbled specimens with tooth side and position (where possible), analysed facet (see **Fig. 3.1**), grain size fraction and tumbling interval.

Taxon	Side	Tooth position	Facet	Original vs. mould	Treatment	Tumbling interval [hrs]
Equus sp.	right	M2	3	original	63-125 µm	0.5, 1, 2, 4, 8, 12, 16, 336
Equus sp.	right	M1	1	original	63-125 µm	
Equus sp.	left	M2	1	original	63-125 µm	
Equus sp.	left	P4	1	original	125-250 µm	
Equus sp.	right	P4	1	original	125-250 µm	
Equus sp.	left	M1	3	original	125-250 µm	
Equus sp.	left	P3	1	original	250-500 µm	
Equus sp.	right	P3	3	original	250-500 µm	
Equus sp.	left	P2	1	original	250-500 µm	
Capreolus capreolus	left	M1	2	original	63-125 µm	4, 8, 12, 16, 336
Capreolus capreolus	left	P2	3	original	63-125 µm	
Capreolus capreolus	right	M3	1	mould	63-125 µm	
Capreolus capreolus	left	M2	3	original	125-250 µm	
Capreolus capreolus	left	P3	4	original	125-250 µm	
Capreolus capreolus	right	P4	1	original	125-250 µm	
Capreolus capreolus	left	M3	4	original	250-500 µm	
Capreolus capreolus	left	P4	4	original	250-500 µm	
Capreolus capreolus	right	M1	3	original	250-500 µm	
Otomys sp.	n.n	n.n	L1	original	63-125 µm	4, 8, 12, 16
Otomys sp.	n.n	n.n	L1	original	63-125 µm	
Otomys sp.	n.n	n.n	L2	original	63-125 µm	
Otomys sp.	n.n	n.n	L1	original	125-250 µm	
Otomys sp.	n.n	n.n	L2	original	125-250 µm	
Otomys sp.	n.n	n.n	L2	original	125-250 µm	
Otomys sp.	n.n	n.n	L1	original	250-500 µm	
Otomys sp.	n.n	n.n	L1	original	250-500 µm	
Otomys sp.	n.n	n.n	L1	original	250-500 µm	

3.3.1 Sample preparation

The teeth were cleaned manually using cotton swabs and water to remove adhering dust, ethanol to remove lipids and acetone to remove any residual acetone-soluble vanishes/superglue. 3DST measurements were taken of the original ante-mortem occlusal texture according to the protocol of Schulz et al. (2013a) for all dental specimens except for three molars of *Capreolus capreolus,* in which the high cusps and steeply inclined wear facets did not allow for direct measurements on the original teeth. For these *C. capreolus* specimens, moulds of the facet surface of each of the three molars were produced using high-resolution silicone-Vinylpolysiloxane precision impression material Provil novo Light regular set EN ISO 4823, type 3, light (Heraeus Kulzer GmbH, Dormagen, Germany).

Two cutmarks were placed on the target facets of the *Equus* sp. and *C. capreolus* (pre-)molars (facets 1-4, **Fig. 3.2**) in order to define a measurement area. Four non-overlapping scans of 160 x 160 µm were taken on all suitable and marked wear facets (**Fig. 3.1**). In order to identify and measure the same areas on the occlusal surface after each tumbling interval,

the wear facet was optically aligned to the referring cutmark and measured at the same relative coordinates as in the previous measurements. Since there were possible inaccuracies during the orientation of the teeth at each measuring interval, a rotation of the wear facet around 5-10° was accepted. *Otomys* teeth were too small and delicate to use cutmarks, however, the small size and number of enamel lamellae enabled precise re-identification of focal measurement positions. (**Fig. 3.2, Table 3.1**). Four non-overlapping scans were measured per tooth.

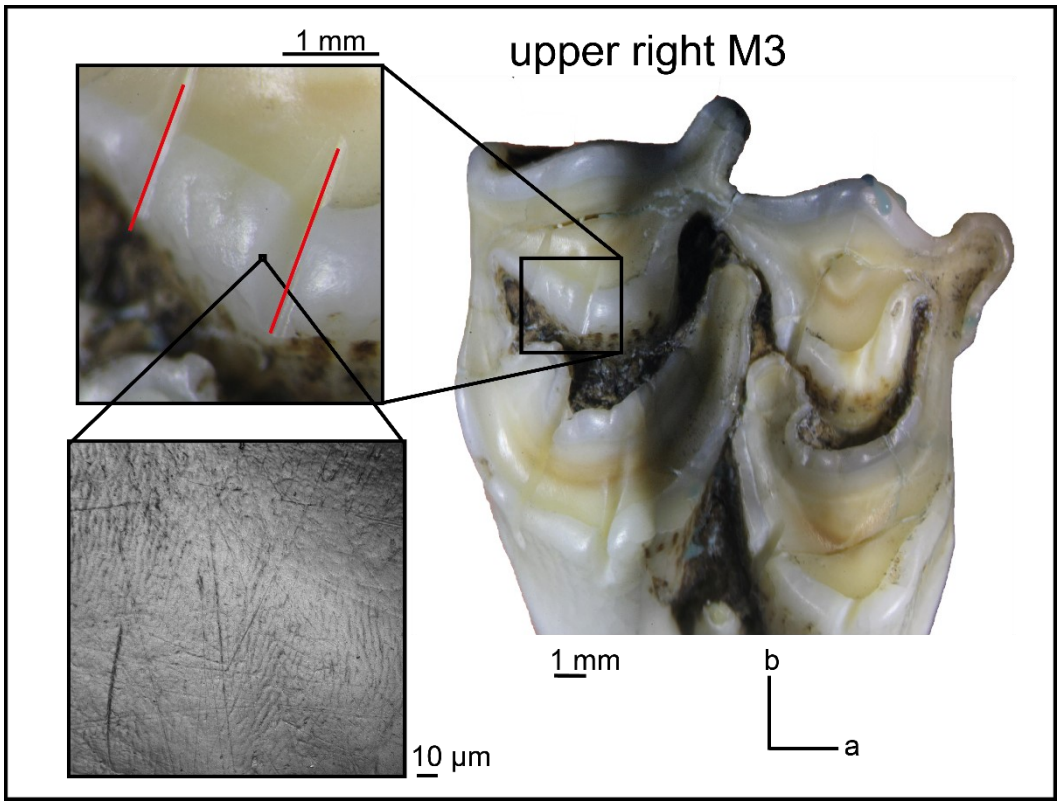

Figure 3.2. Exemplary graphical representation of the measurement position on the chewing facet of the upper third molar (M3) of Capreolus capreolus; and the cut marks (red lines) used for orientation. The area of the 3D scan is 160 x 160 µm. b = buccal, a = anterior.

3.3.2 Sediment

Construction grade joint-sand (Flairstone) was sieved using DIN norm sieves (500 µm, 250 µm, 125 µm and 63 µm), into three different grain size fractions: 63-125 µm, 125-250 µm, 250-500 µm. Based on grain size analysis with laser granulometry, the true grain size fractions have a median of 101 µm (range: 51-168 µm), 200 µm (range: 112-292 µm) and 353 µm (221-513 µm) (**Fig. 3.3**). The grain size fractions thus overlap somewhat, potentially due to aggregate formation and disintegration; nevertheless, the median fits the considered grain size fractions. In the following, the grain size fractions are labelled as follows: very fine sand (51-168 µm), fine sand (112-292 µm) and medium sand (221-513 µm). Based on X-ray diffraction

measurements, quartz is the principle mineral phase in all three sand fractions. In the fine sand, the quartz content is slightly higher (~60 %) than in the other two grain size fractions (~50-55 %). Additionally, feldspar (albite) is a component of the sediment in all three sand fractions.

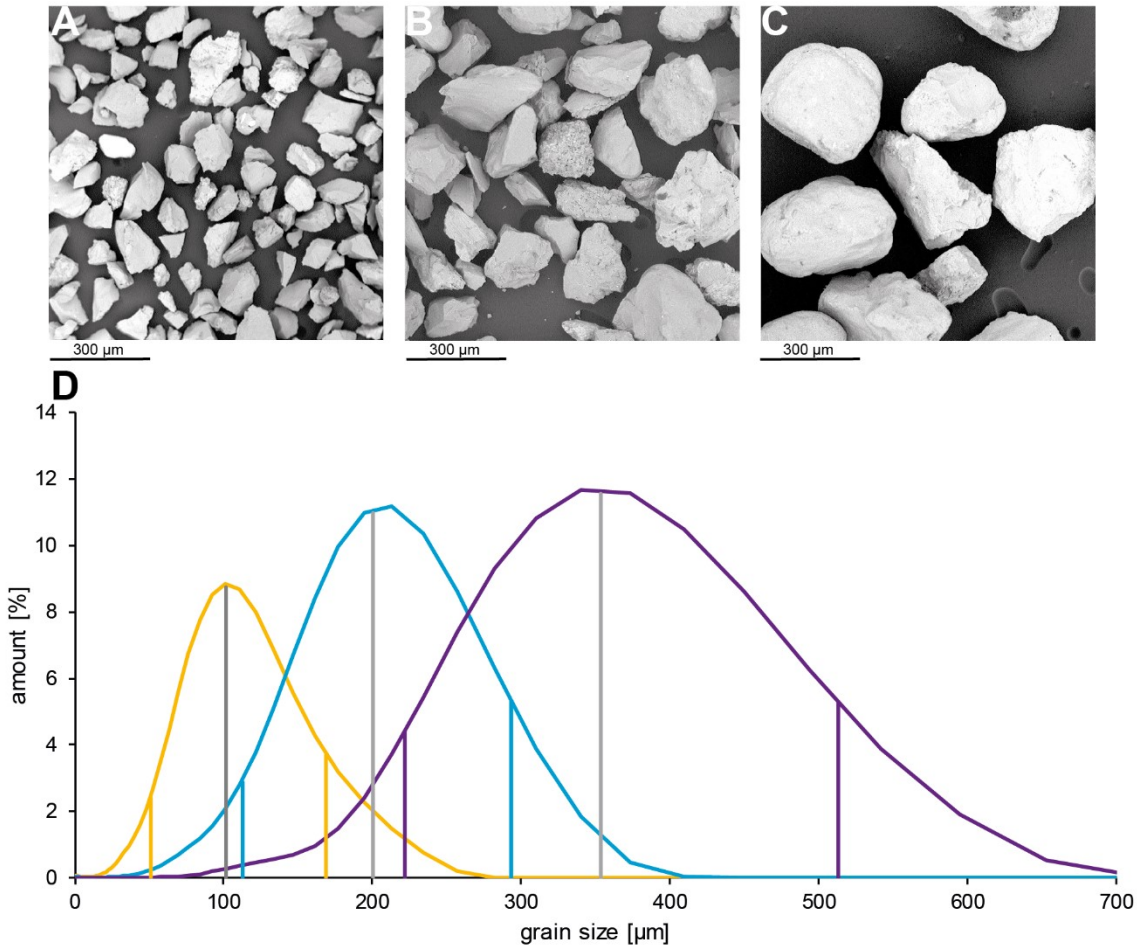

Figure 3.3. Graphical representation of the sediment grain size fractions measured by laser granulometry. SEM photos (275x magnification) of A. very fine sand, median 101 µm (range: 51-168 µm); B. fine sand, median 200 µm (range: 112-292 µm); and C. medium sand, median 353 µm (221-513 µm). D. Grain size distribution according to analysis with laser granulometry. Yellow = very fine sand (51-168 µm), blue = fine sand (112-292 µm), violet = medium sand (221-513 µm).

3.3.3 Tumbling procedure

The effects of fluvial transport in a suspension of sediment particles were simulated using commercial hobby rotary tumblers TYP TRO 2 A (Otto Eigner e.K., Industriebedarf & Hobbyschleifmaschinen, Idar-Oberstein, Germany). Tumbling barrels have a diameter of 10 cm and a capacity of 900 ml. Machines operate at a constant speed of 45 rpm, which equals a transport speed of around 1.08 km per hour. As comparison, the Rhine river flows with a speed of around 2.5 – 10.5 km per h (http://www.wsd-west.wsv.de). In order to ensure a constant suspension of sediment in water during tumbling and to facilitate contact between the tooth and sediment, the barrels were filled with 500 g of sediment and 300 ml of tap water (resulting in a 90 % full barrel). For each barrel, one tooth was added to the sediment-water mixture and each tooth was then tumbled for 0.5, 1, 2, 4, 8, 12 and 16 h (**Table 3.1**). These time intervals were chosen to represent the potential alteration effects on diet-related ante-mortem textures occurring during the first hours (i.e. first kilometres) of simulated fluvial transport. Additionally, teeth of two species (*C. capreolus* and *Equus* sp.) were also tumbled for 336 h to simulate a long distance (362.9 km) transport scenario. The enamel texture of each tooth was scanned prior to tumbling, to establish baseline parameters and document original ante-mortem dental wear. The approximately same surface area was scanned again after each time interval of tumbling (**Table 3.1**).

3.3.4 Data acquisition for enamel surface texture analysis

The surface scans of occlusal enamel facets were performed using the high-resolution disc-scanning confocal 3D-surface measuring system μsurf Custom (NanoFocus AG, Oberhausen, Germany), following the procedure described in Schulz et al. (2010). A square area of 160 x 160 μm was scanned using the x100 long distance lens with a resolution in x, y = 0.16 μm, and z = 0.06 μm. Measurements with a vertical displacement range δz > 60 μm were rejected (i.e. measured surface was oriented too obliquely).

We applied 3D (enamel) surface texture analysis (compare Schulz et al. 2010; 2013a, b; Calandra et al., 2012) and scale-sensitive fractal analysis (SSFA) using parameters after Ungar et al. (2003) and Scott et al. (2006) using MountainsMap Premium v.7.4 software for data evaluation. To test for the impact of imprecision in misalignment of repeated sampling, we performed a nine-time repetition of the same scan for one original and one moulded sample. Percentage variance was below 1 % for ~50 % (moulded sample) and ~57 % (original sample) of the parameters. For the parameters *Spd*, *S10z*, *S5p*, *S5v*, *Shv*, *mea,* and *madf* a percentage variance above 10 % (**Table ES3.1**) was found.

3.3.5 Data processing

3.3.5.1 Dental microwear texture analysis

The measurements were processed using two different templates in MountainsMap Premium v.7.4. 8495 (DigitalSurf, Besançon, France):

I. *Otomys* template. First an extraction sub-surface of 60 x 60 µm was cut out using the extraction operator in MountainsMap, because the enamel bands of this taxon are smaller than the typical measurement field of 160 x 160 µm used for all other teeth. All extracted scans of *Otomys* sp. were treated in the same way without mirroring to account for left/right teeth, since tooth position could not be determined. Most surface texture parameters are, however, expected not to differ between left and right teeth with exception of directional parameters such as *Str*, *Spd*, *Tr1R*, *Tr2R*, *Tr3R*. After tumbling, we expect directional parameters to be altered and hence the inclusion of both left and right teeth with potentially different original surface textures is unproblematic.
II. Large mammal template. This template is designed to analyse scans on original upper right (pre-) molar teeth. Therefore, in order to have the same orientation in all teeth, all scans of original left teeth were mirrored along the y-axis. All moulded surfaces were mirrored along the z-axis, since the measurements first need to be inverted, additionally, all moulded upper right teeth need to be mirrored along the x-axis.

The analysis is based on 3D industrial area surface texture standards (ISO 25178, ISO 12781), with parameters which allow quantification of an area based on surface texture geometry (Schulz et al., 2010; Calandra et al., 2012). Thirty-five 3D-surface roughness parameters (according to ISO 25178): standardised height, functional, spatial, hybrid, and segmentation parameters (Schulz et al., 2013b); and fourteen motif, furrow, isotropy, and ISO 12781 (flatness) parameters integrated in Mountains 7.4 were computed (**Table 3.2**). Additionally, we employed the SSFA parameter *Asfc* (complexity) and *epLsar* (anisotropy) (compare Ungar et al., 2007; 2008), as these are commonly applied to differentiate browsing and grazing herbivores (Scott et al., 2005; 2006; Merceron et al., 2007; DeSantis et al., 2013; Ungar et al., 2012).

Table 3.2. Description of applied surface texture parameters according to ISO 25178, ISO 12781, motif, furrow, texture direction and isotropy.

Category	Parameter	Description (condition)	Standard	Unit
Height	*Sq*	Standard deviation of the height distribution, or RMS surface roughness	ISO 25178	µm
	Ssk	Skewness of the height distribution	ISO 25178	no unit
	Sku	Kurtosis of the height distribution	ISO 25178	no unit
	Sp	Maximum peak height, height between the highest peak and the mean plane	ISO 25178	µm
	Sv	Maximum pit height, depth between the mean plane and the deepest valley	ISO 25178	µm
	Sz	Maximum height, height between the highest peak and the deepest valley	ISO 25178	µm
	Sa	Arithmetic mean height or mean surface roughness	ISO 25178	µm
Function	*Smr*	Areal material ratio	ISO 25178	%
	Smc	Inverse areal material ratio (p = 10%)	ISO 25178	µm
	Sxp	Peak extreme height difference in height between p% and q% (p=50%, q=97.5%)	ISO 25178	µm
	Sk	Core height	ISO 25178	µm
	Svk	Reduced dale height, average height of the protruding dales below the core surface	ISO 25178	µm
	Spk	Reduced peak height, average height of the protruding peaks above the core surface	ISO 25178	µm
	Smr1	Peak areal material ratio	ISO 25178	%
	Smr2	Dale areal material ratio	ISO 25178	%
Spatial	*Sal*	Auto-correlation length (s = 0.2)	ISO 25178	µm
	Str	Texture aspect ratio (s = 0.2)	ISO 25178	no unit
	Std	Texture direction	ISO 25178	no unit
Hybrid	*Sdq*	Root mean square gradient	ISO 25178	no unit
	Sdr	Developed interfacial area ratio	ISO 25178	%
Volume	*Vm*	Material volume at a given material ratio (p = 10%)	ISO 25178	$\mu m^3/\mu m^2$
	Vmc	Material volume of the core at given material ratio (p = 10%, q = 80%)	ISO 25178	$\mu m^3/\mu m^2$
	Vmp	Material volume of the peaks (p=10%)	ISO 25178	$\mu m^3/\mu m^2$
	Vv	Void volume at a given material ratio (p = 10%)	ISO 25178	$\mu m^3/\mu m^2$
	Vvc	Void volume of the core (p = 10%, q = 80%)	ISO 25178	$\mu m^3/\mu m^2$
	Vvv	Void volume of the valley at a given material ratio (p = 80%)	ISO 25178	$\mu m^3/\mu m^2$
Feature	*S10z*	Ten-point height	ISO 25178	µm
	S5p	Five-point peak height	ISO 25178	µm
	*S5*v	Five-point valley height	ISO 25178	µm
	Sda	Closed dale area	ISO 25178	μm^2
	Sdv	Closed dale volume	ISO 25178	μm^3
	Sha	Closed hill area	ISO 25178	μm^2
	Shv	Closed hill volume	ISO 25178	μm^3
	Spc	Arithmetic mean peak curvature	ISO 25178	1/µm
	Spd	Density of peaks	ISO 25178	$1/\mu m^2$
Motif	*nMotif*	Number of motifs	Motif	no unit
	meh	Mean height	Motif	µm
	mea	Mean area	Motif	μm^2
Furrow	*metf*	Mean depth of furrows	Furrow	µm
	medf	Mean density of furrows	Furrow	cm/cm^2
	madf	Maximum depth of furrows	Furrow	µm
Direction	*Tr1R*	First direction	Direction	no unit
	Tr2R	Second direction	Direction	no unit
	Tr3R	Third direction	Direction	no unit
Isotropy	*IsT*	Texture isotropy	Isotropy	%
Flatness	*FLTt*	Peak to valley flatness deviation of the surface (Gaussian Filter, 0.025 mm)	ISO 12781	µm
	FLTp	Peak to reference flatness deviation (Gaussian Filter, 0.025 mm)	ISO 12781	µm
	FLTv	Reference to valley flatness deviation (Gaussian Filter, 0.025 mm)	ISO 12781	µm
	FLTq	Root mean square flatness deviation (Gaussian Filter, 0.025 mm)	ISO 12781	µm
SSFA	*Asfc*	Fractal complexity (Area-scale)	SSFA	no unit
	epLsar	Length-scale anisotropy	SSFA	no unit

3.3.5.2 Statistics

Two datasets which were subjected to different statistical procedures, are described below. The open-source software R v.3.4.1 (R. Development Core Team, 2009) with the packages xlsx, rJava, doBy, R.utils and WRS version 0.12.1 was used for the statistical

analyses. For every specimen, only one measured facet was used. The datasets were calculated equally for all three species (n = 9 teeth) as follows:

I. A mean for each tumbled tooth was calculated from four measured scans for t_0 and for each tumbling interval (**Table 3.1**) (n = 9 mean values).

II. Dataset 1 (**Table ES3.2**), separated after sediment grain size fraction. Here, we used the mean values of step 1 and calculated a mean for each sediment type (n = 3 teeth/mean values).

III. Dataset 2 (**Table ES3.3**), all nine teeth per taxon were pooled (ignoring the grain size fraction with which it was tumbled during the experiment). Here, we used the mean values of step 1 and averaged these nine values for t_0 and per tumbling interval (**Table 3.1**).

For Dataset 1 we only present descriptive statics, because a sample size of n = 3 per species and sediment grain size fraction is not sufficient to draw statistically significant conclusions. However, we discuss visible trends in parameter value development between tumbling intervals. Trends are calculated by the quotient of tumbling time zero (t_0) and the maximum tumbling time (t_{max}) (16 hours for *Otomys* sp., 336 hours for *Equus* sp and *C. capreolus,* **Table ES3.4**). If the value for the quotient (index) is above a value of one outside the standard error, the parameter value is increasing and the trend is described as positive. If the quotient (index) value is below one outside the standard error, the trend is described as negative. In case the quotient (index) value is within the standard error, there is no trend in the parameter.

For Dataset 2, we employ pair-wise comparisons of surface texture parameter values within species between the different tumbling intervals. Dataset 2 also allows us to test for conservation of significant differences between dietary categories (grazer – browser). Previous studies have shown that surface texture data is non-normally distributed and heteroscedastic (e.g. Schulz et al, 2013a). Therefore, we used the procedure of Wilcox (Wilcox, 2003; 2005), applying the robust heteroscedastic Welch-Yuen omnibus test (Welch, 1938; Yuen, 1974) coupled with a heteroscedastic pair-wise comparison test (“Lincon test”, analogous to Dunnett’s T3 test (Dunnett, 1980)). Data were trimmed (15%) to compensate for non-normality. Following the established statistical protocol for 3DST data in dietary analyses (Calandra et al.,2012; Schulz et al., 2013a), we further applied the robust heteroscedastic rank-based test according to Cliff (Cliff, 1996; Schulz et al., 2013a). Due to the heterogeneity of the tooth sample (different tooth positions and suitability of facets for texture analysis), we encountered

a higher variability in diet-related texture parameters than in previous studies. This was evident in the results from the rank-based statistical test (Cliff's method) which did not confirm the significant differences documented by the first robust heteroscedastic pair-wise comparison ("Lincon's test").

3.4 Results

Only texture parameters (**Table 3.2**) showing distinct trends after the tumbling intervals are further described and only parameters with obvious alterations are plotted for the individual species in figures 4, 7 and 8.

3.4.1 Small mammal-*Otomys* sp.

3.4.1.1 Dataset 1: Very fine sand (51-168 µm)

Most intra-specific alterations are observed in this grain size fraction. Three parameters, which reflect the extreme height differences of the surface texture, are decreasing (*Sq, Sv* and *Svk*, **Fig. 3.4**). All parameters (except of *Str*) showing a negative trend (**Fig. 3.5**) (decreasing parameters) are describing the overall surface flatness (*FLTt, FLTp, FLTv, FLTq*), volume (*Vm, Vv, Vmp, Vmc, Vvc, Vvv*), roughness (*Sa*), dales and peaks (*Spd, Spc, S5p, S5v, Shv, Sdv, madf, met*f). Complexity (*Asfc*) vs. heterogeneity (*epLsar*) of the surface texture (**Fig. 3.6**) is decreasing during the first four hours of tumbling, during the last 12 hours of tumbling, no further alteration was observed.

3.4.1.2 Dataset 1: Fine sand (112-292 µm)

Peaks become less voluminous as indicated by decreasing *Vm* and *Vmp* (**Fig. 3.4**), while the volume of valleys and core (*Vv, Vvc, VVv, Vmc,* **Fig. 3.5**) remained almost unaltered after the treatment with the fine sand. The majority of altered parameters (describing overall height and roughness; *Sq, Sa*) show a negative trend for parameter values over the 16 hours of tumbling (**Fig. 3.5**). The parameter related to size of dales (*Sdv*) has an increasing trend. *Asfc* vs. *epLsar* does not change during the course of all tumbling intervals (**Fig. 3.6**).

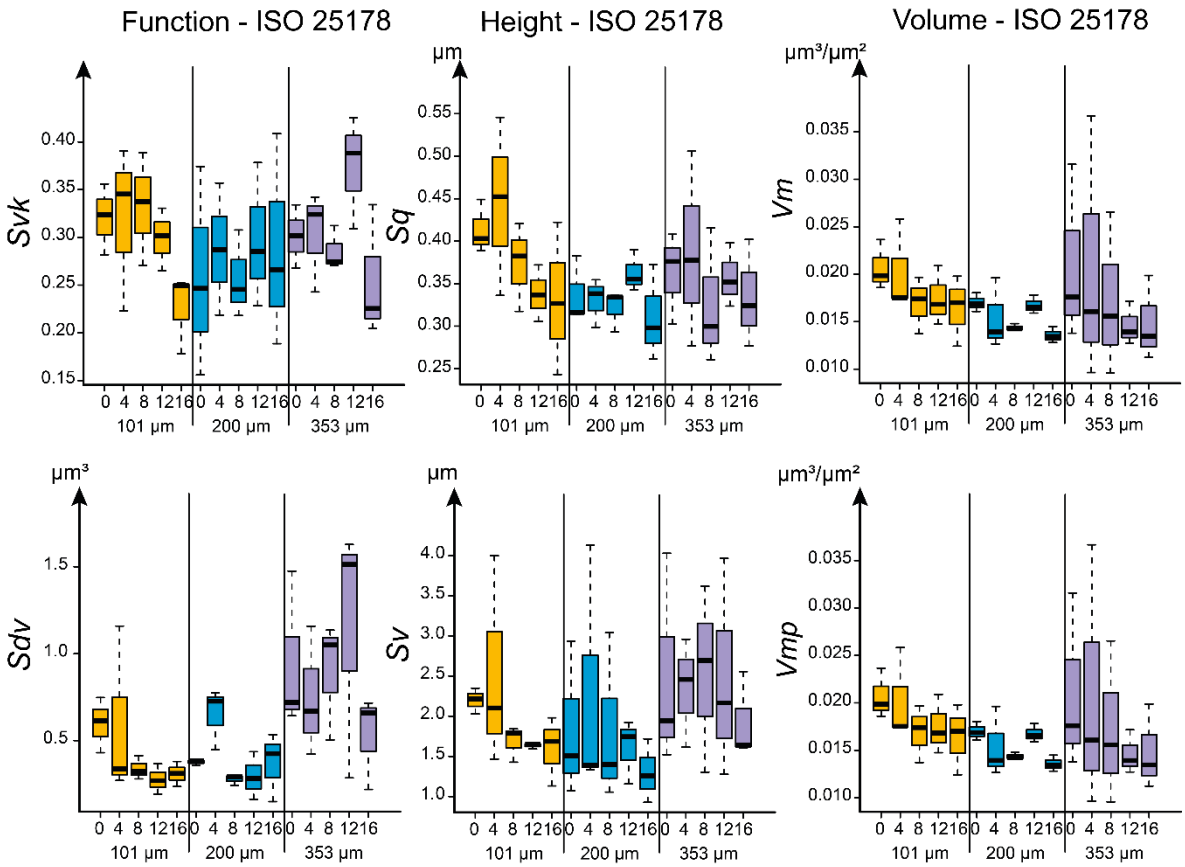

Figure 3.4. Exemplary parameters with strong alteration after tumbling for *Otomys* sp. (Dataset 1). Yellow = Very fine sand (51-168 µm), blue = Fine sand (112-292 µm), violet = Medium sand (221-513 µm). *Svk* = Reduced dale height, *Sq* = Standard deviation of the height distribution, *Vm* = Material volume at a given material ratio (p = 10%), *Sdv* = Closed dale volume, *Sv* = Maximum pit height, depth between the mean plane and the deepest valley, *Vmp* = Material volume of peaks (p = 10).

3.4.1.3 Dataset 1: Medium sand (221-513 µm)

Similar to the two smaller grain size fractions, parameters describing the volume (*Vm, Vv, Vmp, Vmc, Vvc*), general height (*meh, Sq*) and the extreme features (peaks and dales; *Spc, S5p, S5v, Shv*) tend to decrease (**Fig. 3.5**). *Asfc* vs. *epLsar* is not altered after the tumbling treatment with the medium sand (**Fig. 3.6**).

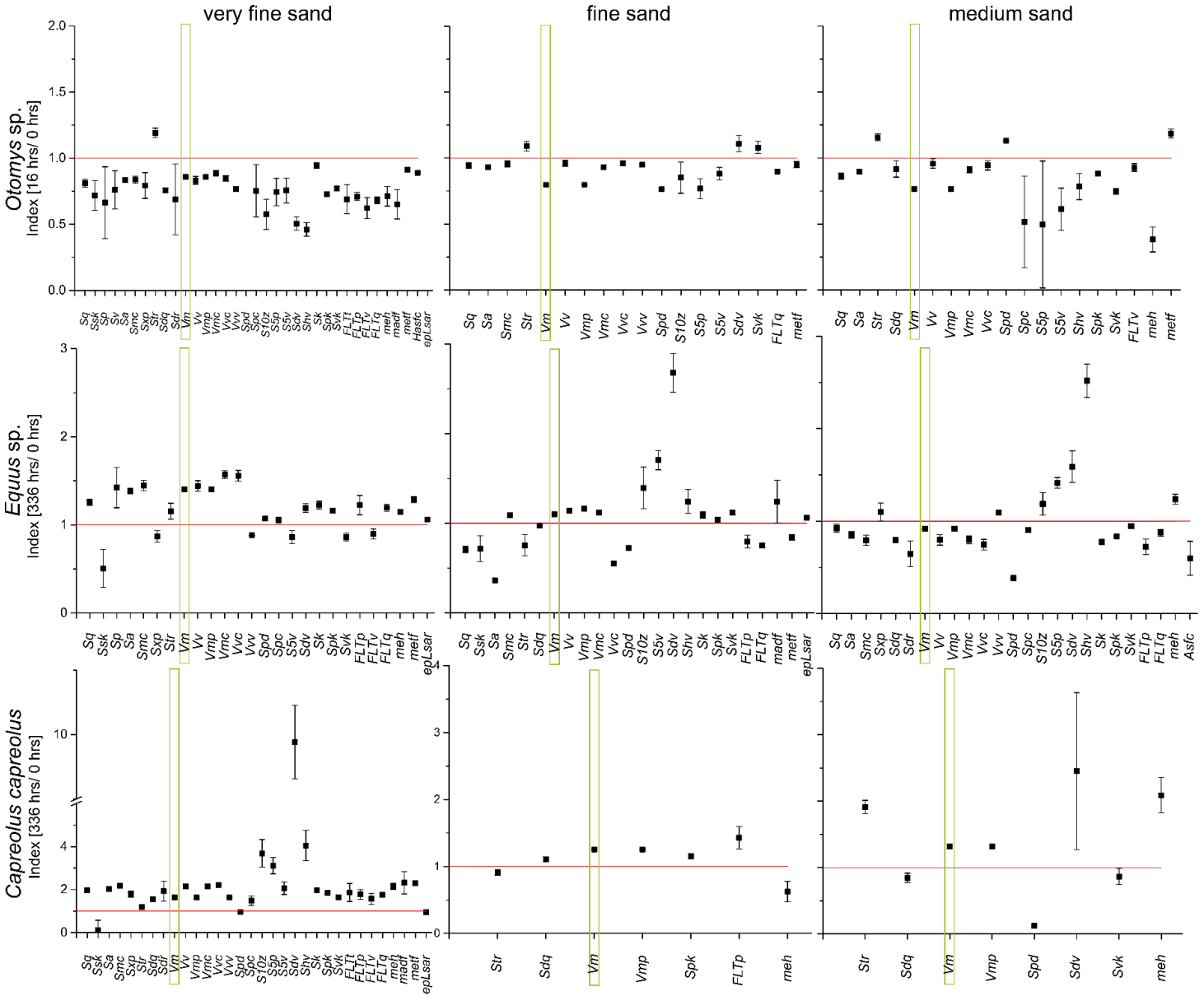
very fine sand
fine sand
medium sand
Otomys sp.
Index [16 hrs/ 0 hrs]
Equus sp.
Index [336 hrs/ 0 hrs]
Capreolus capreolus
Index [336 hrs/ 0 hrs]

Figure 3.5. Trends for Dataset 1 of *Otomys* sp., *Equus* sp. and *C. capreolus*. Index values of t_0 calculated with standard error. Red line = Index value of one. The roughness parameter *Vm* (material volume) shows an index value different from 1 in all treatments (within the standard error), and therefore highlighted to illustrate the intraspecific trends. For *Otomys* sp., *Vm* shows a negative trend (index value below 1) in all three grain size fractions, *Vm* decreases from t_0 to t_{max}. In *Equus* sp. *Vm* increase from t_0 to t_{max} for the two smaller grain size fractions, the index values are above 1. However, for the medium sand, the trend is negative (index value below 1), *Vm* value of t_{max} is lower than t_0. For *C.capreolus Vm* shows an increasing trend in all grain size fractions (index values above 1), *Vm* values are higher in t_{max} than t_0.

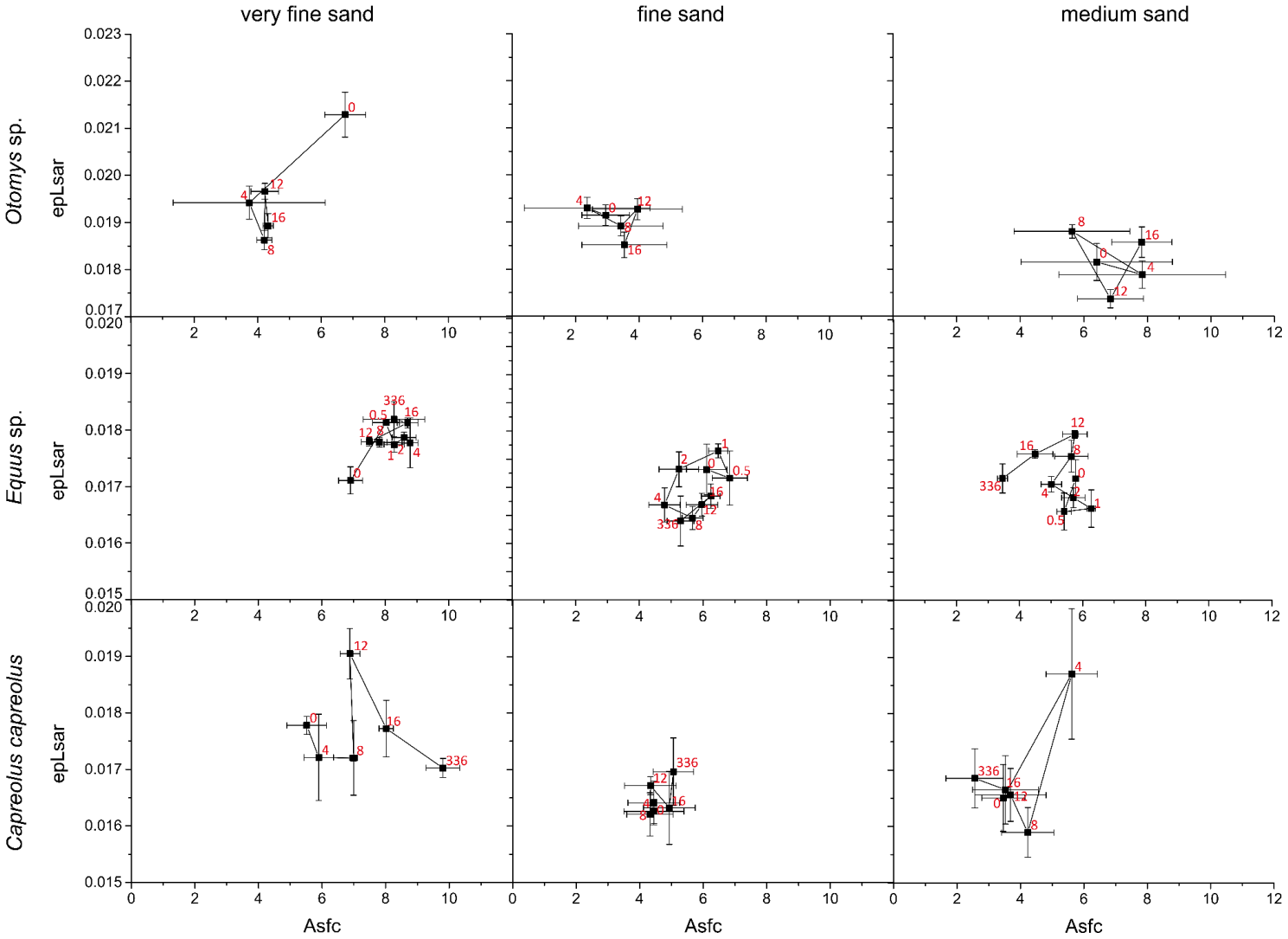

Figure 3.6. Complexity vs. heterogeneity for Dataset 1 of *Otomys* sp., *Equus* sp. and *C. capreolus* at all tumbling intervals (red numbers represent the hours of tumbling).

3.4.2 Large mammals-*Equuus* sp.

The *Equus* sp. (pre-)molars are the only large mammal teeth which show pronounced alterations after the tumbling process.

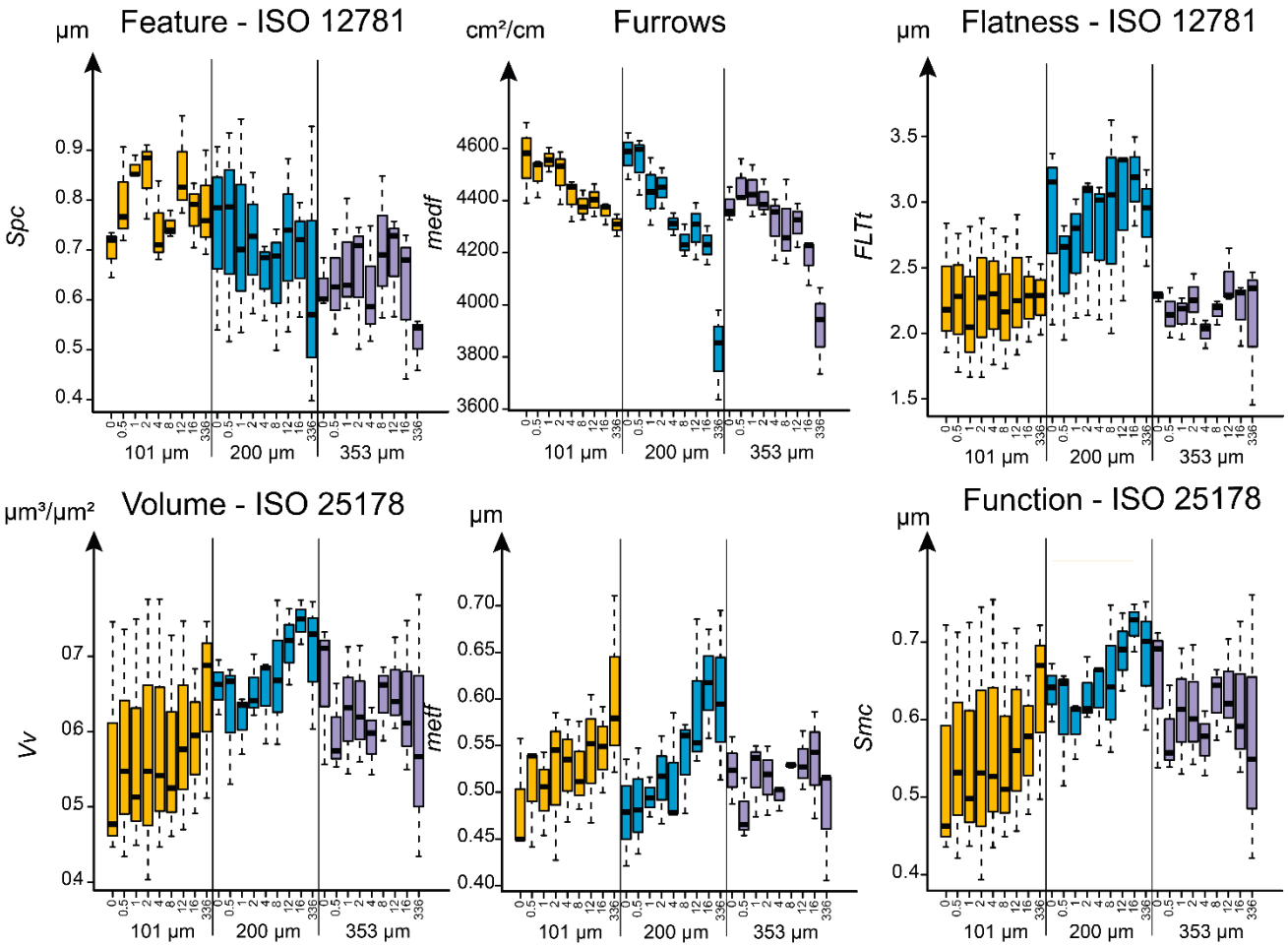

Figure 3.7. Exemplary parameters with strong alteration after tumbling for *Equus* sp. (Dataset 1). Yellow = very fine sand (51-168 µm), blue = fine sand (112-292 µm), violet = medium sand (221-513 µm). *Spc* = Arithmetic mean peak curvature, *medf* = Mean density of furrows, *FLTt* = Peak to valley flatness deviation of the surface, *Vv* = Void volume at a given material ratio (p = 10%), *metf* = Mean depth of furrows, *Smc* = Inverse areal material ratio (p = 10).

3.4.2.1 Dataset 1: Very fine sand (51-168 µm)

In this size fraction almost no alteration on the inner wear facets is observed, even though the tumbled teeth macroscopically display pronounced rounding of cusps and other elevations of the occlusal surface and visible alteration on the facets after 336 hours of tumbling (**Fig. 3.9**). After a tumbling time of 336 hrs, reflecting a transport distance of over 360 km, parameters describing the surface volume (*Vm, Vv, Vmp, Vmc, Vvc*) and general

surface roughness (*Sa*) show positive trends (**Fig. 3.5**). Increasing values are found primarily in the peak and dale parameters (*Sp, Spd, Spc, S5v, Spk, metf*) and additionally in parameters describing the general height (*meh*) (**Fig. 3.5**). Negative trends are found in *Ssk, Sxp, Vvv, S5v, Svk* and *FLTv.* Regarding *Asfc* vs. *epLsar*, both parameters increase after ~540 m of transport (30 minutes of tumbling), however, for longer tumbling intervals no further alteration is visible (**Fig. 3.6**).

3.4.2.2 Dataset 1: Fine sand (112-292 µm)

Equus sp. teeth show strong signs of alteration in surface texture (**Fig. 3.7**). In contrast to the smaller grain size fraction, the whole chewing area shows no obvious macroscopic alteration at the corners. *medf* decreases over the whole tumbling treatment of 336 hours, while the ISO void volume parameter (*Vv*) increases (until 16 hours of tumbling) (**Fig. 3.7**). A positive trend is observed in parameters describing the overall volume (*Vm, Vmp, Vmc, Vvc*) and a strong negative in the general surface roughness (*Sa*) and height (*Sq*) (**Fig. 3.5**). Parameters describing peaks and dales (*Spd, S10z, S5v, Sdv, Shv, Spk, Svk, madf, metf*) of the surface are ambiguous (**Fig. 3.5**).

3.4.2.3 Dataset 1: Medium sand (221-513 µm)

Parameters describing the amount of the dales (*medf,* **Fig. 3.7**) and the complexity (*Asfc,* **Fig. 3.6**) are strongly decreasing over the whole tumbling time (336 hours). Only seven parameters show a positive trend (*Sxp, Vvv, S10z, S5p, Sdv, Shv* and *meh*), while parameters describing the volume (*Vm, Vv, Vmp, Vmc, Vvc*) and the peaks (*Spd, Spc,)* as well as the general roughness (*Sa*) are decreasing in their parameter values over ~362 km of transport (336 hours of tumbling) (**Fig. 3.5**).

3.4.3 Large mammals-*Capreolus capreolus*

The roe deer teeth do show alteration in parameter values and new wear features are visible after tumbling procedure (described below).

3.4.3.1 Dataset 1: Very fine sand (51-168 µm)

The strongest alteration effect on enamel facets can be observed for this grain size fraction (**Fig. 3.5 and 3.8**). *Ssk, Spd* and *epLsar* are the only parameters showing a negative trend over 336 hours of tumbling, while the parameters describing the volume (*Vm, Vmp, Vmc,*

Vvc, Vvv (**Fig. 3.5**), *Vv* (**Fig. 3.8**)), the general surface texture (*Sq, Sa, Sxp, Str* (**Fig. 3.5**), *Smc* (**Fig. 3.8**)), the dales and peaks (*S10z, S5p, S5v, Sdv, Shv, madf* (**Fig. 3.5**), *Spc, metf* (**Fig. 3.8**)) are increasing. *Asfc* vs. *epLsar* of specimens tumbled with this grain size fraction show a broad range of values between the different tumbling intervals (**Fig. 3.6**).

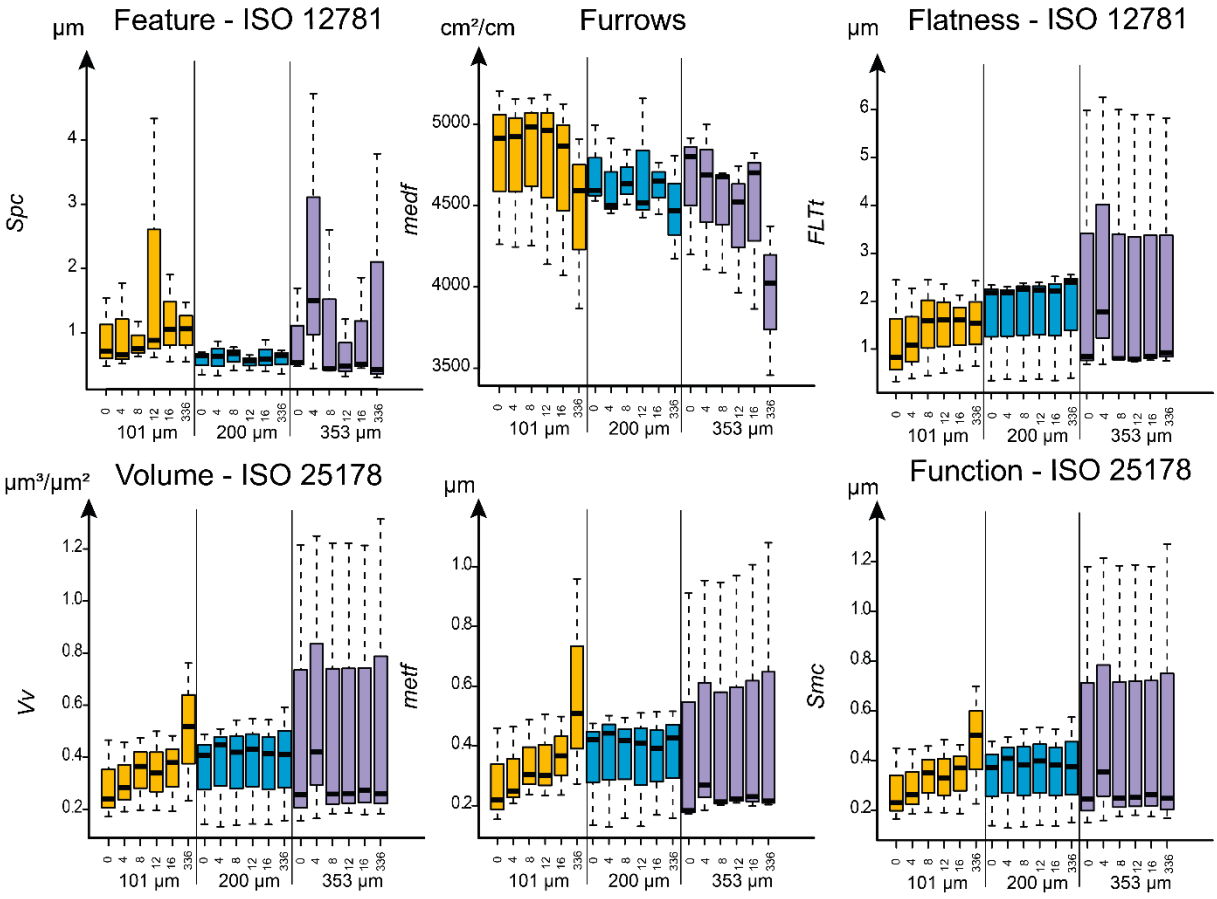

Figure 3.8. Exemplary parameters for *C. capreolus* (Dataset 1). Yellow = very fine sand (51-168 µm), blue = fine sand (112-292 µm), violet = medium sand (221-513 µm). *Spc* = Arithmetic mean peak curvature, *medf* = Mean density of furrows, *FLTt* = Peak to valley flatness deviation of the surface, *Vv* = Void volume at a given material ratio (p = 10%), *metf* = Mean depth of furrows, *Smc* = Inverse areal material ratio (p = 10).

3.4.3.2 Dataset 1: Fine sand (112-292 µm)

The least alteration during the tumbling experiment was found for the medium grain size fraction (112-292 µm). The teeth of *Capreolus capreolus* show a pronounced negative trend in two surface texture parameters, *Str* and *meh* (**Fig. 3.5**). A positive trend is found in five parameters describing the peaks (*Spk, FLTp*) and the volume (*Vm, Vmp*) (**Fig. 3.5**).

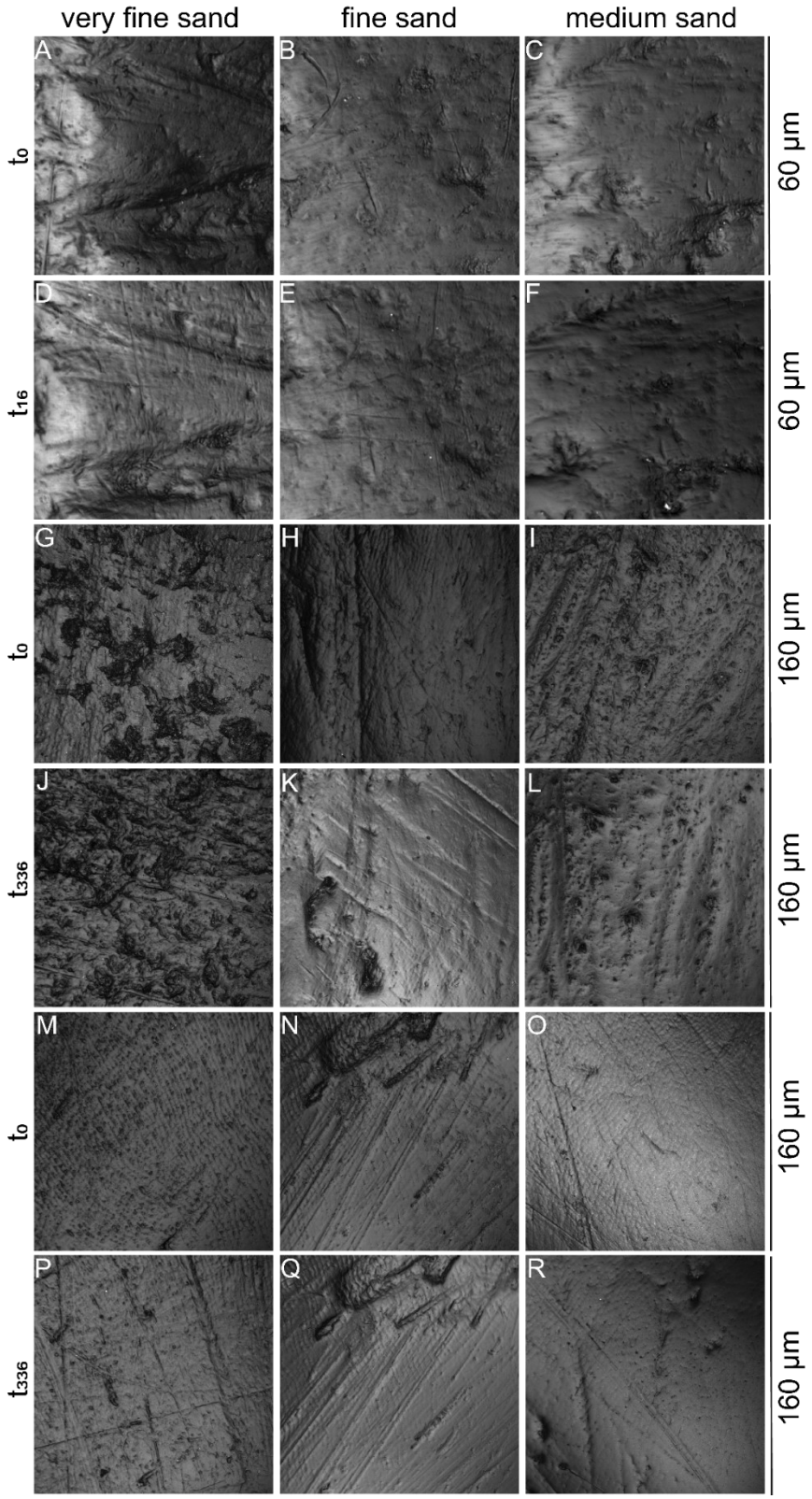

Figure 3.9. Photosimulations 3DMT surface models of single facets of *Otomys* sp (A-F), horse (*Equus* sp.) (G-L) and roe deer (*Capreolus capreolus*) (M-R) teeth. A/D. individual K, lammela 2; B/E. individual J, lamella 2; C/F. indivual L, lamella 1; G/J. upper left M2, facet 1; H/K. upper left M1, facet 3; I/L. upper left P2, facet 1; M/P. upper left M1, facet 2, N/Q. upper left M2, facet 3; O/R. upper right M1, facet 3.

3.4.3.3 Dataset 1: Medium sand (221-513 µm)

Teeth tumbled with this grain size fraction of middle sand show an obvious surface abrasion already visible with the naked eye (**Fig. 3.9**). However, only eight surface texture parameters show pronounced trends. *Sdq, Spd* and *Svk* decrease strongly, while parameters *Str, Vm, Vmp, Sdv* and *meh* increase (**Fig. 3.5**), comparable to the trends observed in the roe deer specimens tumbled with the fine sand. After four hours of tumbling, *Asfc* vs. *epLsar* increases strongly, but then reverts back to the level of time zero during all remain tumbling intervals until 336 hours (**Fig. 3.6**)

3.4.4 Large mammals *Dataset 2* -grazer versus browser

3.4.4.1 Conservation of inferred diet categories at the same tumbling interval

The parameter differences between zebra and roe deer remain stable for the majority of well-differentiating parameters. Overall, in both species alteration is only visible as non-significant trends, which are however more pronounced in *C. capreolus* teeth (Dataset 2) compared to *Equus* sp. (Dataset 2). All ISO 25178 volume parameters are altered towards increasing values for both species (zebra and roe deer), leading to consistently higher parameter values *Vmc, Vvv, Vv* and *Vvc* (exemplary parameter *Vv* **Fig. 3.10**) in the grazer (*Equus* sp.). Additionally, in the ISO 12781 flatness parameters (*FLTp, FLTq* (exemplary parameter *FLTq* **Fig. 3.10**)) and the well separated ISO 25178 parameters *Smc, Sxp and Sa* (**Fig. 3.10**) of the grazer (*Equus* sp.) are consistently higher than those of the browser (*C. capreolus*) and lower in *medf* (**Fig. 3.10**).

3.4.4.2 Diet categories between different tumbling intervals

Besides finding differences between grazer (*Equus* sp.) and browser (*C. capreolus*) at the same tumbling interval, these two diet categories are also still distinguishable when original tooth surface textures are compared to those of tumbled samples (**Fig. 3.10**).

After t_{16}, surface textures of tumbled *C. capreolus* still show smaller flatness parameters (*FLTp, FLTq, FLTt* (exemplary parameter *FLTq* **Fig. 3.10**)) and the ISO 25178 roughness parameters *Sa, Smc,* the volume parameters (*Vmc, Vv* and *Vvc* (exemplary parameter *Vv* **Fig. 3.10**)) than the untreated *Equus* sp. samples (**Fig. 3.10**). After t_{336} of tumbling, only four separating parameters still show pronounced differences between the two diet categories. The flatness parameter *FLTq,* and the parameters *Sa, Sxp* and *Vmc* (**Fig. 3.10**) are still separate clearly.

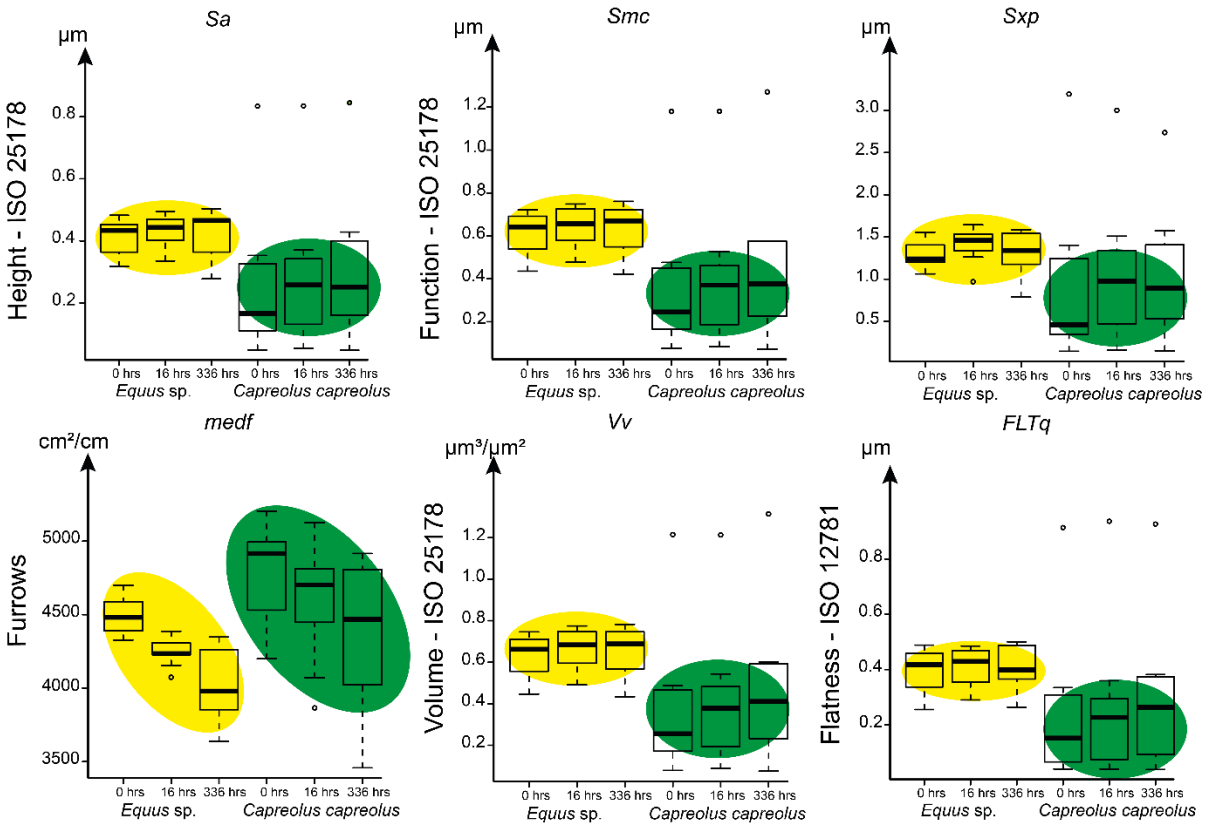

Figure 3.10. Well separating 3D surface texture parameters with well distinguished grazer (horse, yellow) and browser (roe deer, green) specimens. Small open circles represent outliers. *Sa* = Mean surface roughness; *Smc* = Inverse areal material ratio (p = 10%); *Sxp* = Peak extreme height difference in height between p=50% and q=97.5%; *medf* = Mean density of furrows; *Vv* = Void volume at a given material ratio (p = 10%); *FLTq* = Root mean square flatness deviation.

Contrary, at t_{16} for the teeth of the grazer (*Equus* sp.) a higher number of parameters distinguishes them from the teeth of the untreated (pre-tumbled) browser (*C. capreolus*). The values of the surface texture parameters of *Equus* sp. are lower in *medf* than for the browser, even still after 336 hrs of tumbling (**Fig. 3.10**). Flatness (*FLTp, FLTq, FLTt* (exemplary parameter *FLTq* **Fig. 3.10**)), volume (*Vmc, Vv, Vvc* (exemplary parameter *Vv* **Fig. 3.10**)), *Sa* and the function parameters *Sxp* and *Smc* are almost unaltered after the whole tumbling treatment and higher in *Equus* sp. (**Fig. 3.10**, *FLTp, FLTt, Vmc* and *Vvc* in **Table ES3.2**).

3.5 Discussion

Generally, we observe two different patterns in parameter values when comparing the original, unaltered surface textures with those after the subsequent tumbling intervals. “Stable” parameters are either not significantly altered by the tumbling process or follow a distinct trend

with increasing tumbling time (**Fig. 3.11**). “Unstable” parameters show pronounced different values after tumbling and/or follow no distinct trend, alternating between increasing and decreasing parameter values over the tumbling intervals (**Fig. 3.12**). We find the highest number of stable parameters in the tumbling regimes using the two smaller grain size fractions (51-168 µm, 112-292 µm). Altogether, those parameters that appear to be unstable, in all tumbling regimes, regardless of grain size fraction, describe the extreme height and depth characteristics of the enamel surface (peaks and dales). The peaks are most exposed to the sediment, and therefore vulnerable for alteration through abrasion. However, it needs to be taken into account, that some of these unstable parameters are also prone to measurement inconsistencies in repeated measurement approach (see **Table ES3.1**). It is clear that observed post-tumbling alteration in parameter values for the parameters *Spd*, *S10z*, *S5p*, *S5v*, *Shv*, *mea*, and *madf* result from experimental abrasion or are due to the repeated measurement error. However, in all other 44 parameters, the error due to repeated measurements is lower than 5 %. Changes in these parameters are therefore considered to be the result of the experimental abrasion.

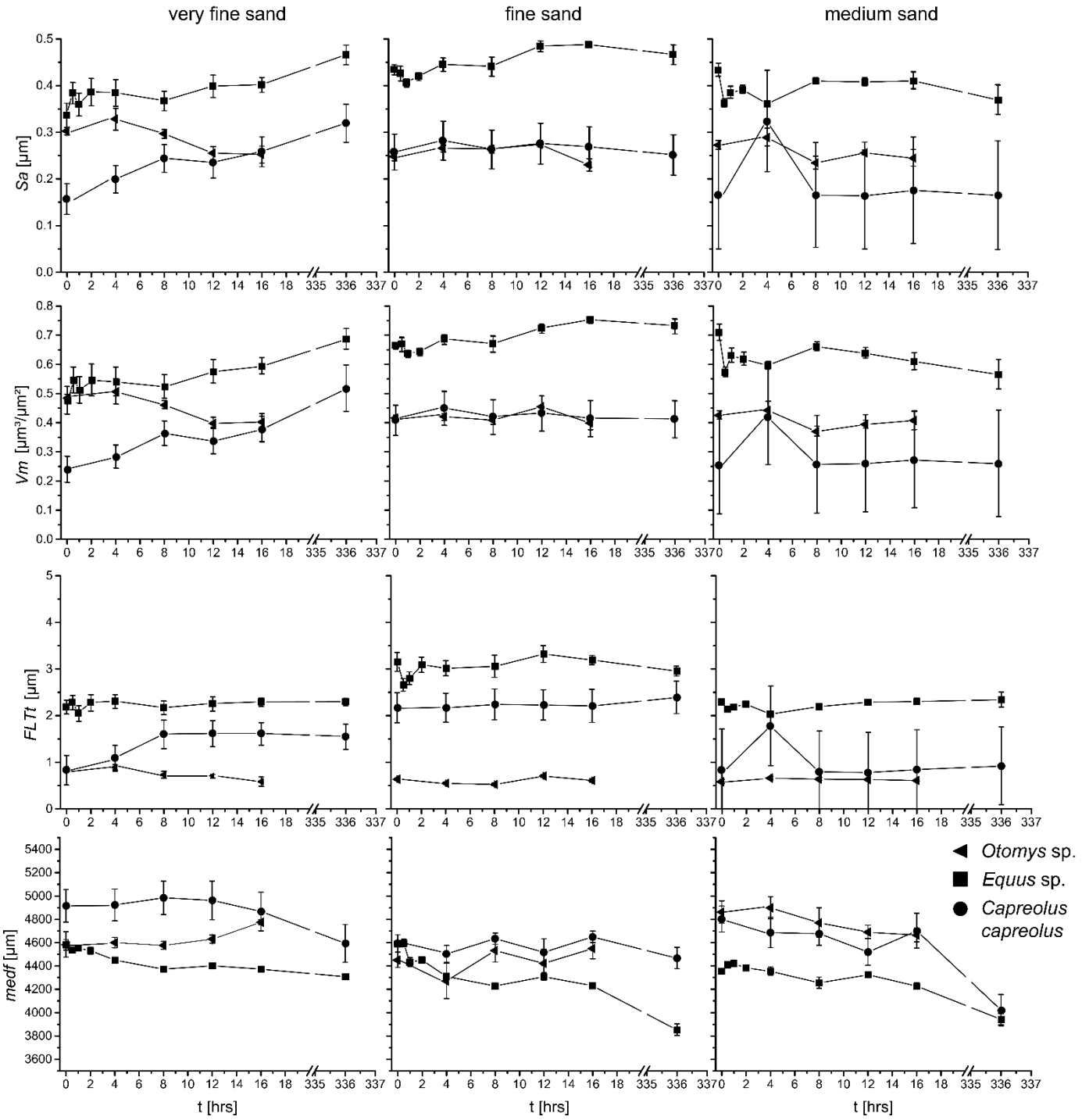

Figure 3.11. Examples of stable parameters over the tumbling experiment for Dataset 1 of *Otomys* sp., *Equus* sp. and *Capreolus capreolus*. *Sa* = Mean surface roughness; *Vm* = Material volume; *FLTt* = Peak to valley flatness deviation of the surface; *medf* = Mean density of the furrows.

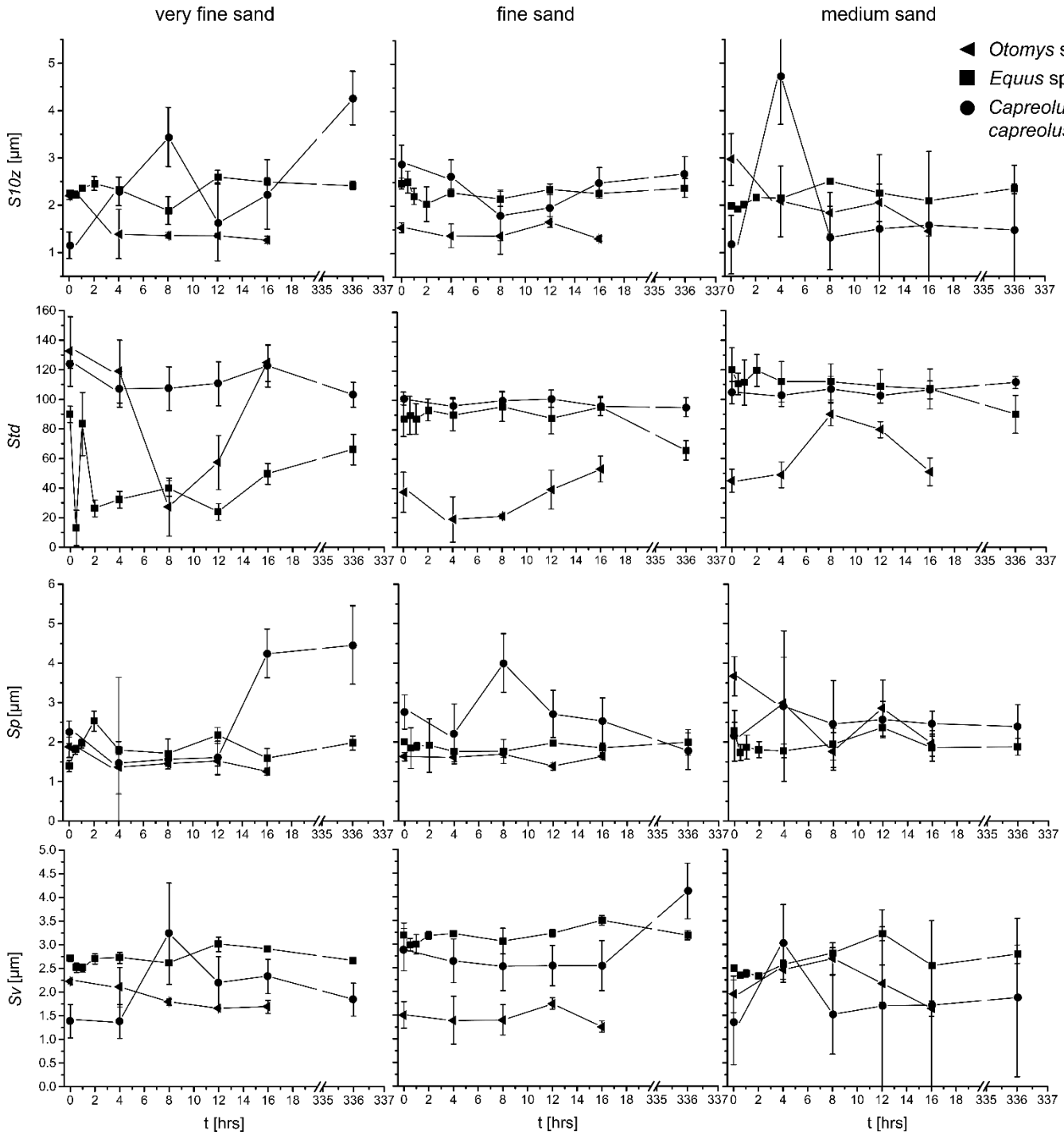

Figure 3.12. Examples of unstable parameters over the tumbling experiment for Dataset 1 of *Otomys* sp., *Equus* sp. and *Capreolus capreolus*. *S10z* = Ten-point peak height; *Std* = Texture direction; *Sp* = Maximum peak height; *Sv* = Maximum pit height.

3.5.1 Differences in sand grain size fractions

3.5.1.1 Small mammal-Otomys sp.

Otomys sp. are specialised herbivores which live in Africa feed primarily on grasses, reeds and sedges (as well as some fruits, roots and bark) (Skinner and Chimimba, 2005; Happold, 2013). Their 3DST is similar to that of rats from an abrasive, dusty environment in SW Madagascar (Winkler et al., 2016). Tumbling in three different grain size fractions results in relatively small alteration effects on the enamel surface. The most general changes caused by the tumbling procedure, that applies for all grain size fractions, is observed in the volume and height of the peaks and size of the dales (**Fig. 3.13**), as indicated by decreasing *Vm* and *Vmp*, *Sp* and *Sv, Sda* and *Sha*. The slightly smaller values for volume parameters, (e.g. the volume of the core (*Vmc*) and the volume of the peaks (*Vmp*)), is likely the result of sediment abrasion (most pronounced in the fine sand) which removed the peaks during the tumbling experiment. In addition, in the two smallest grain size fractions (51-168 and 292 µm), new scratches formed (indicated by increasing *medf)*. However, these scratches are never as deep or as broad (decreasing *Sda*) as those related to ante-mortem wear (**Fig. 3.13**). This can possibly be explained by the small size of *Otomys* enamel lamella, which are less than 80 µm wide. The likelihood of sediment particles leaving scratches on the lamella increases with smaller particle size and decreases with larger particle size. In our case, the 51-168 and 112-292 µm grain size fractions were more effective in producing this abrasive signal on these small specimens.

3.5.1.2 Large mammals-Equus sp.

In contrast to the *Otomys* sp. teeth, the zebra teeth show different patterns of alteration in all the three different grain size fractions. Larger particles have greater potential to leave scratches on the broader enamel bands of the zebra (**Fig. 3.13**). Thus, in addition to the abrasion of peaks, a formation of new scratches in all grain size fractions was caused by the tumbling. There is an increase of the volume of the surface texture in the two smaller grain size fractions, and a decrease of the general surface roughness in the two larger grain size fractions. Apart from a slight polishing effect that occurs in all grain size fractions (**Fig. 3.13**), and a slightly changing roughness, volume and width of the furrows, teeth of *Equus* sp. show few signs of surface texture alteration, after a long distance (> 360 km) fluvial transport (as simulated in the 336 hrs experiment), even though the teeth exhibit macroscopic signs of strong abrasion. The least pronounced alteration was observed during tumbling with the very fine sand (51-168 µm), which caused deepening of furrows (increasing *metf*) after 362 km of transport, the surface tends to become more rough and voluminous.

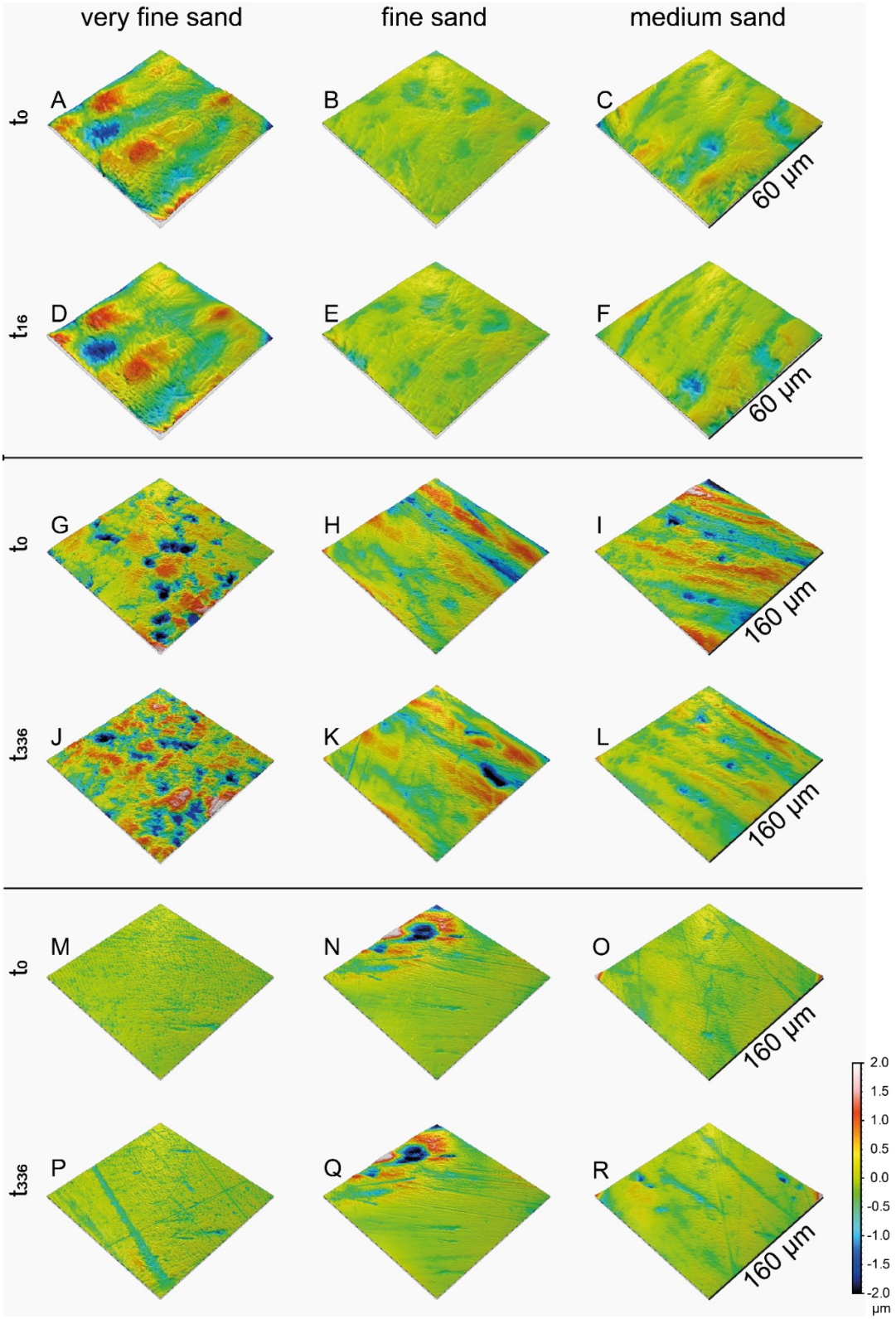

Figure 3.13. 3D simulations of surface models of single facets of *Otomys* sp. (A-F), horse (*Equus* sp.) (G-L) and roe deer (*Capreolus capreolus*) (M-R) teeth. A/D. individual K, lammela 2; B/E. individual J, lamella 2; C/F. individual L, lamella 1; G/J. upper left M2, facet 1; H/K. upper left M1, facet 3; I/L. upper left P2, facet 1; M/P. upper left M1, facet 2, N/Q. upper left M2, facet 3; O/R. upper right M1, facet 3.

Tumbling with the medium sand (221-513 µm) resulted in faster and more intense abrasion of the enamel surface, leading to a less rough and voluminous surface texture (**Fig. 3.13**).

3.5.1.3 Large mammals-Capreolus capreolus

The teeth of the *Capreolus capreolus* do not show pronounced changes of the surface textures in any of the grain size fractions used for the tumbling procedure. Compared to the *Equus* sp. samples, the very fine sand mainly produces deeper scratches on the occlusal surface, while the fine sand only abrades the surface (decreasing *meh*) (**Fig. 3.13**). In contrast to the *Equus* sp. teeth, the strongest alteration trends are observed for the very fine sand (51-168 µm). The pre-existing furrows become deeper (increasing *metf* and *madf*), resulting in a relatively increased peak- and mean height and a slightly rougher surface. There is almost no macroscopically visible alteration in the fine sand (112-292 µm), however, surface texture parameters reveal the slightly levelled towards a less high texture with mainly the peaks abraded, the surface becomes flatter.

3.5.2 Inter-specific differences in mechanical alteration

3.5.2.1 Preservation of different sized teeth

Understanding alteration and stability of surface features is crucial to infer how good the experimental setup is as a model for natural transport in a fluviatile system. Tumbling intended to mimic fluviatile transport and being performed in barrels may potentially introduce systematic errors. This is because the likelihood for a sediment particle (including a tooth) to touch the inner wall of the barrel will depend on the geometry of both, the barrel and the particle (i.e. tooth). A fluviatile system does not have these restrictions. Periodic contact with the barrel wall may introduce directionally non-random signals to scars, in particular, when the sediment filling is not turbulently mixed, but rather slides along the wall, just separated by a fluid layer. We propose this effect to be reduced with larger sediment infill amounts, when the diameter of the tumbling barrel is small as compared to the size of the tooth. The reverse should hold true, if the specimen is small in relation to the diameter of the barrel. Nevertheless, the texture signals of small mammal teeth appear particularly less sensitive to post-mortem abrasive alteration and should thus be robust in maintaining their ante-mortem signatures, although they do have the possibility to move more freely in the barrel, according to the small size of the teeth. This makes them potentially well-suited samples for environmental reconstruction even if the exact post-mortem abrasive impact is unknown.

The zebra teeth tumbled during this experiment show the strongest alteration effects. Considering the geometry of both the barrel and a zebra molar, these large cheek teeth likely overturn along their longitudinal axis, instead of being transported in a randomly oriented fashion in the sediment flow. Our experimental data is thus less well suited to infer fluviatile abrasive effects on such large mammal dental specimens. However, although the roe deer teeth treated during this experiment could potentially move more freely in the barrel than the larger zebra teeth, none of the texture parameters were strongly altered during any of the tumbling treatments. Therefore, medium-sized mammal teeth from fluvial transported fossil assemblages embedded in fine to medium grained siliciclastic sediments, may still preserve their original ante-mortem occlusal surface texture.

3.5.2.2 Alteration versus preservation of dietary signatures in large mammals

Dietary reconstruction through 3DST is usually applied on homologous tooth positions and enamel wear facets. Due to the composition of the tooth sample set for this partially destructive experiment, the teeth were not ideally suited for dietary analysis, as we compared several wear facets among different tooth positions. Nevertheless, prior to tumbling as well as after the two longest tumbling intervals, grazer and browser could still be distinguished by parameter values (**Fig. 3.10**). This supports the applicability of 3DST for dietary reconstruction in fossil species, even on isolated teeth.

Before the tumbling treatment 12 surface texture parameters resulted in excellent separation between grazers and browsers, and nine of these are texture parameters previously demonstrated by Schulz et al. (2013a) to differentiate best between the two feeding traits: *FLTp, FLTq, FLTt, Sa, Smc, Sxp, Vmc, Vv* and *Vvc*. Over a short tumbling period of 16 hrs, the textural differences between grazers and browsers, especially in these well discriminating parameters, are very stable. In contrast, over the very long tumbling interval of 336 hrs, four parameters (*FTLp, FLTt, Vv* and *Vvc*) lost their strength in discriminating those two feeding traits. Six surface texture parameters are very stable, mainly corresponding to the volume of the core, the general roughness and the flatness of the surface. Contrary, parameters corresponding to the peaks, dales and the mean height are unstable. In conclusion, isolated teeth from fossil assemblages deposited in siliciclastic sediment by fluviatile transport, with parameters simulated by our experiments, would still preserve diet-related ante-mortem occlusal textures that allow distinction between grazers and browsers. *Vvc, Sa, Smc, Sxp* and *FLTq* would be the best suited parameters in this case. However, those texture parameters characterising extreme topographic features such as peaks and dales, seem to be preferentially biased by abrasive post-mortem alteration and thus are not reliable predictors for ingesta reconstruction under these circumstances. In contrast, if only one species within a

comparative pair of two was subject to post-mortem alteration, while the other was not, flatness and volume parameters well as the surface roughness still permit distinction between grazing and browsing. Even if teeth from the same depositional setting are not taphonomically altered in the same way, grazers and browsers should still be distinguishable in their mostly unbiased texture parameters corresponding to the form and volume of the occlusal surface.

In general, it can be concluded, that discrimination of the two broad dietary categories browser and grazer can still be performed based on surface texture parameters even after a long tumbling period in siliciclastic very fine to medium sand of 336 hrs (simulating more than 360 km of transport distance in a fluviatile environment). This also applies if those teeth that are tumbled in different grain size fractions of sand. Therefore, it is not necessary to categorically exclude fluvial transported dental specimens from dietary reconstruction based on surface texture analysis and likely also other ingesta related dental wear proxies.

3.6 Conclusion

Tumbling experiments of isolated cheek teeth from large and small mammalian herbivores in siliciclastic sediment demonstrate a high degree of resistance of surface textures against physical post-mortem abrasive alteration during simulated fluvial transport in grain size fractions representing a sandy natural river sediment. The surface texture signatures as measured do not generally respond to post-mortem abrasive alteration as imposed by the tumbling procedure. Macroscopically these modified surfaces appear slightly polished, but we also found newly formed large scratches in different grain size fractions; however, these alteration features do not change the overall surface texture signature significantly. We conclude that there is a difference in the degree of post-mortem abrasive impact related both to sediment particle size and to the morphology and size of an individual dental specimen. Small teeth are less affected compared to larger sized teeth. This effect should relate to the size relation between teeth and sediment grains, where small teeth obviously incur fewer new scratches, if individual grains are at the same size fraction as occlusal enamel structures under study, as indicated by our *Otomys* sample. The larger occlusal facets of the roe deer were most visibly altered in the very fine sand fraction of 51-168 µm, while the zebra samples suffered post-mortem alteration mainly by the coarser grain size fraction of medium sand 221-513 µm grain size fraction. Signs of physical alteration were mainly detected in peak and furrow parameters. No single surface texture parameter could be identified, which can be used as an unambiguous indicator for taphonomic alteration of ante-mortem enamel wear texture. Parameters describing the volume, flatness and roughness of the wear surface only showed slight shifts. These parameters enable us to discriminate between the two feeding categories, even when isolated teeth of grazers and browsers transported in the same sediment.

Therefore, tooth samples need not to be discarded from microtexture analyses even if they are slightly abraded or if the reference tooth position and facet are not preserved, they can still be used for dietary reconstruction, at least to resolve the browser-grazer dichotomy.

3.7 Acknowledgments

The research was funded by the European Research Council (ERC) under the European Union's Horizon 2020 research and innovation programme (ERC CoG grant agreement No 681450) to TT and the Max-Planck Graduate Center. We thank the Center of Natural History (CeNak) and Dr. Irina Ruf (Senckenberg Museum, Frankfurt) for the dental material. We thank Ralf Meffert and Dr. Tobias Häger (Johannes Gutenberg-University Mainz) for the X-ray diffraction-analysis and Prof. Dr. Frank Lehmkuhl (RWTH Aachen University) for the particle size analysis. We would also like to express our gratitude to Dr. Jennifer Leichliter (Johannes Gutenberg-University) for proofreading the manuscript. We further acknowledge the two anonymous reviewers for their helpful comments that greatly helped to improve the manuscript.

3.8 Supplements

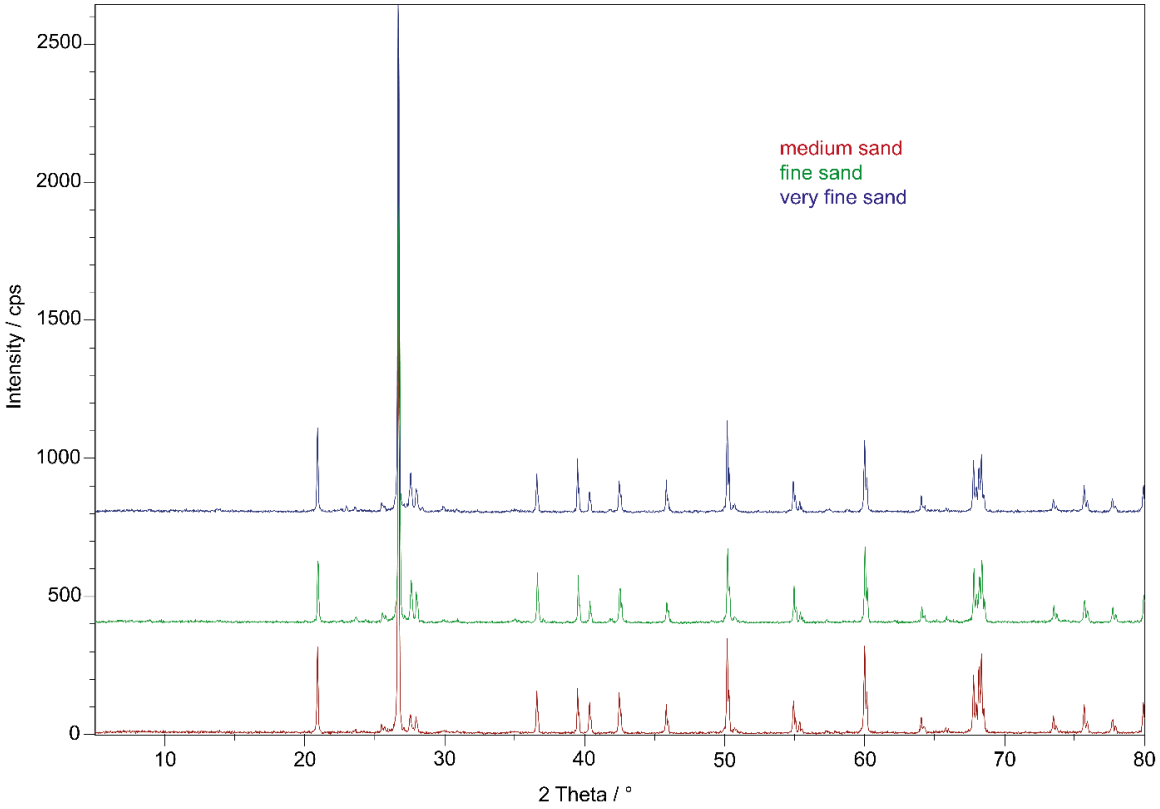

Figure S3.1. X-ray diffraction-analysis of the three different grain size fractions used for the tumbling.

Table ES3.1. Nine-time repetition of the same scan for one original and one moulded sample to test for imprecision in misalignment of repeated sampling. The table is found in the electronic Supplement.

Table ES3.2. Descriptive statistics for Dataset 1 separated after sediment grain size fraction. The table is found in the electronic Supplement.

Table ES3.3. Descriptive statistics for Dataset 2 with all nine teeth per taxon pooled together. The table is found in the electronic Supplement.

Table ES3.4. Trends calculated by the quotient of tumbling time zero (t_0) and the maximum tumbling time (t_{max}) (16 hours for *Otomys* sp., 336 hours for *Equus* sp and *C. capreolus*). The table is found in the electronic Supplement.

Chapter 4 Manuscript II: Post-mortem enamel surface texture alteration during taphonomic processes – do experimental approaches reflect natural phenomena?

Post-mortem enamel surface texture alteration during taphonomic processes – do experimental approaches reflect natural phenomena?

Katrin Weber [1], Daniela E. Winkler [1,2,3], Ellen Schulz-Kornas [2,4,5], Thomas M. Kaiser [2], Thomas Tütken[1]

[1]Applied and Analytical Palaeontology, Institute of Geosciences, Johannes Gutenberg University, Mainz, Germany

[2]Center of Natural History (CeNak), University of Hamburg, Hamburg, Germany

[3]Department of Natural Environmental Studies, Graduate School of Frontier Sciences, The University of Tokyo, Tokyo, Japan

[4]Department of Cariology, Endodontology and Periodontology, University of Leipzig, Leipzig, Germany

[5]Department of Human Evolution, Max Planck Institute for Evolutionary Anthropology, Leipzig, Germany

This manuscript is submitted to *PeerJ.*

4.1 Abstract

Experimental approaches are often used to better understand the mechanisms behind and consequences of post-mortem alteration on proxies for diet reconstruction. Dental microwear texture analysis (DMTA) is such a dietary proxy using dental wear features in extant and extinct taxa to reconstruct feeding behaviour and mechanical food properties. In fossil specimens especially, DMTA can be biased by post-mortem alteration caused by mechanical or chemical alteration of the enamel surface. Here we performed three different dental surface alteration experiments to simulate common taphonomic processes: 1) tumbling in sediment suspension to simulate fluvial transport, 2) sandblasting to simulate mechanical erosion due to aeolian sediment transport, 3) acid etching to simulate chemical dissolution by stomach acid. For tumbling (1) we found alteration to be mainly dependent on sediment grain size fraction and that specimens tumbled with a fine-gravel fraction resembles those of fossil horse teeth of *Hippotherium primigenium* deposited in similar sized sediments of the Dinotheriensande, Germany. Sandblasting (2) with loess caused only negligible alteration however, blasting with fine sand quartz particles resulted in significant destruction of enamel surfaces. Acid etching (3) using diluted HCl in concentrations similar to that of predator stomachs led to a complete etching of the whole dental surface which did not resemble those of teeth from owl pellets. These experimental settings resulted in post-mortem alteration similar, but not identical to post-mortem alteration features occurring during natural taphonomic processes. Nevertheless, this study serves as a first assessment and step towards further, refined taphonomic experiments evaluating post-mortem alteration of DMT.

4.2 Introduction

Dental microwear texture analysis (DMTA) is a common and well-established proxy for reconstructing diet and food properties in extant and extinct vertebrates (Scott et al., 2005; Merceron et al., 2007; Ungar et al., 2003, 2007, 2008, 2020; Scott et al., 2009; Schulz et al., 2010; Winkler et al., 2013, 2016). It has been successfully applied to terrestrial large and small mammals (Ungar et al., 2003; Merceron and Madelaine, 2006; Merceron et al., 2007; Scott et al., 2009; Schulz et al., 2010, 2013b, 2019; Calandra et al., 2012; Purnell et al., 2013; Winkler et al., 2016; Kubo et al., 2017), including (semi-)aquatic mammals (Purnell et al., 2017; Bethune et al., 2019), but also non-mammalian taxa like lepidosaurs (Bestwick et al., 2019; Winkler et al., 2019a), mammal-like reptiles (Kalthoff et al., 2019), and fish (Purnell et al., 2016). Microwear and microwear texture are shown to be powerful proxies for oral behaviour and ingesta-intake in general; however, they can be biased by post-mortem surface alteration resulting in material loss (King et al., 1999; Dauphin et al., 2018). In fossil sample sets, it is often the case that a high number of specimens have to be excluded from analyses, since they

show potential post-mortem alteration, which reduces the sample drastically (Ungar et al., 2008). Chemical or mechanical alteration can be caused by transport, burial and/or different fossilisation processes and the impact of such post-mortem alteration has not been sufficiently explored. Only a few studies have dealt with post-mortem alteration under natural conditions (Dauphin et al., 2003, 2018; Martínez and Pérez-Pérez, 2004) or in different experimental approaches (e.g. Gordon, 1983, 1984; King et al., 1999; Böhm et al., 2019; Kropacheva et al., 2019). However, it is unknown how well natural alteration processes can be simulated and how comparable experimentally induced post-mortem wear alteration is to naturally induced alteration. Here we performed three dental microwear texture (DMT) alteration experiments to recreate three different mechanical and chemical natural taphonomic processes:

I. Fluvial transport in a sediment suspension (tumbling).
II. Aeolian erosion by windblown mineral dust (sandblasting).
III. Stomach digestion erosion in an acidic environment (acid etching).

Fluvial transport (I) of vertebrate fossil remains is a very common post-mortem alteration process in terrestrial depositional settings. It can occur in permanent as well as ephemeral river systems, e.g. in arid settings with heavy rainfall or intense snowmelt events (Milner, 1987; Astin et al., 2010; Cressler et al., 2010; Bennett et al., 2016; Beylich and Gintz, 2016). In high-energy environments and during long fluvial transport processes, water, together with transported sediment, has a strong abrasion effect on objects, e.g. as seen in its rounding effect on sand, stones or bones (Domokos et al., 2014). This type of mechanical post-mortem alteration process modifies skeletal remains of aquatic as well as terrestrial vertebrates transported in fluvial systems as well as reworked fossil specimens. To experimentally simulate fluvial transport, we performed a tumbling experiment with rotary tumblers filled with tap water and siliciclastic sediment of different grain size fractions (fine to medium sand, 63–500 µm; fine gravel, 2–8 mm).

Sandblasting (II) was used to simulate the mechanical effects of aeolian sediment transport. This type of alteration is encountered in fossil or modern vertebrate remains exposed to weathering in arid or desert systems. In such settings vertebrates remains decompose and disarticulate on the sediment surface and face intermittent sandblasting prior to burial. It is not well known if, and how exactly, this “sandblasting” affects the dental surface. Therefore, we performed a sandblasting experiment with loess and fine sand to assess how different grain size fractions of siliciclastic mineral particles alter dental microwear textures. Loess is a widespread silt-sized aeolian sediment that is often deposited during glacial periods (Wright,

2001). The quartz fine sand used in this study is at the upper end of the typical sediment fraction which can be carried by suspension in dust storms (Squires, 2001).

Finally, we performed an acid etching experiment (III). This type of chemical alteration was chosen because it frequently occurs in remains of small mammals and other vertebrates, which are preyed on by raptorial birds, which then regurgitate bones and teeth in pellets. Small vertebrates are common fossils found in coprolites or e.g. owl pellets and they could potentially be affected by the strong stomach acid of the predator. Carnivorous and necrophagous birds, like grey falcon, the bald eagle, vultures and different owl species, have stomach pH-values of ≈ 1.0 – 1.8, while carnivorous mammals have higher pH values, depending on the species (e.g. cat: 3.6, dog: 4.5; Houston and Cooper, 1975; Beasley et al., 2015). Faunivorous sharks (Papastamatiou et al., 2007) and reptiles, such as crocodiles (Pooley and Gans, 1976) and snakes, have low stomach pH-values of around 2, at least during digestion (e.g. *Python molurus,* Secor, 2003). Thus, for the acid-etching experiment, we immersed different vertebrate teeth in specific concentrations of hydrochloric acid matching the chemical (i.e. pH) conditions of typical predator stomach environments.

For the first time, extensive alteration experiments of dental surface texture with teeth from different modern taxa, two large mammals, one small mammal, one fish and one reptile species were performed to cover three key mechanical and chemical post-mortem alteration processes. We intend to address the following two research questions in this study:

I. Is it possible to experimentally reproduce post-mortem wear features similar to those observed on fossil tooth samples altered by natural processes?

II. Are single surface texture parameters or sets of parameters suitable to detect post-mortem alteration?

For this purpose, we applied scale-sensitive fractal analysis (SSFA, e.g. Ungar et al., 2003, 2012; Scott et al., 2006; Scott, 2012) and 3D surface texture analysis (3DST, Schulz et al., 2010, 2013a, 2013b; Purnell and Darras, 2016; Kubo et al., 2017; Purnell et al., 2017; Winkler et al., 2019a), two different DMTA techniques that evaluate 3D representations of the enamel surface at submicron resolution. For addressing the first research question, we measured the experimentally altered dental surface before and after each experiment and compared the resulting surfaces with those of fossil and extant specimens that potentially underwent comparable natural alteration processes. For addressing the second research question, we applied pairwise comparison of the experimentally altered dental surface before

and after the experiment and used principal component analysis (PCA) for evaluation of textural changes.

4.3 Material and methods

4.3.1 Experimental design

4.3.1.1 Tumbling experiment

This dataset includes dental surface measurements of modern cheek teeth from three different large and small mammals (zebra (*Equus* sp.), roe deer (*Capreolus capreolus*) and African vlei rats (*Otomys* sp.)), one archosaur (Nile crocodile, *Crocodilus niloticus*) and a cartilaginous fish (sandbar shark, *Carcharhinus plumbeus*) which were tumbled in commercial hobby rotary tumblers TYP TRO 2 A (Otto Eigner e.K., Industriebedarf & Hobbyschleifmaschinen, Idar-Oberstein, Germany) at University Mainz. Similar to Böhm et al. (2019), two different siliciclastic sediments, a quartz-dominate (~60 %) sand and a fine to medium grained gravel, were sieved into four different grain size fractions for tumbling (Table S5.1): very fine sand (51–168 µm), fine sand (112–292 µm) and medium sand (221–513 µm), and fine to medium-grained gravel (2–8 mm, **Table S4.1**). A single isolated tooth was tumbled in each specific grain size fraction. Experimental tumbling barrels were filled with a mixture of 300 g of sediment and 500 g of tap water. Each tooth was tumbled for 336 hours and surface texture scans were measured on the same, marked area of the tooth enamel surface both before and after the experiment. The duration of 336 hours of tumbling was chosen to simulate an extreme case of constant water-sediment-tooth movement in a fluvial system. Two weeks of experimental tumbling represent a fluvial transport distance of ca. 363 km, using the size of the barrels and the speed of the rotation for calculation of the distance. It has previously been observed that even 10 km of fluvial transport in a tropical montane system reduced the mass of volcaniclastic pebbles to two thirds of their original mass and resulted in an exponential decline in pebble diameter (Miller et al., 2014), thus our calculated transport distance of 363 km represents an extreme case of fluvial transport.

In our experiment, one specimen of roe deer (tx right M3, **Table ES4.2**) was moulded using high-resolution silicone-Vinylpolysiloxane precision impression material Provil novo Light regular set EN ISO 4823, type 3, light (Heraeus Kulzer GmbH, Dormagen, Germany), all other specimens were measured directly on the original dental surface. The occlusal surface of this specimen was to oblique to be measured directly on the original dental surface. Scans on original and moulded dental surface are considered to have similar quality and contain the same information on wear features (Mihlbachler et al., 2019). Sample preparation of mammalian teeth is described in detail in Böhm et al. (2019). To ensure measurement of the

same enamel surface areas after the tumbling experiment, mammalian teeth were marked with cutmarks on enamel bands while crocodile and shark teeth were marked with a small drill hole on the centre of the dental surface. The dental surface was optically aligned to the reference cutmark/drill hole and measured at the same relative coordinates as in the previous measurements. Four non-overlapping scans were taken of all experimentally altered teeth (for details see Supplement **Table ES4.2**).

In comparison to this experimentally altered set of dental surfaces, we also analysed cheek teeth of the fossil horse *Hippotherium primigenium* from the Dinotheriensande, Eppelsheim, Germany. The Dinotheriensande are Late Miocene (~ 10.5 Ma) fluviatile deposits of the ancient Rhine river (Steininger et al., 1996; Andrews and Bernor, 1999). Mammalian fossils in this locality are almost entirely restricted to a siliciclastic, sand- and gravel-dominated horizon close to the base of the sedimentary sequence (Tobien, 1983). The similarity in grain size spectrum of these deposits containing fluvially transported isolated teeth makes them suitable for comparison with our experimentally altered large mammal teeth.

4.3.1.2 Sandblasting experiment

A single fossil tooth of *Mammuthus* sp. from Pleistocene Rhine river deposits was cut several times parallel to the occlusal surface to produce several slices comprised of multiple enamel and dentine bands. The slices were polished using silicon carbide (SiC) of different grain size fractions down to 6.5 µm, to produce large, smooth enamel surfaces where new wear features could easily been identified. These polished enamel surfaces were then sandblasted with two different natural sediments: Late Pleistocene airborne loess (Schwalbenberg outcrop, Remagen, Germany) and Oligocene fluvial fine sand (Feinsand 12c, Dörentrup Quarzwerke, Germany). The silt-sized loess was sieved through a 300 µm mesh and had a mean grain size of 36.87 µm (range: 6.3 to 200 µm, data from laser diffraction size analysis, Table S5.1), with quartz (37.3 wt.-%), calcite (15.7 wt.-%), illite and mica (13.8 wt.-%), plagioclase (9.8 wt.-%), and dolomite (5.4 wt.-%) as main mineral phases. The fine sand 12c had a mean grain size of 166.01 µm (range: 63 to 630 µm, data from laser diffraction size analysis, **Table S4.1**) and was composed of nearly pure quartz (99.5 wt.-%). Four non-overlapping scans were measured on three different enamel bands before and after sandblasting with each of the two sediment types. A sandblasting machine (Renfert, basic quattro IS, Hilzingen, Germany) was used to blast the mineral dust vertically onto the sample from a distance of 30 cm and with a pressure of 3.5 bar for 7 seconds for the fine sand and additionally up to 14 sec for the loess. These experimental conditions were chosen for practical reasons, 3.5 bar is the lowest pressure possible for the sandblaster and a seven-second interval is the shortest human reaction time we could set for turning the sandblaster on and off.

The pressure of 3.5 bar represents an approximate wind speed of 100 m/s when the particles hit the dental surface, which is about 3 to 4 times higher than gusts of wind in very strong naturally occurring dust-storms (e.g. up to 30 m/s measured in Chinese dust-storms, Gengsheng et al., 2001). For comparison, naturally “sandblasted” (i.e. eroded by windblown sand) fossil antelope teeth from the Late Miocene Toros-Menalla fossiliferous area in Chad, approximate 500 km NE of the present-day Lake Chad, were analysed. The fossil-bearing siliciclastic sediments consist of clay and sandstone (Lebatard et al., 2008) with a sediment grain size comparable to that of the fine sand used in our experiment. The majority of present-day wind-speeds for dust-storms in the Chad are 2 to 6 m/s (Cowie et al., 2014). All specimens were measured on the original dental material.

4.3.1.3 Acid etching experiment

After being tumbled for 336 hours in the finest sand fraction, teeth of *Otomys* sp., *Crocodilus niloticus* and *Carcharhinus plumbeus* were *in-vitro* exposed to acid etching simulating pH and temperature conditions experienced in stomach acid of the gastro-intestinal tract of different predators (**Table 4.1 and ES4.2**). The samples were chosen for practical reasons, as they were easily available, and the post-tumbling surface could be re-used representing the pre-etching surface. *Otomys* teeth were kept in trace-metal grade 0.1 mol/L hydrochloric acid of pH ~ 1.3 for 12 hours at a temperature of 45 °C to simulate the stomach conditions of a barn owl prior to the regurgitation of bone and tooth material in the form of pellets (Grémillet and Plös, 1993; Beasley et al., 2015). Crocodile teeth were kept under crocodile stomach conditions, while shark teeth were kept under simulated shark stomach conditions, to simulate stomach conditions of carnivore reptile and predatory fish (**Table 4.1**). These large predators frequently replace their teeth, and potentially swallow some of them. Fossil shark and crocodile teeth may therefore have passed through their respective stomachs. For both crocodile and shark teeth, we used 0.05 mol/L hydrochloric acid (pH ~2) at 25 °C for 48 and 72 hours to simulate passage times through the gastrointestinal tract of each respective taxon (Pooley and Gans, 1976; Hutton, 1987; Papastamatiou et al., 2007, **Table 4.1**). A mixing ratio of 10 ml acid to 1 g dental material was applied, and the acid was renewed after 24 hours to ensure persistence of a low pH.

After the experiment, all teeth were thoroughly rinsed with Milli-Q water (18.2 MΩ) and dried at room temperature. Two different sets of modern *Otomys* teeth from the Cradle of Humankind World Heritage Site, South Africa (collected in 2017) were used as natural reference samples for comparison to those from the acid etching experiment. The first sample set (*Otomys* sp.) of teeth was extracted from barn owl pellets and serves as a direct comparison to the African vlei rat teeth from the etching experiment. The second sample set

of teeth (*Otomys irroratus*) was extracted from skulls of live-trapped animals and provides the natural baseline for non-altered, ingesta-related dental surface textures from the same geographic setting and species. For all specimens DMTA were performed on the original dental material.

Table 4.1. Taxon, number of teeth, pH-value, temperature, and etching interval for the stomach acid alteration experiment. [1] Beasley et al., 2015; [2] Papastamatiou et al., 2007; [3] Pooley and Gans, 1976; [4] Grémillet and Plös, 1993; [5] Hutton, 1987.

Taxon	Number of teeth	pH value	Temperature [°C]	Etching interval [hrs]
Otomys sp.	3	1.3 [1]	42 [4]	12 [4]
Carcharhinus plumbeus	3	2 [2]	25 [2]	48 [2]
Crocodilus niloticus	3	2 [3]	25 [5]	72 [3]
Otomys sp.	8			Barn owl pellet
Otomys irroratus	8			None (live-trapped)

4.3.2 Dental microwear texture analysis

All samples were cleaned prior to moulding or scanning using water to remove adherent dirt, ethanol, and acetone to remove lipids and varnishes or glue from the dental surface. Surfaces were scanned using the high-resolution disc-scanning confocal 3D-surface measuring system μsurf Custom (NanoFocus AG, Oberhausen, Germany) with a blue LED (470 nm) and high-speed progressive-scan digital camera (984 × 984 pixel). Per sample, four non overlapping square areas of 160 × 160 μm were scanned using a x100 long distance lens (numerical aperture 0.8) with a resolution in x, y = 0.16 μm, and z = 0.06 μm. Measurements with an oblique orientation too significant for measurement were rejected (displacement range $\delta z > 60$ μm). Following Böhm et al. (2019) for the experimental settings, a rotation along x-, y- and z-axis of the teeth between individual measurements of 5-10° was accepted. We used 3D (enamel) surface texture analysis (see Schulz et al., 2010, 2013a, 2013b; Calandra et al., 2012) and scale-sensitive fractal analysis (SSFA) with parameters after Ungar et al. (2003) and Scott et al. (2006), implemented in MountainsMap Premium v. 7.4.8676. We used three customized templates in MountainsMap Premium v.7.4.8676 software to generate an S-L surface (noise, waviness, and form removed; for more details see Schulz et al., 2013a). A detailed description of the templates including the pre-processing procedures are given in the supplements. Subsequently a set of 46 surface texture parameters were quantified on the S-L surface using the following analyses: (1) the ISO 25178, (2) motif, (3) furrow, (4) direction, (5) isotropy, and (6) ISO 12871 (flatness) analysis (**Table S4.3**).

4.3.3 Statistics

The open-source software R v.4.0.0 (R. Development Core Team, 2020) with the packages xlsx (Dragulescu, 2014), rJava (Urbanek, 2016), doBy (Højsgaard and Halekoh, 2016), R.utils (Bengtsson, 2016), factoextra (Kassambara, 2017), plyr (Wickham, 2011), ggplot2 (Wickham, 2016), Rcpp (Eddelbuettel, 2011, 2013), rela (Chajewski, 2009) and WRS version 0.12.1 (Wilcox and Schönbrodt, 2010) was used for data processing and all statistical analyses. A median for each tooth was calculated from four measured scans. From this median, a mean was calculated for all experimental datasets for t_0 (before each experiment as a baseline) and t_i (after each experiment) (**Table ES4.4 – ES4.6**). In general, we employed pair-wise comparisons for the following datasets:

I. Pairwise comparison for dependent data of pre- and post-tumbling surfaces in all four grain size fractions, five species in the tumbling experiment (**Table S4.7**).

II. Pairwise comparison dependent data of pre- and post-sandblasted surfaces in the two grain size fractions used in the sandblasting experiment (**Table S4.7**).

III. Pairwise comparison dependent data of pre- and post-etching surfaces in all three species in the acid etching experiment (**Table S4.7**).

IV. Pairwise comparison of independent data from trapped animals (*Otomys irroratus*), *Otomys* sp. extracted from owl pellets and experimentally altered *Otomys* teeth before and after acid etching (**Table ES4.2 and ES4.8**).

For pair-wise comparison of dependent data the Wilcoxon signed rank test with continuity correction was employed (Wilcoxon, 1945). Pairwise comparison of independent data was subjected to the statistical test after Calandra et al. (2012) and Schulz et al. (2013a). We applied the robust heteroscedastic Welch-Yuen omnibus test (Welch, 1938; Yuen, 1974) coupled with a heteroscedastic pairwise comparison test (“Lincon test”, analogous to Dunnett's T3 test (Dunnett, 1980)), according to the procedure of Wilcox (Wilcox, 2003, 2005, 2012). We performed a data trimming of 15 % to remove outliers and compensate for non-normality. Finally, we applied the robust heteroscedastic rank-based test according to Cliff (Cliff, 1996; Schulz et al., 2013a). Before applying principal component analyses, we use the Kaiser-Meyer-Olkin test for sampling adequacy (value>0.5) and Bartlett’s test of sphericity (<0.05) to validate the application of a principal component analysis (PCA) is justified on our data. PCAs were conducted using the built-in function prcomp(). All principal components (PCs) with standard deviation of over 1.0 are considered in the result section. For factor loadings, we choose a cut-

off value of 0.4 (Budaev, 2010), describing the best separating parameters in the different PCs (**Table ES4.9**).

4.4 Results

4.4.1 Tumbling experiment

4.4.1.1 Very fine sand (51–168 µm)

Exemplary scans of experimentally altered dental surfaces are shown in Figure 4.1. The Wilcoxon signed rank test displays significant differences between dental surface before and after the tumbling experiment for *Capreolus capreolus*, *Crocodilus niloticus*, *Carcharhinus plumbeus* and *Otomys* sp., while *Equus* sp. did not show significant surface modifications (**Table S4.7**). Experimental alteration of teeth with very fine sand lead to a higher number of new wear features, such as new scratches and dales (larger anisotropy values of parameters, except for *Otomys*, **Fig. S4.1A and S4.2A**). This coincided with an increase in overall complexity of the surface (larger *Sdr*, *Asfc* values, except for *Otomys*) and an increase in height and volume parameters for the large mammal teeth (*Equus* and *Capreolus*). PCA displayed separation of dental surface before and after tumbling for all five different species along PC1 – PC3 (**Fig. 4.2A and S4.3A**), whereby the isotropy (*IsT*), complexity (*Asfc*), area (*mea*), density (*Spd*) and plateau size (*Smr*) are the best separating parameters (**Table ES4.9**).

4.4.1.2 Fine sand (112–292 µm)

Tumbling the teeth of the five different species with the fine sand resulted in only minor modifications on the dental surface (**Fig. 4.1**), only *Capreolus capreolus* (**Fig. 4.1**) showed significant changes in the Wilcoxon rank test. Quantitative analyses of the surface texture parameter values of teeth tumbled in this grain size fraction indicated only slight changes in the direction of the wear features (texture direction) with changing complexity and fewer peaks and furrows (**Table ES4.2 and S4.3**). The biplot of *metf* vs *medf* displayed a strong separation for *Equus* sp. and slight separation of *Charcharhinus plumbeus*, *Capreolus capreolus* and *Crocodilus niloticus* with a decreasing density of the furrows (*medf*, **Fig. S4.2B**). *Asfc* showed a slight increase of parameter values for *Charcharhinus plumbeus* and *Otomys* sp., while it decreased for *Equus* sp. (**Fig. S4.1B**). The PCA showed no separation of dental surfaces before and after tumbling, except for *Equus* sp. along PC1 and PC2 (**Fig. 4.2B and S4.3B**) and for *Charcharhinus plumbeus* along PC3 (**Fig. S4.3B**). In this grain size fraction, the best separating parameters of the PCA are isotropy (*IsT*), complexity (*nMotif*) and peak curvature (*Spc)* (**Table ES4.9**).

4.4.1.3 Medium sand (221–513 µm)

Similar to the tumbling with the fine sand, tumbling with medium sand resulted mostly in slight surface modifications, only *Otomys* sp. and *Crocodilus niloticus* showed significant surface changes according to the Wilcoxon rank test (**Table ES4.7**). The biplot of *metf* vs *medf* provided good separation for all species, expect for *Otomys* sp., which showed decreasing depth of furrows (**Fig. S4.2C**). The biplot of *Asfc* vs *epLsar* displayed a strong separation only for *Equus* sp. with decreasing complexity (**Fig. S4.1C**). PCA showed a strong separation in PC2 and PC3 (**Fig. 4.2C and S4.3C**) for all specimens expect *Otomys* sp.. The best separating parameters in this PCA are the volume (*Vm*), peak curvature and peak density (*Spc* and *Spd*), complexity (*nMotif*), mean area (*mea*) as well as the isotropy (*IsT*).

4.4.1.4 Fine to medium-grained gravel (2–8 mm)

Tumbling with 2-8 mm-sized gravel lead to major changes in surface texture patterns and resulted in a complete overwriting of the dental surface. More new small dales (**Fig. 4.1**) and very similar texture features on dental surfaces between different species become apparent after the experiment, which indicates significant post-mortem abrasion. Both the complexity (*Asfc*, **Fig. S4.1D**) and the isotropy of the dental surface increased in all specimens (**Table S4.3**). Parameters describing the height, plateau size, slope, and volume showed different trends in the teeth of different species. The specimens tumbled with gravel had a high mean density of furrows with a low depth, plotting as a data cloud in the biplot of *medf* – mean density of furrows vs. *metf* – mean depth of furrows parameter space (**Fig. S4.2D**). The surface texture parameter values for all five species experimentally altered using gravel, displayed a huge overlap with the parameter space of the fluvial transported fossil *Hippotherium primigenium* teeth from the Dinotheriensande (**Fig. S4.2D**). However, the Wilcoxon signed rank test indicated significant changes of the dental surface only for the *Equus* sp., *Crocodilus niloticus* and *Otomys* sp. (**Table S4.7**).

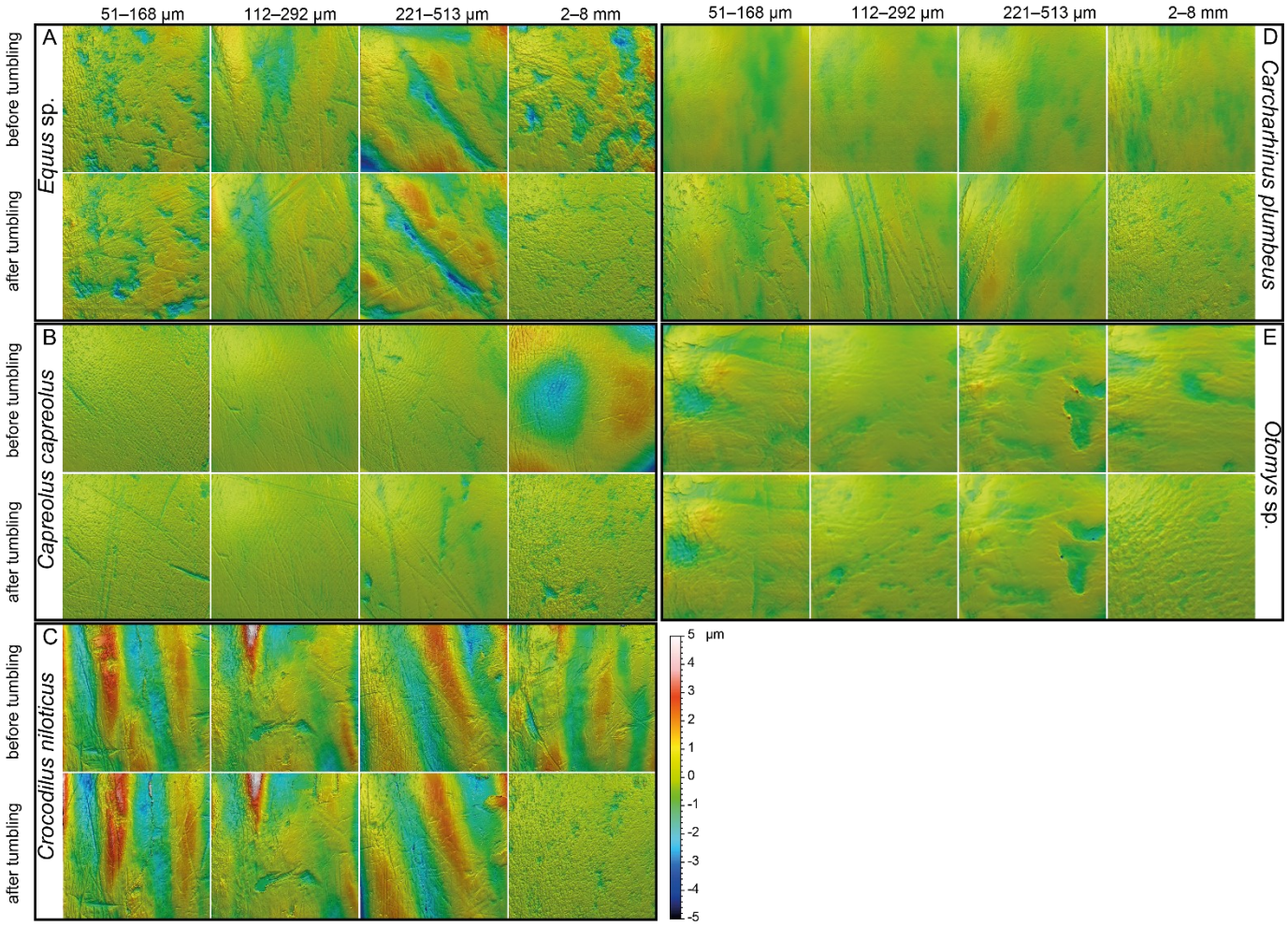

Figure 4.1. Meshed axiomatic 3D models of enamel surfaces (160 x 160 µm, if not specified otherwise) of the 3D models represent experimentally altered teeth before tumbling (left column) and after tumbling for 336 hours (column 2-5) with four different grain size fractions: very fine sand (51–168 µm), fine sand (112–292 µm), medium sand (221–513 µm) and fine to medium gravel (2–8 mm). A. zebra: *Equus* sp.; B. roe deer: *Capreolus capreolus*; C. crocodile: *Crocodilus niloticus*, and D. shark: *Carcharhinus plumbeus*; E. African vlei rat: *Otomys* sp., scan size 60 x 60 µm.

PCA revealed a strong separation of dental surface before and after the tumbling along PC1 for *Capreolus capreolus*, *Crocodilus niloticus*, *Carcharhinus plumbeus* and *Otomys* sp. (**Fig. 4.2D**), along PC2 for *Capreolus capreolus*, *Carcharhinus plumbeus* and *Otomys* sp. (**Fig 4.2D and S4.3D**) as well as along PC3 for *Crocodilus niloticus* (**Fig. S4.3D**). The best separating parameters in the PCA are the peak curvature (*Spc*), complexity (*Asfc*) and isotropy (*IsT*).

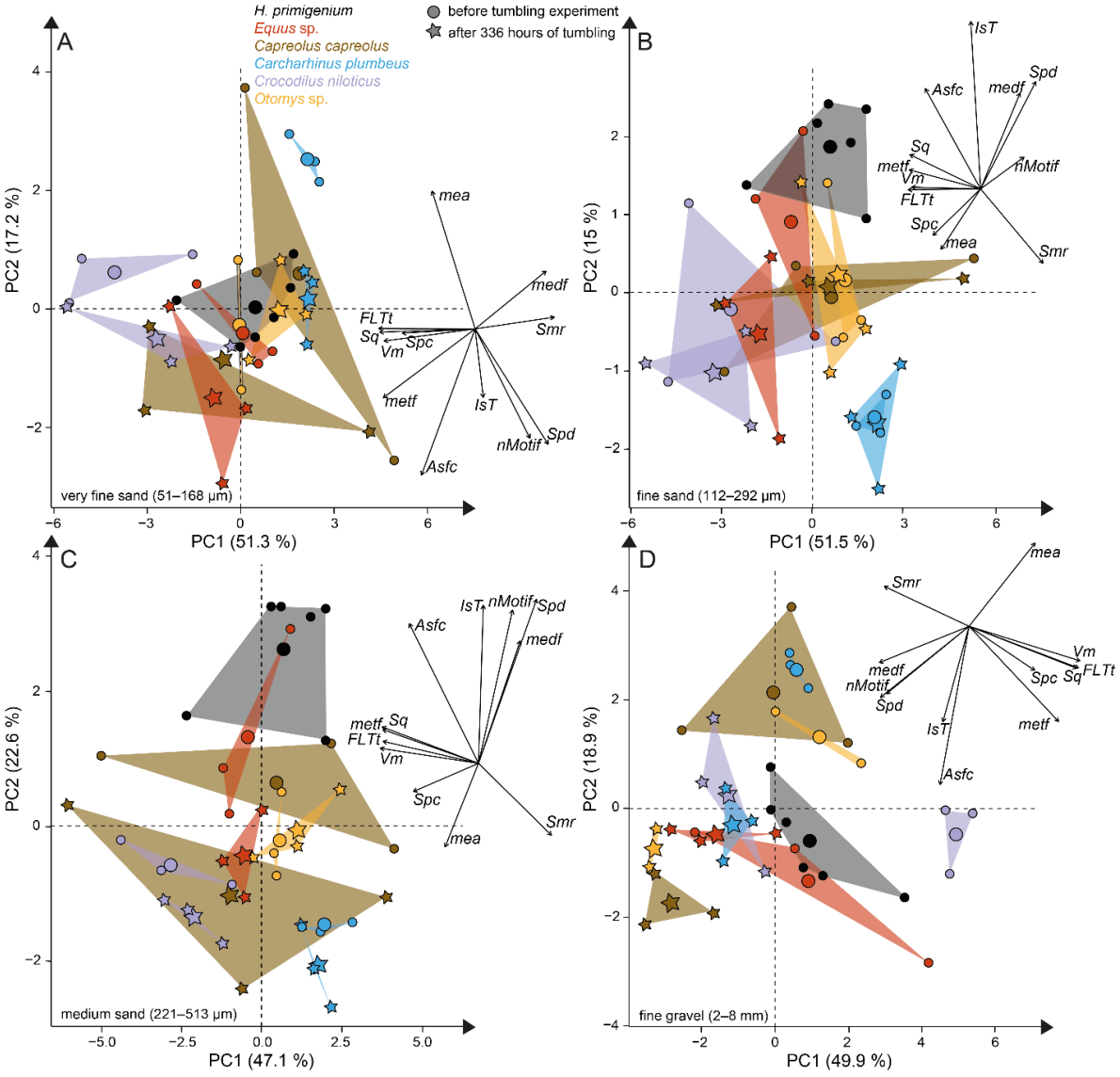

Figure 4.2. PCA results of the tumbling experiment. Principle component analysis (PCA) of surface texture parameters from each category (Table S5.3) with good separation between ante- and post-tumbling dental surfaces. Large symbols in the PCA plot mark the mean area of the different groups; for details about the taxa see Table S5.2. A. very fine sand (51–168 µm, B. fine sand (112–292 µm), C. medium sand (221–513 µm) and D. fine to medium gravel (2–8 mm).

4.4.2 Sandblasting experiment

Sandblasting the *Mammuthus* sp. polished surface with loess did not change the surface texture pattern significantly; at least not after 14 seconds of blasting time (**Fig. 4.3A and 4.4; Table ES4.4 and S4.7**). The impact of the fine sand 12c however, was very prominent, and resulted in a significant difference between dental surface before and after sandblasting with numerous new large dales formed on the surface of the section (**Fig. 4.3B and 4.4, Table S4.7**).

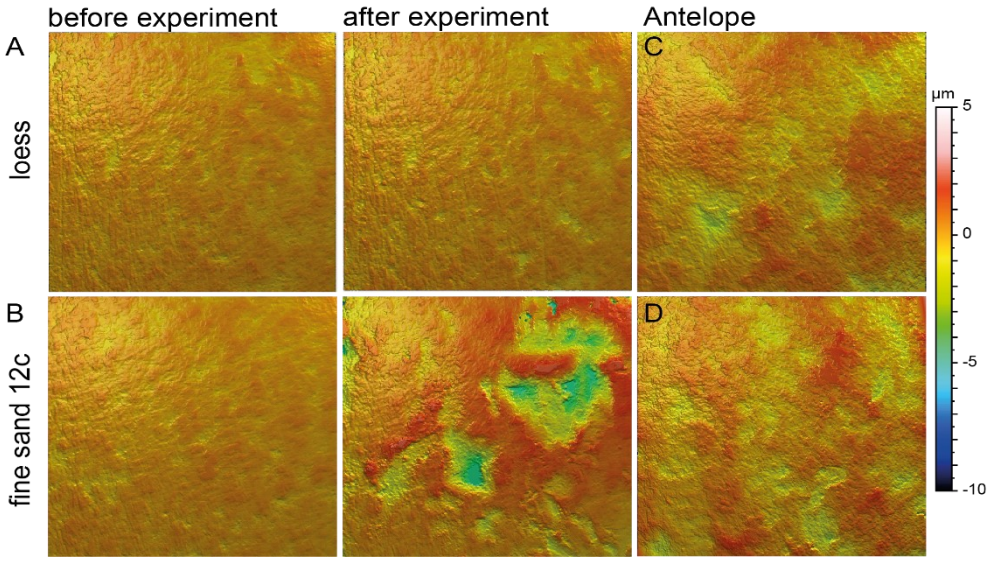

Figure 4.3. Meshed axiomatic 3D models of enamel surfaces (160 x 160 µm) of the experimentally sandblasted teeth of the same area of tooth specimens before (left) and after (right) alteration. A. *Mammuthus* sp. before and after being sandblasted with loess for seven seconds; B. *Mammuthus* sp. before and after being sandblasted with fine sand 12c for seven seconds; C. and D. Miocene antelope tooth from Chad (Lake Chad) as natural example of a fossil tooth that was exposed to windblown mineral dust (comparable to fine sand 12c in particle size) in comparison to tooth surfaces from the sandblasting experiment.

The biplot of *medf* – mean density of furrows vs. *metf* – mean depth of furrows displayed strong separation of surface parameter values before and after the experiment with strongly increasing depth of the furrows (**Fig. 4.4A**). The biplot *Asfc* vs. *epLsar* also showed this strong separation for sandblasting with fine sand, with strongly increasing fractal complexity (*Asfc*, **Fig. 4.4B**). PCA revealed strong separation of dental surface before and after the sandblasting only along PC1 (**Fig. 4.4C**), with volume (*Vm*) and depth of the furrows (*metf*) as best separating parameters. Additionally, we compared the experimentally sandblasted mammoth dental surfaces with naturally “sandblasted” fossil antelope teeth from the Late Miocene Toros-Menalla, Chad. The dental surface of the fossil specimens shows elevated height and volume

parameters. The biplots of *medf* vs. *metf* show high *medf* values, while *metf* is similar to the ones of the mammoth dental surface before and after sandblasting with loess (**Fig. 4.4A**). The PCA reveals a strong separation along PC1 and PC2 from the experimentally altered mammoth teeth (**Fig. 4.4C**).

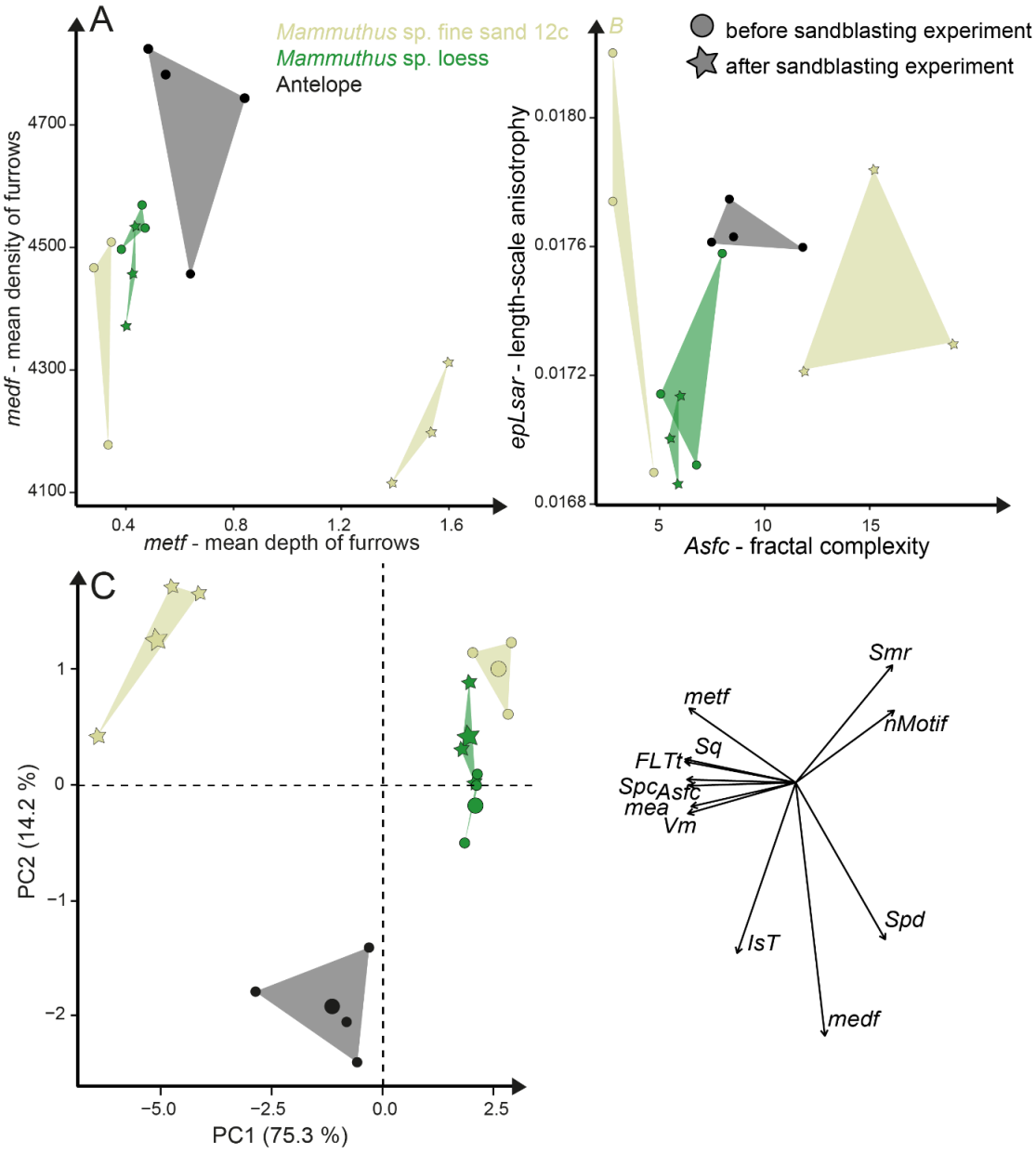

Figure 4.4. Results of the sandblasting experiment. Dental microwear texture parameter A. *metf* (µm) vs *medf* (cm/cm²) values and B. *Asfc* vs. *epLsar* for the experimentally altered mammoth teeth before (circles) and after (stars) the sandblasting experiment. C. Principle component analysis (PCA) of surface texture parameters that best separate surfaces before and after experiment. Large symbols in PCA plot mark the mean area of the different sample sets.

4.4.3 Acid etching experiment

The acid etching experiment was performed with three different species, *Otomys* sp., *Crocodilus niloticus* and *Carcharhinus plumbeus* at different pH-values and temperatures. The three species displayed significant textural surface modification after the acid etching (**Table S4.7**). Overall, it is evident that the outermost layer of enamel (consisting of hydroxylapatite) and enameloid (consisting of fluorapatite) is significantly affected by etching during the experiment (**Fig. 4.5**) and thus the original dental surface is completely overwritten. The biplot *medf* vs. *metf* as well as *Asfc* vs. *epLsar* displayed a strong separation in all three species with increasing density and depth of furrows, as well as increasing complexity of the dental surface after the etching (**Fig. 4.6A and B**). PCA revealed a strong separation only along PC2 (**Fig. 4.6C and S4.5**) with the most separating parameters being density of the peaks (*Spd*), complexity (*nMotif*), depth (*medf*) and area (*mea*) parameters (**Table ES4.9**).

Additionally, we compared two sets of different natural African vlei rat tooth samples - one live-trapped and the other digested and extracted from barn owl pellets - with each other and with the experimentally altered *Otomys* teeth. The two natural samples are barely distinguishable from each other according to all surface texture parameters (**Fig. 4.5D and E, Fig. 4.6, Table ES4.8**). Even though Dunnett`s T3 test displays significant differences between the two natural samples sets as well as the experimentally altered *Otomys* teeth, the overlap of the parameter values is very large and therefore none of the differences were confirmed by Cliff's method (**Table ES4.9**). The biplot *medf* vs. *metf* and *Asfc* vs. *epLsar*, as well as the PCA displayed strong separation of the two natural *Otomys* sample sets from the experimentally altered *Otomys* samples after the acid etching (**Fig. 4.6 and S4.5**).

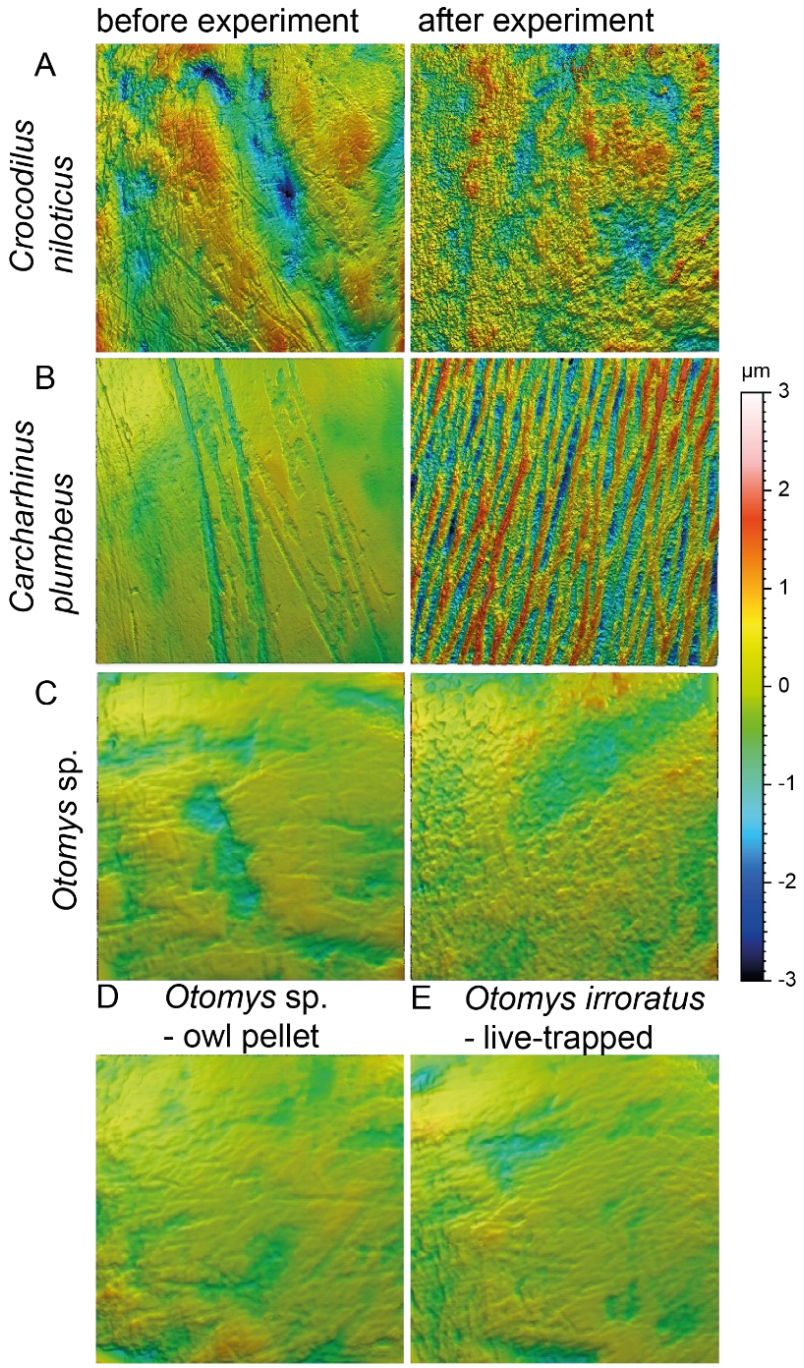

Figure 4.5. Meshed axiomatic 3D models of enamel surfaces (160 x 160 µm) of dental specimens before (left) and after (right) the acid etching experiments. Scan size is 160 x 160 µm except for all *Otomys* sp. for which scan size is 60 x 60 µm. A. *Crocodilus niloticus* before and after experiment at pH 2 for 72 hours; B. *Carcharhinus plumbeus* before and after experiment at pH 2 for 48 hours; C. *Otomys* sp., before and after experiment at pH 1.3 for 12 hours; D. *Otomys* sp. from modern owl pellets as natural comparison to the acid etching experiment; E. *Otomys irroratus* live-trapped as unaltered comparison to the naturally altered *Otomys* sp..

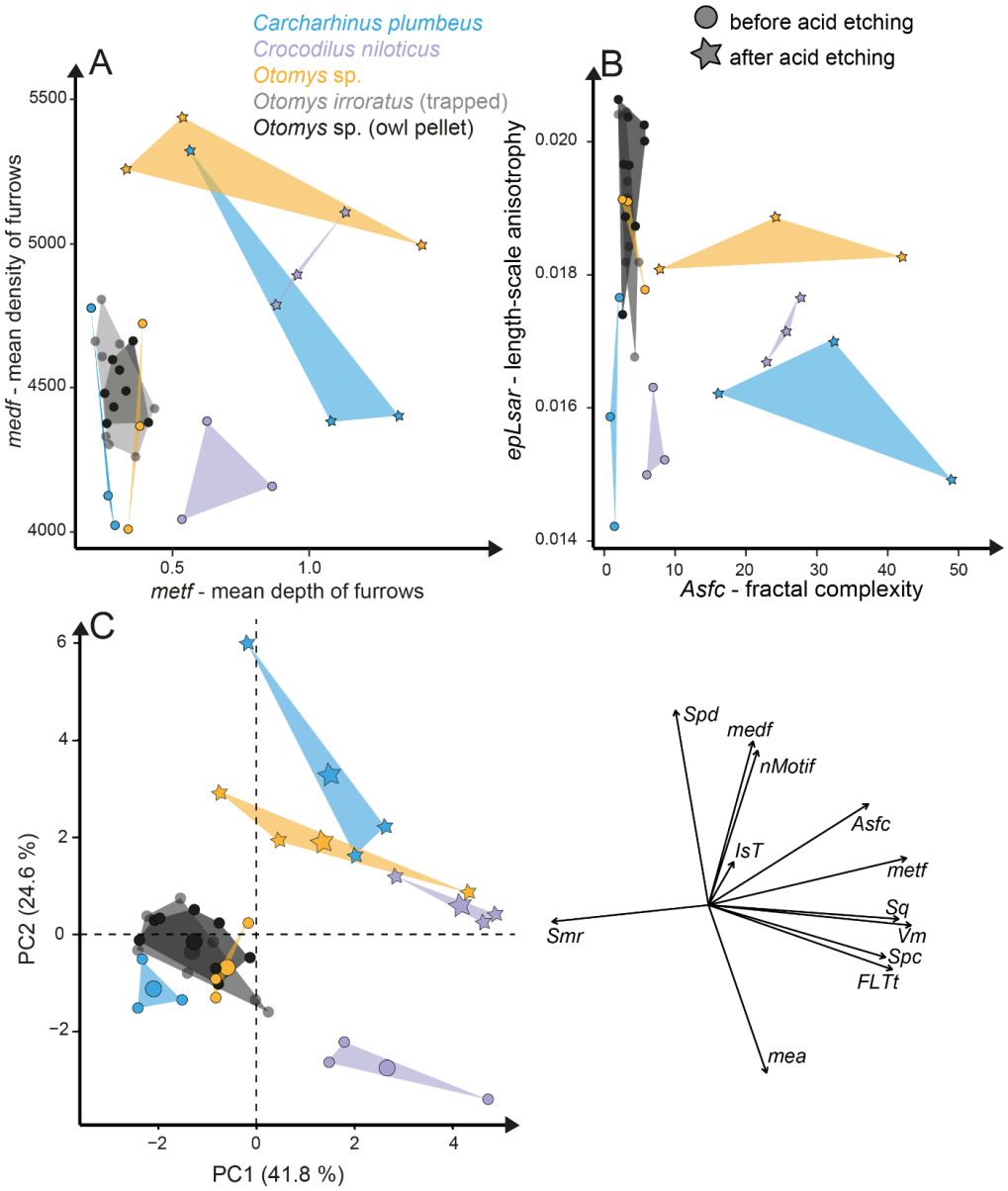

Figure 4.6. Results of the acid etching experiment. Dental microwear texture parameter A. *metf* (µm) vs *medf* (cm/cm²) and B. *Asfc* vs. *epLsar* for the experimentally altered teeth before (circles) and after (stars) the acid etching experiment. C. Principle component analysis (PCA) of surface texture parameters with best separation. Large symbols in PCA plots mark the mean for each taxon/etching interval.

4.5 Discussion

4.5.1 Fluvial transport in a sediment suspension simulated via a tumbling experiment

Tumbling of mammal, reptile and fish teeth shows that mechanical alteration of dental surfaces as characterised by dental microwear texture analysis seems to be more dependent on the sediment particle size than on the type of enamel(-oid) microstructure, tooth morphology or size. In most cases, the mechanical modification of the dental surface during tumbling leads

to changes of surface texture parameters in the same directions for all species (three mammalian, one reptilian, and one fish species). The dental surfaces of different species are strongly affected by sediment abrasion, especially by the small gravel fraction. The surfaces altered by the small gravel fraction look quite similar across species (**Fig. 4.1**) and they share a similar parameter space in the biplot *metf* vs. *medf* (**Fig. S4.2**), as well as in the PCA (**Fig. 4.2**). Very fine sand and gravel have the strongest alteration effects on abrasive texture patterns over the tumbling two-week time interval, with a variety of new texture features forming on the surface and increasing surface complexity (**Fig. S4.1**). In contrast, tumbling with the fine and medium sand have a slight polishing effect resulting in only a few new scratches. In this case, the abrasional effects are mostly undetectable by statistical analyses (**Table S4.6**). In general, all four grain size fractions of both sediment types lead to a variety of new texture features on the teeth of all five species as reflected in the shift of the parameter values before and after tumbling. In a direct comparison of the pre-tumbling with the post-tumbling surfaces, a separation was evident in the finest fine sand and the gravel fraction and for the biplots as well as in the PCA; however, there is still substantial overlap. Volume and overall height parameters seem to be least affected. Parameters from these groups are considered to be among the best for distinguishing between different feeding strategies (e.g. browser-grazer, Schulz et al., 2013a; herbivorous, carnivorous, frugivorous and molluscivorous lepidosaurs, Winkler et al., 2019a). Still, this can be critical for dietary reconstructions using DMTA and requires careful sample selection prior to scanning to exclude taphonomically altered teeth or surface areas. A proper training in DMTA would help to serve this purpose. We recommend that such training should include experience in recognizing various taphonomic alterations, which should ideally be calibrated to a database of surface textures characteristic of poorly preserved enamel surfaces as described in Weber et al. (in review). Here, we provide a first set of surface texture examples that illustrate the alteration effect of fluvial transport in sediment suspension. The comparison of fossil equid teeth *Hippotherium primigenium* from the Dinotheriensande, which were fluvially transported to a certain extent and deposited in sand-gravel sized siliciclastic sediments (Tobien, 1983), with the experimentally altered tooth samples reveals differences as well as similarities between the natural and the experimental surface alteration features. Keeping teeth moving in water-sediment suspension continuously for 336 hrs is an extreme taphonomic scenario, which was chosen to produce clear alteration effects in a short time experiment. Fluvial transport is potentially shorter, depending on different factors, such as size of the fossil and flow rate of the river system, e.g. smaller sediments could be transported over longer distances, in contrast to larger and heavier grains or fossils, where the flow rate has to be much faster to transport the material (Harms et al., 1982). The alteration process could be variable and might include reworking or discontinuous draining and flooding processes, leading not only to various post-mortem alterations, but that might also affect the

proportion of species in a fossil assemblage (Dodson, 1973; Russel et al., 1996; Läng et al., 2013, Pesquero et al., 2013). Still, the mechanical surface modification is rather small; only the tumbling with the fine gravel resulted in strong alteration. Fine-grained gravel leads to similar surface texture parameter values as those observed for fossil teeth from *Hippotherium primigenium* that were found in fine-grained sandy gravels of the fluvial Dinotheriensande deposits. Thus, we can link the *in-vitro* surface texture alteration results with those of fossil *Hippotherium primigenium* teeth that were deposited in a similar type of sediment. Hence, fluvial transport in gravel leads to similar enamel surface alteration features and potentially abrades ante-mortem surface texture. This finding is of high importance for dietary reconstructions because it limits ingesta-related reconstruction of microscopic wear patterns. Our tumbling experiments revealed that fossil teeth transported in fluviatile settings with gravel or sand, could be altered and that ante-mortem wear features might be erased or at least modified mechanically during transport due to post-mortem alteration. This might set limits on reliable dietary reconstruction at least for *Hippotherium primigenium* from the fluviatile environment of the Dinotheriensande. Furthermore, teeth of other species from the Dinotheriensande might be altered when transported in the same grain size fractions.

Thus, dental surfaces must be evaluated very carefully before attempting dietary reconstruction from this and similar fluvial depositional settings. When comparing different species from the same locality within the same depositional setting, dental surface might be altered in the same extant, and offsets between different feeding categories reflect ante-mortem differences, while absolute parameter values might be altered post-mortem (see Böhm et al., 2019). Vice-versa, when comparing the same species from different localities and different depositional settings where offsets between the different groups might be due to different diagenetic alterations.

4.5.2 Aeolian abrasion simulated via sandblasting experiment

Our sandblasting experiment demonstrated the suitability of such experimental approaches for testing the impact of aeolian sand on dental surfaces exposed to post-mortem or post-depositional weathering by airborne mineral dust. However, the air pressure applied in our experiment was very high (e.g. at least 20 times higher than present-day natural wind-speeds in the Chad, Cowie et al., 2014) and constant, leading to excessive alteration by the quartz fine sand.

Loess is a typical silt-sized aeolian sediment predominantly deposited during glacial periods in many areas, and could potentially have altered post-mortem teeth of the contemporaneous fossil fauna. However, despite the high air pressure and fast speed of sediment particles hitting the dental surface, short duration silt-sized (Ø 36 µm) loess blasting

experiments do not lead to any visible alteration or changes of surface texture parameter values (**Fig. 4.3**). Fossil teeth from natural loess deposits are therefore likely usable for diet reconstruction employing DMTA. In contrast, sandblasting of dental surfaces with larger, sand-sized (Ø 166 µm) quartz grains caused major damage to and abrasion of the enamel surface leading to strongly increasing complexity and volume parameters (**Fig. 4.4**). Fossil tooth specimens that were naturally or artificially sandblasted using sand-sized sediment grain size fractions seem to be affected by mechanical surface modification. However, due to our experimental design, it remains unclear which particle size causes the damage. Further experiments using lower air pressure could help to resolve this issue. Additionally, special care needs to be taken if air-abrasive techniques were used for sample preparation, i.e. sandblasting during preparation of fossils from the embedding sediment/rock. In general, various materials, such as Aluminium oxide, crushed glass, plastic, but also walnut shells or wheat starch, with different hardness, shapes and particle size are used for sample preparation (for detailed information see Graham and Allington-Jones, 2018). Air-abrasive techniques should be avoided when dealing with dental surfaces for later dietary analyses using DMTA, however, if is not possible to avoid this, special care needs to be taken to protect the dental surfaces from the blast. Specimens prepared with air-abrasive techniques, especially larger and harder abrasive powders comparable to the quartz finesand (Feinsand 12c) from this study, should be evaluated carefully for potential post-mortem alteration.

4.5.3 Stomach digestion alteration effects simulated via in-vitro acid etching experiments

Acid-etching experiments of mammal, reptile, and fish teeth with diluted HCl alter the original dental surface of enamel (hydroxylapatite: *Otomys* sp., *Crocodilus niloticus*) and enameloid (fluorapatite: *Carcharhinus plumbeus*) by dissolution processes. The complexity and the roughness of the dental surface increase strongly and the textures of the dental surfaces are significantly different before and after the etching experiment (**Fig. 4.6, Table S4.7**). The *in-vitro* stomach acid experiment design performed with isolated teeth directly immersed only in hydrochloric acid do not accounting for the role of digestive enzymes, and therefore resemble more closely the digestive system of crocodiles, where stomach fluids consist almost entirely of hydrochloric acid with almost no enzyme activity (Fisher, 1981). A similar experiment performed by Fernández-Jalvo et al. (2014) showed great similarities between the surface of bones and teeth of small mammals immersed exclusively in hydrochloric acid and bones digested by crocodiles. Additionally, they found differences between hydrochloric acid immersion alone and natural digestion of avian predators as well as mammalian carnivores, which we can confirm with our comparison of experimentally altered versus natural *Otomys* samples from owl pellets. We find the surface textures of the

experimentally altered teeth to be very different from those of small mammal teeth digested by avian predators. For avian predators and mammalian carnivores digestion is driven by the combination of stomach fluids and enzymes. Modifications in form of corrosion and decalcification on bones and teeth of small mammals can be reproduced with experimental approaches, but to a lesser degree and at a slower alteration rate than during natural digestion (Fernández-Jalvo et al., 2014). Our results further support the findings of Fernández-Jalvo et al. (2014), that hydrochloric acid erodes the outer tooth enamel layer almost completely, especially the most exposed areas, such as cusps or lamella of molars.

In contrast, no significant differences in DMT parameters could be detected between digested and non-digested teeth, i.e. from barn owl-pellet (that were digested for at least 10-12 hours (Grémillet and Plös, 1993)) and live-trapped specimens, both from the same area in South Africa. This result is in line with findings that in barn owl stomachs, only 1 % of ingested molars evidence digestion-related acid-etching and supports the categorization of barn owls in the weakest predator category 1 (i.e. exhibit no or minimal acid digestion, Fernández-Jalvo et al., 2016). We conclude that small mammal teeth extracted from barn owl pellets can be used for diet reconstruction studies using DMTA, however, we did not test if this is also the case for other owl species. It is likely that, at least for birds of prey of predator category 1 (see Fernández-Jalvo et al., 2016), ingesta-related enamel surface textures of prey vertebrates can survive the weak acid attack.

4.6 Conclusions

While all of our experiments were well conceived, they nonetheless represent simplified approximations of post-mortem alteration and do not completely reproduce the complex, natural conditions teeth will experience during post-mortem taphonomic processes. Nevertheless, both simplified and extreme experimental conditions, can be very informative in understanding how dental surfaces can be affected by post-mortem wear and alteration processes. An important finding of our tumbling experiment is that surface texture parameter values of naturally or experimentally altered dental surfaces often cannot be unambiguously distinguished from ingesta-related ante-mortem wear by DMTA. This is because the surface texture parameter values of taphonomically biased post-mortem textures often fall within the same parameter space as textures from ingesta-related ante-mortem wear. Therefore, fluvially transported fossil specimens need to be evaluated carefully and categorised according to their degree of post-mortem alteration. Only slightly altered dental surfaces should be considered in a DMTA study for diet reconstruction. Different parameters, including sample size, grade of alteration, and research question should all be considered and should be addressed in the discussion of the dataset. Different species from the same depositional setting might still be

comparable, even when the dental surface is influenced by slight post-mortem alteration, if the degree of alteration is comparable between taxa.

Our sandblasting experiment showed that silt-sized aeolian transported mineral particles do not affect the dental surface and only larger, sand-sized quartz particles cause post-mortem abrasion. Depending on the fossil locality and the associated grain size fraction of the aeolian sediment our experiment suggests that sandblasted specimens can be included in DMTA studies. Special care needs to be taken with specimens altered by aeolian activity with larger grain size fractions.

The acid etching experiment revealed a more complex impact of digestion on the dental surface than expected, at least for avian and mammalian predators. First, the comparison of digested and un-digested *Otomys* teeth suggest that small mammal teeth can also be used for diet reconstruction using DMTA, at least for samples processed by category 1 avian predators (Fernández-Jalvo et al., 2016). Teeth digested by mammalian carnivores or crocodiles, which have much stronger stomach acids should be carefully evaluated prior to DMTA.

Our results demonstrate that, at least for a subset of samples from a given fossil assemblage, it is necessary to identify post-mortem wear features to evaluate the degree of post-mortem alteration. Further, it is important to include dental surfaces displaying moderate post-mortem alteration and to subsequently discuss how the parameter spaces might be shifted by those post-mortem alterations. In this study, we only cover three different post-mortem scenarios (fluvial and aeolian sediment transport, digestion), but more experiments covering other scenarios, such as burial or trampling, are necessary and encouraged. Future experiments should also include sediment mixtures of larger particle size spectra as well as abrasives with different mineralogical compositions. Also, experiments simulating transport in a flow channel instead of tumbling barrels would better approximate natural fluvial depositional settings. In vitro digestion experiments should be performed with better environmental control (i.e. controlled pH, addition of digestive enzymes) and in vivo feeding experiments with actual predators digesting prey and investigation of teeth collected from faeces would complement the dataset.

4.7 Acknowledgment

This project has received funding from the European Research Council (ERC) under the European Union's Horizon 2020 research and innovation programme (grant agreement No 681450) and the Max-Planck Graduate Center. We thank the Center of Natural History (CeNak, Hamburg), Irina Ruf (Senckenberg Museum, Frankfurt), Zivile Zigaite (University of Stockholm), Jean-Michel Male (Pierre Latte Fermes aux Crocodile, Lyon) and Jan Fischer

(Geoskop Kusel) for the dental material used for the experiments. We would also like to express our gratitude to the Hessisches Landesmuseum Darmstadt, Cecile Blondel and Jennifer Leichliter (Johannes Gutenberg-University Mainz) for modern and fossil dental material used for comparison. We thank Marcel Fries for performing the sandblasting experiment, Ralf Meffert and Tobias Häger (both Johannes Gutenberg-University Mainz) for the X-ray diffraction-analysis and Philipp Schulte (RWTH Aachen University) for the grain size analysis. Additionally, we thank Jennifer Leichliter (Johannes Gutenberg-University Mainz, Germany) for proofreading the manuscript.

4.8 Supplement

Operators used in MountainsMap template:

Otomys template. This template applies to all *Otomys* specimens. The enamel ridge of Otomys are very small, therefore, first a sub-surface of 60 × 60 µm was cut out of the texture model using the extraction operator in MountainsMap. The following MountainsMap template was produced for extracted scans of *Otomys* sp. upper right teeth, scanned on the original tooth. All single teeth with unknown position were treated similarly.

1. Orientation of dental surface with LS-surface using subtraction
2. Noise-cancelling median filter, filter size 5 x 5
3. Gaussian filter, filter size 3 x 3
4. Filling of non-measured points
5. Set the threshold using the material-% (0.5-99.5 %) to reduce height and depth
6. Removal of isolated outliers, outliers at the edge and with a maximum allowed inclination (85°), soft strength of the method
7. Removal of form using a 2nd order polynomial.

Mammal template. This template is for analyses of original upper right premolar and molar teeth of all large mammal species in this study and the polished mammoth teeth. All moulded surfaces were mirrored along the z-axis, to be inverted first. Lower jaw teeth were treated the same way.

1. Orientation of dental surface with LS-surface using subtraction
2. Noise-cancelling median filter, filter size 5 x 5
3. Gaussian filter, filter size 3 x 3
4. Filling of non-measured points
5. Set the threshold using the material-% (0.5-99.5 %) to reduce height and depth

6. Removal of isolated outliers, outliers at the edge and with a maximum allowed inclination (85°), soft strength of the method
7. Removal of form using a 2nd order polynomial.

Reptile template. This template is designed for original upper right teeth of crocodile teeth; all teeth were treated the same way.

1. Orientation of dental surface with LS-surface using subtraction
2. Noise-cancelling median filter, filter size 5 x 5
3. Gaussian filter, filter size 3 x 3
4. Filling of non-measured points
5. Set the threshold using the material-% (0.5-99.5 %) to reduce height and depth
6. Removal of isolated outliers, outliers at the edge and with a maximum allowed inclination (85°), soft strength of the method
7. Removal of form using a 4th order polynomial.

Shark template. This template is designed for original upper right teeth of sandbar shark teeth; all teeth were treated the same way.

1. Orientation of dental surface with LS-surface using subtraction
2. Noise-cancelling median filter, filter size 5 x 5
3. Gaussian filter, filter size 3 x 3
4. Filling of non-measured points
5. Set the threshold using the material-% (0.5-99.5 %) to reduce height and depth
6. Removal of isolated outliers, outliers at the edge and with a maximum allowed inclination (85°), soft strength of the method
7. Removal of form using a 2nd order polynomial.

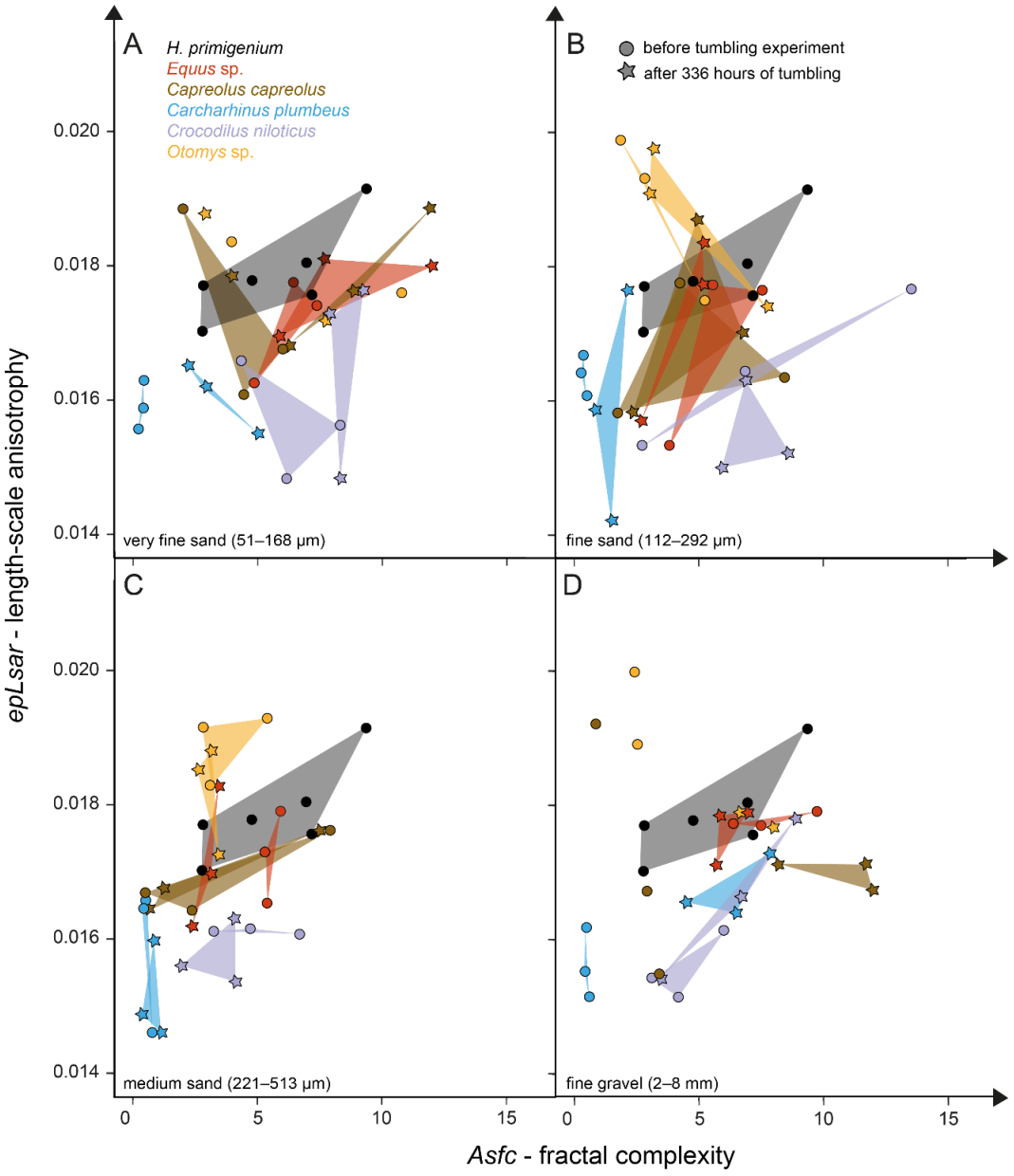

Figure S4.1. Results of *Asfc*-*epLsar* of the tumbling experiment. Biplot of the enamel surface texture parameters *Asfc* – fractal complexity versus *epLsar* – length-scale anisotropy for the experimentally altered teeth of different vertebrate species before (circles) and after (stars) the tumbling experiment with A. very fine sand (51–168 µm), B. fine sand (112–292 µm), C. medium sand (221–513 µm) and D. fine-grained gravel (2–8 mm) as suspension in water.

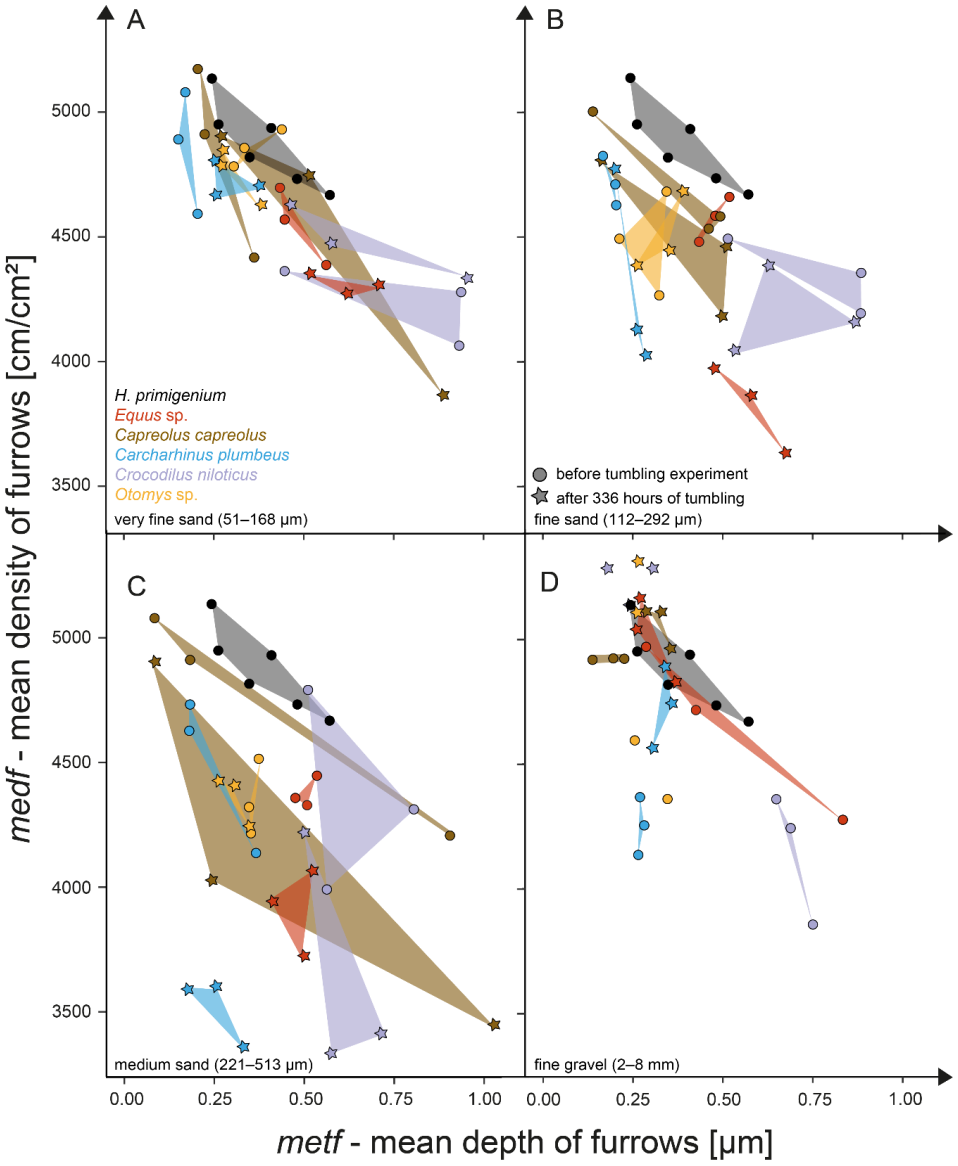

Figure S4.2. Results of *metf-medf* of the tumbling experiment. Biplot of the enamel surface texture parameters *metf* (µm) vs *medf* (cm/cm²) for the experimentally altered teeth of different vertebrate species before (circles) and after (stars) the tumbling experiment with A. very fine sand (51–168 µm), B. fine sand (112–292 µm), C. medium sand (221–513 µm) and D. fine-grained gravel (2–8 mm) as suspension in water.

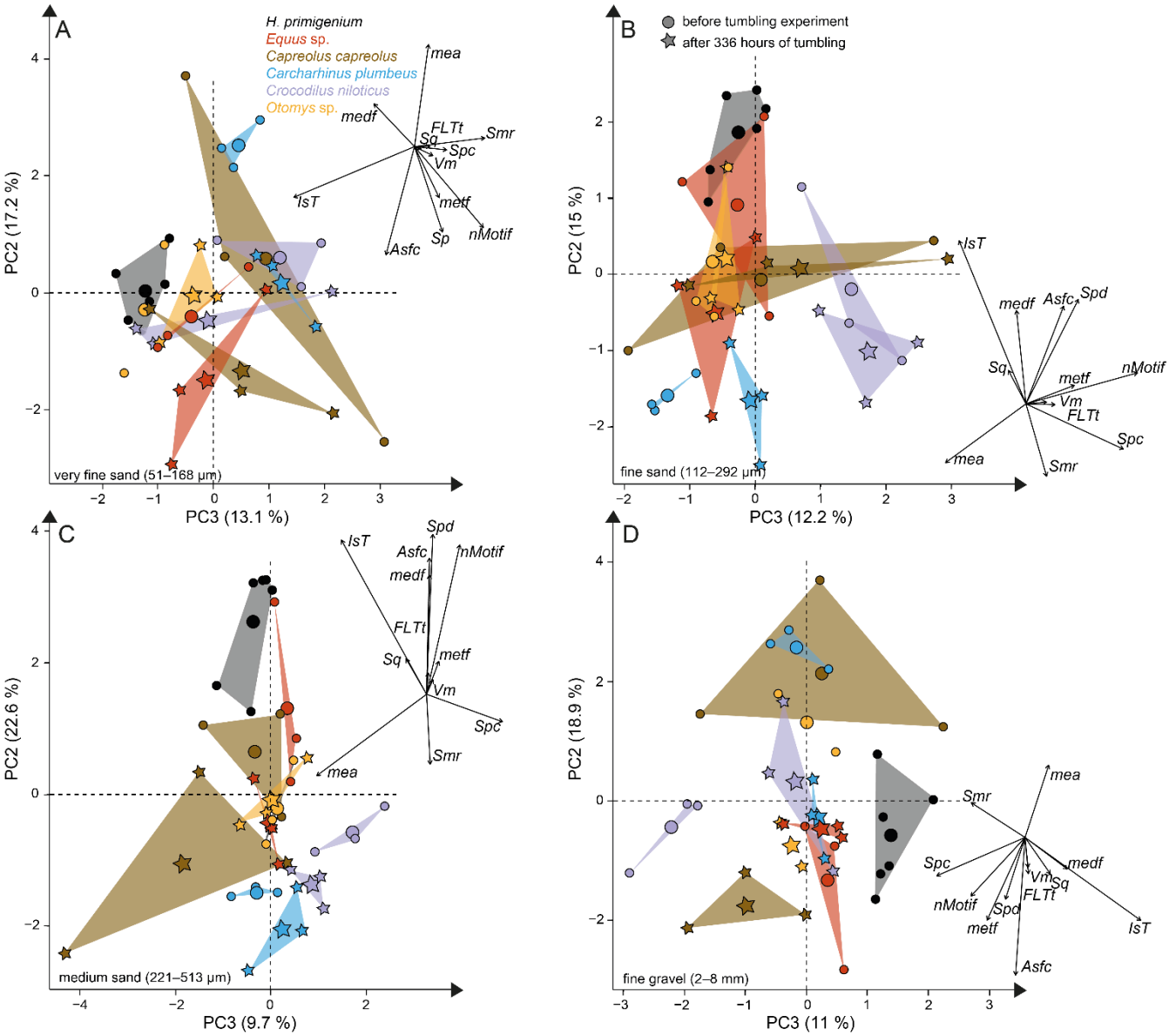

Figure S4.3. Principle component analysis (PC2 and 3) of the tumbling experiment with surface texture parameters that best separate for the experimentally altered teeth of different vertebrate species before (circles) and after (stars) the tumbling experiment with A. very fine sand (51–168 µm), B. fine sand (112–292 µm), C. medium sand (221–513 µm) and D. fine-grained gravel (2–8 mm) as suspension in water. Large symbols in PCA plot mark the mean of the area of the different taxa and tumbling intervals.

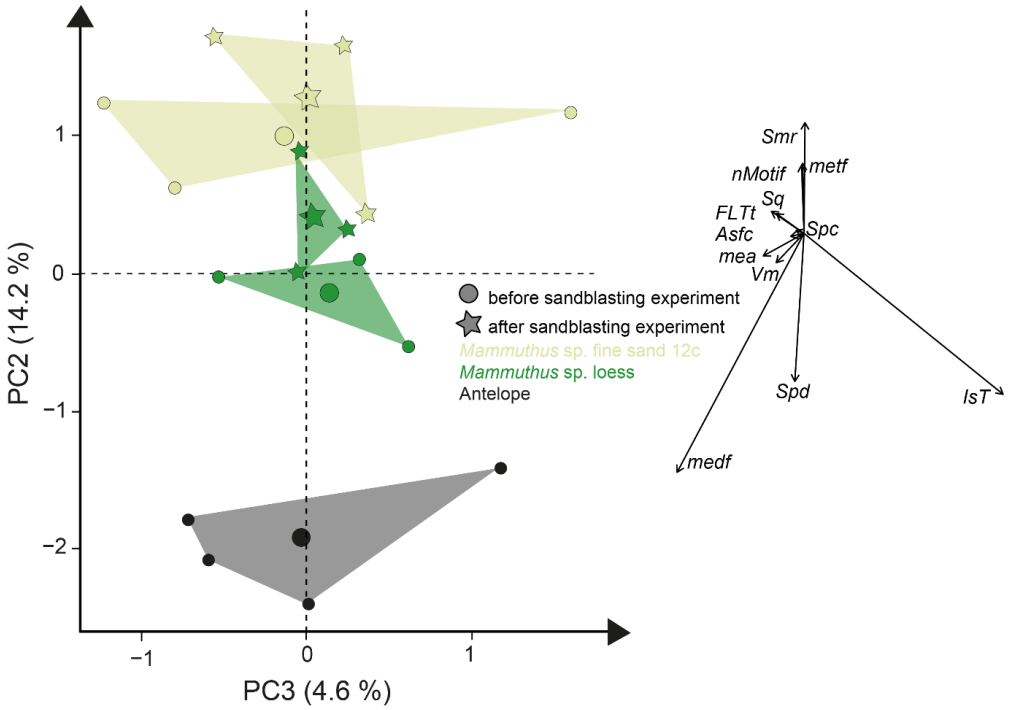

Figure S4.4. Principle component analysis (PC2 and PC3) of the sandblasting experiment with surface texture parameters that best separate for the experimentally altered mammoth teeth before (circles) and after (stars) the sandblasting experiment. Large symbols in PCA plot mark the mean of the area of the taxa and blasting intervals.

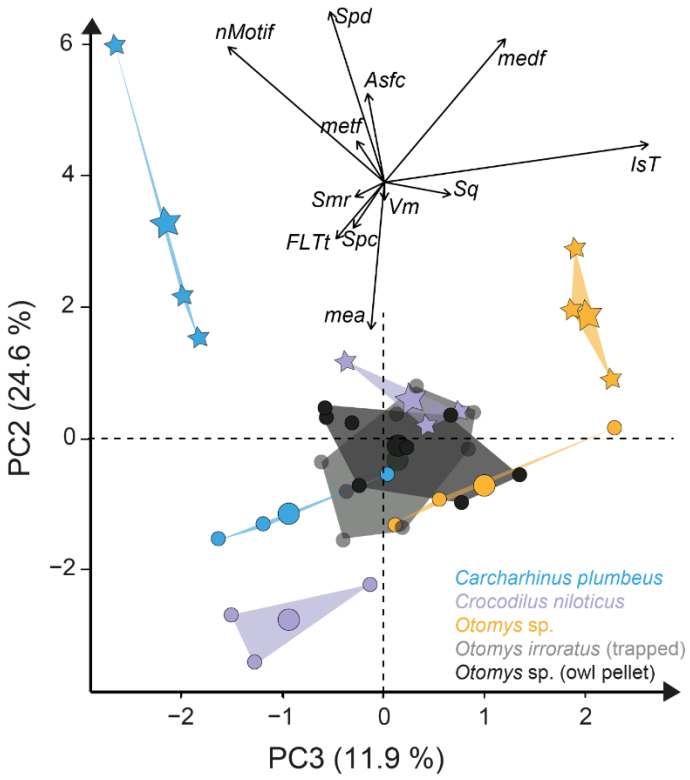

Figure S4.5. Principle component analysis (PC2 and 3) of the acid etching experiment with surface texture parameters that best separate for the experimentally altered teeth before (circles) and after (stars) the acid etching experiment. Large symbols in PCA plot mark the mean of the area of the taxa and blasting intervals.

Table S4.1. Grain size fraction with mean and median of the sediments used for the experiments. The quartz-bearing sand used for the tumbling experiment (measured before and after tumbling) and Feinsand 12c and loess used for the sandblasting experiment, measured by laser granulometry.

	< 0,2 µm [%]	< 0,63 µm [%]	< 2 µm [%]	< 6,3 µm [%]	< 20 µm [%]	< 36 µm [%]	< 63 µm [%]	< 200 µm [%]	< 630 µm [%]	< 2000 µm [%]	mean [µm]	median [µm]
51–168 µm before tumbling	0.03	0.28	0.85	0.50	0.62	2.42	11.94	78.71	4.65	0.00	105.86	101.20
112–292 µm before tumbling	0.12	0.30	0.44	0.21	0.14	0.24	1.18	47.78	49.61	0.00	200.94	200.36
221–513 µm before tumbling	0.10	0.20	0.22	0.08	0.06	0.04	0.10	6.63	90.50	2.09	359.24	353.45
51–168 µm after tumbling	0.00	0.27	1.39	1.98	3.11	3.65	12.71	74.20	2.69	0.00	95.80	94.62
112–292 µm after tumbling	0.14	0.34	0.55	0.52	0.76	0.55	0.80	42.52	53.83	0.00	205.96	207.57
221–513 µm after tumbling	0.09	0.19	0.20	0.07	0.09	0.06	0.09	4.07	92.45	2.70	375.83	369.22
Finesand 12c	0.12	0.32	0.52	0.18	0.11	0.32	1.40	71.72	25.32	0.00	166.01	164.31
loess Schwalbenberg	1.16	2.97	4.51	6.88	16.87	23.81	28.24	15.46	0.10	0.00	36.86	31.97

Table ES4.2. Taxon, amount, information about collection, fossil side and teeth samples and different experimental set ups. n.a. = information not available. The table is found in the electronic Supplement.

Table S4.3. Description of applied surface texture parameters according to ISO 25178, ISO 12781, motif, furrow, texture direction and isotropy.

Category	Parameter	Description (condition)	Standard	Unit
Area	*Sda*	Closed dale area	ISO 25178	μm^2
	Sha	Closed hill area	ISO 25178	μm^2
	mea	Mean area	Motif	μm^2
Complexity	*Sdr*	Developed interfacial area ratio	ISO 25178	%
	nMotif	Number of motifs	Motif	no unit
	Asfc	Fractal complexity (Area-sale)	SSFA	no unit
Density	*Sal*	Auto-correlation length (*s* = 0.2)	ISO 25178	µm
	Spd	Density of peaks	ISO 25178	$1/\mu m^2$
	medf	Mean density of furrows	Furrow	cm/cm^2
Direction	*Str*	Texture aspect ratio (*s* = 0.2)	ISO 25178	no unit
	Std	Texture direction	ISO 25178	no unit
	Tr1R	First direction	Direction	no unit
	Tr2R	Second direction	Direction	no unit
	Tr3R	Third direction	Direction	no unit
	IsT	Texture isotropy	Isotropy	%
	epLsar	Length-sale anisotropy	SSFA	no unit
Height	*S10z*	Ten-point height	ISO 25178	µm
	S5p	Five-point peak height	ISO 25178	µm
	S5v	Five-point valley height	ISO 25178	µm
	Sa	Arithmetic mean height or mean surface roughness	ISO 25178	µm
	Sku	Kurtosis of the height distribution	ISO 25178	no unit
	Sp	Maximum peak height, height between the highest peak and the mean plane	ISO 25178	µm
	Sq	Standard deviation of the height distribution or RMS surface roughness	ISO 25178	µm
	Ssk	Skewness of the height distribution	ISO 25178	no unit
	Sv	Maximum pit height, depth between the mean plane and the deepest valley	ISO 25178	µm
	Sxp	Peak extreme height difference in height between p% and q% (p=50%, q=97.5%)	ISO 25178	µm
	Sz	Maximum height, height between the highest peak and the deepest valley	ISO 25178	µm
	meh	Mean height	Motif	µm
	madf	Maximum depth of furrows	Furrow	µm
	metf	Mean depth of furrows	Furrow	µm
	FLTt	Peak to valley flatness deviation of the surface (Gaussian Filter, 0.025 mm)	ISO 12781	µm
	FLTp	Peak to reference flatness deviation (Gaussian Filter, 0.025 mm)	ISO 12781	µm
	FLTv	Reference to valley flatness deviation (Gaussian Filter, 0.025 mm)	ISO 12781	µm
	FLTq	Root mean square flatness deviation (Gaussian Filter, 0.025 mm)	ISO 12781	µm
Peak sharpness	*Spc*	Arithmetic mean peak curvature	ISO 25178	1/µm
Plateau size	*Smr*	Areal material ratio	ISO 25178	%
	Smc	Inverse areal material ratio (*p* = 10%)	ISO 25178	µm
Slope	*Sdq*	Root mean square gradient	ISO 25178	no unit
Volume	*Sdv*	Closed dale volume	ISO 25178	μm^3
	Shv	Closed hill volume	ISO 25178	μm^3
	Vm	Material volume at a given material ratio (*p* = 10%)	ISO 25178	$\mu m^3/\mu m^2$
	Vmc	Material volume of the core at given material ratio (*p* = 10%, *q* = 80%)	ISO 25178	$\mu m^3/\mu m^2$
	Vmp	Material volume of the peaks (p=10%)	ISO 25178	$\mu m^3/\mu m^2$
	Vv	Void volume at a given material ratio (*p* = 10%)	ISO 25178	$\mu m^3/\mu m^2$
	Vvc	Void volume of the core (*p* = 10%, *q* = 80%)	ISO 25178	$\mu m^3/\mu m^2$
	Vvv	Void volume of the valley at a given material ratio (*p* = 80%)	ISO 25178	$\mu m^3/\mu m^2$

Table ES4.4. Descriptive statistics (mean ±SD) for all DMT parameters for the tumbling experiment (see **Table ES4.3**). For parameter descriptions, see Table S4.3. The table is found in the electronic Supplement.

Table ES4.5. Descriptive statistics (mean ±SD) for all DMT parameters for the sandblasting experiment (see **Table ES4.3**). For parameter descriptions, see Table S4.3. The table is found in the electronic Supplement.

Table ES4.6. Descriptive statistics (mean ±SD) for all DMT parameters for the acid etching experiment (see **Table ES4.3**). For parameter descriptions, see Table S4.3. The table is found in the electronic Supplement.

Table S4.7. Statistical results from Wilcoxon Signed-Rank Test for the different experiments. Significances confirmed are highlighted in red.

	***Equus* sp.**	***Charcharhinus plumbeus***	***Crocodilus niloticus***	***Otomys* sp.**	***Capreolus capreolus***	***Mammuthus sp.***
tumbling experiment with fine sand (51–168 µm)	0.111	0.024	0.006	0.000	0.000	-
tumbling experiment with fine sand (112–292 µm)	0.237	0.335	0.768	0.053	0.039	-
tumbling experiment with medium sand (221–513 µm)	0.704	0.716	0.000	0.029	0.063	-
tumbling experiment with fine-grained gravel (2–8 mm)	0.002	0.804	0.000	0.007	0.076	-
sandblasting experiment with loess	-	-	-	-	-	0.721
sandblasting experiment with fine sand	-	-	-	-	-	0.000
acid etching experiment, pH 1.3, Temperature 42 °C	-	-	-	0.021	-	-
acid etching experiment, pH 2, Temperature 25 °C	-	0.000	0.000	-	-	-

Table ES4.8. Statistical results of the acid etching experiment for all DMT parameters for *Otomys* teeth of trapped (*Otomys irroratus*) species, *Otomys* sp. extracted from owl pellets and experimentally altered *Otomys* teeth before and after acid etching. For parameter description, see Table S4.3. Significances confirmed by Cliff's method are highlighted in bold. The table is found in the electronic Supplement.

Table ES4.9. Importance of components for PCA from the different types of experimentally altered enamel surfaces scans using 12 DMT parameter (*Smr, medf, Spd, nMotif, Asfc, Spc, metf, Vm, Sq, FLTt, IsT, mea*). Factor loadings for the parameter values are represented with values cut-off +/- 0.4 marked in red. The table is found in the electronic Supplement.

Chapter 5 Manuscript III: The good, the bad and the ugly – a trash or treasure hunt for reliable enamel surface textures in vertebrates

The good, the bad and the ugly – a trash or treasure hunt for reliable enamel surface textures in vertebrates

Weber, Katrin[1], Winkler, Daniela E.[1,2], Schulz-Kornas, Ellen[3,2,4], Kaiser, Thomas M.[2], Tütken, Thomas[1]

[1]Applied and Analytical Palaeontology, Institute of Geosciences, Johannes Gutenberg University, Mainz, Germany, daniela.winkler@uni-mainz.de, tuetken@uni-mainz.de

[2]Center of Natural History (CeNak), University of Hamburg, Hamburg, Germany, Thomas.Kaiser@uni-hamburg.de

[3]Department of Cariology, Endodontology and Periodontology, University of Leipzig, Leipzig, Germany, Ellen.Schulz-Kornas@medizin.uni-leipzig.de

[4]Department of Human Evolution, Max Planck Institute for Evolutionary Anthropology, Leipzig, Germany

A similar version of this manuscript is under review in *Palaeogeography, Palaeoclimatology, Palaeoecology.*

5.1 Abstract

Dental microwear texture analysis (DMTA) is a common wear proxy for diet using dental wear features enabling dietary reconstruction in extant and extinct taxa. Dietary reconstructions of extinct species can be biased post-mortem due to mechanical modification. These post-mortem surface alterations can be caused by material loss occurring after death or as the result of burial, excavation or preparation processes. In this study, we are dealing with the latter ones, post-mortem surface alteration occurring during excavation, preparation and conservation processes. We present a first general overview of “bad” and unsuitable dental surface scans and describe them qualitatively as well as by using dental microwear texture (DMT) parameters and compare them to “good”, unaltered ingesta-related dental surfaces. Therefore a dataset was compiled consisting of scans of common surface defects observed in different species. These non-ingesta related “bad” surfaces show a great variety of morphologies, whereby some are easy to distinguish from ante-mortem ingesta-related wear features, such as large post-mortem scratches or cracks in the enamel, while others are more obscured, such as remaining varnish covering the dental surface. The compiled surface defects dataset reveals that “bad and ugly” surfaces often partly overlap with the parameter space of “good” surfaces, but have a number of outliers. However, with sufficient training and a reference database, these surfaces are detectable by an experienced user. At this point, we want to initiate a database for the user of dental microwear texture analysis containing different kinds of non-ingesta related dental wear features, to help identify those and improve future DMTA studies.

5.2 Introduction

For nearly 20 years, dental microwear texture analysis (DMTA) has been a well-established method to estimate dietary tendencies in extant and extinct taxa (e.g. Scott et al., 2005; Merceron et al., 2007; Ungar et al., 2003, 2007, 2008, 2020; Scott et al., 2009; Schulz et al., 2010; Winkler et al., 2013, 2016). Originally developed for terrestrial mammals (Ungar et al., 2003; Schulz et al., 2010; Purnell et al., 2013; Kubo et al., 2017), including lagomorphs (Schulz et al., 2013b), rodents (Winkler et al., 2016), ungulates (Merceron et al., 2007; Merceron and Madelaine, 2006), and primates (Scott et al., 2009; Calandra et al., 2012; Schulz-Kornas et al., 2019), it has gained popularity and been successfully applied to teeth of many extant and extinct vertebrate taxa, such as reptiles (Bestwick et al., 2019; Winkler et al., 2019a), mammal-like reptiles (Kalthoff et al., 2019), fish (Purnell et al., 2016) and (semi-)aquatic mammals (Purnell and Darras, 2017; Bethune et al., 2019). Furthermore, DMTA has proven to be a powerful tool for quantifying wear of bone surfaces, e.g. archaeological use-wear (Martisius et al., 2018) and bone-use (Turcotte et al., 2019). It has long been known that

dental microwear and dental microwear texture are proxies for oral behaviour and environment but that they are also prone to bias from post-mortem alteration, especially in fossil teeth (King et al., 1999; Dauphin et al., 2003, 2018). Taphonomic post-mortem alteration of the occlusal surface can be caused by mechanical and/or chemical agents during transport, burial, and the fossilization process as well as during excavation and preparation of fossils for conservation or study. When surfaces from museum collections are moulded using high-resolution silicones, another potential source of alteration is introduced by moulding errors. Only a few studies address the issue of diagenetic changes in dental wear features under experimental (e.g. Gordon, 1983, 1984; King et al., 1999; Böhm et al., 2019) or natural conditions (Dauphin et al., 2003, 2018; Martínez and Pérez-Pérez, 2004). In general, DMTA relies on surface scans of "good" (i.e. proposed ingesta-related) ante-mortem surfaces, but those scans which appear suspicious are excluded (i.e. the "bad and ugly") and never shown in publications. "Bad" surfaces with dirt (i.e. dust or lint) attached or "ugly" wear surfaces which have been potentially affected by post-mortem surface alteration are usually excluded from analyses (Ungar et al., 2008; Schulz et al., 2010; Purnell et al., 2013). On the one hand, this guarantees higher quality of the selected "good" ingesta-related surface scans, but on the other hand it reduces the sample drastically (Ungar et al., 2008). However, selecting only "good" ingesta-related dental surface depending on the subjective view of the observer does not consequently guarantee "high quality" datasets. This selection can improve datasets, the more experienced the user, and the better be the selection. Further, every DMTA study focused on diet or feeding behaviour of vertebrates relies on user expertise to sort reliable (i.e. ingesta-related) from un-reliable surface scans (negative results) out by recognizing variable and sometimes unknown surface features. Therefore, we see a need to publish these negative results and compile a dataset of scans of obviously altered surfaces to better characterise the "bad and ugly" surface features. Here we provide a first general orientation for researchers applying DMTA, and focus on "bad and ugly" dental surface scans resulting from preparation blunders during collection, cleaning (adherent dirt or remaining varnish or glue), moulding or enamel defects. For the first time, these "bad and ugly" surfaces were not identified and excluded by individual researchers, but instead were included and standardised surface texture parameters were used to quantify "bad and ugly" surfaces using an automated software tools in order to be objective.

To do so, we employed two different DMTA approaches: scale-sensitive fractal analysis (SSFA, Ungar et al., 2003) and 3D surface texture analysis (3DST, Schulz et al., 2010). Both, SSFA and 3DST, use optical topometry at the µm-scale to produce 3D representations of the enamel surface and rate the distribution and geometry of topographic features in three-dimensions. In SSFA, complexity and anisotropy of the surfaces are described, using length-scale and area-scale fractal parameters (e.g. Ungar et al., 2003, 2012; Scott et al., 2006; Scott, 2012). In 3DST, surfaces are characterised using standardised surface texture roughness (ISO

25178) and flatness (ISO 12781) parameters, as well as additional motif, furrow, direction and parameters (Schulz et al., 2010, 2013a, b; Purnell and Darras, 2016; Kubo et al., 2017; Purnell et al., 2017; Winkler et al. 2019).

In this study, we test the hypothesis, that the observer-biased, visual separation of ingesta-related ante-mortem wear, done by the authors, and any kind of post-mortem alteration can statistically be supported by different 3DST and SSFA parameters. We further compile a literature-based overview of thresholds for DMTA parameter values from unaltered, diet-related wear surfaces, and compare them to parameter values obtained for the “bad” post-mortem altered surfaces. We intend to find parameters or sets of parameters, which reliably characterize post-mortem altered surface textures by values falling out of range of the threshold set by literature values, and therefore help to discard “bad” surface scans on objective parameter basis, rather than on subjective, visual basis. In theory, it should be possible to identify extreme post-mortem wear features, such as cracks in the enamel or bubbles in the moulding silicon. However, if the features are very small and/or only cover small areas of the dental surface, they might not affect parameter values significantly and therefore could be concealed. So far, presumably altered, “bad and ugly” surfaces are excluded during the cleaning, moulding and scanning procedure on a qualitative basis by an experienced observer. It is necessary to quantitatively test if DMTA itself can - based on surface features characterised by surface texture parameter values - separate post-mortem altered “bad and ugly” from ante-mortem “good” wear surfaces. This will be helpful in future studies and interpretations based on DMTA to avoid taphonomic artefacts in assessing diet related ante-mortem wear features as well as help to understand the limits of the method in distinguishing ingesta-related and taphonomic wear.

5.3 Material and methods

5.3.1 Dataset structure

Single scans of “bad” post-mortem altered dental surface textures of the selected taxa were included in this study (**Table 5.1 and ES5.1**). Scans were taken between 2003 and 2019 from different, mostly museum specimens (**Table ES5.1**), however, have not been included into published studies according to their badly preserved dental surface or bad quality of the moulds. Some scans are already used as examples for bad surfaces to train students and young researcher fellows in the DMTA lab of Thomas M. Kaiser at the Center of Natural History, University of Hamburg. The dataset includes a large number of mammalian species and additionally reptilian and synapsid samples. All teeth were cleaned with water to remove adherent dust or dirt particles, ethanol for removing lipids and acetone for removing remaining glue or varnish, often applied on museum specimens.

Table 5.1. Sample set for the “bad and ugly” dataset. Type of defect, class, taxon, trivial name and number of specimens and scans per specimen and number of total scans per “bad and ugly” surface category and ingesta-related dental surfaces.

Type	Class	Taxon	Trivial name	n of individuals	n single scans	Scans in total
crack in enamel	mammalia	*Connochaetes taurinus*	blue wildebeest	2	2	
		Canis lupus	grey wolf	1	1	
	diapsida	*Allosaurus*	Allosaurus	2	2	
		Ceratosaurus	Ceratosaurus	1	5	**10**
post-mortem scratches	mammalia	*Propalaeotherium hassiacum*	Primeval horse	2	2	
	diapsida	Theropoda	theropod	1	3	
		Iguanodon	Iguanodon	1	1	
		Allosaurus	Allosaurus	1	3	
		Tyrannosaurus rex	Tyrannosaurus rex	1	1	**10**
varnish	mammalia	*Hippotherium primigenium*	Hipparion	3	22	
		Gorilla gorilla gorilla	western lowland gorilla	3	3	
		Paranthropus robustus	Robust australopithecine	1	1	
	sauropsida/ diadectomorpha /synapsida	*Amblyrhynchus cristatus*	marine iguana	2	2	
		Genovum broilii		1	19	
		Synapsida indet.		1	9	
		Orobates		1	18	
		Pristerognathus		1	2	
		Diadectes		1	5	
		Pareiasauria		1	8	**89**
damage of surface	mammalia	*Propalaeotherium hassiacum*	Primeval horse	2	5	
		Hippotherium primigenium	Hipparion	1	2	
		Bison bison	bison	1	1	
		Canis lupus	grey wolf	5	5	
		Connochaetes taurinus	blue wildebeest	1	14	
		Giraffa camelopardalis	three-horned giraffe	1	1	
		Gorilla gorilla gorilla	western lowland gorilla	5	3	
		Propalaeotherium parvus	Primeval horse	1	1	
		Diceros bicornis	black rhinoceros	1	1	
		Equus grevyi	Grévy's zebra	1	2	
	diapsida	Diplodocidae		1	4	**43**
moulding errors	mammalia	*Candiacervus* sp.		2	2	
		Connochaetes taurinus	blue wildebeest	1	5	
		Canis lupus	grey wolf	1	1	**8**
surface covered	mammalia	*Candiacervus* sp.		5	6	
		Canis lupus	grey wolf	6	28	
		Connochaetes taurinus	blue wildebeest	1	1	
		Equus grevyi	Grévy's zebra	1	1	**36**
surface eroded	mammalia	*Canis lupus*	grey wolf	2	3	**3**
attached dirt	mammalia	*Canis lupus*	grey wolf	2	2	
		Connochaetes taurinus	blue wildebeest	1	8	
	sauropsida	*Iguana iguana*	green iguana	2	3	**13**
drill traces	diapsida/ sauropsida	*Camarasaurus*		2	5	
		Diplodocidae		1	1	
		Crocodylus sp.		1	2	**8**
ingesta-related dental surfaces	mammalia	*Equus* sp.	horse	2	48	
	sauropsida	*Crocodilus niloticus*	Nile crocodile	unknown	48	**96**

The exception from this cleaning procedure are the green iguana teeth. Those teeth were extracted from extant animals having undergone feeding experiments and were cleaned according to a cleaning protocol using 3 % NaOCl (for 2 hrs) and distilled water. Afterwards, sample were dried at 40 °C over night. Scans were either taken on the original dental surface or on moulds of the original facets (Table S1). Moulds were produced using high-resolution silicone-vinylpolysiloxane precision impression material Provil novo Light regular set EN ISO 4823, type 3, light (Heraeus Kulzer GmbH, Dormagen, Germany). Casts were produced using epoxy resin (Injektionsharz EP, Reckli GmbH, Herne, Germany). We did not choose specific sides or tooth positions; therefore, the dataset comprises both sides, teeth and facets for the mammal and reptile/synapsid species (**Table ES5.1**). The different types of post-mortem wear features are not produced on purpose and together with the great variety of different scanning positions, we are able to cover variable expressions of the different “bad” post-mortem wear features.

Scans were sorted into post-mortem feature groups, whereby multiple scans can belong to multiple groups because a dental surface can have more than one typical bad surface structure, e.g. post-mortem scratches together with adherent dirt. Altogether, nine different groups of “bad” post-mortem altered surface defects from different mammalian and reptilian taxa were compiled and compared to one sample set of unaltered *Equus* sp. (Böhm et al., 2019) and one sample set of unaltered *Crocodilus niloticus* teeth (**Table 5.1 and ES5.1**).

5.3.2 Dental microwear texture analysis

Following the protocol described in Schulz et al. (2010), a high-resolution disc-scanning confocal 3D-surface measuring system μsurf Custom (NanoFocus AG, Oberhausen, Germany) with a blue LED (470 nm) and high-speed progressive-scan digital camera (984 × 984 pixel) was used for surface measurements. A x100 long distance lens (numerical aperture 0.8) with a resolution in x, y=0.16 μm, and z=0.06 μm was used, non-overlapping 160 × 160 μm square areas were scanned per specimen. Scans with surface oriented too obliquely were rejected (i.e. vertical displacement range δz > 60 μm). MountainsMap Premium v.7.4.8676 software was used for data evaluation and we applied 3D (enamel) surface texture analysis (compare Schulz et al., 2010, 2013a, 2013b; Calandra et al., 2012) and scale-sensitive fractal analysis (SSFA) after Ungar et al. (2003) and Scott et al. (2006). Selected SSFA parameters (complexity and anisotropy) are implemented as an additional new module in MountainsMap Premium v. 7.4.8676 and are no longer analysed in the sfrax or toothfrax software as described by Ungar et al. (2003). In total, we employed two SSFA, thirty 3D-surface roughness parameters (according to ISO 25178, Schulz et al., 2013b); and fourteen motif, furrow, isotropy, and ISO 12781 (flatness) parameters (**Table S4.3**). All specimens measured are listed in the

supplements (**Table ES5.1**). Detailed description of the MountainsMap templates are included in the supplements. Scans were performed on the original dental surface and casts, or directly on the moulds of facets and dental surfaces. Therefore, all scans performed on moulds were mirrored along the z-axis.

I. Mammal template. For analysis of scans of original upper right molar and premolar teeth. Original upper left teeth were mirrored along the y-axis to obtain the same orientation as in upper right teeth. Casts are treated as original teeth. All moulded upper right teeth were mirrored along the x-axis. Lower jaw teeth were treated the same way.
II. Reptile template. This template is designed for original upper right teeth; all teeth were treated the same way. The main difference to the mammal template is the form removal based on a 4^{th} polynomial function, because the curvature on reptile teeth is stronger as compared to most mammals.

5.3.3 Statistics

Data processing and statistical analyses, including principal component analyses (PCA) were performed with the open-source software R v.4.0.0 (R. Development Core Team, 2020) using the packages xlsx (Dragulescu, 2014), rJava (Urbanek, 2016), doBy (Højsgaard and Halekoh, 2016), R.utils (Bengtsson, 2016), WRS version 0.12.1 (Wilcox and Schönbrodt, 2010), factoextra (Kassambara, 2017), plyr (Wickham, 2011), ggplot2 (Wickham, 2016), Rcpp (Eddelbuettel, 2011, 2013) and rela (Chajewski, 2009). We used only single scans and did not produce any mean or median values, as typically used in 3DST studies (e.g. Schulz et al., 2010, 2013a, b; Winkler et al., 2013, 2016, 2019a). Schulz et al. (2013a) have shown that that surface texture data of mammalian teeth are non-normally distributed and heteroscedastic, which was verified using the Shapiro-Wilk test (Shapiro and Wilk, 1965). We proceed the data using the method of Wilcox (Wilcox, 2003, 2005, 2012), with the robust heteroscedastic Welch-Yuen omnibus test (Welch, 1938; Yuen, 1974) together with a heteroscedastic pairwise comparison test (“Lincon test”, according to Dunnett's T3 test (Dunnett, 1980)). For removing outliers and for non-normality, data were trimmed (15%). Afterwards, we performed the robust heteroscedastic rank-based test in accordance with Cliff (Cliff, 1996; Schulz et al., 2013a). We compared the “good” ingesta-related ante-mortem enamel surfaces with each of the different types of “bad” post-mortem surfaces. No pairwise comparison of the different “bad” post-mortem surfaces was performed. For validation of adequacy and justification of conduction of PCAs on our data, we used the Kaiser-Meyer-Olkin test for sampling adequacy (value>0.5) and Bartlett’s test of sphericity (<0.05). PCAs were built using the function prcomp() with singular value decomposition (SVD). Detailed results for the PCAs are given in the Electronic

Supplement (**Fig. S5.1, Table S5.2**), all principal components (PCs) with standard deviation of over 1.0 are considered in the result section. We set a cut-off value of 0.4 for factor loading (Budaev, 2010), describing the most important parameters in the PCA (**Table S5.2**).

5.4 Results

A great variety of different surface or moulding defects exist (as illustrated in the photosimulations **Fig. 5.1, Fig. S5.2-S5.10**). Several types of post-mortem scratches can be found. These scratches often crosscut other wear features and can be qualitatively described as deeper and straighter than ante-mortem scratches. In contrast, cracks in the surface are not straight although they are frequently deep and wide. Surfaces with varnish residue, as well as eroded ones, result in a blurred dental surface. Adherent dirt, a covered surface and bubbles in the moulding material can produce topographic elevations which are much larger/higher than peaks caused by ante-mortem wear processes. The drill traces produced by diamond studded dill heads show pronounced, deep valleys on the surface, with several, parallel running scratches. The group which includes different kinds of surface damages of unknown origin or cause, shows very rough and unnaturally shaped surface structures in general. This category shows the broadest variability in surface structure and parameter space (**Fig. S5.6 and S5.11**).

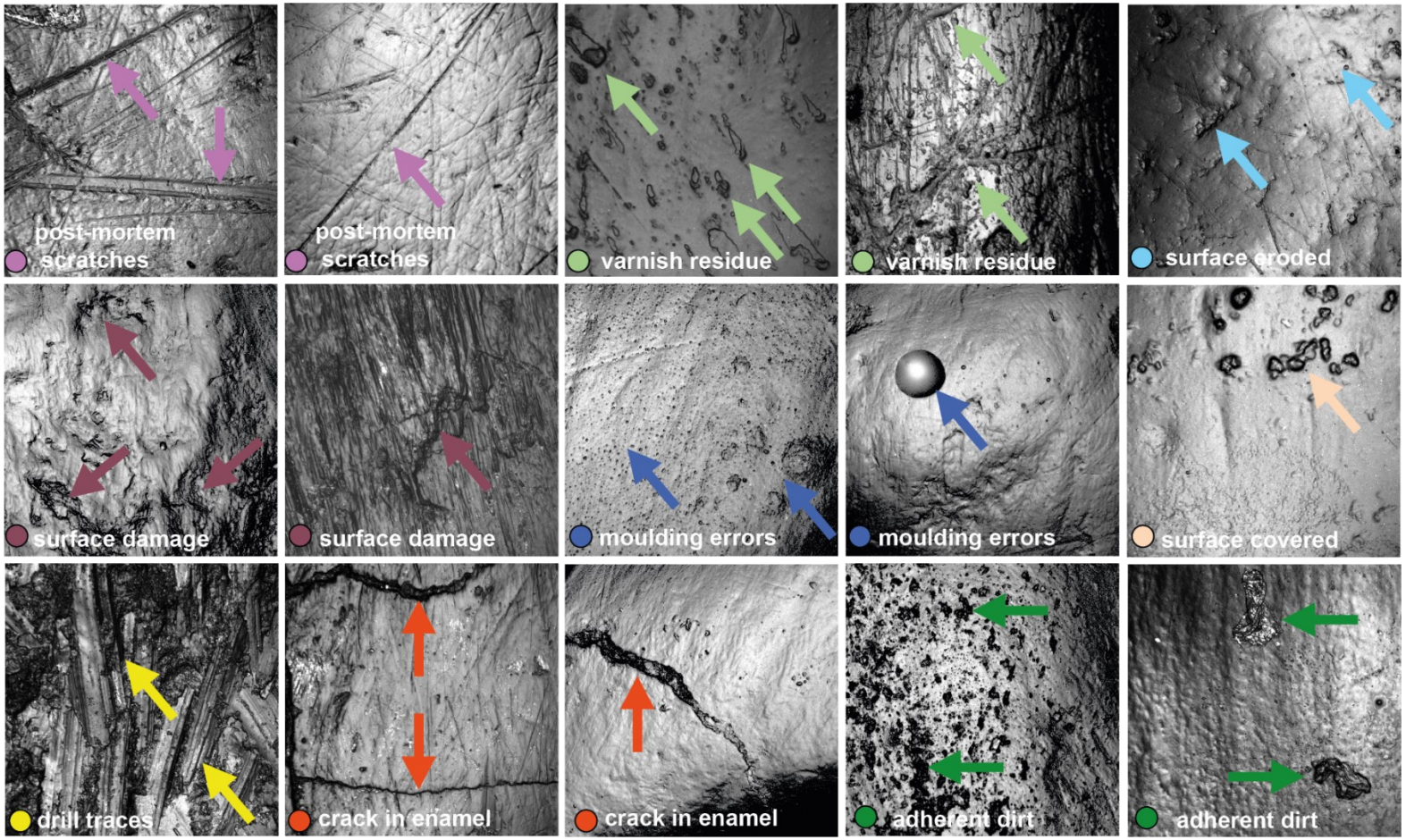

Figure 5.1. Photosimulations of enamel surface scans (160 x 160 µm) of different types of "bad" post-mortem surface textures is shown with arrows pointing to the according alteration features. These "bad" post-mortem surfaces represent examples of common naturally or anthropogenically altered surface textures due to moulding and surface defects: post-mortem scratches, varnish residue, cracks in the enamel, adherent dirt, different kinds of surface damages, drill traces (diamond studded drill bit traces from enamel sampling for isotope analysis), moulding errors (i.e. air bubbles, paraffin sweat out, detailed wear features not visible), and dental surfaces that are covered or eroded.

Table 5.2. Significant DMT parameters (p-value value in brackets derived from "Lincon" test, confirmed by Cliff's method) for the pairwise comparison of the ingesta-related "good" ante-mortem dental surfaces with the different types of "bad" post-mortem dental surfaces.

	Area	**Complexity**	**Density**	**Direction**	**Height**	**Peak sharpness**	**Plateau size**	**Slope**	**Volume**
Moulding errors	*mea* (0.011)				*Sa* (0.060), *Sq* (0.078), *Sxp* (0.086)		*Smc* (0.055)		*Vmc* (0.054), *Vv* (0.051), *Vvc* (0.118), *Vvv* (0.619)
Cracks in the enamel									
Adherent dirt	*mea* (0.699)								
Drill traces									
Post-mortem scratches									
Varnish residue	*mea* (0.024)			*epLsar* (0.005)					
Surface covered									
Surface eroded	*mea* (0.095)				*S5p* (0.039), *Sz* (0.108)	*Spc* (0.209)			
Damage on the surface	*mea* (0.011)				*Sa* (0.038), *Sz* (0.082)				*Vmc* (0.031)

All nine identified groups of “bad” post-mortem surfaces are characterised by many extreme parameter values in the surface texture parameter space (**Fig. S5.11, Table S5.3 and S5.4**). However, due to high parameter variance and the large number of outliers in the parameter groups, “bad” post-mortem surface scans cannot be unambiguously distinguished from one another. Moreover, according to the high variability of the different categories, they are hardly distinguishable from non-altered wear surfaces, although Cliff´s method displays significant differences between “good” ingesta-related and “bad” post-mortem surfaces (**Table 5.2 and S5.3-S5.4**). Cracks in the enamel, drill traces, post-mortem scratches and covered surface are not different in all parameter groups from ingesta-related dental surfaces (**Table 5.2 and S5.4**). For the mean area (*mea*) moulding errors and eroded or damaged surfaces have significantly higher parameter values than ingesta-related dental surfaces, while adherent dirt and remaining varnish is significantly lower than ingesta-related dental surfaces (**Table 5.2 and S5.4**). Remaining varnish is additionally significantly higher in *epLsar* than ingesta-related dental surfaces (**Table 5.2 and S5.4**). The complexity, density and slope parameter groups did not display any significant differences between different groups. In general, moulding errors have significantly larger height (*Sa*, *Sq*, *Sxp*) and volume (*Vmc*, *Vv*, *Vvc*, *Vvv*) parameter values than ingesta-related dental surfaces (**Table 5.2 and S5.4**), while they are lower in *Spc*. Also surface damages of unknown origin show significantly larger height (*Sa*, *Sz*) and volume (*Vmc*) parameters than “good” surface, while eroded dental surface have significantly higher *S5p* and *Spc* parameter values and lower *Sz* parameter values compared to ingesta-related dental surfaces (**Table 5.2 and S5.4**). The biplot of *medf* vs. *metf* indicates that all kinds of “bad” post-mortem surfaces cluster together with the “good”, ingesta-related dental surfaces (**Fig. 5.2A**). In general, the ingesta-related dental surface textures show relatively little variance in parameter values, while those of all other scans show a larger scatter. Importantly, however, no type of “bad” post-mortem surfaces can be clearly separated texturally from “good” (i.e. ingesta-related) surface. The scans with post-mortem scratches tend to show higher *metf* values, while eroded and covered surfaces show lower values (**Fig. 5.2A**). Drill traces show much deeper furrows (higher *metf*, **Fig. 5.2A**), as for example post-mortem scratches or cracks in the enamel, where deeper furrows are expected as well (**Fig. 5.2A**). If the enamel surface is covered with remaining varnish or glue, the parameter space nonetheless largely overlaps with that of the unaltered, ingesta-related enamel surfaces. However, values tend to have much lower *metf* values, while the scatter along the *medf* parameter increases (**Fig. 5.2A**).

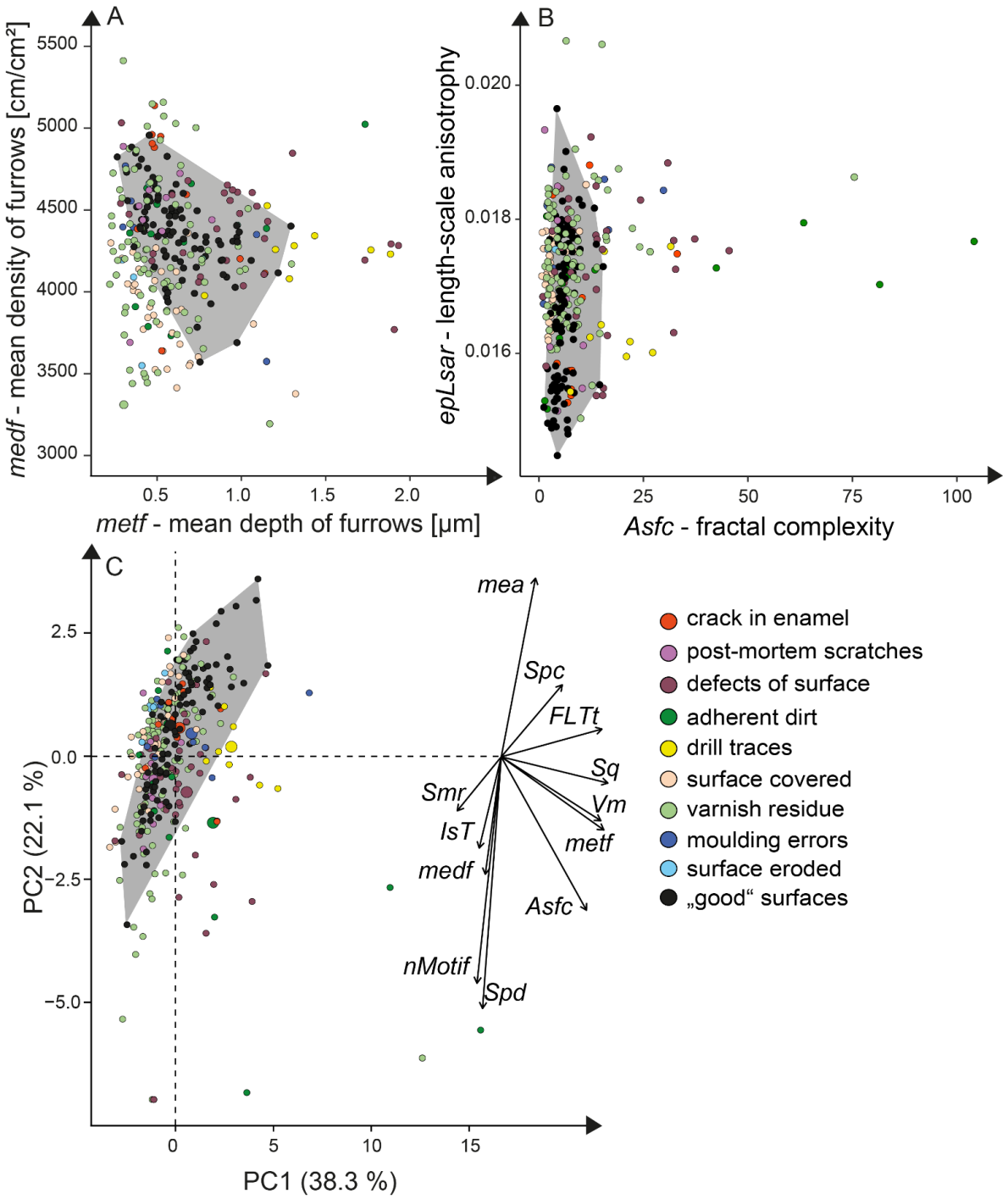

Figure 5.2. Results for the "bad and ugly" dataset. Biplot of A. *metf* (µm) versus *medf* (cm/cm²) and B. *Asfc* vs. *epLsar* for the different types of altered enamel surfaces (coloured circles) in comparison to "good", ingesta-related, well-preserved dental surface scans (black circles) that define the parameter space of ingesta-related surfaces (grey area). C. Principle component analysis (PCA) of surface texture parameters from each category (**Table S4.3**) with good separation. Large symbols in PCA plot mark the mean of the area of the different "bad" post-mortem surface categories. Note the large overlap of all categories in the three plots.

In the SSFA biplot *Asfc* vs. *epLsar*, different kinds of "bad" post-mortem surfaces display high complexity values, however, no single "bad" post-mortem surface category consistently exhibits such a high complexity for all surface scans (**Fig. 5.2B**). In a PCA with a set of 12 different parameters, the ingesta-related surfaces again show a large scatter and overlap with most "bad" post-mortem surfaces. The "bad" post-mortem surface category of drill traces and attached dirt is separated from the ingesta-related surfaces along PC1, explaining 36.8% of the variance with *Sq*, *Vm*, *FLTt* and *metf* considered to be most important (**Table S5.2**). Also, the mean area of the different types of surface defects falls outside the narrow cluster of the majority of scans (**Fig. 5.2C**). PC2 and PC3 describe 21.6 % and 11 % of the variance, but there is almost no separation possible along those two PCs. Only a covered surface is slightly separated along PC3, with isotropy (*IsT*) as best distinguishing parameter (**Table S5.2**).

5.5 Discussion

Blunders during preparation and moulding or errors during measuring of the surface and defects on the surface can be detected by eye, but predominantly still fall in the same broad parameter space as "good" ingesta-related dental surfaces. The most difficult alteration to identify by naked eye is a thin cover of translucent conservation varnish. Dental surfaces coated with varnish have a slightly blurry appearance which has the effect of "smoothing" the relief of normal wear features. In the parameter space of the biplot *metf* – *medf* varnish has a huge overlap with "good" ingesta-related surface scans (**Fig. 5.2A**). This is likely due to the variable thickness of the varnish layer and the detection of gross topography underneath the varnished surface. Most likely, if the layer is thick, wear features and most of the surface roughness can be completely obscured; but if the layer is relatively thin, however, the parameter values are almost similar to "good" ingesta-related surfaces, but slightly shifted towards a reduced depth of furrows. Complete removal of vanish from museum specimens could be a critical and challenging task sometimes, and it is difficult to ensure that all varnish is removed before moulding and measuring.

In general, shifts of parameter spaces and values are detectable for different kinds of dental surface alteration or defects/blunders, but no clear separation of those "bad" post-mortem surfaces from "good" (i.e. diet related) surfaces was possible. Especially in very fragile fossil specimens, e.g. small bubbles in moulds or casts often cannot be avoided. These small bubble-like features in casts created from silicone moulds may result from small bubbles which formed during the moulding or from transpiration of paraffin drops when the silicone is stored under high temperatures. If such minor blunders do not result in significantly different parameter values from surface without obvious defects/blunders, it may be possible to include

them to extend limited datasets. Still, it is advisable to analyse both, surfaces with visible defects/blunders, and surface showing (potentially) only diet-related traces, separately. When the "bad" post-mortem surfaces yield comparable results to the "good" ingesta-related surfaces, including them may be justified, but needs to be evaluated thoroughly on a case by case basis. By no means we want to encourage to include altered surfaces, but for small (fossil) sample sizes, inclusion might be inevitable.

We compiled published values of different dental surface parameters to establish a range of ingesta-related parameter values for small and large mammals, both from wild specimens and feeding experiments as well as for wild lepidosauria (**Table 5.3**). The lepidosauria show a much larger range in parameter values than mammals. Overall, the "good" ingesta-related surface measurements scatter a great deal. According to the high number of outliers in the dataset and the different "bad" post-mortem surface categories, we try to identify those categories which are outside the ingesta-related parameter range of extant mammals and reptiles (**Table 5.3**). The PCA shows that different parameters with factor loading over +/- 0.4, such as *Sq*, *Vm*, *Spd*, *FLTt*, *nMotif* and *metf*, can potentially help to detect ranges of different types of "bad" post-mortem surfaces (**Fig. 5.2C**). In most cases, the "bad" post-mortem surfaces show maximum parameter values that surpass those of the ingesta-related parameter space, especially for the parameters *Asfc, FLTp, metf, Sa, Shv, Smc, Sq, Sz, Vmc,* while the parameters *Spd* and *medf* vary within the literature parameter space. For *medf* the minimum values in the categories moulding errors and surface defect are much lower than for the ingesta-related parameter space (**Table 5.3**). Interestingly, the drill traces caused by enamel sampling for isotope analyses do not show higher maximum values than the published values for extant vertebrates. However, they show lower minimum parameter values thus, the range of parameter space for this "bad" post-mortem surface category is smaller than the literature range (**Table 5.3**). We combine the information about surface texture parameters from each category with good separation and factor loadings of lower -0.4 and higher 0.4 from the PCA (following Budaev, 2010) the range of published ingesta-related parameter values. For this threshold, we calculated 10 % of the mean literature value for mammals and lepidosaurs and added this 10 % to the maximum parameter value and subtracted it from the minimum parameter value (**Table 5.3**). Parameter values which exceed this threshold may potentially indicate dental surfaces that were overprinted through post-mortem mechanical and/or chemical alteration processes as they fall outside of the known ingesta-related parameter space.

Table 5.3. Compilation of published minimum and maximum parameter values for different large and small mammal species from the wild and feeding experiments as well as different extant lepidosauria compared to different categories of surface defects and errors. Based on these literature values a threshold for "good", ingesta-related parameter values for mammals and lepidosauria was defined. n.a. = not available, min = minimum parameter value, max = maximum parameter value. For parameter description see Table S4.3. Parameter values in the different surface categories, which greatly exceed literature range are highlighted in bold, whereby the "bad" post-mortem surface categories moulding errors, surface covered, surface eroded, adherent dirt and surface damages are mostly compiled on mammalian data and are compared to the mean of the mammal studies, while the "bad" post-mortem surface categories remaining varnish, cracks in the enamel, post-mortem scratches and drill traces mostly compiled reptile data and are compared to the study of Winkler et al., 2019b.

Data	**Taxon**	***Asfc***		***FLTp* [µm]**		***IsT* [%]**		***medf* [cm/cm²]**		***metf* [µm]**		***Sa* [µm]**	
		min	max	min	max	min	max	min	max	min	max	min	max
Catz et al. 2020*	*Rangifer tarandus*	0.394	5.36	n.a.	n.a.	n.a.	n.a.	n.a.	n.a.	n.a.	n.a.	n.a.	n.a.
Ackermans et al. 2020	*Ovis aries*	0	25	n.a.	n.a.	n.a.	n.a.	4050	4800	0.3	0.9	0.3	1
Schulz et al. 2019*	*Pan troglodytes verus*	n.a.	n.a.	0.44	4.98	17	79	1840	3003	0.1	1.1	0.1	1.3
Hullot et al. 2018*	*Diceros bicornis, Ceratotherium simum, Dicerorhinus sumatrensis, Rhinoceros unicornis , Rhinoceros sondaicus*	0.32	10.51	n.a.	n.a.	n.a.	n.a.	n.a.	n.a.	n.a.	n.a.	n.a.	n.a.
Kubo et al. 2017 *	*Cervus nippon*	3.56	7	n.a.	n.a.	n.a.	n.a.	n.a.	n.a.	n.a.	n.a.	0.6	1.3
Schulz et al. 2013a	*Connochaetes taurinus, Diceros bicornis, Equus grevyi, Giraffa camelopardalis*	n.a.	n.a.	0	2.2	20	75	4400	5400	0.2	1.2	0.1	1.1
mean of large mammal studies		1	14	0	4	18	77	3430	4401	0	1	0	1
Robinet et al. 2020	caviomorphs (Rodentia)	0.12	8.87	n.a.	n.a.	n.a.	n.a.	n.a.	n.a.	n.a.	n.a.	n.a.	n.a.
Winkler et al. 2019bb*	*Cavia porcellus*	n.a.	n.a.	n.a.	n.a.	n.a.	n.a.	n.a.	n.a.	n.a.	n.a.	n.a.	n.a.
Winkler et al. 2016	*Rattus rattus*	n.a.	n.a.	n.a.	n.a.	n.a.	n.a.	n.a.	n.a.	n.a.	n.a.	0.1	0.4
mean of small mammal studies		0.12	8.87	n.a.	n.a.	n.a.	n.a.	n.a.	n.a.	n.a.	n.a.	0.1	0.4
mean of mammal studies		1	13	0	4	18	77	3430	4401	0	1	0	1
moulding errors	only mammalia	1.09	29.45	1.02	8.79	21.07	77.83	2042	4783	0.29	3.29	0.37	2.86
surface covered	only mammalia	0.45	11.04	0.21	156.06	9.3	91.14	3380	4659	0.14	100.33	0.1	79.79
surface eroded	only mammalia	1.95	3.98	0.8	1.85	61.69	73.03	3540	4171	0.3	0.41	0.37	0.53
attached dirt	mostly mammalia	1.43	103.47	0.59	11.97	9.15	80.95	3676	5026	0.3	5.47	0.27	4.19
surface defects	mostly mammalia	0.98	74.75	0.28	15.59	8.62	88.72	3181	5034	0.17	4.19	0.12	2.74
Winkler et al. 2019a*	Lepidosauria	0.4	41.19	0.38	9.16	5.52	86.21	2825	5447	0.19	1.23	0.13	1.42
varnish	mostly synapsids	1.49	74.75	0.33	15.59	9.02	89.37	3181	5413	0.22	4.19	0.13	2.74
cracks in the enamel	more reptilia	3.31	32.82	0.75	4.61	5	57.99	3638	5140	0.39	1.12	0.26	1.59

post-mortem scratches	more reptilia	1.39	10.61	0.61	16.3	70.77	0.79	3704	4890	0.3	0.83	0.15	0.51
drill traces	only reptilia	7.55	31.53	2.36	11.08	69.84	2.17	3978	4528	0.78	1.89	0.58	1.36
preliminary threshold from	mammals	0.9	14	0.2	3.95	16.56	84.7	3087	4841	0.19	1.18	0.23	1.11
literature	lepidosauria	0.36	45.3	0.34	10.07	4.97	94.83	2542	5991	0.17	1.36	0.12	1.57

Table 5.3. (continued)

Data	**Taxon**	***Shv* [µm³]**		***Smc* [µm]**		***Spd* [1/µm²]**		***Sq* [µm]**		***Sz* [µm]**		***Vmc* [µm³/µm²]**	
		min	max	min	max	min	max	min	max	min	max	min	max
Catz et al. 2020*	*Rangifer tarandus*	n.a.	n.a.	n.a.	n.a.	n.a.	n.a.	n.a.	n.a.	n.a.	n.a.	n.a.	n.a.
Ackermans et al. 2020	*Ovis aries*	n.a.	n.a.	0.4	1.6	n.a.	n.a.	n.a.	n.a.	n.a.	n.a.	0.3	1.1
Schulz et al. 2019*	*Pan troglodytes verus*	1	87	0.2	1.7	0	0.022	0.174	1.798	1.513	13.334	0.1	1.3
Hullot et al. 2018*	*Diceros bicornis, Ceratotherium simum, Dicerorhinus sumatrensis, Rhinoceros unicornis , Rhinoceros sondaicus*	n.a.	n.a.	n.a.	n.a.	n.a.	n.a.	n.a.	n.a.	n.a.	n.a.	n.a.	n.a.
Kubo et al. 2017 *	*Cervus nippon*	5	24	0.94	2	0	0	0.84	1.6	5.61	9.65	0.6	1.4
Schulz et al. 2013a	*Connochaetes taurinus, Diceros bicornis, Equus grevyi, Giraffa camelopardalis*	0	20	0.25	1.45	0	1.7	0.25	1.5	n.a.	n.a.	0	1
mean of large mammal studies		2	44	0	2	0	1	0	2	4	11	0	1
Robinet et al. 2020	caviomorphs (Rodentia)	n.a.	n.a.	n.a.	n.a.	n.a.	n.a.	n.a.	n.a.	n.a.	n.a.	n.a.	n.a.
Winkler et al. 2019bb*	*Cavia porcellus*	0	2	n.a.	n.a.	0.01	0.04	0.15	0.55	1	5	0.1	0.5
Winkler et al. 2016	*Rattus rattus*	n.a.	n.a.	0.1	0.6	n.a.	n.a.	0.1	0.5	n.a.	n.a.	0.1	0.4
mean of small mammal studies		0	1.5	0.1	0.6	0.01	0.04	0.13	0.53	1	5	0.1	0.45
mean of mammal studies		1	33	0	1	0	0	0	1	3	9	0	1
moulding errors	only mammalia	0.5	94.34	0.61	4.52	0	0.02	0.5	3.42	5.06	18.17	0.39	3.21
surface covered	only mammalia	0.07	10.9	0.14	110.57	0	0.03	0.14	111.26	1.13	826.69	0.08	1.27
surface eroded	only mammalia	0.48	4.45	0.58	0.95	0	0.01	0.46	0.69	2.66	9.49	0.43	0.55
attached dirt	mostly mammalia	0.49	33.15	0.38	6.81	0	0.06	0.38	5.71	3.49	44.14	0.25	4.34
surface defects	mostly mammalia	0.19	14.1	0.18	3.82	0	0.06	0.17	3.99	1.57	28.31	0.12	2.53
Winkler et al. 2019a*	Lepidosauria	0.1	327.76	0.22	2.17	0	0.01	0.16	1.89	1.86	30.74	0.14	1.52
varnish	mostly synapsids	0.18	13.63	0.22	3.82	0	0.06	0.17	3.99	1.74	28.57	0.14	2.53
cracks in the enamel	more reptilia	1	26.21	0.39	2.98	0	0.01	0.34	2.06	3.42	17.63	0.25	1.94
post-mortem scratches	more reptilia	0.76	3.95	0.23	0.79	0	0.02	0.21	0.69	2.21	6.76	0.15	0.5
drill traces	only reptilia	4.07	9.34	0.89	2.17	0	0.01	0.87	1.82	9.67	22.51	0.5	1.41
preliminary threshold from	mammals	1.34	36.43	0.34	1.63	0	0.49	0.27	1.32	2.44	10.26	0.19	1.06
literature	lepidosauria	0.09	360.54	0.2	2.39	0	0.01	0.15	2.08	1.68	33.81	0.13	1.67

Nevertheless, it was still not possible to find a single surface parameter or combination of parameters to clearly and unambiguously identify altered dental surfaces of any specific kind. Therefore, the observed surface alteration defects cannot be clearly distinguished via the selected texture parameters as proxies for alteration, even though such surface alteration features are readily visually identified by the naked eye and a threshold might give information about the validity of a given surface. The mismatch between visual and DMTA identification of altered enamel surfaces might be due to the fact that alteration defects do not cover the whole enamel surface scan area in many cases. Often, especially when only a few suspicious scratches or one enamel crack are present, the good surface area covers more than 80%. The majority of ISO parameters evaluate the whole surface and report a mean value (e.g. *Sa* – mean surface roughness), therefore the importance of small, altered areas, may be less preponderate. Moreover, all "bad" post-mortem surfaces included in this study were treated like "good" ingesta-related surfaces, i.e. subjected to the same post-scanning filtering protocol. This includes several filters to remove noise, non-measured points, and outliers. The impact of non-diet related surface artefacts is therefore minimized by the filtering routine, and only extreme alterations can be seen in the parameter values, obscuring minor defects.

Still the trained eye of an experienced user is able to differentiate easily between different ingesta-related ("good") and taphonomically altered ("bad") surfaces, such as post-mortem scratches, cracks, drill traces, dirt, or bubbles in moulds. Even if the presence of most defects/blunders may be negligible, it is still desirable to be aware of their presence, so that the researchers are aware of potential effects on their data. This differentiation can be difficult, therefore, experience in surface texture analysis as well as a representative reference database of badly preserved/altered enamel surfaces is necessary. Where DMTA is used, such a database of good and bad surfaces is needed during the training of new unexperienced users as well as a helpful reference tool for experienced users. Here, we provide an example and we would like to encourage other working groups to start collecting and share data, to enlarge the exemplary database and provide an resource for DMTA for various laboratory and measurement systems. We want to encourage a discussion about what is the best way to share cross-laboratory DMT data and scans. As reliability of dental wear studies hugely benefits from assessing intra-species or intra-population variation, the volume of DMTA data expands continuously. It is our vision and hope that standards for data quality control could and need to be established beyond the borders of individual working groups and measurement systems to train future generations of researchers and foster data exchange. Consequently, this would allow as a logical next step for the future direction of dental microwear research to establish and share large databases of this type to facilitate "big data" analysis. Big data analysis can use various approaches, e.g. using machine learning or neural network algorithms on artificially produced surface textures in order to detect patterns of surface

textures of fossil taxa. Training neural networks could also be an option to detect those suspicious alteration features visible to the naked eye, but not detectable by the currently available DMT parameters. Furthermore, other computer algorithms, e.g. machine-learning approaches could facilitate diet reconstruction in identifying diet characteristics as well as altered surface features to identify wear patterns that are beyond parameter values.

5.6 Conclusions

Surface texture parameter values of altered dental surfaces often cannot be unambiguously distinguished from ingesta-related ante-mortem wear by DMTA. This is due to the surface texture parameter values of post-mortem altered textures often falling within the same parameter space as ingesta-related ante-mortem wear. Thus, there seems to be no single surface texture parameter and no specific set of parameters that can be used as alteration proxies to sort out altered “bad” surfaces using the DMTA method itself. However, it was possible to set thresholds for some DMT parameters, based on literature values for the surface parameter space of “good” ingesta-related enamel surfaces. This helps to identify at least strongly altered dental surface areas and exclude them after measurement. Even if surface damage due to cracks or post-mortem scratches or the impact of attached dirt seems to be minor, it is still strongly recommended to exclude such altered surfaces from DMTA, even if they share a similar parameter space with well-preserved specimens. This will ensure the best possible DMTA results. In general, an experienced DMTA user can more easily and quickly visually distinguish between “good” and “bad” enamel surfaces than software. Ideally, teeth or enamel surface areas with alteration artefacts or defects should be excluded by experienced researchers directly before measurement and DMTA rather than a post-hoc using the surface texture parameters themselves. However, if a small amount of enamel surface scans with unavoidable blunders during preparation slip through the sort out process, they do not seem to reduce the sample quality massively.

5.7 Acknowledgment

This project has received funding from the European Research Council (ERC) under the European Union's Horizon 2020 research and innovation programme (grant agreement No 681450) and the Max-Planck Graduate Center. We thank Jennifer Leichliter (Johannes Gutenberg-University Mainz, Germany) for proofreading the manuscript and Jean-Michel Male (Pierre Latte Fermes aux Crocodile, Lyon) for the dental material.

5.8 Supplement

Operators used in MountainsMap template:

Mammal template

1. Orientation of dental surface with LS-surface using subtraction
2. Noise-cancelling median filter (5 x 5) and Gaussian filter (3 x 3)
3. Filling of non-measured points
4. Threshold to reduce height and depth using the material-% (0.5-99.5 %)
5. Soft strength removal of isolated outliers, outliers at the edge and with a maximum allowed inclination (85°)
6. Form removal using a 2nd order polynomial.

Reptile template

1. Orientation of dental surface with LS-surface using subtraction
2. Noise-cancelling median filter (5 x 5) and Gaussian filter (3 x 3)
3. Filling of non-measured points
4. Threshold to reduce height and depth using the material-% (0.5-99.5 %)
5. Soft strength removal of isolated outliers, outliers at the edge and with a maximum allowed inclination (85°)
6. Form removal using a 4th order polynomial.

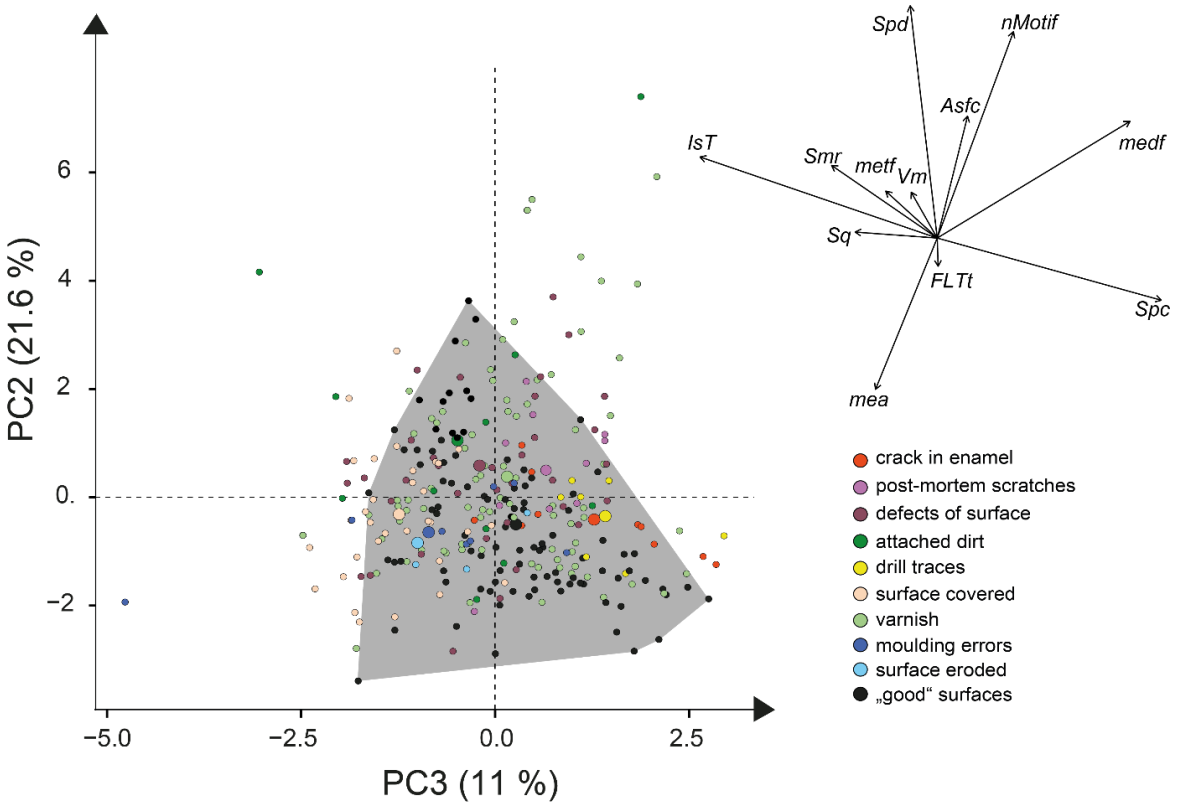

Figure S5.1. Principle component analysis (PC2 and 3) for the “bad and ugly” dataset of surface texture parameters from each category (**Table S4.3**) with good separation. Large symbols in PCA plot mark the mean of the area of the different “bad” post-mortem surface categories. Note the large overlap of all categories.

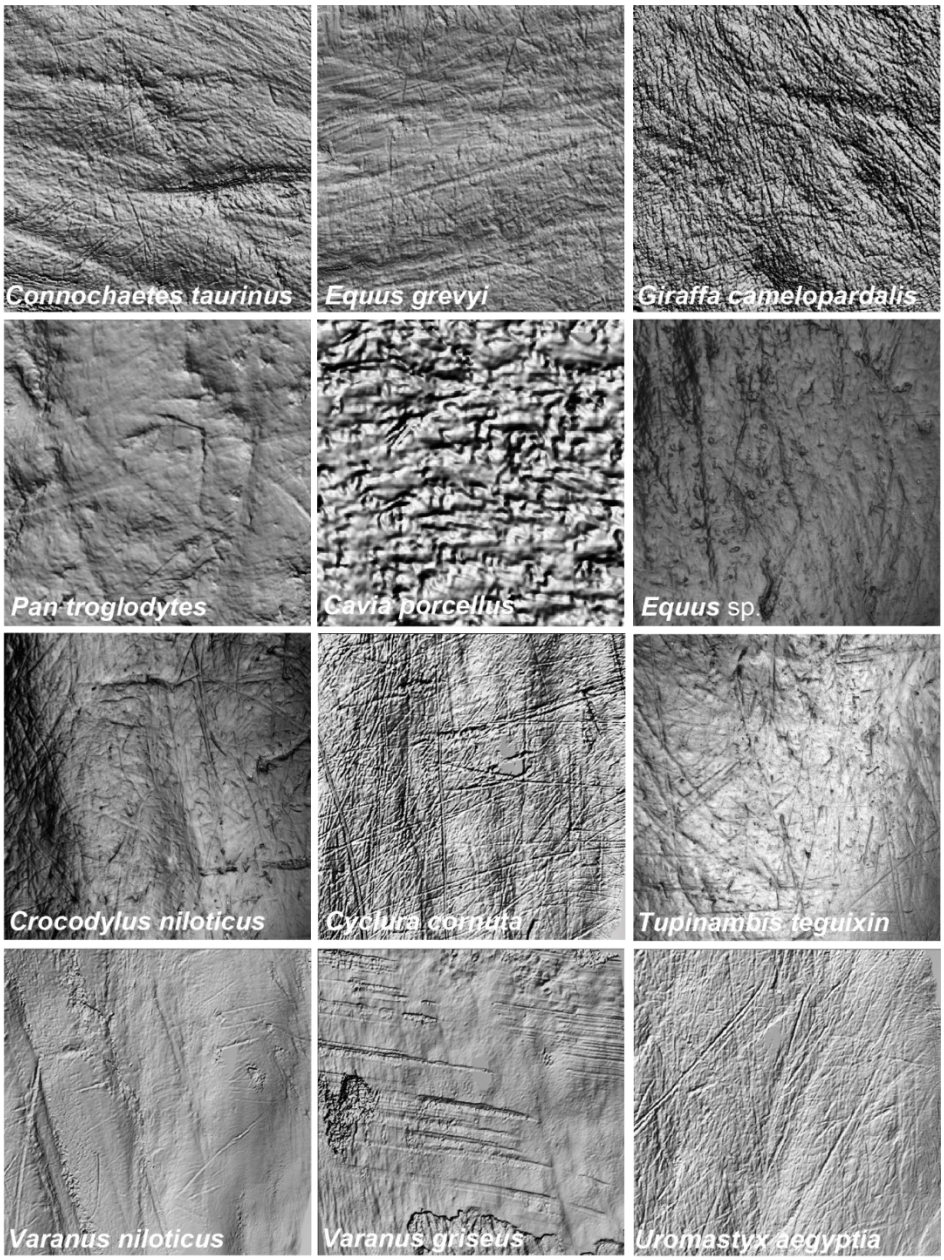

Figure S5.2 Exemplary photosimulations of "good" diet-related enamel surface scans (160 x 160 µm if not mentioned otherwise). Large mammals: *Connochaetes taurinus*, *Giraffa camelopardalis*, *Equus grevyi* (Schulz et al., 2013a); primates: *Pan troglodytes* (Schulz-Kornas et al., 2019); small mammals (scan size 60 x 60 µm): *Cavia porcellus* (Winkler et al., 2019a); comparison for this study: *Equus* sp. (Böhm et al., 2019), *Crocodylus niloticus*; lepidosaurs: *Cyclura cornuta, Tupinambis teguixin, Varanus niloticus, Varanus griseus, Uromastyx aegyptia* (Winkler et al., 2019b). Note that some reptile species have very pronounced scratches, which are considered to be ante-mortem, since their enamel is very thin. Especially in faunivorous taxa, scratches are often aligned at almost 90° towards the tooth apex, and likely result from a pulling/tearing motion during prey capture. If only one deep scratch is present, and is aligned differently from the main texture pattern, this is likely a sign of post-mortem wear (compare **Fig. S9**).

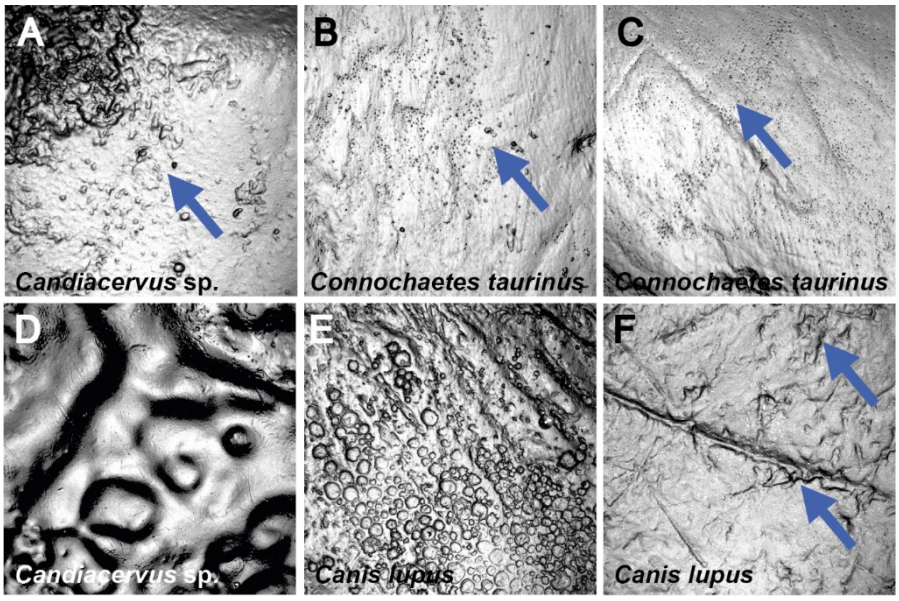

Figure S5.3. Exemplary photosimulations of enamel surface scans (160 x 160 µm) of moulding errors are shown. In A–C. a large number of small air bubbles are included in the silicone. These small bubbles are expressed as dark dots, lower in the moulds, with sharp edges. In D–F. the first two scans show larger bubbles and places, where the moulding material did not cover the dental surface perfectly. In the last scan of *Canis lupus*, two different defects are visible, a large post-mortem scratch, as well as moulding material, which deliver a more blurry dental surface.

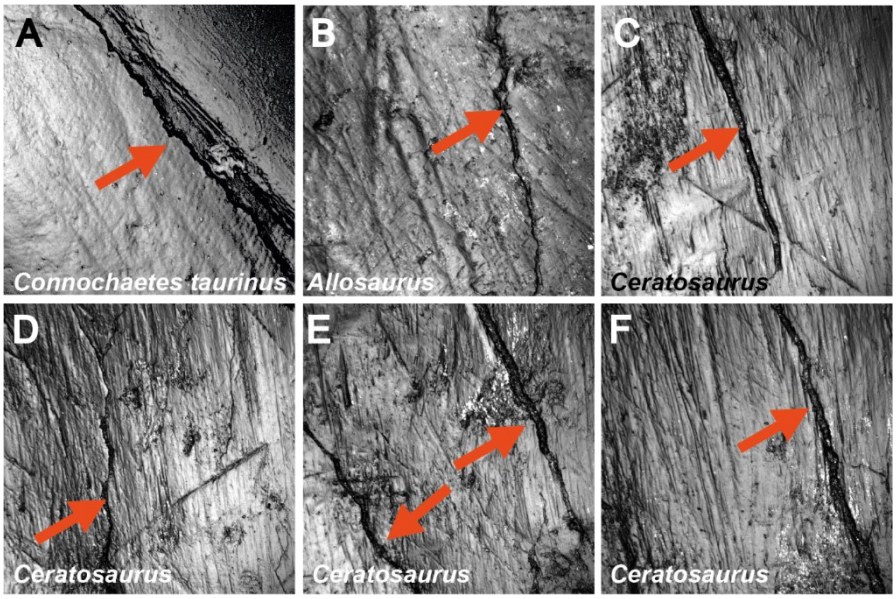

Figure S5.4. Exemplary photosimulations of enamel surface scans (160 x 160 µm) of cracks in the enamel are shown. This type of surface defect is often the case in fossil material, especially in dinosaurs with thin enamel layers (B–F), Cracks are relatively large, long and show “frayed” edges.

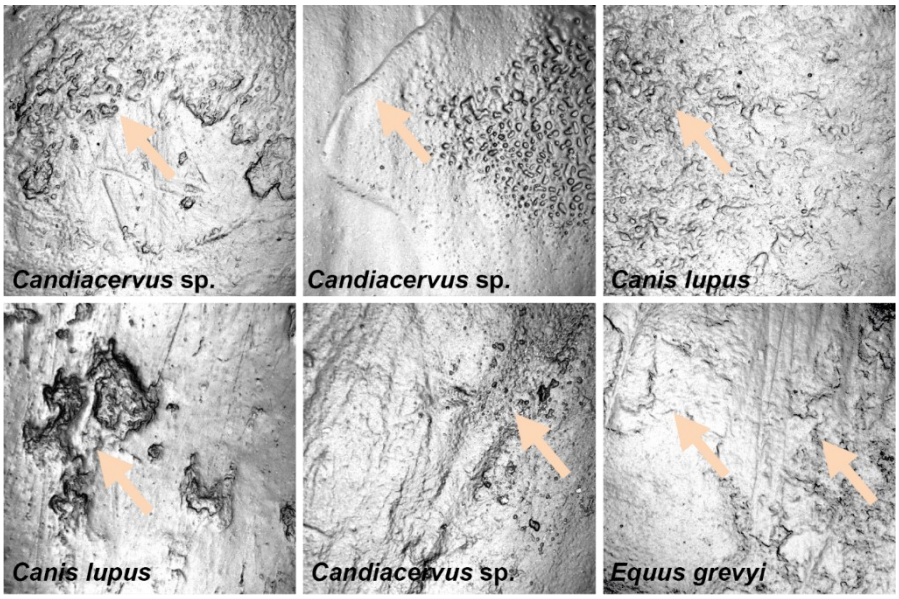

Figure S5.5. Exemplary photosimulations of enamel surface scans (160 x 160 µm) of dental surfaces that are covered with substances of unknown origin are shown. These moulded specimens show partly extensive thin or thick covers of the surface, moulded in form of elevations. This category can be also mistaken for moulding errors.

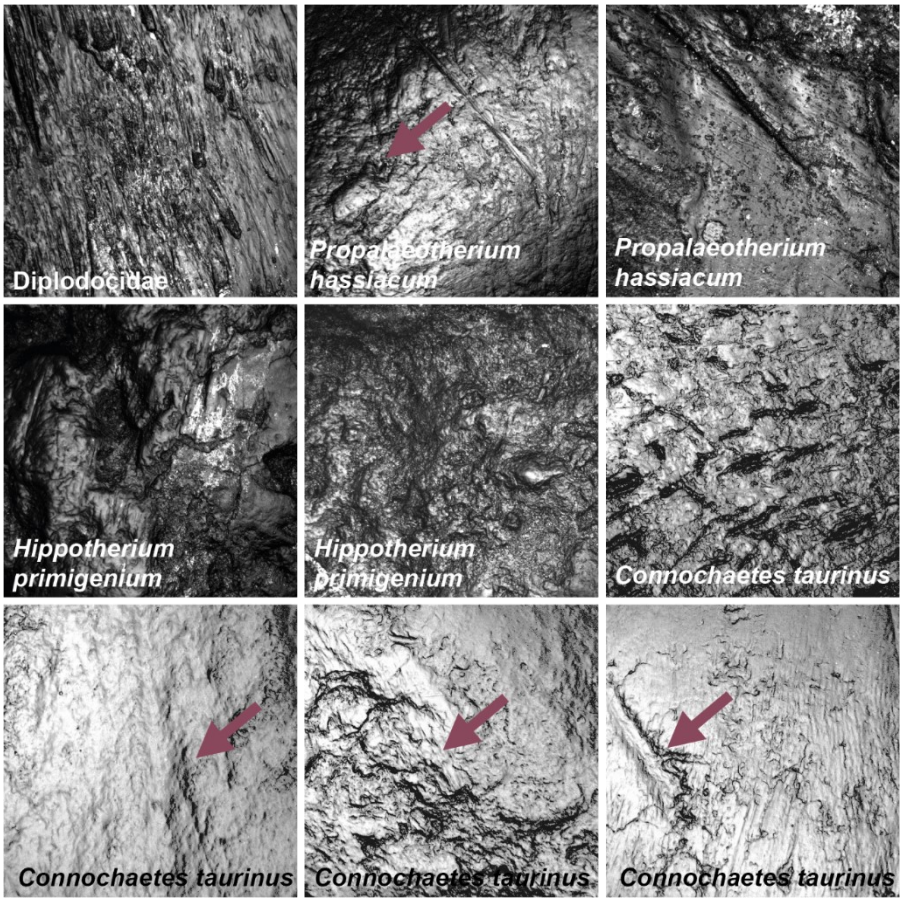

Figure S5.6. Exemplary photosimulations of enamel surface scans (160 x 160 µm) of different kind of surface damages are shown. This category shows very rough surface, partly large

dales in the dental surface. The dental surfaces are looking generally strange and post-mortem.

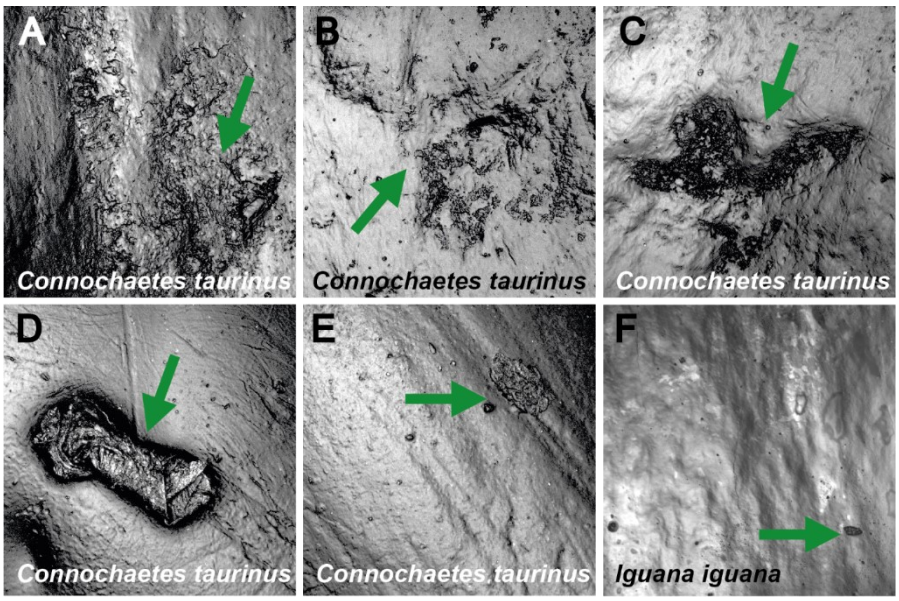

Figure S5.7. Exemplary photosimulations of enamel surface scans (160 x 160 µm) of adherent dirt are shown. This category also shows a great variety of different expressions. A. and C. shows large, extensive layers of some kind of dirt. D. and F. shows only single, small bits of attached dirt, expressed as little dark dots. Similar to bubbles, dirt on the dental surface in moulds is lower, while it is elevated on original dental surfaces. It mostly has sharp edges and could be clearly separated from wear features B. and E. are showing really large, single bits of dust or maybe frays from the cleaning procedure. Those extreme features are easily distinguishable from normal wear features according to their enormous size.

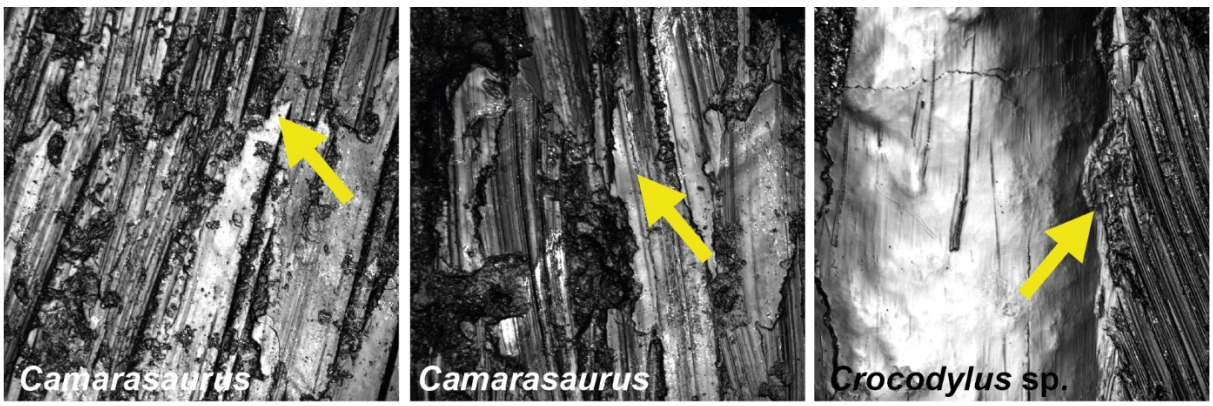

Figure S5.8. Exemplary photosimulations of enamel surface scans (160 x 160 µm) of drill traces (diamond studded drill traces from enamel sampling for isotope analysis) are shown. This kind of post-mortem wear is very unusual and shows parallel straight and deep scratches on the dental surface.

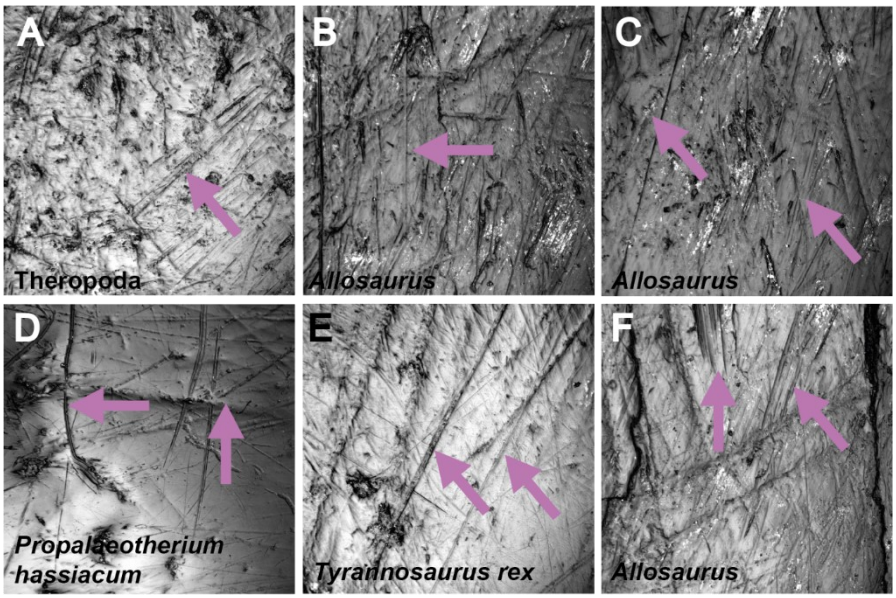

Figure S5.9. Exemplary photosimulations of enamel surface scans (160 x 160 µm) of post-mortem scratches are shown. This category has a great variety of different expressions and is sometimes hardly to describe and differentiate from ante-mortem, ingesta-induced scratches. Post-mortem scratches can be relatively small, however, still deeper and straighter than the surrounding ante-mortem wear features (A). They can also be very long, deep and straight and crossing all ingesta-related wear features. (B–D, F). In E. several short, but parallel post-mortem scratches are shown, crossing ingesta-related wear features.

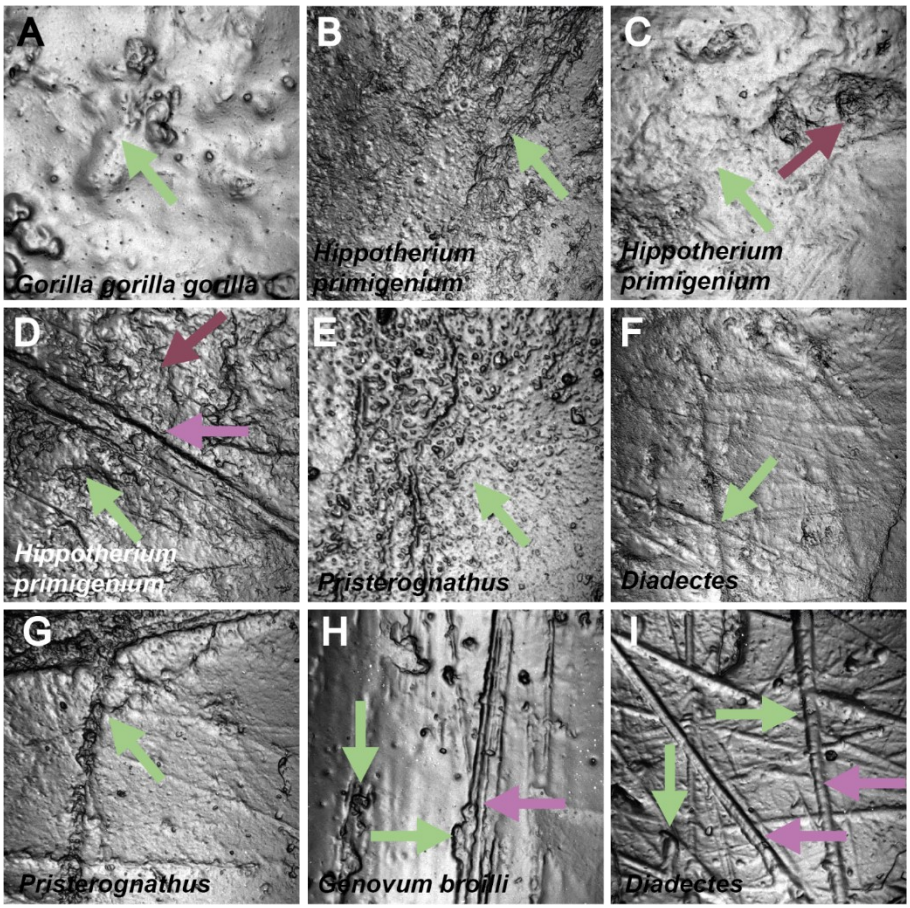

Figure S5.10. Exemplary photosimulations of enamel surface scans (160 x 160 µm) of varnish residue are shown. This category can be difficult to identify and describe. It can also include different other post-mortem alteration features, such as post-mortem scratches (D, F, G–I), or surface damages of unknown source (C–D). In general, the dental surface appears to be blurred, wear features are not as clear as without a varnish cover. Depending on the thickness of the varnish layer, the ingesta-related wear features disappear completely (A).

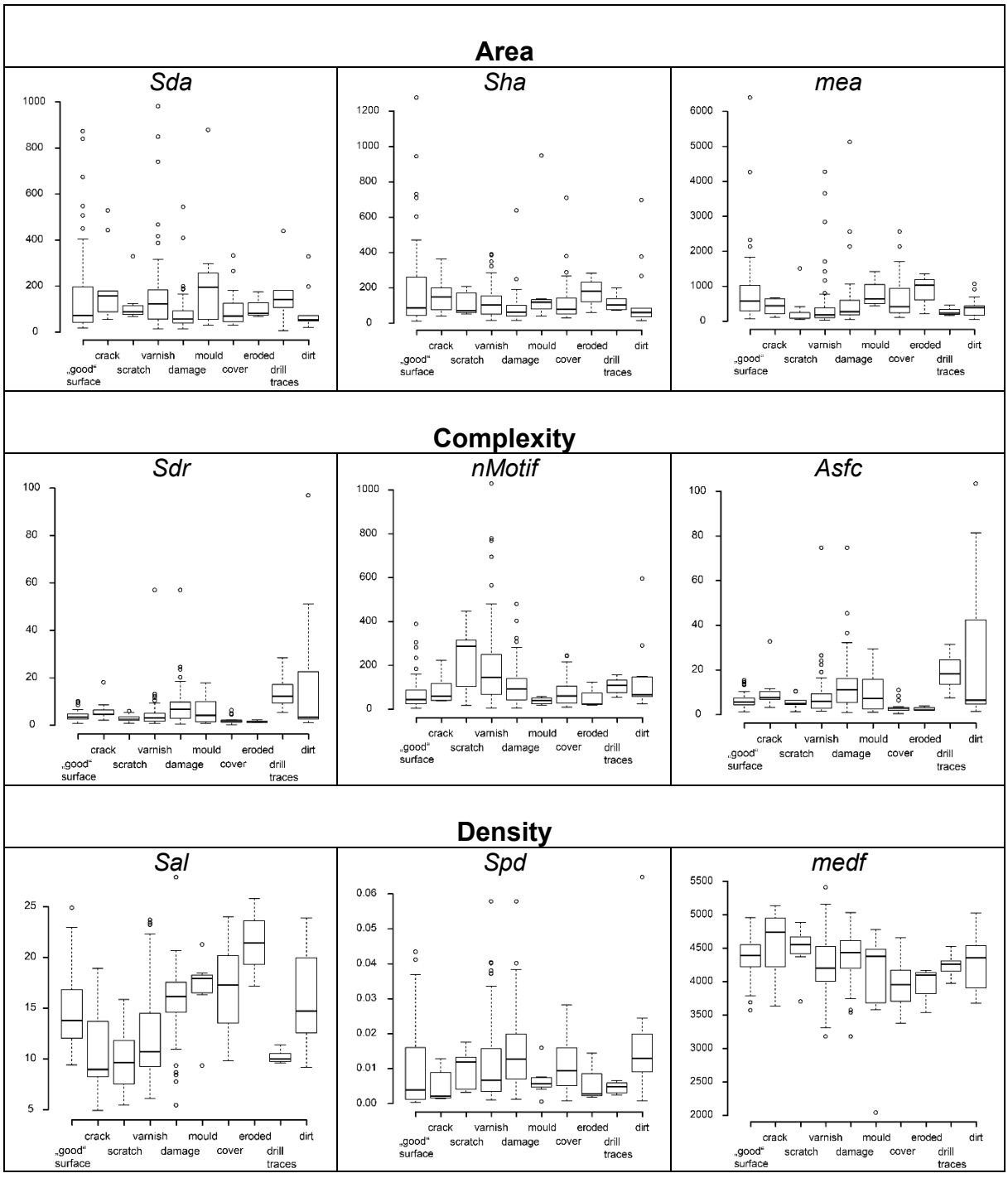
Area
Sda
Sha
mea
Complexity
Sdr
nMotif
Asfc
Density
Sal
Spd
medf
„good“ surface
crack
scratch
varnish
damage
mould
cover
eroded
drill traces
dirt

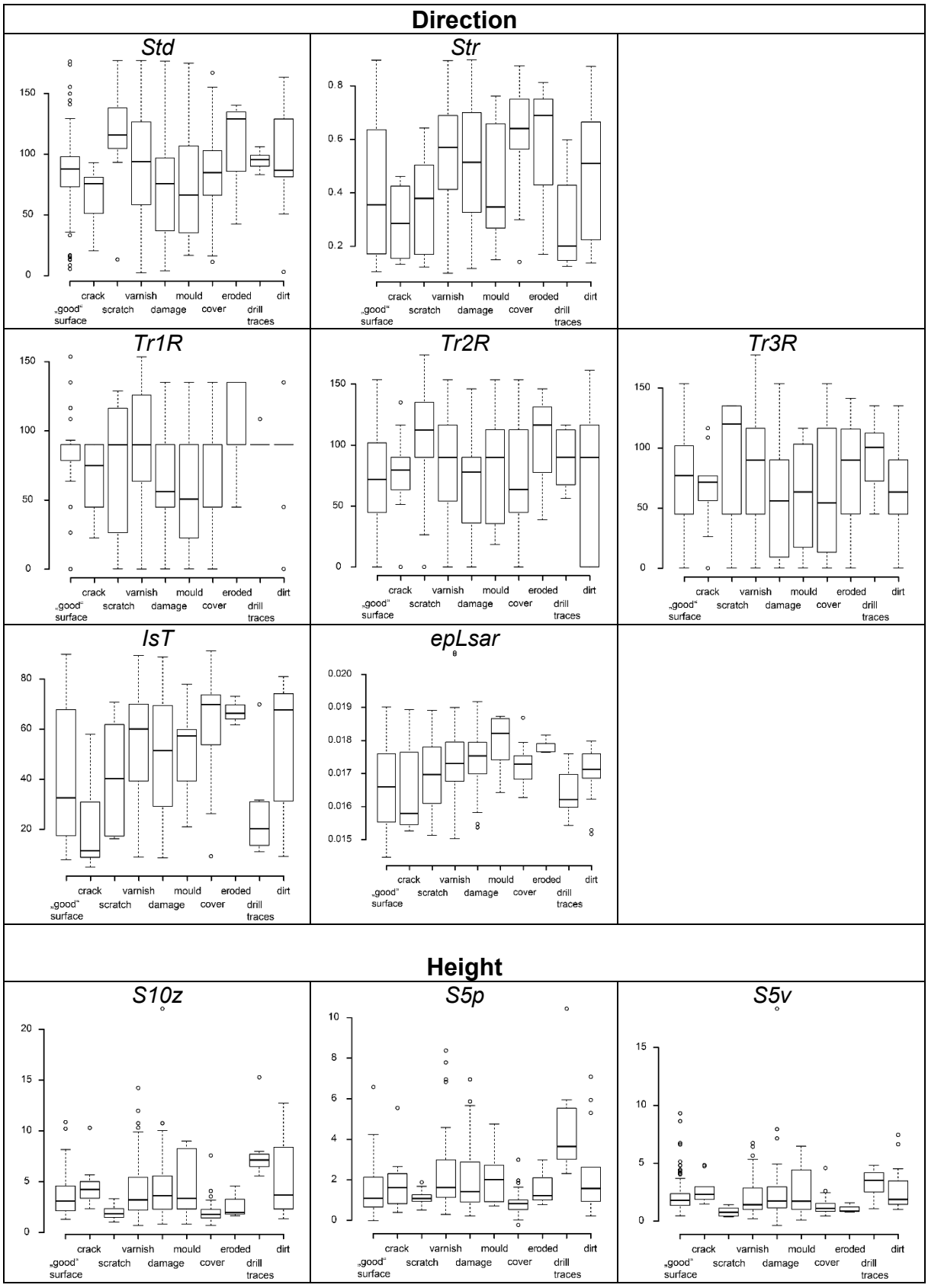
Direction
Std
Str
Tr1R
Tr2R
Tr3R
IsT
epLsar
Height
S10z
S5p
S5v
„good" surface
crack
scratch
varnish
damage
mould
cover
eroded
drill traces
dirt

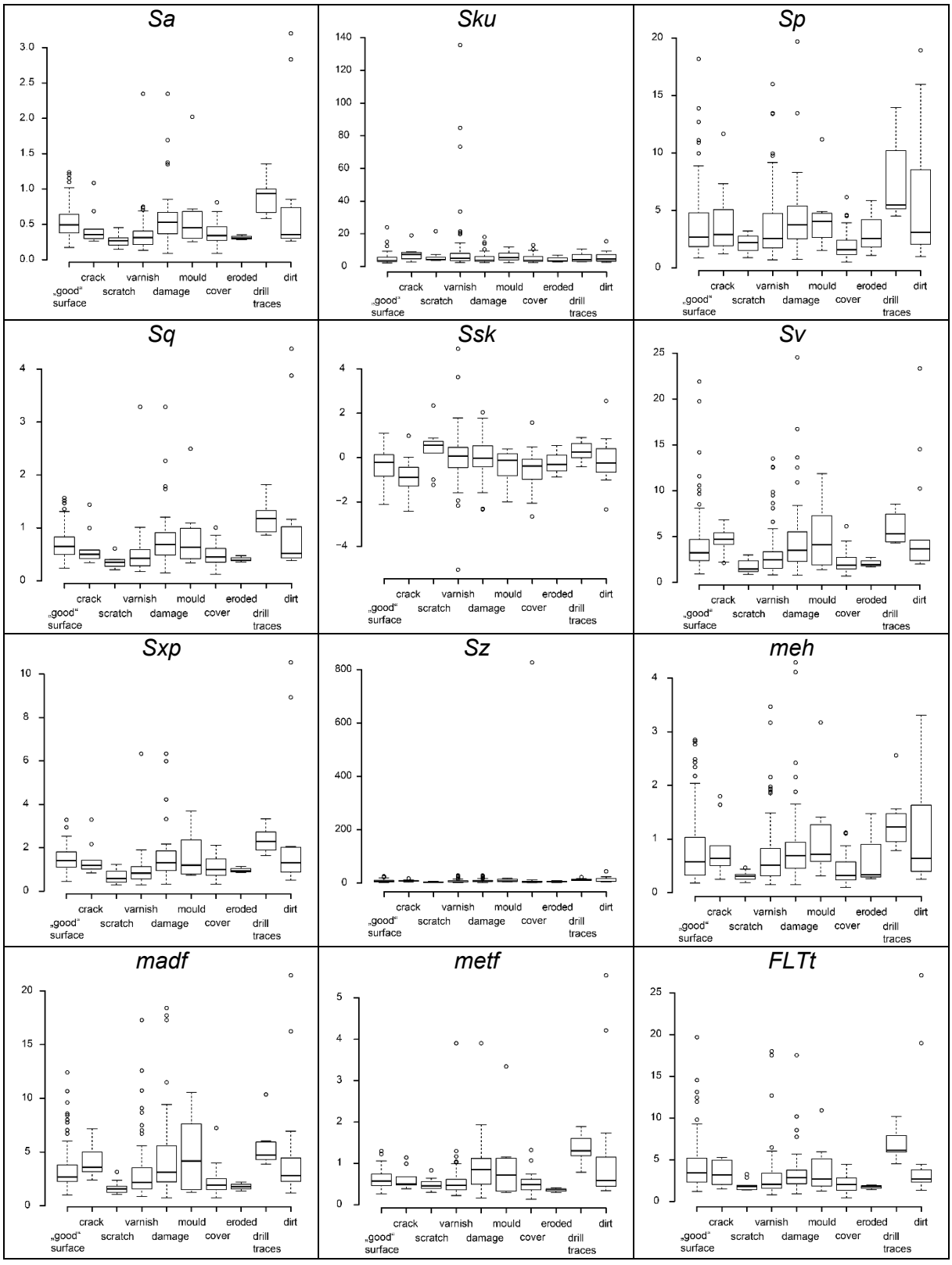
Sa
Sku
Sp
Sq
Ssk
Sv
Sxp
Sz
meh
madf
metf
FLTt
„good“ surface
crack
scratch
varnish
damage
mould
cover
eroded
drill traces
dirt

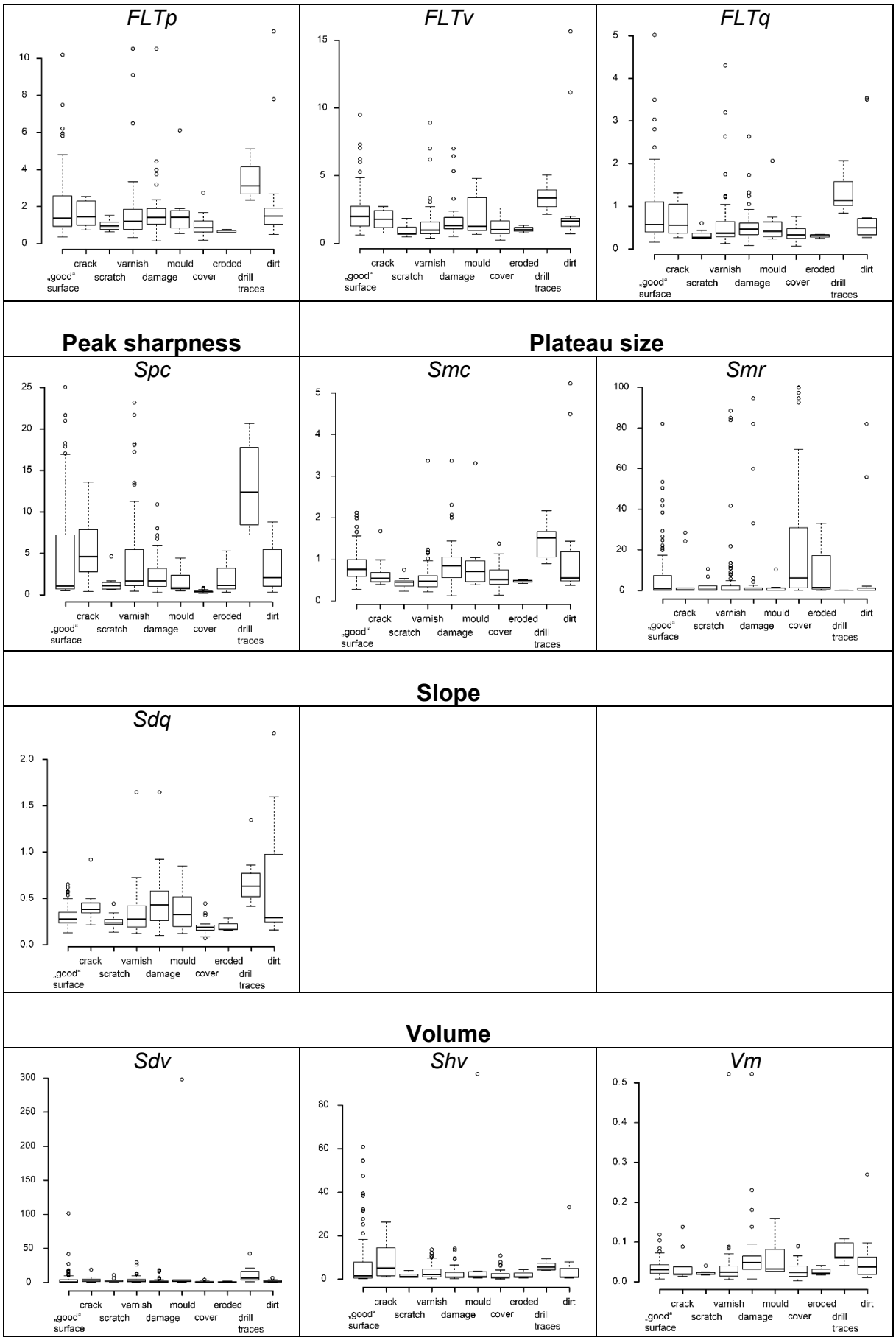
FLTp
FLTv
FLTq
Peak sharpness
Plateau size
Spc
Smc
Smr
Slope
Sdq
Volume
Sdv
Shv
Vm
„good" surface
crack
scratch
varnish
damage
mould
cover
eroded
drill traces
dirt

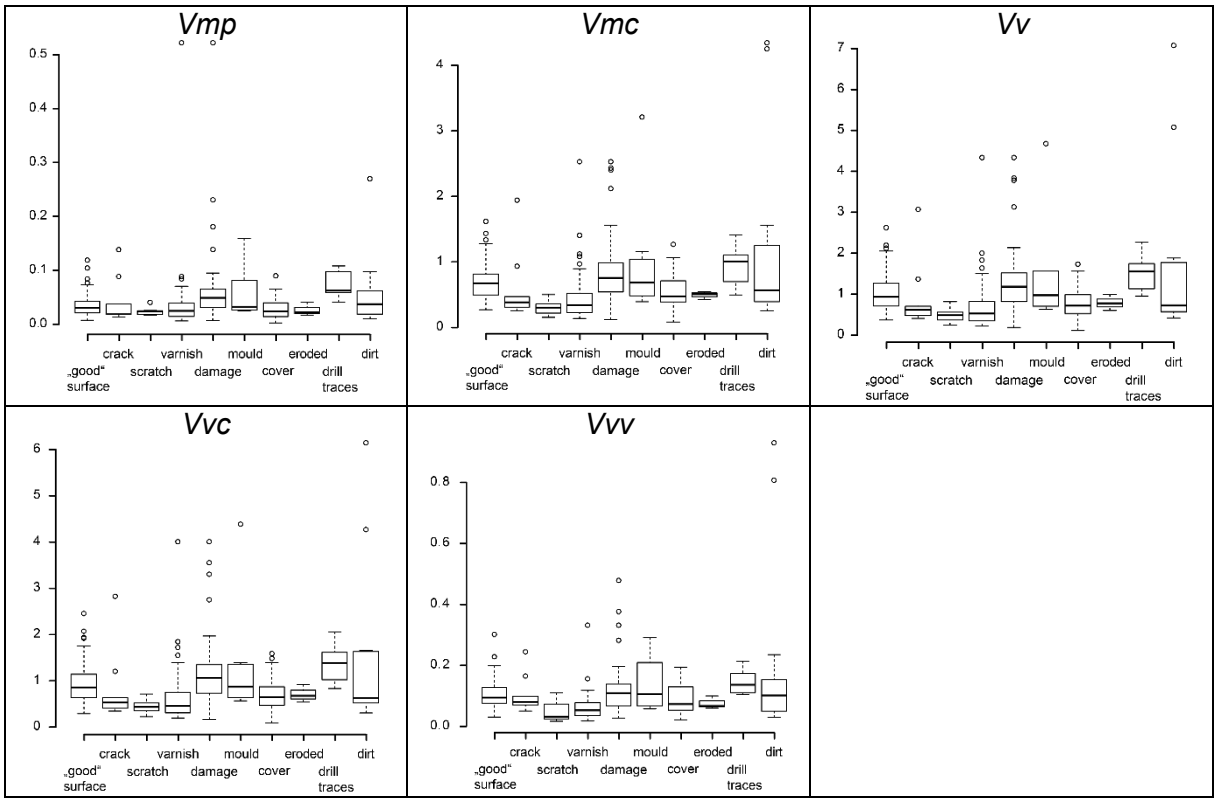

Figure S5.11. Boxplots for all dental microwear texture parameters for the “bad and ugly” surfaces. The thick horizontal bar represents the median; the box encloses the first (25%) and third (75%) quartiles; the whiskers extend to 1.5 times the length of the box (the interquartile range); the small open circles represent outliers.

Table ES5.1. Type of defect, class, taxon and amount of scans per specimen and number of total scans per “bad and ugly” surface category. n.a. = information not available. Table is found in the electronic supplement.

Table S5.2. Importance of components for PCA from the different types of altered enamel surfaces and the "good", well-preserved dental surface scans using 12 DMT parameter (*Smr, medf, Spd, nMotif, Asfc, Spc, metf, Vm, Sq, FLTt, IsT, mea*). Factor loadings for the parameter values are represented in line 8-19.

	PC1	**PC2**	**PC3**	**PC4**	**PC5**	**PC6**	**PC7**	**PC8**	**PC9**	**PC10**	**PC11**	**PC12**
Standard deviation	2.102	1.611	1.148	0.966	0.916	0.828	0.650	0.512	0.480	0.415	0.284	0.205
Proportion of Variance	0.368	0.216	0.110	0.078	0.070	0.057	0.035	0.022	0.019	0.014	0.007	0.003
Cumulative Proportion	0.368	0.584	0.694	0.772	0.842	0.899	0.934	0.956	0.975	0.990	0.997	1.000
Sq	-0.445	0.015	-0.196	0.077	-0.060	0.093	-0.091	0.177	-0.214	-0.101	-0.520	-0.616
Smr	0.172	0.177	-0.252	-0.036	-0.884	-0.237	0.023	-0.079	-0.111	0.131	0.004	-0.007
Vm	-0.411	0.112	-0.062	-0.006	-0.051	0.162	-0.050	-0.810	0.312	-0.006	0.140	-0.104
Spd	0.028	0.565	-0.065	0.111	-0.049	0.070	0.022	0.311	0.646	-0.357	-0.104	0.051
Spc	-0.213	-0.151	0.534	-0.148	-0.066	-0.659	0.221	-0.031	0.261	0.007	-0.256	-0.048
FLTt	-0.435	-0.069	0.002	0.105	-0.126	-0.167	0.064	0.175	-0.254	-0.582	0.555	0.067
nMotif	0.079	0.502	0.182	-0.044	0.112	0.116	0.709	-0.152	-0.381	-0.021	-0.027	-0.092
mea	-0.109	-0.368	-0.147	0.674	-0.105	0.118	0.500	0.075	0.219	0.197	-0.031	0.095
metf	-0.447	0.114	-0.123	-0.134	-0.020	0.072	-0.017	0.038	-0.174	0.081	-0.388	0.748
medf	0.055	0.284	0.459	0.656	-0.040	-0.058	-0.422	-0.132	-0.247	0.019	-0.087	0.080
Asfc	-0.380	0.297	0.072	-0.045	0.038	-0.032	-0.064	0.332	0.070	0.676	0.406	-0.129
IsT	0.063	0.197	-0.565	0.205	0.403	-0.636	-0.016	-0.143	-0.072	0.048	0.000	0.008

Table S5.3. Descriptive statistics (mean ±SD) for all DMT parameters for the “bad and ugly” surfaces (see **Table S4.3**). Specimens of *Equus* sp. and *Crocodilus niloticus* are unaltered and compiled as diet-related "good" surface, see Table ES5.1. Table is found in the electronic supplement.

Table S5.4. Statistical results (p-values) for pair-wise comparison in all DMT parameters for diet-related “good” surface scans and all different categories of “bad and ugly” surface scans (see **Table ES5.1**). For parameter description, see Table S4.3. Significant p-values derived by Welch-Yuen test ($p < 0.05$) are highlighted in bold. Significant differences between pairs (by “Lincon’s” test) confirmed by Cliff’s method are highlighted in bold. Table is found in the electronic supplement.

Chapter 6 Manuscript IV: Dental microwear texture analysis on extant and extinct sharks: Ante - or post-mortem tooth wear?

Dental microwear texture analysis on extant and extinct sharks: Ante - or post-mortem tooth wear?

Weber, Katrin[1]; Winkler, Daniela E.[1,2]; Kaiser, Thomas M.[2]; Žigaitė, Živilė[3]; Tütken, Thomas[1]

[1]Applied and Analytical Palaeontology, Institute of Geosciences, Johannes Gutenberg University, Mainz, Germany. daniela.winkler@uni-mainz.de, tuetken@uni-mainz.de

[2]Center of Natural History (CeNak), University of Hamburg, Hamburg, Germany. thomas.kaiser@uni-hamburg.de

[3]Department of Organismal Biology, Uppsala University, Uppsala, Sweden. zivile.zigaite@ebc.uu.se

A similar version of this paper is in Press in *Palaeogeography, Palaeoclimatology, Palaeoecology, Available online 24 November 2020, 110147.*

6.1 Abstract

Sharks are apex-predators that play an important role in past and present aquatic food webs. However, their diet - especially in extinct species - is often not well constrained. Dental microwear texture analysis (DMTA) has been successfully applied to reconstruct diet and feeding behaviours of different aquatic and terrestrial vertebrates. However, unlike in mammals, food-to-tooth contact in sharks is rather limited because only larger prey is manipulated before swallowing. Together with a fast tooth replacement rate, this reduces wear on individual teeth. Here, we present an explorative study of dental microwear texture on extant and extinct sharks to test whether ante-mortem wear is related to ingested diet or habitat preferences and resistant to post-mortem alteration processes. Shark teeth from 24 modern species and 12 fossil species from different localities were measured. As an additional comparison, extant shark teeth of *Carcharhinus plumbeus* were tumbled in sediment-water suspensions to simulate post-mortem mechanical alteration by sediment transport. Only three of the twelve extant shark species with three or more specimens had significantly different dental surface textures. Furthermore, no clear relation between food or habitat preferences and ante-mortem dental wear features was detected for this sample set. Tumbling modern shark teeth with siliciclastic sediment of four different grain size fractions led to increasing complexity of the dental surface. Fossil specimens resemble these experimentally altered shark teeth more in complexity and roughness. Thus, fossil shark teeth seem to display either very different (e.g. harder) diet-related wear or a strong degree of post-mortem alteration. Based on our restricted sample size, dental wear of shark teeth does overall not seem to simply reflect dietary differences; hence, it is difficult to use DMTA as reliable dietary reconstruction, in either extant nor extinct sharks.

6.2 Introduction

Sharks (Galeo- and Squalomorphs) belong to the subclass Elasmobranchii, which has a complex and long evolutionary history (Compagno, 1990; Maisey et al., 2004; Wilga et al., 2007). After the Late Devonian mass extinction, the subclass diversified and radiated quickly and become the oceanic apex-predators during the Carboniferous (Wilga et al., 2007; Long, 2011; Maisey, 2012). Sharks themselves evolved during the Lower Jurassic and after a loss of genera during the end of the Cretaceous, they again radiated during the Lower Palaeocene, reaching a high diversity during the Eocene (Guinot et al., 2012; Maisey, 2012). Today, there are around 500 extant shark species (Compagno, 1990).

Still, relatively little is known about the ecology of sharks and their dietary preferences are not well constrained beyond the fact that most sharks are zoophagous, with a few exceptions (e.g. Leigh et al., 2018). Dietary information for extant sharks are predominantly

derived from stomach content analyses (e.g. Ellis and Musick, 2006; Sommerville et al., 2011; Espinoza et al., 2015), field observations (e.g. Ebert, 1991; Klimley, 1994), tooth morphology (e.g. Tricas and McCosker, 1984; Simpfendorfer et al., 2001; Markaida and Sosa-Nishizaki, 2010), bite marks from shark attacks on prey remains (e.g. Ehret et al., 2009; Bianucci et al., 2010) and stable isotope analyses of (hard-)tissues (Vennemann et al., 2001; Hussey et al., 2012; Žigaitė and Whitehouse, 2014; Churchill et al., 2015; Martin et al., 2015a). For fossil sharks, information on feeding behaviour is sparse; fossilized stomach contents are rarely preserved (e.g. Kriwet et al., 2007). In general, sharks are rarely fossilized because unlike bony fish they have a less mineralized cartilaginous skeleton. In contrast, shark teeth are highly mineralized, and are thus often well preserved as fossils. The teeth consist of an enameloid layer of fluorapatite on top of dentin (Enax et al., 2012, 2014). Shark enameloid has similar hardness values as compared to mammalian enamel (Whitenack et al. 2010), which is composed of hydroxylapatite and also usually well preserved in the fossil record. As sharks have a revolver dentition and permanently replace their teeth, shark teeth are very common in the fossil record. Although taxonomy based on the morphology of isolated shark teeth sometimes yields controversial results, the shape and serration of fossil teeth nonetheless provides taxonomic information (e.g. Adnet and Cappetta, 2001; Straube et al., 2007) and can show significant differences between species (Shimada, 2005; Marramà and Kriwet, 2017). Although tooth morphology can also be a useful proxy for diet reconstruction, this method is hampered by several different factors. For instance, individuals of the same species of modern elasmobranchs can have nearly the same tooth morphology, although consuming a different diet, and, conversely, the same diet can be consumed by different species with varying tooth morphologies (Tricas and McCosker, 1984; Simpfendorfer et al., 2001; Markaida and Sosa-Nishizaki, 2010). Furthermore, when teeth of extinct species are compared to extant species, tooth morphology may be similar but differs in main features, such as presence or absence of cusplets or serration characteristics (Welton and Farish, 1993; Purdy et al., 2001). Bite marks on fossil prey bones, as proxy for diet reconstruction in extinct sharks, can be difficult to assign to specific species (Kent, 2018). However, stable isotope analysis of carbon and nitrogen isotopes (Hussey et al., 2012; Tamburin et al., 2020) as well as calcium isotopes (Martin et al., 2015a) in shark teeth can yield information about the diet ingested and their trophic level in food webs.

Dental microwear texture analysis (DMTA) is also a well-established, powerful dietary proxy for mechanical food properties of the last meals. Abrasion and/or attrition cause material loss and wear features at the µm-scale on the enamel surface (Dahlberg and Kinzey, 1962). DMTA has successfully been applied to differentiate dietary groups in mammalian herbivores (e.g., grazer and browser; Schulz et al., 2010; Fraser and Theodor, 2011; Calandra and Merceron, 2016) and carnivores (e.g. Schubert et al., 2010; DeSantis et al. 2012, 2015, 2017;

Stynder et al., 2019). The diet-related enamel microwear texture of mammal teeth seem to be not significantly changed by mechanical diagenetic alteration during sediment transport, at least for sandy substrates as demonstrated experimentally (Böhm et al., 2019). This is encouraging for application of DMTA on fossil teeth. So far, DMTA has mainly been performed on extant and fossil terrestrial mammalian species and has only recently been applied to reptiles (Bestwick et al, 2019; Winkler et al., 2019a), aquatic mammals (Purnell et al., 2017) and fish (e.g. Purnell et al., 2012; Purnell and Darras, 2016; McLennan, 2017).

However, there are potential issues with DMTA on shark teeth. Shark species with broad, serrated teeth, such as great whites, tear or cut chunks of flesh from large prey. Those teeth are also suitable for cracking hard items, such as turtle shells. Species with long, pointed teeth, like the sandtiger shark, use their teeth to quickly grab and swallow smaller prey (e.g. Lucifora et al., 2001; Ferrara et al., 2011). Some shark species like the nurse shark have conical or flattened teeth for crushing crustaceans or molluscs. Similarly, molariform teeth, found in e.g. *Heterodontus*, are for crushing and grinding prey (e.g. Whitenack and Motta, 2010). However, no mammal-like true chewing takes place in sharks, resulting in only brief tooth-to-prey contact. This limits the food-to-tooth contact and hence dental wear. Another potential issue is the fast tooth replacement rate (again reducing food-to-tooth contact), which varies between different shark species (e.g. 8-10 days in lemon shark (*Negaprion brevirostris*; Moss, 1967), a few weeks in leopard shark (*Trikias semifasciata*; Reif et al., 1978), or up to several months in great white shark (*Carcharodon carcharias*; Fraser and Thiery, 2018). The replacement rate is also related to different parameters such as ontogeny, diet type, and frequency of feeding events (Fraser and Thiery, 2018) and is unknown for extinct species (Strasburg, 1963; Litvinov et al., 1983; Overstrom, 1991). Therefore, cross-species comparison might be problematic, because the degree of dental wear can vary even for the same diet or within the same species, depending on the time period during which the teeth were in use. Moreover, tooth position could affect tooth-to-food contact (Purnell et al., 2012). It can be difficult or sometimes impossible to assign and sample the same tooth position for isolated fossil shark teeth, as is common practice when sampling mammalian dentitions for DMTA. Tooth replacement and reduced food-tooth contact also occur in many reptiles, nevertheless, DMTA was successfully applied for diet inference (Bestwick et al., 2019; Winkler et al., 2019a). However, tooth replacement rate in sharks is potentially faster and feeding categories are more general than in reptiles. This could challenge the application of DMTA on extant shark species. Independent of tooth position and replacement rate, mechanical alteration during post-mortem transport processes, especially in high-energy depositional environments, such as sandy or rocky shores with breaking waves, could play a major role in potential alteration or even complete overwriting possible ante-mortem wear patterns on shark teeth. A single study (McLennan, 2017) explored the use of DMTA on fossil and modern shark

teeth and found a relationship between distinct ingested diets and dental wear on enameloid surfaces in two different modern populations of *Carcharias taurus* nonetheless. Sharks from the Sea Life London Aquarium, who received a diet of whole 'white fish' and occasional tropical fish (*Caranx* sp.), could be clearly separated from sharks captured in the western Atlantic, which presumably fed on a more diverse, mostly unknown diet. McLennan also postulates that there is diet-related ante-mortem wear preserved on fossil *Carcharodon carcharias* and *Carcharocles megalodon* teeth. Similarly, a 2D microwear study using stereomicroscopy to count the number of ante-mortem scratches on fossil teeth of the Carboniferous shark *Edestus minor* found a relationship between abundance and orientation of scratches near the tooth apex to hunting and feeding behaviour (Itano, 2019).

Here, we perform an explorative study to test the applicability of DMTA for determining diet in sharks by analysing extant, fossil, and experimentally altered extant shark tooth specimens. To quantify dental wear on shark teeth we employ two different DMTA methods: scale-sensitive fractal analysis (SSFA) and 3D surface texture analysis (3DST). The aim was to assess if the teeth of extant sharks with known dietary habits have characteristic, diet-related surface textures and if such diet-related dental wear features are still preserved in fossil shark teeth. First, extant shark teeth from known tooth positions within complete jaws from wild caught collection specimens were analysed to test for the influence of tooth position on wear features along the upper and lower jaw, as well as to compare textures from buccal and lingual sides of the same teeth. Second, tooth specimens from the same species but from individuals of different ontogenetic stages were compared. A third dataset of extant shark species generated by these analyses was then employed as a reference framework to assess dietary differences. Fourth, we performed a taphonomic experiment with siliciclastic sediments of four different sediment grain size fractions (very fine sand, 51-168 µm; fine sand, 112-292 µm; medium sand, 221-513 µm: fine gravel, 2-8 mm) and different tumbling time periods (from 0.5 to 336 h) using the setup of Böhm et al. (2019), in order to simulate the effect of sediment transport on dental wear features of modern sandbar shark (*Carcharhinus plumbeus*) teeth. Finally, a set of isolated fossil shark teeth from different species and depositional settings were measured, to infer whether taphonomic transport processes overprinted ante-mortem wear features.

6.3 Material and methods

All tooth samples were cleaned with tap water to remove dust and any adhering dirt, ethanol and acetone to remove organic remains and potential glue and varnishes sometimes applied to museum specimens.

6.3.1 Modern shark tooth dataset

The modern dataset comprises 89 teeth from 24 shark species of different ontogenetic stages and sizes (**Table 6.1, Table ES6.1**). The DMTA was directly performed on the original tooth surface for teeth in smaller jaws and single teeth (aquarium specimens), while for specimens with larger jaws, teeth were moulded using high-resolution silicone-vinylpolysiloxane precision impression material Provil novo Light regular set EN ISO 4823, type 3, light (Heraeus Kulzer GmbH, Dormagen, Germany).

The modern shark teeth were used for three main aims of this study, including testing the:

I. *Influence of tooth position on DMT.* For this purpose, multiple teeth along the buccal side of the complete first, functional upper tooth row (see **Fig. 6.1**) of six specimens belonging to four different species were scanned and analysed to assess the variance of the dental surface texture among teeth along the jaw. One sample specimen was measured directly on the original enameloid, while the remaining five specimens needed to be moulded due to their large jaw size. Additionally, some lower jaw teeth and a few lingual tooth sides were also scanned for the moulded samples (Supplement **Table ES6.1**).

II. *Influence of ontogeny on DMT.* For the species *Galeocerdo cuvier* it was possible to obtain central teeth from three different ontogenetic stages, classified according to jaw and body size (Lowry et al., 2009) as juvenile (n = 4, all from Florida, U.S.A.), mid-age (n = 5, three from Florida, U.S.A., two from south-east Asia) and adult (n = 2, unknown origin). This sub-dataset is used to exemplarily assess the range of DMT for shark teeth from individuals of different ontogenetic ages.

III. *Influence of diet on DMT.* One central upper tooth was measured on the buccal side per specimen and included in further analyses. The buccal side was favoured due to practical reason, the lingual side is often difficult to reach, since the space between the in-use tooth row and the second row is often narrow. First, dental surface textures of modern wild specimens, with a diverse and mostly unknown diet were compared with those of modern aquarium sharks from the Blackpool Sea Life centre, which were fed with a mixed shrimp and white fish pellet-based diet. From this diet type, no wear features are expected for the aquarium specimens. Additionally, for all modern wild shark species with three or more teeth analysed, literature information regarding their respective food spectra and habitat were compiled (**Table 6.2**) and compared to DMT parameter values of the same species. For *Galeocerdo cuvier*, the four juvenile

specimens were excluded from the diet reference frame dataset. These data were then used as a reference framework for assessing the diets of fossil sharks (**Table 6.3**).

Table 6.1. Shark taxon, number and type of modern specimen. All wild specimens are included in the modern wild dataset, which is compared to the modern aquarium dataset (including all aquarium specimens) and to the fossil dataset (including all fossil specimen, **Table 6.3**). Note that when testing for diet differences, only extant species represented by 3 or more specimens were included.

Taxon	Common name			n	DMT reference frame for		
					Diet	Ontogeny	Tooth position
Alopias vulpinus	common thresher	wild	jaw	3	x		
Carcharhinus brevipinna	spinner shark	wild	jaw	2			
Carcharhinus falciformis	silky shark	wild	jaw	6	x		
Carcharhinus galapagensis	galapagos shark	wild	jaw	3	x		
Carcharhinus leucas	bull shark	wild	jaw	2			2
Carcharhinus obscurus	dusky shark	wild	jaw	3	x		
Carcharhinus plumbeus	sandbar shark	aquarium	single teeth	15			
Carcharhinus sorrah	spot-tail shark	wild	jaw	10	x		1
Carcharias taurus	sand tiger shark	aquarium	single teeth	2			
Centrophorus granulosus	gulper shark	wild	jaw	3	x		
Galeocerdo cuvier	tiger shark	wild	jaw	11	x	11	2
Hemipristis elongata	snaggletooth shark	wild	jaw	1			
Isurus oxyrinchus	shortfin mako shark	wild	jaw	2			
Isurus paucus	longfin mako shark	wild	jaw	1			
Mustelus manazo	starspotted smooth-hound	wild	jaw	10	x		
Negaprion sp.	lemon shark	wild	jaw	1			
Prionace glauca	blue shark	wild	jaw	3	x		1
Rhizoprionodon acutus	milk shark	wild	jaw	1			
Rhizoprionodon sp.	sharpnose shark	wild	jaw	1			
Somniosus microcephalus	greenland shark	wild	tooth row	1			
Sphyrna lewini	scalloped hammerhead	wild	jaw	1	x		
Sphyrna tiburo	bonnethead shark	wild	jaw	1	x		
Sphyrna zygaena	smooth hammerhead	wild	jaw	1	x		
Triaenodon obesus	whitetip reef shark	wild	jaw	2			
Triaenodon obesus	whitetip reef shark	aquarium	single teeth	3			

Table 6.2. Habitat, body size and diet of the 12 modern shark species used for establishing an enameloid surface texture dietary reference framework. Three different *Sphyrna* species are later pooled into *Sphyrna*. Data were compiled from the following literature resources: [1] Last and Stevens (2009); [2] Compagno (1984a); [3] Preti et al. (2004); [4] Compagno (1984b); [5] Clarke et al. (2011); [6] Cabrera-Chavez-Costa et al. (2010); [7] Meyer et al. (2010); [8] Florida Museum of Natural History (2005); [9] Compagno et al. (2005); [10] Hoffmayer et al. (2014); [11] Dicken et al. (2015); [12] Carpenter and Valdestamon (2017); [13] White et al. (2006); [14] Last and Stevens (1994); [15] Randall et al. (1990); [16] White et al. (2013); [17] Megalofonou and Chatzispyrou (2006); [18] Heithaus et al. (2002); [19] Werry et al. (2014); [20] Heithaus, et al. (2002); [21] Heithaus (2001); [22] Heithaus et al. (2007); [23] Compagno and Niem (1998); [24] Yamaguchi and Taniuchi (2000); [25] Taniuchi et al. (1983); [26] Vaske et al. (2009); [27] Kubodera et al. (2007); [28] Schluessel et al. (2008); [29] Sommer et al. (1996); [30] Myers (1999); [31] Smith (1997); [32] Cortes et al. (1996); [33] Cortes and Parsons (1996); [34] Ebert (2003); [35] Cortés (1999).

Taxon	Habitat	Diet	Size
Alopias vulpinus	pelagic and outer shelf waters [1] in depths up to 366 m [2]	mostly small teleosts; also squids; octopuses; pelagic crustaceans; rarely seabirds [2; 3; 4]	up to 600 cm [2; 4]
Carcharhinus falciformis	pelagic and continental shelf edge waters in depths up of 500 m [1; 5]	mostly teleosts; squid; paper nautiluses; pelagic crustaceans [2; 4; 6]	up to 330 cm [2; 4]
Carcharhinus galapagensis	isolated, oceanic islands and reefs from surface waters to depths of 280 m [7; 8]	mostly bottom teleosts (e.g. eels, flying fish); squid; octopi; other sharks; sea lions; marine iguana; occasional garbage [2; 4; 9]	up to 370 cm [2; 4]
Carcharhinus obscurus	coastal and pelagic waters from the surface to depths of 400 m [4; 10]	wide variety of reef, bottom and pelagic teleosts; octopi; squid; crustaceans; other shark species; whale meat; sea turtles; occasional garbage (uncommon) [2; 4; 11]	up to 400 cm [2; 4; 10; 12]
Carcharhinus sorrah	continental and insular shelf waters from the intertidal to depths of 140 m [1; 4; 13]	mostly teleosts; octopi; crustaceans [2; 4; 14]	up to 160 cm [2; 4; 15]
Centrophorus granulosus	upper continental slopes and outer continental shelves at depths to 1700 m [4; 16]	mostly teleosts (e.g. hake, epigonids and lanternfish); cephalopods; crustaceans [2; 4; 17]	up to 170 cm [16]
Galeocerdo cuvier	coral reefs, continental shelves and offshore islands and atolls from very shallow waters to depths of 1200 m [18; 19]	variety of marine life (mammals, seabirds, sea turtles,…) and garbage; potent predator-scavenger, very opportunistic [2; 4; 20, 21]	up to 750 cm [2; 4; 22]
Mustelus manazo	mud and sand bottoms of continental waters in the intertidal and subtidal regions [4; 9], up to 360 m [23]	mostly bottom invertebrates; teleosts; crustacean; eggs; bivalve molluscs [2; 4; 24; 25]	up to 120 cm [2; 4; 9]
Prionace glauca	oceanic and pelagic waters to depths of 1000 m [1]	mostly relatively small teleosts; squid; invertebrates; small sharks; mammalian carrion; seabirds [2; 4; 26; 27]	up to 380 cm [2; 4]
Sphyrna lewini	continental and insular shelves and in deep water from intertidal zone up to 275 m depth [4; 28]	variety of teleosts; invertebrates (e.g. cephalopods); crustaceans; other shark species [2; 4; 14; 29; 30]	up to 420 cm [2; 4; 31]
Sphyrna tiburo	mud and sand bottoms of inshore, coastal, continental and insular shelf and coral reefs [4]	mostly small teleosts; crustacean; bivalves; octopi [2; 4; 32]	up to 100 cm [2; 4; 33]
Sphyrna zygaena	coastal-pelagic and semi-oceanic to depths of 200 m [34]	variety of teleosts; cephalopods; crustaceans;small sharks (favoured) [2; 4; 33; 35]	up to 400 cm [2; 4]

Table 6.3. Fossil shark teeth with locality, stratigraphic age, geological formation, sediment type. For more detailed information see supplement and Table S6.1.

Taxon	Stratigraphic age	Geological formation	Locality	Predominant sediment fraction	n
Hemipristis serra	Middle Miocene	Torreya Fm.	Milwhite Gunnfarm Mine, Florida, U.S.A. (30.584844°, -084.620819°)	Clay to sand	2
	Lower Pliocene	Bone Valley Fm.	Polk County, Florida, U.S.A. (27.9600°, -081.7000°)	Sand (sand-gravel particle)	1
Negaprion brevirostris	Middle Miocene	Torreya Fm.	Milwhite Gunnfarm Mine, Florida, U.S.A. (30.584844°, -084.620819°)	Clay to sand	1
	Lower Miocene	Parachucla Fm.	White springs east quad., Florida, U.S.A. (30.331647°, -082.756008°)	Sand	1
	Lower Pliocene	Bone Valley Fm.	Polk County, Florida, U.S.A. (27.9600°, -081.7000°)	Sand (sand-gravel particle)	5
Carcharhinus sp.	Lower Pliocene	Bone Valley Fm.	Polk County, Florida, U.S.A. (27.9600°, -081.7000°)	Sand (sand-gravel particle)	1
Carcharhinus taurus	Lower Pliocene	Bone Valley Fm.	Polk County, Florida, U.S.A. (27.9600°, -081.7000°)	Sand (sand-gravel particle)	1
Carcharodon carcharias	Lower Pliocene		Hillsborough County, Florida, U.S.A. (27.9100°, -082.3500°)	Sand (sand-gravel particle)	1
	Pliocene	Yorktown Fm.	North Carolina, U.S.A. (35.782169°, -080.793457°)	Clay to sand	5
Carcharocles megalodon	Miocene	Bone Valley Fm.	Polk County, Florida, U.S.A. (27.9600°, -081.7000°)	Sand (sand-gravel particle)	1
	Pliocene	Yorktown Fm.	North Carolina, U.S.A. (35.782169°, -080.793457°)	Clay to sand	7
Cosmopolitodus hastalis	Pliocene	Yorktown Fm.	North Carolina, U.S.A. (35.782169°, -080.793457°)	Clay to sand	5
Galeocerdo aduncus	Middle Miocene	Torreya Fm.	Milwhite Gunnfarm Mine, Florida, U.S.A. (30.584844°, -084.620819)	Sand	1
Isurus hastalis	Pliocene/Miocene	Sands of Kattendijk	Antwerpen/Doel, Belgium (51.260197°, 004.402771°)	Clay to sand	3
Isurus sp.	Pliocene/Miocene	Sands of Kattendijk	Antwerpen/Doel Steendorp, Belgium (51.260197°, 004.402771°)	Clay to sand	3
	Pliocene/Miocene	Glaukonitsande	Rumst, clay pit Svendsen, Belgium (51.08153°, 004.42217°)	Clay to sand	4
	Lower Oligocene	Alzey Fm.	Eckelsheim, Germany (49.794982°, 007.983155°)	Sand (sand-gravel particle)	2
Odontaspis sp.	Lower Oligocene	Alzey Fm.	Wöllstein, Germany (49.811878°, 007.960753°)	Sand (sand-gravel particle)	7
unknown	Lower Oligocene	Alzey Fm.	Eckelsheim, Germany (49.794982°, 007.983155°)	Sand (sand-gravel particle)	2

6.3.2 Fossil shark tooth dataset

All fossil specimens are isolated shark teeth from different locations in Europe and North America representing different geological time periods (Oligocene to Pliocene) and marine sedimentary settings (**Table 6.3 and Table ES6.1**). For more detailed description of the depositional settings, see Table 6.3 and supplement. Since several specimens were used for isotopic analyses in previous studies (Tütken, 2003), some buccal surfaces had been destructively sampled, therefore, for those specimens, lingual sides were used for DMTA. The whole pooled fossil dataset was compared to the whole modern dataset, for comparison to ante-mortem wear.

6.3.3 Experimental shark tooth dataset

To test for the effect of fluvial transport on the enameloid surface, modern shark tooth specimens from unknown position in the upper jaw of *Carcharhinus plumbeus* were subjected to five tumbling intervals between 0.5 and 336 h (**Table 6.4**) in water-sediment suspension using commercial hobby rotary tumblers TYP TRO 2 A (Otto Eigner e.K., Industriebedarf & Hobbyschleifmaschinen, Idar-Oberstein, Germany). Teeth were marked with a drill hole on the centre of the lingual dental surface to identify the same areas for DMTA between the different tumbling intervals. A rotation of the dental surface according to possible inaccuracies during the orientation of the teeth of ~ 5-10° was accepted. A tumbling procedure as described in Böhm et al. (2019) was performed using siliciclastic sand (quartz-content 50-60 %) in three different grain size fractions, very fine sand (51-168 µm), fine sand (112-292 µm), medium sand (221-513 µm), and fine gravel (2-8 mm). Rotary tumbler barrels were filled with 500 g of tap water and 300 g sediment, one tooth per tumbling barrel. Per sediment type, three teeth were tumbled subsequently for 30 minutes, 1, 2, 4, and 336 h, and scans were taken on the lingual side of each tooth per tumbling interval.

Table 6.4. Modern shark teeth tumbled with different grain size fractions and tumbling intervals.

Taxon	n	Sediment grain size fraction	Tumbling interval [h]
Carcharhinus plumbeus	12	before tumbling	0
Carcharhinus plumbeus	3	51-168 µm	0.5, 1, 2, 4, 336
Carcharhinus plumbeus	3	112-292 µm	0.5, 1, 2, 4, 336
Carcharhinus plumbeus	3	221-513 µm	0.5, 1, 2, 4, 336
Carcharhinus plumbeus	3	2-8 mm	0.5, 1, 2, 4, 336

The experimental and fossil dataset were employed for a secondary aim of this study, comparison of ante- and post-mortem wear on fossil shark teeth. The DMTA data of the fossil shark teeth from different localities were compared to the dataset of experimentally altered teeth that were tumbled in different grain size fractions.

6.3.4 Dental microwear texture analysis

Following the procedure of Schulz et al. (2010) surface scans were conducted using a high-resolution disc-scanning confocal 3D-surface measuring system μsurf Custom (NanoFocus AG, Oberhausen, Germany) with a high-speed progressive-scan digital camera (984 x 984 pixel) and a blue LED (470 nm). The measurements were processed using the software package of MountainsMap Premium v.7.4.8676 (DigitalSurf, Besançon, France). All teeth were scanned with the tip pointing in the same direction. For detailed description of the MountainsMap template and a detailed description of DMTA, please see supplement.

We employed scale-sensitive fractal analysis (SSFA) and 3D surface texture analysis (3DST), both techniques use optical profilometry to receive 3D pictures of the enamel surface at submicron resolution and evaluate the general three-dimensional geometry of wear features. In total we computed two SSFA, thirty 3D-surface roughness parameters (standardised height, functional, spatial, hybrid, and segmentation parameters according to ISO 25178 (Schulz et al., 2013b) and fourteen motif, furrow, isotropy, and flatness (ISO 12781) parameters included in MountainsMap 7.4.8676 (**Table S4.3**).

6.3.5 Statistics

Data processing and statistical analyses were performed using the open-source software R v.4.0.0 (R. Development Core Team, 2020). A detailed description of the packages and calculations can be found in the electronic supplement. Detailed results for the PCAs including graphical representations of principal components with a standard deviation >1 are given in the electronic supplement (**Table S6.2-S6.6, Fig. S6.1-S6.5**).

For all teeth of the modern, fossil and experimental datasets (**Table 6.1, 6.3 and 6.4**), a median for each tooth was calculated from four measured scans. For testing the influence of tooth position and ontogenetic age on DMT (**Table 6.1**), no inferential statistics were performed. In the experimental dataset, a median was calculated for t0 and for each tumbling interval, for each sediment grain size fraction. The median values for each tooth were used to calculate a mean for each sediment type (n = 3 teeth/median values). No further statistics were performed for the experimental dataset.

Only species with n ≥ 3 in the datasets of fossil and modern sharks were included in statistical tests. Pairwise comparisons of dental surface texture parameter values were performed between:

I. twelve different modern wild shark species with an n ≥ 3, to test for possible differences in dental surface wear among these (**Table 6.1 and 6.2**),

II. modern aquarium specimens of *Carcharhinus plumbeus* before the tumbling experiment with the same teeth after the tumbling experiment in four different grain size fractions (336 h) and the fossil shark teeth (**Table 6.1 and 6.4**),

III. modern wild, modern aquarium and fossil specimens (**Table 6.1 and 6.3**), to test for possible significant variation in DMT signals between species with an unknown but presumably broader range of diet and specimens with a pellet-based diet and to see, if there are significant differences between ante- and potentially post-mortem wear from transport, deposition and reworking.

6.4 Results

6.4.1 Influence of tooth position on DMT

Teeth of modern sharks from multiple tooth positions along the jaw of two different individuals of *Galeocerdo cuvier* and *Carcharhinus leucas* and one each of *Carcharhinus sorrah* and *Prionace glauca* were analysed. All DMTA data are reported in the supplements (**Table ES6.7-S6.12, Fig. ES6.6-ES6.11**).

All teeth (n = 20) of the most complete foremost upper tooth row of a *Carcharhinus sorrah* were measured (**Fig. 6.1A**). The scans show differences between tooth positions along the upper jaw, also DMT parameters show a certain variation along the tooth row (**Fig. 6.1A**). The PCA shows however, that the different teeth along a tooth row are grouped species-specific. All measured teeth of the two individuals of *Galeocerdo cuvier* grouped together, the same is true for the two individuals of *Carcharhinus leucas*. Additionally, the different species could be distinguished along PC1, PC2 and PC3 (**Fig. 6.2A and S6.1A**). No systematic textural differences between lingual and buccal side of the analysed specimens were found, as well as only slight differences between teeth from the upper and lower jaw (**Table ES6.8-S6.12**). Overall, the parameter space measured for one central tooth position in the modern wild sharks covers mostly the parameter variance measured for single teeth along the jaw of one individual.

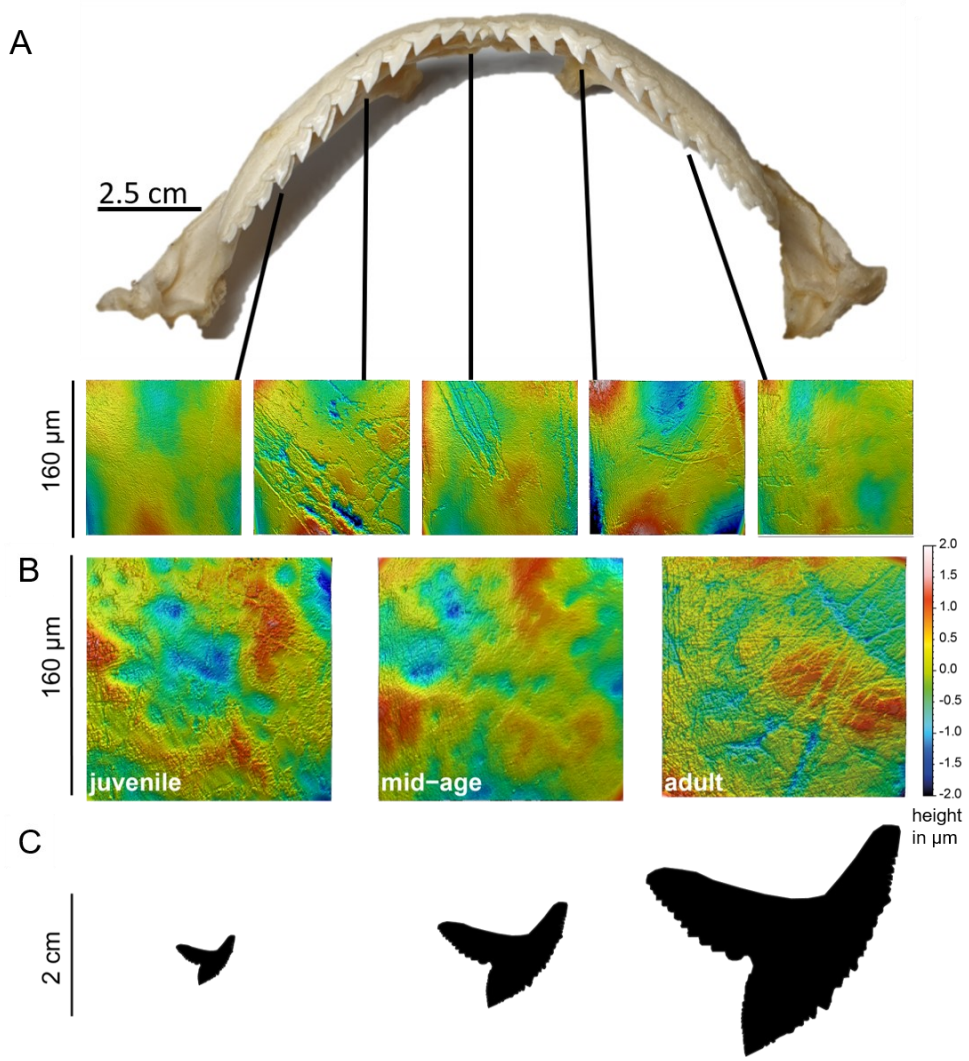

Figure 6.1. Illustration of influence of tooth position and ontogeny on the dental surface of *Carcharhinus sorrah*. A. Photo of the complete upper jaw tooth row of a modern *Carcharhinus sorrah* with 3D enameloid surface texture models shown for five different tooth positions. B. Typical 3D photosimulations for one tooth of a juvenile, mid-age, and adult specimen. C. Schematic outline of the typical tooth size for different ontogenetic stages.

6.4.2 Influence of ontogenetic stage on dental wear patterns

One central tooth per specimen from three different ontogenetic stages, juvenile (n = 4), mid-age (n = 5), and adult (n = 2) of *Galeocerdo cuvier* was measured (**Fig. 6.1B and C**) and showed no surface texture differences in the area, density, and direction parameters (**Table ES6.13, Fig. ES6.12**). In parameters describing the height and volume, a trend towards lower values for the two adult specimens occurs (**Fig. ES6.12**). The PCA revealed a distinct separation of the different ontogenetic stages, whereby the juvenile specimens were separated along PC2 from the adult and mid-age individuals, and the adult specimens were separated along PC1 from the other two ontogenetic stages (**Fig. 6.2B**). However, it needs to be noted

here, that the sample size per stage is very small and, at least the mid-age individuals show a high scatter in the PCA (**Fig. 6.2B and S6.2**)

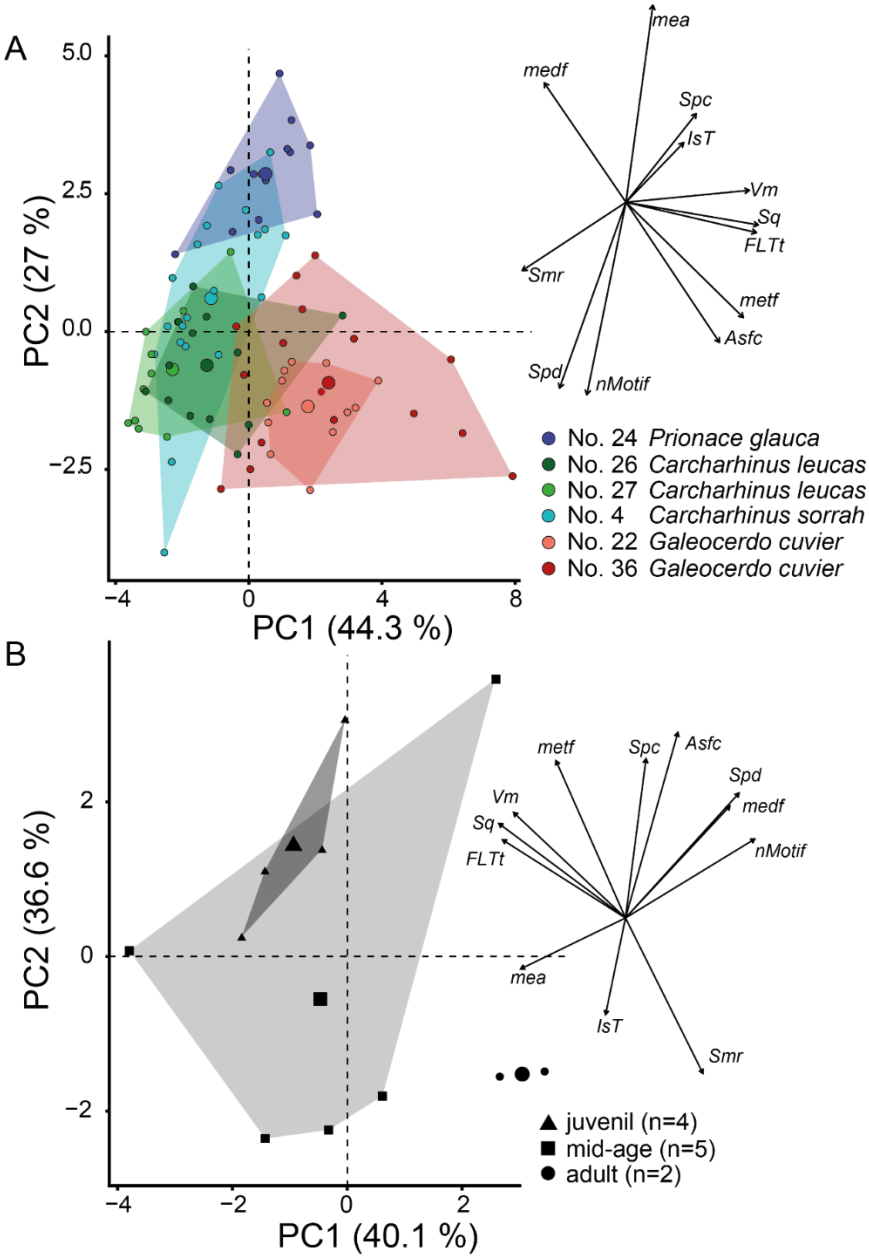

Figure 6.2. Results of the test for the influence of tooth position on DMT. Principle component analysis (PCA) of surface texture parameters from each category (**Table S4.3**) with good separation. Large symbols in PCA plot mark the mean of the area of the different groups. A. All measured modern shark teeth of *Galeocerdo cuvier* (specimen No. 22 and No. 36), *Carcharhinus leucas* (specimen No. 26 and No. 27), *Carcharhinus sorrah* (specimen No. 4) and *Prionace glauca* (specimen No. 24) for testing the influence of tooth position; for details about the taxa see Table S6.1. B. All *Galeocerdo cuvier* specimens according to their ontogenetic age to assess whether dental wear differs in different ontogenetic stages.

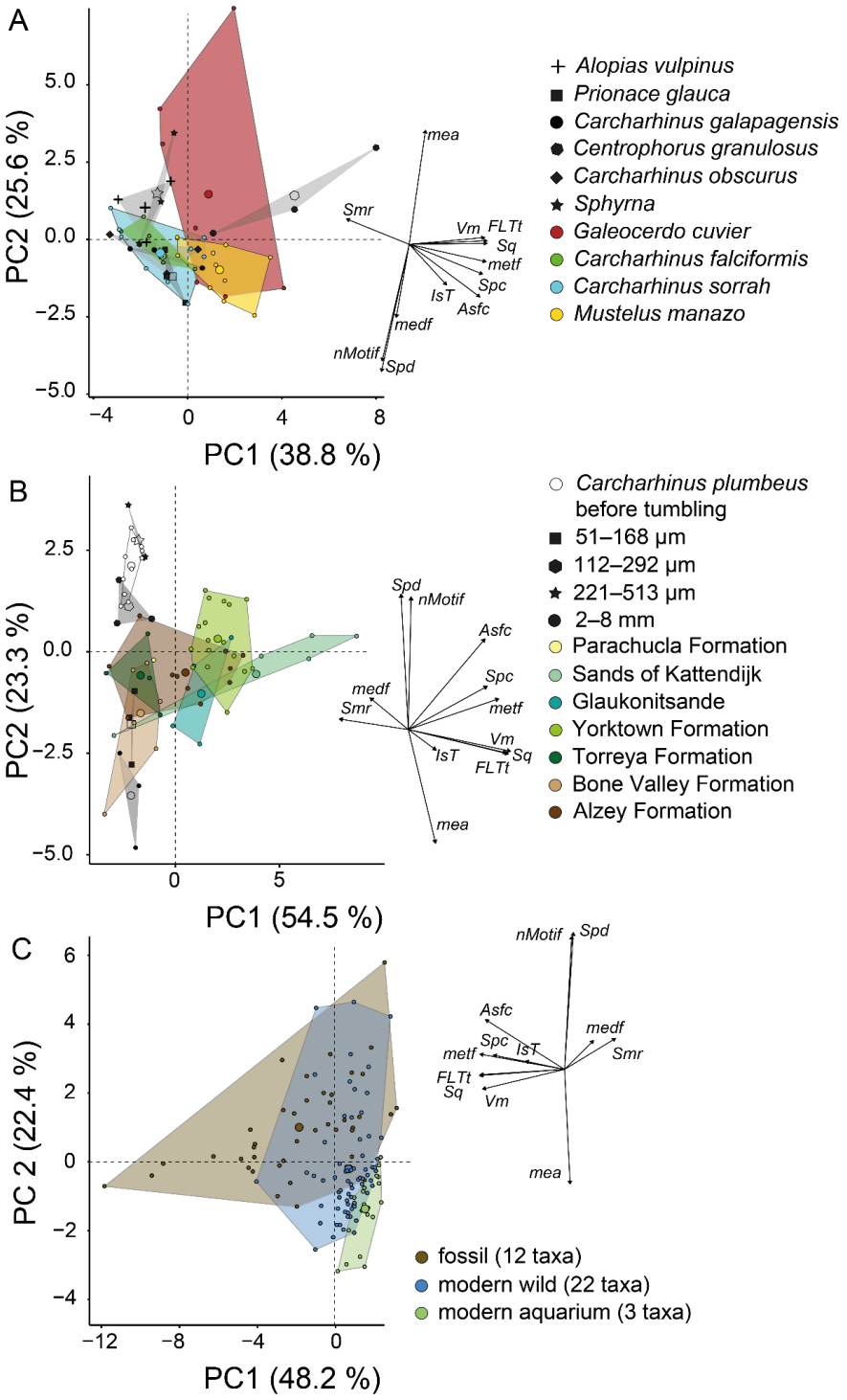

Figure 6.3. DMT results for the shark teeth. Principle component analysis (PCA) of surface texture parameters from each category (**Table S4.3**) with good separation. Large symbols in PCA plot mark the mean of the area for the different groups. A. 12 wild shark species, three different Sphyrna species are pooled into Sphyrna; for details about the taxa see Table 6.2 and S1. B. Modern *Carcharhinus plumbeus* tooth specimens from aquarium sharks used for tumbling experiments. Parameter values of teeth tumbled for 336 hrs in all four different sediment grain size fractions are plotted. Additionally, the values of all fossil shark tooth

specimens are plotted, divided according to their locality. C. All different modern wild, modern aquarium and fossil sharks analysed in this study.

6.4.3 Influence of diet on DMT of shark teeth

Twelve different species (with three *Sphyrna* species pooled together under *Sphyrna*) with three or more individuals used for DMTA were included in the analysis of diet-related wear parameters of the modern wild sharks (**Fig. 6.3A and 6.4, Table 6.5**). All DMTA data and parameter boxplots are reported in the supplements (**Table ES6.14, Fig. ES6.13**). Only significances confirmed by Cliff´s method are accepted (**Table 6.5 and ES6.15**). Two groups could be identified along PC1, with *Mustelus manazo*, *Centrophorus granulosus* and *Galeocerdo cuvier* separated by higher complexity, height, volume, and density parameters from the other taxa. *Mustelus manazo* and *Centrophorus granulosus* were additionally clearly separated along PC4 (**Fig. S6.3A**). The remaining taxa overlapped and were almost not distinguishable from each other, whereby *Alopias vulpines* and *Sphyrna* showed higher values along PC2 (**Fig. 6.3A**). The DMT parameters, however, revealed only significant differences between *Mustelus manazo* and *Galeocerdo cuvier* and all remaining taxa, though, there were no significant differences between *Mustelus manazo* and *Galeocerdo cuvier*. These two taxa showed the largest height, complexity and volume parameter values. Additionally, only *Centrophorus granulosus* was significantly different from *Mustelus manazo* and *Galeocerdo cuvier*, but also from *Carcharhinus sorrah*. All other taxa showed no significant differences between each other (**Table 6.5 and ES6.15**).

Table 6.5. Significant DMT parameters (confirmed by Cliff's method) for the analysis of diet-related wear parameters of the modern wild sharks.

Alopias vulpines	*Alopias vulpines*									
Prionace glauca		*Prionace glauca*								
Carcharhinus falciformis			*Carcharhinus falciformis*							
Carcharhinus galapagensis				*Carcharhinus galapagensis*						
Centrophorus granulosus					*Centrophorus granulosus*					
Carcharhinus obscurus						*Carcharhinus obscurus*				
Carcharhinus sorrah					*Asfc, Sv, Sz, madf, metf, Spc, Vvv*		*Carcharhinus sorrah*			
Sphyrna (including S. lewini, S. tiburo, S. zygaena)								*Sphyrna (including S. lewini, S. tiburo, S. zygaena)*		
Mustelus manazo	*Smr*	*Asfc,*	*Asfc, Sku, Sv, Sxp, Sz, madf, FLTt, FLTv, Vm, Vvv*	*Tr1R, Tr3R, IsT, epLsar, Sku, Sv, Sz, Spc, Smr*	*Asfc, Tr1R, metf, Spc*	*Tr1R, Sku, epLsar, Vvv*	*Tr1R, Sv, Sz, Vm, Vvv*	*mea, IsT, epLsar, Sku, Sv, Vvv*	*Mustelus manazo*	
Galeocerdo cuvier	*metf, FLTt*	*metf*	*madf, metf*	*Sv*	*Sv*	*madf, metf*	*epLsar, madf, metf*	*madf, metf*		*Galeocerdo cuvier*

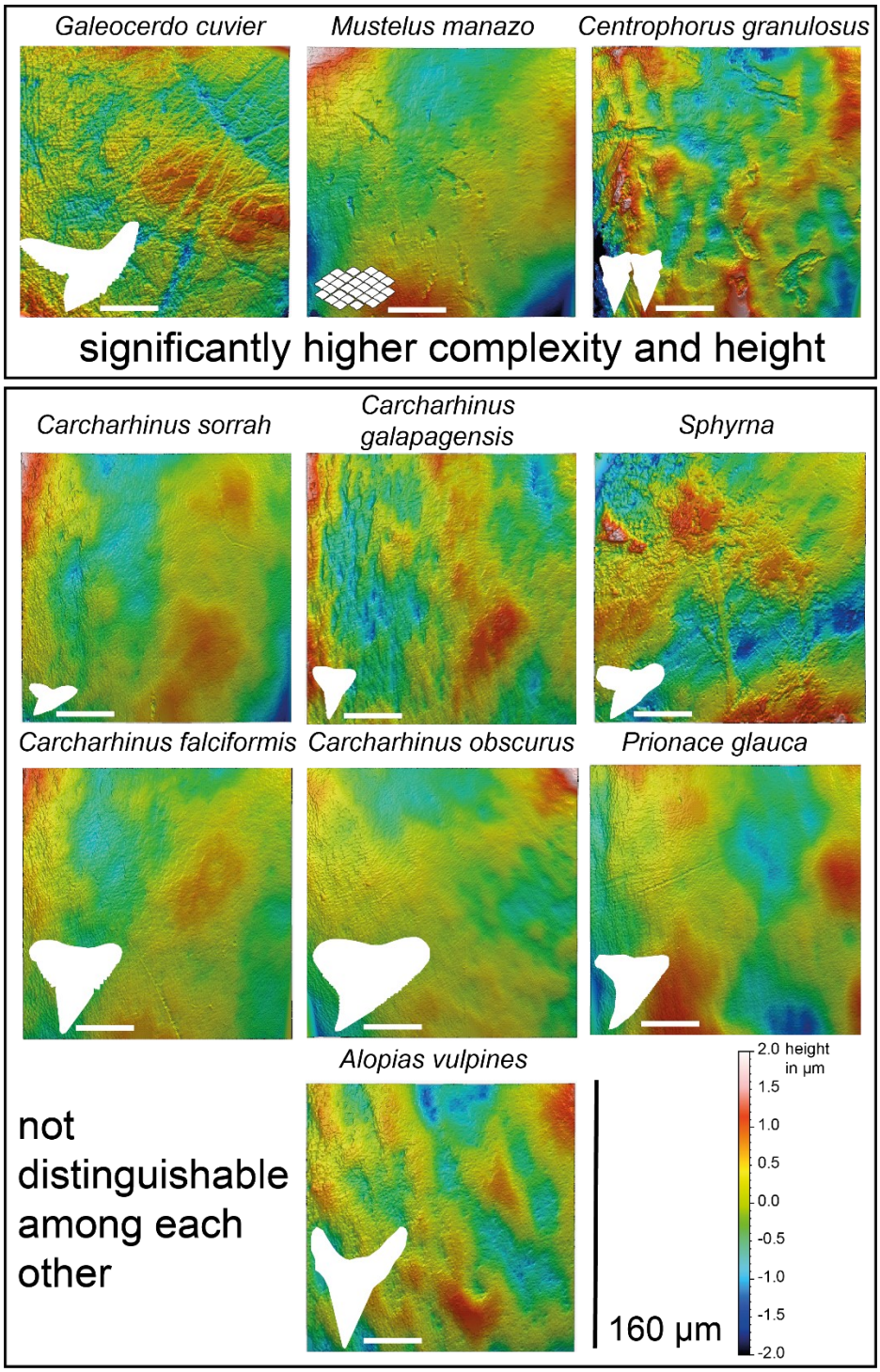

Figure 6.4. Representative 3D surface models of single teeth (including a schematic outline of a typical tooth for each modern shark species) employed to establish a dietary reference frame for modern sharks. *Mustelus manazo* (scale bar 0.5 cm), *Centrophorus granulosus* (scale bar 0.5 cm) and *Galeocerdo cuvier* (scale bar 2 cm) have significantly different (i.e. larger) complexity and height values while the remaining seven taxa (scale bar 1 cm) have similar parameter values.

6.4.4 Ante- or post-mortem wear on fossil shark teeth

6.4.4.1 Tumbling experiment of shark teeth with siliciclastic sediments of different grain size fractions

For the experimentally altered shark teeth (**Table ES6.16, Fig. ES6.14**), an increase of the surface complexity (*Sdr*, *nMotif*, *Asfc*) was evident. The strongest increase occurred in the gravel group, followed by the finest fine sand group (**Fig. 6.5**). The same was true for the area parameters *mea*, *Spc* and *Spd*, which decreased over the duration (up to 336 h) of the tumbling experiment in all four grain size groups. Height parameters exhibited increasing variance after tumbling intervals for all four sediment groups compared to before the experiment. However, not all of them showed clear trends towards increasing or decreasing parameter values (**Fig. 6.5 and ES6.14**). *S10z*, *S5p*, *S5v*, *Sv*, *Sz*, *meh*, *madf* and *metf* were increasing over the tumbling time **(Fig. ES6.14**), with the strongest increase of parameter values in the gravel group, followed by the very fine sand group. The parameters *Ssk,* as well as *FLTt*, *FLTp*, *FLTv* and *FLTq,* were decreasing only in the gravel group, while they did not change in the three sand groups. The volume parameter group was the only set of parameters exhibiting changes towards both decreasing and increasing values during the tumbling experiment for the different grain size fractions. While the fine and medium sand fractions did not cause changes in the parameter values, the smallest, very fine sand fraction showed a trend during the experiment towards higher volume values. Tumbling with the gravel fraction already resulted in lower volume parameter values after the first interval of 0.5 h (**Fig. 6.5**). However, the changes in parameter values after the tumbling experiment deviated only slightly from the large parameter range of the modern wild shark species (**Fig. 6.5**).

The PCA (**Fig. 6.3B and S6.4A**) revealed, that there is no distinct difference between the pre-tumbling dental surface and the dental surface after tumbling with fine and medium sand fraction. The teeth tumbled with the very fine sand and the fine gravel are well separated along PC2 after tumbling and share a similar PCA space as the fossil specimens form the Bone Valley Formation (sand with gravel-sized particles). Fossils from the Torreya Formation (sand with clay fractions) lie between the specimens tumbled with fine and very fine sand, according to PC2 (**Fig. 6.3B**). Fossils from the Alzey Formation (sand with gravel-sized particles), Yorktown Formation (sand with clay fractions), Sand of Kattendijk (sand with clay fractions) and the Glaukonitsande (sand with clay fractions) are well separated from all tumbled specimens and the fossil specimens from Bone Valley and Torreya Formation.

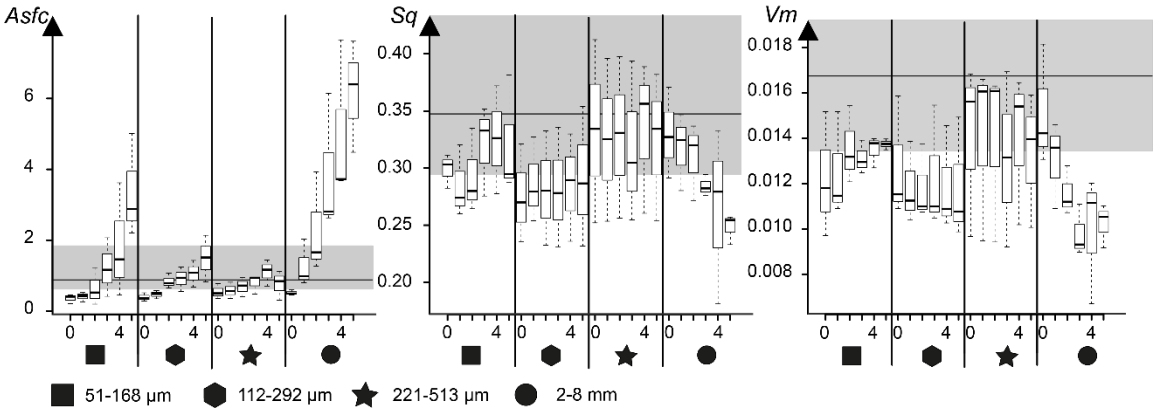

Figure 6.5. Results for the experimentally altered shark teeth. Boxplots for *Asfc* – fractal complexity, *Sq* – standard deviation of height distribution (µm) and *Vm* – material volume (µm³/µm²). Parameter values of all six tumbling time intervals (0, 0.5, 1, 2, 4, 336 h) with all the four different grain size fractions ranging from fine sand to fine gravel. The thick horizontal bar represents the median; the box encloses the first (25%) and third (75%) quartiles; the whiskers (extend to 1.5 times the length of the box (the interquartile range); the dots represent outliers. The grey box marks the parameter space of all modern wild shark species.

6.4.4.2 Fossil and modern shark specimens

There were several significant differences between modern shark species kept in an aquarium on the same pellet-based diet and different wild shark species with variable but unknown diet (**Table ES6.17, Fig. ES6.15**). However, both groups had a high overlap, with the wild shark group showing much higher variance (**Fig. 6.3C and ES6.15**). The comparison of fossil and modern wild shark teeth revealed high variability in texture parameters for both groups, however, they differed significantly in 35 DMT parameters. Six dental surface parameters (*Sda*, *Sha*, *mea*, *Sal*, *Tr3R*, *Ssk*) were significantly lower in the fossil group, while all other significant parameters describing height, area, peak sharpness, plateau size, slope and volume were lower in the modern wild group. The PCA of the 12 best separating DMT parameters (**Fig. 6.3C and S6.5A**), showed an overlap between all three data clouds, whereby the core area of the fossil group was separated along PC1 by higher complexity, height, volume and density parameters from the core area of the two modern groups.

6.5 Discussion

6.5.1 Effects of tooth position and ontogeny on dental surface wear

Non-systematic differences in surface textures exist between different tooth positions, upper and lower jaw, and measurements on opposing tooth sides (buccal vs. lingual). The

more posterior tooth positions along both jaws showed more variance (**Fig. ES6.6-S6.11**), which might be due to higher bite forces generated at the back of the jaw (Huber et al. 2005). However, this variability appears to be individual and species specific and rather independent from the tooth position in the jaw. We also found differences between different ontogenetic stages in *Galeocerdo cuvier* (**Fig. 6.2B**). Especially the juvenile specimens showed quite different DMT and were therefore excluded for the dietary dataset. This variability might be caused by several life history variables, such as changing tooth replacement rate and bite force with age (Fraser and Thiery, 2019), as well as changing diet (e.g. size and hardness of prey, Lowe et al., 1996) or habitat preferences (Lowry and Motta, 2008). The variability could also be a result of the variation of provenance of the different samples. Hence, our data imply that the effect of tooth position and ontogeny introduce certain variability to dental surface texture and that it is advisable to constrain sampling to one tooth position and a narrow age range. DMTA further seems to be a useful tool to help with the identification of shifting ecological factors during the ontogeny. However, to verify this hypothesis it would be necessary, to sample different ontogenetic stages of one species from the same spatiotemporal origin.

6.5.2 Suitability of dental surface texture on shark teeth for diet reconstruction

Sharks have only short food-to-tooth contact due to limited oral food processing and fast tooth replacement rates. However, some species, such as the bull shark, great white shark and tiger shark have a strong bite force able to even crack shells of sea turtles (e.g. Wroe et al., 2008; Habegger, 2009; Ferrara et al., 2011; Ferrara, 2012), which leads, at least for short periods, to forceful contact between teeth and prey items and/or the opposing teeth. Thus, depending on the type, hardness, and size of ingested prey, various degrees of food-tooth or tooth-tooth interaction are expected. This should presumably leave some wear features on the enameloid surface of shark teeth; however, the results of this study indicate that such wear is not indicative of the type of ingested diet.

McLennan (2017) found different surface textures between two different populations of modern wild and aquarium *Carcharias taurus* and concluded that dental surface texture on shark teeth is diet-related. We also found some significant differences in dental surface textures between wild specimens and those kept in an aquarium, indicating even lower tooth wear in the aquarium sharks. This was expected, since the aquarium species had a pellet-based diet, digested as bolus. However, the two groups showed a huge variance and overlap in dental wear parameter space, making clear separations between potential diet groups difficult (**Fig. 6.3C, Table ES6.17-S6.18**). Currently, our data for the same species from a wild and an aquarium setting is too limited to directly confirm or rebut this conclusion.

The results of the PCA for the extant wild shark species (with teeth from n ≥ 3 individuals analysed) indicated significant DMT differences between two groups of sharks (**Fig. 6.3A**). In particular, in one group containing *Mustelus manazo, Centrophorus granulosus* and *Galeocerdo cuvier*, the volume, height, and complexity parameters showed higher values. This reflects an overall rougher and more complex dental surface texture in these three taxa than for the other seven taxa and likely indicates the ingestion of harder food items. Further support for this interpretation comes from the mean density of furrows versus their mean depth, which showed a trend for *Centrophorus granulosus* and *Galeocerdo cuvier* towards fewer but deeper furrows (**Fig. S6.3B**), that clearly separated them from other shark taxa. A similar pattern was also observed for extant hard-object feeding lepidosaurs, which have a very different tooth morphology, but also limited oral food processing behaviour (Winkler et al., 2019a).

Centrophorus granulosus showed the most prominent differences in height and volume parameters and the clearest separation from all other shark taxa with n ≥ 3. This species has compressed, interlocking teeth and tends to live in water depths of up to 1700 m. Its diet consisting mostly of different species of small- and medium-sized teleost fish appears to be relatively soft. However, a relatively small part of the soft teleost fish are potentially soleidea or flatfishes (Megalofonou and Chatzispyrou, 2006), which are living directly on the sea floor covered by sediment. It is plausible, that sediment might be ingested together with this bottom-dwelling prey, which could potentially lead to complex and rough enameloid surface textures in this taxon. However, other species, such as *Carcharhinus galapagensis* and *Carcharhinus obscurus* might also ingest a high amount of sediment together with their prey (**Table 6.2**) and did not show more complex or rougher surface textures. Together with teleosts, around one third of *Centrophorus granulosus* diet seems to be cephalopods, which are overall very soft, but also possess gladium and rostrum consisting of relatively hard chitin (Megalofonou and Chatzispyrou, 2006). The ingestion of this hard material could cause increased surface roughness and complexity, if it comes to contact with teeth. Additionally, another smaller taxon with a similar diet, *Carcharhinus sorrah* (**Table 6.2**), showed lower and less complex surface textures than *Centrophorus granulosus* in the same parameter groups. In contrast to *Centrophorus granulosus*, *Carcharhinus sorrah* was not clearly separated from other shark taxa in PCA (**Fig. 6.3A**). *Mustelus manazo*, a small-sized shark with small teeth not suitable for cutting prey, lives mostly on sandy and muddy ocean bottoms and feeds on benthic crustaceans and molluscs (**Table 6.2**). This durophagous diet could explain a rougher and more complex surface texture, due to the hardness of the food (invertebrates with mineralized exoskeletons) and/or potentially a high amount of sediment ingested alongside the benthic prey. However, for example *Sphyrna tiburo* (as a part of *Sphyrna*) showed less rough and complex surface textures, although it is also a durophagous benthic species and mostly feeds

on hard crustaceans and bivalves (**Table 6.2**). The last species with distinct surface textures is *Galeocerdo cuvier*, which is one of the largest shark species in the modern dataset (**Table 6.2**). However, this species represented by adult and mid-age individuals in the dataset, had a higher variance of surface texture parameter values. Nevertheless, it was well separated from other sharks in the PCA (**Fig. 6.3A**), as well as in mean density versus mean depth of the furrows (**Fig. S6.3B**), due to deeper furrows in *G. cuvier*. *Galeocerdo cuvier*'s serrated teeth are suitable for cracking hard prey, as well as for cutting though flesh (Ferrara et al., 2011). The latter feeding is hypothesized as a potential reason for several scratches on *Edestus minor* teeth (Itano, 2019), therefore, it could potentially cause also furrows on the dental surface on *G. cuvier*. *Galeocerdo cuvier* has the most opportunistic diet of all investigated shark species, including fish, marine mammals, birds, as well as carrion and even garbage into its diet (**Table 6.2**). It is known from the literature, that large sharks, such as *G. cuvier*, *Carcharodon carcharias* or *Carcharhinus leucas* prey on larger and harder prey than smaller sharks (e.g. Cliff and Dudley 1991; Lowe et al. 1996; Cortés, 1999; Ebert, 2002; Lucifora et al., 2009; Habegger, 2009), so a rougher surface is expected. However, other large species in this dataset, such as *Carcharhinus obscurus* and *Carcharhinus galapagensis*, which feed on larger bony fish, marine mammals and sometimes garbage (**Table 6.2**), do not show significantly different surface textures. Additionally, *G. cuviers* enameloid surface clearly shows not as high roughness and complexity as *Centrophorus granulosus* with a potentially softer diet.

In general, almost all our tested shark species feed on teleost fish and some species of cephalopods, which are overall a softer diet, however, include some harder body parts. Crustaceans are also included in most shark's diets and are presumably harder but would only leave wear features on the dental surfaces if they were processed orally. Larger shark species in this dataset partly prey on other sharks, mammals, or even sea turtles, which are expected to be processed, e.g. during shell cracking or ripping apart a carcass. It is likely, that mode of food processing, hardness and size of prey, and ingestion of sediment together with prey, have some effect on DMTA. Consequently, a variable mixture of these factors leads to unsystematic differences between species, or even within one species. Based on our dataset, no clear correlation between diet or environment and enameloid surface texture can be established for modern sharks feeding on different or similar prey. Even sharks feeding predominantly on a durophagous diet did not show characteristic surfaces textures different from more soft-prey or opportunistic feeding sharks. Sharks seem to display a species-specific DTM pattern rather than a diet-specific one. However, at this point it is worth to mention the limitations of this study: a small sample size and a potentially high number of variables influencing DMTA. This study aims to give a broad overview over a variety of shark species, and we note that for further studies, it is worth focussing on fewer species with higher specimen numbers.

6.5.3 Ante- or post-mortem wear

Another important aspect is if ante-mortem surface textures are robust against taphonomic processes during sediment transport and deposition. As shark tooth enameloid consists of fluorapatite (e.g. Enax et al., 2012, 2014), a chemically resistant apatite, and shows similar hardness to mammal teeth, shark teeth are frequently preserved in the fossil record. Analysis of fossil shark teeth from different taphonomic/depositional settings indicated that their enameloid surface is often not well preserved and shows signs of post-mortem alteration often being different from DMT of modern shark teeth.

The tumbling experiments with modern shark teeth in aqueous suspension of siliciclastic sediment showed that transport with constant tooth-to-sediment contact leads to strong changes in some DMT parameters (e.g. *nMotif*, *Asfc, Spc, Spd*, *mea, meh*) while others remain mostly unchanged (e.g. *Ssk, FLTt*, *FLTp*, *FLTv* in the sand fractions). In most parameter sets, the direction of changes is similar for all four experimental grain size fractions. Surface complexity increased dramatically after tumbling in all grain size fractions. This was likely caused by the addition of new wear features and material removal, which is supported by increased density of peaks (*Spd*) and depth of furrows (*madf*) (**Fig. ES6.14**). Such an increase in complexity was also observed for mammalian teeth in a tumbling experiment with the same siliciclastic sediments (Böhm et al., 2019). Height parameters were not obviously altered and the most prominent differences between dental surfaces of non-tumbled and tumbled shark teeth were found in the parameters describing the valleys and furrows, e.g. increasing depth of the furrows. Again, this post-tumbling condition was also found in mammalian teeth (Böhm et al., 2019), which indicates that shark enameloid and mammalian enamel react similarly when subjected to sediment transport. We find that modern shark enameloid surface textures after tumbling resemble the surface textures of fossil shark teeth in this study.

The comparison of different Paleogene/Neogene fossil shark species found in different sedimentary settings revealed difference in DMT parameters between fossil shark teeth from different localities as well as from the experimentally altered teeth (**Fig. 6.3B**). Specimens from the Yorktown Formation (North Carolina, U.S.A.), with clayey and medium to coarse quartz sands were distinctively different from the Bone Valley and Alzey Formation with gravel-sized sediments. However, they were also different from other sedimentary settings with clay components, such as the Glaukonitsande and Sands of Kattendijk (Antwerp, Belgium) and the Torreya Formation (Florida, U.S.A.).Presumably, the hydrodynamics of the depositional setting during burial and potential reworking processes of the fossil site, as well as the grain size of the embedding sediment play a major role in dental surface texture formation of shark teeth.

However, based on our limited dataset, a final conclusion cannot be drawn and needs further investigation in the future.

The comparison of the fossils from the different localities with the experimentally altered modern shark teeth, before and after the tumbling experiment, shows that tumbling shifted the dental surfaces towards the parameter space of the fossil specimens from Florida, especially for the specimens tumbled in the very fine sand and the fine gravel fraction. This is due to an increasing complexity and depth of wear features on the experimentally altered dental surface. This likely reflects a taphonomic alteration of the fossil shark teeth during post-mortem transport, overprinting the original ante-mortem wear features. Different from the ante- and post-tumbling surface are the fossils of the Yorktown Formation and from silty sands of the Glaukonitsande and Sands of Kattendijk and of the Alzey Formation. Thus, the fossil shark teeth from these sediments are most likely overprinted by diagenetic (i.e. mechanical) surface alteration during marine transport processes in near-coastal settings with sediments, which might differ from the sediments (e.g. grain size fraction, composition,…) used in this tumbling experiment. The fossil shark teeth from mudstones and silt-to-clay containing sediments (e.g. Yorktown Formation, North Carolina, U.S.A.; Sands of Kattendijk, Antwerp, Belgium), are presumably taphonomically altered by contact with smaller grain size fractions than those which were used for the tumbling experiments in this study. These very small grain size fractions (clay/silt) seem to have a greater alteration impact on dental surface wear in the form of strongly increasing complexity, height/roughness, and volume, than the larger sand fractions used in this experiment (**Fig. 6.5**).

The DMTA data of all fossil specimens compiled showed a high number of significant differences compared with all the modern wild specimens, despite a large overlap between the two groups (**Fig. 6.3C**). The fossil shark teeth had more complex surfaces, together with larger height and furrow values than the modern wild shark teeth. Hence, there were more deep wear features, such as furrows and scratches on the dental surface of the fossil specimens than observed on modern wild shark teeth. However, it also demonstrates that some modern wild shark species, as *Mustelus manazo* or *Galeocerdo cuvier*, had very rough and complex dental surface textures. Some fossil shark teeth even fall clearly outside the surface texture parameter space of ante-mortem dental wear of modern wild shark teeth (**Fig. 6.3C**). The large overlap between the two groups in the mean density vs. mean depth of the furrows as well as in the PCA demonstrates that there are potentially some well-preserved ante-mortem dental surface areas on the fossil shark tooth specimens, independent of their sedimentary setting. Regardless, fossil and modern specimens are still distinguishable in the PCA, suggesting either a high amount of post-mortem alteration of ante-mortem dental wear on fossil shark teeth or different unknown diet in the fossil species. Especially for extinct large species, such as *Carcharocles megalodon*, the diet is potentially larger and harder than for smaller species.

However, the high complexity and roughness of the dental surface in almost all species, independent of taxonomy, gives a hint towards diagenetic alteration rather than differences in diet.

6.6 Conclusions

Dental microwear texture analysis of extant shark teeth demonstrates that enameloid surface wear can occur *in vivo*, despite minimal tooth-food or tooth-tooth contact and rapid tooth replacement rates. However, it needs to be taken into account, that the sample size of the analysed species in this study is quite small. At this point, it was not possible to relate a clear dietary or environmental signal to the observed wear features. We theorize that a potentially more complex interaction between type and size of prey, food processing or attrition, and ingested sediment exists, which together with a variable carnivorous diet result in highly variable DMT. DMTA in shark species seems to be not as diet-specific as in mammals or even reptiles, which have similar unfavourable characteristics for development of diet-related dental wear, such as reduced oral processing and fast tooth replacement rates. These circumstances could be caused by the potentially faster rates in shark species. Additionally, feeding categories in mammals and reptiles are more distinct and diverse than in sharks, which have a generalist, but variable carnivorous or piscivorous diet.

DMTA of fossil shark teeth revealed that hydrodynamic transport regime and grain size of the embedding siliciclastic sediment seems to influence the surface texture differently. The surfaces of fossil shark teeth were much more complex and rougher than those of modern shark teeth. Thus, the microwear textures of fossil shark teeth either reflect a certain diet or habitat interaction quite different from extant species or post-mortem mechanical alteration during sediment transport. However, fossil shark teeth of different species from the same localities had very similar microwear textures. In contrast, fossil shark teeth of the same species from different localities had very different microwear textures. This is a strong indication for taphonomic processes being the main agent in DMT formation (i.e. overwriting) post-mortem, although our results indicate that preservation of some ante-mortem wear features might be possible. In fossil sedimentary settings, sediments of mixed grain sizes (from clay to sand) seemed to lead to a stronger alteration effect on texture than could be simulated by use of narrow grain size fractions (very fine to medium sand) in the tumbling experiment. All experimentally altered shark teeth have more complex surfaces after tumbling, resembling the fossil shark teeth in this respect. Microwear textures of extant specimens tumbled in fine gravel most closely resembled those observed in fossil shark teeth. Taphonomic post-mortem wear is different from what can be experimentally simulated. Therefore, the complex interaction between small and large sediment particles of natural depositional settings potentially together

with different (i.e. longer) time-spans leaves microscopic wear traces that cannot exactly be reproduced by a simple tumbling experiment.

6.7 Acknowledgements

This project has received funding from the European Research Council (ERC) under the European Union's Horizon 2020 research and innovation programme (grant agreement no 681450 to T.T.), the European Commission FP-07 Individual Marie Curie Fellowship (2012, Ž.Ž.), and the Junior Researcher Grant from the Swedish Research Council VR 2014-4367 (2015, Ž.Ž). This work was supported by the Max Planck Graduate Center with the Johannes Gutenberg-Universität Mainz (MPGC). We would also like to express our gratitude to Jürgen Kriwet (Universität Wien, Austria), Niklas Löffler (University Frankfurt, Germany), Michael Griffiths (William Paterson University, U.S.A.) and Torsten Vennemann (University of Lausanne, Switzerland) for providing fossil and modern wild shark teeth. We are grateful to Scott Blacker (Blackpool Sea Life, UK) and Ivan Sansom (University of Birmingham, UK) for providing access to shed shark teeth from aquaria used in this study. We thank Jennifer Leichliter (Johannes Gutenberg-University Mainz, Germany) for proofreading the manuscript. We further acknowledge the reviews of Ivan Calandra, Jürgen Kriwet and Gildas Merceron that greatly helped to improve the manuscript.

6.8 Supplement

6.8.1 Detailed description of depositional settings of the fossil shark teeth

6.8.1.1 Sands of Kattendijk and Glaukonitsande

The two fossiliferous sedimentary settings are located near Steendorp and Rumst, south-west of Antwerp, Belgium. During the Miocene this area in the Belgian Basin at the north-western border of the European continental shelf was covered by a shallow sea and a huge amount of different vertebrate fossils were deposited together with sand during the Miocene. Due to global sea-level-rise during the Pliocene (Haq et al., 1987), these deposits were eroded and fossils were re-worked and re-deposited as Kattendijk Formation. The basis of the formation is a 10 cm thick bonebed, rich in Miocene and Pliocene vertebrate fossils. The fossil shark fauna is especially rich suggesting abundant food resources. This bonebed layer is overlain by the Glaukonitsande, black and grey-green fine to medium glauconite sands, with a clay component and a shell-rich layer on top of the Kattendijk Formation (Laenen, 1997; Tütken, 2003).

6.8.1.2 Parachucla Formation

The Parachucla Formation contains coastal marine deposits from the Late Oligocene and Lower Miocene together with a rich fossil vertebrate fauna of different sizes. The sediment of the Parachucla Formation contains sandstones formed by fine to middle sand (Morgan, 1989; Tütken, 2003).

6.8.1.3 Bone Valley Formation and Torreya Formation

The Bone Valley Formation in central Florida, as well as the Torreya Formation, belong to the Hawthorn Group. Shark teeth from the Bone Valley Formation are found in the upper part of the formation in phosphate-bearing sands with sand-gravel sized particles and a rich fossil fauna (Palmetto-Fauna, including shark teeth) deposited during a sea-level rise in the Lower Pliocene (Scott and MacGill, 1981; Woodburne, 1987; Scott, 1988; Tütken, 2003). The Torreya Formation contains a rich vertebrate fauna from the Lower to Middle Miocene (Bryant, 1991). The formation consists of siliciclastic sediments with variable carbonate and phosphate content with clay to sand grain size and the fossil bearing layer was deposited during a sea-level high (Bryant, 1991).

6.8.1.4 Alzey Formation

The Alzey Formation is located in the Mainzer Basin west of the Rhine Graben fault in Germany and consists of siliciclastic, coarse-grained, fossil-bearing sands and gravels that were deposited in a marine coastal facies during the Lower Oligocene (Grimm et al., 2000).

6.8.1.5 Yorktown Formation

The shark specimens from the Yorktown Formation are found in North Carolina, U.S.A.. The sediments of this formation were deposited during multiple transgressions in the Lower to Middle Pliocene and interpreted as basement of the Chesapeake Bay (Hobbs, 2004). The Formation is divided into the lower Yorktown and upper Yorktown, whereby the lower consists of muddy, medium to coarse, phosphatic quartz sands and the upper Yorktown has gray, clayey quartz sands with occasional interbeds of sandy clay (Snyder and Riggs, 1993).

6.8.2 Detailed description of dental microwear texture analysis

Four non-overlapping square areas of 160 x 160 µm in close proximity to the apex of the tooth were scanned using a x100 long distance lens (numerical aperture 0.8, resolution in

x, y of 0.16 µm, and z of 0.06 µm). We employed the SSFA parameters *Asfc* (complexity) and *epLsar* (anisotropy), implemented in a new MountainsMap module, where surface features are characterised using length-scale and area-scale fractal analyses (e.g. Ungar et al., 2003, 2012; Scott et al., 2006; Scott, 2012). Additionally, we used standardised roughness (ISO 25178) and flatness (ISO 12781) parameters together with motif, furrow and direction parameters to characterise wear features (Schulz et al., 2013a, 2013b; Purnell and Darras, 2016; Kubo et al., 2017; Purnell et al., 2017).

A MountainsMap template for scans of upper and lower original right shark teeth and moulded left teeth on the buccal side, and moulded upper left teeth on the lingual side was created. In general, all moulded tooth surfaces were mirrored along the z-axis prior to analysis. All scans of upper and lower jaw teeth original left buccal side and moulded right buccal side were mirrored along the x-axis, as well as moulded upper right teeth on the lingual side. All isolated teeth of unknown position were treated as upper right teeth.

Operators used in MountainsMap template:

1. Orientation of dental surface with LS-surface using subtraction
2. Noise-cancelling median filter, filter size 5 x 5
3. Gaussian filter, filter size 3 x 3
4. Filling of non-measured points
5. Set the threshold using the material-% (0.5-99.5 %) to reduce height and depth
6. Removal of isolated outliers, outliers at the edge and with a maximum allowed inclination (85°), soft strength of the method
7. Removal of form using a 2nd order polynomial.

6.8.3 Statistics

For data processing and statistical analyses, the open-source software R v.4.0.0 (R. Development Core Team, 2020) using the packages xlsx (Dragulescu, 2014), rJava (Urbanek, 2016), doBy (Højsgaard and Halekoh, 2016), R.utils (Bengtsson, 2016), factoextra (Kassambara, 2017), plyr (Wickham, 2011), ggplot2 (Wickham, 2016), Rcpp (Eddelbuettel, 2011, 2013), rela (Chajewski, 2009), WRS version 0.12.1 (Wilcox and Schönbrodt, 2010) and the function prcomp() was employed. Surface texture data are usually non-normally distributed and heteroscedastic (e.g. Schulz et al., 2013a), therefore we applied the robust heteroscedastic Welch-Yuen omnibus test (Welch, 1938; Yuen, 1974) paired with a heteroscedastic pairwise comparison (“Lincon test”, analogous to Dunnett's T3 test; Dunnett, 1980) according to the method of Wilcox (Wilcox, 2003, 2005, 2012). A data trimming of 15 %

was performed to remove outliers and compensate for non-normality. We further used the robust heteroscedastic rank-based test according to Cliff (Cliff, 1996; Schulz et al., 2013a), according to the established statistical protocol for 3DST data (Calandra et al., 2012; Schulz et al., 2013a). Finally, before calculating principal component analyses (PCA), we performed the Kaiser-Meyer-Olkin criteria of sampling adequacy (value>0.5) and Bartlett's test of sphericity (<0.05) to validate that PCAs are justified on the current dataset.

6.8.4 Detailed description of results modern wild and aquarium specimens

This dataset compares the DMT of three modern shark species (*Carcharias taurus, Carcharhinus plumbeus, Triaenodon obesus*) kept in an aquarium on the same pellet-based diet with a range of 22 different wild shark species with variable but unknown diet. The data show a high overlap between these two groups with a much higher variance in the wild shark group (**Fig. 6.3C, Table ES6.17-S6.18**). However, 17 DMT parameters show significant differences between aquarium and wild specimens (**Table ES6.18**). In 15 parameters describing the complexity of the surface (*Sdr, nMotif, Asfc*), density (*Spd*), direction (*Tr2R*, *Tr3R, IsT, epLsar*) and height (*S5p, Sku, Sp, FLTv*) of wear features, peak sharpness (*Spc*), slope (*Sdq*) and volume (*Vvv*), the values of aquarium sharks are significantly lower than those of the wild sharks. Only in the parameters *mea* (mean area) and *Smr* (areal material ratio), do the wild sharks have significantly lower values (**Table ES6.18, Fig. ES6.15**).

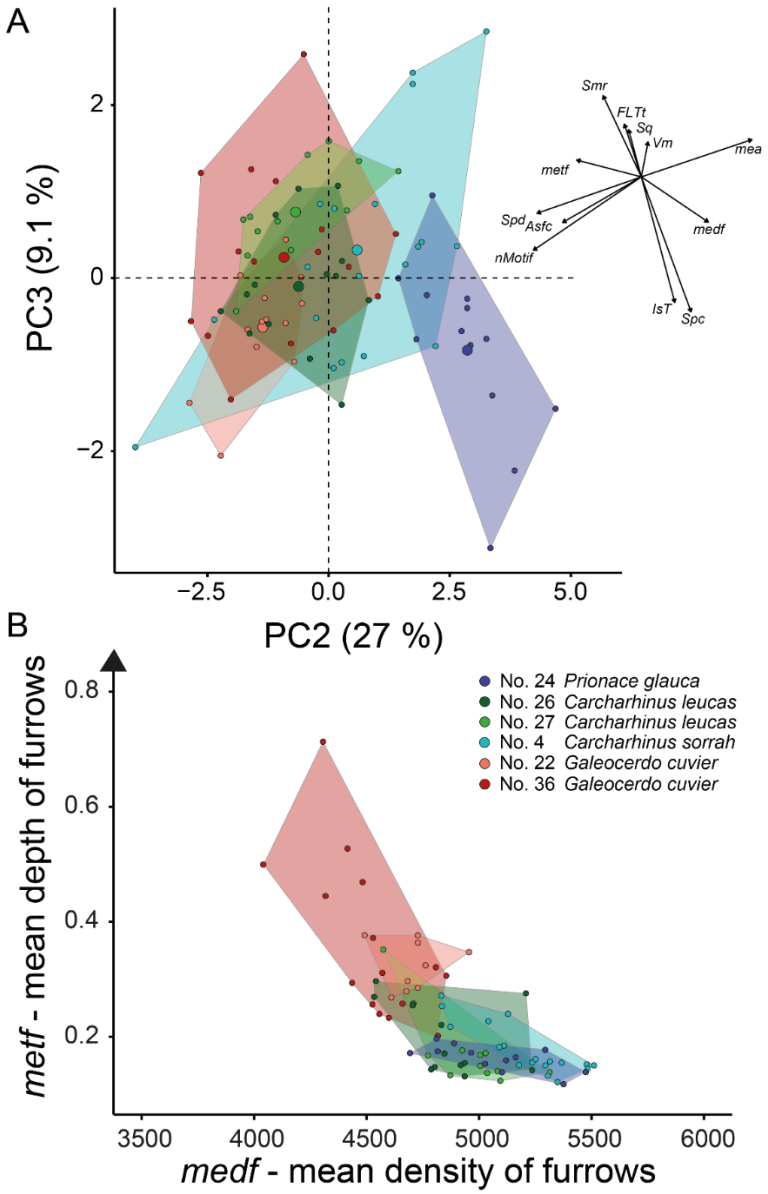

Figure S6.1. Results for the influence of tooth position on DMT. All measured modern shark teeth of *Galeocerdo cuvier* (specimen No. 22 and No. 36), *Carcharhinus leucas* (specimen No. 26 and No. 27), *Carcharhinus sorrah* (specimen No. 4) and *Prionace glauca* (specimen No. 24) for testing the influence of tooth position; for details about the taxa see Table S6.1. A. Principle component analysis (PCA) of surface texture parameters from each category (**Table S4.3**) with good separation of different taxa. Large symbols in PCA plot mark the mean of the area of the different shark taxa. B. Dental microwear texture parameter *metf* [µm] vs *medf* [cm/cm²] values.

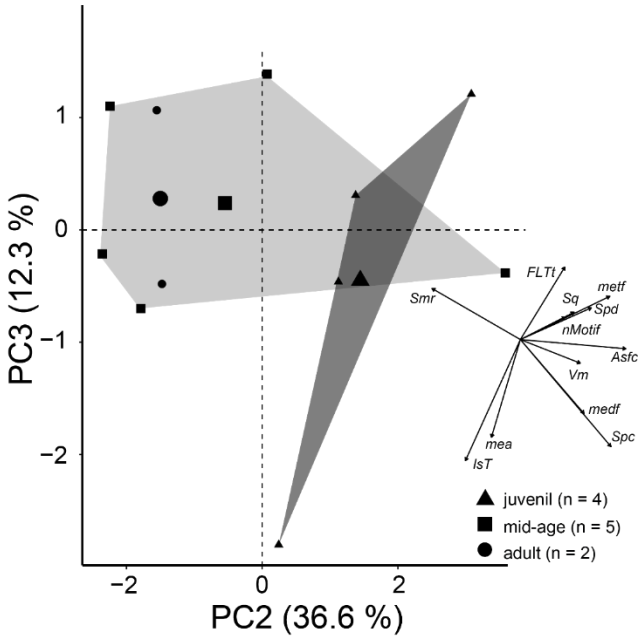

Figure S6.2. Results for the influence of ontogenetic age on DMT. Principle component analysis (PCA) of surface texture parameters from each category (**Table S4.3**) with good separation of all *Galeocerdo cuvier* specimens according to their ontogenetic age to assess whether dental wear differs in different ontogenetic stages. Large symbols in PCA plot mark the mean of the area of the different groups; for details about the taxa see Table S6.1.

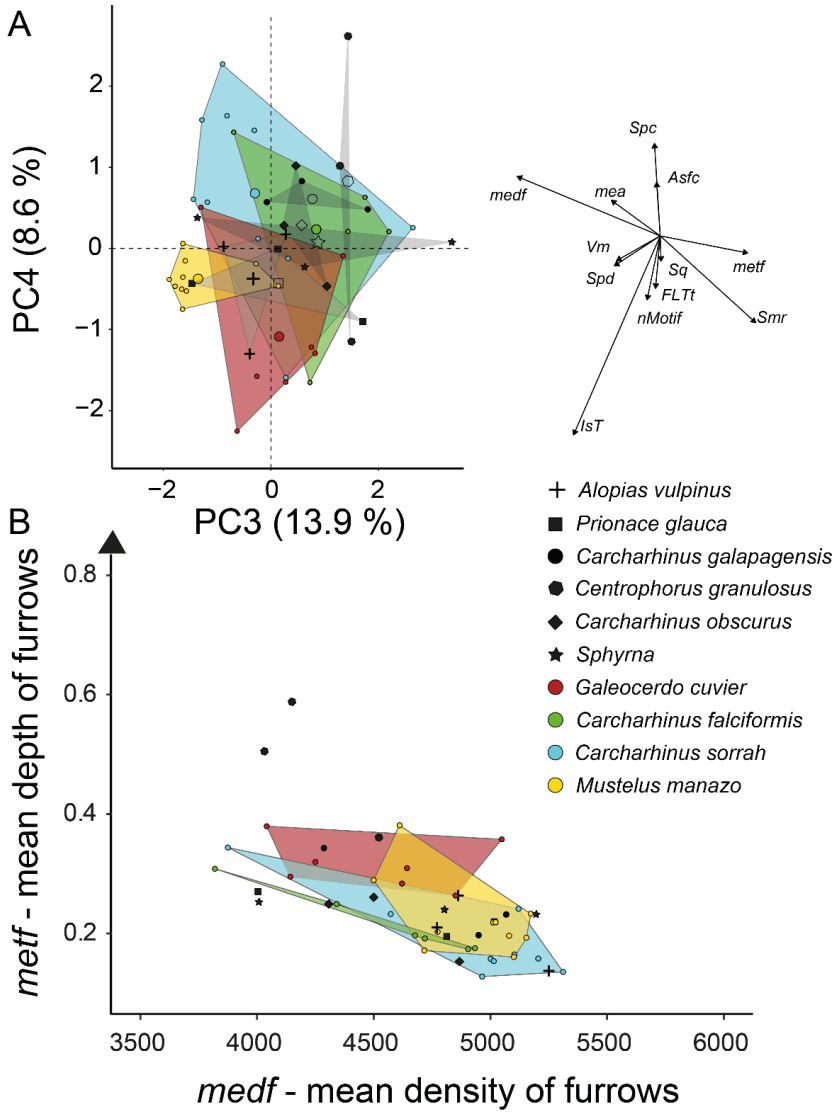

Figure S6.3. Results for the 12 wild shark species; for details about the taxa see Table 6.2 and S6.1. A. Principle component analysis (PCA) of surface texture parameters. Large symbols in PCA plot mark the mean of the area of the different groups. B. Dental microwear texture parameter *metf* [µm] vs *medf* [cm/cm²] values.

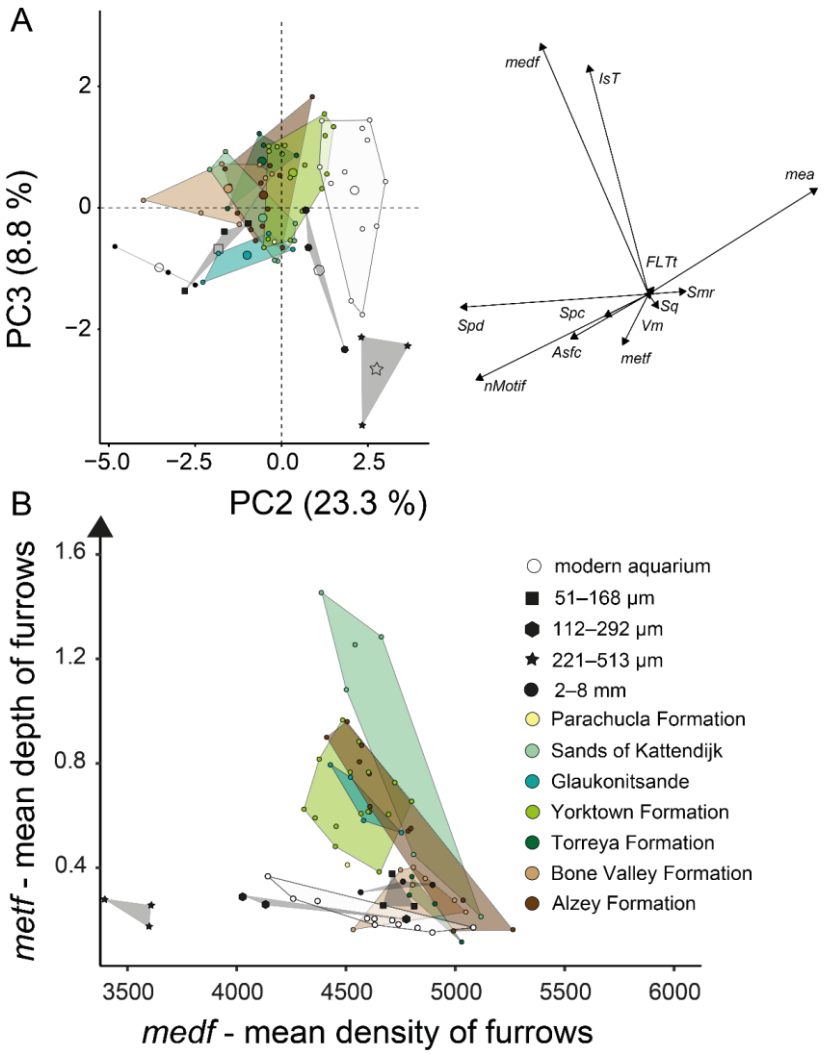

Figure S6.4. Results for the fossil and experimentally altered shark teeth. Modern *Carcharhinus plumbeus* tooth specimens from aquarium sharks used for tumbling experiments. Parameter values of teeth tumbled for 336 h in all four different sediment grain size fractions are plotted. Additionally, the values of all fossil shark tooth specimens are plotted, divided according to their locality.; for details about the taxa see Table S6.1. A. Principle component analysis (PCA) of surface texture parameters. Large symbols in PCA plot mark the mean of the area of the different groups. B. Dental microwear texture parameter *metf* [µm] vs *medf* [cm/cm²] values.

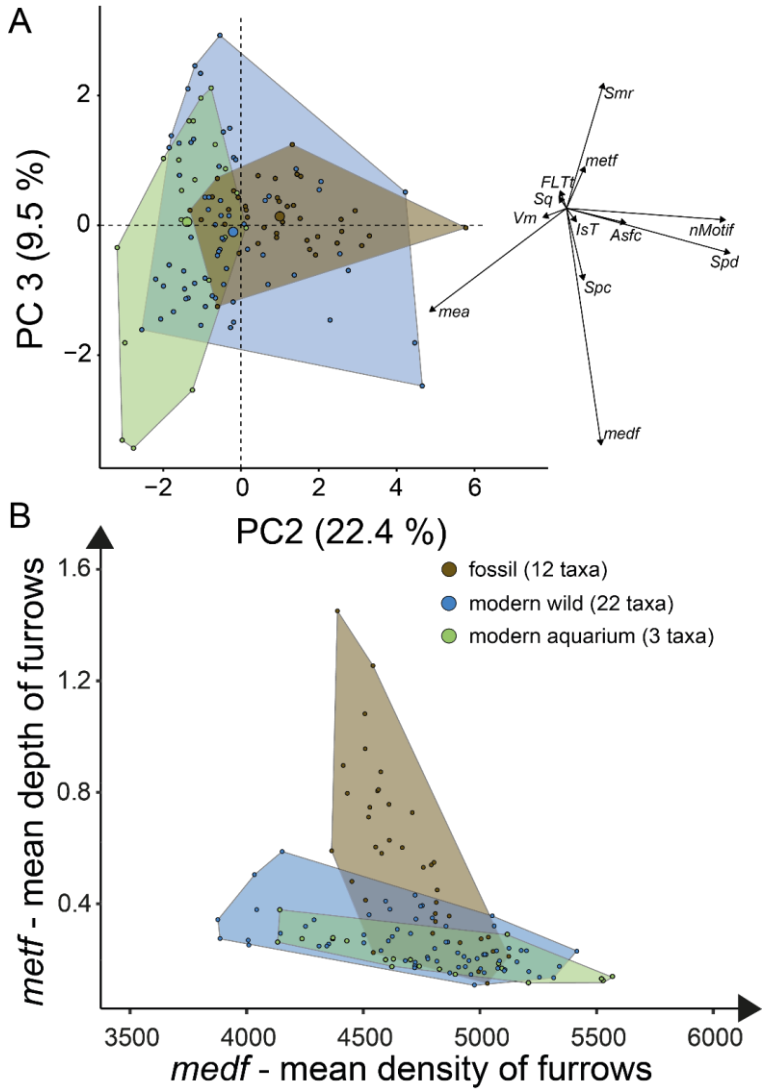

Figure S6.5. All measured modern wild/aquarium and fossil shark teeth; for details about the taxa see Table S6.1. A. Principle component analysis (PCA) of surface texture parameters. Large symbols in PCA plot mark the mean of the area of the different groups. B. Dental microwear texture parameter *metf* [µm] vs *medf* [cm/cm²] values.

Figure ES6.6. Values for all dental microwear texture parameters for *Carcharhinus sorrah* (specimen 4). The thick horizontal bar represents the median of four measured sans per tooth. Data for 20 teeth of the foremost upper tooth row. The figure is found in the electronic Supplement.

Figure ES6.7. Values for all dental microwear texture parameters for *Carcharhinus leucas* (specimen 26). The thick horizontal bar represents the median of four measured sans per tooth. Data for 3 lingual and 9 buccal teeth of foremost upper tooth row and 2 teeth of the foremost lower tooth row. The figure is found in the electronic Supplement.

Figure ES6.8. Values for all dental microwear texture parameters for *Carcharhinus leucas* (specimen 27). The thick horizontal bar represents the median of four measured sans per tooth. Data for 3 lingual and 6 buccal teeth of foremost upper tooth row and 4 teeth of the foremost lower tooth row. The figure is found in the electronic Supplement.

Figure ES6.9. Values for all dental microwear texture parameters for *Prionace glauca* (specimen 24). The thick horizontal bar represents the median of four measured sans per tooth. Data for 2 lingual and 8 buccal teeth of foremost upper tooth row and 3 teeth of the foremost lower tooth row. The figure is found in the electronic Supplement.

Figure ES6.10. Values for all dental microwear texture parameters for *Galeocerdo cuvier* (specimen 22). The thick horizontal bar represents the median of four measured scans per tooth. Data for 2 lingual and 7 buccal teeth of the foremost upper tooth row and 3 teeth of the foremost lower tooth row. The figure is found in the electronic Supplement.

Figure ES6.11. Values for all dental microwear texture parameters for *Galeocerdo cuvier* (specimen 36). The thick horizontal bar represents the median of four measured scans per tooth. Data for 2 lingual and 9 buccal teeth of the foremost upper tooth row and 5 teeth of the foremost lower tooth row. The figure is found in the electronic Supplement.

Figure ES6.12. Boxplots for all dental microwear texture parameters for different ages of *Galeocerdo cuvier*. The thick horizontal bar represents the median; the box encloses the first (25%) and third (75%) quartiles; the whiskers (extend to 1.5 times the length of the box (the interquartile range); the dots represent outliers. The figure is found in the electronic Supplement.

Figure ES6.13. Boxplots for all dental microwear texture parameters for upper central tooth of *Alopias vulpines* (*A. v.*), *Prionace glauca* (*P. g*), *Carcharhinus falciformis* (*Ca. f.*), *Carcharhinus galapagensis* (*Ca. gal.*), *Centrophorus granulosus* (*Ce. g.*), *Carcharhinus obscurus* (*Ca. o.*), *Carcharhinus sorrah* (*Ca. s.*), *Mustelus manazo* (*M. m.*), *Sphyrna* (*S.*), *Galeocerdo cuvier* (*G. c*). The thick horizontal bar represents the median; the box encloses the first (25%) and third (75%) quartiles; the whiskers (extend to 1.5 times the length of the box (the interquartile range); the dots represent outliers. The figure is found in the electronic Supplement.

Figure ES6.14. Boxplots for all dental microwear texture parameters for the experimentally altered *Carcharhinus plumbeus* teeth (see **Table 6.2**). For parameter description, see Table S4.3. FFS = 51-168 µm; FS = 112-292 µm; S = 221-513 µm; G = 221-513 µm. The thick horizontal bar represents the median; the box encloses the first (25%) and third (75%) quartiles; the whiskers (extend to 1.5 times the length of the box (the interquartile range); the dots represent outliers. The figure is found in the electronic Supplement.

Figure ES6.15. Boxplots for all dental microwear texture parameters for fossil and modern wild shark tooth specimens. The thick horizontal bar represents the median; the box encloses the first (25%) and third (75%) quartiles; the whiskers (extend to 1.5 times the length of the box (the interquartile range); the dots represent outliers. The figure is found in the electronic Supplement.

Table ES6.1. Shark taxon, sample ID, dataset and type of specimen. The table is found in the electronic Supplement.

Table S6.2. Importance of components for PCA from different tooth positions (*Smr, medf, Spd, nMotif, Asfc, Spc, metf, Vm, Sq, FLTt, IsT, mea*).

	PC1	PC2	PC3	PC4	PC5	PC6	PC7	PC8	PC9	PC10	PC11	PC12
Standard deviation	2.305	1.8	1.045	0.9199	0.6321	0.6	0.559	0.4368	0.3581	0.23223	0.19577	0.1658
Proportion of Variance	0.443	0.27	0.091	0.0705	0.0333	0.03	0.026	0.0159	0.0107	0.00449	0.00319	0.00229
Cumulative Proportion	0.443	0.713	0.804	0.8742	0.9074	0.937	0.963	0.9793	0.99	0.99452	0.99771	1

Table S6.3. Importance of components for PCA from different ontogenetic stages (*Smr, medf, Spd, nMotif, Asfc, Spc, metf, Vm, Sq, FLTt, IsT, mea*).

	PC1	PC2	PC3	PC4	PC5	PC6	PC7	PC8	PC9	PC10	PC11	PC12
Standard deviation	2.193	2.095	1.213	0.7609	0.5572	0.5119	0.29719	0.28266	0.3581	0.10493	0.02917	2.59E-16
Proportion of Variance	0.401	0.366	0.123	0.0483	0.0259	0.0218	0.00736	0.00666	0.0107	0.00092	0.00007	0.00E+00
Cumulative Proportion	0.401	0.766	0.889	0.9373	0.9631	0.985	0.99235	0.99901	0.99	0.99993	1	1.00E+00

Table S6.4 Importance of components for PCA from 12 wild shark species (*Smr, medf, Spd, nMotif, Asfc, Spc, metf, Vm, Sq, FLTt, IsT, mea*).

	PC1	PC2	PC3	PC4	PC5	PC6	PC7	PC8	PC9	PC10	PC11	PC12
Standard deviation	2.158	1.753	1.29	1.0185	0.7846	0.58	0.5191	0.3865	0.26812	0.2401	0.20075	0.16081
Proportion of Variance	0.388	0.256	0.139	0.0864	0.0513	0.028	0.0225	0.0124	0.00599	0.0048	0.00336	0.00215
Cumulative Proportion	0.388	0.644	0.783	0.8694	0.9207	0.949	0.9712	0.9837	0.98968	0.9945	0.99785	1

Table S6.5 Importance of components for PCA from the experimentally altered teeth. Modern *Carcharhinus plumbeus* tooth specimens from aquarium sharks used for tumbling experiments and all fossil shark tooth specimens, divided according to their locality (*Smr, medf, Spd, nMotif, Asfc, Spc, metf, Vm, Sq, FLTt, IsT, mea*).

	PC1	PC2	PC3	PC4	PC5	PC6	PC7	PC8	PC9	PC10	PC11	PC12
Standard deviation	2.583	1.678	0.9534	0.8021	0.6046	0.5316	0.34275	0.29465	0.23403	0.1867	0.10561	0.08225
Proportion of Variance	0.556	0.235	0.0757	0.0536	0.0305	0.0236	0.00979	0.00723	0.00456	0.0029	0.00093	0.00056
Cumulative Proportion	0.556	0.791	0.8664	0.92	0.9505	0.974	0.9838	0.99104	0.9956	0.9985	0.99944	1

Table S6.6. Importance of components for PCA from fossil and modern shark species (*Smc, medf, Spd, nMotif, Asfc, Spc, metf, Vm, Sq, FLTt, IsT, mea*).

	PC1	PC2	PC3	PC4	PC5	PC6	PC7	PC8	PC9	PC10	PC11	PC12
Standard deviation	2.406	1.641	1.0689	0.9183	0.774	0.6063	0.565	0.3625	0.22164	0.21534	0.11409	0.08844
Proportion of Variance	0.482	0.224	0.0952	0.0703	0.05	0.0306	0.0266	0.0109	0.00409	0.00386	0.00108	0.00065
Cumulative Proportion	0.482	0.707	0.8019	0.8722	0.922	0.9527	0.9794	0.9903	0.9944	0.99826	0.99935	1

Table ES6.7. Descriptive statistics (mean) for all DMTA parameters for *Carcharhinus sorrah* (specimen 4) at different tooth positions (see **Table ES6.1**). For parameter description, see Table S4.3. The table is found in the electronic Supplement.

Table ES6.8. Descriptive statistics (mean) for all DMTA parameters for *Carcharhinus leucas* (specimen 26) at different tooth positions (see **Table ES6.1**). For parameter description, see Table S4.3. The table is found in the electronic Supplement.

Table ES6.9. Descriptive statistics (mean) for all DMTA parameters for *Carcharhinus leucas* (specimen 27) at different tooth positions (see **Table ES6.1**). For parameter description, see Table S4.3. The table is found in the electronic Supplement.

Table ES6.10. Descriptive statistics (mean) for all DMTA parameters for *Prionace glauca* (specimen 24) at different tooth positions (see **Table ES6.1**). For parameter description, see Table S4.3. The table is found in the electronic Supplement.

Table ES6.11. Descriptive statistics (mean) for all DMTA parameters for *Galeocerdo cuvier* (specimen 22) at different tooth positions (see **Table ES6.1**). For parameter description, see Table S4.3. The table is found in the electronic Supplement.

Table ES6.12. Descriptive statistics (mean) for all DMTA parameters for *Galeocerdo cuvier* (specimen 36) at different tooth positions (see **Table ES6.1**). For parameter description, see Table S4.3. The table is found in the electronic Supplement.

Table ES6.13. Descriptive statistics (mean ±SD) for all DMTA parameters for different ages of *Galeocerdo cuvier* (see **Table ES6.1**). For parameter description, see Table S4.3. The table is found in the electronic Supplement.

Table ES6.14. Descriptive statistics (mean ±SD) for all DMTA parameters of the wild taxa. For upper central tooth of *Alopias vulpines* (*A.v.*), *Prionace glauca* (*P.g*), *Carcharhinus falciformis* (*Ca. f.*), *Carcharhinus galapagensis* (*Ca.gal.*), *Centrophorus granulosus* (*Ce. g.*), *Carcharhinus obscurus* (*Ca.o.*), *Carcharhinus sorrah* (*Ca. s.*), *Mustelus manazo* (*M. m.*), *Sphyrna* (*S.*), *Galeocerdo cuvier* (*G. c*) (see **Table 6.1**). For parameter description, see Table S4.3. The table is found in the electronic Supplement.

Table ES6.15. Statistical results for all DMTA parameters of the wild taxa. For upper central tooth of *Alopias vulpines* (*A.v.*), *Prionace glauca* (*P.g*), *Carcharhinus falciformis* (*Ca. f.*), *Carcharhinus galapagensis* (*Ca.gal.*), *Centrophorus granulosus* (*Ce. g.*), *Carcharhinus obscurus* (*Ca.o.*), *Carcharhinus sorrah* (*Ca. s.*), *Mustelus manazo* (*M. m.*), *Sphyrna* (*S.*), *Galeocerdo cuvier* (*G. c*). For parameter description, see Table S4.3. The table is found in the electronic Supplement.

Table ES6.16. Descriptive statistics (mean ±SD) for all DMTA parameters for the experimentally altered *Carcharhinus plumbeus* teeth (see **Table 6.2**). For parameter description, see Table S4.3. FFS = 51-168 µm; FS = 112-292 µm; S = 221-513 µm; G = 221-513 µm. The table is found in the electronic Supplement.

Table ES6.17. Descriptive statistics (mean ±SD) for all DMTA parameters for fossil and modern wild/aquarium specimens (see **Table S6.1**). For parameter descriptions, see Table S4.3. The table is found in the electronic Supplement.

Table ES6.18. Statistical results for all DMTA parameters for fossil (f) and modern wild (w)/aquarium (a) specimens. For parameter descriptions, see Table S4.3. The table is found in the electronic Supplement.

Chapter 7 Manuscript V: Diagenetic stability of non-traditional stable isotope systems (Ca, Sr, Mg, Zn) in teeth – an in-vitro alteration experiment of biogenic apatite in isotopically enriched tracer solution

Diagenetic stability of non-traditional stable isotope systems (Ca, Sr, Mg, Zn) in teeth – an *in-vitro* alteration experiment of biogenic apatite in isotopically enriched tracer solution

Weber, Katrin[1], Weber, Michael[1], Menneken, Martina[2], Kral, Anna G.[2], Mertz-Kraus, Regina[1], Geisler, Thorsten[2], Vogl, Jochen[3], Tütken, Thomas[1]

[1]Institute of Geosciences, Johannes Gutenberg University, J.-J.-Becher-Weg 21, 55128 Mainz, Germany

[2]Institute of Geoscience, Rheinische Friedrich-Wilhelms University Bonn, Poppelsdorfer Schloß, 53115 Bonn, Germany

[3]Bundesanstalt für Materialforschung und -prüfung (BAM), Berlin, Germany

This manuscript is submitted to *Geochimica et Cosmochimica Acta.*

7.1 Abstract

Stable isotope ratios and trace element concentrations of fossil bones and teeth are important geochemical proxies for the reconstruction of diet and past environment in archaeology and palaeontology. However, since diagenesis can significantly alter primary diet-related isotope signatures and elemental compositions, it is important to understand and quantify alteration processes. Here, we present the results of *in-vitro* alteration experiments of dental tissues from a modern African elephant molar reacted in aqueous solutions at 30 °C and 90 °C for 4 to 63 days. Dental cubes with ≈ 3 mm edge length, comprising both enamel and dentin, were placed into 2 mL of acidic aqueous solution enriched in different isotopes (^{25}Mg, ^{44}Ca, ^{67}Zn, ^{86}Sr). Element and isotope distribution profiles across the reacted cubes were measured with LA-(MC-)ICP-MS and EMPA, while potential effects on the bioapatite crystal structure were characterised by Raman spectroscopy. In all experiments isotope ratios measured by LA-(MC-)ICP-MS revealed an alteration of the enamel in the outer ≈ 200-300 µm. In contrast, dentin was fully altered after one week at 90 °C. Then, the tracer solution started also to penetrate through the enamel-dentin junction into the innermost enamel, however, leaving the central part of the enamel unaltered, even after three months. The Raman spectra suggest an initial demineralisation in the acidic environment while organic matter (i.e. collagen) is still preserved. In the 90 °C experiment, Raman spectra of the $v_1(PO_4)$ band of the dentin shift over time towards synthetic hydroxylapatite patterns and the Ca (and Sr) concentrations in the respective solutions decrease. This indicates precipitation of newly formed apatite. Isotope and element concentration profiles across the dental tissues reveal different exchange mechanisms for different isotope systems. Magnesium is leached from enamel and dentin, while Zn is incorporated into the apatite crystal structure. However, the distribution of both elements is not affected in the innermost enamel where their concentrations do not change over the whole duration of the experiments. We found no correlation of reaction depth in the cubes and experimental duration, which might be caused by natural variability of the dental material already at the beginning of the experiment. Our alteration experiments in a closed system at high temperatures ≤90 °C and low initial pH demonstrate that at least the central part of mm-thick mammalian enamel apatite seems to be resistant against alteration preserving its pristine bioapatite mineral structure as well as its in vivo elemental and isotopic composition. The experiments in the presented study demonstrate that the isotopes Ca, Sr, Zn and Mg in the dentin are prone for diagenetic alteration, while enamel is more resistant against alteration and could be used for dietary and physiological reconstructions in fossil teeth.

7.2 Introduction

Bones and teeth are important proxy archives for the reconstruction of diet, ecology, habitat use, and environment of extant and extinct vertebrates. Both traditional and non-traditional stable isotopes in bones and teeth have become important proxies for the reconstruction of diet ($\delta^{13}C$: e.g. DeNiro and Epstein, 1978; $\delta^{15}N$: DeNiro and Epstein, 1981; Leichliter et al., under review), diet and trophic level ($\delta^{44}Ca$: Skulan et al., 1997; Clementz et al., 2003; Heuser et al., 2011; Melin et al., 2014; Tacail et al., 2020; $\delta^{26}Mg$: Martin et al., 2014, 2015b; $\delta^{66}Zn$: Jaouen et al., 2013, 2016a, b, 2020; Bourgon et al., 2020; $\delta^{88/86}Sr$: Knudson et al., 2010; Lewis et al., 2017) and migration ($^{87}Sr/^{86}Sr$: Ericson, 1985; Price et al., 1994; Sillen et al., 1995; Hoppe et al., 1999), respectively. Environment- and diet-related element or isotope compositions are ingested from food and water and via metabolic processes incorporated into bones and teeth. Bones and teeth are hard tissues composed predominantly of bioapatite, a non-stoichiometric, carbonate-bearing hydroxylapatite with the formula $Ca_{10}–x[(PO_4)_6–x(CO_3)x]\ (OH)_2–x\cdot nH_2O$, where n ranges between 0.1 and 0.3 (Pasteris et al., 2014). The OH group in bioapatite is partly replaced by F, whereas Ca is partly substituted by, e.g., Mg, Zn, Sr, Na, and K due to their similar chemical behaviour and ion radii (e.g., Kohn et al., 1999; Boanini et al., 2010). Bone and tooth apatite is a complex solid solution that is further characterised by a small crystallite size in the order of 20 to 150 nm. Dental enamel has on average, larger bioapatite crystallites than bone and dentin, a significantly lower organic content (≈ 1 %) of phosphoproteins and amelogenins, and negligible intrinsic porosity (Hillson, 2005). This makes tooth enamel much less prone to diagenetic alteration than bone and dentin, the latter which has similar properties as bone and is thus similarly susceptible to aqueous alteration and diagenetic changes (see overview in: Tütken and Vennemann, 2011). Due to its crystal-chemical properties, bioapatite is a highly reactive phase that, if its physical and chemical environment is changing, for instance, after death of the individual, has a high thermodynamic driving force to dissolve (Berna et al., 2004). In teeth, the organic and inorganic components vary significantly between different hard tissues such as enamel, dentin, and cement. While enamel contains about 960-990 mg/g hydroxylapatite, dentin and cement contain about 200 mg/g and ≈ 300 mg/g of collagen, respectively (Hillson, 2005). According to its different protein content, crystallite size, and porosity, enamel apatite is less vulnerable to diagenetic alteration than dentin and bone (Wang and Cerling, 1994; Hedges et al., 1995; Kohn et al., 1999; Hedges, 2002; Pfretzschner, 2004). However, also enamel, especially its trace element composition, can be altered during the fossilization process (e.g., Kohn et al., 1999; Schoeninger et al., 2003), while stable light isotope composition such as C and O (CO_3^{2-} or PO_4^{3-} group) are not prone to diagenetic alteration (Lee-Thorp et al., 1989, 2000; Ayliffe et al., 1994), except if microbes are involved (Zazzo et al., 2004a, b).

Diagenetic alteration of the isotopic composition in bioapatite depends on several variables such as temperature, pH, chemical and isotopic compositions of the surrounding fluid and/or sediment as well as of the biogenic apatite itself. Some elements are more prone for diagenetic alteration than others, therefore every element or isotope system has to be checked for alteration individually. In general, systematic studies on the effect of diagenesis on trace element composition are rare. A good overview about the current knowledge of various isotope systems, such as Ca, Mg, Cu, Zn and Fe, as well as their diagenetic vulnerability in biological apatite and potential applications for vertebrate palaeobiology are given by Martin et al. (2017a). Heuser et al. (2011) measured the calcium isotope composition of fossil dinosaur enamel as well as dentin from the same teeth and could not detect any diagenetic alteration of $\delta^{44/40}$Ca values in both dental tissues, which was further supported by mass balance considerations. However, especially trace elements, such as Sr, Mg and Zn, are more prone to diagenetic alteration compared to the major element Ca. A trace element study performed on Plio-Pleistocene South African australopithecine teeth displayed dramatically increased Zn levels in the fossil enamel samples, compared to Sr/Ca, Ba/Ca and Pb/Ca ratios, which were not significantly altered during fossilization (Sponheimer and Lee-Thorp, 2006). Different trace elements seem to be affected differently during diagenesis. Generally, the effect on Zn in fossil enamel seem to vary from site to site (Bocherens et al., 1994; Sponheimer and Lee-Thorp, 2006; Hinz and Kohn, 2010). Bourgon et al. (2020) measured enamel Zn isotope ratios of a diverse fossil Late Pleistocene fauna from the Tam Hay Marklot cave and found the δ^{66}Zn values still reflecting trophic level differences similar to modern mammals, supporting that the ante-mortem Zn isotope composition and concentration was still preserved. Both, in modern and fossil teeth they found the outermost enamel layer of <200 µm displaying higher Zn concentration. This Zn concentration increase towards the outermost enamel was also found in teeth of other large mammals and seems to be caused by the process of enamel maturation (Müller et al., 2019). Based on mass balance considerations a diagenetic Mg uptake seems to be unlikely, at least for terrestrial settings, since the Mg concentration in fresh water fluids (5 – 20 µg/mL, Shalev et al., 2017; Potasznik and Szymczyk, 2015) is negligible in comparison to the typical at least 100-fold higher Mg concentration in bioapatite (2000 – 10000 µg/g, Martin et al., 2017a). In contrast, because of the higher Mg concentration in seawater (~1300 mg/mL, Shalev et al., 2017), a diagenetic alteration of Mg in bioapatite deposited in marine settings is more likely. Overall, alteration of the trace element composition and isotope ratios can vary from one setting to another, according to the type of surrounding sediment, stratigraphic age as well as taphonomical and environmental conditions (e.g., Wang and Cerling, 1994; Kohn et al., 1999; Hedges, 2002). A study by Copeland et al. (2010) on Sr isotopes (^{87}Sr/^{86}Sr) in fossil rodent teeth from South Africa suggest little contamination of tooth enamel with diagenetic Sr, however, dentin was observed to have ≈ 50 % diagenetic Sr. Another study by Budd et al.

(2000) on archaeological human teeth also found a common, but highly variable diagenetic alteration of Sr in the dentin, potentially derived from the surrounding soil. Hoppe et al. (2003) demonstrate, that pretreatment can eliminate around 20 % of diagenetic Sr from Holocene seal bones, and nearly 95 % from fossil tooth enamel.

The understanding of alteration processes is paramount for the reconstruction of palaeoenvironmental or palaeodietary information from fossil teeth. However, still little is known about these processes and mechanisms driving those chemical and mineralogical alterations, such as recrystallization or isotope exchange processes. Thus far, only few diagenetic alteration experiments were made. Snoeck et al. (2015) performed an alteration experiment, where they put fragments of tooth enamel and calcined bones in ^{87}Sr-spiked solution for up to 1 year at room temperature and afterwards cleaned the samples using acetic acid washing and ultrasonic. $^{87}Sr/^{86}Sr$ was measured before and after the cleaning treatment, whereby all samples showed elevated ratios of $^{87}Sr/^{86}Sr$ before cleaning. After cleaning, only enamel remained significantly elevated in ^{87}Sr, indicating that porosity allows Sr to penetrate into the dental material, however, higher crystallinity of calcined bones in comparison to pristine bones and tooth enamel did not allow an incorporation of Sr into the crystal lattice. This is showing that apatite crystallinity plays a major role during diagenesis (Snoeck et al., 2015). There is only a small number of alteration experiments, dealing with the alteration of stable isotope compositions and apatite crystallinity changes. In most cases, alteration experiments are performed on bone material (e.g. Stiner and Kuhn, 1995; Berna et al., 2004; Pucéat et al., 2004; Munro et al., 2007; Kohn and Moses, 2013; Keenan and Engel, 2017; Aufort et al., 2019). Berna et al. (2004) performed dissolution experiments in aqueous and buffered solution with synthetic hydroxylapatite and bone samples at 25 °C with the purpose of measuring the solubilities and therefore the stabilities of fossil bone under quasi-natural conditions. The so-called recrystallization window, the chemical conditions under which bone apatite can recrystallize into authigenic apatite, is restricted to a narrow pH range between 7.6 and 8.1. Preservation is best at a pH of above 8.1, whereby minerals will undergo recrystallization in alkaline to neutral pH conditions. This, together with precipitation of additional apatite, will generally increase the crystallinity of the bone material. Berna et al. (2004) found, that under a pH of 7.5, the original bone mineral was totally recrystallized. An experiment on alligator bones buried in wetland soils and in experimental mesocosms with and without microbial colonization performed by Keenan and Engel (2017) found that this recrystallization into a more stable apatite phase occurred already after one month of burial when microbial colonization was inhibited. Preservation of stable isotope compositions in bone were experimentally investigated by Munro et al. (2007) or Aufort et al. (2019). Munro et al. (2007) tested the effects of heating bone in air on the isotopic composition of phosphate oxygen, whereby the original $\delta^{18}O_{PO4}$ values were preserved at <300 °C and strongly shifts towards

lower $\delta^{18}O_{PO4}$ values at higher temperatures, potentially due to ^{18}O exchanges with an external low-^{18}O reservoir in the phosphate oxygen. Whereas Aufort et al. (2019) performed immersion experiments of modern bones in aqueous NaF solution at pH 9 - 10 for up to three weeks at up to 70 °C and measured F, Ca and P concentrations, C and O isotopes, as well as vibrational (ATR-FTIR, Raman) and solid-state (H-1, C-13, F-19) NMR spectroscopies. They found a transformation mechanism by partial dissolution of biogenic apatite and precipitation of secondary apatite. There are only a few experiments on enamel hydroxylapatite (e.g., Koch et al., 1997; Zazzo et al., 2004a, b). Zazzo et al. (2004a) measured $\delta^{13}C$ and $\delta^{18}O$ of bone and tooth enamel powders after immersing the samples in ^{13}C- and ^{18}O-labelled water with the result of rapid and significant isotopic changes in the bone material, while tooth enamel is more resistant, however not exempt of alteration. Especially in the presence of microbial activity, even $\delta^{18}O_{PO4}$ values can alter in both, bone and tooth enamel. From the Raman spectroscopy perspective, spectra reveal modifications of the position and the full width at half maximum of the $v_1(PO_4^{3-})$ band caused by aqueous alteration (Thomas et al., 2007). In general, Raman spectroscopy is used in palaeontology for identification of mineralogical contents (Schweitzer et al., 1997), crystallinity changes (Person et al., 1995) and diagenetically induces ion concentration (MacFadden et al., 2010). Thomas et al. (2011) were able to detect io exchanges in apatite chemistry in fossil enamel and dentin samples indicating significant diagenetic alteration using Raman spectroscopy. They found Raman spectroscopy to be very useful a non-destructive tool for pre-screening fossil samples for diagenetic alteration (particularly CO_3^{2-}, F^- and Sr^{2+}).

To our knowledge, there are so far no experiments performed to assess the stability of original element and isotope compositions of enamel and dentin by exposing tooth pieces to aqueous solutions. Here we present an extensive *in-vitro* alteration experiment assessing the resistance of non-traditional stable isotopes against diagenetic alteration in enamel and dentin by immersing tooth pieces in an isotope tracer solution enriched in ^{25}Mg, ^{44}Ca, ^{67}Zn, and ^{86}Sr. For this purpose, cubes cut from a modern elephant molar comprising both enamel and dentin were placed into the acidic tracer solution at 30 °C and 90 °C and for different time intervals (up to three months). This experimental approach allows to assess the diagenetic stability of these non-traditional isotope systems used for dietary reconstruction and to characterize the physico-chemical mechanisms involved in tooth diagenesis. Changes of the chemical composition and isotopic composition in the reacted samples are measured *in-situ* with high spatial resolution using LA-ICP-MS, LA-MC-ICP-MS, electron microprobe and Raman spectroscopy on the dental cubes before and after the alteration experiments.

7.3 Material and methods

7.3.1 Dental material

A molar of a wild modern African elephant (*Loxodonta africana*) from Africa of unknown provenance (AG-Lox: Gehler et al., 2012) was cut into mm-sized dental cubes with a mean edge length of about 3.3 mm ± 0.3 mm (1SD). Enamel thickness is on average 1.8 mm ± 0.2 mm (1SD), that of the dentin portion from the enamel dentin junction (EDJ) is on average about 1.4 mm ± 0.2 mm (1SD). The mean weight of the cubes was 63.8 mg ± 3.5 mg (1SD) (Table 7.1). An overview of the sampling locations on the dental cubes of the *in-situ* element and isotope analyses is provided in Figure 7.1.

7.3.2 Isotope tracer solution

For all alteration experiments, an aqueous solution isotopically enriched in ^{25}Mg, ^{44}Ca, ^{67}Zn and ^{86}Sr was used (**Table S7.1**). The different isotopes ^{25}Mg, ^{67}Zn and ^{86}Sr (in HNO_3 solution) were mixed and evaporated at 80 °C down to a volume of ≈ 500 µL. ^{44}Ca was added (as carbonate powder, 34.8 mg $CaCl_2$, 97 % ^{44}Ca) and evaporated at ≈ 55 °C to a volume of ≈ 100 µL. Afterwards 1 mL of $H_2{}^{18}O$ (Sigma-Aldrich, 97 atom-% ^{18}O) was added and the solution was filled up to 30 ml with D_2O (Sigma-Aldrich, 99.9 atom-% D). The final acidic tracer solution (pH of ≈ 1) was shaken and equilibrated for three hours before entering the experiment. The element concentrations of the tracer solution after different time intervals of the dental immersion experiments and an aliquot of the starting solution were measured using a Thermo Element 2/XR ICP-MS system (University Bonn). Results are presented in Figure 7.2 and Table S7.1.

7.3.3 *In-vitro* alteration experiment

The alteration experiments were performed in custom-made 3 mL teflon beakers, self-sealed autoclaves with custom-made furnaces. The dental cube samples were weighted before and after the experiment to determine the weight loss. For each beaker, the temperature was constantly monitored during the experiment using a Digital Multimeter Voltcraft 840. Room temperature and relative humidity were monitored during the whole experiment, using a Tinytag Ultra 2 Datalogger – TGU-4500 (Gemini Data Loggers, Chichester, United Kingdom). The room temperature over the whole duration of the experiment was always below 26 °C (average 22.6 °C ± 2.0 °C). Each 3 mL teflon autoclave was filled with 2 mL of aqueous tracer solution. One dental cube was added to each teflon autoclave (**Fig. 7.1**).

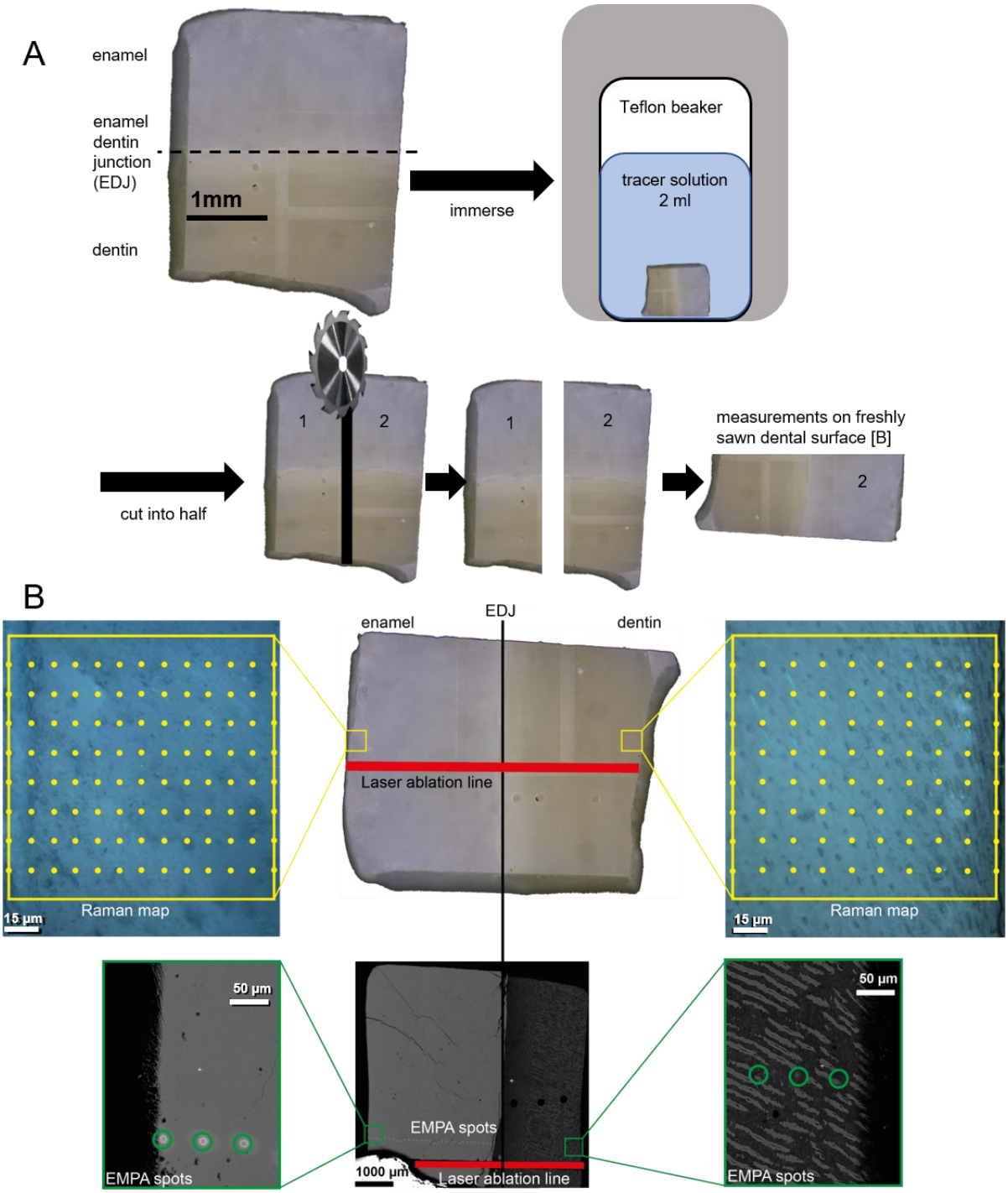

Figure 7.1. Illustration of the experimental setup. A. Dental cubes, containing enamel and dentin, were immersed in isotopic tracer solution enriched in ^{25}Mg, ^{44}Ca, ^{67}Zn and ^{86}Sr and afterwards cut into half for in situ trace element and Sr isotope analysis. B. Illustration of the scans and maps measured with different in situ analytical techniques on the freshly sawn surface of one of the two halves of the dental cube. Red: Laser ablation lines of ICP-MS and MC-ICP-MS across the EDJ. Yellow: Raman maps, covering the outer 120 µm rim of both dental tissues, different number of rows for dentine (n = 10) and enamel (n = 13). Yellow dots indicate one Raman measurement respectively. Green: EMPA spots across EDJ, parallel to the laser ablation lines.

Table 7.1. Sample list of dental cubes with size and weight (before and after experiment).

Sample ID	Experiment	Temperature [°C]	Duration [days]	Length [mm]	Length after Experiment [mm]	Length loss [%]	Weight before Experiment [mg]	Weight after Experiment [mg]	Weight loss [%]
G	Isotopic tracer solution	30	4	3.52	3.42	2.8	59.5	49.1	17.5
K	Isotopic tracer solution	30	7	3.3	3.11	5.8	62	51.9	16.3
N	Isotopic tracer solution	30	14	3.25	2.91	10.5	64.8	54.6	15.7
C	Isotopic tracer solution	30	21	2.95	2.75	6.8	66.7	56.9	14.7
E	Isotopic tracer solution	30	64	3.14	2.91	7.3	66.8	56.5	15.4
A	Isotopic tracer solution	90	4	2.98	2.73	8.4	61.2	47.5	22.4
H	Isotopic tracer solution	90	7	3.17	2.81	11.4	62.9	48.2	23.4
I	Isotopic tracer solution	90	14	3.49	3.23	7.4	66.2	49.2	25.7
J	Isotopic tracer solution	90	21	3.01	2.86	5.0	67.8	52.9	22.0
F	Isotopic tracer solution	90	64	3.77	3.65	3.2	66.8	49.6	25.7
D	untreated reference sample	-	-	3.23			57.3	-	-
L	untreated reference sample	-	-	3.75			116.3	-	-
M	untreated reference sample	-	-	3.25			93.8	-	-

The experiments were carried out at 30 °C and 90 °C (± 1 °C) over a period of 4, 7, 14, 21 and 64 days (**Table 7.1**). After the experiment, the samples were washed three times with ultrapure water and dried in a desiccator for one day at room temperature. After drying, the samples were cut in half, perpendicular to the enamel-dentin junction (**Fig. 7.1**). On the first half, first LA-ICP-MS and LA-ICP-MC-MS measurements were performed, afterwards, after embedding and polishing, the same halves were used for Raman spectroscopy and electron microprobe measurement (**Table S7.2**). For further description of the embedding see section "Electron microprobe analysis" and "Raman spectroscopy".

7.3.4 Laser ablation inductively coupled plasma mass spectrometry (LA-ICP-MS)

Trace element measurements were performed using an ArF Excimer laser system (193 nm wavelength, NWR193 by ESI/NewWave) equipped with a TwoVol^2 ablation cell and coupled to an Agilent 7500ce quadrupole ICP-MS (Agilent Technologies) at the Institute of Geoscience, University of Mainz. Laser repetition rate was set to 10 Hz. Line scans with a transition speed of 5 µm/s, using a fluence of 3.5 J/cm^{2}were carried out with a rectangular spot size of 130 µm x 30 µm. Pre-ablation was performed prior to each analysis to clean the surface. Background signals were acquired for 20 s during laser warm-up prior to each scan. ^{43}Ca was used as internal standard and synthetic NIST SRM 612 was used for calibration, using the preferred values from the GeoReM Database (Jochum et al., 2005). Data reduction was performed using an in-house Excel spreadsheet (Jochum et al., 2007). Details of the calculations are given in Mischel et al. (2017). For each day of measurement basaltic USGS BCR-2G and Durango Apatite were used as quality control materials to test accuracy and reproducibility of the measurements (**Table S7.3**). All reference materials were measured prior and after each sample block, three lines of 100 µm length respectively per reference material. Measured isotopes of interest are ^{24}Mg, ^{25}Mg, ^{26}Mg, ^{42}Ca, ^{44}Ca, ^{64}Zn, ^{66}Zn, ^{67}Zn, ^{68}Zn, ^{86}Sr and ^{88}Sr. The dental cubes were analysed prior to the experiment at the outer surface with one long line scan across the EDJ (start and end point beyond the cube). After the experiment, the freshly sawn surface was analysed in the same way, to determine the reaction depth of the solution into both dental tissues. The scans before and after the experiment differs slightly in length, since we measured on different plains of the same cube. The same untreated dental cube (cube D) was measured each time together with the altered cubes as reference cube to test the reproducibility and comparability between different measuring days (**Table S7.4**). Each line on this cube D was placed in close proximity to the previous one.

7.3.5 Laser ablation multi collector inductively coupled plasma mass spectrometry (LA-MC-ICP-MS)

In-situ analyses of Sr isotopes have been performed for all dental cubes after the experiment by LA-MC-ICP-MS. A first generation Nu Plasma MC-ICP-MS (Nu Instruments™) was coupled to a 213 nm Nd:YAG laser ablation system (New Wave Research™ UP-213) at the Max Planck Institute for Chemistry, Mainz, following the methods described by Weber et al. (2017, 2018). Data acquisition was performed in line scan analysis, covering the whole transect and across the EDJ. A circular spot size of 100 µm, a transition rate of 5 µm/s and a laser repetition rate of 10 Hz have been applied. Energy output was set to 100 %, resulting in a fluence of 15 – 20 J/cm^2. Prior to each analysis, a pre-ablation of the sample surface was performed for cleaning purposes.

The following m/z ratios were monitored during analysis: 82, 83, 84, 85, 86, 87 and 88 and half masses 83.5, 85.5 and 86.5 (monitoring ^{167}Er, ^{171}Yb and ^{173}Yb, respectively) using time-resolved analysis (0.2 s integration time). To correct for Kr, we used the “on peak zero” method by measuring a 45 s gas background prior to each analysis without the laser firing (^{82}Kr <0.2 mV). Calcium argide and dimer formation was found to be negligible by monitoring m/z 82 (<0.2 mV). Potential signals of doubly-charged REEs corrected by using constant isotope ratios for ^{167}Er and ^{171}Yb (Berglund and Wieser, 2011). To correct for the occurrence of ^{87}Rb on mass 87, we used the natural constant ^{87}Rb/^{85}Rb ratio of 0.3857 (Berglund and Wieser, 2011) and assume the same mass bias for Rb as for Sr. Mass bias correction was performed using the exponential law (Ingle et al., 2003) assuming a constant ^{86}Sr/^{88}Sr ratio of 0.1194. Standard-bracketing was used as calibration protocol, applying the same laser parameters for the reference material and the samples (Irrgeher et al., 2016, Weber et al., 2017). An in-house marine shark tooth was used as reference material, using a modern-day seawater ^{87}Sr/^{86}Sr ratio of 0.70918 ± 0.00001 (McArthur et al., 2001) as reference value. This is in the range of modern-day marine organisms (e.g. marine carbonate reference materials JCt-1 (giant clam, *Tridacna gigas*) and JCp-1 (coral, *Porites* sp.), yielding ^{87}Sr/^{86}Sr ratios of 0.709169 ± 0.000009 (2SE, n = 3) and 0.709170 ± 0.000006 (2SE, n = 3, Weber et al., 2018), respectively, and a modern Great white shark tooth having an average ^{87}Sr/^{86}Sr ratio of 0.709167 ± 0.000009 (2SE, n = 10, Vennemann et al., 2001).

Since the original tooth (AG-Lox) from which the dental cubes were processed is used as in-house reference material, additional analyses of the unaltered sample have been performed in the framework of further analyses, using a Neptune Plus MC-ICP-MS system (ThermoFisher Scientific) coupled with an ArF Excimer laser system (193 nm wavelength, NWR193 by ESI/NewWave) at the Institute of Geosciences, University of Mainz. All analyses using this system have been performed using a 500 µm long line scan, a transition speed of

5 µm/s and 0.262 s integration time. Due to different applications, the other laser parameters varied accordingly (spot size 70 – 110 µm, laser repetition rate 20 – 50 Hz and fluence of 3.5 – 5 J/cm^2). Data evaluation has been performed offline, using an in-house R-script, following the methods described below.

7.3.6 Laser ablation data processing

For calculation of the isotope ratios of interest, the background corrected raw data measurements obtained from the LA-(MC-)ICP-MS analyses were used.

The calculation was performed in a similar way for all isotope ratios and is therefore only described in detail once for the Sr isotope system as an example. The $^{87}Sr/^{86}Sr$ was chosen since it is widely used in geochemical studies of tooth enamel and dentin to determine habitat-use and migration patterns in palaeontology and archaeology (e.g. Clarke et al., 2007; Vroon et al., 2008). The $^{87}Sr/^{86}Sr$ was only corrected for mass bias and isobaric interference of Rb following the methods described for LA-MC-ICP-MS measurements in the section above.

Calculation of $^{44}Ca/^{42}Ca$, $^{25}Mg/^{24}Mg$ and $^{67}Zn/^{64}Zn$ ratios were performed similar to the $^{87}Sr/^{86}Sr$ using the exponential law for mass bias correction with the literature values for $^{42}Ca/^{44}Ca = 0.3102$, $^{24}Mg/^{26}Mg = 7.1728$ and $^{64}Zn/^{66}Zn = 1.7732$ (Berglund and Wieser, 2011). Then a 100-point running mean was calculated for all isotope ratios.

To evaluate if there are alteration effects on the element concentration independent or dependent on the isotope of interest for the respective element, ^{n}element/Ca ratio have been calculated based on the element concentrations, with n = mass number of the specific isotope the concentration was calculated with, e.g. $^{86}Sr/Ca$ vs. $^{88}Sr/Ca$. For undoped samples, those ratios are expected to be identical, while doped parts should yield diverging results.

7.3.7 Solution MC-ICP-MS analysis

To further evaluate the initial isotopic values of Sr ($^{87}Sr/^{86}Sr$) and Ca ($^{44}Ca/^{42}Ca$ expressed as $\delta^{44/42}Ca$) of the original dental material (AG-Lox) solution-based MC-ICP-MS analyses have been performed on enamel bulk powder samples. Purification of Sr and Ca has been performed using a prep*FAST* MC (ESI Elemental Scientific) using a 1 mL Sr-Ca ion chromatographic column following the default Sr-Ca separation protocol. Mass spectrometric analyses have been performed using a Neptune Plus MC-ICP-MS coupled with an Aridus3 (CETAC Technology) for Sr isotopes and an Apex Omega HF (ESI Elemental Scientific) for Ca isotopes at the Institute of Geosciences, University of Mainz. Strontium isotopes were measured following the methods described by Weber et al. (2018), using NIST SRM 987

(Strontium carbonate isotopic standard) as reference material for standard bracketing (long-term $^{87}Sr/^{86}Sr$ = 0.710279 ± 0.000027 (1SD, n = 506) and normalizing measured values to a $^{87}Sr/^{86}Sr$ of 0.710248 (McArthur et al., 2001). Calcium isotope analyses were made following the protocol of Tacail et al. (2014), using an Alfa Aesar plasma standard solution (Lot.Nr. 8142996) as reference material for standard bracketing of the Ca isotope ratio. Sample solutions have been prepared to match the concentration of the reference solution within 10 % (10 µg/L for Sr, 2 mg/L for Ca).

7.3.8 Raman spectroscopy

For Raman spectroscopic measurements, the same halves of the dental cubes were embedded in the fast hardening resin Technovit 5071 and polished. The measurements were performed at the Institute of Geoscience, University of Bonn, using a Horiba Scientific HR800 confocal Raman equipped with an Olympus BX41 microscope and an electron-multiplier CCD detector. A 200 mW, 784 nm diode-pumped solid-state laser was applied as excitation source. A 50 times objective with a numerical aperture of 0.75 and a confocal hole of 1000 µm were used for all measurements, resulting in a theoretical, diffraction limited lateral and axial resolution in the order of about 1.3 and 5.5 µm, respectively. The scattered light passed a 100 µm spectrometer entrance slit and was dispersed by a grating with 600 grooves/mm. The 520.7 cm^{-1} line of a silicon standard was used for initial calibration of the spectrometer, while the 985.43 cm^{-1} line of a neon lamp (Saloman, 2006) was used as an internal standard to be able to correct for any spectrometer shift occurring during analysis by placing a Ne lamp alongside the beam path of the scattered light. The 520.7 cm^{-1} line of a silicon standard was used for initial calibration, while the 985.43 cm^{-1} Ne line was then used as an internal standard to correct for any linear shift occurring during analysis, e.g., due to small temperature fluctuation in the laboratory (± 0.5 °C). With these settings, the spectral resolution was 2.478 ± 0.006 cm^{-1} as estimated from the width of the Ne line. Point-by-point measurements were performed with an acquisition time of 60 s and three accumulations per point in the frequency range between 360 and 1200 cm^{-1} for enamel and between 750 and 1450 cm^{-1} for the dentin, due to the different structures of enamel and dentin. With 10 spots parallel to the cubes edge and 10 (dentin) and 13 (enamel) spots into the sample, an area of 120 x 120 μm^2 was covered for all samples. To observe changes in crystallinity of the hydroxylapatite or potential incorporation of isotopes from the tracer solution the $v_1(PO_4)$ symmetric stretching band near 960 cm^{-1} of apatite was fitted using the LabSpec 6 program of Horiba Scientific. In case of isotope incorporation shifts in $v_1(PO_4)$ band position and width (e.g. Thomas et al., 2011). In all samples a slight asymmetry of the $v_1(PO_4)$ band was observed. To quantify changes in the width Γ (given as full width at half maximum, FWHM) and frequency of the $v_1(PO_4)$ band, an

asymmetric Gauss-Lorentz function was used. All other bands were fitted with symmetric Gauss-Lorentz function along with a linear background function between 900 and 1200 cm^{-1}. Furthermore, finite slit width effects on the width of the Raman bands were corrected using the following equation (Tanabe and Hiraishi 1980):

$$\Gamma_c = \Gamma_m[1 - (S/\Gamma_m)^2]$$

with Γ_m and Γ_c representing measured and corrected bandwidth, respectively, and S the spectra resolution (= 2.478cm^{-1}).

7.3.9 Electron microprobe analysis

For electron microprobe analysis (EMPA), the halves of the dental cubes (already embedded in Technovit) were further embedded in epoxy resin, polished, cleaned and sputtered with a ≈ 20 nm layer of carbon. Experimentally altered dental cubes were solely measured after the experiment, together with untreated samples D, L and M (Table 7.1). Analyses were carried out at the Institute of Geosciences, University of Mainz, using a Jeol JXA 8200 electron microprobe in wavelength-dispersive spectrometry (WDS) mode. A beam current of 12 nA and an acceleration potential of 15 kV were chosen, with the electron beam defocused to 10 µm. Peak counting times were 30 s for Ca, P and Mg, 120 s for Zn and 80 s for Sr. Raw element concentration data were corrected using the routine by Armstrong (1995) and an in-house apatite reference material was chosen for calibration. A profile of 10 µm spot measurements with a distance of 40 µm between the spot centres was analysed across the enamel thickness across the EDJ into to the dentin (**Fig. 7.1**).

7.4 Results

7.4.1 Changes in physical properties of the dental cubes

All dental cubes react very brittle during the preparation after immersion in the tracer solution at 90 °C, indicating higher porosity, especially sample I (14 days, 90 °C) shows a clear dissolution of dentin, especially at the boundary to the enamel (**Fig. S7.1**). All cubes have a few µm-thick, pale whitish coating on the dental surface, which was too thin to be detected in the different measurement methods used in this study. All cubes have a weight loss of around 15.5 % ± 1.5 % (30 °C) and 23.5 % ± 2.3 % (90 °C), which is also reflected in an average size decrease of the dental cubes leading to an average length loss (length across enamel dentin junction) of 6.6 % ± 2.5 % (30 °C) and 7.1 % ± 2.8 % (90 °C), respectively.

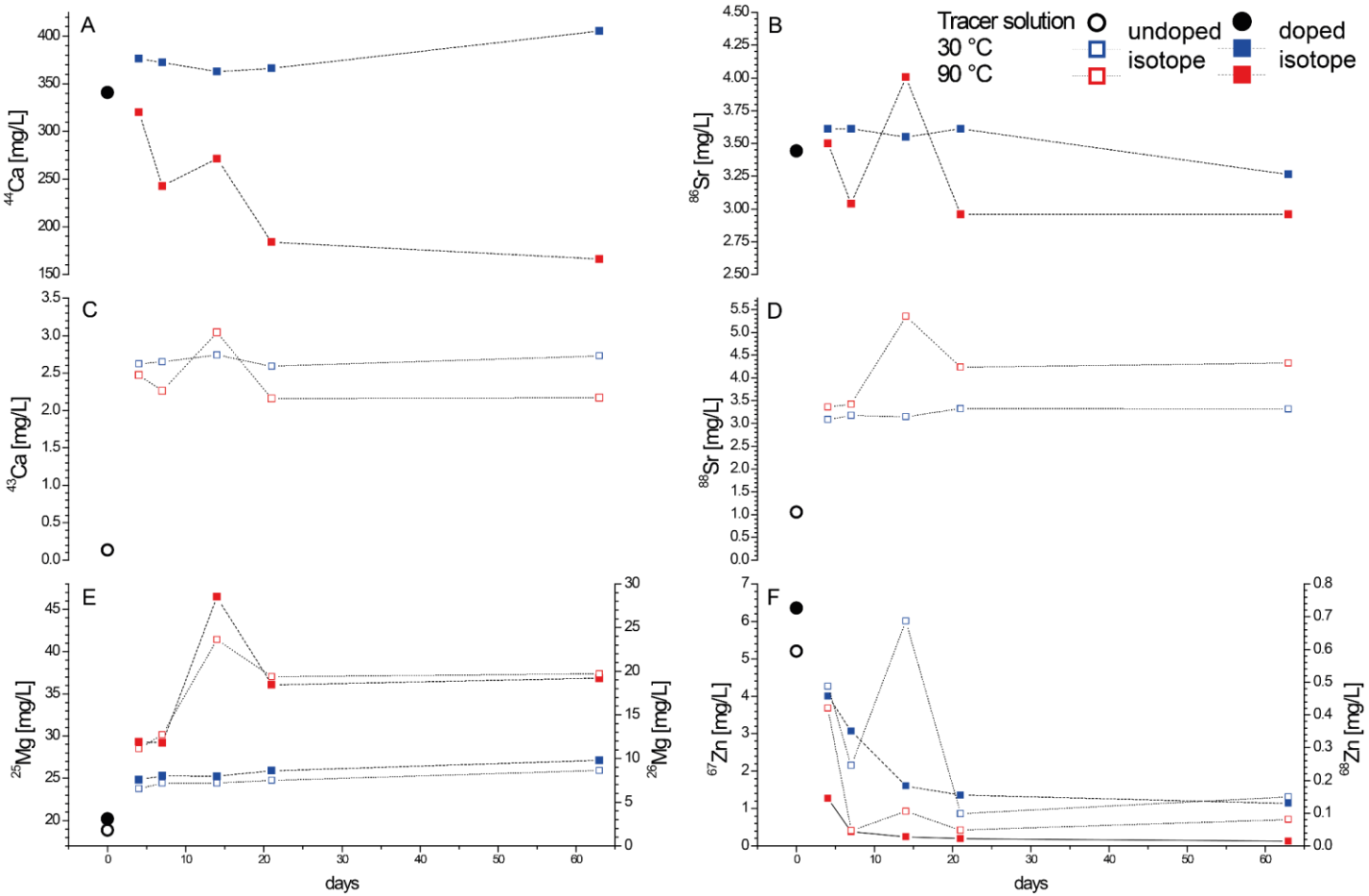

Figure 7.2. Evolution of the doped isotopes in the isotopic tracer solution over the experiments. Closed circles/rectangles indicate the concentration of the doped isotope (^{44}Ca (A), ^{86}Sr (B), ^{25}Mg (E), ^{67}Zn (F)) in the solution, while open circles/rectangles represent the concentration of the undoped isotope (^{43}Ca (C), ^{88}Sr (D), ^{26}Mg (E), ^{68}Zn (F)). In (E) and (F) the doped isotope (^{25}Mg (E), ^{67}Zn (F)) are plotted against the primary axis, while the undoped isotope (^{26}Mg (E), ^{68}Zn (F)) are plotted against the secondary axis. The initial concentration is represented as a black circle, the evolution during the 30 °C experiment is shown by blue rectangles and the 90 °C experiment by red rectangles.

7.4.2 Tracer solution composition

The pH value of the solution rose already during the first week of experiment from pH ≈ 1 to pH ≈ 6-7 and stayed relatively constant afterwards. The evolution of the elemental and isotopic composition of the tracer solution is shown in Figure 7.2 and Table S7.1.

7.4.2.1 Calcium

The Ca of the raw tracer solution consisted almost purely of the doped isotope ^{44}Ca (340 mg/L, **Fig. 7.2A**), while the ^{43}Ca content was almost negligible (0.14 mg/L, **Fig. 7.2C**). During the 30 °C experiment, ^{44}Ca increased up to 376 mg/L after four days and remained rather constant and only increased up to 405 mg/L after 63 days. A contrasting evolution is visible during the 90 °C experiment, where ^{44}Ca decreased (nearly exponential, apart from cube I, 14 days, see **Fig. S7.1**) in the tracer solution during the whole experiment down to a concentration of 166 mg/L after 63 days. The undoped ^{43}Ca shows a similar behaviour for both experiments, with a strong initial increase towards 2.62 mg/L (30 °C) and 2.47 mg/L (90 °C), with almost constant concentrations afterwards (apart from cube I, 14 days, 90 °C, see above).

7.4.2.2 Strontium

In comparison to the other used element solutions enriched in a specific isotope, the ^{86}Sr-enriched solution was not as pure and contained also a significant amount of ^{88}Sr. Therefore, the tracer solution has ^{86}Sr (3.44 mg/L, **Fig. 7.2B**) and ^{88}Sr (1.05 mg/L, **Fig. 7.2D**). Overall, the Sr concentration in the solution displays a similar behaviour as Ca. For the 30 °C experiment, a slight increase in the ^{86}Sr is visible after four days (3.61 mg/L), which then remains almost constant, except for a small decrease after 63 days (3.26 mg/L). During the 90 °C experiment, the ^{86}Sr concentration decreases over the experimental duration (except for cube I, 14 days, 90 °C) down to 2.96 mg/L after 63 days (**Fig. 7.2B**). This decrease is not as strong as for Ca, however, the general trend is similar. The ^{88}Sr increases already after four days of experiment up to 3.09 mg/L (30 °C) and 3.36 mg/L (90 °C) and increases slightly over time (**Fig. 7.2D**).

7.4.2.3 Magnesium

The evolution of the Mg concentrations is almost identical for both analysed isotopes and at the two different temperatures (**Fig. 7.2E**). Both, the doped ^{25}Mg (24.8 mg/L 30 °C and 29.3 mg/L 90 °C), as well as the undoped ^{26}Mg (6.6 mg/L 30 °C and 11.1 mg/L 90 °C), increase significantly after four days in comparison to the starting solution (^{25}Mg 20.2 mg/L and ^{26}Mg

1.8 mg/L). Afterwards, the concentration for both Mg isotopes increases slightly during the experimental period. In addition, the concentration increases strongly during the 90 °C experiment.

7.4.2.4 Zinc

The evolution of Zn in the tracer solution is similar for both isotopes and temperatures (**Fig. 7.2F**). While the raw solution has the highest concentration for the doped ^{67}Zn (6.35 mg/L) and undoped ^{68}Zn (0.59 mg/L), the concentration in the solution decreases during the whole experimental duration (except cube I, 14 days, 90 °C and cube N, 14 days, 30 °C) down to 0.15 mg/L (30 °C) and 0.08 mg/L (90 °C) for ^{68}Zn and 1.14 mg/L (30 °C) and 0.13 mg/L (90 °C) for ^{67}Zn (**Fig. 7.2F**).

7.4.2.5 Phosphorus

Phosphorus concentrations were measured only qualitatively using a Spectro Vision ICP-OES at the Institute of Geosciences, University of Mainz (**Fig. S7.2**). The absolute concentration values could not be established, because the analytical procedure was not validated for this high concentrations of phosphorous, but the trend can be used as the matrix of the samples did not change significantly and reproducibility of the measurements was ensured. Phosphorous was absent in the initial tracer solution but increased strongly after the first days of experiment. However, P tends to decrease in the progression of the experiment, especially for the 90 °C experiment.

7.4.3 Element concentration profiles across dental cubes

Concentration of Ca, P, Mg, Zn, and Sr were measured using electron microprobe analysis. In both, enamel and dentin the concentrations do not show significant changes within the EPMA uncertainties of approximately 3 % (Weber et al., 2020) during the 63 days of the 30 °C experiment (**Fig. S7.3**). Dental cubes placed in the 90 °C solutions show for the dentin slightly higher Ca (≈ 10 %) and P (≈ 14 %) concentrations after 21 days (**Fig. 7.3**). The Mg and Zn concentration of the inner dentin immersed for four days still shows an unreacted core area, while the outer ≈ 200 µm are clearly altered. After seven days of treatment, Mg and Zn in the dentin are altered throughout. While Zn concentration in dentin increases (up to 90 times above the range of natural variability), Mg decreases down to about 80 % less Mg than the unaltered dental cube and the range of natural variability (**Fig. 7.3**). The enamel does not show significant changes during the 90 °C experiment (**Fig. 7.3**).

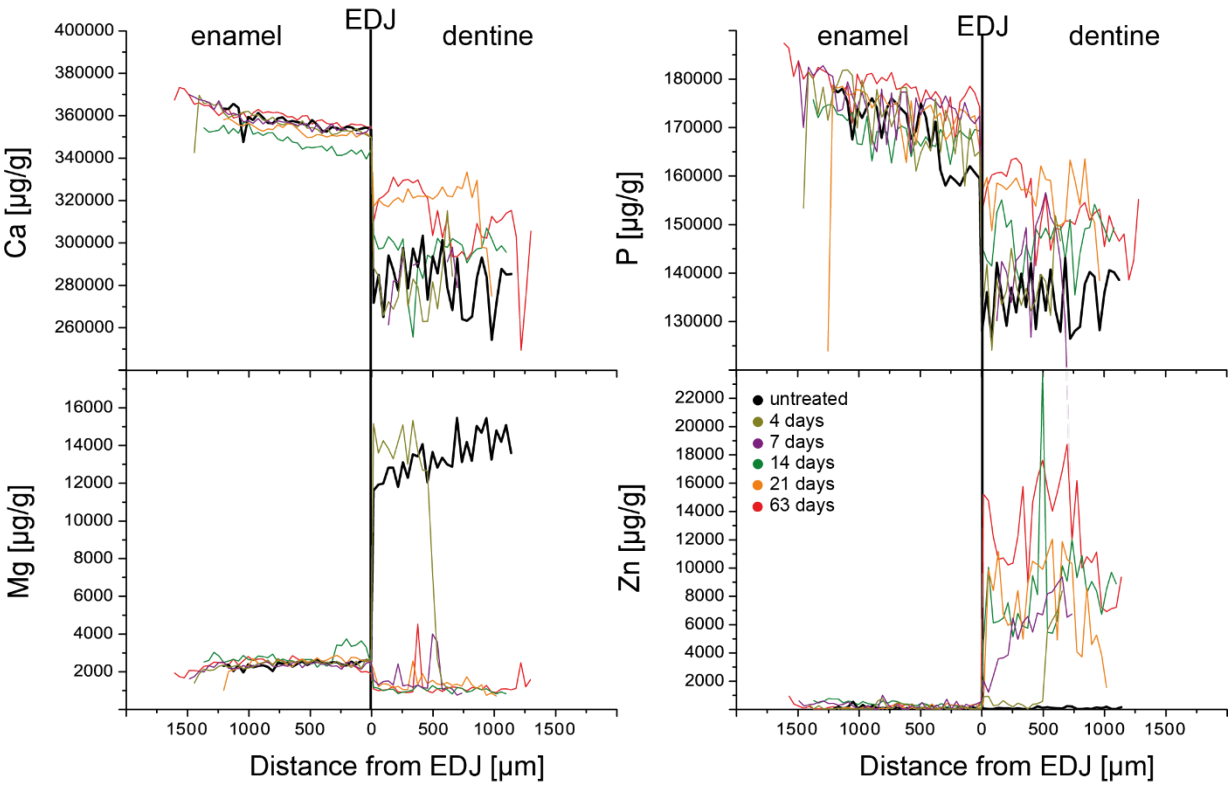

Figure 7.3. Element (Ca, P, Mg and Zn) concentration profiles across the full enamel and dentin length of the dental cubes determined by EMPA perpendicular to the enamel-dentin junction (EDJ) (Fig. 1) on samples from the 90 °C experiments of different duration (4 to 63 days). Data are all centred [0 µm] to the EDJ.

7.4.4 Isotope ratios of Mg, Ca, Zn and Sr across dental cubes

Isotope ratios were measures using the count rates conducted by LA-ICP-MS. Solutions bases Ca and Sr, as well as *in-situ* $^{87}Sr/^{86}Sr$ profiles were measured using (LA-)MC-ICP-MS. The untreated dental cube D was analysed as a reference material together with the treated samples to test the reproducibility of the measurements between different days of analysis. For the isotopes of interest, the mean values of the concentration of enamel and dentin lie within one standard deviation for all days of analysis (**Table S7.4**). Therefore, the LA-ICP-MS data of the different days of analysis are comparable among each other.

Solution based $^{87}Sr/^{86}Sr$ analyses of the unaltered enamel (AG-Lox) yielded an average value of 0.70999 ± 0.00003 (1SD, n = 6, MC-ICP-MS), in perfect agreement with LA-MC-ICP-MS results of 0.71003 ± 0.00009 (1SD, n = 23). Stable Sr ($\delta^{88/86}Sr_{NIST987}$) analysis of the unaltered enamel (AG-Lox) yield an average of -0.31 ± 0.05 ‰ (1SD, n = 5) and Ca isotope analyses yielded an average $\delta^{44}Ca_{NIST\text{-}SRM\ 915a}$ ($^{44}Ca/^{42}Ca$) of -1.82 ± 0.06 ‰ (1SD, n = 10). Both Sr and Ca isotope composition were measured using MC-ICP-MS.

The calculated isotope ratios of all four elements Mg, Ca, Zn and Sr in the dental tissues indicate that the dentin generally shows more pronounced alteration effects in comparison to the enamel during the experiment duration for both temperatures (**Fig. 7.4-7.6 and S7.4-S7.15**). However, samples immersed at 30 °C in the tracer solution show only slight alteration effects in both enamel and dentin. Generally, the enamel shows only a narrow alteration rim of 25 – 50 µm for $^{44}Ca/^{42}Ca$, $^{67}Zn/^{64}Zn$ and $^{87}Sr/^{86}Sr$ (**Fig. 7.4 and S7.4**) in comparison to the dentin with an alteration rim of up to 150 – 200 µm from the outer tissue surface (**Fig. S7.5**). No correlation between the alteration depth and the duration of the experiment was detected. For $^{25}Mg/^{24}Mg$, no distinct alteration is detectable in enamel (**Fig. 7.4**). However, a small decrease in all $^{n}Mg/Ca$ during the 30 °C experiment is visible for the outer 50 – 75 µm in the enamel (**Fig. S7.6**). Since all $^{n}Mg/Ca$ ratios decrease the same way, no change in the isotopic ratio occur. In addition, an increase of all $^{n}Zn/Ca$ ratios has been observed in the outer part of both enamel (up to 100 µm) and dentin (up to 150 µm), with the $^{67}Zn/Ca$ being at least one order of magnitude more enriched than the other $^{n}Zn/Ca$ ratios (**Fig. S7.7 and S7.8**). This is in accordance with the increase in $^{67}Zn/^{64}Zn$ shown in Figure 7.4 and S7.9, as well as with the data of the tracer solution, which is reflecting a loss of ^{67}Zn from the solution. The enamel of the sample immersed for seven days (sample K), however, shows a different alteration pattern in the isotope ratio and the alteration depth, up to 100 µm in Ca, Sr and Zn and only a very minor (≈ 20-25 µm) alteration depth in Mg. This pattern is not visible in the dentin of sample K (**Fig. S7.5**). The dentin of samples treated up to 63 days at 30 °C show alteration rims up to 200 µm for $^{44}Ca/^{42}Ca$, $^{67}Zn/^{64}Zn$ and $^{87}Sr/^{86}Sr$. The $^{25}Mg/^{24}Mg$ shows an alteration in the outer 150 µm, but not as pronounced as for the other three isotope ratios (**Fig. S7.5**). This agrees with the $^{n}Mg/Ca$ ratios for the outer dentin, which also show a decrease of $^{n}Mg/Ca$ for at least 150 µm. However, the $^{25}Mg/Ca$ is slightly elevated in comparison to the other $^{n}Mg/Ca$ ratios (**Fig. S7.9**), which is in line with the increase in $^{25}Mg/^{24}Mg$. The innermost part of all dental cubes treated with the solution at 30 °C does not show any sign of alteration of the enamel and dentin in the area around the EDJ.

The enamel of dental cubes immersed at 90 °C in tracer solution show alteration rims in the outer part of the samples. The highest degree of alteration occurs in the experiment with the longest duration (cube F) for all isotope ratios, with alteration depths of ≈ 100 µm for $^{25}Mg/^{24}Mg$ and $^{67}Zn/^{64}Zn$, ≈ 150 µm for $^{44}Ca/^{42}Ca$ (**Fig. S7.10**) and up to 350 µm for $^{87}Sr/^{86}Sr$ (LA-MC-ICP-MS) (**Fig. 7.5**). All other experiments of different, shorter durations show consistently an alteration rim of around 50-100 µm for Ca, Zn and Sr isotopes and almost no alteration of the $^{25}Mg/^{24}Mg$. In contrast, the $^{n}Mg/Ca$ is significantly lower than for the untreated sample (**Fig. S7.11**), while the $^{25}Mg/Ca$ is again higher compared to other $^{n}Mg/Ca$ ratios. No systematic increase of the alteration depth is visible with prolonged experimental duration.

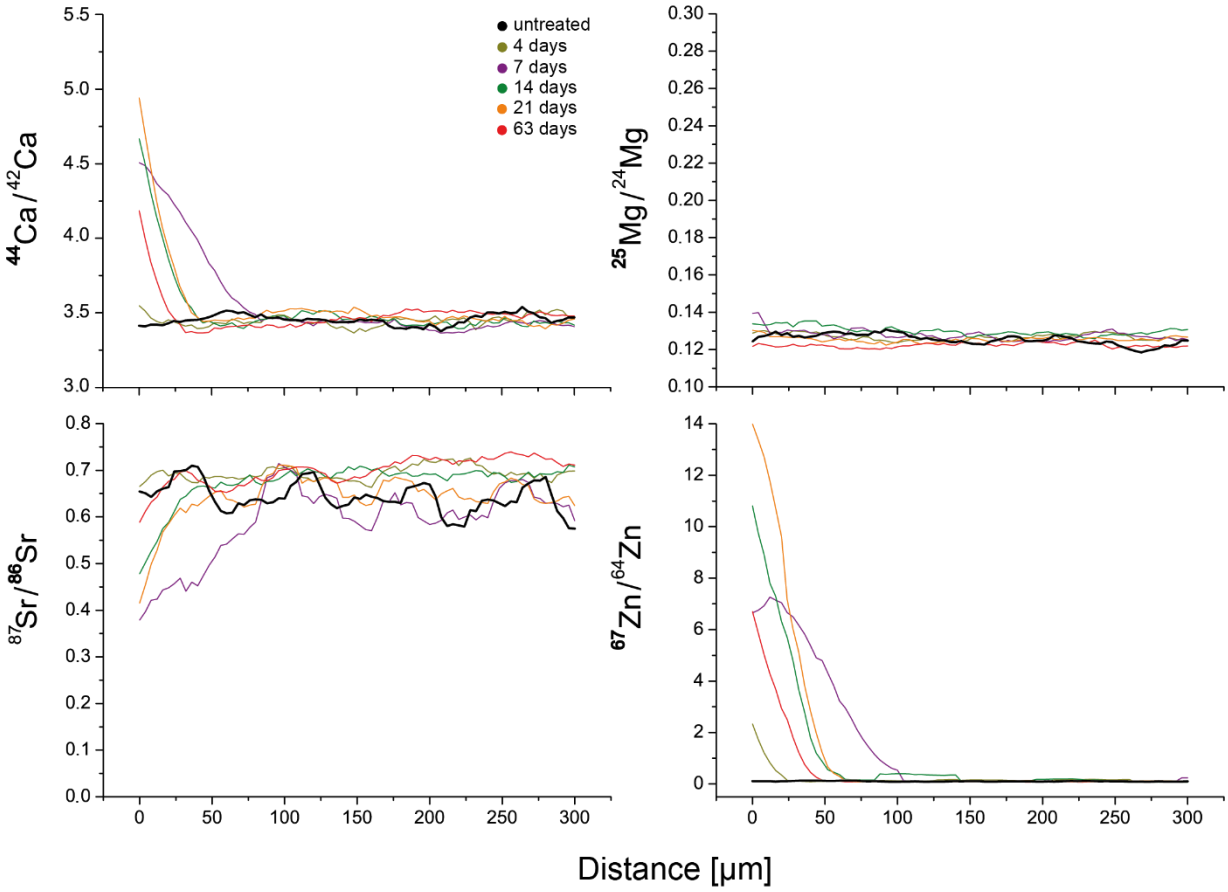

Figure 7.4. Profiles of Ca, Mg, Sr and Zn isotope ratios measured in-situ by LA-ICP-MS from the outer enamel boundary 300 µm into the enamel of experimentally altered dental cubes. The cubes were immersed in isotopically (^{44}Ca, ^{26}Mg, ^{86}Sr, ^{67}Zn) enriched tracer solution at 30 °C for increasing durations from 4 to 63 days.

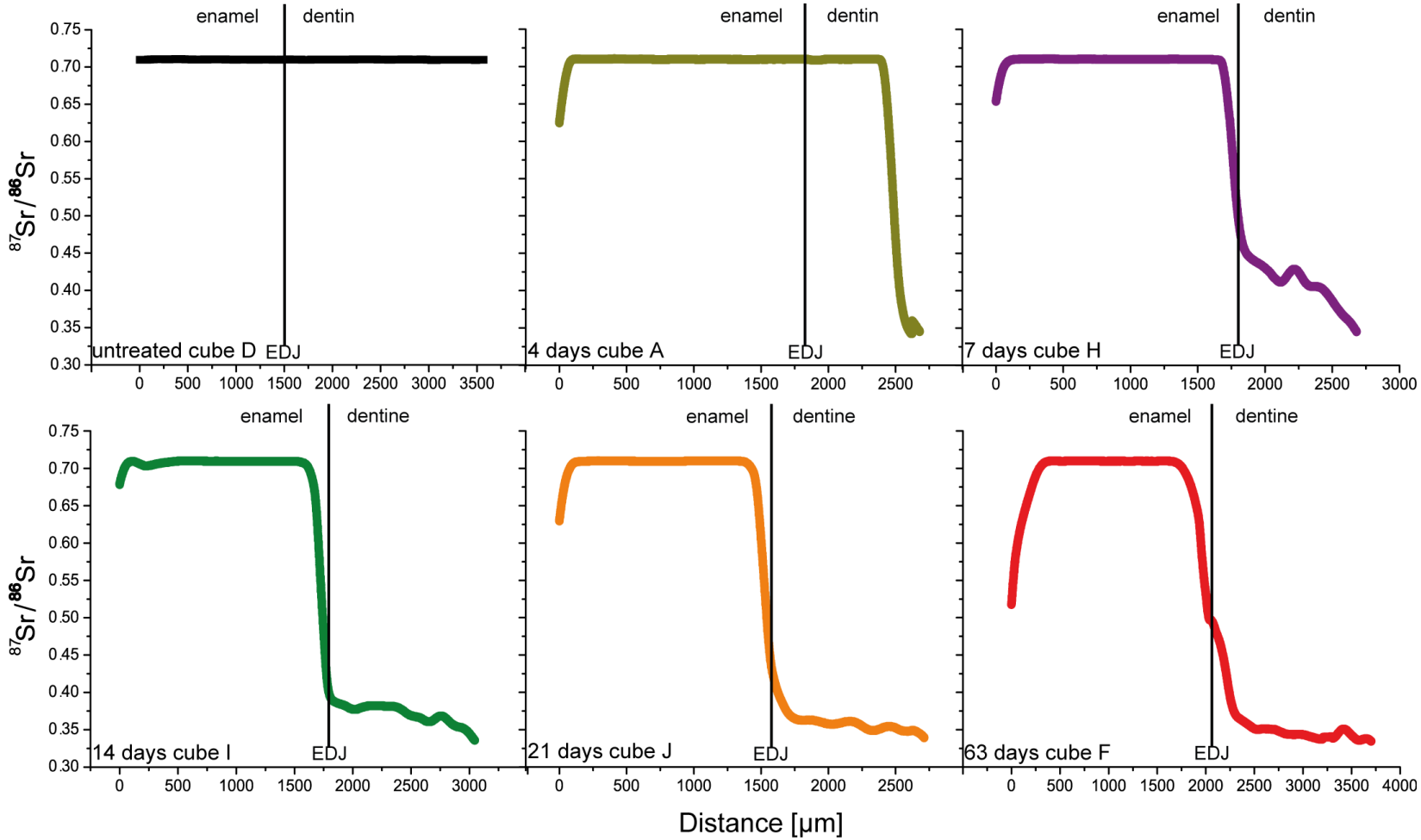

Figure 7.5. The $^{87}Sr/^{86}Sr$ profiles measured in-situ by LA-MC-ICP-MS across experimentally altered dental cubes starting from the outer boundary of the enamel perpendicular across the enamel-dentin junction (EDJ). The unaltered sample (black bold line) is plotted in comparison to those from the 90 °C experiments of increasing durations from 4 to 63 days.

Samples kept at 90 °C in the tracer solution show strong alteration effects, especially in the dentin. Only the sample with the shortest experimental duration (cube A, 4 days) still has an unaltered zone in the inner dentin and an alteration rim of ≈ 150 µm visible in the $^{44}Ca/^{42}Ca$, $^{87}Sr/^{86}Sr$, and $^{25}Mg/^{24}Mg$ (**Fig. 7.6**). Samples treated for a longer duration of a week or more do not have any unaltered dentin remaining (**Fig. 7.5**). Solution based Sr isotope analysis dentin from the altered dental cube H (7 days) yield a $^{87}Sr/^{86}Sr$ of 0.35680 ± 0.00001 (2SE, n = 1) and a $\delta^{88/86}Sr$ of -720.62 ± 0.03 ‰ (1SD, n = 1) showing the strong alteration of the dentin. Also, the $\delta^{44/42}Ca$ value of 2941.5 ± 1.4 ‰ (1SD, n = 1) is strongly altered. However, $^{67}Zn/^{64}Zn$ shows only a narrow alteration rim of 50 µm even for the shortest experimental duration (cube A, **Fig. 7.6**). For samples treated for seven and 14 days, a gradual increase of the $^{67}Zn/^{64}Zn$ towards the inner dentin until ≈ 250-300 µm is observed. Only the sample with the longest experimental duration (sample F, 63 days) shows fully altered dentin in $^{67}Zn/^{64}Zn$. This is in agreement with the $^{n}Zn/Ca$ ratios, which show an alteration rim for $^{67}Zn/Ca$ of 300 µm after 14 days (**Fig. S7.12**). Interestingly, the $^{n}Mg/Ca$ decreased in comparison to the initial ratio in all dentin cubes treated in the 90 °C experiment, indicating a Mg loss (**Fig. S7.13**). Nevertheless, the $^{25}Mg/Ca$ is higher than the two other $^{n}Mg/Ca$ ratios, confirming the increase in $^{25}Mg/^{24}Mg$ (**Fig. 7.6**). The LA-MC-ICP-MS $^{87}Sr/^{86}Sr$ clearly shows a fully altered dentin after seven days. At this point, the alteration starts to penetrate across the EDJ into the enamel, clearly visible in the longest duration experiment (cube F, **Fig. 7.5**). An interesting feature is visible for Sr in the $^{n}Sr/Ca$ ratios of the dentin (**Fig. S7.14**). While the $^{86}Sr/Ca$ is increased in the treated samples, the $^{88}Sr/Ca$ ratio is slightly decreased. This feature is especially pronounced in the dentin and only slightly occurring in the enamel (**Fig. S7.15**).

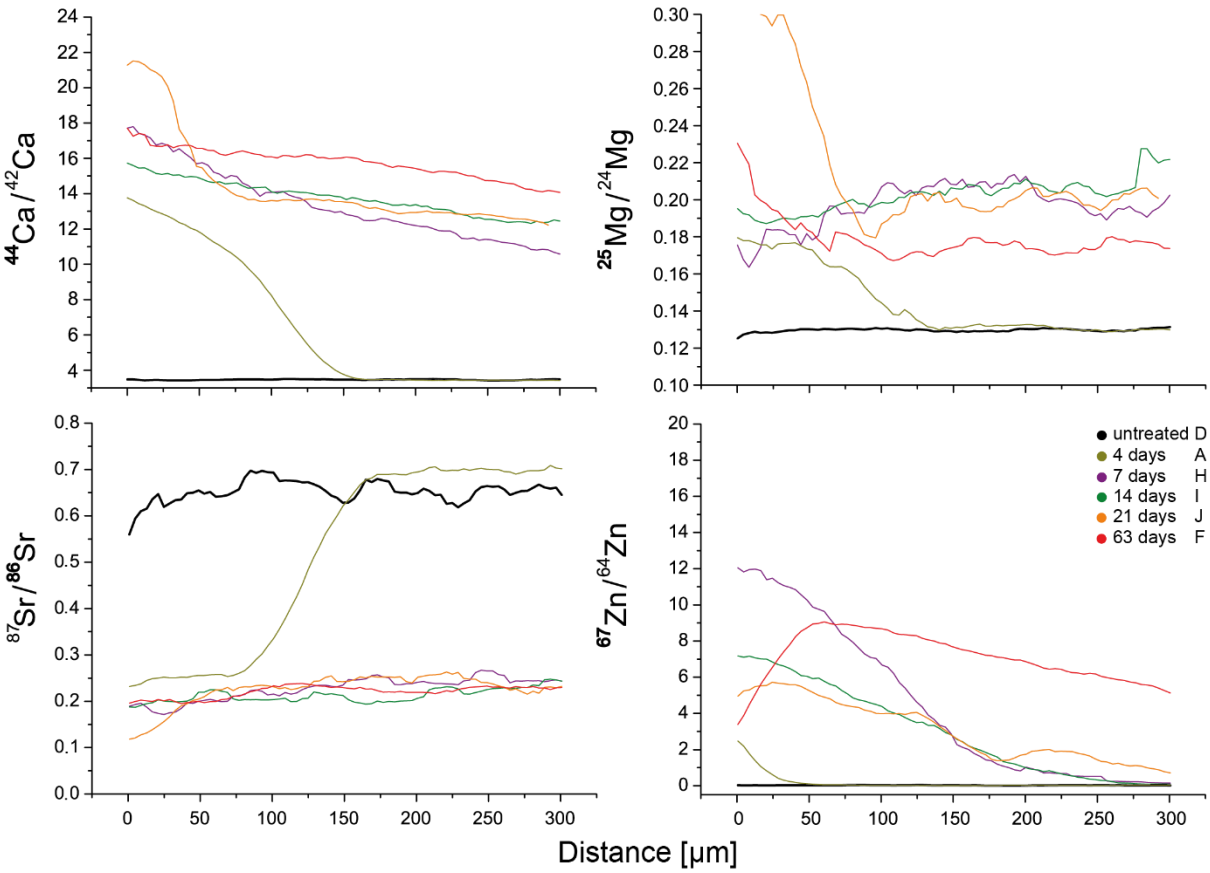

Figure 7.6. Profiles of isotope ratios for Ca, Mg, Sr and Zn measured in-situ by LA-ICP-MS from the outer boundary of the dentin 300 µm into the dentin for dental cubes of the *in-vitro* alteration experiments in isotopically (^{44}Ca, ^{26}Mg, ^{86}Sr, ^{67}Zn) enriched tracer solution at 90 °C for increasing durations from 4 to 63 days.

7.4.5 Changes in bioapatite mineralogy assessed by Raman spectroscopy

Raman spectroscopy was used to investigate potential modifications of the biogenic apatite in both dental tissues, enamel and dentin, of each sample (**Fig. 7.7 and 7.8**). Figure 7.7 shows Raman spectra in the frequency range of 700-1450 cm^{-1} taken from the outer 120 µm of the dentin (**Fig. 7.7A**). A frequency range of 360-1200 cm^{-1} was chosen for spectra from the outer rim of the enamel (**Fig. 7.7B**). Reference spectra of untreated dentin and enamel as well as synthetic hydroxylapatite (HAp) are also included.

A comparison made of the reference spectra of both tissue types and the synthetic HAp (**Fig. 7.7**) reveal that the most intense feature is a band at ~960 cm^{-1}, which is attributed to the fully symmetric stretching mode of phosphate ($v_1(PO_4^{3-})$). In HAp the shape of this band is symmetric, whereas in dentin and enamel spectra, on the lower frequency side, a slight asymmetry of the $v_1(PO_4^{3-})$ band can be observed, which is most likely caused by an underlying band at 950 cm^{-1} that has also been observed in other studies on bone apatite (Pasteris and

Ding, 2009; Asjad et al., 2019). Broad and less intense Raman bands between 1040 and 1090 cm^{-1} are attributed to the PO_4^{3-} antisymmetric stretching modes. However, the v_3 band 1070 cm^{-1} overlaps with v_1 band of the carbonate unit near 1079 cm^{-1} ($v_1(CO_3^{2-})$). Dentin is further distinguished by a number of broad bands that are related to collagen vibrations: proline (853 and 917 cm^{-1}), hydroxyproline (873 cm^{-1}), phenylalanine (~1001 cm^{-1}) and amid III, consisting of v(C-N) and δ(N-H) modes (1243-3120 cm^{-1}).

The treatment in solutions at 30 °C and 90 °C affected the dental hard tissues differently, enamel experienced distinctly less modifications than dentin (**Fig. 7.7**). For dentin, representative spectra were selected from different locations on the sawed surface of the treated cubes for different reaction durations and at different temperatures (**Fig. 7.7A**). The exact locations of the spectra are displayed as circle on the hyperspectral images in Figure 7.7C, where the colour of the respective circle corresponds to the colour of the spectrum. Each hyperspectral image covers an area of 120 x 120 µm with one collected spectrum each 10 µm. Spectra 1 and 2 were taken close to the rim of the dentin sample which was exposed for 4 days at 30 °C to the tracer solution. Here, the collagen bands are still detectable in the peripheral areas, whereas the initially most intense $v_1(PO_4)$ band is not detectable (spectrum 1) or shows only weak intensities (spectrum 2). The $v_1(CO_3)$ band is also not detectable anymore in both spectra. These spectral observations demonstrate that the inorganic component (i.e. bioapatite) of dentin dissolved, whereas the organic material was preserved.

Spectrum 3 was collected from the inner part of the 120 µm thick rim of a sample reacted for 63 days at 30 °C. This spectrum is comparable to those of the untreated sample, suggesting that no significant alteration occurred. In the hyperspectral image shown in Figure 7.6C, however, it is clearly observed that within the outermost 50 µm the dentin has been strongly altered, i.e., this area is characterized by a low intensity ratio between the v_1 phosphate and the collagen bands. Spectra 4 and 5 were taken from dentin samples reacted at 90 °C for 14 and 63 days, respectively, and were taken from the inner part of the mapped area. The most prominent feature is again the $v_1(PO_4)$ band near 960 cm^{-1}, which, however, became sharper and blue shifted with increasing reaction time. The narrowing of this band is evident in spectrum 5 by the appearance of a small shoulder near 948 cm^{-1} (grey arrow in **Fig. 7.7A**). This band is also present in spectra from synthetic HAp, but has not yet been convincingly assigned, but could possibly reflect the splitting of the $v_1(PO_4)$ vibration of the free tetrahedron by the crystal field (Asjadi et al., 2019). It is usually hidden below the $v_1(PO_4)$ band (Pasteris and Ding, 2009), which was accounted for in this study by using an asymmetric Gauss-Lorenz function to fit the overall profile of this band. Moreover, both spectra do not anymore exhibit the broad $v_1(CO_3)$ band near 1070 cm^{-1}, suggesting the loss of carbonate from the dentine bioapatite phase and thus complete reorganisation of its apatite crystal lattice. It is

also noteworthy that the v(C-C) vibration of the aromatic phenylalanine ring near 1001 cm^{-1} is clearly detectable but this is the only significant remaining collagen-related Raman signal.

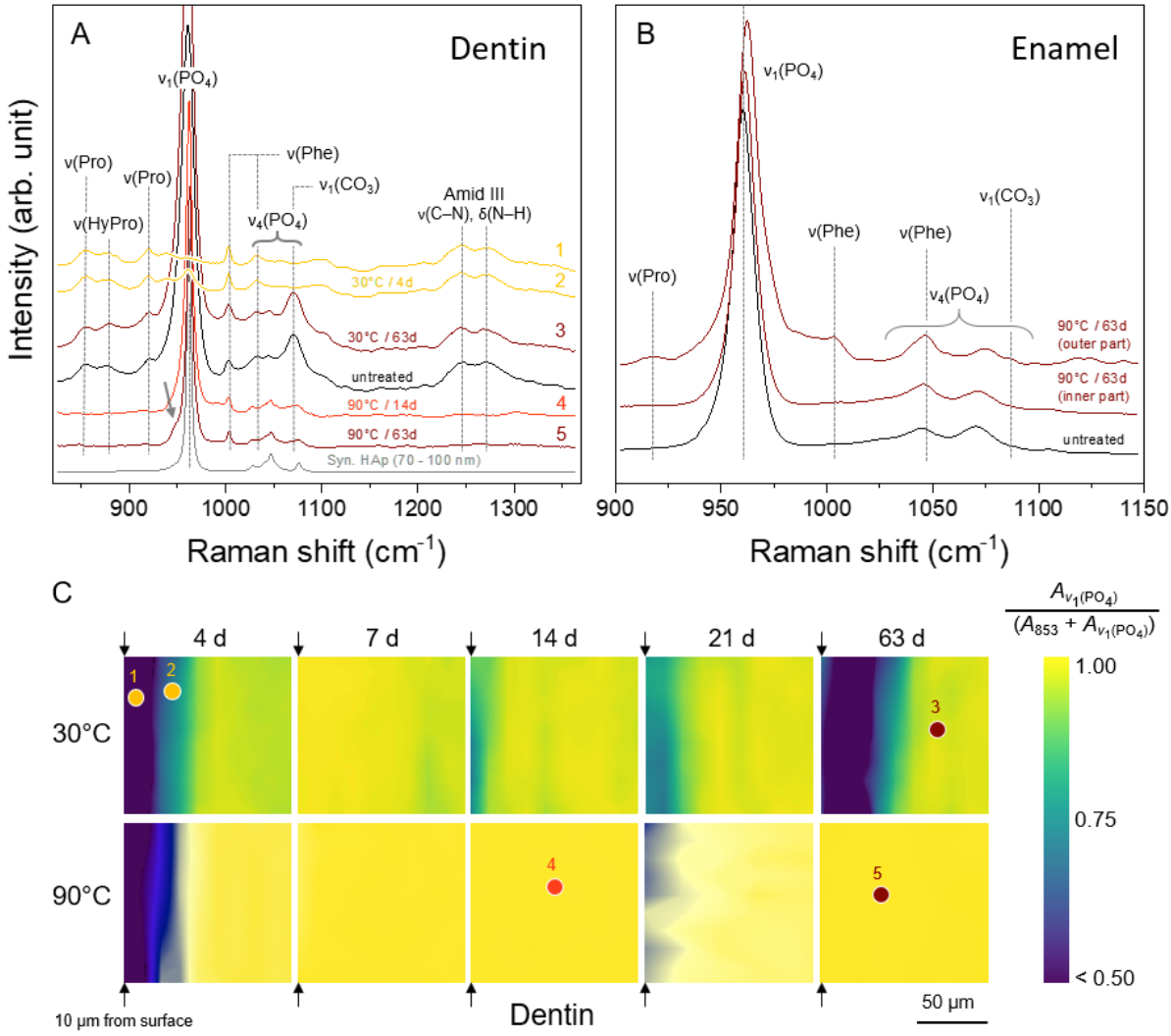

Figure 7.7. Results of Raman spectroscopy. Raman spectra of dentin A. and enamel B. for different experimental durations and temperatures. Spectra were normalized to the $\nu_1(PO_4)$ intensity. Location of respective Raman spectra in the dentin are displayed as circle on the hyperspectral images shown in C. Each hyperspectral image represents an area of 120 x 120 µm. The colour coding shows the integrated intensity of the $\nu_1(PO_4)$ band relative to the proline band near 853 cm^{-1}.

The only significant visible spectral changes in enamel were observed on the rim of the enamel sample treated at 90 °C for the longest reaction duration (**Fig. 7.7B**). The spectra from the outer part of this sample have a distinctly blue shifted $\nu_1(PO_4)$ band compared to the spectra of the inner part and the untreated enamel reference. Furthermore, two weak bands at 917 cm^{-1} (proline) and 1001 cm^{-1} (phenylalanine) as well as weak amid III bands, all assigned to

collagen vibrations, are significantly more intense than in the spectra from the inner part of the enamel and the untreated enamel reference.

In order to quantify potential modifications within the bioapatite lattice, the position and width of the $v_1(PO_4)$ band were determined by least-squares fitting of an asymmetric Gauss-Lorentz function and plotted against each other in Figure 7.8. Raman data from fossil dentin and enamel, modern and fluoridated fossil lizard bone, modern fluoridated shark tooth, magmatic fluorapatite (FAp), as well as synthetic HAp are plotted as references in Figure 7.8C.

As already observed in the Raman spectra, enamel is distinctly less reactive than dentin. Especially, the Raman spectra from the enamel samples reacted at 30 °C for different durations (**Fig. 7.8A**, blue symbols) do not reveal any significant changes, as the samples, irrespective of the experimental duration, all plot in the same area. Any difference merely reflects the natural variability of the starting material. Similarly, samples treated at 90 °C for up to 21 days do not show any significant changes (**Fig. 7.8B**). However, after an experimental duration of 63 days, the $v_1(PO_4)$ band position increased significantly by about 1 cm^{-1}, whereas the bandwidth did not change significantly. This frequency shift is also directly visible in the Raman spectrum shown in Figure 7.7B.

Under the microscope differently pronounced but clear reaction rims are visible in the dentin part of all samples treated at 30 °C (**Fig. S7.16**). However, there is no clear correlation between the width of the reaction rim and the duration of the experiment, as also deducible from Figure 7.7C. In any case, all samples from the 30 °C experiments have preserved an apparently unreacted zone within the measured areas (**Fig. 7.7C**). Data points from this zone cluster in the diagram frequency versus width of the $v_1(PO_4)$ band between about 960.5 and 961.7 cm^{-1} and between 12.0 and 15.5 cm^{-1}, respectively (marked area in **Fig. 7.8A and B**). These ranges essentially represent the natural, spectral variability of the starting dentin material. In the measured outer part of the treated dentin samples, substantially band parameter changes occurred with increasing reaction time both at 30 °C and 90 °C (**Fig. 7.8A and B**). At 90 °C and reaction times larger than 7 days, the measured area has completely been altered, particularly recognizable by a significant reduction of the bandwidth (**Fig. 7.8B**), whereas for samples treated at 90 °C for 4 days only the data pattern is still comparable to that observed for the 30 °C experiments (**Fig. 7.8A**).

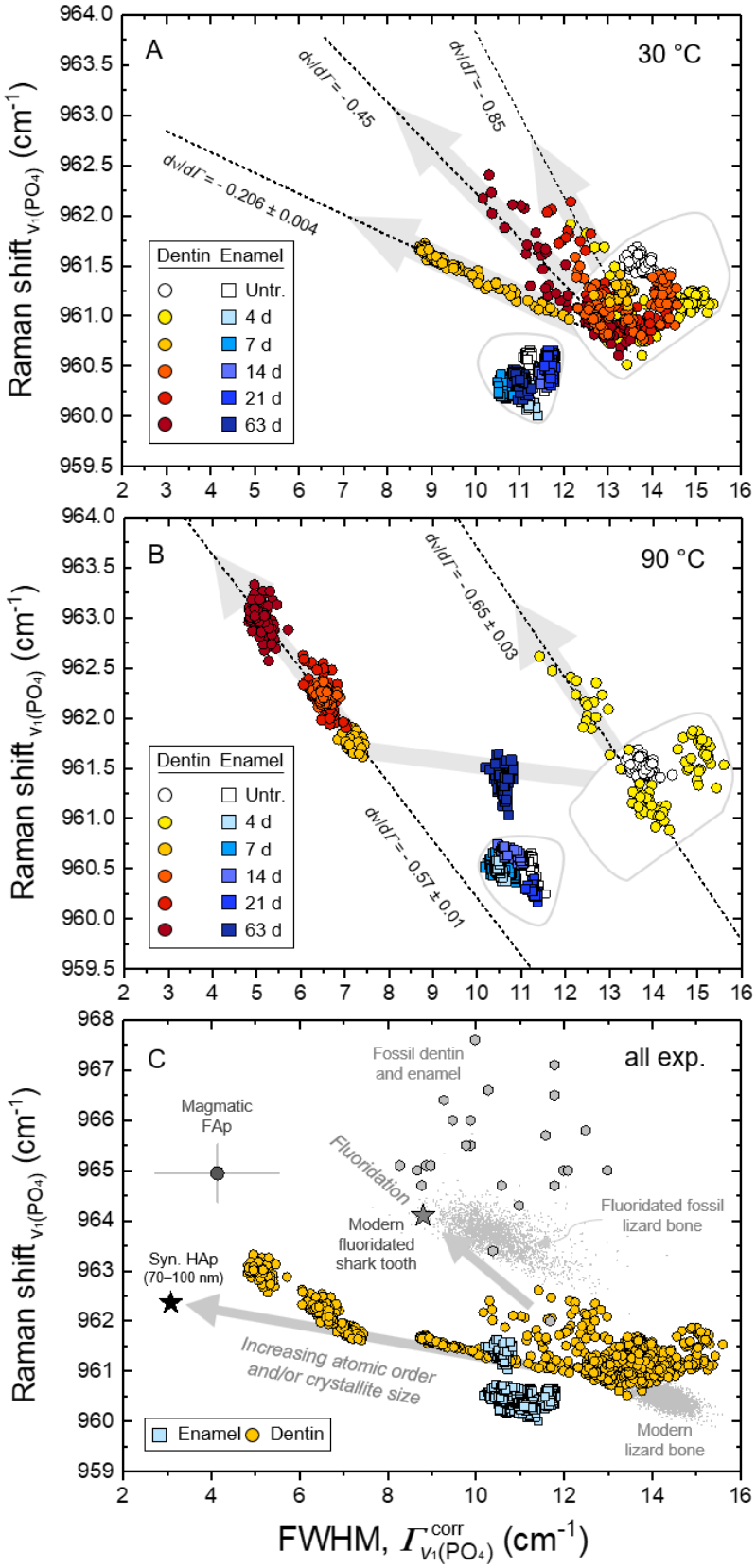

Figure 7.8. The Raman shift of the $\nu_1(PO_4)$ band as a function of its width (corrected FWHM, $\Gamma^{corr}\nu_1(PO_4)$) for dentin (yellow to red colours) and enamel (blue colours). A. Data from the 30 °C

experiment, B. from the 90 °C experiment, and C. from both experiments in comparison with data from different modern and fossil bones (Pasteris and Ding, 2009; Barthel et al., 2020) and teeth (Thomas et al., 2007), as well as from synthetic HAp (Asjadi et al., 2019) and magmatic FAp (own, unpubl. data). Arrows mark distinct trends that show different slopes of dν/dΓ in A and B enclose the field for untreated and unaltered dentin and enamel, respectively.

The overall pattern is complex and cannot be explained by a single process. Whereas in a perfect crystalline solid the long-range order of the lattice makes the correlation length of the normal-mode vibration infinite, limiting Raman scattering to zone-centre (q = 0) optical phonon modes, in defect-rich or nano-crystalline materials, such as dentin apatite, the relaxation of the momentum selection rule allows a greater range of vibrational modes to contribute to Raman scattering. This results in a redshift of the phonon frequency and a decrease in the phonon lifetimes, i.e., a broadening of Raman bands. In the anharmonic approximation, the phonon frequency (real part) and the phonon lifetime (imaginary part) should be linearly related to each other via Kramers-Kronig relationship. Indeed, we observe different, nearly linear data arrays in the data set of dentin treated at 30 °C that are characterized by different slopes dν/dΓ, ranging from -0.206 ± 0.004 to about -0.85 (**Fig. 7.8A and B**). In particular, the dentin altered for 7 days at 30°C shows an evolution of Raman spectral parameters towards synthetic hydroxylapatite (crystallite sizes between 70 and 100 nm) with a slope dν/dΓ of -0.206 ± 0.004, whereas all other experiments resulted in steeper trends that point then towards fluoridated fossil tooth and bone references as shown in Figure 7.8C. We also note that after 7 days at 90 °C, the dentin band parameters plot at the trend towards synthetic HAp, but for longer durations the slope dν/dΓ again became steeper, i.e., dν/dΓ = -0.57 ± 0.01, indicating a change in the recrystallization process.

7.5 Discussion

7.5.1 Weight loss and mass balance

The weight loss observed in samples immersed in acidic (≈ pH 1) tracer solutions at 30 °C and 90 °C is the result of material loss by dissolution of dental material (preferentially bioapatite), as indicated by increasing Ca and P content in the remnant solution (**Table S7.1, Fig. 7.2 and S7.3**). This dissolution of bioapatite caused an increase of solution pH from 1 to about 6-7. The degree of alteration observed at 30 °C and 90 °C seem to be different for the elements of interest. While both Ca and Sr concentrations show a similar temporal evolution in the tracer solution, both at 30 °C and 90 °C, Mg and especially Zn seem to be controlled by different reaction mechanisms. This becomes evident by the differences in material loss of the dental cubes between both experimental temperatures and by comparing those data with the

changes in solution composition over time. Based on the observed concentrations of the doped and undoped isotopes of interest in the solution, it is possible to calculate the expected material loss of the dental cubes by calculating a mass balance based on the solution concentrations (**Table S7.5**). However, this approach is limited by some assumptions, i.e. (a) the natural variability in element concentrations across the dental cubes, resulting in uncertainties of the average concentration of the dissolved material, (b) the uneven surface of the dental cubes, which can cause an enhanced dissolution of one cube in comparison to the other, due to differences in surface area, (c) the concentration difference of the isotope/element of interest in the initial solution and in the solutions from different time intervals of the immersion experiment. The latter is especially crucial for ^{44}Ca, which has already a high concentration in the raw solution and does not increase as much as the ^{43}Ca, i.e. resulting in a high background concentration in the starting solution. These limitations also explain the non-linear behaviour of the material loss with increasing time. However, there are as well several points affecting the accuracy in weighing, i.e. varying water content in the dental cube. Based on the results from the solution (**Fig. 7.2**), we calculated the absolute amount of each isotope (^{25}Mg, ^{26}Mg, ^{43}Ca, ^{44}Ca, ^{67}Zn, ^{68}Zn, ^{86}Sr, ^{88}Sr), based on their concentration, the known volume of each solution (2 mL, see “Materials and Methods, Tracer solution”), the natural abundance of each isotope (Berglund and Wieser, 2011), the elemental concentrations of the unaltered dental cube (**Table S7.4**) and the weight of each dental cube (**Table 7.1**). Calculations for Zn have not been performed, since the Zn concentration in the solution is decreasing with time, i.e. there is no Zn dissolution from the dental cube. The same trend was observed for the calculations using ^{44}Ca and ^{86}Sr during the 90 °C experiment. Therefore, these calculations have also been excluded from the Figure 7.9. For the 30 °C experiment, the calculations based on ^{43}Ca, ^{88}Sr, ^{25}Mg and ^{26}Mg show the best agreement with the measured weight loss, while ^{44}Ca and ^{86}Sr seem to underestimate the dissolved apatite material. During the 90 °C experiment, both Mg concentration calculations, as well as the calculation based on ^{43}Ca, overestimate the weight loss. The best agreement was found between the measured weight loss and the mass balance model based on the ^{88}Sr. This is especially interesting, since we observe a decrease of the ^{88}Sr/Ca in the dental cubes in the 90 °C experiment (**Fig. S7.14 and S7.15**). This evolution indicates, that ^{88}Sr seems to most accurately reflect the bioapatite dissolution process of the dental cubes during this experiment. In contrast, ^{44}Ca and ^{86}Sr show a decreasing trend in the solution data and are most likely involved in an opposing trend and increase due to mineral re-precipitation along the dental surface.

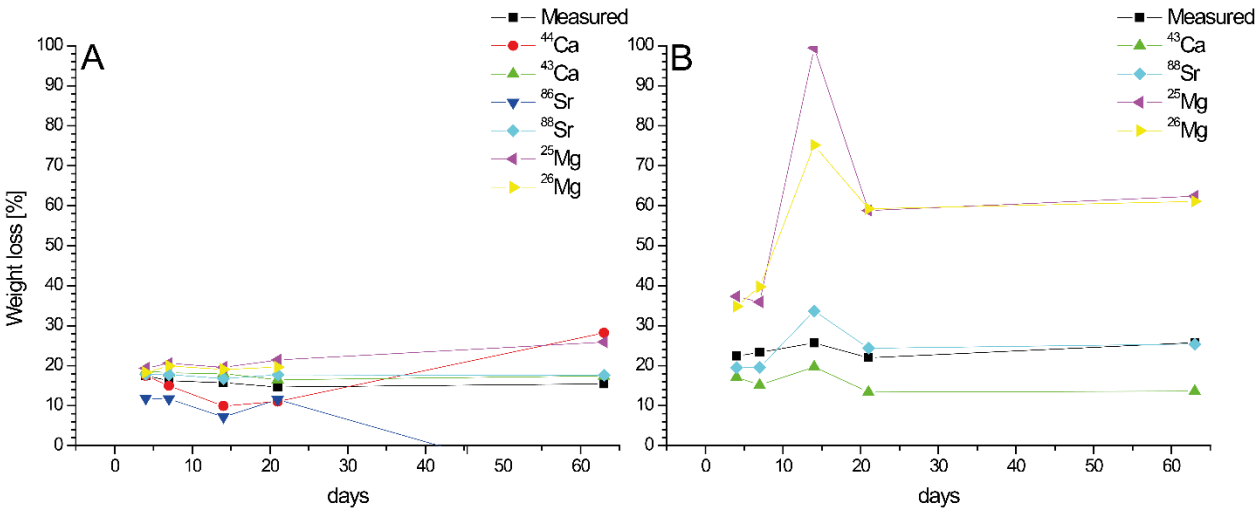

Figure 7.9. Weight loss of the dental cubes based on the mass balance model for the A. 30 °C experiment and the B. 90 °C experiment. Note that in B, the calculations based on ^{44}Ca and ^{86}Sr are not shown due to negative values (see text for details).

7.5.2 Evolution of the tracer solution and dental cubes

The composition of the tracer solution evolves differently for the elements enriched therein, but also for different isotopes of the element of interest at 30 °C and 90 °C, whereby slight positive shifts in the mass fraction might be due to some evaporation loss of the tracer solution during the experiment, especially during the 90 °C experiment. For Mg, a clear increase for both isotopes ^{25}Mg (doped) and ^{26}Mg (undoped) in the solution is observed at both temperatures. Interestingly, the increase in ^{25}Mg (~4.6 mg/L for 30 °C and ~9.1 mg/L for 90 °C) and ^{26}Mg (~4.8 mg/L for 30 °C and ~9.3 mg/L for 90 °C) reflects the natural isotopic composition of Mg (^{25}Mg ~10 % and ^{26}Mg ~11 %), proofing that Mg is leached from the dental cubes. In general, during the 90 °C experiment the Mg concentration in the solution increased more than during the 30 °C experiment, indicating a higher dissolution of the dental material (**Fig. 7.1**). This is in agreement with the weight loss data of the dental cubes at 90 °C and 30 °C displaying a higher loss of 23.5 ± 2.3 % compared to 15.5 ± 1.5 %, respectively (**Table 7.1**). Magnesium is further dissolved with increasing duration of the experiment, which is in agreement with the decreasing ^{n}Mg/Ca in the dental cubes. All ^{n}Mg/Ca ratios decrease in altered dental tissue compared to the starting values of each dental cube before the experiment, especially in the dentin, which is completely overprinted in the 90 °C experiment and lost about 80 % of its Mg content (**Fig. S7.9**). However, the doped ^{25}Mg shows the highest ^{n}Mg/Ca ratio, both in the dentin and enamel after the 90 °C experiment. Since both, the lighter ^{24}Mg and the heavier ^{26}Mg are lower concentrated in comparison to the ^{25}Mg with intermediate weight, no clear trend towards a preferential dissolution of heavier/lighter isotopes is detectable. This implies, that the dissolution process out of the dental cube for the Mg is

(mainly) controlled by the concentration gradient between solid dental material and the tracer solution, the latter being highly enriched in ^{25}Mg.

Zinc shows a completely different alteration behaviour, both in the solution and in the dental tissues, than Ca, Sr and Mg. Apart from two outliers for the 14 days experiment (**Fig. 7.2**), the Zn concentration in the solution shows an exponential decrease for the whole experimental duration for both temperatures (**Fig. S7.17**). In addition, all $^{n}Zn/Ca$ ratios increase in the outer parts of the dental cubes, both for enamel and dentin (**Fig. S7.7, S7.8 and S7.12**). However, the $^{67}Zn/Ca$ increases the most, leading to an increased $^{67}Zn/^{64}Zn$ (**Fig. 7.4, 7.5, S7.5, S7.10**). This implies, that Zn is absorbed from the solution and incorporated into the apatite crystal lattice. If any Zn dissolution from the dental material occurs, this amount is several orders of magnitude lower than that of the Zn precipitation, i.e. there is a net accumulation of Zn in the outer rim of the dental tissues, both dentin and enamel. However, it is not possible to evaluate the amount of Zn dissolved in comparison to Zn incorporated. It is assumed that Zn is taken up into the dental material, substituting for the leached out divalent cations, such as Ca^{2+}, Mg^{2+} and Sr^{2+} in the crystal lattice of the apatite. Zinc distribution patterns comparable to our experiment have also been postulated for fossil aurochs bone fragments from the Neolithic (Reiche et al., 2003). The increase in $^{n}Zn/Ca$ ratios in the outermost parts of the dentin and enamel could be caused by incorporation of Zn from the tracer solution into the dental tissue or the possibility of contamination of Zn from either laboratory gloves during the handling of the samples (Garçon et al., 2017), or from the resin Technovit 5071 in which the samples have been embedded. An incorporation from the tracer solution, however, seems to be more likely, since there is no increase in $^{n}Zn/Ca$ ratios in the untreated cube, which were handled similar to the treated cubes.

The evolution of Sr and Ca isotopes is rather similar during the experimental duration and the two temperatures, as expected from their similar chemical properties. However, the concentration changes of Ca in the tracer solution are even more pronounced during the 90 °C experiment. The ^{43}Ca and ^{88}Sr, which were not enriched in the tracer solution, both increase rapidly after the experiment started and almost stay constant during the full experimental duration (**Fig. 7.2**). Only for the 90 °C experiment, ^{43}Ca might show a slight decrease with increasing experimental duration (**Fig. 7.2C**). This indicates that Sr and Ca are both dissolved from the dental material into the solution, as shown by the increased ^{88}Sr and ^{43}Ca concentration in the tracer solution. This dissolution is mostly happening during the first four days of the experiment and is significantly reduced afterwards. Due to buffering of the tracer solution by bioapatite dissolution, the pH increases up to 6 to 7 and the solution is no longer acidic, preventing any significant further dissolution, since hydroxylapatite dissolution is highly dependent on pH and almost not soluble in neutral aqueous solutions (Fassbender et al., 1966; Berna et al., 2004). The same changes are visible during the 30 °C experiment for the doped

^{44}Ca and ^{86}Sr. After initial dissolution within the first four days, the solution concentration varies only slightly. However, for the 90 °C experiment, the doped isotopes of ^{44}Ca and ^{86}Sr tend to decrease significantly in the tracer solution. Since there is no other sink (no precipitates that formed in the Teflon beaker) for the Ca and Sr than the dental cubes, the only explanation is that both are incorporated into the dental material, i.e. by re-precipitation as newly formed (synthetic) hydroxlyapatite (**Fig. 7.8**). The differences in the concentration for the specific time intervals (i.e., 14 days at the 90 °C experiment) are again most likely due to the natural variance in the trace element composition of the dental material between the different individual cubes. The imperfections of the crystal structure of bioapatite can therefore favour the mineral dissolution (Mayer and Featherstone, 2000). As soon as hydroxylapatite starts to re-precipitate from the solution, the rate of precipitation is not only controlled by the availability of Ca^{2+} and PO_4^{3-} ions, but also by the surface area (Inskeep and Silvertooth, 1988), which likely differs between the different dental cubes. This re-precipitation is only visible during the 90 °C experiment and therefore seems to be controlled mainly by temperature, i.e. a specific thermal activation energy is needed to induce the re-precipitation. Especially for supersaturated solutions, an equilibrium state can only be achieved when long experimental durations and/or highly elevated temperatures are used (Chander and Fuerstenau, 1984). Nevertheless, in the 90 °C experiment, the doped isotopes (^{44}Ca, ^{86}Sr, ^{25}Mg) of the according elements show a different evolution. There is no clear trend regarding the preferred precipitation of a lighter/heaver isotope. For Ca, the heavier ^{44}Ca is preferentially removed from the solution into the newly precipitated mineral, while for Sr, the lighter ^{86}Sr is preferentially incorporated. For the 90 °C experiment, the ^{88}Sr/Ca is lower than before the experiment, while the ^{86}Sr/Ca is increased. This trend is especially visible in the dentin, but also slightly visible for the outer enamel (**Fig. S7.14 and S7.15**), which would imply a preferred incorporation of the lighter ^{86}Sr in comparison to the heavier ^{88}Sr. While this trend is known for fractionation along trophic food chains (Knudson et al., 2010), i.e. due to biological processes, the experimental setup is entire inorganic and therefore should not favour the lighter isotope. Stable isotope fractionation in biological processes is typically in in the permil or sub-permil range. In our *in-vivo* experiment probably no stable isotope fractionation might be visible for the precipitation of Sr (for Ca and Mg as well) from the tracer solution to the solid dental material, because the difference in the ^{86}Sr/Ca ratio is dominated by the excess of ^{86}Sr in the solution. We observe preferred isotopic incorporation not dependent on isotopic weight, but rather on concentration of the isotope in the enriched tracer solution. This is true for Ca (^{44}Ca preferentially incorporated versus ^{43}Ca), Sr (^{86}Sr preferentially incorporated versus ^{88}Sr), but also for Mg, where the intermediate, but higher concentrated ^{25}Mg in preferentially incorporated in contrast to the lighter ^{24}Mg or the heavier ^{26}Mg (**Fig. S7.11 and S7.13**). Considering, that all three elements belong to the same group of earth alkaline elements they should react in a similar way in natural processes. Due

to the fact that there is no, or at least no detectable, preferred isotopic incorporation for a lighter or heavier isotope during the alteration experiments, it seems more plausible, that the re-precipitation process at higher temperatures is induced due to the oversaturation in the solution of solved calcium phosphate and the unproportionally higher abundance of the enriched ^{25}Mg, ^{44}Ca and ^{86}Sr in the solution, compared to ^{24}Mg, ^{26}Mg, ^{43}Ca and ^{88}Sr, respectively.

7.5.3 Implications for sampling of dental tissues for isotope or trace element analysis

Based on the laser ablation profiles isotope ratios of all four different isotope systems Ca, Sr, Mg and Zn display alteration rims of enriched concentrations in the outer enamel of at least ≈ 100 µm for both temperatures. For the lower temperature experiment (30 °C) no systematic extension of the alteration rim (i.e. penetration depth of the reaction zone) with increasing experiment duration was observed. Since the dental cubes are biological materials, natural variation in chemical composition and structural properties is likely. Therefore, deeper penetration depth of the alteration rim in single samples could be explained with a crack or more porous enamel, which might function as a fluid pathway for the isotopic tracer solution deeper into the dental material. In the higher temperature experiment (90 °C), the deepest reaction depth of around 150 µm was observed in the longest lasting experiment (cube F, 63 days). For all other experimental durations, no systematic increase could be detected, implying that a significant difference in alteration depth of the enamel only occurs at higher temperatures and long experimental durations. It could also be concluded that the main alteration processes took place during the first few days of experiment, while the pH value was only 1. As soon as the pH increases, the dissolution process likely stopped. *In-situ* LA-MC-ICP-MS $^{87}Sr/^{86}Sr$ analysis allows for a more sensitive and higher spatially resolved assessment of diagenetic alteration than LA-ICP-MS analysis. During LA-ICP-MS analysis, the high number of isotopes measured per cycle, resulting in a temporal resolution of 0.8 s, limits the temporal resolution. Based on the transition rate of 5 µm/s, the calculated spatial resolution for the LA-ICP-MS data is 6 – 8 µm (Sanborn and Telmer, 2003). In contrast, the data acquisition in multi-collection mode solely for Sr enables the LA-MC-ICP-MS methodology to achieve a spatial resolution of up to 1 µm (based on a transition rate of 5 µm/s and an integration time of 0.2 s in the time resolved analysis of the Nu Plasma software). Therefore, the higher spatially resolved LA-MC-ICP-MS $^{87}Sr/^{86}Sr$ data shows, independent of experiment duration, an enamel alteration rim of 300 µm at 30 °C (**Fig. S7.4**) and up to 500 µm at 90 °C. Therefore, for sampling of fossil teeth for isotope analysis the removal of the outer few 100 µm of enamel is recommended to ensure the analysis of the least altered central part of the enamel. This may work well for mammal teeth with thick enamel but can be problematic and not feasible for reptilian teeth with thin enamel is for small-sized teeth. However, as the innermost enamel,

along the EDJ, is also altered due to a penetration of the tracer fluid through the whole dentin and across the EDJ into the innermost few 100 µm of enamel (**Fig. 7.5**), this zone should ideally also be avoided for geochemical analysis assessing in vivo compositions. The innermost, pristine zone in the central part of the enamel is shrinking from both sides with the duration of the alteration experiments (**Fig. 7.5**). After 63 days at 90 °C, there remains only a zone of ≈ 1 mm unaltered enamel, which is about ≈ 56 % of the original enamel thickness of ≈ 1.8 mm. In contrast, dentin is much more prone to alteration than the enamel. Especially during the higher temperature experiment, a complete alteration of the ≈ 1.4 mm thick dentin is observed for all doped isotopes (^{25}Mg, ^{44}Ca, ^{67}Zn and ^{86}Sr) already after 7 days. This is probably caused by the lower apatite crystallinity, higher porosity, lower degree of mineralisation and higher content of organic matter (i.e. collagen) in the dentin compared to the enamel, making it much more prone to diagenetic alteration.

7.5.4 Dissolution and precipitation processes

The Raman spectra of enamel and the extracted spectral parameters, bandwidth and position, of the $v_1(PO_4)$ band display a higher resistance of enamel against alteration, matching with the expected higher apatite crystallinity of enamel compared to dentin. According to the high crystallinity, the enamel is less vulnerable to changes during the lower temperature experiment (30 °C), where no changes in the Raman spectral parameters in the outer 120 µm were observed. Even at higher temperatures (90 °C experiment), only the enamel in the sample with longest exposure to the tracer solution show an increase of the $v_1(PO_4)$ band position in the outer 120 µm (**Fig. 7.7 and S7.18**). Note that band position is determined from the average P–O bond length involved in the symmetric stretching of phosphate (i.e. Popović et al., 2005). The higher band positions indicate a shorter P–O bond length, which could be caused by the incorporation of light ions from the doped isotope tracer solution on the Ca crystal lattice position. Fluorine is known to substitute on the OH- position in the apatite lattice and can cause also such a shift of the $v_1(PO_4)$ band to higher wavenumbers (Thomas et al., 2011). However, the tracer solution initially did not contain any F, therefore, in this special experimental setup, the only possible source of F are the reaction beakers consisting of Teflon, which is a synthetic fluoropolymer of tetrafluoroethylene. This is further supported by the fact that a notable shift only occurred in the enamel experiment that ran for 63 days at 90 °C. The different dν/dΓ trends are potentially a result of different F concentrations dissolved from the Teflon beakers, expect for the dν/dΓ trends going towards synthetic HAp (**Fig. 7.8C**).

Modifications of the dentin Raman spectra and of the $v_1(PO_4)$ band confirm that dentin is much less resistant against alteration compared to enamel. Furthermore, the alteration processes of dentin samples progress continuously and are temperature-dependent. The

reaction time seems to have only little influence at low temperatures, however, a clear tendency to a dissolution of hydroxylapatite and a preservation of organic material exists. It is indicated, that the partial dissolution of the apatite component in the outer part of the samples, which relatively increased the amount of collagen with respect to the bioapatite, as also observed for the dentin samples but here even at lower temperatures. Raman spectra of the dental cubes from the 30 °C experimental series display the dissolution of apatite in the outer dentin area exposed to the solution already after 4 days, while collagen is predominantly still preserved, indicating a preferred preservation of organic matter in this specific acidic environment at low temperatures (**Fig. 7.7**). In the 90 °C experimental series, the outer 120 µm of dentin were also completely altered already after 4 days. At higher temperature, also degradation of the organic matter can be observed, while the bioapatite component remains preserved, even after long experimental durations. This is reflected by a strong shift of the $v_1(PO_4)$ band towards higher wavenumbers in samples with longer reaction duration at 90 °C (**Fig. 7.8B**), which hints towards a dissolution-recrystallization process. From unaltered dentin Raman shift and FWHM display two different trends, one towards values of high bandwidth and slightly increasing band position and the other one displaying increasing band position accompanied by a strongly decreasing bandwidth, reaching minimum values close to synthetic HAp (**Fig. 7.8C**).

A dissolution-recrystallization process of the bioapatite resulting in higher apatite crystallinity would lead to such an increasing $v_1(PO_4)$ band position and decreasing bandwidth. During the dissolution and recrystallization of the apatite F and Zn got incorporated. Zinc is known (independent of Zn concentration) to reduce the acid reactivity, causing less dissolution of the dental cubes after the initial experimental phase, as well as the formation of new and larger crystals (Featherstone and Nelson, 1980) with less structural defects (Nelson et al., 1982; Mayer and Featherstone, 2000). This would lead to the observed increased crystallinity and the decreased bandwidth in the Raman spectra. Furthermore, the lower Mg/Ca in the newly precipitated hydroxylapatite could also cause a higher crystallinity (Legfros et al., 1996). Since Mg is leached out of the dentin, Sr and/or Zn seems most likely to substitute for Ca instead of Mg, causing the increase of the band position, when comparing Raman spectra with the laser ablation results.

The dissolution behaviour of Ca-apatites in acids, such as hydroxylapatite in HNO_3, can be described by different models and is still a matter of debate (see Dorozhkin, 2012 and references therein for a literature review of different models). However, all of these models are generally limited by several assumptions, they usually only use the stoichiometric hydroxylapatite (Ca/P = 1.67) and only consider ions of Ca^{2+}, PO_4^{3-} and OH^- or F^-, respectively. In addition, the initial surface of the model-apatite is always perfectly smooth, even from a molecular point of view, i.e. no dissolution nuclei are modelled. Furthermore, those models

usually do not consider whether the specific anions of an acid such as Cl^- vs. NO_3^- for hydrochloric and nitric acid, respectively, might have unknown specific effects. Therefore, such models are only of limited use to explain dissolution and precipitation of the bioapatite of the dental cubes used in this study. Furthermore, these models are not valid for experimental conditions with pH of < 2 and temperatures above 70 °C (Dorozhkin, 2012). Since isotopic fractionation seems to be only of minor importance for the processes observed during the experiment, we mainly use concentration differences and diffusion effects on the solid/liquid interface as explanation. As soon as the solid material (i.e. the dental cube) gets in contact with the tracer solution, a small layer of solid/liquid interface develops (DePaolo, 2011). This induces the chemical interaction of the solution with the apatite (Pearce, 1988), and the exchange of ions from both reservoirs within the solid/liquid interface. The components of the solution will absorb onto the surface of the dental cubes and induce a chemical exchange of the surface layer, i.e. causing the crystal surface to lose some of its components, such as Ca^{2+}, Sr^{2+}, Mg^{2+} and PO_4^{3-}. Depending on the ionic diffusion gradient, ions from the bulk solution or the dental material are exchanged within this interface layer and ultimately either transported into the solution, or incorporated into recrystallized dental material (Dorozhkin, 2012). Therefore, the large concentration differences in the tracer solution between the different isotopes, ^{44}Ca vs. ^{43}Ca and ^{88}Sr vs. ^{86}Sr, will ultimately be responsible for the different isotope evolution, while the element concentration stays consistent during the 90 °C experiment.

Our experiments demonstrate that non-traditional isotopes such as Ca, Sr, Zn and Mg increasingly used for dietary and physiological reconstructions are prone for diagenetic alteration in fossil teeth. Especially dentin is vulnerable for alteration and should be avoided. But also enamel, exposed to diagenetic fluids, can be altered especially the outer and innermost few hundred micrometres, depending on the time of burial and the physico-chemical conditions in the diagenetic setting. The enamel along the EDJ can be affected by alteration of solutions penetrating into the enamel from the dentin. To obtain pristine, in vivo isotope compositions it is thus important to carefully assess the chemical and mineralogical preservation state of enamel ideally by spatially resolved *in-situ* techniques such as Raman and LA-(MC)-ICP-MS. By analysing profiles across the enamel, the least altered zones can be identified and sampled from fossil tooth specimens. This is especially important for the application of non-traditional stable isotope systems such as $\delta^{44}Ca$, $\delta^{88}Sr$, $\delta^{26}Mg$ and $\delta^{64}Zn$ values used as trophic level indicators for the reconstruction of fossil food chains (Knudson et al., 2010; Jaouen and Pons, 2017; Martin et al., 2015b, 2017a; Bourgon et al., 2020). For these isotopes displaying trophic level differences in the sub-permil range, even small degrees of diagenetic alteration can strongly bias original compositions. Due to the experimental setup of this study, it is not possible to evaluate differences in the isotopic behaviour within a specific element, due to the high concentration in the tracer solution. To further evaluate the differences

during the 90 °C experiment between heavier and lighter isotopes, another experimental and analytical setup would be necessary, i.e. by using single element solutions with reduced isotopic concentration gradients (i.e. only near-natural isotopic enrichment). Besides the analysed Sr, Mg and Zn, there are several further elements that are contained in natural hydroxylapatite, such as Na, K, Ba, etc., which might influence the chemical properties during the experimental setup. In an independent experiment to evaluate isotopic fractionation effects during dissolution and/or precipitation of hydroxylapatite, single element solutions should be used at different temperatures, using high-resolution analytical techniques, such as MC-ICP-MS or TIMS, to further assess changes in the isotopic composition in the per mil range, which is relevant for palaeoecological and palaeoenvironmental applications using isotope compositions of fossil teeth.

7.6 Conclusion

In general, low, near Earth-surface temperatures (30 °C) do not affect the chemical alteration of dental tissues in acidic aqueous solution as much as higher temperatures of 90 °C (representing about 3 km of burial depth). Enamel isotope composition and apatite crystallinity are both much less affected by the *in-vitro* alteration experiment in the isotopically enriched tracer solution than in dentin. The isotopic ratios of dentin are fully altered at 90 °C after only few days. Calcium, Mg, Zn and Sr concentrations and isotope composition indicate that only the outermost ≈ 100-200 µm of the enamel are affected by reaction processes, probably diffusion and re-precipitation. High-resolution *in-situ* LA-MC-ICP-MS $^{87}Sr/^{86}Sr$ profiles across the dental cubes indicate that the central part of mm-thick enamel preserves original isotope compositions (even after 63 days at 90 °C), while dentin is fully altered after one week. This finding has implications for only few 100 µm thick enamel of certain fossil reptiles or small vertebrates. To measure pristine, *in-vivo* isotope compositions, we recommend to either remove the outermost ≈ 100-200 µm of enamel, as well as not to sample too close to the EDJ, or work with spatially resolving methods such as SIMS or laser ablation (MC-)ICP-MS to identify and avoid diagenetically altered zones. Magnesium and Zn show a different behaviour than Ca and Sr during the experimental bioapatite alteration. Zinc is incorporated into the dentin, while Mg is leached out of the dentin. The incorporation of Zn into the hydroxylapatite could be the reason for a decreasing Raman shift, causing the precipitation of crystals with less structural defects. Due to the lack of correlation between the reaction depth of the apatite (i.e. changes in isotope ratio and Raman spectra) and the duration of the experiments, it is not possible to determine the kinetic mechanism causing the alteration reaction. In contrast, it was possible to explain the different evolutions for the doped isotopes of Sr and Ca during the 90 °C experiment in the alteration zones of the bioapatite. Probably a diffusion gradient controlled

mechanism at the solid/liquid interface around the dental cubes due to the highly elevated concentration of the doped isotopes caused the altered isotope ratios in the outer few 100 µm enamel and throughout the dentin.

7.7 Acknowledgement

This project has received funding from the European Research Council (ERC) under the European Union's Horizon 2020 research and innovation programme (grant agreement No 681450) and the DFG grant nr. TU 148/9-1. This is contribution 30 of the DFG-funded research unit FOR 2685 "The Limits of the Fossil Record: Analytical and Experimental Approaches to Fossilization". We also acknowledge funding by the Max-Planck Graduate Center. We thank Alexander Gehler (University of Göttingen) who kindly supplied the tooth fragments of the African elephant molar (AG-Lox) from which dental cubes were cut and used for the alteration experiments. We thank Klaus Peter Jochum (Max-Planck Institute for Chemistry, Mainz) for the access to the LA-MC-ICP-MS laboratory.

7.8 Supplement

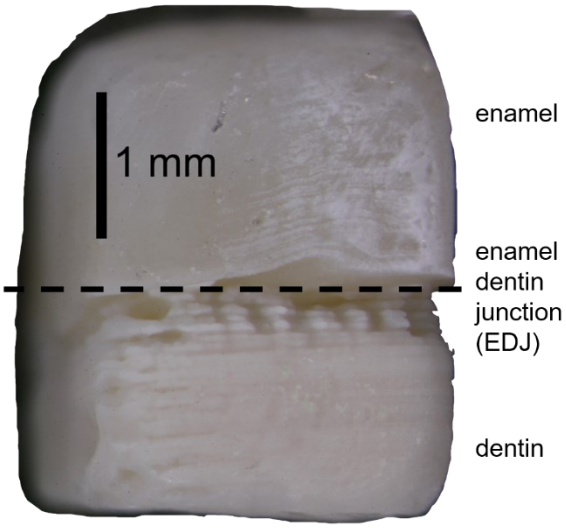

Figure S7.1. Dental cube I (14 days, 90 °C) after the experiment. A clear dissolution scar around the enamel dentin junction (EDJ) is visible, resulting in a higher concentration of Ca, P, Mg and other apatite-derived trace elements in the tracer solution. This picture was taken prior to the cutting and does not represent the area where the LA-(MC-)ICP-MS, EMPA and Raman analyses have been performed.

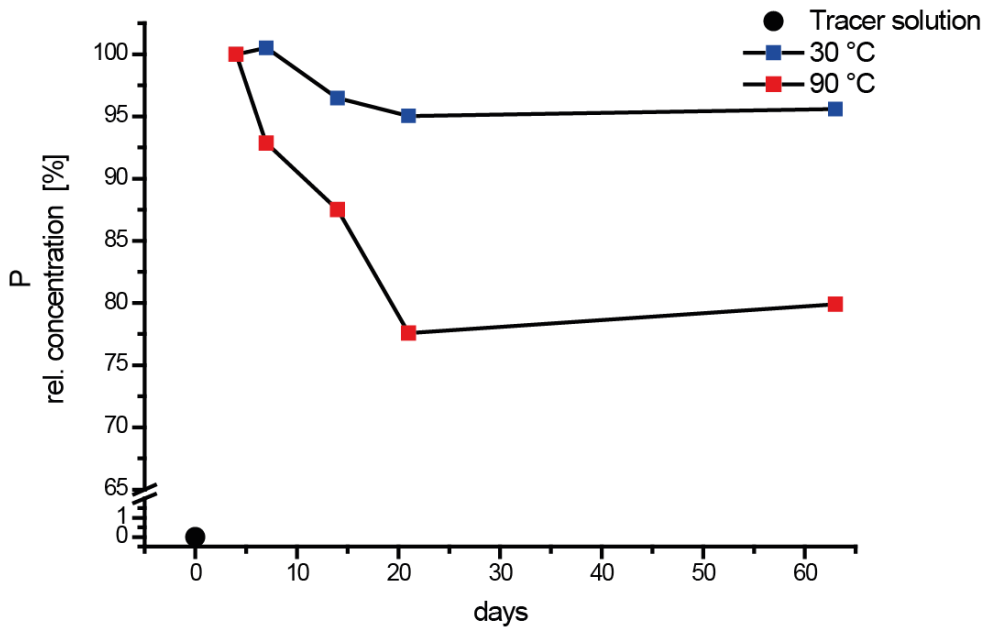

Figure S7.2. Qualitative evolution of the P concentration in the tracer solution. While P is absent in the raw solution, a significant amount is dissolved into the solution already after 4 days, which decreases afterwards, especially during the 90°C experiment. Note that the Y-axis is interrupted.

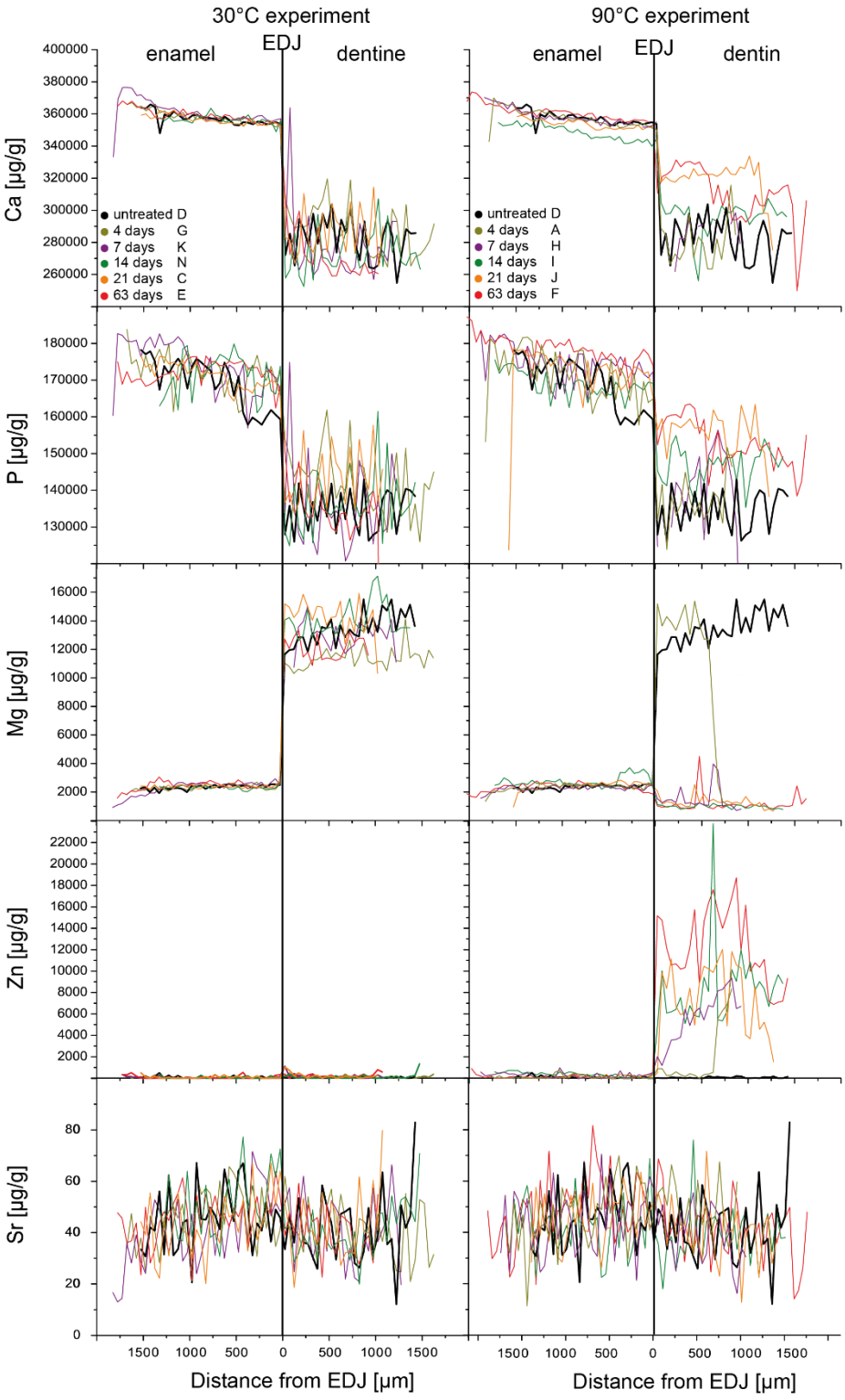

Figure S7.3. Results from EMPA for the *in-vitro* experiment. Major and trace element concentration profiles of enamel and dentin across the enamel dentin junction (EDJ) determined by EMPA, lines are centred to the EDJ. Concentration profiles of dental cubes immersed for different reaction times of 4–63 days in to ^{25}Mg, ^{44}Ca, ^{67}Zn and ^{86}Sr enriched tracer solution are given for both reaction temperatures 30 °C and 90 °C.

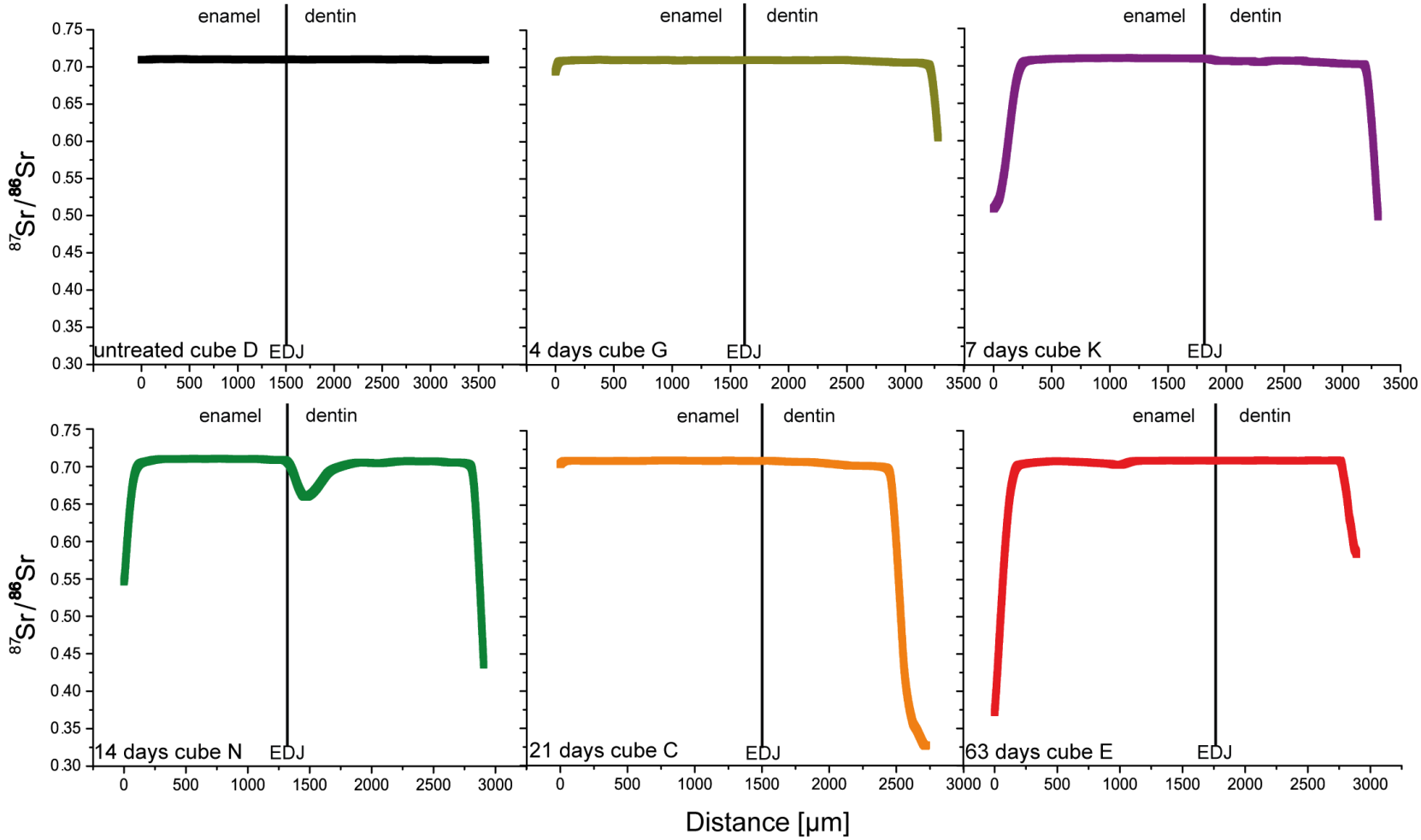

Figure S7.4. In situ $^{87}Sr/^{86}Sr$ LA-MC-ICP-MS profiles across the enamel and dentin perpendicular to the enamel dentin junction (EDJ) of the cubes from the 30 °C experiment. Note that only the outer rims of both enamel and dentin were altered and shifted to lower $^{87}Sr/^{86}Sr$ due to ^{86}Sr incorporation from the tracer solution. Note also the decrease of $^{87}Sr/^{86}Sr$ in the dentin close to the EDJ in the 14 days experiment, which is in line with the strong dissolution of dentin visible in this cube (**Fig S7.2**). The zero point is defined as the outer boundary of the enamel.

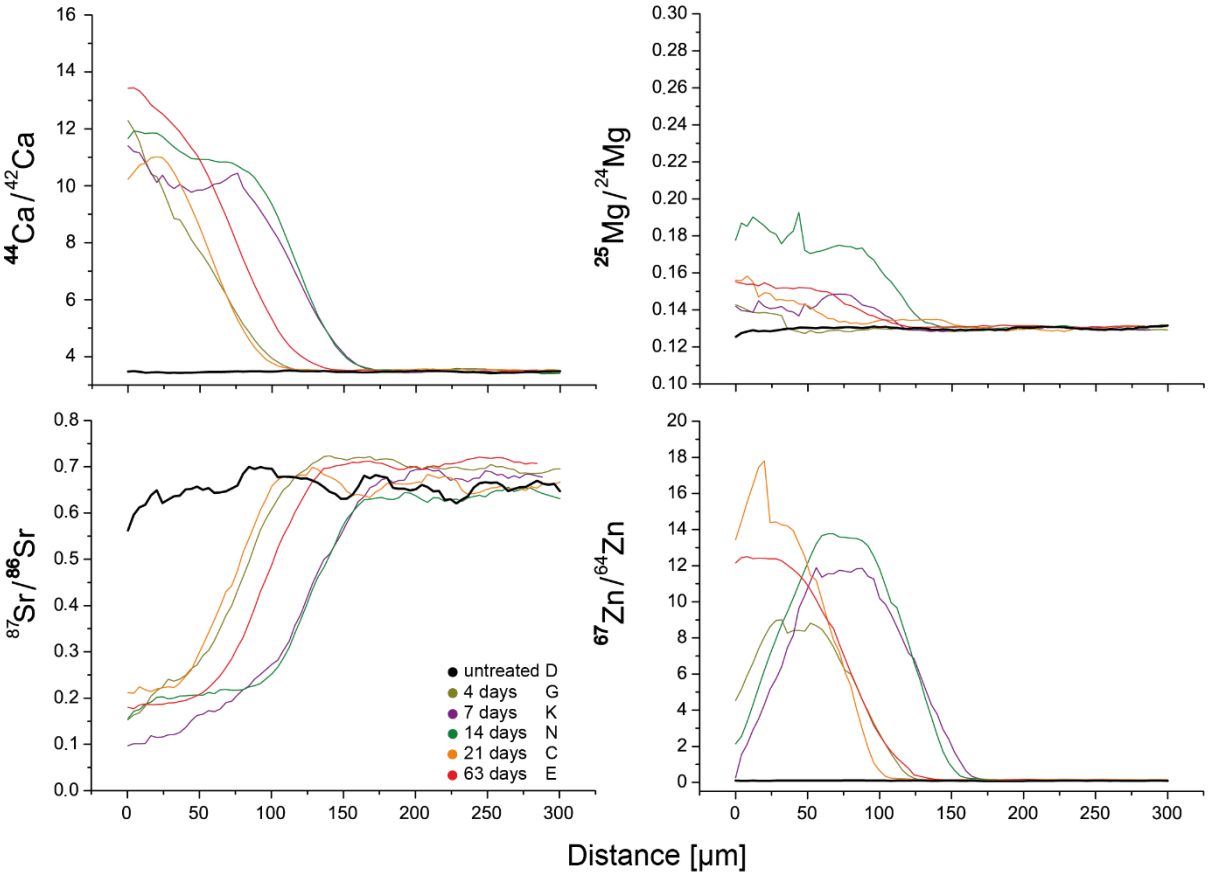

Figure S7.5. Isotope ratios of Ca, Mg, Sr and Zn measured by LA-ICP-MS in the outer 300 µm of dentin from the *in-vitro* alteration experiments at 30 °C for 4 to 63 days in isotopically (^{44}Ca, ^{26}Mg, ^{86}Sr, ^{67}Zn) enriched tracer solution. The zero point is defined as the outer boundary of the dentin.

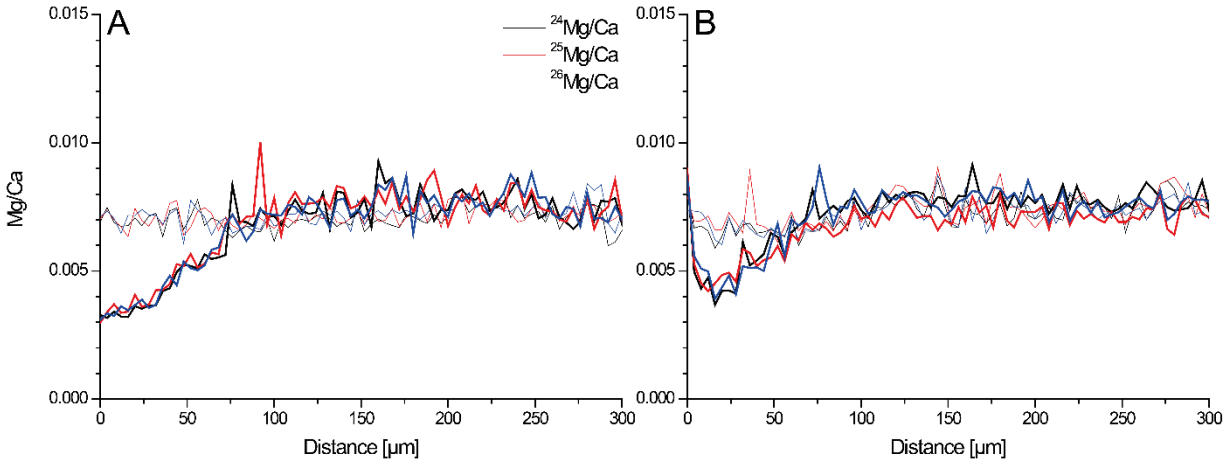

Figure S7.6. ^{n}Mg/Ca ratios measured by LA-ICP-MS in the outer 300 µm enamel of dental cubes from the 30 °C experiment after 14 (A) and 63 days (B). Thick lines indicate the ^{n}Mg/Ca ratios after the experiment, while thin lines show the initial ^{n}Mg/Ca prior to the experiment. The zero point is defined as the outer boundary of the enamel.

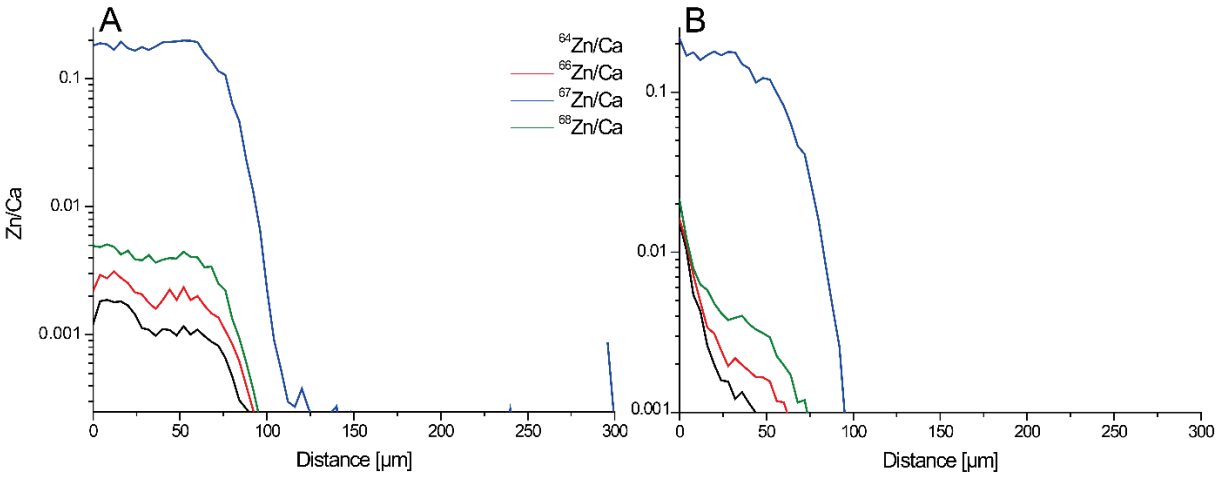

Figure S7.7. ^{n}Zn/Ca ratios measured by LA-ICP-MS in the outer 300 µm enamel of dental cubes from the 30 °C experiment after 14 (A) and 63 days (B). Thick lines indicate the ^{n}Zn/Ca ratios after the experiment, while initial ^{n}Zn/Ca prior to the experiment are almost 0 and not visible in this plot. Note that both y-axes are plotted on a logarithmic scale. The zero point is defined as the outer boundary of the enamel.

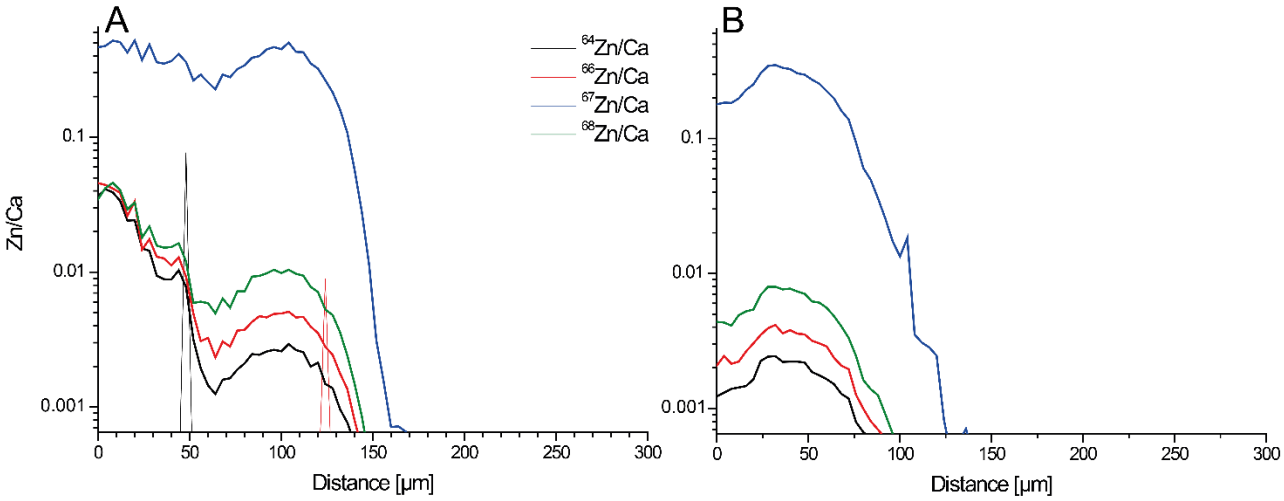

Figure S7.8. ^{n}Zn/Ca ratios measured by LA-ICP-MS in the outer 300 µm dentin of dental cubes from the 30 °C experiment after 14 (A) and 63 days (B). Thick lines indicate the ^{n}Zn/Ca ratios after the experiment, while initial ^{n}Zn/Ca prior to the experiment are almost 0 and not visible in this plot. The zero point is defined as the outer boundary of the dentin.

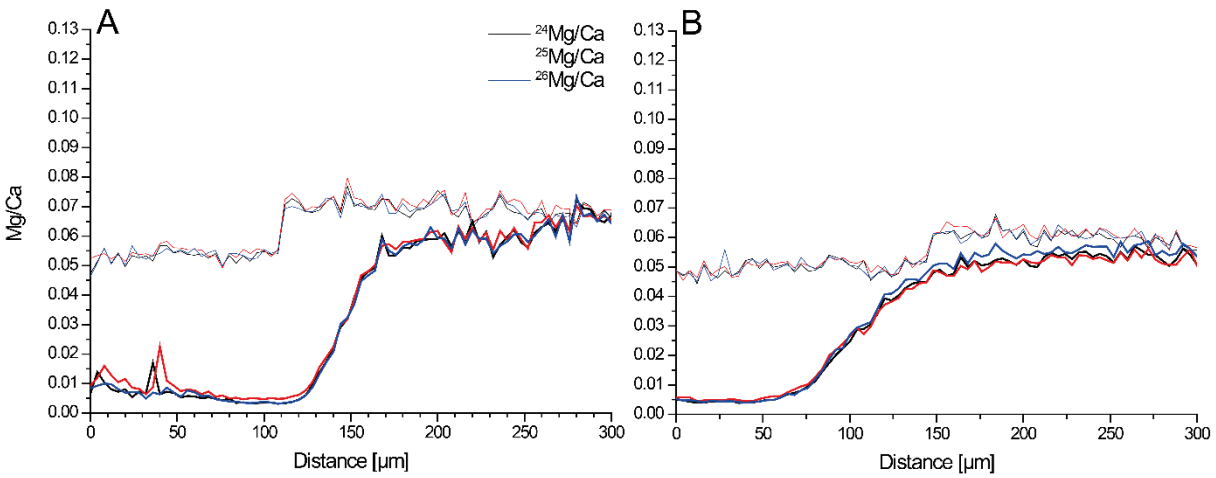

Figure S7.9. ^{n}Mg/Ca ratios measured by LA-ICP-MS in the outer 300 µm dentin of dental cubes from the 30 °C experiment after 14 (A) and 63 days (B). Thick lines indicate the ^{n}Mg/Ca ratios after the experiment, while thin lines show the initial ^{n}Mg/Ca prior to the experiment. The zero point is defined as the outer boundary of the dentin.

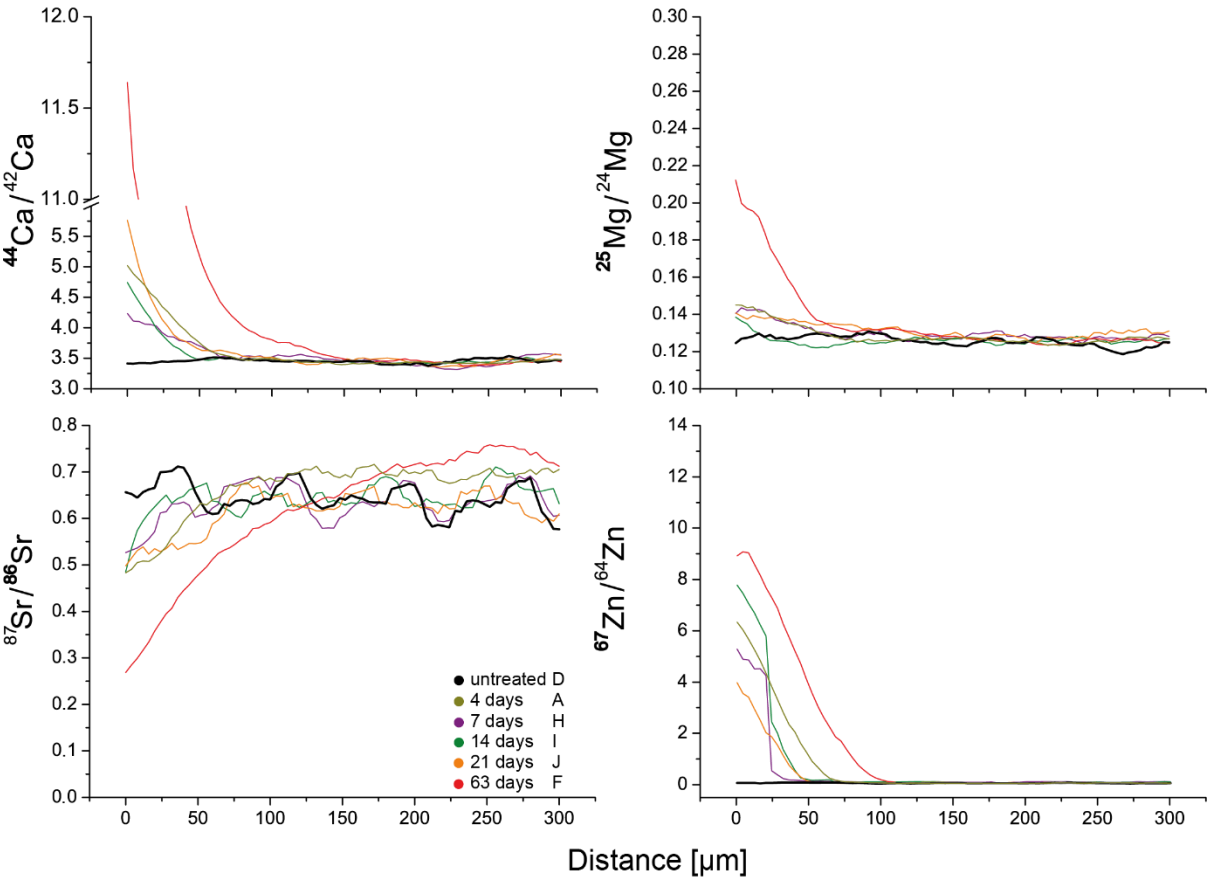

Figure S7.10. Isotope ratios of Ca, Mg, Sr and Zn measured by LA-ICP-MS in the outer 300 µm of enamel from the in-vitro alteration experiments at 90 °C for 4 to 63 days in isotopically (^{44}Ca, ^{26}Mg, ^{86}Sr, ^{67}Zn) enriched tracer solution. The zero point is defined as the outer boundary of the dentin.

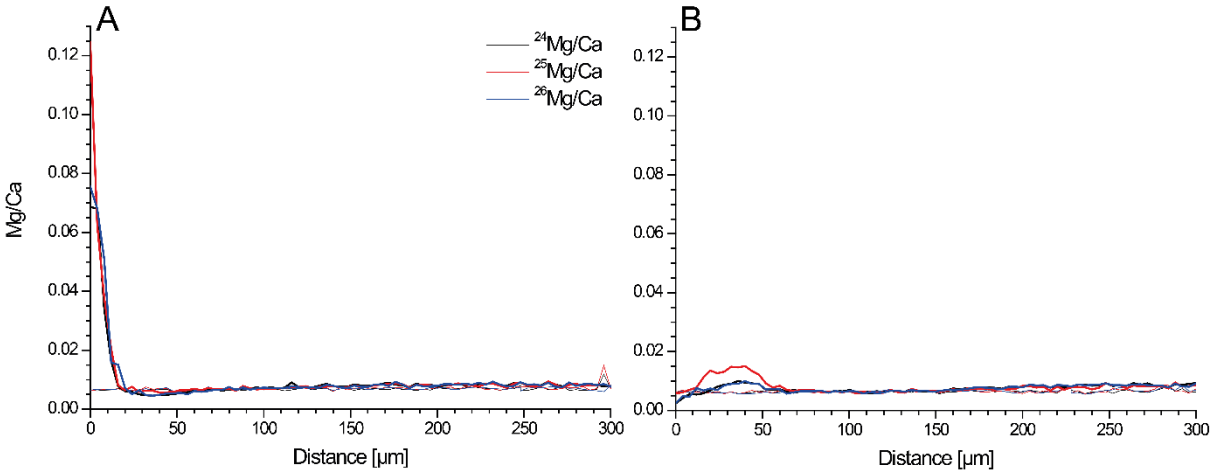

Figure S7.11. ^{n}Mg/Ca ratios measured by LA-ICP-MS in the outer 300 µm enamel during the 90 °C experiment after 14 (A) and 63 days (B). Thick lines indicate the ^{n}Mg/Ca ratios after the experiment, while thin lines show the initial ^{n}Mg/Ca prior to the experiment. The zero point is defined as the outer boundary of the enamel.

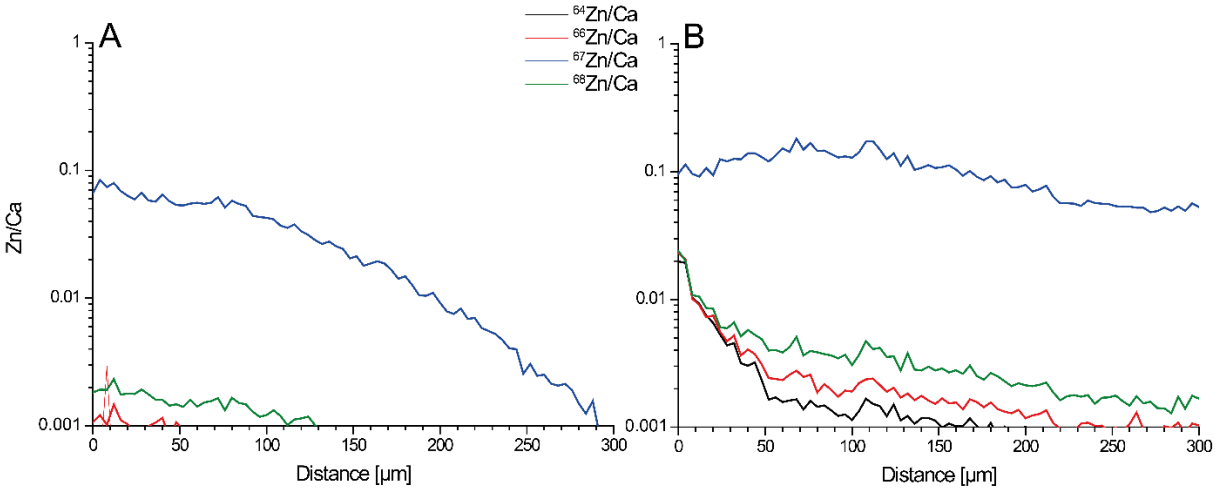

Figure S7.12. ^{n}Zn/Ca ratios measured by LA-ICP-MS in the outer 300 µm dentin during the 90 °C experiment after 14 (A) and 63 days (B). Thick lines indicate the ^{n}Zn/Ca ratios after the experiment, while thin lines show the initial ^{n}Zn/Ca prior to the experiment. The zero point is defined as the outer boundary of the dentin.

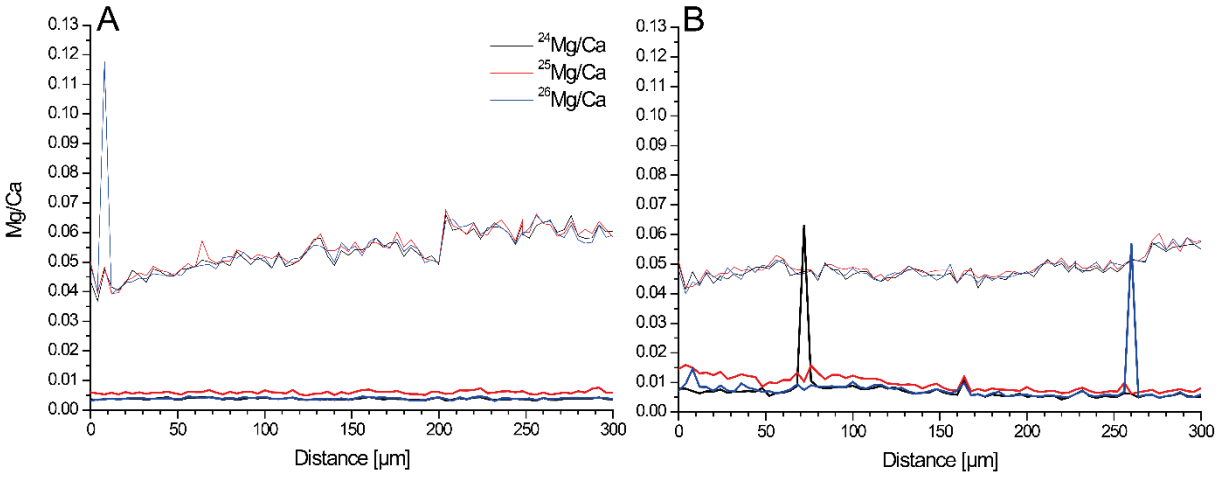

Figure S7.13. ^{n}Mg/Ca ratios measured by LA-ICP-MS in the outer 300 µm dentin during the 90 °C experiment after 14 (A) and 63 days (B). Thick lines indicate the ^{n}Mg/Ca ratios after the experiment, while thin lines show the initial ^{n}Mg/Ca prior to the experiment. The zero point is defined as the outer boundary of the dentin.

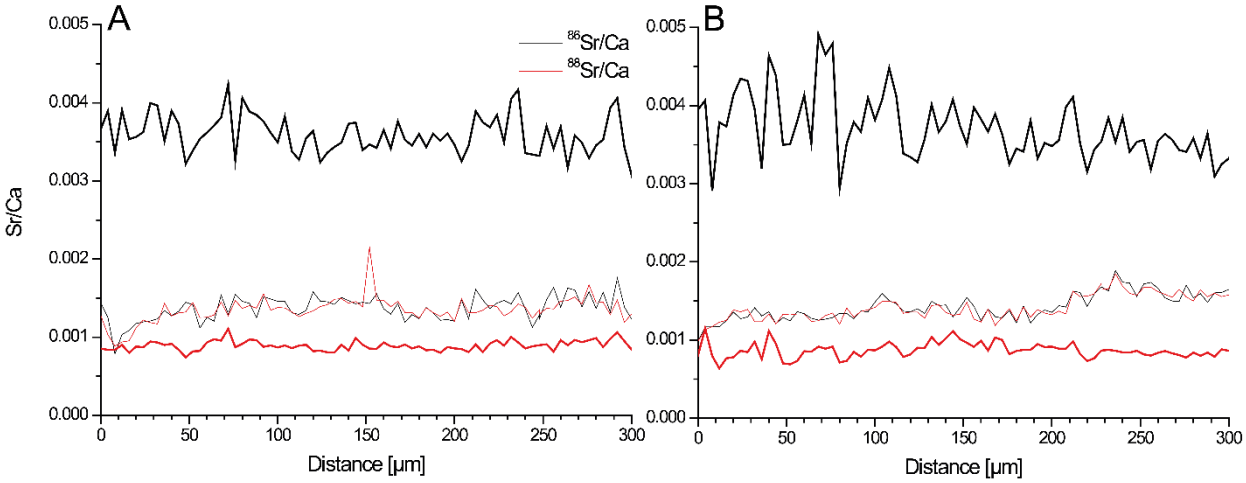

Figure S7.14. ^{n}Sr/Ca ratios measured by LA-ICP-MS in the outer 300 µm dentin during the 90 °C experiment after 14 (A) and 63 days (B). Thick lines indicate the ^{n}Sr/Ca ratios after the experiment, while thin lines show the initial ^{n}Sr/Ca prior to the experiment. The zero point is defined as the outer boundary of the dentin.

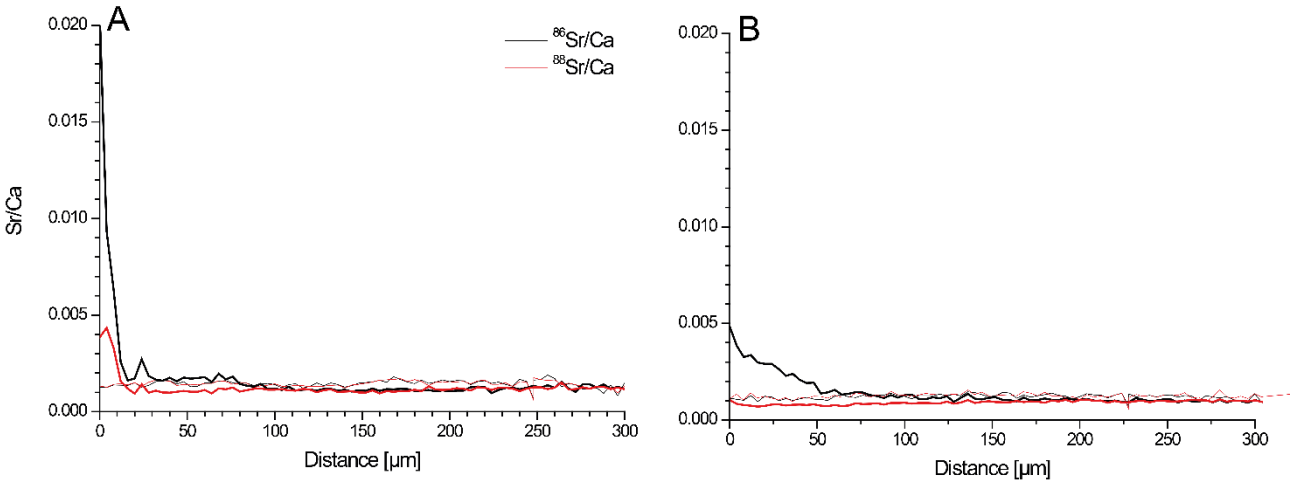

Figure S7.15. ^{n}Sr/Ca ratios measured by LA-ICP-MS in the outer 300 µm enamel during the 90°C experiment after 14 (A) and 63 days (B). Thick lines indicate the ^{n}Sr/Ca ratios after the experiment, while thin lines show the initial ^{n}Sr/Ca prior to the experiment. The zero point is defined as the outer boundary of the enamel.

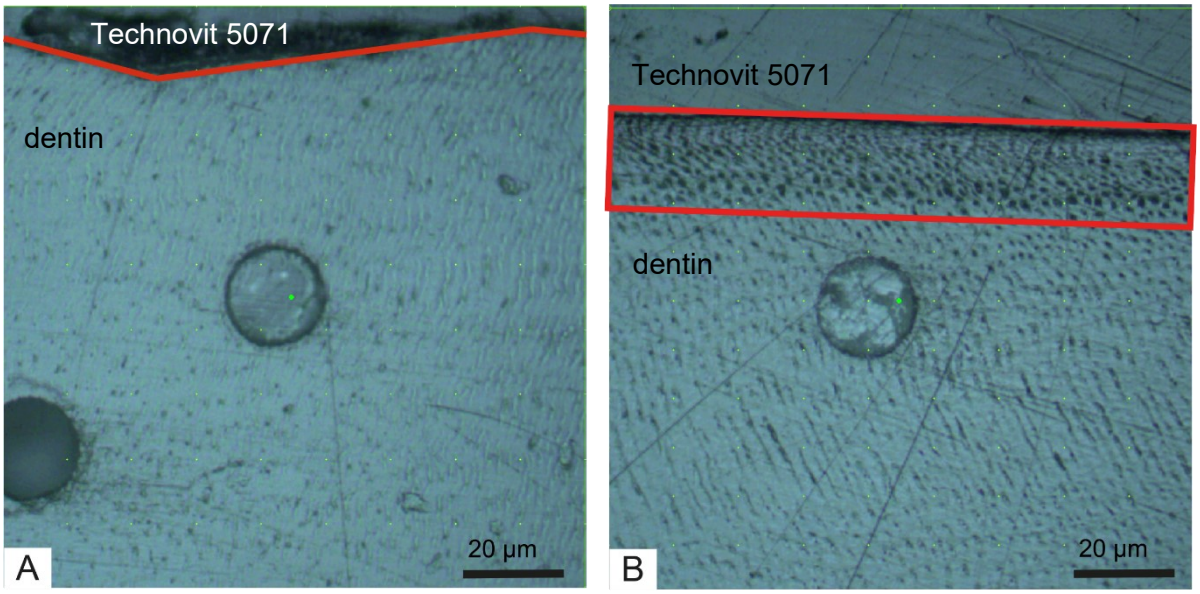

Figure S7.16. Example of the alteration rim (red box) visible in the dentin after the experiment. A. untreated reference cube D, B. 63 days, 30 °C experimental cube E.

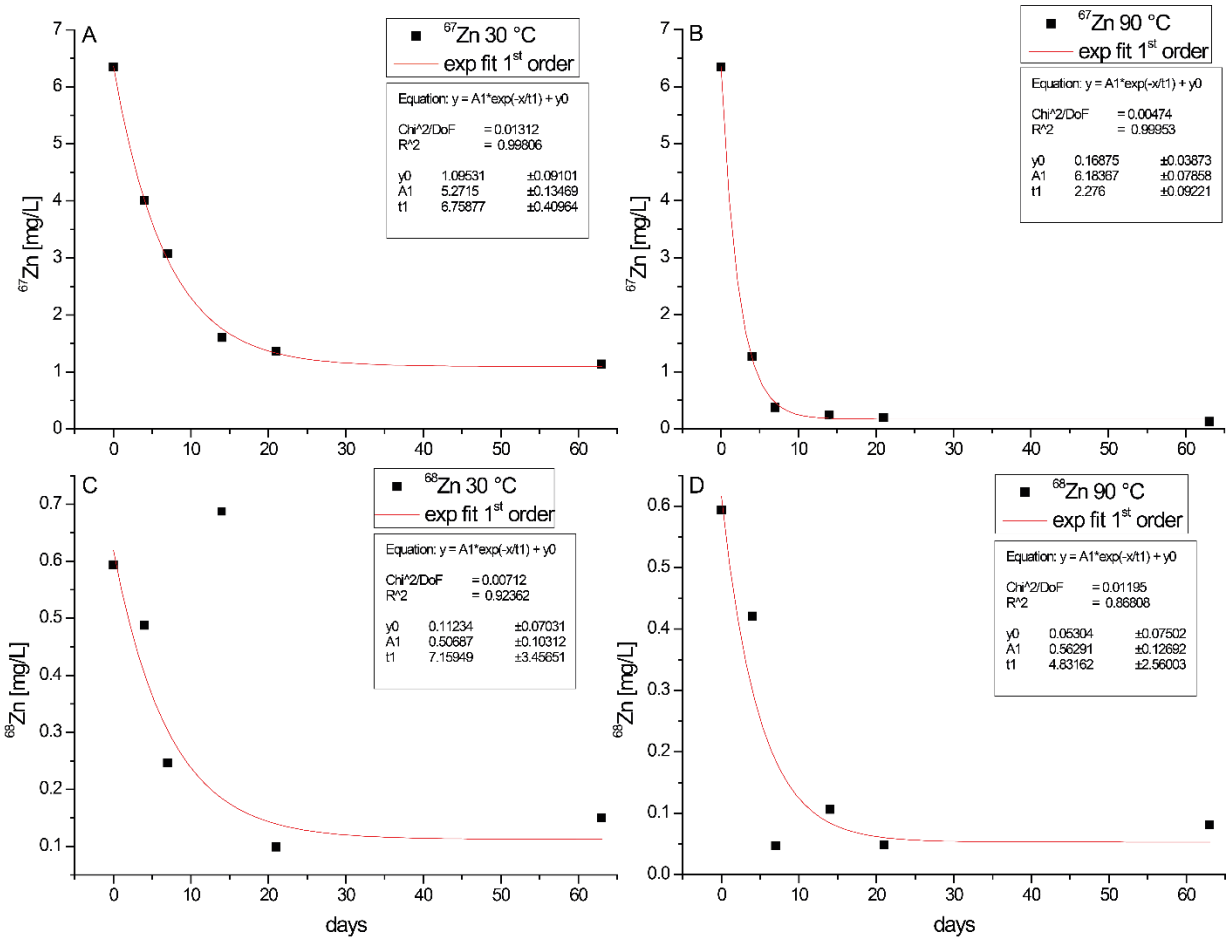

Figure S7.17. Exponential decrease of the Zn concentration in the tracer solutions for 30 °C (A) and (C) and 90 °C (B) and (D). Equations for every plot are given in the figure and are plotted as a red line. Please note that in C, the 14 days experiment was excluded from the calculations (red circle), due to its unusual dissolution behaviour (see **Fig. S7.2**).

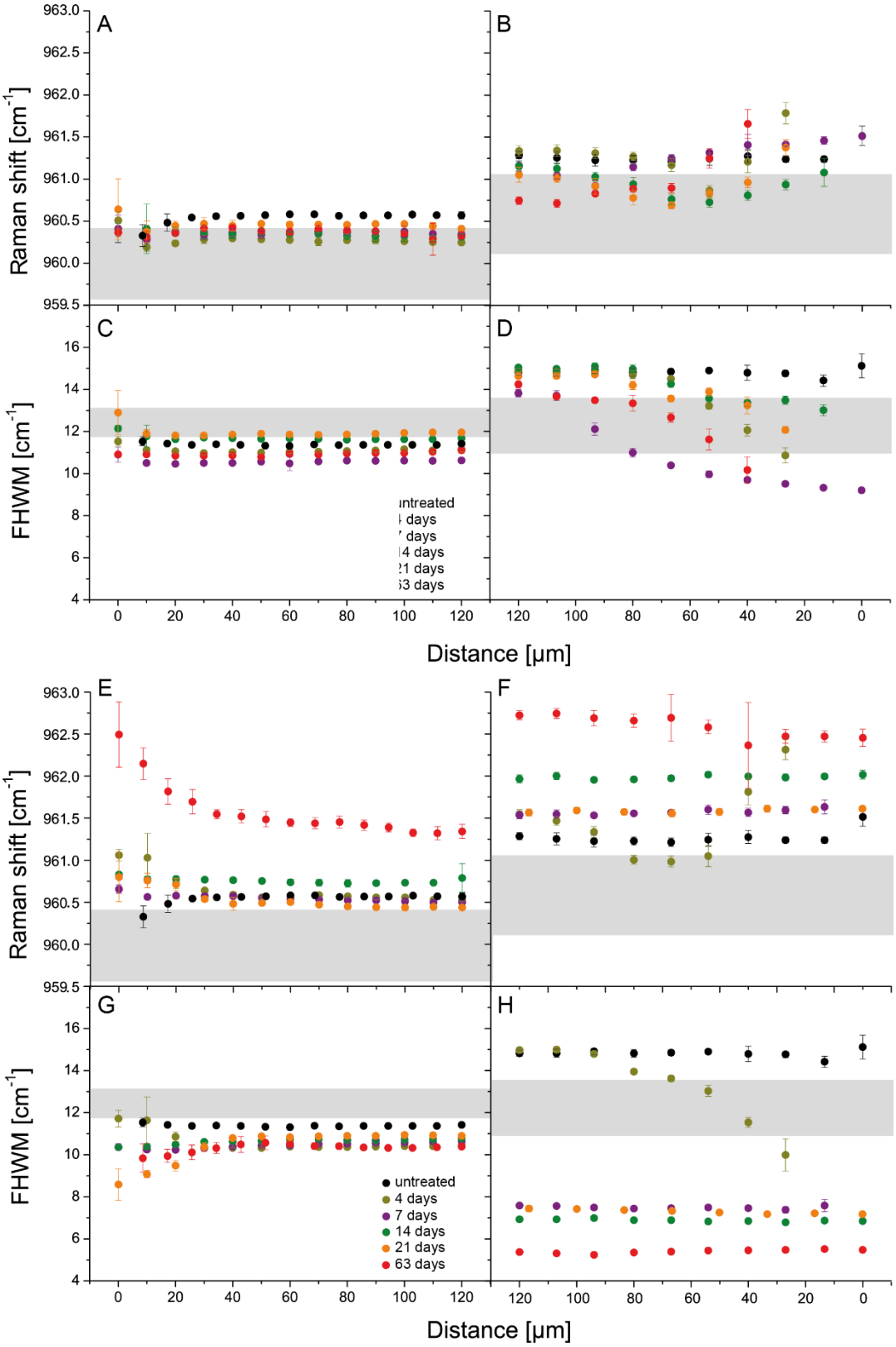

Figure S7.18. Raman shift and full width at half maximum (FHWM) of the outer 120 µm of the enamel (A), (C) of the 30 °C and (E), (G) of the 90 °C experiment and the outer 120 µm of the dentin (B), (D) of the 30 °C and (F), (H) of the 90 °C experiment. Grey bars show the natural variability of different unaltered dental samples from the same modern African elephant (*Loxodonta africana*) molar of unkown provenance (AG-Lox: Gehler et al., 2012).

Table S7.1. Concentration of the isotopic tracer solutions, the raw solution and those from the different time intervals during the 30 °C and the 90 °C alteration experiments. A. shows the isotopic concentration of the enriched isotopes (^{44}Ca, ^{86}Sr, ^{25}Mg, ^{67}Zn), while B. shows the isotopic concentration of the non-doped isotopes (^{43}Ca, ^{88}Sr, ^{26}Mg, ^{68}Zn), which have not been added on purpose to the raw solution, but are comprised as impurities.

A [mg/l]	**raw solution**	**day 4, 30 °C**	**day 7, 30 °C**	**day 14, 30 °C**	**day 21, 30 °C**	**day 63, 30 °C**	**day 4, 90 °C**	**day 7, 90 °C**	**day 14, 90 °C**	**day 21, 90 °C**	**day 63, 90 °C**
^{44}Ca	340.6	376.4	372.6	362.8	366.0	405.4	320.0	242.5	271.5	184.0	166.2
± SD	1.1	1.9	2.2	1.1	7.0	0.5	2.1	0.5	0.6	2.0	0.2
^{86}Sr	3.443	3.612	3.610	3.550	3.620	3.262	3.500	3.040	4.004	2.960	2.959
± SD	0.036	0.023	0.030	0.030	0.050	0.058	0.023	0.040	0.019	0.020	0.011
^{25}Mg	20.20	24.80	25.30	25.27	25.90	27.10	29.31	29.22	46.47	36.10	36.82
± SD	0.20	0.20	0.30	0.15	0.30	0.20	0.15	0.06	0.02	0.40	0.22
^{67}Zn	6.350	4.010	3.070	1.600	1.362	1.140	1.270	0.374	0.247	0.194	0.127
± SD	0.050	0.050	0.020	0.020	0.001	0.010	0.020	0.007	0.002	0.002	0.001

B [mg/l]	**raw solution**	**day 4, 30 °C**	**day 7, 30 °C**	**day 14, 30 °C**	**day 21, 30 °C**	**day 63, 30 °C**	**day 4, 90 °C**	**day 7, 90 °C**	**day 14, 90 °C**	**day 21, 90 °C**	**day 63, 90 °C**
^{43}Ca	0.14	2.62	2.65	2.74	2.59	2.73	2.47	2.26	3.04	2.16	2.17
± SD	0.00	0.06	0.03	0.00	0.04	0.02	0.01	0.02	0.01	0.01	0.00
^{88}Sr	1.05	3.09	3.18	3.15	3.33	3.32	3.36	3.42	5.35	4.24	4.32
± SD	0.01	0.05	0.00	0.07	0.02	0.01	0.07	0.05	0.05	0.02	0.01
^{26}Mg	1.78	6.56	7.21	7.21	7.54	8.63	11.13	12.76	23.61	19.40	19.70
± SD	0.03	0.04	0.11	0.03	0.12	0.07	0.05	0.01	0.05	0.50	0.30
^{68}Zn	0.59	0.49	0.25	0.69	0.10	0.15	0.42	0.05	0.11	0.05	0.08
± SD	0.01	0.00	0.02	0.02	0.00	0.01	0.00	0.00	0.00	0.00	0.00

Table S7.2. Overview of dental cube samples and analytical methods used to measure isotope and chemical compositions in the dental tissues.

Time of measurement	Sample	Data	Method
before and after *in-vitro* experiment	D, G, K, N, C, E, A, H, I, J, F	$^{44}Ca/^{42}Ca$, $^{25}Mg/^{24}Mg$, $^{67}Zn/^{64}Zn$ and $^{87}Sr/^{86}Sr$ ^{n}element/Ca	Laser ablation inductively coupled plasma mass spectrometry (LA-ICP-MS)
after *in-vitro* experiment	D, G, K, N, C, E, A, H, I, J, F	$^{87}Sr/^{86}Sr$	Laser ablation multi collector inductively coupled plasma mass spectrometry (LA-MC-ICP-MS)
after *in-vitro* experiment	D, L, M, G, K, N, C, E, A, H, I, J, F	Concentration of Ca, P, Mg, Zn, and Sr	Electron microprobe analysis (EMPA)
after *in-vitro* experiment	D, G, K, N, C, E, A, H, I, J, F	Changes in bioapatite mineralogy	Raman spectroscopy
after *in-vitro* experiment	original dental material (AG-Lox)	$^{87}Sr/^{86}Sr$ $\delta^{44/42}Ca$	Solution multi collector inductively coupled plasma mass spectrometry (MC-ICP-MS)
before and after *in-vitro* experiment	raw solution, experimental solutions from different temperatures and durations	Tracer solution composition	Thermo Element 2/XR inductively coupled plasma mass spectrometry (ICP-MS) and Spectro Vision ICP-OES

Table S7.3. Trace element data for quality control materials (QCMs) USGS BCR-2G and Durango Apatite, during each day of LA-ICP-MS analysis.

		Magnesium			Calcium		Zinc				Strontium	
total concentration based on measured isotope		**^{24}Mg**	**^{25}Mg**	**^{26}Mg**	**^{42}Ca**	**^{44}Ca**	**^{64}Zn**	**^{66}Zn**	**^{67}Zn**	**^{68}Zn**	**^{86}Sr**	**^{88}Sr**
BCR-2G	GeoReM*	21471			50458		125				342	
1st	Mean [µg/g]	21644	21842	21626	50132	52479	152	154	168	162	335	328
	RSF	1.01	1.02	1.01	0.99	1.04	1.21	1.24	1.34	1.30	0.98	0.96
2nd	Mean [µg/g]	23821	23838	23829	50614	50082	152	150	170	144	324	321
	RSF	1.11	1.11	1.11	1.00	0.99	1.21	1.20	1.36	1.15	0.95	0.94
3rd	Mean [µg/g]	25356	24982	26654	50600	48656	157	153	179	156	325	325
	RSF	1.18	1.16	1.24	1.00	0.96	1.26	1.23	1.43	1.25	0.95	0.95

		Magnesium			Calcium		Zinc				Strontium	
total concentration based on measured isotope		**^{24}Mg**	**^{25}Mg**	**^{26}Mg**	**^{42}Ca**	**^{44}Ca**	**^{64}Zn**	**^{66}Zn**	**^{67}Zn**	**^{68}Zn**	**^{86}Sr**	**^{88}Sr**
Durango	GeoReM*	229			390444		NA				524	
1st	Mean [µg/g]	182	182	179	389247	405573	0.3	0.4	3.3	1.4	471	461
	RSF	0.80	0.79	0.78	1.00	1.04	NA	NA	NA	NA	0.90	0.88
2nd	Mean [µg/g]	192	190	190	413513	406890	BDL	BDL	BDL	BDL	451	440
	RSF	0.84	0.83	0.83	1.06	1.04	NA	NA	NA	NA	0.86	0.84
3rd	Mean [µg/g]	186	177	176	434803	405648	BDL	BDL	BDL	BDL	458	459
	RSF	0.81	0.77	0.77	1.11	1.04	NA	NA	NA	NA	0.87	0.88

*Reference values obtained from the GeoReM database (Jochum et al., 2005) and the provided references therein for the different reference materials.

Table S7.4. Trace element data measured for the unaltered dental cube during different days of LA-ICP-MS analysis. The elemental concentration [µg/g] was calculated based on the isotope in superscript for every day of analysis.

	total concentration based on measured isotope	Enamel [µg/g]				Dentin [µg/g]			
		1st	2nd	3rd	Mean	1st	2nd	3rd	Mean
Magnesium	^{24}Mg	2806	2986	2990	2927	13200	13148	12289	12879
	± SD	265	320	246	277	1542	945	1172	1220
	^{25}Mg	2893	2978	2751	2874	13428	13267	12174	12956
	± SD	314	335	242	297	1531	960	1183	1224
	^{26}Mg	2892	2990	2968	2950	13244	13283	13025	13184
	± SD	305	304	240	283	1549	948	1222	1240
Calcium	^{42}Ca	377322	399458	418486	398422	275958	292278	294270	287502
	± SD	28227	28021	21077	25775	10424	9603	15398	11808
	^{44}Ca	389620	395194	388455	391090	286109	289139	273807	283018
	± SD	27497	25603	19112	24071	11245	9344	14443	11677
Zinc	^{64}Zn	59	62	58	59	46	54	44	48
	± SD	15	15	10	14	12	16	9	12
	^{66}Zn	58	64	51	58	47	57	41	48
	± SD	17	17	12	16	13	19	9	14
	^{67}Zn	59	65	60	62	48	55	46	50
	± SD	37	36	24	32	18	26	15	20
	^{68}Zn	59	62	56	59	47	52	43	47
	± SD	20	18	13	17	13	15	9	12
Strontium	^{86}Sr	554	505	509	523	428	403	408	413
	± SD	116	74	67	86	50	44	44	46
	^{88}Sr	547	499	508	518	419	395	430	415
	± SD	106	68	65	80	45	39	46	43

Table S7.5. Measured and calculated weight loss based on the mass balance model explained in the main text.

Weight loss [%]	day 4, 30 °C	day 7, 30 °C	day 14, 30 °C	day 21, 30 °C	day 63, 30 °C	day 4, 90 °C	day 7, 90 °C	day 14, 90 °C	day 21, 90 °C	day 63, 90 °C
Measured	17.5	16.3	15.7	14.7	15.4	22.4	23.4	25.7	22.0	25.7
^{44}Ca	17.5	15.0	10.0	11.1	28.2	-9.8	-45.3	-30.3	-67.1	-75.9
^{86}Sr	11.8	11.7	7.2	11.5	-11.8	4.0	-27.8	36.8	-30.9	-31.5
^{25}Mg	19.4	20.6	19.6	21.4	25.9	37.3	36.0	99.5	58.8	62.4
^{43}Ca	18.7	18.2	18.0	16.5	17.4	17.1	15.2	19.7	13.4	13.7
^{88}Sr	17.8	17.8	16.8	17.7	17.6	19.6	19.5	33.7	24.4	25.4
^{26}Mg	18.3	19.9	19.1	19.7	NA	34.8	39.8	75.1	59.2	61.1

Chapter 8 DMTA and isotopes in the fossil record

After experimentally testing the resistance of DMTA (Chapter 3-5) and non-traditional stable isotopes (Chapter 7) against diagenetic alteration these dietary proxies are applied in the following chapter to Permo-Carboniferous tetrapod fossil to assess their diet. In the fossil record, skeletal hard tissues are usually the only available source for inferring the dietary preferences, however, even though DMTA and non-traditional isotopes seems to be relatively resistant against diagenetic alteration this needs to be assessed for 300 Ma old fossils. In general, DMTA could help to infer mechanical food properties (e.g. Calandra and Merceron, 2016), while $\delta^{44/42}$Ca and $\delta^{88/86}$Sr are promising proxies for distinguishing faunivores from herbivores (Knudson et al., 2010; Tacail et al., 2020). A combination of both approaches should be able to infer dietary preferences and feeding behaviours more precisely and provide a clearer picture of trophic spacing and niche partitioning in fossil ecosystems. In the following, preliminary DMTA, $\delta^{44/42}$Ca and $\delta^{88/86}$Sr data of Permo-Carboniferous tetrapods from different localities (**Fig. 2.7**) are presented to assess the suitability of these proxies for diet reconstruction in deep time.

8.1 Material

The first DMTA, $\delta^{44/42}$Ca and $\delta^{88/86}$Sr dataset comprises a large variety of different species from the Late Carboniferous and lower Permian of the Remigiusberg Fm., the Bromacker Quarry (Tambach Fm.) and the Briar Creek Bonebed in Texas together with upper Permian taxa from the Karoo Basin and the Korbach fissure filling. Not for all taxa DMTA and stable isotope data are analysed (**Table ES8.1, S8.2 and 8.1**). The stable isotope dataset comprises tooth enamel and bone samples of fossil specimens (**Table S8.2**). As comparative dataset for the non-traditional isotopes (Ca and Sr) a preliminary dataset of extant lepidosaurs from a broad variety of feeding strategies (insectivorous, herbivorous, algaevorous, omnivorous, ovivorous and carnivorous) was measured (**Table ES8.1**). All measured extant lepidosaur taxa have continuous tooth replacement. The lepidosaur dataset includes tooth samples (whole tooth and powdered enamel) as well as powdered bone samples (**Table ES8.1 and S8.2**).

For DMTA it was not possible to include all measured specimens in the dataset, due to the poor quality of some dental surfaces. Herbivore species from the lower Permian are mostly represented by *Diadectes* (Sues and Reisz, 1998), *Orobates* (Berman et al., 2004) and *Edaphosaurus* (Spindler et al., 2020) and additionally the Caseidae *Martensius bromackerensis* including one potentially juvenile specimen. This is of particular interest, since Caseidae are assumed to undergo a diet switch from an insectivorous to a more herbivorous diet during ontogeny (Berman et al., 2020). Furthermore, one Bolosauridae (*Eudibamus*

cursoris) from the Bromacker Quarry with a plant-based or potentially insect-based diet (Reisz, 2006) and *Tseajaia* (Tseajaiidae; Berman et al., 1992) from the Remigiusberg Fm. with an assumed omnivorous (Hotton et al., 1997) or faunivorous (Kissel, 2010; Reisz and Fröbisch, 2014) diet was sampled. Faunivorous species from the lower Permian are mainly represented by *Dimetrodon* (Sphenacodontidae; Brink and Reisz, 2014) as apex-predators and additionally Varanopidae, Seymouridae and Eryopidae specimens (Benton and Pfretzschner, 2007). *Archeria* (Archeriidae) and *Varanosaurus acutirostris* (Ophiacodontidae) are considered to be carnivorous or piscivorous (Holmes, 1989; Brocklehurst, 2015). The sampled exclusively herbivorous upper Permian taxa are pareiasaurs (Benton and Pfretzschner, 2007) and Dicynodontia (e.g. Cox and Angielczyk, 2015), while *Gansurhinus* (Captorhinidae) are considered to have an herbivorous/omnivorous diet (Reisz et al., 2011). An omnivorous (Shelton et al., 2017) or herbivorous (Nicolas and Rubidge, 2010) species in the dataset is *Jonkeria* (Titanosuchidae) from the Karoo Supergroup, South Africa. The sampled upper Permian faunivorous are mainly Gorgonopsidae and Therocephalia (Rubidge and Sidor, 2001; Kammerer et al., 2015). *Procynosuchus* (Procynosuchidae) from the Korbach fissure filling are considered to have fed on small vertebrates and/or insects (Sues and Munk, 1996). Diadectomorphs (*Diadectes* and *Orobates*), Seymouridae and most basal amniotes (e.g. Sphenacodontidae, pareiasaurs, Dicynodontia, Gorgonopsia, Therocephalia, Captorhinidae) experience a permanent tooth replacement in labial-vertical direction (e.g. Romer and Price, 1940; Edmund, 1960; Hopson, 1964; Kermack, 1956; Bolt and DeMar, 1985; Laurin, 1996; Luo et al., 2004; Cabeira and Cisneros, 2009; Macdougall and Modesto, 2011; LeBlanc and Reisz, 2013, 2015; Benton et al., 2015; Bendel et al., 2017; Bertin et al, 2018; LeBlanc et al., 2018). Cynodonts exhibit a treadmill-like tooth replacement, where newly formed teeth are regularly added to the tooth row to maintain a relatively precise dental occlusion. This replacement pattern evolved probably due to highly abrasive intakes (Bertin et al, 2018). Across the amniote clade the rate of tooth replacement is reduced towards the mammalian clade (Sánchez-Villagra, 2010; Bertin et al, 2018).

8.2 Methods

8.2.1 Dental microwear texture analyses

Specimens from the Remigiusberg Fm. (collection Geoskop Kusel), Briar Creek Bonebed in Texas (Museum für Naturkunde, Berlin), Korbach fissure filling (Naturkundemuseum Karlsruhe), Karoo Supergroup Africa (Museum für Naturkunde, Berlin and Palaeontological Collection, University Tübingen) and the Bromacker Quarry (Tambach Fm., Museum der Natur, Gotha) were moulded or directly measured on the original dental surface (**Table ES8.1**). All samples were manually cleaned with water to remove dust and

afterwards with ethanol and acetone to remove any adherent lipids, varnish or glue. In case of multiple teeth still associated in a tooth row several teeth were moulded using high-resolution silicone-Vinylpolysiloxane precision impression material Provil novo Light regular set EN ISO 4823, type 3, light (Heraeus Kulzer GmbH, Dormagen, Germany). All specimens were scanned using the high-resolution disc-scanning confocal 3D-surface measuring system µsurf Custom (NanoFocus AG, Oberhausen, Germany) with a high-speed progressive-scan digital camera (984 × 984 pixel) and a blue LED (470 nm). In general, several non-overlapping scans (160 x 160 µm) were taken in close proximity to the tip or the edge of the tooth, if still preserved. In isolated, not in matrix embedded teeth, scans were taken from the lingual and buccal side, while in shed teeth which are still embedded in the sediment only one side (often orientation was not identifiable) was measured. When fragments of the jaw or the whole skull were preserved, measurements were taken on the whole tooth row to address differences in DMT along the jaw. Both lingual and buccal as well as upper and lower jaw were measured, if possible. As described in Chapter 3-6 3DST (Schulz et al., 2010, 2013a, b; Calandra et al., 2012) and SSFA (after Ungar et al., 2003; Scott et al., 2006) are employed using MountainsMap Premium v. 7.4.8676. In order to reduce the amount of post-mortem alteration on the dental surface and increase the data quality, a reduced surface of 120 x 120 µm was extracted from all scans prior to analyses. All moulded scans were mirrored along the z-axis, all scans of upper jaw left teeth were mirrored along the x-axis, while all lower jaw teeth were first mirrored along the y-axis and right teeth additionally along the x-axis. Upper right teeth and single teeth were not mirrored at all. The reptile template of Chapter 4.8 (Supplement) was used for data acquisition. All statistical analyses were performed as described in Chapter 6.3.5. using the open-source software R v.4.0.0 (R. Development Core Team, 2020), with inferential statistics calculated between:

I. Pooled herbivorous (n = 19), carnivorous (n = 18) and insectivorous (n = 3) feeding categories,
II. *Dimetrodon* (n = 10), *Diadectes* (n = 11), pareiasaurs (n = 3) and *Procynosuchus* (n = 3).

Only significances confirmed by “Lincon’s” test (equivalent to Dunnett’s T3) and Cliff’s method are considered as significant, however, several parameters only significant in Cliff’s method still well separate different groups and are therefore considered in the result section.

8.2.2 Non-traditional stable isotopes

Samples for Ca and Sr stable isotope analyses were either bone or tooth fragments or drilled from bones and teeth (i.e. enamel) using a hand drill with a diamond drill head, size 1 mm., Depending on the available sample amount, between 0.3 and 10 mg of material were used for analysis (**Table S8.2**). Powdered and fragmented samples were dissolved using distilled concentrated HNO_3 on a hot plate at 120 °C overnight. Afterwards samples were dried down and dissolved in 2 mol/L HNO_3. Chemical separation and purification of Ca and Sr was performed using prep*FAST*-MC (ESI Elemental Scientific) with a 1 mL Sr-Ca ion chromatographic column (see Chapter 7.2.7). The Ca and Sr fractions were dried down, dissolved in concentrated suprapure H_2O_2 and HNO_3 to destroy all remaining organic matter, dried down and finally dissolved in 0.5 mol/L HNO_3 (Ca) or 0.8 mol/L (Sr), respectively. Calcium and Sr isotope analyses were performed using a Neptune Plus MC-ICP-MS coupled with an Apex Omega HF (ESI Elemental Scientific) for Ca and Sr isotopes at the Institute of Geosciences, University of Mainz. Measurements were performed equivalent to Chapter 7.2.7. For data evaluation the open-source software R v.4.0.0 (R. Development Core Team, 2020) with an in-house R-script, following the calculations presented by Tacail et al. (2014) for Ca and Weber et al. (2017) for Sr. Delta values for Ca ($\delta^{44/42}$Ca, relative to Ca ICP-Std MZ) and Sr ($\delta^{88/86}$Sr, relative to NIST SRM 987) were calculated using a standard-sample-bracketing approach. A mean value was calculated for all duplicate measurements and for all samples from one specimen if available (including bone and tooth measurements, **Table ES8.1 and S8.2**). Uncertainty ranges include analytical uncertainty and intra-individual variability, given as Standard Deviation (SD). Inferential statistics were calculated using the Wilcoxon signed rank test only between extinct carnivorous (n = 10) and herbivorous (n = 7) taxa.

8.3 Results

8.3.1 Dental microwear texture analysis

Only a fraction of 43 out of 93 sampled specimens from 17 taxa were suitable for dental microwear texture measurements in extinct non-mammalian Permian tetrapods (**Table 8.1 and ES8.1**). Species such as *Martensius bromackerensis, Eudibamus cursoris* and *Archeria* had no suitable preserved ante-mortem dental surfaces. In the measurable 43 specimens, dental surfaces were relatively well preserved (**Fig. 8.1**), with only minor post-mortem erosion features.

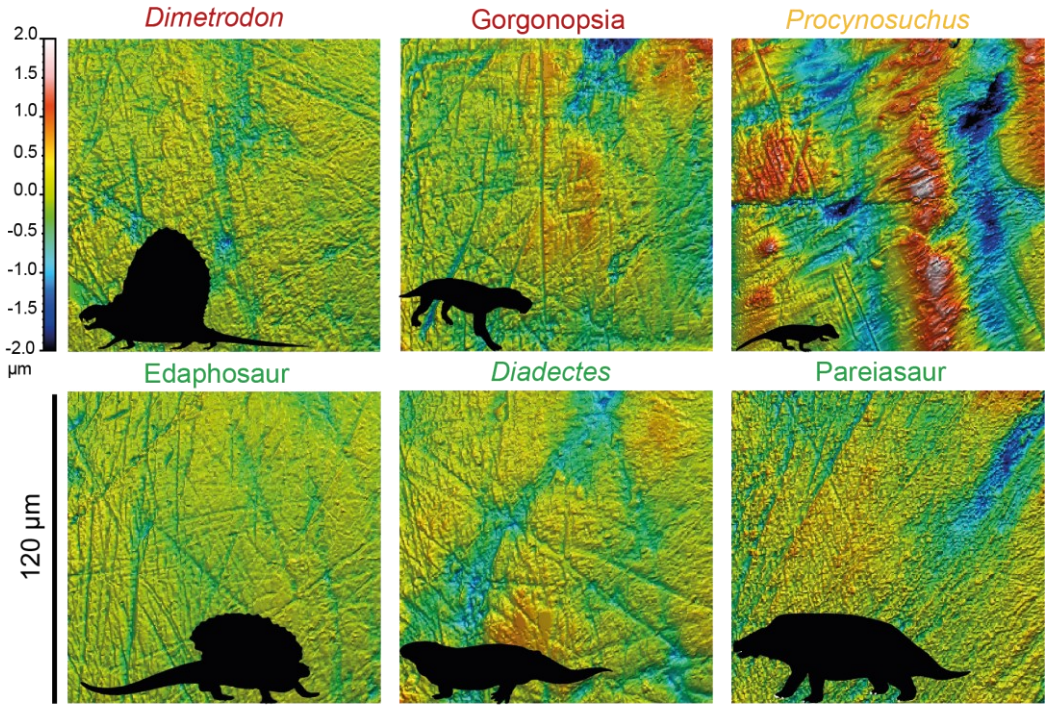

Figure 8.1. 3D simulations (120 x 120 µm) of the enamel surface with associated silhouettes (scaled to approximate species size for better comparison) of the animals. *Dimetrodon* (≈ 3 m), Gorgonopsia (≈ 1.5 m), *Procynosuchus* (≈ 0.6 m), edaphosaur (≈ 3 m), *Diadectes* (≈ 3 m) and pareiasaur (≈ 3 m).

In general, herbivorous and carnivorous taxa are only significantly distinguishable among each other in the MountainsMap parameter second texture direction (*Tr2R,* **Table S4.3**). Both, plant- and meat-based feeding categories show relatively low parameter values for most height and area parameters (e.g. *mea*, *madf*, *FLTt*, *FLTq*, *FLTp*, *FLTv*, **Fig. 8.2, Table ES8.3**), the complexity parameter *nMotif* and the isotropy (*IsT*) are relatively high (**Fig. 8.2, Table ES8.3**). The enamel surface is characterized by a high number of shallow furrows, indicated by higher *medf* and low *metf* and *madf*. The insectivorous feeding category, however, can be separated significantly from herbivorous and carnivorous taxa by lower complexity (*nMotif*) and density (*Spd*) of the dental surface and lower direction (*Tr2R*) values.

Additionally, insectivores can be separated significantly from carnivorous species by a lower isotropy of the surface (*IsT*) and higher values for the parameters *Sdq* and *Sdr*. Insectivores also have fewer but deeper furrows than the other two categories, indicated by lower *medf* and significantly higher *madf* values than both carnivores and herbivores (**Fig. 8.2A, Table 8.2 and ES8.4**).

Table 8.1. Taxon, locality, geological period, and presumed diet of samples included in the DMTA dataset.

Taxon	Locality	Period	Presumed diet	Number of specimens
Diadectes sp.	Remigiusberg Formation, Germany	Late Carboniferous, lower Permian	herbivore	1
Eryopide indet.	Remigiusberg Formation, Germany	Late Carboniferous, lower Permian	carnivore	1
Tseajaia	Remigiusberg Formation, Germany	Late Carboniferous, lower Permian	omnivore	1
Diadectes absitus	Bromacker Quarry, Germany	lower Permian	herbivore	4
Diadectes sp.	Bromacker Quarry, Germany	lower Permian	herbivore	3
Orobates pabsti	Bromacker Quarry, Germany	lower Permian	herbivore	1
Orobates sp.	Bromacker Quarry, Germany	lower Permian	herbivore	1
Diadectes sp.	Briar Creek Bonebed, Texas	lower Permian	herbivore	2
Dimetrodon sp.	Briar Creek Bonebed, Texas	lower Permian	carnivore	11
Edaphosaurus	Briar Creek Bonebed, Texas	lower Permian	herbivore	1
Varanosaurus acutirostris	Craddock Bonebed, Texas	lower Permian	piscivore	1
Gansurhinus	Korbach fissure filling	upper Permian	herbivore	2
Gorgonopsia indet.	Korbach fissure filling	upper Permian	carnivore	1
Procynosuchus	Korbach fissure filling	upper Permian	insectivore	3
Aelurognathus	Karoo Supergroup, Africa	upper Permian	carnivore	1
Bolotridon frerensis	Karoo Supergroup, Africa	Lower Triassic	carnivore	1
Cyniscops broomianus	Karoo Supergroup, Africa	upper Permian	carnivore	1
Genovum broilii	Karoo Supergroup, Africa	upper Permian	carnivore	1
Gorgonopsia indet.	Karoo Supergroup, Africa	upper Permian	carnivore	1
Jonkeria sp.	Karoo Supergroup, Africa	upper Permian	omnivore	1
Pareisaur indet.	Karoo Supergroup, Africa	upper Permian	herbivore	3
Pristerognathus sp.	Karoo Supergroup, Africa	upper Permian	carnivore	1

In addition, the height and volume parameter values are higher in insectivorous taxa. The only piscivorous taxon *Varanosaurus acutirostris* (Ophiacodontidae) included in the dataset is characterized by a smaller number of deeper furrows (low *medf*, high *metf* and *madf*) and relatively large height and volume parameters (**Fig. 8.2A**). The two omnivorous taxa are characterized by low area, height and volume and high complexity and direction parameters. In contrast to piscivorous and insectivorous taxa, *Jonkeria* and *Tseajaia* have a high density of shallow furrows (high *medf*, low *metf* and *madf*, **Fig. 8.2B**). The PCA shows a separation of insect-feeders from carnivores, omnivores and herbivores along PC1 and PC3 (**Fig. 8.3, Table ES8.5**), with the best separating parameters for PC3 being *IsT*. This is also true for the piscivorous specimen. Herbivores can be separated along PC2 and PC4 from carnivores, with the best separating parameters in PC2 being *Sdq* and *Sdr*, while *Tr2R* and *IsT* best separate in PC4. Omnivores are only represented by two individuals which are highly variable and fall in between carnivores and herbivores but are only separated by PC4 from the two feeding categories (**Fig. 8.3, Table ES8.5**).

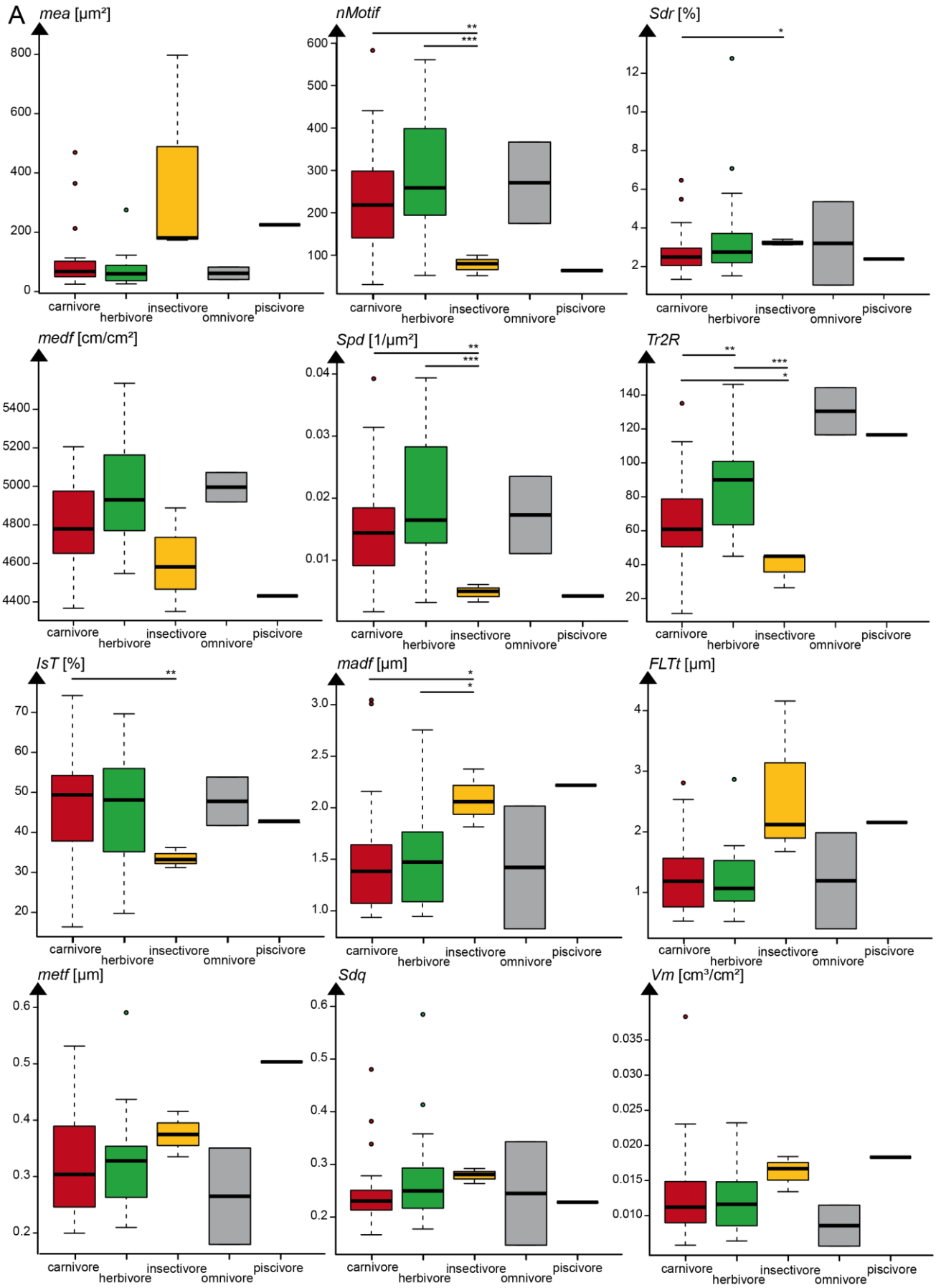
A
mea [µm²]
nMotif
Sdr [%]
medf [cm/cm²]
Spd [1/µm²]
Tr2R
IsT [%]
madf [µm]
FLTt [µm]
metf [µm]
Sdq
Vm [cm³/cm²]
carnivore
herbivore
insectivore
omnivore
piscivore

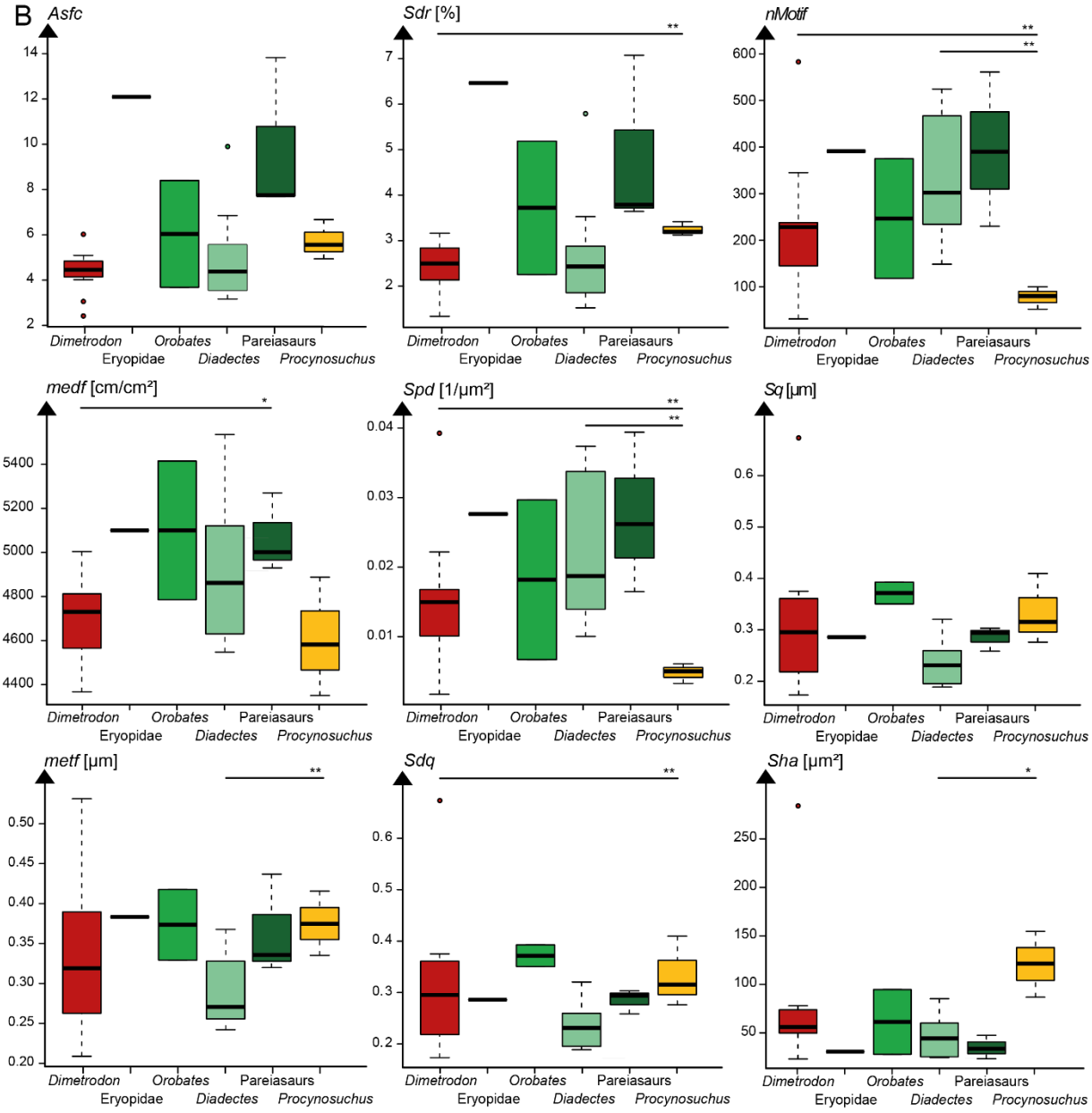

Figure 8.2. Best separating parameters for Permo-Carboniferous non-mammalian tetrapods: A. herbivore (n = 19), carnivore (n = 18), insectivore (n = 4), omnivore (n = 2) and piscivore (n = 1) feeding categories; B. *Dimetrodon* (n = 11), eryopid (n = 1), *Orobates* (n = 2), *Diadectes* (n = 10), pareiasaurs (n = 3), *Procynosuchus* (n = 3). Significance levels from "Lincon's" test: 0.05 = *, 0.01 = **, 0.001 = ***. *mea* = mean height, *Asfc* = fractal complexity (Area-scale), *nMotif* = number of motifs, *Sdr* = developed interfacial area ratio, *medf* = mean density of furrows, *Spd* = density of peaks, *Tr2R* = second direction, *IsT* = texture isotropy, *Sq* = RMS surface roughness, *madf* = maximum depth of furrows, *FLTt* = peak to valley flatness deviation of the surface (Gaussian Filter, 0.025 mm), *medf* = mean depth if furrows, *Sdq* = root mean square gradient, *Vm* = material volume at a given material ratio (p = 10 %), *Sha* = closed hill area.

On the species level, statistics could only be calculated for *Dimetrodon* (n = 10), *Diadectes* (n = 11), pareiasaurs (n = 3) and *Procynosuchus* (n = 3) (**Table 8.2, Fig. 8.2B**). Carnivorous *Dimetrodon* have significantly shallower furrows (*medf*) and additionally significantly less complex dental surface (*Asfc*) and lower values for *Sdr* and *Sdq* than herbivorous pareiasaurs. Additionally, *Dimetrodon* are among the carnivorous species with the lowest *medf* and *Asfc* values, while the single eryopid is among species with the highest density of furrows and highest complexity of the surface. No statistics could be calculated here, according to the low sample number for the eryopid (n = 1). Interestingly, within the herbivorous feeding category, *Diadectes* and pareiasaurs differ strongly in the complexity of the surface (*Asfc* and *Sdr*), with *Diadectes* having a less complex surface. The same is true for *Orobates*, however, according to the low sample size (n = 2) of *Orobates*, no inferential statistics were performed. Additionally, *Diadectes* have a lower height and less rough surface, with a lower density of furrows (*medf*) and peaks (*Spd*). Contrary, *Orobates* have larger height, roughness and density (*medf*) parameter values than pareiasaurs. The only insectivorous species, *Procynosuchus* differs significantly from *Diadectes* and *Dimetrodon* with lower values for *Procynosuchus* in *nMotif* and *Spd. Metf*, *madf* and *Sha* are significantly higher in *Procynosuchus* than in *Diadectes*, while *Sdq* and *Sdr* are significantly higher *Procynosuchus* than in *Dimetrodon*.

Table 8.2. Inferential statistics for A. carnivore, herbivore and insectivore feeding categories and B. *Dimetrodon*, *Diadectes*, pareiasaurs and *Procynosuchus*. Only significant parameters confirmed by both, “Lincon’s” test and Cliff’s method are reported here.

A

carnivore	carnivore		
herbivore	*Tr2R*	herbivore	
insectivore	*IsT, madf, nMotif, Sdq, Sdr, Spd, Tr2R*	*madf, nMotif, Spd, Tr2R*	insectivore

B

Dimetrodon	*Dimetrodon*			
Diadectes	*Tr2R*	*Diadectes*		
pareiasaurs	*medf*		pareiasaurs	
Procynosuchus	*nMotif, Sdq, Sdr, Spd*	*metf, madf, nMotif, Sha, Spd, Tr2R*		*Procynosuchus*

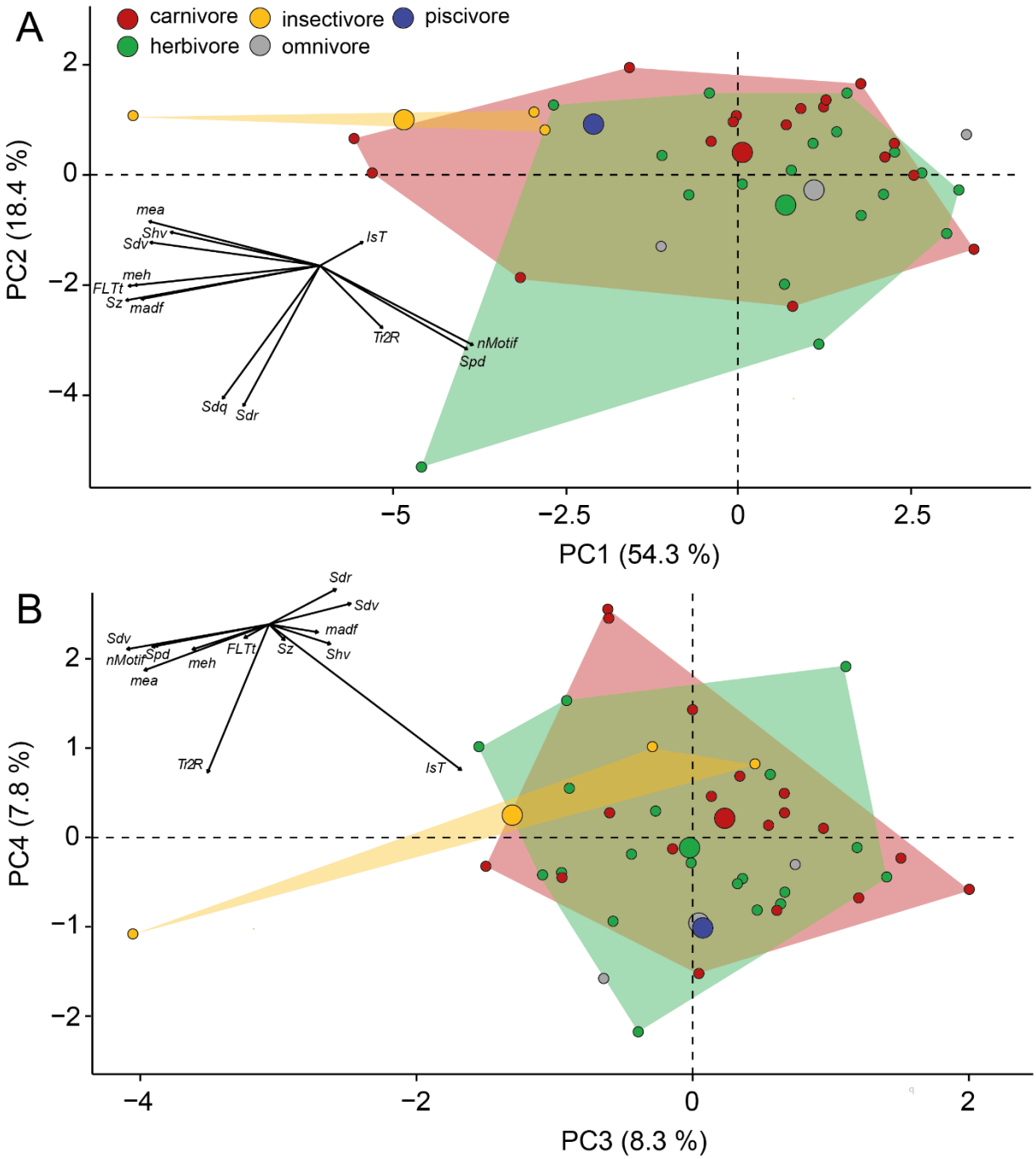

Figure 8.3. Principle component analysis (PCA) of surface texture parameters with best separation between different feeding categories. A. for PC1 and PC2, B. for PC2 and PC3. Large symbols in the PCA plot mark the mean area of the different groups.

8.3.2 Ca and Sr isotope data

In extant lepidosaurs, except for the insectivorous giant girdled lizard (*Cordylus giganteus*) and extinct *Dimetrodon*, *Arctops*, eryopids and *Diadectes*, $\delta^{44/42}Ca$ and $\delta^{88/86}Sr$ values were measured in both, bone and tooth samples. In all other species, only tooth or bone samples were available (**Table 8.3 and ES8.2**).

Table 8.3. Presumed diet, number of samples and $\delta^{44/42}Ca_{vs.\ MZ\text{-}STD}$ and $\delta^{88/86}Sr_{vs.NIST987}$ values with 1SD of the extant wild lepidosaur and extinct non-mammalian tetrapod feeding categories, bone and tooth samples separated.

	Diet	Number of samples	Tooth sample		Bone sample		Tooth sample		Bone sample	
			$\delta^{44/42}Ca_{vs.\ MZ\text{-}STD}$ [‰]	1SD [‰]	$\delta^{44/42}Ca_{vs.\ MZ\text{-}STD}$ [‰]	1SD [‰]	$\delta^{88/86}Sr_{vs.NIST987}$ [‰]	1SD [‰]	$\delta^{88/86}Sr_{vs.NIST987}$ [‰]	1SD [‰]
extant lepidosaurs	algaevore	2	-0.79	0.02	-0.78	0.04	-0.39	0.02	-	-
	insectivore	2	-	-	-0.68	0.06	-	-	-0.20	0.03
	herbivore	2	-0.83	0.02	-0.87	0.03	-0.29	0.03	-	-
	ovivore	1	-0.73	0.04	-0.98	0.06	-0.25	0.07	-	-
	omnivore	3	-1.07	0.06	-1.03	0.03	-0.42	0.04	-	-
	carnivore	2	-1.10	0.03	-1.04	0.04	-0.55	0.05	-	-
extinct non-mammalian tetrapods	herbivore	Bone 10 Enamel 3	-0.56	0.08	-0.52	0.03	0.43	0.15	0.36	0.20
	omnivore	Bone 1 Enamel 2	-0.42	0.02	-0.35	0.06	0.19	0.06	0.38	0.04
	carnivore	Bone 6 Enamel 11	-0.66	0.09	-0.59	0.10	0.31	0.08	0.45	0.10

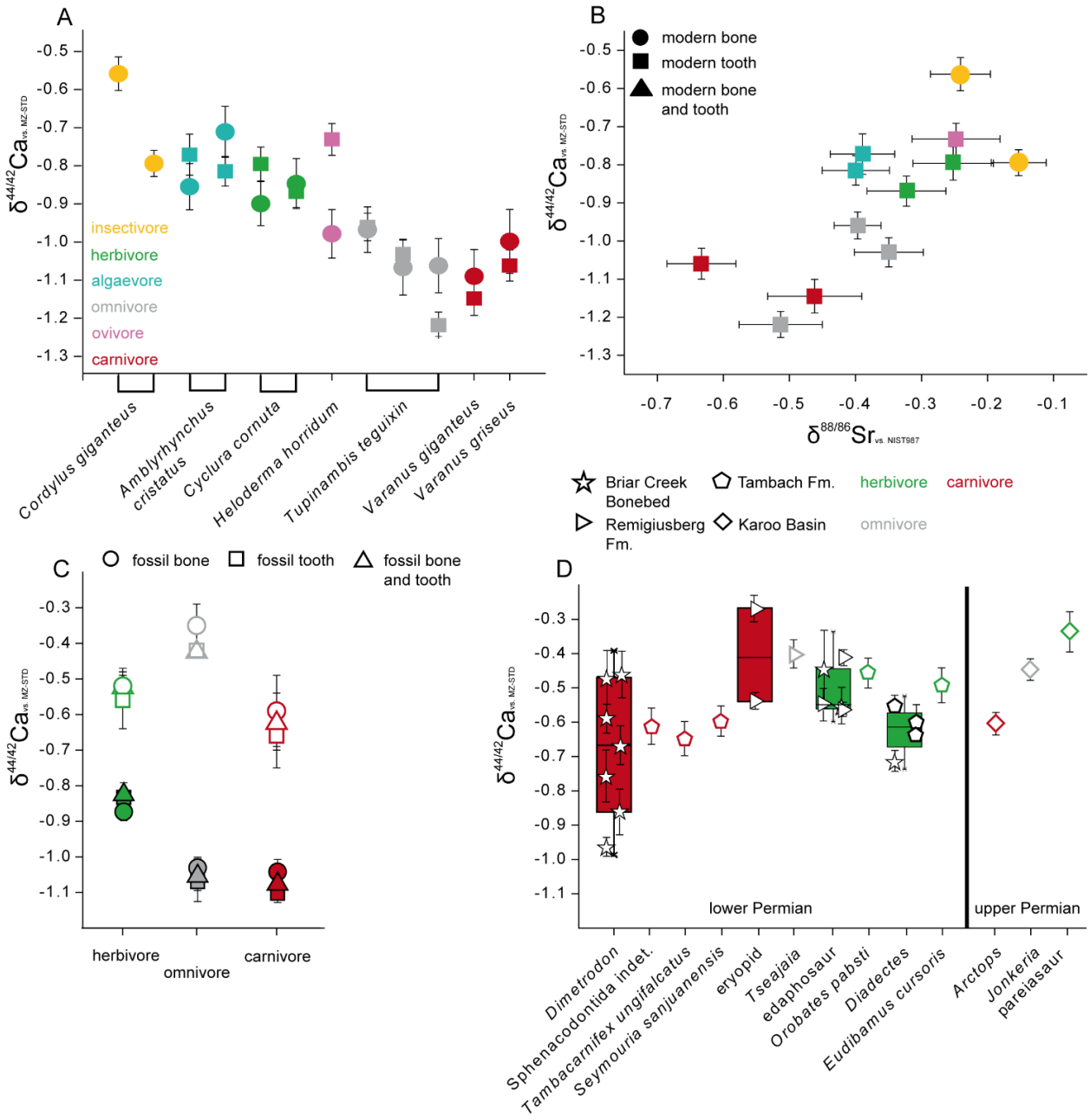

Figure 8.4. Ca and Sr isotope results of extant lepidosaurs and extinct non-mammalian tetrapods: A. individual $\delta^{44/42}$Ca values of bone and teeth/tooth enamel of extant wild lepidosaurs (**Table ES8.2**), B. biplot of $\delta^{44/42}$Ca and $\delta^{88/86}$Sr values of extant lepidosaurs (**Table ES8.2**), C. mean $\delta^{44/42}$Ca values of bones, teeth and tooth enamel, and combined teeth and bones of herbivorous, omnivorous and carnivorous extant lepidosaurs in comparison to herbivorous, omnivorous and carnivorous extinct non-mammalian tetrapods (**Table 8.3**), D. $\delta^{44/42}$Ca values for different fossil species (bone and enamel, **Table 8.4 and ES8.2**) from the lower Permian Briar Creek Bonebed, Bromacker Quarry and Remigiusberg Fm., and the upper Permian Karoo Basin.

$\delta^{44/42}$Ca values in extant lepidosaurs were obtained for insectivorous, herbivorous, omnivorous, ovivorous and carnivorous species (**Fig. 8.4A, Table 8.3**). Tooth and bone samples were available for herbivorous, omnivorous, ovivorous and carnivorous species, for the insectivorous species, only bone powder was available. For the herbivorous Rhinoceros iguana (*Cyclura cornuta*) and marine iguana (*Amblyrhynchus cristatus*), omnivorous gold tegu (*Tupinambis teguixin*) and carnivorous perentie (*Varanus giganteus*) and desert monitor (*Varanus griseus*), $\delta^{44/42}$Ca values of bones and teeth differ about 0.01 to 0.06 ‰ with teeth being less negative in herbivorous *Cyclura cornuta* (0.04‰) and being more negative in algaevorous *Amblyrhynchus cristatus* (0.01 ‰), omnivorous *Tupinambis teguixin* (0.04 ‰) and the carnivorous species (0.06 ‰, **Table 8.3**). However, the tooth in the ovivorous Mexican beaded lizard (*Heloderma horridum*) yields 0.24 ‰ less negative $\delta^{44/42}$Ca values that the bone (**Fig. 8.4, Table 8.3**). Bone of the insectivorous species yield the least negative values (*Cordylus giganteus,* mean bone -0.68 ‰, 1SD 0.12 ‰, n = 2, **Table 8.3 and S8.2**), followed by tooth of *Heloderma horridum* (-0.73 ‰, 1SD 0.04 ‰, n = 1, **Table 8.3 and S8.2**). Herbivorous (*Cyclura cornuta*) and algaevorous (*Amblyrhynchus cristatus*) taxa have slightly more negative $\delta^{44/42}$Ca values (mean tooth -0.81 ‰, 1SD 0.02 ‰, n = 4, mean bone -0.83 ‰, 1SD 0.04 ‰, n = 4, **Table 8.3**) and omnivorous taxa (*Tupinambis teguixin*, mean tooth -1.07 ‰, 1SD 0.06 ‰, n = 3, mean bone -1.03 ‰, 1SD 0.04 ‰, n = 3, **Table 8.3**) yield even more negative $\delta^{44/42}$Ca values. The omnivorous taxa have the largest inter-species variability among the measured specimens (0.26 ‰), followed by the insectivorous taxa with around 0.23 ‰ (**Table S8.2**). Bone of *Heloderma horridum* yields very negative values (-0.98 ‰, 1SD 0.06 ‰, n = 1, **Table 8.3**. The most negative $\delta^{44/42}$Ca values are visible in the carnivorous taxa (*Varanus griseus*, *Varanus giganteus*) with -1.06 to -1.14 ‰ (1SD 0.04 ‰, respectively) in teeth and -1.00 to -1.09 ‰ (1SD 0.07 ‰, and 0.08 ‰, **Table S8.2**) in bones. Extant lepidosaurs show an average trophic spacing between exclusively herbivorous and carnivorous species of 0.29 ‰ in teeth and 0.21 ‰ in bones. Due to the small sample size, no inferential statistics were calculated (**Table 8.3)**.

Tooth enamel was not available for all extinct non-mammalian tetrapods, only in *Dimetrodon*, *Arctops*, *Diadectes* and *Jonkeria* specimens both enamel and bone were sampled in the same individual (**Table S8.2**). For all four species, tooth enamel yield more negative values than bone (0.16 – 0.20 ‰, **Table S8.2**). Additionally, for two *Dimetrodon* and one *Diadectes* specimens tooth enamel of two different teeth within one jaw were measured (**Table S8.2**). The two *Diadectes* teeth yield within uncertainties identical $\delta^{44/42}$Ca values of -0.72 ‰ (1SD 0.05 ‰) and -0.71 ‰ (1SD 0.04 ‰), while the *Dimetrodon* teeth differ strongly with -0.59 ‰ (1SD 0.04 ‰) and -0.86 ‰ (1SD 0.07 ‰) for specimen DIM BRI 2 and -0.74 ‰ (1SD 0.04 ‰) and -1.19 ‰ (1SD 0.05 ‰) for specimen DIM BRI 3. For the following dataset (**Table 8.4**), the two enamel samples per specimen were pooled into one mean value. $\delta^{44/42}$Ca

values show a tendency towards less negative values in the herbivorous taxa (mean tooth -0.56 ‰, 1SD 0.08 ‰, n = 2, mean bone -0.52 ‰, 1SD 0.03 ‰, n = 11) and towards slightly more negative values in the carnivorous species (mean tooth -0.66 ‰, 1SD 0.09 ‰, n = 7, mean bone -0.59 ‰, 1SD 0.10 ‰, n = 12, **Table 8.4**), however no significant difference between the two feeding categories were detected. There is an offset between extant herbivorous lepidosaurs (including algaevores) and extinct tetrapods of 0.31 ‰ in bones and 0.25 ‰ in teeth and for the carnivores of 0.45 ‰ in bones and 0.44 ‰ in teeth (**Fig. 8.4B, Table 8.3**).

Table 8.4. Taxon, presumed diet, number of samples and $\delta^{44/42}Ca_{vs.\ MZ\text{-}STD}$ and $\delta^{88/86}Sr_{vs.NIST987}$ values with 1SD of extinct non-mammalian tetrapod feeding categories and species.

Taxon	Diet	Number of samples	$\delta^{44/42}Ca_{vs.\ MZ\text{-}STD}$ [‰]	1SD [‰]	$\delta^{88/86}Sr_{vs.NIST987}$ [‰]	1SD [‰]
extinct non-mammalian tetrapods	herbivore	12	-0.52	0.05	-0.52	0.03
	omnivore	13	-0.42	0.02	-0.35	0.06
	carnivore	2	-0.62	0.08	-0.59	0.10
Dimetrodon sp.	carnivore	7	-0.68	0.09	0.52	0.14
Sphenacodontida indet.	carnivore	1	-0.61	0.05	-	-
Tambacarnifex ungifalcatus	carnivore	1	-0.65	0.05	-	-
Arctops	carnivore	1	-0.60	0.03	0.09	0.09
eryopids	carnivore	2	-0.41	0.06	0.54	0.05
Seymouria sanjuanensis	carnivore	1	-0.59	0.04	-	-
pareiasaur	herbivore	1	-0.34	0.06	0.45	0.11
edaphosaurs	herbivore	5	-0.50	0.04	0.47	0.10
Diadectes	herbivore	4	-0.62	0.03	0.17	0.06
Orobates pabsti	herbivore	1	-0.46	0.04	-	-
Eudibamus cursoris	herbivore	1	-0.49	0.05	-	-
Jonkeria	omnivore	1	-0.45	0.03	0.22	0.12
Tseajaia	omnivore	1	-0.40	0.05	0.30	0.07

In the following, only tooth enamel is included into the dataset, if both tissue types, i.e. bone and tooth enamel, were available for one specimen (**Table S8.2 and 8.4**). Within the extinct carnivore feeding group, *Dimetrodon* (mean -0.68 ‰, 1SD 0.09 ‰, n = 7) with a large variability displays the most negative $\delta^{44/42}Ca$ values, followed by *Tambacarnifex ungifalcatus* (Varanopidae, -0.65 ‰, 1SD 0.05 ‰, n = 1), Sphenacodontida indet. (-0.61 ‰, 1SD 0.05 ‰, n = 1), *Arctops* (-0.60 ‰, 1SD 0.03 ‰, n = 1) and *Seymouria sanjuanensis* (-0.59 ‰, 1SD 0.04 ‰, n = 1, **Fig. 8.4C, Table 8.4**). The eryopid specimens yield less negative values (mean -0.41 ‰, 1SD 0.07 ‰, n = 2) overlapping with the omnivorous *Jonkeria* (-0.45 ‰, 1SD 0.03 ‰, n = 1) and *Tseajaia* (-0.40 ‰, 1SD 0.04 ‰, n = 1, **Table 8.4**). Within the herbivore feeding group,

Diadectes yields the most negative value (mean -0.62 ‰, 1SD 0.03 ‰, n = 4) therefore overlapping with all carnivorous species, except the eryopids. Contrary, pareiasaur yields the least negative $\delta^{44/42}$Ca value (-0.34 ‰, 1SD 0.03 ‰, n = 1, **Table 8.4**). Intermediate to low $\delta^{44/42}$Ca values are displayed by *Orobates pabsti* (-0.46 ‰, 1SD 0.04 ‰, n = 1, **Fig. 8.4C**, **Table 8.4**), *Eudibamus cursoris* (-0.49 ‰, 1SD 0.05 ‰, n = 1) and edaphosaurs (mean -0.50 ‰, 1SD 0.03 ‰, n = 5) with a large variability $\delta^{44/42}$Ca values (**Fig. 8.4C**, **Table 8.4 and S8.2**).

Stable Sr in extant lepidosaurs was only measured in tooth samples, with the exception of the insectivorous giant girdled lizard (*Cordylus giganteus*), where only bone was available (**Fig. 8.4A, Table 8.3**). The biplot of $\delta^{88/86}$Sr vs. $\delta^{44/42}$Ca therefore includes only tooth samples and bone samples of *Cordylus giganteus*. $\delta^{88/86}$Sr values of insectivorous (*Cordylus giganteus,* mean bone -0.20 ‰, 1SD 0.03 ‰, n = 2) and herbivorous taxa in extant lepidosaurs yield the least negative values (*Cyclura cornuta,* mean tooth -0.29 ‰, 1SD 0.03 ‰, n = 2, **Table 8.3 and S8.2**). The two carnivorous specimens have a large inter-species variability (*Varanus giganteus* -0.46, 1SD 0.07 and *Varanus griseus* -0.63 ‰, 1SD 0.05 ‰), however, carnivores are in general more negative in $\delta^{88/86}$Sr (**Table 8.3 and S8.2**). The omnivorous taxa (*Tupinambis teguixin,* mean -0.42 ‰, 1SD 0.07 ‰, n = 3) have intermediate $\delta^{88/86}$Sr values (**Table 8.3**). The herbivorous taxon feeding on algae (*Amblyrhynchus cristatus*) yield a mean $\delta^{88/86}$Sr value of -0.39 ‰ (1SD 0.01 ‰, n = 2) and is therefore more negative than *Cyclura cornuta* (**Table 8.3**). The biplot of $\delta^{88/86}$Sr vs. $\delta^{44/42}$Ca show a clear separation of carnivore taxa from insectivorous, ovivorous and herbivorous taxa, while omnivorous taxa yield intermediate values. In all fossil tetrapods, independent of age, excavation site and sampled tissue, i.e. bone or tooth, $\delta^{88/86}$Sr values are positive (carnivores: mean tooth 0.43 ‰, 1SD 0.15 ‰, n = 9, mean bone 0.36 ‰, 1SD 0.20 ‰, n = 7; herbivores: mean tooth 0.31 ‰, 1SD 0.08 ‰, n = 2, mean bone 0.45 ‰, 1SD 0.10 ‰, n = 6, **Table 8.3 and 8.4**), with the exception of bone of a single *Arctops* and *Dimetrodon* specimen, which yield slightly negative values of -0.30 ‰ (1SD 0.04 ‰, n = 1) and -0.13 ‰ (1SD 0.06 ‰, n = 1, **Table 8.4**). For comparison, geological rock and soil samples yield $\delta^{88/86}$Sr values ranging from -0.42 ‰ in limestone (-0.42 to 0.38 ‰) to 0.42 ‰ in basalt (de Souza et al., 2010; Hajj et al., 2017).

8.4 Discussion

8.4.1 Diet related DMT

Diagenesis (i.e. mechanical and/or chemical alteration) can be a problem in dental microwear texture analysis as diet-related ante-mortem wear surfaces can be taphonomically modified. Even though the influence of small blunders and post-mortem alteration on the dataset were tested in previous chapters (Chapter 3-5), the observed defects and preparation traces on the dental surfaces of non-mammalian tetrapods were often too extreme to include

them into the diet reconstruction. The main issue of the Karoo specimens, especially in those preserved as complete crania, was a thick, unremovable layer of varnish and/or glue (applied to the specimens for sample preservation), which covered the whole dental surfaces. DMT measurements with layers of remaining varnish could shift the resulting parameter space towards lower roughness and height of the dental surface (see Chapter 5.5) and therefore lead to biased inferences drawn when comparing to extant reference data or other, unaltered synapsids. Furthermore, several specimens showed no ante-mortem dental surface preservation, but instead unnaturally rough dental surfaces, deep furrows and cracks in the enamel, or the thin enamel layer was completely missing at all. These massive ante-mortem alterations of the dental surface would distort the analyses and were therefore removed. Especially the majority of the Bromacker specimens showed badly preserved dental surfaces. This was unexpected, since the preservation at this locality should be rather favourable, especially in excellently preserved articulated specimens that were fast embedded by mudflow events. Due to a short exposure of the carcass and assumed limited reworking, obvious causes for post-mortem alteration were not expected (Eberth et al., 2000). The reason for the badly preserved dental surfaces in non-mammalian tetrapods in general could be any kind of post-mortem alteration during burial or transport, as well as during excavation and preparation. However, the precise cause for the post-mortem erosion cannot be clarified here. This issue is currently limiting the possibility of testing e.g. the influence of tooth position or ontogeny in single specimens or between species. So far, only scans from one single tooth or pooled scans of several teeth were included into the dataset, in order to analyse as many specimens as possible. Also, dental surfaces with minor signs of post-mortem alteration are included into the dataset, therefore conclusions drawn from the data have to be treated with caution.

Based on the 17 fossil taxa suitable for DTMA it can be concluded that ante-mortem tooth wear is reflecting the feeding behaviour of these extinct non-mammalian tetrapods. The effect of tooth replacement on DMTA could not be tested in the following dataset due to the low number of specimens. However, DMTA studies on extant lepidosaurs (Bestwick et al., 2019; Winkler et al., 2019a) and extant and extinct crocodiles (Winkler et al., 2020b) have demonstrated the suitability of dental microwear for diet reconstruction in taxa with comparable reduced oral food processing and fast tooth replacement rate as seen in Diadectomorphs and the basal amniotes (e.g. *Dimetrodon*, edaphosaurs, pareiasaur). Distinct surface textures were found between insectivores and herbivores/carnivores independent of the fossil locality and stratigraphic age (**Fig. 8.2 and 8.3**). The preliminary data suggest that DMTA on extinct non-mammalian tetrapods is a potential dietary proxy to differentiate insect from plant and meat feeding taxa, which might help to assess the evolution from insectivory to herbivory (Reisz and Sues, 2000; Modesto et al., 2009). This could also help to assess ontogenetic diet shifts, such as hypothesized for caseids (Berman et al., 2020). The large height and *metf* and *madf* values

in insectivorous *Procynosuchus* (**Fig. 8.2**) would hint towards relatively hard material properties of the ingesta, potentially due to the insect's chitinous exoskeleton. The low number of scratches together with the less complex dental surface (**Fig. 8.2**) would suggest a less pronounced food processing behaviour and prey size reduction in insectivorous compared to carnivorous and herbivorous taxa, possibly according to a smaller size of the ingested insects. This is similar to extant carnivorous monitor lizards and *Heloderma*, where a low density of furrows implies a reduced tooth-food contact during capturing, killing and swallowing the prey (Winkler et al., 2019a). Feeding behaviour in extant carnivorous lepidosaurs and extinct non-mammalian insectivorous *Procynosuchus* appears to be relatively similar. The only piscivorous species (*Varanosaurus acutirostris*) falls within the same parameter space (**Fig. 8.2**), suggesting a reduced food processing, however, more data are needed. No distinct differences were found between carnivorous and herbivorous feeding strategy in general, which might be caused by e.g. similar material properties of the diet or very similar oral processing (**Fig. 8.2**). Both feeding categories are characterised by a higher number of shallow furrows and a more complex dental surface, which would suggest a more pronounced oral processing compared to insectivorous *Procynosuchus*. This more pronounced food processing is also found in extant herbivorous, omnivorous and insectivorous lepidosaurs (Winkler et al., 2019a). Differences between extant and extinct carnivores might be caused by different types of prey size reduction. While extant carnivorous lepidosaurs only capture and swallow their prey, extinct carnivores potentially reduced prey size orally, possibly due to differences in prey size. Large extant carnivorous monitor lizards feed on smaller prey (other reptiles, birds, small mammals), while extinct carnivores, such as *Dimetrodon*, fed on larger prey like edaphosaurs, which needed to be at least torn apart, increasing the tooth-to-prey contact. This feeding behaviour might be more comparable to extant and extinct crocodiles, which show distinctive prey-processing behaviour, and consequently more pronounced dental wear as compared to carnivorous lepidosaurs (Winkler et al. 2020b, Winkler pers. comm.). Single species within the carnivorous and herbivorous feeding categories, however, are showing distinct differences in DMT parameters. The single carnivorous eryopid seems to have had a pronounced oral processing behaviour. Low height and roughness of the DMT data (**Fig. 8.2**) furthermore suggest limited consumption of hard tissue, i.e. bone, in carnivorous species, such as *Dimetrodon* or Gorgonopsidae, both considered to have been active hunters and apex-predators in Permian food webs. The extinct herbivore dataset includes lower Permian *Diadectes*, *Orobates* and *Edaphosaurus* as well as the upper Permian pareiasaurs and *Gansurhinus*. Herbivory among extant taxa in general is a vast feeding category, including e.g. grazing and browsing, ingestion of fruits or nuts, which differ in their material properties, however, among the early herbivores during the Permian, the herbivore diet was probably characterized by the ingestion of e.g. leaves or needles, stems or roots of e.g. early conifers,

ginkgo trees and ferns (Sues and Reisz, 1998, Reisz and Fröbisch, 2014). The extant flora and it's material properties are probably not comparable to the Permian flora, even though e.g. woody conifers (e.g. *Agathoxylon*), *Calamites*, ferns (e.g. *Asterotheca*) and seed ferns (e.g. *Lepidopteris*) colonised the ecosystems (Bamford, 2004; Uhl and Jasper, 2016), therefore it is difficult to draw conclusion on the material properties of ingested plants in the fossil record, compared to the modern ones. In general, early herbivore diet included more high fibre-plant matter and few harder ingesta, which would have led to more food processing and a complex dental surface, which can be observed in the current dataset. Differences were detected in the complexity of the dental surface between lower Permian *Diadectes, Orobates* and upper Permian pareiasaurs (**Fig. 8.2**), indicating differences in the ingested plant matter, either due to ingestion of different parts of plants or ingestion of different plant species, or different oral processing behaviour. Since different localities and time scales were compared, i.e. lower and upper Permian (~ 298 – 251 Ma), differences in floral composition between the ecosystems were not accounted for in the analysis, but might be an important factor leading to the observed variability in Permian herbivore DMTA. More specimens from specific localities, e.g. Bromacker Quarry or Karoo Basin, are needed to exclude the possibility of major differences in vegetation and to draw conclusion about niche partitioning within one single ecosystem. The slightly higher density of wear features together with a higher complexity of the dental surface and larger depth of the furrows in pareiasaurs and *Orobates* compared to *Diactectes* (**Fig. 8.2**) would suggest a more pronounced food processing behaviour or at least a larger proportion of harder diet (e.g. roots, rhizome, branches) or a combination of both. *Diadectes* seems to have had less pronounced food processing or ingestion of different, maybe softer plant-matter (e.g. young plant shoots, leaves). However, especially in case of ingestion of e.g. roots or young plant shoots near the ground, external mineral abrasives attached to the plant matter could influence DMT, as seen in experiments with guinea pigs (Winkler et al., 2020c). While fine-grained quartz (>5/<50 µm), loess and kaolin seems to have no significant effect on DMT, ingestion of coarse grained volcanic ashes increase the complexity significantly and ingestion of fine sand (130 – 166 µm) increases the roughness significantly. Ingestion of fine silt-sized quartz (~ 5µm) has a polishing effect on DMT. Hence, depending on the sediment grain size fraction surrounding the roots, ingestion of high loads of mineral dust can influence DMT towards higher as well as lower surface complexity and roughness. Differences in dental surface texture between the analysed herbivores demonstrate that the Permian herbivorous taxa seem to differ at least slightly in oral processing behaviour and probably slight preferences towards ingestion of different plant parts, possibly together with mineral dust. For the omnivorous species *Jonkeria* and *Tseajaia* the data show, that at least the two measured specimens were different in their ingested diet and their way to process their diet, with *Tseajaia* showing a less complex dental surface (**Fig. 8.2**). However, no assumption can be drawn for

the proportion of plant- versus meat-based diet ingested, since carnivorous and herbivorous species cannot be separated clearly and both specimens overlap with the carnivore and herbivore parameter spaces.

8.4.2 Diet specific isotope composition

The $\delta^{44/42}Ca$ in teeth and bones of extant lepidosaurs showed no distinct offset between bone and tooth, therefore is assumed, that there is no systematic fractionation offset between them. This is in contrast to studies in modern sheep, where a systematic offset of Ø 0.15 ‰ between bone and tooth enamel was measured (Tacail et al., 2014) These differences might be explained by different physiological process in mammals compared to reptiles, lepidosaurs in particular. Only the ovivorous Mexican beaded lizard (*Heloderma horridum*, Beck and Lowe, 1991) showed a large offset in $\delta^{44/42}Ca$ values, with the bone being more negative (-0.98 ‰) than the tooth (-0.73 ‰, **Fig. 8.4A**). Ovivores (i.e. egg-feeding), when consuming egg yolk and white, are expected to have more positive $\delta^{44/42}Ca$ values, since egg white has very positive values (Skulan and DePaolo, 1999). This enrichment in $\delta^{44/42}Ca$ is visible in the tooth sample, however, not in the bone sample, which displayed $\delta^{44/42}Ca$ values similar to carnivorous species. The reason for the offset between *Heloderma horridum* bone and tooth is probably a difference in ingested diet during the formation and remodelling time. During bone formation and remodelling this *Heloderma horridum* specimen fed on a meat-based diet, while it was feeding on eggs during tooth formation. Since *Heloderma* shed their teeth regularly, tooth $\delta^{44/42}Ca$ values would represent the more recent diet preference before death in comparison to the bone. Therefore, in species with regular tooth replacement, such as reptiles and non-mammalian tetrapods, different teeth within one jaw might display significantly different $\delta^{44/42}Ca$ values, depending on the diet ingested during formation. Also, in the fossil record differences between two different tooth enamel samples from the same specimens were detected in *Dimetrodon*, however, not in *Diadectes*. Extinct non-mammalian tetrapods had tooth replacement just like extant lepidosaurs, therefore differences in the $\delta^{44/42}Ca$ value along the tooth row might be expected, if changes in the diet occurred. In *Diadectes* however, both measured teeth were either formed during the same time or diet preferences did not changed, at least for this individual.

$\delta^{44/42}Ca$ showed differences between herbivorous (including algaevore, having higher $\delta^{44/42}Ca$) and carnivore species (having lower $\delta^{44/42}Ca$) with omnivores in between, which is in line with the expected TLE in Ca isotopes for e.g. terrestrial extant mammals or extinct dinosaurs (**Fig. 8.4A**, e.g. Heuser et al., 2011; Hassler et al. 2018, Tacail et al., 2020). The extant Rhinoceros Iguana (*Cyclura cornuta*) is not a strict herbivore, as they are frequently feeding on animal matter, especially as juveniles (Cooper and Vitt, 2002; Hines, 2016);

however, the $\delta^{44/42}$Ca data show that the two specimens were feeding on herbivorous diets during the formation times of the analysed teeth. Ingested animal tissue, especially bones and teeth, would have shifted the $\delta^{44/42}$Ca value to more negative values. In contrast, *Cyclura cornuta* yielded the same $\delta^{44/42}$Ca value as the marine iguana (*Amblyrhynchus cristatus*), which is feeding exclusively on marine algae (Cooper and Vitt, 2002). This supports the assumption that all measured *Cyclura* specimens were feeding on a plant-based diet during tooth formation. This implies that early ontogenetic stages are potentially not represented in the available teeth (ontogenetic age of sampled specimens unknown, according to the size they were assumed to be adult). The omnivorous gold teju (*Tupinambis teguixin,* Colli et al., 1998) had $\delta^{44/42}$Ca values closer to the two carnivorous *Varanus* specimens (Reilly et al., 2007), leading to the assumption that a larger proportion of its diet is composed of vertebrates, rather than a plant-based or even insect-based diet (**Fig. 8.4A**). The ingestion of insects seems to shift the $\delta^{44/42}$Ca value towards less negative values, as suggested by the other two measured insect feeding specimens (*Cordylus giganteus*, **Fig. 8.4A**). The high $\delta^{44/42}$Ca values of the insect feeders were also expected since mammalian insectivores tend towards less negative $\delta^{44/42}$Ca values than carnivores or herbivores (Gussone and Heuser, 2016; Weber et al., 2020).

In general, there was no distinct offset between fossil bone and tooth enamel $\delta^{44/42}$Ca values of herbivorous (including pareiasaur, edaphosaurs, *Orobates pabsti*, *Eudibamus cursoris* and *Diadectes*) and carnivorous (*Tambacarnifex ungifalcatus*, Sphenacodontida indet., *Dimetrodon*, *Arctops* and eryopide) feeding categories (**Table 8.4, Fig. 8.4C**). However, on the species level, in specimens where bone and tooth enamel samples from the same specimen were available, bone samples displayed less negative $\delta^{44/42}$Ca values than tooth enamel samples in *Dimetrodon*, *Diadectes*, *Arctops* and *Jonkeria*. Such a systematic offset was not observed in extant lepidosaurs, however in e.g. extant sheep, with bones on average being higher in $\delta^{44/42}$Ca than enamel (Tacail et al., 2014). Physiological fractionation effects between bone and dental tissues might be one explanation for this offset. Another explanation might also be diagenetic alteration of the ante-mortem isotope composition. Calcium is the main component in hydroxylapatite and is generally less prone to diagenetic alteration than trace elements, such as Sr (Chapter 2.2.1 and 2.4). Overprinting of biogenic Ca with diagenetic Ca is unlikely, however, in bone is a higher risk to measure diagenetically overprinted $\delta^{44/42}$Ca due to secondary calcite infilling in the pore space (Martin et al., 2017a), which was not addressed in the current dataset. Contrary, enamel is according to its lower porosity and higher inorganic proportion less prone to diagenetic alteration (Chapter 2.4 and 7.5.3). The taphonomic settings of the fossil specimens employed in this thesis show different potential for diagenetic alteration. The Permo-Carboniferous Remigiusberg Fm. contains sedimentary lacustrine and floodplain deposits together with volcaniclastic deposits (Schindler, 2007) that have been hydrothermally altered due to the kuselite sill intrusion a few meters beneath the

fossil-bearing sediments (Voigt et al., 2014; Uhl and Jasper, 2016). The Remigiusberg Fm. bore fossils with exceptionally white-coloured preservation (Voigt et al., 2014), which might be biased diagenetically due to hydrothermal activity and contact metamorphism. Trace elements measured in white *Lebachacanthus* teeth (Permian shark) from the Remigiusberg Fm., such as U, Cu, Fe and Al associated with hydrothermal fluid activity, as well as REE are enriched and the crystallite dimensions are elevated, however the fossil are still preserved as carbonate fluorapatite. It is assumed, that these fossils altered in contact with hydrothermal fluids at temperatures above 500 °C (Arns et al., 2020). In contrast, the continental red bed sediments of the Beauford Group, Karoo Basin, as well as from the Briar Creek Bonebed, Texas, consist mainly of sedimentary mud-, silt-, and sandstones (Nicolas and Rubidge, 2010; Konietzko-Meier et al., 2016; Neveling et al., 2016) and were probably not altered much by diagenetic fluids. Diagenesis cannot be excluded entirely, however, fossils from localities, such as the Remigiusberg Fm., showed no distinct or systematic differences compared with the same species from other localities, e.g. edaphosaurs from the Remigiusberg Fm and the Briar Creek Bonebed or *Diadectes* from the Bromacker Quarry and the Briar Creek Bonebed (**Table 8.5 and Table S8.2, Fig. 8.4D**), which makes a strong diagenetic overprint unlikely.

Comparing $\delta^{44/42}$Ca values of extant lepidosaurs with those of extinct non-mammalian tetrapods, a systematic offset between extant and extinct carnivorous and herbivorous species exists (**Fig. 8.4C**). This could be best explained by different $\delta^{44/42}$Ca values of the primary food source. It is known from extant terrestrial ecosystems, that different plant tissues, such as roots, stems or leaves, as well as different plant species have different $\delta^{44/42}$Ca values (e.g. Schmitt, 2016, and references therein; Tacail et al., 2020). Generally, roots of e.g. beech, spruce or pine trees display the most negative $\delta^{44/42}$Ca values in trees, while leaves or needles have around 0.5 ‰ higher $\delta^{44/42}$Ca values (Cenki-Tok et al., 2009; Holmden and Bélanger, 2010). The same is true for extant dicotyledons, where root and trunk display similar $\delta^{44/42}$Ca values, while leaves and fruits are around 0.5 ‰ higher (Tacail et al., 2020). However, different plant parts still show a large variability in $\delta^{44/42}$Ca values and therefore also a large overlap (Schmitt, 2016, and references therein; Tacail et al., 2020). Additionally, different species yield different $\delta^{44/42}$Ca values, e.g. Jack pines (*Pinus banksiana*) display very high $\delta^{44/42}$Ca values of about 0.15 ‰, while Norway spruce (*Picea abies*) have values of about 0 ‰ and black spruce (*Picea mariana*) and trembling aspen (*Populus tremuloides*) displays $\delta^{44/42}$Ca values of -0.15 ‰. Extant European beech (*Fagus sylvatica*) displays very negative values with a large variance (-0.25 ‰ to -1.0 ‰) overlapping with the sugar maple (*Acer saccharum*, -1.0 ‰, Page et al., 2008; Cenki-Tok et al.,2009; Holmden and Bélanger, 2010). Therefore, the ingestion of different plant species and/or plant parts could vary the $\delta^{44/42}$Ca values greatly. Additionally, if the $\delta^{44/42}$Ca value of the primary producers (plants) differ between different localities, different $\delta^{44/42}$Ca values for the primary consumers and finally the apex-predators are expected. In the

fossil ecosystems analysed in this thesis $\delta^{44/42}$Ca values of different plant species, e.g. ferns and seed ferns, and plants parts are unknown, therefore it is difficult to infer differences in the ingested plant matter and species from differences in $\delta^{44/42}$Ca values of the herbivorous taxa. Generally, it is assumed that fractionation between root and leaves is similar to modern plants.

Fossil carnivorous and herbivorous non-mammalian tetrapods yielded an offset of around 0.10 ‰, with herbivores having higher $\delta^{44/42}$Ca values, which is in line with a plant-based diet, while carnivorous taxa have more negative values, indicating more meat/bone consumption (as bone is Ca-rich and ^{44}Ca-depleted, **Table 8.5**). The overlap in $\delta^{44/42}$Ca between the two feeding categories is large and no significant differences could be detected. In lower Permian ecosystems, i.e. Briar Creek Bonebed, Bromacker Quarry and Remigiusberg Fm., no clear separation of trophic levels are shown in the $\delta^{44/42}$Ca values (**Fig. 8.4D**). Within the carnivorous feeding group *Dimetrodon*, *Tambacarnifex ungifalcatus*, Sphenacodontida indet. and *Seymouria sanjuanensis* yielded the most negative $\delta^{44/42}$Ca values, supporting the assumption of them being apex-predators in Permian ecosystems. Lower Permian eryopids are also assumed to be carnivorous, however the $\delta^{44/42}$Ca results yielded less negative values, overlapping strongly with omnivorous *Tseajaia* and herbivorous edaphosaurs from the same locality (**Fig. 8.4D**). Several hypotheses could explain the higher values of eryopids, first, diagenesis cannot be unambiguously excluded, especially in the Remigiusberg Fm., as described above. However, the edaphosaur bones from the Remigiusberg Fm. do not differ isotopically from the edaphosaur bones from the Briar Creek Bonebed, therefore, taphonomical alteration seems unlikely (**Fig. 8.4D**). Secondly, eryopids were amphibians living in lakes or swamps (Quémeneur et al., 2013; Witzmann, 2013) and their physiology was potentially different from those of synapsid, such as e.g. *Dimetrodon*. Thirdly, their diet might have been different from other carnivores, maybe also including invertebrates or fish. Generally, the lower Permian carnivores overlap greatly with the lower Permian herbivores, within the herbivorous feeding group *Diadectes* (from Briar Creek Bonebed and Bromacker Quarry) displayed the most negative $\delta^{44/42}$Ca values, comparable to those of the carnivorous species. Edaphosaurs, *Orobates pabsti* and *Eudibamus cursoris* yielded higher $\delta^{44/42}$Ca values than *Diadectes* and were therefore slightly elevated compared to carnivorous *Tambacarnifex ungifalcatus*, Sphenacodontida indet. and *Seymouria sanjuanensis*. $\delta^{44/42}$Ca values of the different lower Permian herbivorous species generally showed two things, firstly they did not show a clear trophic spacing compared to lower Permian carnivorous species (**Fig. 8.4D**). During the lower Permian a new trophic structure only started to evolve and was not comparable modern day ecosystems, and the physiology of non-mammalian lower Permian synapsids differed from those of extant mammals or reptiles, and therefore, no clear trophic spacing is visible in lower Permian bone and tooth enamel. Secondly, and most interestingly, there were differences in $\delta^{44/42}$Ca values and therefore potentially in ingested plant-based diet

lower Permian herbivores (**Fig. 8.4D**). In modern ecosystems higher $\delta^{44/42}$Ca values, as seen in edaphosaurs, *Orobates pabsti* and *Eudibamus cursoris,* would suggest ingestion of e.g. leaves or species with higher $\delta^{44/42}$Ca values such as Jack Pine, as described above. Lower $\delta^{44/42}$Ca values (as measured in *Diadectes*), however, would suggest ingestion of branches or even roots or species with low $\delta^{44/42}$Ca values, e.g. sugar maple. In lower Permian ecosystems $\delta^{44/42}$Ca values of plants and tissue types are unknown, therefore, no clear conclusion about ingested plant matter or species can be done at this point. The only assumption which can be done so far is that edaphosaurs (from Briar Creek Bonebed and Remigiusberg Fm.), *Orobates pabsti* and *Eudibamus cursoris* (both from Bromacker Quarry) potentially fed on isotopically lighter (^{44}Ca-enriched) plant species and/or plant tissues (e.g. leaves or needles), while *Diadectes* (from Briar Creek Bonebed and Bromacker Quarry) lived in the same ecosystems, however fed on isotopically heavier (^{44}Ca-depleted) plants and/or tissues (e.g. roots, branches, trunks). Compared to the lower Permian localities, the upper Permian ecosystem of the Karoo Basin, South Africa, showed a very distinct trophic level effect (TLE), with carnivorous *Arctops* (n = 1) having a low $\delta^{44/42}$Ca value due to potential bone ingestion, while herbivorous pareiasaur (n = 1) is very high in $\delta^{44/42}$Ca suggesting a plant-based diet. Omnivorous *Jonkeria* (n = 1) yielded an intermediate $\delta^{44/42}$Ca value (**Fig. 8.4D**). Differences in physiological effects in lower and upper Permian taxa might lead to the pronounced TLE (**Fig. 8.4D**). However, the upper Permian carnivorous therapsid yielded a comparable $\delta^{44/42}$Ca value like the lower Permian carnivores (including synapsids and Seymouriidae), suggesting ingestion of ^{44}Ca-depleted bone in all carnivores. Also, the two presumed omnivorous species (lower Permian *Tseajaia* (Tseajaidae) and upper Permian *Jonkeria* (Therapsida)) yielded similar $\delta^{44/42}$Ca values, suggesting either similar diet, i.e. similar proportion of meat- and plant-based diet, or in general similar physiological effects between lower Permian and upper Permian species, at least for carnivores and omnivores (**Fig. 8.4D**). The upper Permian herbivore pareiasaur (Sauropsida, Pareiasauridae), however, is on average 0.18 ‰ above the lower Permian herbivores in $\delta^{44/42}$Ca (including Synapsida, Diadectidae and Bolosauridae (Sauropsida), **Fig. 8.4D**). During the Permian especially herbivory as feeding strategy diversified greatly, upper Permian herbivores might have had different or more efficient ways to access nutrients and Ca from ingested plant matter, compared to the early herbivores from the lower Permian. However, all Karoo Basin taxa are only represented by one specimen, therefore these preliminary results should be cautiously interpreted. Contrary, the differences in herbivorous taxa could also be an effect of the ingestion of isotopically lighter plant species and/or plant tissues (e.g. needles). More faunal specimens from lower and upper Permian ecosystems need to be measured and analysed locality-wise, to test, if the $\delta^{44/42}$Ca values represent diet specific Ca signals due to different diet preferences, differences in the flora assemblage

between the localities or differences in physiological fractionation processes between synapsids, diadectids, therapsids, sauropsids and also amphibs, i.e. *Seymouria* and eryopids.

$\delta^{88/86}$Sr in the extant lepidosaurs teeth and bone (insectivorous *Cordylus giganteus*) showed, similar to $\delta^{44/42}$Ca, the expected trophic level effect (TLE) effect, however the offset is smaller than in Ca, with 0.26 ‰ between carnivores and herbivores (**Fig. 8.4A**). In general, the biplot $\delta^{44/42}$Ca vs. $\delta^{88/86}$Sr showed a clear TLE, with omnivores between carnivores and herbivores. One omnivorous specimen yielded more negative $\delta^{44/42}$Ca and $\delta^{88/86}$Sr values, suggesting a more meat-based diet of this single specimen. Similar to $\delta^{44/42}$Ca, insectivores and the single ovivorous specimen were elevated in $\delta^{88/86}$Sr values, both plotting at the upper end of the Ca versus stable Sr isotope biplot (**Fig. 8.4A**). The most interesting offset, which could not be detected in Ca isotopes, is between the terrestrial herbivore *Cyclura cornuta* and the marine algaevore *Amblyrhynchus cristatus*. In general, seawater has slightly lower $\delta^{88/86}$Sr values (0.31 – 0.38 ‰, Halicz et al., 2008; Knudson et al., 2010) than fresh water lakes (0.40 ‰, Knudson et al., 2010), therefore plants growing in sea water would yield slightly lower $\delta^{88/86}$Sr values than plants growing in freshwater ecosystems. This could be an explanation for the slightly more negative values in the algaevorous marine iguana *Amblyrhynchus cristatus*. Therefore $\delta^{88/86}$Sr might be an additional proxy to distinguish the source of plant ingesta in terrestrial herbivores. The $\delta^{88/86}$Sr in fossil non-mammalian tetrapods, however, yielded with one exception, only positive, geogenic values instead of expected trophically fractionated negative $\delta^{88/86}$Sr values. Siliciclastic sedimentary rocks yield mean $\delta^{88/86}$Sr of around 0.25 ‰, also volcanic rocks and hydrothermal waters yield mean values of around 0.16 ‰ and 0.32 ‰, while plants would typically have mean $\delta^{88/86}$Sr values of around 0 ‰ and secondary consumers such as humans and animals would yield negative $\delta^{88/86}$Sr values (mean around -0.2 ‰ with a large variability, Hajj et al., 2017; and references therein). Therefore, it seems more plausible that the fossil tetrapod remains rather reflect a diagenetically overprinted Sr isotope composition caused by the hydrothermal fluids and thus reflecting bedrock/soil compositions, rather than biological ante-mortem $\delta^{88/86}$Sr values. This is well in line with the taphonomic setting of the fossil specimens, as described above.

8.4.3 Combination of Ca isotopes and DMTA as dietary proxies

Combining the two independent dietary proxies DMTA (reflecting mechanical food properties) and $\delta^{44/42}$Ca (reflecting chemical/isotopic food properties) have the potential to separate different feeding strategies more precisely and therefore reconstruct trophic niche partitioning in more detail than a single proxy approach. This could be particularly interesting for species with ontogenetic dietary shifts, omnivorous species, or different herbivorous species with variable (unknown) plant matter as diet and will potentially allow refined dietary

reconstructions of past food webs and feeding behaviour of extinct taxa. Therefore, a principal component analysis (PCA) was conducted using the DMT parameters *Asfc* and *metf* as indicators for harder components or more abrasives in the ingesta and therefore for a more pronounced tooth-to-food contact, e.g. through more pronounced oral processing, and stable Ca ($\delta^{44/42}$Ca) as indicator for the trophic level. Carnivorous lower Permian *Dimetrodon* and eryopid, herbivorous lower Permian *Diadectes*, *Orobates*, edaphosaurs and upper Permian pareiasaurs, as well as omnivorous lower Permian *Tseajaia* and upper Permian *Jonkeria* were included into the PCA, mean parameter and $\delta^{44/42}$Ca values per species were calculated because the overlap of DMTA and stable isotope dataset was too small on the individual level (**Table S8.5**).

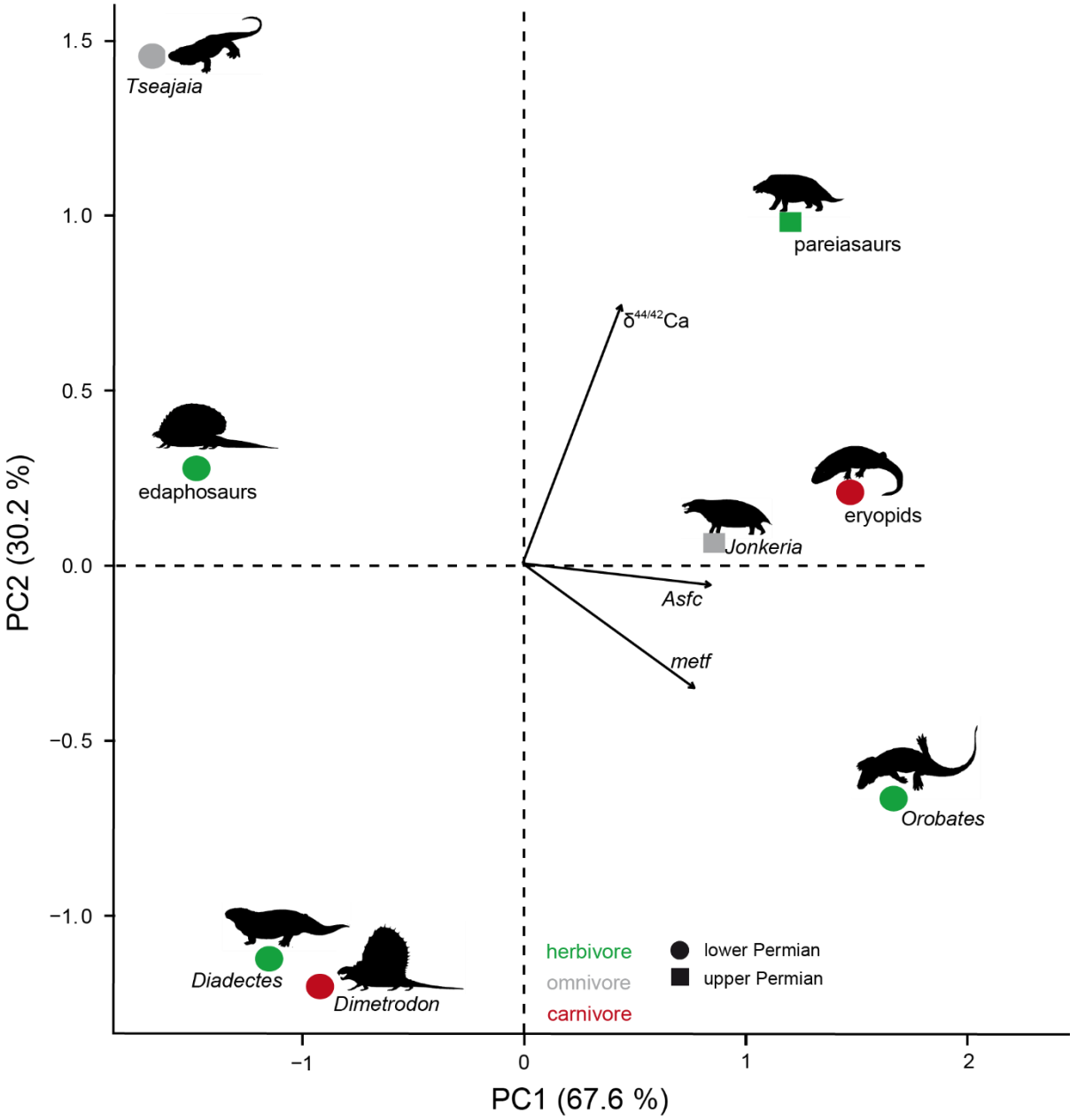

Figure 8.5. Principle component analysis (PCA) for the combination of Ca isotopes and DMTA for different lower (circles) and upper (squares) Permian non-mammalian tetrapods with associated silhouettes of the animals.

The PCA reveals a clear separation of two groups along PC1, with *metf* and *Asfc* as separating parameters. DMTA showed that extinct non-mammalian tetrapods in general showed an oral processing behaviour similar to extant herbivorous, omnivorous and insectivorous lepidosaurs (Winkler et al., 2019a), however, there were differences within the feeding groups. On the one side of PC1, with low *metf* and *Asfc* values, are *Dimetrodon*, *Diadectes*, *Tseajaia* and edaphosaurs, with potentially softer diet and less pronounced food processing behaviour compared to the other species (**Table S8.6 and S8.7**). On the other side of PC1, with higher *metf* and *Asfc* values, are pareiasaurs, eryopide, *Jonkeria* and *Orobates* (**Table S8.6 and S8.7**). Along PC2, with $\delta^{44/42}$Ca and *metf* as best separating parameters are *Diadectes, Orobates* and *Dimetrodon* with low $\delta^{44/42}$Ca values, eryopids, *Jonkeria* and edaphosaurs with intermediate and pareiasaurs and *Tseajaia* with less negative $\delta^{44/42}$Ca values (**Table S8.6 and S8.7**). This separation was already seen in the single stable isotope approach (Chapter 8.4.2). The PCA shows, that carnivorous *Dimetrodon* and eryopids are separated by material and isotopic food properties. $\delta^{44/42}$Ca values differs, possibly due to the different $\delta^{44/42}$Ca values of the ingested diet. It could be assumed that even though both species lived in the same ecosystems, they hunted different types of prey, potentially at different positions in the trophic web (i.e. primary consumers, other carnivores). Potentially, eryopids did not ingest the bones (Ca-rich and ^{44}Ca-depleted) of their prey, which could also explain the higher $\delta^{44/42}$Ca values. More data are needed to validate this hypothesis.

The lower Permian carnivorous *Dimetrodon* and herbivorous *Diadectes* clearly plot together, therefore the material, as well as the isotopic food properties seem to have been similar, with low $\delta^{44/42}$Ca values and low abrasiveness. It is unclear what exactly was ingested by *Diadectes* to cause such negative $\delta^{44/42}$Ca values with low abrasiveness. The ingestion of roots would explain low $\delta^{44/42}$Ca values, however, this would increase *metf* and *Asfc*, since roots are supposed to be relatively hard and external abrasives would potentially be attached to the roots (expect of external abrasives with very low grain sizes). This is not the case in *Diadectes*, however, in *Orobates*, high *metf* and *Asfc* together with relatively low $\delta^{44/42}$Ca values could indicate ingestion of root material. This hypothesis might be supported by traces of digging, as they were found in the Bromacker Quarry and were probably produced by Diadectomorphs (Martens, 2005a; Nyakatura et al., 2015), possibly in search of food. Within the same lower Permian ecosystems, the large herbivorous edaphosaurs showed signs of diet with low abrasiveness and low $\delta^{44/42}$Ca values (not as low as *Diadectes*). The PCA of lower Permian herbivorous taxa suggested distinct differences in ingested plant parts or even plant species e.g. early conifers and ferns, however, since $\delta^{44/42}$Ca values of Permian plants species

are unknown, it is so far not possible to draw conclusion of what plant species were consumed by which tetrapod species. Lower Permian potentially omnivorous *Tseajaia* from the Remigiusberg Fm. also showed signs of ingesta with low abrasiveness, however, with very high $\delta^{44/42}$Ca values, suggesting a more leave-based diet of $\delta^{44/42}$Ca high plants. Therefore, *Tseajaia*'s ecological niche differs from all other lower Permian species measured so far. Upper Permian omnivorous *Jonkeria*'s diet had a higher abrasiveness compared to lower Permian *Tseajaia*, with slightly lower $\delta^{44/42}$Ca values, at least for this specific individual. So far, it is unclear, if the reason for these differences were distinct differences in ingested diet, i.e. different plant species or meat-based diet, differences between mechanical and isotopic properties of lower and upper Permian plants or even different physiological processes between lower Permian *Tseajaia* (Diadectomorphs) and upper Permian *Jonkeria* (Therapsida, Dinocephalia). More individuals of more species from the same localities are needed to test if a combined proxy approach would be able to exclude or validate one of these reasons. Finally, there are distinct differences between lower Permian herbivores, i.e. *Diadectes, Orobates* and edaphosaurs, and upper Permian pareiasaurs. Upper Permian pareiasaurs showed signs of a highly abrasive ingesta, however with very positive $\delta^{44/42}$Ca values. However, these differences might be explained with the same reasons as already explained for *Tseajaia* and *Jonkeria*, differences in physiological processes or ingested plant species cannot be excluded. Despite the issues with the preliminary dataset, PCA of combined DMTA and $\delta^{44/42}$Ca generally was able to draw a complex picture lower and upper Permian ecological niche partitioning and positions in the trophic webs.

8.5 Conclusion and Outlook

The measurements of stable Ca and Sr in extant lepidosaurs showed that both systems are able to resolve a TLE, especially the biplot of $\delta^{44/42}$Ca vs. $\delta^{88/86}$Sr showed that carnivorous species have more negative values in both systems, while herbivores and insectivores are higher in Ca and Sr values (**Fig. 8.4**). Especially Sr might be a valuable proxy to distinguish between aquatic and terrestrial plant matter as diet in extant herbivorous lepidosaurs. Preliminary data showed no offset in $\delta^{44/42}$Ca values between bone and tooth samples in general, only in ovivorous *Heloderma horridum*, where potential differences in diet during formation of bone and tooth are assumed. The preliminary dataset of fossil specimens showed that both methods are applicable to Permo-Carboniferous tetrapods, but with some limitations due to preservation. While DMTA seem to differentiate between insectivores and carnivores/ herbivores, Ca isotopes seem to preserve the ante-mortem, presumably diet-related isotope signal and differentiate between carnivorous and herbivorous species. A more pronounced TLE was found in upper Permian taxa, compared to lower Permian taxa, where herbivores

yielded $\delta^{44/42}Ca$ more similar to those of carnivorous taxa. Several hypothesises, such as identification of proportion of different ingesta in omnivorous species, ontogenetic diet shifts or expected diet niche occupation in specific species could not be tested yet due to the small sample size and badly preserved dental surfaces. First results suggest distinct differences in ingested plant matter between *Diadectes*, *Orobates,* edaphosaurs and pareiasaurs, and in prey-preferences between *Dimetrodon* and eryopids (**Fig. 8.2B, 8.4 and 8.5**). For DMTA and Ca isotope datasets, more samples from the same localities are needed to assess physiological processes and differences in flora assemblages between the localities. Additionally, more insectivores are needed to further assess if insect-feeding can be distinguished from the other feeding categories. If the size and biodiversity of the ecosystem allow it, specific lower and upper Permian food webs should be analysed and compared among each other, i.e. Bromacker Quarry and Texas Bonebed, as well as terrestrial and aquatic food webs withing one locality, i.e. from the Remigiusberg Fm.. Nevertheless, the first attempt in combining both independent proxies in a PCA showed huge potential to distinguish more precisely what kind of plant matter or animal tissue was ingested and will enable more sophisticated diet reconstructions of fossil food webs and niche partitioning in the future. In a next step, trophic niche partitioning at the Permo-Carboniferous boundary, during the Permian and beyond the Permo-Triassic mass extinction should be tracked and the evolution, changes and stability (especially over the Permo-Triassic mass extinction) of the early trophic web should be analysed.

8.6 Supplement

Table ES8.1. Sampled taxon, sample ID, collection ID, collection, locality, Period, presumed diet and sampled tissue types for extinct non-mammalian tetrapods and extant wild lepidosaurs. The table is found in the electronic Supplement.

Table S8.2. Taxon, trivial name, presumed diet, sample weight and $\delta^{44/42}Ca_{vs.\ MZ\text{-}STD}$ and $\delta^{88/86}Sr_{vs.\ NIST987}$ values with 1SD of the extant wild lepidosaur and extinct non-mammalian tetrapod specimens, bone and tooth samples separated.

Sample ID	Taxon	Trivial name	Diet		Tooth sample						Bone sample				
					sample amount [mg]	$\delta^{44/42}Ca_{vs.\ MZ\text{-}STD}$ [‰]	1SD [‰]	$\delta^{88/86}Sr$ vs.NIST987	1SD [‰]		sample amount [mg]	$\delta^{44/42}Ca_{vs.\ MZ\text{-}STD}$ [‰]	1SD [‰]	$\delta^{88/86}Sr$ vs.NIST987	1SD [‰]
ZFMK_84181	*Amblyrhynchus cristatus*	Marine iguana	algaevore	whole tooth	4.91	-0.77	0.05	-0.39	0.05	lower jaw bone	9.1	-0.86	0.06	-	-
ZFMK_84199	*Amblyrhynchus cristatus*	Marine iguana	algaevore	whole tooth	4.96	-0.81	0.04	-0.40	0.05	lower jaw bone	8.5	-0.71	0.07	-	-
ZFMK_7816	*Cordylus giganteus*	Giant girdled lizard	insectivore	-	-	-	-	-	-	lower jaw bone	2.91	-0.56	0.04	-0.24	0.05
ZFMK_7817	*Cordylus giganteus*	Giant girdled lizard	insectivore	-	-	-	-	-	-	crania	5.05	-0.79	0.03	-0.15	0.04
ZFMK_5223	*Cyclura cornuta*	Rhinoceros iguana	herbivore	whole tooth	2.78	-0.80	0.04	-0.25	0.06	lower jaw bone	2.8	-0.90	0.06	-	-
ZFMK_86078	*Cyclura cornuta*	Rhinoceros iguana	herbivore	whole tooth	7.62	-0.87	0.04	-0.32	0.06	lower jaw bone	3.4	-0.85	0.06	-	-
ZFMK_7846	*Heloderma horridum*	Mexican beaded lizard	ovivore	whole tooth	1.82	-0.73	0.04	-0.25	0.07	lower jaw bone	5.2	-0.98	0.06	-	-
ZFMK_7859	*Tupinambis teguixin*	Gold tegu	omnivore	whole tooth	2.12	-0.96	0.04	-0.40	0.04	lower jaw bone	2.6	-0.97	0.06	-	-
ZFMK_53531	*Tupinambis teguixin*	Gold tegu	omnivore	whole tooth	9.91	-1.03	0.04	-0.35	0.05	humerus	3.7	-1.06	0.07	-	-
ZFMK_53532	*Tupinambis teguixin*	Gold tegu	omnivore	enamel powder	0.27	-1.22	0.03	-0.51	0.06	lower jaw bone	2.9	-1.06	0.07	-	-
ZFMK_14882	*Varanus giganteus*	Perentie	carnivore	enamel powder	3.17	-1.14	0.04	-0.46	0.07	lower jaw bone	2.9	-1.09	0.07	-	-
ZFMK_7484	*Varanus griseus*	Desert monitor	carnivore	enamel powder	0.98	-1.06	0.04	-0.63	0.05	lower jaw bone	2.1	-1.00	0.08	-	-
DIM BRI 1	*Dimetrodon* sp.	-	carnivore	-	-	-	-	-	-	jaw bone	3.7	-0.67	0.06	0.42	0.06
DIM BRI 2	*Dimetrodon* sp.	-	carnivore	enamel (distal and	1.0 / 0.6	-0.73	0.10	0.32	0.08	jaw bone	1.6	-0.60	0.05	-0.13	0.06
DIM BRI 3	*Dimetrodon* sp.	-	carnivore	enamel (distal and	1.2 /0.5	-0.96	0.16	0.02	0.04	jaw bone	4.0	-0.76	0.05	0.19	0.05
DIM BRI 4	*Dimetrodon* sp.	-	carnivore	enamel	1.5	-0.76	0.08	0.61	0.04	jaw bone	1.9	-0.77	0.05	0.40	0.03
DIM TX 1	*Dimetrodon* sp.	-	carnivore	enamel	3.1	-0.47	0.08	0.93	0.11	vertebrae	0.5	-0.94	0.12	0.19	0.04
DIM TX 2	*Dimetrodon* sp.	-	carnivore	enamel	4.3	-0.46	0.07	0.59	0.05	unspecified fragment	5.6	-0.19	0.06	1.05	0.05
DIM TX 3	*Dimetrodon* sp.	-	carnivore	-	-	-	-	-	-	unspecified fragment	4.4	-0.24	0.08	0.76	0.04
MNG 10226	Sphenacodontida indet.	-	carnivore	-	-	-	-	-	-	right femur	1.5	-0.64	0.06	-	-
MNG 10596	*Tambacarnifex ungifalcatus*	-	carnivore	-	-	-	-	-	-	rib	7.5	-0.64	0.05	-	-
ARC KA 1	*Arctops*	-	carnivore	enamel	5.2	-0.60	0.06	0.09	0.09	unspecified fragment	4.1	-0.50	0.05	-0.30	0.04
UGKU 2564	Eryopidae	-	carnivore	-	-	-	-	-	-	crania (3 samples)	2.0 / 1.7 / 2.4	-0.53	0.06	0.62	0.09
UGKU L-21	Eryopidae	-	carnivore	enamel	0.3	-0.28	0.04	0.45	0.05	-	-	-	-	-	-
MNG 7727	*Seymouria sanjuanensis*	-	carnivore	-	-	-	-	-	-	crania	0.7	-0.59	0.04	-	-
PAR KA 1	Pareiasaur	-	herbivore	enamel	2.5	-0.34	0.03	0.45	0.11	-	-	-	-	-	-
EDA BRI 1	edaphosaur	-	herbivore	-	-	-	-	-	-	unspecified fragment	2.4	-0.55	0.05	0.37	0.06
ED RM 1	edaphosaur	-	herbivore	-	-	-	-	-	-	unspecified fragment	3.2	-0.56	0.05	0.48	0.03
ED TX 2	edaphosaur	-	herbivore	-	-	-	-	-	-	spine	3.6	-0.44	0.11	0.22	0.07
UGKU-1997	*Remigiomontanus robustus*	-	herbivore	-	-	-	-	-	-	unspecified fragments (n	6.1 / 6.0 / 0.3	-0.56	0.04	0.37	0.06
UGKU-2551	edaphosaur	-	herbivore	-	-	-	-	-	-	spine (3 samples)	1.9 / 0.7 / 1.3	-0.41	0.05	0.86	0.07
DIA BRI 1	*Diadectes* sp.	-	herbivore	enamel (distal and	1.2 /3.2	-0.71	0.05	0.17	0.06	jaw bone (2 samples)	4.4 / 4.8	-0.55	0.07	0.40	0.05
MNG 14473	*Diadectes* sp.	-	herbivore	-	-	-	-	-	-	rib (2 samples)	4.3 / 1.5	-0.55	0.04	-	-
MNG 11134(3)	Diadectidae	-	herbivore	enamel	0.9	-0.63	0.03	-	-	-	-	-	-	-	-
MNG 11240	Diadectidae	-	herbivore	-	-	-	-	-	-	unspecified fragment	0.5	-0.66	0.05	-	-
MNG 8980	*Orobates pabsti*	-	herbivore	-	-	-	-	-	-	rib	1.3	-0.46	0.04	-	-
MNG 12895-3	*Eudibamus cursoris*	-	herbivore	-	-	-	-	-	-	pelvic bone	2.6	-0.49	0.05	-	-
JON BRI 1	*Jonkeria*	-	omnivore	enamel	3.5	-0.45	0.03	0.07	0.04	unspecified fragment	2.4	-0.35	0.06	0.38	0.04
UGKU 2566	*Tseajaia*	-	omnivore	enamel	0.9	-0.40	0.04	0.30	0.07	-	-	-	-	-	-

Table ES8.3. Descriptive statistics (mean ±SD) for all DMT parameters for the extinct non-mammalian tetrapods (see **Table 8.1**). For parameter descriptions, see Table S4.3. The table is found in the electronic Supplement.

Table ES8.4. Statistical results for all DMT parameters for non-mammalian tetrapod. For parameter description, see Table S4.3. Significances confirmed by Cliff's method are highlighted in bold. The table is found in the electronic Supplement.

Table S8.5. Importance of components for PCA using 13 DMT parameter (*Sz, Sdq, Sdr, Spd, Sdv, Shv, FLTt, nMotif, meh, mea, madf, Tr2R, IsT*). Factor loadings for the parameter values are represented with values cut-off +/- 0.4 marked in red.

		PC1	PC2	PC3	PC4	PC5	PC6	PC7	PC8	PC9	PC10	PC11	PC12	PC13
Standard deviation		2.66	1.55	1.04	1.01	0.87	0.57	0.39	0.31	0.25	0.20	0.10	0.10	0.06
Proportion of Variance		0.54	0.18	0.08	0.08	0.06	0.02	0.01	0.01	0.00	0.00	0.00	0.00	0.00
Cumulative Proportion		0.54	0.73	0.81	0.89	0.95	0.97	0.98	0.99	1.00	1.00	1.00	1.00	1.00
Factor loadings	*Sz*	-0.36	-0.14	0.04	-0.07	0.05	-0.04	0.01	-0.25	0.24	-0.23	0.76	-0.23	0.18
	Sdq	-0.18	-0.53	0.23	0.09	0.07	-0.04	-0.13	-0.28	0.01	-0.11	-0.49	-0.52	0.03
	Sdr	-0.14	-0.56	0.19	0.16	0.03	0.06	-0.18	0.32	-0.32	0.47	0.26	0.27	0.00
	Spd	0.27	-0.34	-0.32	-0.10	0.16	-0.36	0.28	0.08	0.06	-0.08	-0.08	0.16	0.65
	Sdv	-0.32	0.09	-0.40	-0.11	0.24	0.09	-0.03	0.04	-0.74	-0.29	-0.01	-0.11	0.03
	Shv	-0.28	0.13	0.17	-0.09	-0.48	-0.77	-0.08	0.01	-0.18	-0.03	-0.05	0.08	-0.03
	FLTt	-0.36	-0.08	-0.07	-0.06	0.10	0.01	-0.17	0.69	0.40	-0.38	-0.16	0.07	-0.09
	nMotif	0.29	-0.32	-0.33	-0.10	0.14	-0.33	0.15	0.01	0.04	-0.05	0.17	-0.12	-0.71
	meh	-0.35	-0.08	-0.22	-0.11	0.23	-0.03	-0.21	-0.50	0.20	0.07	-0.19	0.60	-0.12
	mea	-0.32	0.18	-0.35	-0.21	0.08	-0.07	0.09	0.11	0.19	0.69	-0.08	-0.39	0.06
	madf	-0.33	-0.13	0.14	-0.04	-0.19	0.19	0.85	-0.01	-0.03	-0.03	-0.10	0.16	-0.13
	Tr2R	0.12	-0.25	-0.17	-0.66	-0.56	0.32	-0.19	-0.03	-0.01	-0.04	-0.01	0.00	0.03
	IsT	0.08	0.10	0.54	-0.65	0.49	-0.11	0.06	0.06	-0.08	0.04	-0.01	0.02	-0.02

Table S8.6. Pooled data of non-mammalian tetrapods for PCA of combined DMTA and $\delta^{44/42}Ca_{vs.\ MZ\text{-}STD}$.

Taxon	*Asfc*	*metf*	$\delta^{44/42}Ca_{vs.\ MZ\text{-}STD}$
Diadectes	5.110	0.291	-0.626
Dimetrodon	4.372	0.335	-0.612
Edaphosaurs	4.274	0.210	-0.513
Orobates	11.860	0.446	-0.473
Jonkeria	10.599	0.351	-0.446
Eryopidae	12.090	0.383	-0.409
Tseajaia	2.054	0.180	-0.401
Pareiasaurs	9.755	0.364	-0.336

Table S8.7. Importance of components for PCA using 2 DMT parameter (*Asfc*, *metf*) and $\delta^{44/42}Ca_{vs.\ MZ\text{-}STD}$. Factor loadings for the parameter values are represented with values cut-off +/- 0.4 marked in red.

		PC1	PC2	PC3
Standard deviation		1.42	0.95	0.25
Proportion of Variance		0.68	0.30	0.02
Cumulative Proportion		0.68	0.98	1.00
Factor loadings	*Asfc*	0.69	-0.08	0.72
	metf	0.63	-0.43	-0.65
	$\delta^{44/42}Ca_{vs.\ MZ\text{-}STD}$	0.36	0.90	-0.25

Chapter 9 Conclusion

The main focus of this thesis was the evaluation of the effects of and mechanisms behind mechanical and chemical diagenesis on dental microwear texture analyses and non-traditional isotopes. With the help of the experimental approaches presented in this thesis it was possible to better understand the mechanisms of mechanical and chemical post-mortem alteration of vertebrate teeth and its effects on dental microwear texture analyses and non-traditional stable isotopes as dietary proxies. By performing alteration experiments for simulating three different types of post-mortem diagenesis on dental microwear, the understanding of the impact of post-mortem erosion on DMT parameters was improved. The experiments on fluvial transport and aeolian sediment transport showed that the degree of alteration is mostly dependent on sediment grain size fraction. While very fine sand and gravel had the strongest abrasion effects, fine to medium sand had a slight polishing effect (smoother dental surface) during the tumbling experiment. Very fine-grained loess, however, did not affect the dental surface during the sandblasting, while sand-sized quartz particles causes strong alteration effects. In general, the experiments showed that natural alteration processes are more complex than initially thought, especially in the case of acid etching during digestion. Extant *Otomys* teeth and those extracted from owl pellets showed no differences in their dental surfaces, while experimentally altered *Otomys* teeth showed signs of strong chemical alteration. Together with the first steps towards a database including varies kinds of badly preserved dental surfaces resulted by e.g. excavation or preparation, it is shown, that the influence of blunders, defects and post-mortem erosions on the DMT parameters is not as large as expected. They could not be unambiguously separated from diet-related ante-mortem wear features by using ISO and SSFA parameter values alone. A combination of careful evaluation of wear features by the observers and the use of cut-off values for different parameters is the basis for improving and enlarging sample size and datasets in general, and in the fossil record in particular. Generally, fossils with signs of small post-mortem alteration on the dental surface, might provide reliable results. Additionally, this thesis highlights potential limits of DMTA for dietary reconstruction in species with fast tooth replacement rates and/or very limited tooth-food contact due to reduced oral food processing behaviour. Although there are some differences in diet preferences of extant (generally opportunistic) faunivorous sharks, no ingesta-related ante-mortem wear was detectable. Therefore, sharks seem to be unsuitable for dietary reconstruction using DMTA according to its fast tooth replacement rate and reduced prey processing behaviour.

Post-mortem alteration of the isotope composition is not so easy to access and *in-vitro* alterations experiment, as performed in this thesis, set the basis for better understanding and evaluating the grade of potential post-mortem alteration of tooth chemistry. The *in-vitro* experiments showed that different isotope systems were showing different signs of alteration,

while there is a loss of Mg during the experimental duration in dentin and enamel, Zn is incorporated into the newly formed hydroxylapatite crystal lattice. Calcium and Sr were showing a similar alteration behaviour, probably due to a diffusion gradient controlled mechanism caused by the highly elevated concentration of the doped isotopes. In general, it is assumed, that diffusion and re-precipitation causes the alteration of Ca, Mg, Zn and Sr isotope composition, however even at higher temperatures only the outermost ≈ 200 µm of the enamel are affected. Dentin is more resistant than expected, at least for lower temperatures. During higher temperatures the original isotopic composition are completely altered. The results prove what is already known about the higher vulnerability of dentin in contrast to enamel. These are important findings for the fossil application, even though the isotope concentrations (especially ^{44}Ca) in the tracer solution were extremely elevated, a proportion of inner enamel (~ 200 µm apart from EDJ and enamel edge) preserves ante-mortem original isotopic composition and therefore this part should be suitable for diet reconstruction.

The second part of the presented thesis highlights the possibilities of applying DMTA and non-traditional stable isotopes to fossil non-mammalian taxa. First results of DMTA on extinct Permo-Carboniferous non-mammalian tetrapods show significant differences between insectivorous and herbivorous/carnivorous taxa. DMTA also displays differences in material properties and therefore potential preferences in ingested diet for different taxa within one feeding category, i.e. between the herbivorous *Diadectes, Orobates*, *Edaphosaurus* and pareiasaurs and between carnivorous eryopid and *Dimetrodon*. Furthermore, the first $\delta^{44/42}Ca$ and $\delta^{88/86}Sr$ values of extant lepidosaurs presented in this thesis yielded a trophic spacing between feeding categories with carnivores being more negative than herbivores, which also applies on extinct non-mammalian tetrapods, at least in $\delta^{44/42}Ca$ while the $\delta^{88/86}Sr$ appeared to be diagenetically overprinted. So far, no systematic offset in $\delta^{44/42}Ca$ between bones and teeth of extant lepidosaurs were detected, while extinct non-mammalian tetrapods showed less negative $\delta^{44/42}Ca$ values bone samples compared to enamel. It is not clear yet, if the offset is caused by different physiological processes or by diagenesis. The offset in $\delta^{44/42}Ca$ values between extant carnivorous and herbivorous lepidosaurs and fossil carnivorous and herbivorous taxa implies potential differences in the Ca isotope composition of primary producers, i.e. plants, between modern and Permo-Carboniferous ecosystems. $\delta^{44/42}Ca$ reveals differences in chemical food properties and therefore, similar to DMTA potential preferences in ingested diet within one feeding category, i.e. herbivorous and carnivorous groups, as well as differences between lower and upper Permian herbivores. More data are needed to evaluate the effect of differences in the ingesta, i.e. ingestion of different plant species, and differences in physiological fractionation processes between lower and upper Permian non-mammalian tetrapods. In general, the first combined dental microwear texture and non-traditional stable isotope dataset on Permo-Carboniferous tetrapods yielded distinct

differences between herbivorous, omnivorous and carnivorous non-mammalian tetrapods and indicate the colonization of different niches within the same ecosystem. Therefore, this combined toolset could be able to provide more precise information about fossil food webs and niche portioning and should be further extended in the future.

Chapter 10 References

Abdala, F., Allinson, M. (2005). The taxonomic status of *Parathrinaxodon proops* (Therapsida: Cynodontia), with comments on the morphology of the palate in basal cynodonts. Palaeontologia africana 41, 45–52.

Ackermans, N. L. (2020). The history of mesowear: a review. PeerJ 8, e8519.

Adnet, S., Cappetta, H. (2001). A palaeontological and phylogenetical analysis of squaliform sharks (Chondrichthyes: Squaliformes) based on dental characters. Lethaia 34(3), 234–248.

Agerbaek, M. O., Eriksen, E. F., Kragstrup, J., Mosekilde, L., Melsen, F. (1991). A reconstruction of the remodelling cycle in normal human cortical iliac bone. Bone and mineral 12(2), 101–112.

Akhtar, A. A., Santi, L. M., Griffiths, M. L., Becker, M., Eagle, R. A., Kim, S., Kocsis, L., Rosenthal, Y., Higgins, J. A. (2020). A record of the $\delta^{44/40}$Ca and [Sr] of seawater over the last 100 million years from fossil elasmobranch tooth enamel. Earth and Planetary Science Letters 543, 116354.

Algeo, T. J., Twitchett, R. J. (2010). Anomalous Early Triassic sediment fluxes due to elevated weathering rates and their biological consequences. Geology 38(11), 1023–1026.

Algeo, T. J., Kuwahara, K., Sano, H., Bates, S., Lyons, T., Elswick, E., Honniv, L., Ellwood, B., Moser, J., Maynard, J. B. (2011). Spatial variation in sediment fluxes, redox conditions, and productivity in the Permian–Triassic Panthalassic Ocean. Palaeogeography, Palaeoclimatology, Palaeoecology 308(1-2), 65–83.

Ambrose, S. H. (1986). Stable carbon and nitrogen isotope analysis of human and animal diet in Africa. Journal of Human Evolution 15(8), 707–731.

Ambrose, S. H. (1990). Preparation and characterization of bone and tooth collagen for isotopic analysis. Journal of archaeological science 17(4), 431–451.

Ambrose, S. H., Krigbaum, J. (2003). Bone chemistry and bioarchaeology. Journal of Anthropological Archaeology 22(3), 193–199.

Amiot, R., Lécuyer, C., Buffetaut, E., Escarguel, G., Fluteau, F., Martineau, F. (2006). Oxygen isotopes from biogenic apatites suggest widespread endothermy in Cretaceous dinosaurs. Earth and Planetary Science Letters 246(1–2), 41–54.

Amiot, R., Wang, X., Zhou, Z., Wang, X., Buffetaut, E., Lécuyer, C., Ding, Z., Fluteau, F., Hibino, T., Kusuhashi, N., Mo, J., Suteethorn, V., Wang, Y., Xu, X., Mo, J. (2011). Oxygen isotopes of East Asian dinosaurs reveal exceptionally cold Early Cretaceous climates. Proceedings of the National Academy of Sciences 108(13), 5179–5183.

Amson, E., Laurin, M. (2011). On the affinities of Tetraceratops insignis, an Early Permian synapsid. Acta Palaeontologica Polonica 56(2), 301–312.

Anderson, J. S., Reisz, R. R. (2004). *Pyozia mesenensis*, a new, small varanopid (Synapsida, Eupelycosauria) from Russia:“pelycosaur” diversity in the Middle Permian. Journal of Vertebrate Paleontolog, 24(1), 173–179.

Anderson, J. S., Henrici, A. C., Sumida, S. S., Martens, T., Berman, D. S. (2008). *Georgenthalia clavinasica*, a new genus and species of dissorophoid temnospondyl from the Early Permian of Germany, and the relationships of the family Amphibamidae. Journal of Vertebrate Paleontology 28(1), 61–75.

Andrews, P., Bernor, R. L. (1999). Vicariance biogeography and paleoecology of Eurasian Miocene hominoid primates. The Evolution of Neogene Terrestrial Ecosystem in Europe, 454–487.

Angielczyk, K. D. (2001). Preliminary phylogenetic analysis and stratigraphc congruence of the dicynodont anomodonts (Synapsida: therapsida). Palaeontologia Africana 37, 53–79.

Armstrong, J. T. (1995). Citzaf-a package of correction programs for the quantitative Electron Microbeam X-Ray-Analysis of thick polished materials, thin-films, and particles. Microbeam Analysis 4(3), 177–200.

Arns, A., Tomaschek, F., Alig, E., Weber, K., Vonhof, H., Fischer, J., Voigt, S., Tütken, T. (2020). Metamorphosed Permian vertebrate fossils: geochemistry and mineralogy of" white" sharks. In EGU General Assembly Conference Abstracts (p. 18533).

Asjadi, F., Geisler, T., Salahi, I., Euler, H., Mobasherpour, I. (2019). Ti-Substituted Hydroxylapatite Precipitated in the Presence of Titanium Sulphate: A Novel Photocatalyst? American Journal of Chemistry and Applications 6(1), 1.

Astin, T. R., Marshall, J. E. A., Blom, H., Berry, C. M. (2010). The sedimentary environment of the Late Devonian East Greenland tetrapods. Geological Society, London, Special Publications 339(1), 93–109.

Aufort, J., Gervais, C., Segalen, L., Labourdette, N., Coelho-Diogo, C., Baptiste, B., Beyssac, O., Amiot, R., Lécuyer, C., Balan, E. (2019). Atomic scale transformation of bone in controlled aqueous alteration experiments. Palaeogeography, Palaeoclimatology, Palaeoecology 526, 80–95.

Avci, R., Schweitzer, M. H., Boyd, R. D., Wittmeyer, J. L., Terán Arce, F., Calvo, J. O. (2005). Preservation of bone collagen from the late Cretaceous period studied by immunological techniques and atomic force microscopy. Langmuir 21(8), 3584–3590.

Ayliffe, L. K., Chivas, A. R., Leakey, M. G. (1994). The retention of primary oxygen isotope compositions of fossil elephant skeletal phosphate. Geochimica et Cosmochimica Acta 58(23), 5291–5298.

Baker, G., Jones, L. H. P., Wardrop, I. D. (1959). Cause of wear in sheeps' teeth. Nature 184(4698), 1583–1584.

Balter, V. (2004). Allometric constraints on Sr/Ca and Ba/Ca partitioning in terrestrial mammalian trophic chains. Oecologia 139(1), 83–88.

Balter, V., Bocherens, H., Person, A., Labourdette, N., Renard, M., Vandermeersch, B. (2002). Ecological and physiological variability of Sr/Ca and Ba/Ca in mammals of West European mid-Würmian food webs. Palaeogeography, Palaeoclimatology, Palaeoecology 186(1–2), 127–143.

Balasse, M. (2002). Reconstructing dietary and environmental history from enamel isotopic analysis: time resolution of intra-tooth sequential sampling. International Journal of Osteoarchaeology 12(3), 155–165.

Bamford, M. K. (2004). Diversity of the woody vegetation of Gondwanan Southern Africa. Gondwana Research 7(1), 153–164.

Barthel, H. J., Fougerouse, D., Geisler, T., Rust, J. (2020). Fluoridation of a lizard bone embedded in Dominican amber suggests open-system behavior. PLoS ONE 15(2), e0228843.

Beasley, D. E., Koltz, A. M., Lambert, J. E., Fierer, N., Dunn, R. R. (2015). The evolution of stomach acidity and its relevance to the human microbiome. PLoS ONE 10(7), e0134116.

Becker, F. (2002). Zechsteinkalk und Unterer Werra-Anhydrit (Zechstein 1) in Hessen: Fazies, Sequenzstratigraphie und Diagenese (Vol. 109). Hessisches Landesamt für Umwelt und Geologie.

Bedaso, Z. K., Wynn, J. G., Alemseged, Z., Geraads, D. (2013). Dietary and paleoenvironmental reconstruction using stable isotopes of herbivore tooth enamel from middle Pliocene Dikika, Ethiopia: Implication for Australopithecus afarensis habitat and food resources. Journal of human evolution 64(1), 21–38.

Bendel, E. M., Kammerer, C. F., Kardjilov, N., Fernandez, V., Fröbisch, J. (2017). Cranial anatomy and systematic position of *Aelurosaurus* (Synapsida, Gorgonopsia) based on a CT-reconstruction. Vertebrate Anatomy Morphology Palaeontology 4, 10.

Bengtsson, H. (2010). R. utils: Various programming utilities. R package version, 1(0).

Bengtsson, H. (2016). R.utils: Various programming utilities. R package, version 2.4.0. Available at https://CRAN.Rproject.org/package=R.utils.

Bennett, C. E., Kearsey, T. I., Davies, S. J., Millward, D., Clack, J. A., Smithson, T. R., Marshall, J. E. (2016). Early Mississippian sandy siltstones preserve rare vertebrate fossils in seasonal flooding episodes. Sedimentology 63(6), 1677–1700.

Bennett, S. C. (1996). Aerodynamics and thermoregulatory function of the dorsal sail of *Edaphosaurus*. Paleobiology, 496–506.

Benoit, J., Manger, P. R., Fernandez, V., Rubidge, B. S. (2016). Cranial bosses of *Choerosaurus dejageri* (Therapsida, Therocephalia): earliest evidence of cranial display structures in eutheriodonts. PLoS ONE 11(8), e0161457.

Benson, R. B. (2012). Interrelationships of basal synapsids: cranial and postcranial morphological partitions suggest different topologies. Journal of Systematic Palaeontology 10(4), 601–624.

Benson, R. B., Upchurch, P. (2013). Diversity trends in the establishment of terrestrial vertebrate ecosystems: interactions between spatial and temporal sampling biases. Geology 41(1), 43–46.

Bentley, R. A. (2006). Strontium isotopes from the earth to the archaeological skeleton: a review. Journal of archaeological method and theory 13(3), 135–187.

Benton, M. J. (1983). Dinosaur success in the Triassic: a noncompetitive ecological model. The Quarterly Review of Biology 58(1), 29–55.

Benton, M. J. (2012). No gap in the Middle Permian record of terrestrial vertebrates. Geology 40(4), 339–342.

Benton, M. J., Pfretzschner, H. U. (2007). Paläontologie der Wirbeltiere (pp. 472). München, Friedrich Pfeil.

Benton, M. J., Twitchett, R. J. (2003). How to kill (almost) all life: the end-Permian extinction event. Trends in Ecology and Evolution 18(7), 358–365.

Benton, M. J., Donoghue, P. C., Asher, R. J., Friedman, M., Near, T. J., Vinther, J. (2015). Constraints on the timescale of animal evolutionary history. Palaeontologia Electron 18(1), 1–106.

Berglund, M., Wieser, M. E. (2011). Isotopic compositions of the elements 2009 (IUPAC Technical Report). Pure and applied chemistry 83(2), 397–410.

Berkovitz, B. K., Shellis, R. P. (2016). The teeth of non-mammalian vertebrates (pp.342). London, San Diego, Cambridge: Academic Press.

Berkovitz, B. K., Shellis, R. P. (2018). The teeth of mammalian vertebrates (pp.334). London, San Diego, Cambridge: Academic Press.

Berman, D. S., Sumida, S. S., Lombard, R. E. (1992). Reinterpretation of the temporal and occipital regions in *Diadectes* and the relationships of diadectomorphs. Journal of Paleontology 481–499.

Berman, D. S., Sumida, S. S., Martens, T. (1998). *Diadectes* (Diadectomorpha: Diadectidae) from the Early Permian of central Germany, with description of a new species. Annals-carnegie Museum Pittsburgh 67, 53–93.

Berman, D. S., Reisz, R. R., Scott, D., Henrici, A. C., Sumida, S. S., Martens, T. (2000a). Early Permian bipedal reptile. Science 290(5493), 969–972.

Berman, D. S., Henrici, A. C., Sumida, S. S., Martens, T. (2000b). Redescription of *Seymouria sanjuanensis* (Seymouriamorpha) from the Lower Permian of Germany based on complete, mature specimens with a discussion of paleoecology of the Bromacker locality assemblage. Journal of Vertebrate Paleontology 20(2), 253–268.

Berman, D. S., Reisz, R. R., Martens, T., Henrici, A. C. (2001). A new species of *Dimetrodon* (Synapsida: Sphenacodontidae) from the Lower Permian of Germany records first occurrence of genus outside of North America. Canadian Journal of Earth Sciences 38(5), 803–812.

Berman, D. S., Henrici, A. C., Kissel, R. A., Sumida, S. S., Martens, T. (2004). A new diadectid (Diadectomorpha), *Orobates pabsti*, from the Early Permian of central Germany. Bulletin of Carnegie Museum of Natural History 2004(35), 1–36.

Berman, D. S., Henrici, A. C., Martens, T., Sumida, S. S., Anderson, J. S. (2011). *Rotaryus gothae*, a new trematopid (Temnospondyli: Dissorophoidea) from the Lower Permian of Central Germany. Annals of Carnegie Museum 80(1), 49–65.

Berman, D. S., Henrici, A. C., Sumida, S. S., Martens, T., Pelletier, V. (2014). First European record of a varanodontine (Synapsida: Varanopidae): Member of a unique Early Permian upland paleoecosystem, Tambach Basin, central Germany (p. 69–86). In: Kammerer C., Angielczyk K., Fröbisch J. (eds) Early Evolutionary History of the Synapsida. Vertebrate Paleobiology and Paleoanthropology. Springer, Dordrecht.

Berman, D. S., Maddin, H. C., Henrici, A. C., Sumida, S. S., Scott, D., Reisz, R. R. (2020). New Primitive Caseid (Synapsida, Caseasauria) from the Early Permian of Germany. Annals of Carnegie Museum 86(1), 43–75.

Berna, F., Matthews, A., Weiner, S. (2004). Solubilities of bone mineral from archaeological sites: the recrystallization window. Journal of archaeological Science 31(7), 867–882.

Bernardi, M., Petti, F. M., Kustatscher, E., Franz, M., Hartkopf-Fröder, C., Labandeira, C. C., Wappler, T., van Konijenburg-van Cittert, J. H. A., Peecook, B. R., Angielczyk, K. D. (2017). Late Permian (Lopingian) terrestrial ecosystems: a global comparison with new data from the low-latitude Bletterbach Biota. Earth-Science Reviews 175, 18–43.

Bernard, A., Lécuyer, C., Vincent, P., Amiot, R., Bardet, N., Buffetaut, E., Cuny, G., Fourel, F., Martineau, F., Mazin, J. M., Prieur, A. (2010). Regulation of body temperature by some Mesozoic marine reptiles. Science 328(5984), 1379–1382.

Bertin, T. J., Thivichon-Prince, B., LeBlanc, A. R., Caldwell, M. W., Viriot, L. (2018). Current perspectives on tooth implantation, attachment, and replacement in amniota. Frontiers in Physiology 9, 1630.

Bestwick, J., Unwin, D. M., Purnell, M. A. (2019). Dietary differences in archosaur and lepidosaur reptiles revealed by dental microwear textural analysis. Scientific reports 9(1), 1–11.

Bestwick, J., Unwin, D. M., Butler, R. J., Purnell, M. A. (2020). Dietary diversity and evolution of the earliest flying vertebrates revealed by dental microwear texture analysis. Nature communications 11(1), 1–9.

Bethune, E., Kaiser, T. M., Schulz-Kornas, E., Winkler, D. E. (2019). Multiproxy dietary trait reconstruction in Pleistocene Hippopotamidae from the Mediterranean islands. Palaeogeography, Palaeoclimatology, Palaeoecology 533, 109210.

Beylich, A. A., Gintz, D. (2004). Effects of high-magnitude/low-frequency fluvial events generated by intense snowmelt or heavy rainfall in arctic periglacial environments in northern Swedish Lapland and northern Siberia. Geografiska Annaler: Series A, Physical Geography 86(1), 11–29.

Bianucci, G., Sorce, B., Storai, T., Landini, W. (2010). Killing in the Pliocene: shark attack on a dolphin from Italy. Palaeontology 53(2), 457–470.

Black, B. A., Neely, R. R., Lamarque, J. F., Elkins-Tanton, L. T., Kiehl, J. T., Shields, C. A., Bardeen, C. (2018). Systemic swings in end-Permian climate from Siberian Traps carbon and sulfur outgassing. Nature Geoscience 11(12), 949–954.

Blakey, R. C. (2003). Carboniferous–Permian paleogeography of the assembly of Pangaea (p.443 – 456). In: Wong, Th. E. (ed) Proceedings of the XVth International Congress on Carboniferous and Permian Stratigraphy. Utrecht.

Blum, J. D., Taliaferro, E. H., Weisse, M. T., Holmes, R. T. (2000). Changes in Sr/Ca, Ba/Ca and 87Sr/86Sr ratios between trophic levels in two forest ecosystems in the northeastern USA. Biogeochemistry 49(1), 87–101.

Boanini, E., Gazzano, M., Bigi, A. (2010). Ionic substitutions in calcium phosphates synthesized at low temperature. Acta biomaterialia 6(6), 1882–1894.

Bocherens, H., Brinkman, D. B., Dauphin, Y., Mariotti, A. (1994). Microstructural and geochemical investigations on Late Cretaceous archosaur teeth from Alberta, Canada. Canadian Journal of Earth Sciences 31(5), 783–792.

Bolt, J. R., DeMar, R. E. (1986). Computer simulation of tooth replacement with growth in lower tetrapods. Journal of Vertebrate Paleontology 6(3), 233–250.

Boonstra, L. D. (1969). The fauna of the Tapinocephalus Zone (Beaufort beds of the Karoo). Annals of the South African Museum 56, 1–73.

Boskey, A. L., Posner, A. S. (1976). In vitro nucleation of hydroxyapatite by a bone calcium-phospholipid-phosphate complex. Calcified Tissue Research 22(1), 197–201.

Botha, J., Smith, R. M. (2006). Rapid vertebrate recuperation in the Karoo Basin of South Africa following the end-Permian extinction. Journal of African Earth Sciences 45(4–5), 502–514.

Botha, J., Smith, R. M. (2007). Lystrosaurus species composition across the Permo–Triassic boundary in the Karoo Basin of South Africa. Lethaia 40(2), 125–137.

Botha, J., Lee-Thorp, J., Chinsamy, A. (2005). The palaeoecology of the non-mammalian cynodonts *Diademodon* and *Cynognathus* from the Karoo Basin of South Africa, using stable light isotope analysis. Palaeogeography, Palaeoclimatology, Palaeoecology 223(3–4), 303–316.

Bourdon, B., Turner, S., Henderson, G. M., Lundstrom, C. C. (2003). Introduction to U-series geochemistry. Reviews in mineralogy and geochemistry 52(1), 1–21.

Bourgon, N., Jaouen, K., Bacon, A. M., Jochum, K. P., Dufour, E., Duringer, P., Ponche, J. L., Joannes-Boyau, R., Boesch, Q., Antoine, P. O., Hullot, M. (2020). Zinc isotopes in Late Pleistocene fossil teeth from a Southeast Asian cave setting preserve paleodietary information. Proceedings of the National Academy of Sciences 117(9), 4675–4681.

Boy, J. A. (2003). Paläoökologische Rekonstruktion von Wirbeltieren: Möglichkeiten und Grenzen. Paläontologische Zeitschrift 77(1), 123–152.

Boy, J. A. (2007). Als die Saurier noch klein waren: Tetrapoden im Permokarbon. In: Schindler, T .and Heidtke, U. H. J. (eds.), Kohlesümpfe, Seen und Halbwüsten, 256–286. Pollichia Sonderveröffentlichungen 10, Bad Dürkheim.

Boy, J. A., Schindler, T. (2000). Ökostratigraphische Bioevents im Grenzbereich Stephanium/Autunium (höchstes Karbon) des Saar-Nahe-Beckens (SW-Deutschland) und benachbarter Gebiete. Neues Jahrbuch für Geologie und Paläontologie-Abhandlungen, 89–152.

Boy, J. A., Schindler, T. (2012). Ökostratigraphie des Rotliegend. Schriftenreihe der Deutschen Gesellschaft für Geowissenschaften, 143–160.

Bökenschmidt, S. (2006). Die Fossillagerstätte Korbacher Spalte—ihre Entstehung und Einordnung in den Zechstein Nord-Hessens. Dissertation Philipps Universität Marburg, Germany.

Bökenschmidt, S., Braun, A., Heggemann, H., Zankl, H. (1999). Oberpermische Spaltensedimente bei Dorfitter südlich von Korbach und ihre Beziehungen zur Fossillagerstätte Korbacher Spalte. Geologisches Jahrbuch Hessen 127, 19–31.

Böhm, K., Winkler, D. E., Kaiser, T. M., Tütken, T. (2019). Post-mortem alteration of diet-related enamel surface textures through artificial biostratinomy: a tumbling experiment using mammal teeth. Palaeogeography, Palaeoclimatology, Palaeoecology 518, 215–231.

Brand, U., Blamey, N., Garbelli, C., Griesshaber, E., Posenato, R., Angiolini, L., Azmy, K., Farabegoli, E., Came, R. (2016). Methane Hydrate: Killer cause of Earth's greatest mass extinction. Palaeoworld 25(4), 496–507.

Brink, K. S. (2015). Case 3695 *Dimetrodon* Cope, 1878 (Synapsida, sphenacodontidae): proposed conservation by reversal of precedence with *Bathygnathus* Leidy, 1853. The Bulletin of Zoological Nomenclature 72(4), 297–299.

Brink, K. S., Reisz, R. R. (2014). Hidden dental diversity in the oldest terrestrial apex predator *Dimetrodon*. Nature Communications 5(1), 1–9.

Brink, K. S., Maddin, H. C., Evans, D. C., Reisz, R. R. (2015). Re-evaluation of the historic Canadian fossil *Bathygnathus borealis* from the Early Permian of Prince Edward Island. Canadian Journal of Earth Sciences 52(12), 1109–1120.

Brink, K. S., MacDougall, M. J., Reisz, R. R. (2019). *Dimetrodon* (Synapsida: Sphenacodontidae) from the cave system at Richards Spur, OK, USA, and a comparison of Early Permian–aged vertebrate paleoassemblages. The Science of Nature 106(1–2), 2.

Brocklehurst, N. (2015). The early evolution of Synapsida (Vertebrata, Amniota) and the quality of their fossil record. Dissertation, Humboldt-Universität zu Berlin, Germany.

Brocklehurst, N. (2019). Morphological evolution in therocephalians breaks the hypercarnivore ratchet. Proceedings of the Royal Society B 286(1900), 20190590.

Brocklehurst, N., Fröbisch, J. (2017). A re-examination of the enigmatic Russian tetrapod *Phreatophasma aenigmaticum* and its evolutionary implications. Fossil Record 20(1), 87–93.

Brocklehurst, N., Kammerer, C. F., Fröbisch, J. (2013). The early evolution of synapsids, and the influence of sampling on their fossil record. Paleobiology 39(3), 470–490.

Bronk Ramsey, C. (2008). Radiocarbon dating: revolutions in understanding. Archaeometry 50(2), 249–275.

Brügmann, G., Krause, J., Brachert, T. C., Kullmer, O., Schrenk, F., Ssemmanda, I., Mertz, D. F. (2012). Chemical composition of modern and fossil Hippopotamid teeth and implications for paleoenvironmental reconstructions and enamel formation-Part 1: Major and minor element variation. Biogeosciences 9(1), 119.

Budaev, S. V. (2010). Using principal components and factor analysis in animal behaviour research: caveats and guidelines. Ethology 116(5), 472–480.

Budd, P., Montgomery, J., Barreiro, B., Thomas, R. G. (2000). Differential diagenesis of strontium in archaeological human dental tissues. Applied geochemistry 15(5), 687–694.

Bulanov, V. V., Yashina, O. V. (2005). *Elginiid pareiasaurs* of eastern Europe. Paleontological Journal C/C of Paleontologicheskii Zhurnal 39(4), 428.

Burgess, S. D., Bowring, S. A. (2015). High-precision geochronology confirms voluminous magmatism before, during, and after Earth's most severe extinction. Science advances 1(7), e1500470.

Burgess, S. D., Bowring, S., Shen, S. Z. (2014). High-precision timeline for Earth's most severe extinction. Proceedings of the National Academy of Sciences 111(9), 3316–3321.

Burkhardt, R., Bartl, R., Frisch, B., Jager, K., Mahl, C., Hill, W., Kettner, G. (1984). The structural relationship of bone forming and endothelial cells of the bone marrow (p. 2–14). In: Arlet J, Ficat RP, Hungerford DS (eds) Bone circulation. Williams and Wilkins Baltimore.

Burton, J. H., Price, T. D., Middleton, W. D. (1999). Correlation of bone Ba/Ca and Sr/Ca due to biological purification of calcium. Journal of Archaeological Science 26(6), 609–616.

Bryant, J. D. (1991). New early Barstovian (middle Miocene) vertebrates from the upper Torreya Formation, eastern Florida panhandle. Journal of Vertebrate Paleontology 11(4), 472–489.

Bryant, J. D., Froelich, P. N. (1995). A model of oxygen isotope fractionation in body water of large mammals. Geochimica et Cosmochimica Acta 59(21), 4523–4537.

Cabreira, S. F., Cisneros, J. C. (2009). Tooth histology of the parareptile *Soturnia caliodon* from the Upper Triassic of Rio Grande do Sul, Brazil. Acta Palaeontologica Polonica 54(4), 743–748.

Cabrera-Chávez-Costa, A. A., Galván-Magaña, F., Escobar-Sánchez, O. (2010). Food habits of the silky shark *Carcharhinus falciformis* (Müller and Henle, 1839) off the western coast of Baja California Sur, Mexico. Journal of Applied Ichthyology 26(4), 499–503.

Calandra, I., Merceron, G. (2016). Dental microwear texture analysis in mammalian ecology. Mammal Review 46(3), 215–228.

Calandra, I., Göhlich, U. B., Merceron, G. (2008). How could sympatric megaherbivores coexist? Example of niche partitioning within a proboscidean community from the Miocene of Europe. Naturwissenschaften 95(9), 831–838.

Calandra, I., Schulz, E., Pinnow, M., Krohn, S., Kaiser, T. M. (2012). Teasing apart the contributions of hard dietary items on 3D dental microtextures in primates. Journal of Human Evolution 63(1), 85–98.

Campbell, I. H., Czamanske, G. K., Fedorenko, V. A., Hill, R. I., Stepanov, V. (1992). Synchronism of the Siberian Traps and the Permian-Triassic boundary. Science 258(5089), 1760–1763.

Campione, N. E., Reisz, R. R. (2010). *Varanops brevirostris* (Eupelycosauria: Varanopidae) from the Lower Permian of Texas, with discussion of varanopid morphology and interrelationships. Journal of Vertebrate Paleontology 30(3), 724–746.

Carpenter, K., Valdestamon, R. (2017). "*Carcharhinus obscurus*" (Online). FishBase. Accessed November 21, 2017 at http://www.fishbase.org/summary/Carcharhinus-obscurus.html.

Carroll, R. L. (1964). The earliest reptiles. Zoological Journal of the Linnean Society 45(304), 61–83.

Carter, D. O., Yellowlees, D., Tibbett, M. (2007). Cadaver decomposition in terrestrial ecosystems. Naturwissenschaften 94(1), 12–24.

Case, E. C. (1915). The Permo-Carboniferous red beds of North America and their vertebrate fauna (Vol. 207). Carnegie Institution of Washington.

Catuneanu, O., Wopfner, H., Eriksson, P. G., Cairncross, B., Rubidge, B. S., Smith, R. M. H., Hancox, P. J. (2005). The Karoo basins of south-central Africa. Journal of African Earth Sciences 43(1–3), 211–253.

Catz, N., Bignon-Lau, O., Merceron, G. (2020). Reindeer feeding ecology and hunting strategies by Magdalenians from Pincevent (Paris Basin, France): New insights from dental microwear textural analyses. International Journal of Osteoarchaeology 30(4), 519–528.

Cenki-Tok, B., Chabaux, F., Lemarchand, D., Schmitt, A. D., Pierret, M. C., Viville, D., Bagard, M.-L., Stille, P. (2009). The impact of water–rock interaction and vegetation on calcium isotope fractionation in soil-and stream waters of a small, forested catchment (the Strengbach case). Geochimica et Cosmochimica Acta 73(8), 2215–2228.

Chajewski, M. (2009). rela: Scale item analysis. R package version, 4.

Chander, S., Fuerstenau, D. W. (1984). Solubility and interfacial properties of hydroxyapatite: a review (p. 29–49). In: Misra D.N. (ed) Adsorption on and surface chemistry of hydroxyapatite. Springer, Boston, MA.

Child, A. M. (1995). Microbial taphonomy of archaeological bone. Studies in conservation 40(1), 19–30.

Chu, N. C., Henderson, G. M., Belshaw, N. S., Hedges, R. E. (2006). Establishing the potential of Ca isotopes as proxy for consumption of dairy products. Applied geochemistry 21(10), 1656–1667.

Churchill, D. A., Heithaus, M. R., Vaudo, J. J., Grubbs, R. D., Gastrich, K., Castro, J. I. (2015). Trophic interactions of common elasmobranchs in deep-sea communities of the Gulf of Mexico revealed through stable isotope and stomach content analysis. Deep Sea Research Part II: Topical Studies in Oceanography 115, 92–102.

Clack, J. A. (2012). Gaining ground: the origin and evolution of tetrapods (pp. 526). Indiana University Press.

Clarke, A. D., Telmer, K. H., Mark Shrimpton, J. (2007). Elemental analysis of otoliths, fin rays and scales: a comparison of bony structures to provide population and life-history information for the Arctic grayling (*Thymallus arcticus*). Ecology of Freshwater Fish 16(3), 354–361.

Clarke, C., Lea, J. S. E., Ormond, R. F. G. (2011). Reef-use and residency patterns of a baited population of silky sharks, *Carcharhinus falciformis*, in the Red Sea. Marine and Freshwater Research 62(6), 668–675.

Clarkson, M. O., Kasemann, S. A., Wood, R. A., Lenton, T. M., Daines, S. J., Richoz, S., Ohnemueller, F., Meixner, A., Poulton, S. W., Tipper, E. T. (2015). Ocean acidification and the Permo-Triassic mass extinction. Science, 348(6231), 229–232.

Clementz, M. T., Holden, P., Koch, P. L. (2003). Are calcium isotopes a reliable monitor of trophic level in marine settings? International Journal of Osteoarchaeology 13(1-2), 29–36.

Cliff, G., Dudley, S. F. J. (1991). Sharks caught in the protective gill nets off Natal, South Africa. 4. The bull shark *Carcharhinus leucas* Valenciennes. South African Journal of Marine Science 10(1), 253–270.

Cliff, N. (1996). Ordinal Methods for Behavioral Data Analysis (pp. 196). Erlbaum, Mahwah, New Jersey.

Cliff, N. (2014). Ordinal methods for behavioral data analysis (pp. 196). East Sussex, Psychology Press.

Clissold, F. J. (2007). The biomechanics of chewing and plant fracture: mechanisms and implications. Advances in insect physiology 34, 317–372.

Cobaugh, K. L., Schaeffer, S. M., DeBruyn, J. M. (2015). Functional and structural succession of soil microbial communities below decomposing human cadavers. PLoS ONE 10(6), e0130201.

Collins, M. J., Riley, M. S., Child, A. M., Turner-Walker, G. (1995). A basic mathematical simulation of the chemical degradation of ancient collagen. Journal of Archaeological Science 22(2), 175–183.

Collins, M. J., Gernaey, A. M., Nielsen-Marsh, C. M., Vermeer, C., Westbroek, P. (2000). Osteocalcin in fossil bones: evidence of very slow rates of decomposition from laboratory studies. Geology 28(12), 1139–1142.

Collins, M. J., Nielsen–Marsh, C. M., Hiller, J., Smith, C. I., Roberts, J. P., Prigodich, R. V., Wess, T. J., Csapò, J., Millard, A. R. Turner–Walker, G. (2002). The survival of organic matter in bone: a review. Archaeometry 44(3), 383–394.

Compagno, L. J. V. (1984a). Vol. 4. Sharks of the world. An annotated and illustrated catalogue of shark species known to date. Part 1 - Hexanchiformes to Lamniformes (pp. 249). In: FAO species catalogue.

Compagno, L. J. V. (1984b). Vol. 4. Sharks of the world. An annotated and illustrated catalogue of shark species known to date. Part 2. Carcharhiniformes FAO species catalogue, 251–655.

Compagno, L. J. V. (1990). Alternative life-history styles of cartilaginous fishes in time and space. Environmental Biology of Fishes 28(1–4), 33–75.

Compagno, L. J. V., Niem, V. H. (1998). Triakidae. Houndsharks, smoothhounds, topes. In: K.E. Carpenter and V.H. Niem (eds) FAO identification guide for fishery purposes. The Living Marine Resources of the Western Central Pacific (p. 1297–1304). Rome.

Compagno, L. J. V., Dando, M., Fowler, S. (2005). A field guide to the sharks of the world (pp. 368). Princeton University Press, New Jersey.

Connolly, R. M., Guest, M. A., Melville, A. J., Oakes, J. M. (2004). Sulfur stable isotopes separate producers in marine food-web analysis. Oecologia 138(2), 161–167.

Cook, P. J., Shergold, J. H. (1984). Phosphorus, phosphorites and skeletal evolution at the Precambrian—Cambrian boundary. Nature 308(5956), 231–236.

Cooper Jr, W. E., Vitt, L. J. (2002). Distribution, extent, and evolution of plant consumption by lizards. Journal of Zoology 257(4), 487–517.

Cope, E. D. (1878). Descriptions of extinct Batrachia and Reptilia from the Permian formation of Texas. Proceedings of the American Philosophical Society 17(101), 505–530.

Copeland, S. R., Sponheimer, M., Lee-Thorp, J. A., le Roux, P. J., de Ruiter, D. J., Richards, M. P. (2010). Strontium isotope ratios in fossil teeth from South Africa: assessing laser ablation MC-ICP-MS analysis and the extent of diagenesis. Journal of Archaeological Science 37(7), 1437–1446.

Cortés, E. (1999). Standardized diet compositions and trophic levels of sharks. ICES Journal of marine science 56(5), 707–717.

Cortes, E., Parsons, G. R. (1996). Canadian Journal of Fisheries and Aquatic Sciences. National Research Council of Canada, Canada.

Cortes, E., Manire, C. A., Hueter, R. E. (1996). Diet, feeding habits, and diel feeding chronology of the bonnethead shark, *Sphyrna tiburo*, in southwest Florida. Bulletin of Marine Science 58(2), 353–367.

Cowie, S. M., Knippertz, P., Marsham, J. H. (2014). A climatology of dust emission events from northern Africa using long-term surface observations. Atmospheric Chemistry and Physics 14(16), 8579–8597.

Cox, C. B., Angielczyk, K. D. (2015). A new endothiodont dicynodont (Therapsida, Anomodontia) from the Permian Ruhuhu Formation (Songea Group) of Tanzania and its feeding system. Journal of Vertebrate Paleontology 35(4), e935388.

Cressler, W. L., Daeschler, E. B., Slingerland, R., Peterson, D. A. (2010). Terrestrialization in the Late Devonian: a palaeoecological overview of the Red Hill site, Pennsylvania, USA. Geological Society, London, Special Publications 339(1), 111–128.

Crompten, A. W., Hotten, N. (1967). Functional morphology of the masticatory apparatus of two dicynodonts (Reptilia, Therapsida). Postilla 109, 1–51.

Currey, J. D. (2003). Role of collagen and other organics in the mechanical properties of bone. Osteoporosis International 14(5), 29–36.

Dahl, T. W., Hammarlund, E. U., Anbar, A. D., Bond, D. P., Gill, B. C., Gordon, G. W., Knoll, A. H., Nielsen, A.T., Schovsbo, N. H., Canfield, D. E. (2010). Devonian rise in atmospheric oxygen correlated to the radiations of terrestrial plants and large predatory fish. Proceedings of the National Academy of Sciences 107(42), 17911–17915.

Dahlberg, A. A., Kinzey, W. (1962). Etude microscopique de l'abrasion et de l'attrition sur la surface des dents. Bulletin du Groupement International pour la Recherche Scientifique en Stomatologie et Odontologie (Bruxelles) 5, 242–251.

Damiani, R. J., Rubidge, B. S. (2003). A review of the South African temnospondyl amphibian record. Palaeontologia Africana 39, 21 – 36.

Damuth, J., Janis, C. M. (2011). On the relationship between hypsodonty and feeding ecology in ungulate mammals, and its utility in palaeoecology. Biological Reviews 86(3), 733–758.

Dauphin, Y., Andrews, P., Denys, C., Jalvo, Y. F., Williams, T. (2003). Structural and chemical bone modifications in a modern owl pellet assemblage from Olduvai Gorge (Tanzania). Journal of taphonomy 1(4), 209–232.

Dauphin, Y., Castillo-Michel, H., Denys, C., El Hajraoui, M. A., Nespoulet, R., Stoetzel, E. (2018). Diagenetic alterations of *Meriones* incisors (Rodentia) of El Harhoura 2 cave, Morocco (late Pleistocene–middle Holocene). PalZ 92(1), 163–177.

DeNiro, M. J., Epstein, S. (1978). Influence of diet on the distribution of carbon isotopes in animals. Geochimica et cosmochimica acta 42(5), 495–506.

DeNiro, M. J., Epstein, S. (1981). Influence of diet on the distribution of nitrogen isotopes in animals. Geochimica et cosmochimica acta 45(3), 341–351.

Denys, C. (2002). Taphonomy and experimentation. Archaeometry 44(3), 469–484.

DePaolo, D. J. (2011). Surface kinetic model for isotopic and trace element fractionation during precipitation of calcite from aqueous solutions. Geochimica et cosmochimica acta 75(4), 1039–1056.

DeSantis, L. R., Schubert, B. W., Scott, J. R., Ungar, P. S. (2012). Implications of diet for the extinction of saber-toothed cats and American lions. PLoS ONE 7(12), e52453.

DeSantis, L. R., Scott, J. R., Schubert, B. W., Donohue, S. L., McCray, B. M., Van Stolk, C. A., Winburn, A. A., Greshko, M.A., O'Hara, M. C. (2013). Direct comparisons of 2D and 3D dental microwear proxies in extant herbivorous and carnivorous mammals. PLoS ONE 8(8), e71428.

DeSantis, L. R., Schubert, B. W., Schmitt-Linville, E., Ungar, P. S., Donohue, S. L., Haupt, R. J. (2015). Dental microwear textures of carnivorans from the La Brea Tar Pits, California and potential extinction implications. Contributions in Science, Los Angeles County Museum of Natural History 42, 37–52.

DeSantis, L. R., Tseng, Z. J., Liu, J., Hurst, A., Schubert, B. W., Jiangzuo, Q. (2017). Assessing niche conservatism using a multiproxy approach: dietary ecology of extinct and extant spotted hyenas. Paleobiology 43(2), 286–303.

de Souza, G. F., Reynolds, B. C., Kiczka, M., Bourdon, B. (2010). Evidence for mass-dependent isotopic fractionation of strontium in a glaciated granitic watershed. Geochimica et Cosmochimica Acta 74(9), 2596–2614.

Dicken, M. L., Kock, A. A., Hardenberg, M. (2015). First observations of dusky sharks (*Carcharhinus obscurus*) attacking a humpback whale (*Megaptera novaeangliae*) calf. Marine and Freshwater Research 66(12), 1211–1215.

DiMichele, W. A., Hook, R. W., Beerbower, R., Boy, J. A., Gastaldo, R. A., Hotton III, N., Phillips, T. L., Scheckler, S. E., Shear, W. A., Sues, H. D. (1992). Paleozoic terrestrial ecosystems. In: Behrensmeyer A. K., Damuth, J. D., DiMichelle, W. A. (eds) Terrestrial ecosystems through time (p. 205–325). University of Chicago Press, Chicago.

Dodick, J. T., Modesto, S. P. (1995). The cranial anatomy of the captorhinid reptile *Labidosaurikos meachami* from the Lower Permian of Oklahoma. Palaeontology 38(3), 687.

Dodson, P. (1973). The significance of small bones in paleoecological interpretation. Rocky Mountain Geology 12(1), 15–19.

Domokos, G., Jerolmack, D. J., Sipos, A. Á., Török, Á. (2014). How river rocks round: resolving the shape-size paradox. PLoS ONE 9(2), e88657.

Dorozhkin, S. V. (2012). Dissolution mechanism of calcium apatites in acids: A review of literature. World journal of methodology 2(1), 1.

Dorozhkin, S. V., Epple, M. (2002). Biological and medical significance of calcium phosphates. Angewandte Chemie International Edition 41(17), 3130–3146.

Doubleday, Z. A., Cliff, J., Izzo, C., Gillanders, B. M. (2018). Untapping the potential of sulfur isotope analysis in biominerals. Marine Ecology Progress Series 598, 159–166.

Dragulescu, A. A. (2014). Read, write, format Excel 2007 and Excel 97/2000/XP/2003 files. R package, version 0.5.7. Available at https://CRAN.R-project.org/package=xlsx.

Dunnett, C. W. (1980). Pairwise multiple comparisons in the unequal variance case. Journal of the American Statistical Association 75(372), 796–800.

Ebert, D. A. (1991). Observations on the predatory behaviour of the sevengill shark *Notorynchus cepedianus*. South African Journal of Marine Science 11(1), 455–465.

Ebert, D. A. (2002). Ontogenetic changes in the diet of the sevengill shark (*Notorynchus cepedianus*). Marine and Freshwater Research 53(2), 517–523.

Ebert, D.A. (2003). The sharks, rays and chimaeras of California (p. 103 – 104). University of California Press.

Eberth, D. A., Berman, D. S., Sumida, S. S., Hopf, H. (2000). Lower Permian terrestrial paleoenvironments and vertebrate paleoecology of the Tambach Basin (Thuringia, central Germany): the upland holy grail. Palaios 15(4), 293–313.

Eddelbuettel, D.F. (2011). Rcpp: Seamless R and C++ Integration. Journal of Statistical Software 40, 1–18.

Eddelbuettel, D.F. (2013). Seamless R and C++ Integration with Rcpp (pp. 220). Springer, New York.

Edler, A. L. (2000). Late Triassic dicynodonts: their anatomy, relationships, and paleobiogeography. Dissertation, Texas Tech University, U.S.A..

Eagle, R., Schauble, E., Tripati, A., Tütken, T., Fricke, H., Hulbert, R., Eiler, J. (2010). 'Clumped isotope'thermometry in bioapatite. Geochimica et Cosmochimica Acta 74(12), A256.

Eagle, R. A., Tütken, T., Martin, T. S., Tripati, A. K., Fricke, H. C., Connely, M., Cifelli, R. L., Eiler, J. M. (2011). Dinosaur body temperatures determined from isotopic (13C-18O) ordering in fossil biominerals. Science 333(6041), 443–445.

Edmund, A. G. (1960). Tooth replacement phenomena in the lower vertebrates. Life sciences contributions. Royal Ontario Museum 52, 1–190.

Ehret, D. J., MacFadden, B. J., Salas-Gismondi, R. (2009). Caught in the act: trophic interactions between a 4-million-year-old white shark (*Carcharodon*) and mysticete whale from Peru. Palaios 24(5), 329–333.

Ellis, J. K., Musick, J. A. (2007). Ontogenetic changes in the diet of the sandbar shark, *Carcharhinus plumbeus*, in lower Chesapeake Bay and Virginia (USA) coastal waters. Environmental biology of fishes 80(1), 51–67.

Enax, J., Prymak, O., Raabe, D., Epple, M. (2012). Structure, composition, and mechanical properties of shark teeth. Journal of structural biology 178(3), 290–299.

Enax, J., Janus, A. M., Raabe, D., Epple, M., Fabritius, H. O. (2014). Ultrastructural organization and micromechanical properties of shark tooth enameloid. Acta biomaterialia 10(9), 3959–3968.

Ericson, J. E. (1985). Strontium isotope characterization in the study of prehistoric human ecology. Journal of human evolution 14(5), 503–514.

Eriksen, E. F. (1986). Normal and pathological remodelling of human trabecular bone: three dimensional reconstruction of the remodelling sequence in normal and in metabolic bone disease. Endocrine reviews 7(4), 379–408.

Eriksen, E. F. (2010). Cellular mechanisms of bone remodelling. Reviews in Endocrine and Metabolic Disorders 11(4), 219–227.

Erwin, D. H. (1990). The end-Permian mass extinction. Annual Review of Ecology and Systematics 21(1), 69–91.

Erwin, D. H. (2015). Extinction: How Life on Earth Nearly Ended 250 Million Years Ago-Updated Edition (Vol. 37, pp. 295). Princeton and Oxford, Princeton University Press.

Espinoza, M., Munroe, S. E., Clarke, T. M., Fisk, A. T., Wehrtmann, I. S. (2015). Feeding ecology of common demersal elasmobranch species in the Pacific coast of Costa Rica inferred from stable isotope and stomach content analyses. Journal of Experimental Marine Biology and Ecology 470, 12–25.

Fassbender, H. W., Lin, H. C., Ulrich, B. (1966). Löslichkeit und Löslichkeitsprodukt von Hydroxylapatit und Rohphosphaten. Zeitschrift für Pflanzenernährung, Düngung, Bodenkunde 112(2), 101–113.

Featherstone, J. D. B., Nelson, D. G. A. (1980). The effect of fluoride, zinc, strontium, magnesium and iron on the crystal-structural disorder in synthetic carbonated apatites. Australian Journal of Chemistry 33(11), 2363–2368.

Fernández-Jalvo, Y., Andrews, P., Sevilla, P., Requejo, V. (2014). Digestion versus abrasion features in rodent bones. Lethaia 47(3), 323–336.

Fernández-Jalvo, Y., Andrews, P., Denys, C., Sesé, C., Stoetzel, E., Marin-Monfort, D., Pesquero, D. (2016). Taphonomy for taxonomists: implications of predation in small mammal studies. Quaternary Science Reviews 139, 138–157.

Ferrara, T. L., Clausen, P., Huber, D. R., McHenry, C. R., Peddemors, V., Wroe, S. (2011). Mechanics of biting in great white and sandtiger sharks. Journal of biomechanics 44(3), 430–435.

Ferrara, T. L. (2012). Bite me: Mechanics of feeding in five species of sharks. Dissertation, University of New South Wales, Australia.

Fichter, J. (1983). Tetrapodenfährten aus dem saarpfälzischen Rotliegenden (Ober-Karbon-Unter-Perm; SW-Deutschland), Teil II: Die Fährten der Gattungen Foliipes, Varanopus, Ichniotherium, Dimetropus, Palmichnus, Phalangichnus, cf. Chelichnus, cf. Laoporus und Anhomoiichnium. Mainzer Naturwissenschaftliches Archiv 21, 125–186.

Fischer, J., Schneider, J. W., Hodnett, J. P. M., Elliott, D. K., Johnson, G. D., Voigt, S., Joachimski, M. M., Tichomirowa, M., Götze, J. (2014). Stable and radiogenic isotope analyses on shark teeth from the Early to the Middle Permian (Sakmarian–Roadian) of the southwestern USA. Historical Biology 26(6), 710–727.

Fisher, D. C. (1981). Taphonomic interpretation of enamel-less teeth in the Shotgun local fauna (Paleocene, Wyoming). The University of Michigan, Contributions from the Museum of Paleontology 25(13), 259–275.

Florida Museum of Natural History, 2005. Biological profiles: Galapagos shark. Retrieved on 26 August 2005, from www.flmnh.ufl.edu/fish/Gallery/Descript/GalapagosShark/Galapagosshark.html. Ichthyology at the Florida Museum of Natural History: Education-Biological Profiles. FLMNH, University of Florida.

Fortelius, M., Solounias, N. (2000). Functional characterization of ungulate molars using the abrasion-attrition wear gradient: a new method for reconstructing paleodiets. American Museum Novitates 2000(3301), 1–36.

Fraser, D., Theodor, J. M. (2011). Comparing ungulate dietary proxies using discriminant function analysis. Journal of Morphology 272(12), 1513–1526.

Fraser, G. J., Thiery, A. P. (2018). Evolution, Development and Regeneration of Fish Dentitions (p. 16 –172). In: Johanson, Z., Underwood, C., Richter, M. (eds) Evolution and Development of Fishes.

Fricke, H. C., O'Neil, J. R. (1996). Inter-and intra-tooth variation in the oxygen isotope composition of mammalian tooth enamel phosphate: implications for palaeoclimatological and palaeobiological research. Palaeogeography, Palaeoclimatology, Palaeoecology 126(1–2), 91–99.

Fröbisch, J. (2008). Global taxonomic diversity of anomodonts (Tetrapoda, Therapsida) and the terrestrial rock record across the Permian-Triassic boundary. PLoS ONE 3(11), e3733.

Fröbisch, J., Schoch, R. R., Müller, J., Schindler, T., Schweiss, D. (2011). A new basal sphenacodontid synapsid from the Late Carboniferous of the Saar-Nahe Basin, Germany. Acta Palaeontologica Polonica 56(1), 113–120.

Garbelli, C., Angiolini, L., Brand, U., Shen, S. Z., Jadoul, F., Posenato, R., Azmy, K., Cao, C. Q. (2016). Neotethys seawater chemistry and temperature at the dawn of the end Permian mass extinction. Gondwana Research 35, 272–285.

Garbelli, C., Angiolini, L., Shen, S. Z. (2017). Biomineralization and global change: A new perspective for understanding the end-Permian extinction. Geology 45(1), 19–22.

Garçon, M., Sauzeat, L., Carlson, R. W., Shirey, S. B., Simon, M., Balter, V., Boyet, M. (2017). Nitrile, latex, neoprene and vinyl gloves: a primary source of contamination for trace element and Zn isotopic analyses in geological and biological samples. Geostandards and Geoanalytical Research 41(3), 367–380.

Gengsheng, Y., Honglang, X., Wanquan, T. (2001). Black windstorm in northwest china: a case study of the strong sand-dust storm on may 5th 1993 (p. 45–77). In Global alarm: dust and sandstorms from the World's Drylands. RCU of the United Nations Convention to Combat Desertification (UNCCD), Bangkok.

George, D., Blieck, A. (2011). Rise of the earliest tetrapods: an early Devonian origin from marine environment. PLoS ONE 6(7), e22136.

Goedert, J., Fourel, F., Amiot, R., Simon, L., Lécuyer, C. (2016). High-precision 34S/32S measurements in vertebrate bioapatites using purge-and-trap elemental analyser/isotope ratio mass spectrometry technology. Rapid Communications in Mass Spectrometry 30(18), 2002–2008.

Goldberg, M., Smith, A. J. (2004). Cells and extracellular matrices of dentin and pulp: a biological basis for repair and tissue engineering. Critical Reviews in Oral Biology and Medicine 15(1), 13–27.

Gordon, K. D. (1983). Taphonomy of dental microwear-Can fossil microwear be studied productively. American Journal of Physical Anthropology 60(2), 200–200.

Gordon, K. D. (1984). Taphonomy of dental microwear. 2. American Journal of Physical Anthropology 63(2), 164–165.

Gordon, K. D. (1988). A review of methodology and quantification in dental microwear analysis. Scanning microscopy 2(2), 1139–1147.

Graham, M., Allington-Jones, L. (2018). The air-abrasive technique: a re-evaluation of its use in fossil preparation. Palaeontologia Electronica 21.2.2T, 1–15

Green, J. L., Resar, N. A. (2012). The link between dental microwear and feeding ecology in tree sloths and armadillos (Mammalia: Xenarthra). Biological Journal of the Linnean Society 107(2), 277–294.

Grémillet, D. J., Plös, A. L. (1994). The use of stomach temperature records for the calculation of daily food intake in cormorants. Journal of Experimental Biology 189(1), 105–115.

Grimm, K. I., Grimm, M. C., Schindler, T. (2000). Lithostratigraphische Gliederung im Rupelium/Chattium des Mainzer Beckens, Deutschland. Neues Jahrbuch für Geologie und Paläontologie-Abhandlungen, 343–397.

Grine, F. E., Ungar, P. S., Teaford, M. F. (2002). Error rates in dental microwear quantification using scanning electron microscopy. Scanning: The Journal of Scanning Microscopies 24(3), 144–153.

Guinot, G., Adnet, S., Cappetta, H. (2012). An analytical approach for estimating fossil record and diversification events in sharks, skates and rays. PLoS ONE 7(9), e44632.

Gussone, N., Heuser, A. (2016). Biominerals and biomaterial (p. 111–144). In Gussone, N., Schmitt, A. D., Heuser, A., Wombacher, F., Dietzel, M., Tipper, E., Schiller, M. (eds) Calcium Stable Isotope Geochemistry. Springer, Berlin, Heidelberg.

Habegger, M. L. (2009). Bite force in two top predators, the great barracuda, *Sphyraena barracuda* and bull shark, *Carcharhinus leucas*, during ontogeny. Dissertation University of South Florida, U.S.A..

Hackett, C. J. (1981). Microscopical focal destruction (tunnels) in exhumed human bones. Medicine, Science and the Law 21(4), 243–265.

Hajj, F., Poszwa, A., Bouchez, J., Guérold, F. (2017). Radiogenic and “stable” strontium isotopes in provenance studies: A review and first results on archaeological wood from shipwrecks. Journal of Archaeological Science 86, 24–49.

Halicz, L., Segal, I., Fruchter, N., Stein, M., Lazar, B. (2008). Strontium stable isotopes fractionate in the soil environments? Earth and Planetary Science Letters 272(1–2), 406–411.

Hancox, P. J., Rubidge, B. S. (1996). The first specimen of the Mid–Triassic dicynodont *Angonisaurus* from the Karoo of South Africa: implications for the dating and biostratigraphy of the Cynognathus Assemblage Zone, Upper Beaufort Group. South African Journal of Science 92(8), 391–392.

Hancox, P. J., Rubidge, B. S. (1997). The role of fossils in interpreting the development of the Karoo Basin. Palaeontologia Africana 33, 41–54.

Hancox, P. J., Rubidge, B. S. (2001). Breakthroughs in the biodiversity, biogeography, biostratigraphy, and basin analysis of the Beaufort Group. Journal of African Earth Sciences 33(3–4), 563–577.

Hancox, P. J., Angielczyk, K. D., Rubidge, B. S. (2013). *Angonisaurus* and *Shansiodon*, dicynodonts (Therapsida, Anomodontia) from subzone C of the Cynognathus assemblage zone (Middle Triassic) of South Africa. Journal of Vertebrate Paleontology 33(3), 655–676.

Happold, D. C. D. (2013). Mammals of Africa. Volume III: Rodents, hares and rabbits (pp. 783). London, Bloomsbury Publishing.

Haq, B. U., Hardenbol, J. A. N., Vail, P. R. (1987). Chronology of fluctuating sea levels since the Triassic. Science 235(4793), 1156–1167.

Harms, J. C., JB, S., RG, W. (1982). Structures and sequences in clastic rocks. SEPM Society for Sedimentary Geology, SEPM Short Course Notes 9.

Hartmann-Weinberg, A. (1930). Zur Systematik der Nord-Düna-Pareiasauridae. Paläontologische Zeitschrift 12(1), 47–59.

Harvey, V. L., Egerton, V. M., Chamberlain, A. T., Manning, P. L., Buckley, M. (2016). Collagen fingerprinting: a new screening technique for radiocarbon dating ancient bone. PLoS ONE 11(3), e0150650.

Hassler, A., Martin, J. E., Amiot, R., Tacail, T., Godet, F. A., Allain, R., Balter, V. (2018). Calcium isotopes offer clues on resource partitioning among Cretaceous predatory dinosaurs. Proceedings of the Royal Society B: Biological Sciences 285(1876), 20180197.

Haughton, S. H., Boonstra, L. D. (1929). Pareiasaurian studies. Part I. An attempt at a classification of the Pareiasauria based on skull features. Annals of the South African Museum 28, 79–87.

Hedges, R. E. (2002). Bone diagenesis: an overview of processes. Archaeometry 44(3), 319–328.

Hedges, R. E., Millard, A. R., Pike, A. W. G. (1995). Measurements and relationships of diagenetic alteration of bone from three archaeological sites. Journal of Archaeological Science 22(2), 201–209.

Heithaus, M. R. (2001). The biology of tiger sharks, *Galeocerdo cuvier*, in Shark Bay, Western Australia: sex ratio, size distribution, diet, and seasonal changes in catch rates. Environmental Biology of Fishes 61(1), 25–36.

Heithaus, M., Dill, L., Marshall, G., Buhleier, B. (2002). Habitat use and foraging behavior of tiger sharks (*Galeocerdo cuvier*) in a seagrass ecosystem. Marine Biology 140(2), 237–248.

Heithaus, M. R., Frid, A., Wirsing, A. J., Dill, L. M., Fourqurean, J. W., Burkholder, D., Thomson, J., Bejder, L. (2007). State-dependent risk-taking by green sea turtles mediates top-down effects of tiger shark intimidation in a marine ecosystem. Journal of Animal Ecology 76(5), 837–844.

Henrici, A. C., Martens, T., Berman, D. S., Sumida, S. S. (2011). An ostodolepid 'microsaur'(Lepospondyli) from the Lower Permian Tambach Formation of central Germany. Journal of Vertebrate Paleontology 31(5), 997–1004.

Hesslein, R. H., Capel, M. J., Fox, D. E., Hallard, K. A. (1991). Stable isotopes of sulfur, carbon, and nitrogen as indicators of trophic level and fish migration in the lower Mackenzie River basin, Canada. Canadian Journal of Fisheries and Aquatic Sciences 48(11), 2258–2265.

Heuser, A., Tütken, T., Gussone, N., Galer, S. J. (2011). Calcium isotopes in fossil bones and teeth—Diagenetic versus biogenic origin. Geochimica et Cosmochimica Acta 75(12), 3419–3433.

Hill, P. A. (1998). Bone remodelling. British journal of orthodontics 25(2), 101–107.

Hillson, S. (2005). Teeth, second edition (pp. 388). Cambridge, Cambridge University Press.

Hines, K. N. (2016). Food habits of Northern Bahamian rock iguanas (*Cyclura cychlura*) in the Exuma Islands, with a dietary review of rock iguanas (genus Cyclura). Herpetological Conservation and Biology 11, 121–138.

Hinz, E. A., Kohn, M. J. (2010). The effect of tissue structure and soil chemistry on trace element uptake in fossils. Geochimica et Cosmochimica Acta 74(11), 3213–3231.

Hirata, T., Tanoshima, M., Suga, A., Tanaka, Y. K., Nagata, Y., Shinohara, A., Chiba, M. (2008). Isotopic analysis of calcium in blood plasma and bone from mouse samples by multiple collector-ICP-mass spectrometry. Analytical Sciences 24(11), 1501–1507.

Hobbs III, C. H. (2004). Geological history of Chesapeake Bay, USA. Quaternary Science Reviews 23(5–6), 641–661.

Hoffmayer, E. R., Franks, J. S., Driggers, W. B., McKinney, J. A., Hendon, J. M., Quattro, J. M. (2014). Habitat, movements and environmental preferences of dusky sharks, *Carcharhinus obscurus*, in the northern Gulf of Mexico. Marine biology 161(4), 911–924.

Holmden, C., Bélanger, N. (2010). Ca isotope cycling in a forested ecosystem. Geochimica et Cosmochimica Acta 74(3), 995–1015.

Hoppe, K. A., Koch, P. L., Carlson, R. W., Webb, S. D. (1999). Tracking mammoths and mastodons: reconstruction of migratory behavior using strontium isotope ratios. Geology 27(5), 439–442.

Hoppe, K. A., Koch, P. L., Furutani, T. T. (2003). Assessing the preservation of biogenic strontium in fossil bones and tooth enamel. International Journal of Osteoarchaeology 13(1-2), 20–28.

Hoppe, K. A., Stover, S. M., Pascoe, J. R., Amundson, R. (2004). Tooth enamel biomineralization in extant horses: implications for isotopic microsampling. Palaeogeography, Palaeoclimatology, Palaeoecology 206(3–4), 355–365.

Hopson, B. J. A. (1964). Tooth replacement in cynodont, dicynodont and therocephalian reptiles. Proceedings of the Zoological Society of London 142 (4), 625–654.

Hotton, N. (1986). Dicynodonts and their role as primary consumers (p 71–82). In: Hotton, N., MacLean, P. D., Roth, J. J., Roth, E. C. (eds). The ecology and biology of mammal-like reptiles. Washington, Smithsonian Institutional Press.

Hotton, N., Olson, E. C., Beerbower, R. (1997). Amniote origins and the discovery of herbivory (p. 207–264). In: Sumida, S., Martin, K. L. M. (eds) Amniote Origins: Completing the Transition to Land. Burlington, San Diego, London, Elsevier Academic Press.

Houston, D. C., Cooper, J. E. (1975). The digestive tract of the whiteback griffon vulture and its role in disease transmission among wild ungulates. Journal of Wildlife Diseases 11(3), 306–313.

Højsgaard, S., Halekoh, U. (2016). doBy: Groupwise statistics, LSmeans, linear contrasts, utilities. R package, version 4.5-15. Available at https://CRAN.R-project.org/package=doBy.

Huber, D. R., Eason, T. G., Hueter, R. E., Motta, P. J. (2005). Analysis of the bite force and mechanical design of the feeding mechanism of the durophagous horn shark *Heterodontus francisci*. Journal of Experimental Biology 208(18), 3553–3571.

Hullot, M., Antoine, P. O., Ballatore, M., Merceron, G. (2019). Dental microwear textures and dietary preferences of extant rhinoceroses (Perissodactyla, Mammalia). Mammal Research 64(3), 397–409.

Hussey, N. E., McCann, H. M., Cliff, G., Dudley, S. F., Wintner, S. P., Fisk, A. T. (2012). Size-based analysis of diet and trophic position of the white shark (*Carcharodon carcharias*) in South African waters. Global perspectives on the biology and life history of the white shark, 27–49.

Huttenlocker, A. K., Sidor, C. A. (2016). The first karenitid (Therapsida, Therocephalia) from the upper Permian of Gondwana and the biogeography of Permo-Triassic therocephalians. Journal of Vertebrate Paleontology 36(4), e1111897.

Hutton, J. M. (1987). Growth and feeding ecology of the Nile crocodile *Crocodylus niloticus* at Ngezi, Zimbabwe. The Journal of Animal Ecology, 25–38.

Ingle, C. P., Sharp, B. L., Horstwood, M. S., Parrish, R. R., Lewis, D. J. (2003). Instrument response functions, mass bias and matrix effects in isotope ratio measurements and semi-quantitative analysis by single and multi-collector ICP-MS. Journal of Analytical Atomic Spectrometry 18(3), 219–229.

Inskeep, W. P., Silvertooth, J. C. (1988). Kinetics of hydroxyapatite precipitation at pH 7.4 to 8.4. Geochimica et Cosmochimica Acta 52(7), 1883–1893.

Irrgeher, J., Galler, P., Prohaska, T. (2016). $^{87}Sr/^{86}Sr$ isotope ratio measurements by laser ablation multicollector inductively coupled plasma mass spectrometry: Reconsidering matrix

interferences in bioapatites and biogenic carbonates. Spectrochimica Acta Part B: Atomic Spectroscopy 125, 31–42.

Itano, W. M. (2019). Oriented microwear on a tooth of *Edestus minor* (Chondrichthyes, Eugeneodontiformes): implication for dental function. Palaeontologia Electronica 22(39), 10–26879.

Jackes, M., Sherburne, R., Lubell, D., Barker, C., Wayman, M. (2001). Destruction of microstructure in archaeological bone: a case study from Portugal. International Journal of Osteoarchaeology 11(6), 415–432.

Jaouen, K., Pons, M. L. (2017). Potential of non-traditional isotope studies for bioarchaeology. Archaeological and Anthropological Sciences 9(7), 1389–1404.

Jaouen, K., Pons, M. L., Balter, V. (2013). Iron, copper and zinc isotopic fractionation up mammal trophic chains. Earth and Planetary Science Letters 374, 164–172.

Jaouen, K., Szpak, P., Richards, M. P. (2016a). Zinc isotope ratios as indicators of diet and trophic level in arctic marine mammals. PLoS ONE 11(3), e0152299.

Jaouen, K., Beasley, M., Schoeninger, M., Hublin, J. J., Richards, M. P. (2016b). Zinc isotope ratios of bones and teeth as new dietary indicators: results from a modern food web (Koobi Fora, Kenya). Scientific reports 6(1), 1–8.

Jaouen, K., Trost, M., Bourgon, N., Colleter, R., Le Cabec, A., Tütken, T., Elias Oliveira, R., Pons, M. L., Méjean, P., Steinbrenner, S., Chmeleff, J. (2020). Zinc isotope variations in archeological human teeth (Lapa do Santo, Brazil) reveal dietary transitions in childhood and no contamination from gloves. PLoS ONE 15(5), e0232379.

Jasinoski, S. C., Rayfield, E. J., Chinsamy, A. (2009). Comparative feeding biomechanics of Lystrosaurus and the generalized dicynodont Oudenodon. The Anatomical Record: Advances in Integrative Anatomy and Evolutionary Biology: Advances in Integrative Anatomy and Evolutionary Biology 292(6), 862–874.

Jernvall, J., Thesleff, I. (2012). Tooth shape formation and tooth renewal: evolving with the same signals. Development 139(19), 3487–3497.

Jochum, K. P., Nohl, U., Herwig, K., Lammel, E., Stoll, B., Hofmann, A. W. (2005). GeoReM: a new geochemical database for reference materials and isotopic standards. Geostandards and Geoanalytical Research 29(3), 333–338.

Jochum, K. P., Stoll, B., Herwig, K., Willbold, M. (2007). Validation of LA-ICP-MS trace element analysis of geological glasses using a new solid-state 193 nm Nd: YAG laser and matrix-matched calibration. Journal of Analytical Atomic Spectrometry 22(2), 112–121.

Johnson, G. A. L. (1981). Geographical evolution from Laurasia to Pangaea. Proceedings of the Yorkshire Geological Society 43(3), 221–252.

Jones, A. M., O'Connell, T. C., Young, E. D., Scott, K., Buckingham, C. M., Iacumin, P., Brasier, M. D. (2001). Biogeochemical data from well preserved 200 ka collagen and skeletal remains. Earth and Planetary Science Letters 193(1–2), 143–149.

Jürgensen, J., Drucker, D. G., Stuart, A. J., Schneider, M., Buuveibaatar, B., Bocherens, H. (2017). Diet and habitat of the saiga antelope during the late Quaternary using stable carbon and nitrogen isotope ratios. Quaternary Science Reviews 160, 150–161.

Kaiser, T. M. (2000). Tooth mesowear analysis on *Hippotherium primigenium* from the Vallesian Dinotheriensande (Germany). Carolinea: Beiträge zur naturkundlichen Forschung in Südwestdeutschland 58, 103–114.

Kalthoff, D. C., Schulz-Kornas, E., Corfe, I., Martin, T., McLoughlin, S., Schultz, J. A. (2019). Complementary approaches to tooth wear analysis in Tritylodontidae (Synapsida, Mammaliamorpha) reveal a generalist diet. PLoS ONE 14(7), e0220188.

Kammerer, C. F. (2015). Cranial osteology of *Arctognathus curvimola*, a short-snouted gorgonopsian from the Late Permian of South Africa. Papers in Palaeontology 1(1), 41–58.

Kammerer, C. F. (2016). A new taxon of cynodont from the Tropidostoma Assemblage Zone (upper Permian) of South Africa, and the early evolution of Cynodontia. Papers in Palaeontology 2(3), 387–397.

Kammerer, C. F., Masyutin, V. (2018). Gorgonopsian therapsids (*Nochnitsa* gen. nov. and *Viatkogorgon*) from the Permian Kotelnich locality of Russia. PeerJ 6, e4954.

Kammerer, C. F., Angielczyk, K. D., Fröbisch, J. (2011). A comprehensive taxonomic revision of *Dicynodon* (Therapsida, Anomodontia) and its implications for dicynodont phylogeny, biogeography, and biostratigraphy. Journal of Vertebrate Paleontology 31(1), 1–158.

Kammerer, C. F., Smith, R. M., Day, M. O., Rubidge, B. S. (2015). New information on the morphology and stratigraphic range of the mid-Permian gorgonopsian *Eriphostoma microdon* Broom, 1911. Papers in Palaeontology 1(2), 201–221.

Kammerer, C. F., Deutsch, M., Lungmus, J. K., Angielczyk, K. D. (2020). Effects of taphonomic deformation on geometric morphometric analysis of fossils: a study using the dicynodont Diictodon feliceps (Therapsida, Anomodontia). PeerJ, 8, e9925.

Karlsruhe, W.M., Sues, H. D. (1993). Gut contents of Parasaurus (Pareiasauria) and Protorosaurus (Archosauromorpha) from the Kupferschiefer (Upper Permian) of Hessen, Germany. Paläontologische Zeitschrift 67(1–2), 169–176.

Kassambara, M.A. (2017). factoextra: Extract and Visualize the Results of Multivariate Data Analyses. R package version 1.0.5. https://CRAN.R-project.org/package=factoextra.

Keenan, S. W. (2016). From bone to fossil: A review of the diagenesis of bioapatite. American Mineralogist 101(9), 1943–1951.

Keenan, S. W., Engel, A. S. (2017). Early diagenesis and recrystallization of bone. Geochimica et Cosmochimica Acta 196, 209–223.

Kemp, T. S. (1969). On the functional morphology of the gorgonopsid skull. Philosophical Transactions of the Royal Society of London. B, Biological Sciences 256(801), 1–83.

Kemp, T. S. (2006). The origin and early radiation of the therapsid mammal-like reptiles: a palaeobiological hypothesis. Journal of evolutionary biology 19(4), 1231–1247.

Kent, B. W. (2018). The cartilaginous fishes (chimaeras, sharks and rays) of Calvert Cliffs, Maryland, USA. Geology and Vertebrate Paleontology of Calvert Cliffs. Smithsonian Contributions to Paleobiology 100, 45–160.

Kermack, K. A. (1956). Tooth replacement in mammal-like reptiles of the suborders Gorgonopsia and Therocephalia. Philosophical Transactions of the Royal Society of London. Series B, Biological Sciences 240(670), 95–133.

King, G. M. (1990). Dicynodonts: a study in palaeobiology (pp. 246). London, Springer.

King, G. M., Oelofsen, B. W., Rubidge, B. S. (1989). The evolution of the dicynodont feeding system. Zoological Journal of the Linnean Society 96(2), 185–211.

King, T., Andrews, P., Boz, B. (1999). Effect of taphonomic processes on dental microwear. American Journal of Physical Anthropology: The Official Publication of the American Association of Physical Anthropologists 108(3), 359–373.

Kissel, R. A., Lehman, T. M. (2002). Upper Pennsylvanian tetrapods from the Ada Formation of Seminole County, Oklahoma. Journal of Paleontology 76(3), 529–545.

Kissel, R. A., Reisz, R. R. (2004). Synapsid fauna of the Upper Pennsylvanian Rock Lake Shale near Garnett, Kansas and the diversity pattern of early amniotes. Recent advances in the origin and early radiation of vertebrates, 409–428.

Kissel, R. (2010). Morphology, phylogeny, and evolution of Diadectidae (Cotylosauria: Diadectomorpha). Dissertation, University of Toronto, Canada.

Klimley, A. P. (1994). The predatory behavior of the white shark. American Scientist 82(2), 122–133.

Knudson, K. J., Williams, H. M., Buikstra, J. E., Tomczak, P. D., Gordon, G. W., Anbar, A. D. (2010). Introducing $\delta^{88/86}$Sr analysis in archaeology: a demonstration of the utility of strontium isotope fractionation in paleodietary studies. Journal of Archaeological Science 37(9), 2352–2364.

Koch, G., Poulsen, S., Espelid, I., Haubek, D. (2017). Pediatric dentistry: a clinical approach (pp. 393). Copenhagen, John Wiley & Sons.

Koch, P. L., Fisher, D. C., Dettman, D. (1989). Oxygen isotope variation in the tusks of extinct proboscideans: a measure of season of death and seasonality. Geology 17(6), 515–519.

Kocsis, L., Ősi, A., Vennemann, T., Trueman, C. N., Palmer, M. R. (2009). Geochemical study of vertebrate fossils from the Upper Cretaceous (Santonian) Csehbánya Formation (Hungary): Evidence for a freshwater habitat of mosasaurs and pycnodont fish. Palaeogeography, Palaeoclimatology, Palaeoecology 280(3–4), 532–542.

Kohn, M. J. (2008). Models of diffusion-limited uptake of trace elements in fossils and rates of fossilization. Geochimica et Cosmochimica Acta 72(15), 3758–3770.

Kohn, M. J., Cerling, T. E. (2002). Stable isotope compositions of biological apatite. Reviews in mineralogy and geochemistry 48(1), 455–488.

Kohn, M. J., Moses, R. J. (2013). Trace element diffusivities in bone rule out simple diffusive uptake during fossilization but explain in vivo uptake and release. Proceedings of the National Academy of Sciences 110(2), 419–424.

Kohn, M. J., Schoeninger, M. J., Barker, W. W. (1999). Altered states: effects of diagenesis on fossil tooth chemistry. Geochimica et cosmochimica acta 63(18), 2737–2747.

Kohn, M. J., Morris, J., Olin, P. (2013). Trace element concentrations in teeth–a modern Idaho baseline with implications for archeometry, forensics, and palaeontology. Journal of Archaeological Science 40(4), 1689–1699.

Konietzko-Meier, D., Shelton, C. D., Sander, P. M. (2016). The discrepancy between morphological and microanatomical patterns of anamniotic stegocephalian postcrania from the Early Permian Briar Creek Bonebed (Texas). Comptes Rendus Palevol 15(1–2), 103–114.

Kowalewski, M., Kelley, P. H., Bambach, Richard K., Baumiller, T. K., Bengtson, S., Brett, C. E., Chin, K., Culver, Stephen J., Dietl, G. P., Farlow, J. O., Gahn, F. J., Haynes, G., Holtz, Thomas Richard, Jr., Jenkins, I., Labandeira, Conrad C., Lipps, J. H., van Valkenburgh, B., Vermeij, G. J., and Walker, S. E. (2002). The fossil record of predation: methods, patterns, and processes. Paleontological Society Special Papers 8, 395–398.

Kreiborg, S., Jensen, B. L. (2018). Tooth formation and eruption–lessons learnt from cleidocranial dysplasia. European journal of oral sciences 126, 72–80.

Kriwet, J., Witzmann, F., Klug, S., Heidtke, U. H. (2008). First direct evidence of a vertebrate three-level trophic chain in the fossil record. Proceedings of the Royal Society B: Biological Sciences 275(1631), 181–186.

Kropacheva, Y. E., Zykov, S. V., Smirnov, N. G., Salimov, R. M. (2019, May). Dental microwear and mesowear of the *Microtus* voles molars before and after experimental feeding of owls. Doklady Biological Sciences 486(1), 79–82.

Kubo, T., Kubo, M. O. (2014). Dental microwear of a Late Triassic dinosauriform, *Silesaurus opolensis*. Acta Palaeontologica Polonica 59(2), 305–312.

Kubo, M. O., Yamada, E., Kubo, T., Kohno, N. (2017). Dental microwear texture analysis of extant sika deer with considerations on inter-microscope variability and surface preparation protocols. Biosurface and Biotribology 3(4), 155–165.

Kubodera, T., Watanabe, H., Ichii, T. (2007). Feeding habits of the blue shark, *Prionace glauca*, and salmon shark, *Lamna ditropis*, in the transition region of the Western North Pacific. Reviews in Fish Biology and Fisheries 17(2–3), 111.

Kulick, J. (1997). Erläuterungen zur Geologischen Karte von Hessen 1: 25.000, Blatt 4719 Korbach, 272 S.

Kulick, J., Paul, J. (1987). Zechsteinaufschlüsse in der Hessischen Senke und am westlichen Harzrand. *Internationales Symposium Zechstein*.

Labandeira, C. C., Allen, E. G. (2007). Minimal insect herbivory for the Lower Permian Coprolite Bone Bed site of north-central Texas, USA, and comparison to other Late Paleozoic floras. Palaeogeography, Palaeoclimatology, Palaeoecology 247(3–4), 197–219.

Laenen, B. (1997). Inorganic and organic geochemistry of a cyclic deposit: the Boom Clay, stratotype of the Rupelian (Belgium). Dissertation, KU Leuven, Belgium.

Last, P. R., Stevens, J. D. (1994). Sharks and rays of Australia (pp.513). Australia, Collingwood, CSIRO Publishing.

Last, P. R. Stevens, J. D. (2009). Sharks and Rays of Australia (pp.513). Second Edition. Australia, Collingwood, CSIRO Publishing.

Laurin, M. (1996). A redescription of the cranial anatomy of *Seymouria baylorensis*, the best known seymouriamorph (Tetrapoda: Batracho− sauria). Paleobios 17, 1–16.

Laurin, M., Reisz, R. R. (1990). Tetraceratops is the oldest known therapsid. Nature 345(6272), 249–250.

Laurin, M., Reisz, R. R. (1995). A reevaluation of early amniote phylogeny. Zoological Journal of the Linnean Society 113(2), 165–223.

Laurin, M., Reisz, R. R. (1996). The osteology and relationships of Tetraceratops insignis, the oldest known therapsid. Journal of Vertebrate Paleontology 16(1), 95–102.

Laurin, M., Reisz, R. R. (1997). A new perspective on tetrapod phylogeny. Amniote origins: completing the transition to land, 9–59.

Laurin, M., Reisz, R. R. (1999). A new study of *Solenodonsaurus janenschi*, and a reconsideration of amniote origins and stegocephalian evolution. Canadian Journal of Earth Sciences 36(8), 1239–1255.

Läng, E., Boudad, L., Maio, L., Samankassou, E., Tabouelle, J., Tong, H., Cavin, L. (2013). Unbalanced food web in a Late Cretaceous dinosaur assemblage. Palaeogeography, Palaeoclimatology, Palaeoecology 381, 26–32.

Lebatard, A. E., Bourles, D. L., Duringer, P., Jolivet, M., Braucher, R., Carcaillet, J., Schuster, M., Arnaud, N., Monie, P., Lihoreau, F., Likius, A., Mackaye, H. T., Vignaud, P., Brunet, M. (2008). Cosmogenic nuclide dating of Sahelanthropus tchadensis and *Australopithecus bahrelghazali*: Mio-Pliocene hominids from Chad. Proceedings of the National Academy of Sciences 105(9), 3226–3231.

LeBlanc, A. R., Reisz, R. R. (2013). Periodontal ligament, cementum, and alveolar bone in the oldest herbivorous tetrapods, and their evolutionary significance. PLoS ONE 8(9), e74697.

Leblanc, A. R., Reisz, R. R. (2015). Patterns of tooth development and replacement in captorhinid reptiles: a comparative approach for understanding the origin of multiple tooth rows. Journal of Vertebrate Paleontology 35(3), e919928.

LeBlanc, A. R., Brink, K. S., Whitney, M. R., Abdala, F., Reisz, R. R. (2018). Dental ontogeny in extinct synapsids reveals a complex evolutionary history of the mammalian tooth attachment system. Proceedings of the Royal Society B 285(1890), 20181792.

Lee, M. S. (1997). A taxonomic revision of pareiasaurian reptiles: implications for Permian terrestrial palaeoecology. Modern Geology 21(3), 231–298.

Lee, M. S., Spencer, P. S. (1997). Crown-clades, key characters and taxonomic stability: when is an amniote not an amniote (p. 61–84)? Amniote origins—Completing the transition to land. London, San Diego, Cambridge: Academic Press.

Lee, Y. C., Chiang, C. C., Huang, P. Y., Chung, C. Y., Huang, T. D., Wang, C. C., Chen, C. I., Chang, R. S., Liao, C. H., Reisz, R. R. (2017). Evidence of preserved collagen in an Early Jurassic sauropodomorph dinosaur revealed by synchrotron FTIR microspectroscopy. Nature communications 8(1), 1–8.

Lee-Thorp, J. A., Van Der Merwe, N. J., Brain, C. K. (1989). Isotopic evidence for dietary differences between two extinct baboon species from Swartkrans. Journal of Human Evolutio, 18(3), 183–189.

Lee-Thorp, J., Thackeray, J. F., van der Merwe, N. (2000). The hunters and the hunted revisited. Journal of Human Evolution 39(6), 565–576.

Lee-Thorp, J. A., Sponheimer, M., Passey, B. H., de Ruiter, D. J., Cerling, T. E. (2010). Stable isotopes in fossil hominin tooth enamel suggest a fundamental dietary shift in the Pliocene. Philosophical Transactions of the Royal Society B: Biological Sciences 365(1556), 3389–3396.

Legfros, R. Z., Sakae, T., Bautista, C., Retino, M., LeGeros, J. P. (1996). Magnesium and carbonate in enamel and synthetic apatites. Advances in Dental Research, 10(2), 225–231.

Leichliter, J. N., Luedecke, T., Foreman, A. D., Duprey, N., Winkler, D., Kast, E. R., Vonhof, H., Sigman, D. M., Haug, G. H., Clauss, M., Tütken, T., Martinez-Garcia, A. (In Review at

Chemical Geology). Nitrogen isotopes in tooth enamel record diet and trophic level enrichment: results from a controlled feeding experiment.

Leigh, S. C., Papastamatiou, Y. P., German, D. P. (2018). Seagrass digestion by a notorious 'carnivore'. Proceedings of the Royal Society B: Biological Sciences 285(1886), 20181583.

Lewis, J., Pike, A. W. G., Coath, C. D., Evershed, R. P. (2017). Strontium concentration, radiogenic ($^{87}Sr/^{86}Sr$) and stable ($\delta^{88}Sr$) strontium isotope systematics in a controlled feeding study. STAR: Science and Technology of Archaeological Research 3(1), 45–57.

Litvinov, F. F., Agapov, S. N., Katalimov, V. G., Mironov, S. G. (1983). Rate of tooth replacement in blue shark, *Prionace glauca* (Carcharhinidae), in relation to feeding. Journal of Ichthyology 23(1), 143–145.

Long, J.A. (2011). The Rise of Fishes; 500 million years of evolution (pp. 287). John Hopkins University Press, Baltimore.

Longinelli, A. (1984). Oxygen isotopes in mammal bone phosphate: a new tool for paleohydrological and paleoclimatological research? Geochimica et cosmochimica Acta 48(2), 385–390.

Lowe, C. G., Wetherbee, B. M., Crow, G. L., Tester, A. L. (1996). Ontogenetic dietary shifts and feeding behavior of the tiger shark, *Galeocerdo cuvier*, in Hawaiian waters. Environmental Biology of Fishes 47(2), 203–211.

Lowenstam, H. A. (1980). Bioinorganic constituents of hard parts. Biogeochemistry of amino acids, 3–16.

Lowenstam, H. A., Margulis, L. (1980). Evolutionary prerequisites for early Phanerozoic calcareous skeletons. Biosystems 12(1–2), 27–41.

Lowenstam, H. A., Weiner, S. (1983). Mineralization by organisms and the evolution of biomineralization (p. 191–203). In: Westbroek P., de Jong E.W. (eds) Biomineralization and Biological Metal Accumulation. Springer, Dordrecht.

Lowenstam, H. A., Weiner, S. (1989). On biomineralization (pp. 323). Oxford University Press on Demand.

Lowry, D., Motta, P. J. (2008). Relative importance of growth and behaviour to elasmobranch suction-feeding performance over early ontogeny. Journal of the Royal Society Interface 5(23), 641–652.

Lowry, D., de Castro, A. L. F., Mara, K., Whitenack, L. B., Delius, B., Burgess, G. H., Motta, P. (2009). Determining shark size from forensic analysis of bite damage. Marine Biology 156(12), 2483–2492.

Lucas, S.G. (2005). PANGAEA (p. 225–228). In: R.C. Selley, L.R.M. Cocks and I.R. Plimer (eds) Encyclopedia of Geology. London, San Diego, Cambridge: Academic Press.

Lucas, S. G. (2006). Global Permian tetrapod biostratigraphy and biochronology. Geological Society, London, Special Publications 265(1), 65–93.

Lucas, S. G. (2009). Timing and magnitude of tetrapod extinctions across the Permo-Triassic boundary. Journal of Asian Earth Sciences 36(6), 491–502.

Lucas, S. G., Heckert, A. B. (2001). Olson's gap: a global hiatus in the record of Middle Permian tetrapods. Journal of Vertebrate Paleontology 21(3), 75A.

Lucifora, L. O., Menni, R. C., Escalante, A. H. (2001). Analysis of dental insertion angles in the sand tiger shark, *Carcharias taurus* (Chondrichthyes: Lamniformes). Cybium 25(1), 23–31.

Lucifora, L. O., García, V. B., Menni, R. C., Escalante, A. H., Hozbor, N. M. (2009). Effects of body size, age and maturity stage on diet in a large shark: ecological and applied implications. Ecological Research 24(1), 109–118.

Luo, Z. X., Kielan-Jaworowska, Z., Cifelli, R. L. (2004). Evolution of dental replacement in mammals. Bulletin of Carnegie Museum of Natural History 2004(36), 159–175.

Lyman, R. L., Lyman, C. (1994). Vertebrate taphonomy (pp. 524). Cambridge, Cambridge University Press.

Maas, M. C., Dumont, E. R. (1999). Built to last: the structure, function, and evolution of primate dental enamel. Evolutionary Anthropology: Issues, News, and Reviews 8(4), 133–152.

Macdougall, M. J., Modesto, S. P. (2011). New information on the skull of the Early Triassic parareptile *Sauropareion anoplus*, with a discussion of tooth attachment and replacement in procolophonids. Journal of Vertebrate Paleontology 31(2), 270–278.

Maddin, H. C., Sidor, C. A., Reisz, R. R. (2008). Cranial anatomy of *Ennatosaurus tecton* (Synapsida: Caseidae) from the Middle Permian of Russia and the evolutionary relationships of Caseidae. Journal of Vertebrate Paleontology 28(1), 160–180.

Maddin, H. C., Mann, A., Hebert, B. (2020). Varanopid from the Carboniferous of Nova Scotia reveals evidence of parental care in amniotes. Nature ecology and evolution 4(1), 50–56.

Mainland, I. L. (2003a). Dental microwear in grazing and browsing Gotland sheep (*Ovis aries*) and its implications for dietary reconstruction. Journal of Archaeological Science 30(11), 1513–1527.

Mainland, I. (2003b). Dental microwear in modern Greek ovicaprids: identifying microwear signatures associated with a diet of leafy-hay. British School at Athens Studies, 45–50.

Maisch, M. W. (2002). Observations on Karoo and Gondwana vertebrates. Part 3: Notes on the gorgonopsians from the Upper Permian of Tanzania. Neues Jahrbuch für Geologie und Paläontologie-Monatshefte, 237–251.

Maisey, J. G. (2012). What is an 'elasmobranch'? The impact of palaeontology in understanding elasmobranch phylogeny and evolution. Journal of Fish Biology 80(5), 918–951.

Maisey, J. G., Naylor, G. J., Ward, D. J. (2004). Mesozoic elasmobranchs, neoselachian phylogeny and the rise of modern elasmobranch diversity. Mesozoic fishes 3, 17–56.

Mann, A., McDaniel, E. J., McColville, E. R., Maddin, H. C. (2019). *Carbonodraco lundi* gen et sp. nov., the oldest parareptile, from Linton, Ohio, and new insights into the early radiation of reptiles. Royal Society open science 6(11), 191191.

Markaida, U., Sosa-Nishizaki, O. (2010). Food and feeding habits of the blue shark *Prionace glauca* caught off Ensenada, Baja California, Mexico, with a review on its feeding. Marine Biological Association of the United Kingdom. Journal of the Marine Biological Association of the United Kingdom 90(5), 977.

Marramà, G., Kriwet, J. (2017). Principal component and discriminant analyses as powerful tools to support taxonomic identification and their use for functional and phylogenetic signal detection of isolated fossil shark teeth. PLoS ONE 12(11), e0188806.

Martens, T. (2005a). First burrow cast of tetrapod origin from the Lower Permian (Tambach Formation) in Germany. Abstract book 65th Annual Meeting Society of Vertebrate Paleontology, 89.

Martens, T., Berman, D. S., Henrici, A. C., Sumida, S. S. (2005b). The Bromacker quarry—the most important locality of Lower Permian terrestrial vertebrate fossils outside of North America. New Mexico Museum of Natural History and Science Bulletin 30, 214–215.

Martin, J. E., Vance, D., Balter, V. (2014). Natural variation of magnesium isotopes in mammal bones and teeth from two South African trophic chains. Geochimica et Cosmochimica Acta 130, 12–20.

Martin, J. E., Tacail, T., Adnet, S., Girard, C., Balter, V. (2015a). Calcium isotopes reveal the trophic position of extant and fossil elasmobranchs. Chemical Geology 415, 118–125.

Martin, J. E., Vance, D., Balter, V. (2015b). Magnesium stable isotope ecology using mammal tooth enamel. Proceedings of the National Academy of Sciences 112(2), 430–435.

Martin, J. E., Deesri, U., Liard, R., Wattanapituksakul, A., Suteethorn, S., Lauprasert, K., Tong, H., Buffetaut, E., Suteethorn, V., Suan, G., Telouk, P., Telouk, P. (2016). Strontium isotopes and the long-term residency of thalattosuchians in the freshwater environment. Paleobiology 42(1), 143–156.

Martin, J. E., Tacail, T., Balter, V. (2017a). Non-traditional isotope perspectives in vertebrate palaeobiology. Palaeontology 60(4), 485–502.

Martin, J. E., Vincent, P., Tacail, T., Khaldoune, F., Jourani, E., Bardet, N., Balter, V. (2017b). Calcium isotopic evidence for vulnerable marine ecosystem structure prior to the K/Pg extinction. Current Biology 27(11), 1641–1644.

Martin, J. E., Tacail, T., Cerling, T. E., Balter, V. (2018). Calcium isotopes in enamel of modern and Plio-Pleistocene East African mammals. Earth and Planetary Science Letters 503, 227–235.

Martínez, L. M., Pérez-Pérez, A. (2004). Post-mortem wear as indicator of taphonomic processes affecting enamel surfaces of hominin teeth from Laetoli and Olduvai (Tanzania): implications to dietary interpretations. Anthropologie. International Journal of Human Diversity and Evolution 42(1), 37–42.

Martisius, N. L., Sidéra, I., Grote, M. N., Steele, T. E., McPherron, S. P., Schulz-Kornas, E. (2018). Time wears on: Assessing how bone wears using 3D surface texture analysis. PLoS ONE 13(11), e0206078.

Mayer, I., Featherstone, J. D. B. (2000). Dissolution studies of Zn-containing carbonated hydroxyapatites. Journal of Crystal Growth 219(1–2), 98–101.

Mazierski, D. M., Reisz, R. R. (2010). Description of a new specimen of *Ianthasaurus hardestiorum* (Eupelycosauria: Edaphosauridae) and a re-evaluation of edaphosaurid phylogeny. Canadian Journal of Earth Sciences 47(6), 901–912.

McArthur, J. M., Howarth, R. J., Bailey, T. R. (2001). Strontium isotope stratigraphy: LOWESS version 3: best fit to the marine Sr-isotope curve for 0–509 Ma and accompanying look-up table for deriving numerical age. The Journal of Geology 109(2), 155–170.

McLennan, L. (2017). Tooth wear, microwear and diet in elasmobranchs. Dissertation, University of Leicester, UK.

Megalofonou, P., Chatzispyrou, A. (2006). Sexual maturity and feeding of the gulper shark, *Centrophorus granulosus*, from the eastern Mediterranean Sea. Cybium 30(4), 67–74.

Melin, A. D., Crowley, B. E., Brown, S. T., Wheatley, P. V., Moritz, G. L., Yit Yu, F. T., Bernard, H., DePaolo, D. J., Jacobson, A. D., Dominy, N. J. (2014). Calcium and carbon stable isotope ratios as paleodietary indicators. American journal of physical anthropology 154(4), 633–643.

Merceron, G., Madelaine, S. (2006). Molar microwear pattern and palaeoecology of ungulates from La Berbie (Dordogne, France): environment of Neanderthals and modern human populations of the Middle/Upper Palaeolithic. Boreas 35(2), 272–278.

Merceron, G., Blondel, C., Brunet, M., Sen, S., Solounias, N., Viriot, L., Heintz, E. (2004). The Late Miocene paleoenvironment of Afghanistan as inferred from dental microwear in artiodactyls. Palaeogeography, Palaeoclimatology, Palaeoecology 207(1–2), 143–163.

Merceron, G., Blondel, C., De Bonis, L., Koufos, G. D., Viriot, L. (2005). A new method of dental microwear analysis: application to extant primates and *Ouranopithecus macedoniensis* (Late Miocene of Greece). Palaios 20(6), 551–561.

Merceron, G., Zazzo, A., Spassov, N., Geraads, D., Kovachev, D. (2006). Bovid paleoecology and paleoenvironments from the Late Miocene of Bulgaria: evidence from dental microwear and stable isotopes. Palaeogeography, Palaeoclimatology, Palaeoecology 241(3–4), 637–654.

Merceron, G., Schulz, E., Kordos, L., Kaiser, T. M. (2007). Paleoenvironment of *Dryopithecus brancoi* at Rudabánya, Hungary: evidence from dental meso-and micro-wear analyses of large vegetarian mammals. Journal of Human Evolution 53(4), 331–349.

Merceron, G., Escarguel, G., Angibault, J. M., Verheyden-Tixier, H. (2010). Can dental microwear textures record inter-individual dietary variations? PLoS ONE 5(3), e9542.

Meyer, C. G., Papastamatiou, Y. P., Holland, K. N. (2010). A multiple instrument approach to quantifying the movement patterns and habitat use of tiger (*Galeocerdo cuvier*) and Galapagos sharks (*Carcharhinus galapagensis*) at French Frigate Shoals, Hawaii. Marine biology 157(8), 1857–1868.

Mihlbachler, M. C., Foy, M., Beatty, B. L. (2019). Surface replication, fidelity and data loss in traditional dental microwear and dental microwear texture analysis. Scientific reports 9(1), 1–13.

Miller, K. L., Szabó, T., Jerolmack, D. J., Domokos, G. (2014). Quantifying the significance of abrasion and selective transport for downstream fluvial grain size evolution. Journal of Geophysical Research: Earth Surface 119(11), 2412–2429.

Mischel, S. A., Mertz-Kraus, R., Jochum, K. P., Scholz, D. (2017). TERMITE: An R script for fast reduction of laser ablation inductively coupled plasma mass spectrometry data and its application to trace element measurements. Rapid Communications in Mass Spectrometry 31(13), 1079–1087.

Modesto, S. P. (1995). The skull of the herbivorous synapsid *Edaphosaurus boanerges* from the Lower Permian of Texas. Palaeontology 38(1), 213.

Modesto, S., Sidor, C. A., Rubidge, B. S., Welman, J. (2001). A second varanopseid skull from the Upper Permian of South Africa: implications for Late Permian ‘pelycosaur’evolution. Lethaia 34(4), 249–259.

Modesto, S. P., Scott, D. M., Reisz, R. R. (2009). Arthropod remains in the oral cavities of fossil reptiles support inference of early insectivory. Biology Letters 5(6), 838–840.

Morgan, G. S. (1989). Miocene vertebrate faunas from the Suwannee River Basin of north Florida and South Georgia. Miocene Paleontology and Stratigraphy of the Suwannee River Basin of North Florida and South Georgia: Tallahassee, Florida, Southeastern Geological Society, Guidebook 30, 26–53.

Moss, S. A. (1967). Tooth replacement in the lemon shark, *Negaprion brevirostris*. Sharks, skates and rays, 319–329.

Munro, L. E., Longstaffe, F. J., White, C. D. (2007). Burning and boiling of modern deer bone: effects on crystallinity and oxygen isotope composition of bioapatite phosphate. Palaeogeography, Palaeoclimatology, Palaeoecology 249(1–2), 90–102.

Murdock, D. J., Donoghue, P. C. (2011). Evolutionary origins of animal skeletal biomineralization. Cells Tissues Organs 194(2–4), 98–102.

Müller, A. H. (1992). Lehrbuch der Paläozoologie. 1. Allgemeine Grundlagen (pp. 514). Stuttgart, Fischer.

Müller, J., Berman, D. S., Henrici, A. C., Martens, T., Sumida, S. S. (2006). The basal reptile *Thuringothyris mahlendorffae* (Amniota: Eureptilia) from the Lower Permian of Germany. Journal of Paleontology 80(4), 726–739.

Müller, J., Li, J. L., Reisz, R. R. (2008). A new bolosaurid parareptile, *Belebey chengi* sp. nov., from the Middle Permian of China and its paleogeographic significance. Naturwissenschaften 95(12), 1169–1174.

Müller, W., Nava, A., Evans, D., Rossi, P. F., Alt, K. W., Bondioli, L. (2019). Enamel mineralization and compositional time-resolution in human teeth evaluated via histologically-defined LA-ICPMS profiles. Geochimica et Cosmochimica Acta 255, 105–126.

Myers, R. F. (1999). Micronesian reef fishes: a comprehensive guide to the coral reef fishes of Micronesia, 3rd revised and expanded edition (pp. 330). Coral Graphics, Barrigada, Guam.

Nelson, D. G. A., Featherstone, J. D. B., Duncan, J. F., Cutress, T. W. (1982). Paracrystalline disorder of biological and synthetic carbonate-substituted apatites. Journal of dental research 61(11), 1274–1281.

Neveling, J., Gastaldo, R. A., Kamo, S. L., Geissman, J. W., Looy, C. V., Bamford, M. K. (2016). A review of stratigraphic, geochemical, and paleontologic data of the terrestrial end-Permian record in the Karoo Basin, South Africa (p. 151–157). In: Linol B., de Wit M. (eds) Origin and Evolution of the Cape Mountains and Karoo Basin. Regional Geology Reviews. Springer, Cham.

Newsome, S. D., Clementz, M. T., Koch, P. L. (2010). Using stable isotope biogeochemistry to study marine mammal ecology. Marine Mammal Science 26(3), 509–572.

Neymark, L. A., Premo, W. R., Mel'nikov, N. N., Emsbo, P. (2014). Precise determination of $\delta^{88}Sr$ in rocks, minerals, and waters by double-spike TIMS: a powerful tool in the study of geological, hydrological and biological processes. Journal of Analytical Atomic Spectrometry 29(1), 65–75.

Nicolas, M. V. M. (2007). Tetrapod biodiversity through the Permo-Triassic Beaufort Group (Karoo Supergroup) of South Africa. Dissertation, University of the Witwatersrand, South Africa.

Nicolas, M., Rubidge, B. S. (2010). Changes in Permo-Triassic terrestrial tetrapod ecological representation in the Beaufort Group (Karoo Supergroup) of South Africa. Lethaia 43(1), 45–59.

Nielsen-Marsh, C. M., Hedges, R. E. (2000). Patterns of diagenesis in bone I: the effects of site environments. Journal of Archaeological Science 27(12), 1139–1150.

Nyakatura, J. A., Allen, V. R., Lauströer, J., Andikfar, A., Danczak, M., Ullrich, H. J., Hufenbach, W., Martens, T., Fischer, M. S. (2015). A three-dimensional skeletal reconstruction of the stem amniote *Orobates pabsti* (Diadectidae): analyses of body mass, centre of mass position, and joint mobility. PLoS ONE 10(9), e0137284.

Olroyd, S. L., Sidor, C. A. (2017). A review of the Guadalupian (middle Permian) global tetrapod fossil record. Earth-Science Reviews 171, 583–597.

Olson, E. C. (1962). Late Permian terrestrial vertebrates, USA and USSR. Transactions of the American Philosophical Society 52(2), 1–224.

Olson, E. C. (1966). Community evolution and the origin of mammals. Ecology 47(2), 291–302.

Olszta, M. J., Cheng, X., Jee, S. S., Kumar, R., Kim, Y. Y., Kaufman, M. J., Douglas, E. D., Gower, L. B. (2007). Bone structure and formation: A new perspective. Materials Science and Engineering: R: Reports 58(3–5), 77–116.

Overstrom, N. A. (1991). Estimated tooth replacement rate in captive sand tiger sharks (*Carcharias taurus* Rafinesque, 1810). Copeia 2, 525–526.

Owen, R. (1876). Descriptive and illustrated catalogue of the fossil Reptilia of South Africa in the collection of the British Museum (pp. 86). London, Order of the Trustees.

O'Grady, S. P., Morando, M., Avila, L., Dearing, M. D. (2005). Correlating diet and digestive tract specialization: examples from the lizard family Liolaemidae. Zoology 108(3), 201–210.

Page, B. D., Bullen, T. D., Mitchell, M. J. (2008). Influences of calcium availability and tree species on Ca isotope fractionation in soil and vegetation. Biogeochemistry 88(1), 1–13.

Papastamatiou, Y. P., Purkis, S. J., Holland, K. N. (2007). The response of gastric pH and motility to fasting and feeding in free swimming blacktip reef sharks, *Carcharhinus melanopterus*. Journal of Experimental Marine Biology and Ecology 345(2), 129–140.

Pasteris, J. D., Ding, D. Y. (2009). Experimental fluoridation of nanocrystalline apatite. American Mineralogist 94(1), 53–63.

Pasteris, J. D., Yoder, C. H., Wopenka, B. (2014). Molecular water in nominally unhydrated carbonated hydroxylapatite: The key to a better understanding of bone mineral. American Mineralogist 99(1), 16–27.

Payne, J. L., Boyer, A. G., Brown, J. H., Finnegan, S., Kowalewski, M., Krause, R. A., Lyons, S. K., McClain, C. R., McShea, D. W., Novack-Gottshall, P. M., Smith, F. A., Stempien, J. A., Smith, F. A. (2009). Two-phase increase in the maximum size of life over 3.5 billion years reflects biological innovation and environmental opportunity. Proceedings of the National Academy of Sciences 106(1), 24–27.

Pearce, E. I. F. (1988). On the dissolution of hydroxyapatite in acid solutions. Journal of dental research 67(7), 1056–1058.

Pearson, M. R., Benson, R. B., Upchurch, P., Fröbisch, J., Kammerer, C. F. (2013). Reconstructing the diversity of early terrestrial herbivorous tetrapods. Palaeogeography, Palaeoclimatology, Palaeoecology 372, 42–49.

Pesquero, M. D., Alcalá, L., Fernández-Jalvo, Y. (2013). Taphonomy of the reference Miocene vertebrate mammal site of Cerro de la Garita, Spain. Lethaia 46(3), 378–398.

Pfretzschner, H. U. (1998). Frühdiagenetische Prozesse bei der Fossilisation von Knochen. Neues Jahrbuch für Geologie und Paläontologie-Abhandlungen, 369–397.

Pfretzschner, H. U. (2000). Microcracks and fossilization of Haversian bone. Neues Jahrbuch für Geologie und Paläontologie-Abhandlungen, 413–432.

Pfretzschner, H. U. (2001). Pyrite in fossil bone. Neues Jahrbuch für Geologie und Paläontologie-Abhandlungen, 1–23.

Pfretzschner, H. U. (2004). Fossilization of Haversian bone in aquatic environments. Comptes Rendus Palevol 3(6–7), 605–616.

Polozov, A. G., Svensen, H. H., Planke, S., Grishina, S. N., Fristad, K. E., Jerram, D. A. (2016). The basalt pipes of the Tunguska Basin (Siberia, Russia): High temperature processes and volatile degassing into the end-Permian atmosphere. Palaeogeography, Palaeoclimatology, Palaeoecology 441, 51–64.

Pooley, A. C., Gans, C. (1976). The nile crocodile. Scientific American 234(4), 114–125.

Popović, L., De Waal, D., Boeyens, J. C. A. (2005). Correlation between Raman wavenumbers and P-O bond lengths in crystalline inorganic phosphates. Journal of Raman Spectroscopy: An International Journal for Original Work in all Aspects of Raman Spectroscopy, Including Higher Order Processes, and also Brillouin and Rayleigh Scattering 36(1), 2–11.

Posner, A. S. (1969). Crystal chemistry of bone mineral. Physiological reviews 49(4), 760–792.

Potasznik, A., Szymczyk, S. (2015). Magnesium and calcium concentrations in the surface water and bottom deposits of a river-lake system. Journal of Elementology 20(3), 677–692.

Price, T. D., Johnson, C. M., Ezzo, J. A., Burton, J. H., Ericson, J. A. (1994). Residential mobility in the prehistoric southwest United States: a preliminary study using strontium isotope analysis. Journal of archaeological Science 21, 315–315.

Price, S. A., Hopkins, S. S., Smith, K. K., Roth, V. L. (2012). Tempo of trophic evolution and its impact on mammalian diversification. Proceedings of the National Academy of Sciences 109(18), 7008–7012.

Preti, A., Smith, S. E., Ramon, D. A. (2004). Diet differences in the thresher shark (*Alopias vulpinus*) during transition from a warm-water regime to a cool-water regime off California-Oregon, 1998-2000. California Cooperative Oceanic Fisheries Investigations Report 45, 118.

Pucéat, E., Reynard, B., Lécuyer, C. (2004). Can crystallinity be used to determine the degree of chemical alteration of biogenic apatites? Chemical Geology 205(1–2), 83–97.

Purdy, R. W., Schneider, V. P., Applegate, S. P., McLellan, J. H., Meyer, R. L., Slaughter, B. H. (2001). The neogene sharks, rays, and bony fishes from Lee Creek Mine, Aurora, North Carolina. Smithsonian Contributions to Paleobiology 90, 71–202.

Purnell, M. A., Darras, L. P. (2016). 3D tooth microwear texture analysis in fishes as a test of dietary hypotheses of durophagy. Surface Topography: Metrology and Properties 4(1), 014006.

Purnell, M., Seehausen, O., Galis, F. (2012). Quantitative three-dimensional microtextural analyses of tooth wear as a tool for dietary discrimination in fishes. Journal of the Royal Society Interface 9(74), 2225–2233.

Purnell, M. A., Crumpton, N., Gill, P. G., Jones, G., Rayfield, E. J. (2013). Within-guild dietary discrimination from 3-D textural analysis of tooth microwear in insectivorous mammals. Journal of Zoology 291(4), 249–257.

Purnell, M. A., Goodall, R. H., Thomson, S., Matthews, C. J. (2017). Tooth microwear texture in odontocete whales: variation with tooth characteristics and implications for dietary analysis. Biosurface and Biotribology 3(4), 184–195.

Quemeneur, S., De Buffrenil, V., Laurin, M. (2013). Microanatomy of the amniote femur and inference of lifestyle in limbed vertebrates. Biological Journal of the Linnean Society 109(3), 644–655.

Racki, G., Lucas, S. G. (2020). Timing of dicynodont extinction in light of an unusual Late Triassic Polish fauna and Cuvier's approach to extinction. Historical Biology 32(4), 452–461.

Rand, A. J., Nehlich, O. (2018). Diet and sulfur isotopes (p. 1–4). In: López Varela, S. L. (ed) The Encyclopedia of Archaeological Sciences. Wiley-Blackwell.

Randall, J. E., Allen, G. R., Steene, R. C. (1997). Fishes of the great barrier reef and coral sea (pp. 594). Hawaii, University of Hawaii Press.

Reiche, I., Favre-Quattropani, L., Vignaud, C., Bocherens, H., Charlet, L., Menu, M. (2003). A multi-analytical study of bone diagenesis: the Neolithic site of Bercy (Paris, France). Measurement Science and technology 14(9), 1608.

Reichow, M. K., Saunders, A. D., White, R. V., Al'Mukhamedov, A. I., Medvedev, A. Y. (2005). Geochemistry and petrogenesis of basalts from the West Siberian Basin: an extension of the Permo–Triassic Siberian Traps, Russia. Lithos 79(3–4), 425–452.

Reichow, M. K., Pringle, M. S., Al'Mukhamedov, A. I., Allen, M. B., Andreichev, V. L., Buslov, M. M., Davies, C. E., Fedoseev, G.,S., Fitton, J.,G., Inger, S., Medvedev, A.,Y., Mitchell, C., Puchkov, V. N., Safonova, I. Y., Scott, R. A., Medvedev, A. Y. (2009). The timing and extent of the eruption of the Siberian Traps large igneous province: Implications for the end-Permian environmental crisis. Earth and Planetary Science Letters 277(1–2), 9–20.

Reif, W. E, McGill, D., Motta, P. (1978). Tooth replacement rates of the sharks *Triakis semifasciata* and *Ginglymostoma cirratum*. Zoologische Jahrbücher Abteilung für Anatomie und Ontogenie der Tiere 99, 151–156.

Reisz, R. (1972). Pelycosaurian reptiles from the middle Pennsylvanian of North America (pp. 61). Bulleton of the Museum of Comparative Zoology, Cambridge, Harvard University.

Reisz, R. R. (1997). The origin and early evolutionary history of amniotes. Trends in ecology evolution 12(6), 218–222.

Reisz, R. R. (2006). Origin of dental occlusion in tetrapods: signal for terrestrial vertebrate evolution? Journal of Experimental Zoology Part B: Molecular and Developmental Evolution 306(3), 261–277.

Reisz, R. R., Berman, D. S. (1986). *Ianthasaurus hardestii* n. sp., a primitive edaphosaur (Reptilia, Pelycosauria) from the Upper Pennsylvanian Rock Lake Shale near Garnett, Kansas. Canadian Journal of Earth Sciences 23(1), 77–91.

Reisz, R. R., Fröbisch, J. (2014). The oldest caseid synapsid from the Late Pennsylvanian of Kansas, and the evolution of herbivory in terrestrial vertebrates. PLoS ONE 9(4), e94518.

Reisz, R. R., Kuhn, O. (1986). Handbuch Der Paläoherpetologie: Pelycosauria A17 (pp. 102). München, Friedrich Pfeil.

Reisz, R. R., Sues, H. D. (2000). Herbivory in late Paleozoic and Triassic terrestrial vertebrates (p. 9–41). In: Sues, H. D. (ed) Evolution of herbivory in terrestrial vertebrates. Cambridge, U.K: Cambridge University Press.

Reisz, R. R., Barkas, V., Scott, D. (2002). A new Early Permian bolosaurid reptile from the Richards Spur Dolese Brothers Quarry, near Fort Sill, Oklahoma. Journal of Vertebrate Paleontology 22(1), 23–28.

Reisz, R. R., Mueller, J., Tsuji, L., Scott, D. (2007). The cranial osteology of *Belebey vegrandis* (Parareptilia: Bolosauridae), from the Middle Permian of Russia, and its bearing on reptilian evolution. Zoological Journal of the Linnean Society 151(1), 191–214.

Rensberger, J. M. (1973). An occlusion model for mastication and dental wear in herbivorous mammals. Journal of Paleontology 47 (0003), 515–528.

Resar, N. A., Green, J. L., McAfee, R. K. (2013). Reconstructing paleodiet in ground sloths (Mammalia, Xenarthra) using dental microwear analysis. Kirtlandia 58, 61–72.

Reynard, B., Balter, V. (2014). Trace elements and their isotopes in bones and teeth: Diet, environments, diagenesis, and dating of archeological and paleontological samples. Palaeogeography, Palaeoclimatology, Palaeoecology 416, 4–16.

Richards, M. P., Fuller, B. T., Hedges, R. E. (2001). Sulphur isotopic variation in ancient bone collagen from Europe: implications for human palaeodiet, residence mobility, and modern pollutant studies. Earth and Planetary Science Letters 191(3–4), 185–190.

Robinet, C., Merceron, G., Candela, A. M., Marivaux, L. (2020). Dental microwear texture analysis and diet in caviomorphs (Rodentia) from the Serra do Mar Atlantic forest (Brazil). Journal of Mammalogy 101(2), 386–402.

Romer, A. S., Price, L. W., Price, L. I. (1940). Review of the Pelycosauria (Vol. 28). Geological Society of America, Special Papers. New York, Arno Press.

Rothe, P. (2000). Erdgeschichte: Spurensuche im Gestein (pp. 240). Darmstadt, Wissenschaft Buchgesellschaft.

Rubidge, B. S. (1995). Biostratigraphy of the Beaufort Group (Karoo Supergroup). Biostratigraphic series (pp. 45). Pretoria, Government Printer.

Rubidge, B. S. (2005). 27th Du Toit Memorial Lecture: re-uniting lost continents–fossil reptiles from the ancient Karoo and their wanderlust. South African Journal of Geology 108(1), 135–172.

Rubidge, B. S., Sidor, C. A. (2001). Evolutionary patterns among Permo-Triassic therapsids. Annual Review of Ecology and Systematics 32(1), 449–480.

Rubinstein, C. V., Gerrienne, P., de la Puente, G. S., Astini, R. A., Steemans, P. (2010). Early Middle Ordovician evidence for land plants in Argentina (eastern Gondwana). New Phytologist 188(2), 365–369.

Rubinstein, C. V., Vajda, V. (2019). Baltica cradle of early land plants? Oldest record of trilete spores and diverse cryptospore assemblages; evidence from Ordovician successions of Sweden. GFF 141(3), 181–190.

Russel, D. A. (1996). Isolated dinosaur bones from the Middle Cretaceous of the Tafilalt, Morocco. Bulletin du Muséum national d'Histoire naturelle, 4ème série–section C–Sciences de la Terre, Paléontologie, Géologie, Minéralogie 18, 2–3.

Ruta, M., Cisneros, J. C., Liebrecht, T., Tsuji, L. A., Mueller, J. (2011). Amniotes through major biological crises: faunal turnover among Parareptiles and the end-Permian mass extinction. Palaeontology 54(5), 1117–1137.

Sahney, S., Benton, M. J. (2008). Recovery from the most profound mass extinction of all time. Proceedings of the Royal Society B: Biological Sciences 275(1636), 759–765.

Sahney, S., Benton, M. J., Falcon-Lang, H. J. (2010). Rainforest collapse triggered Carboniferous tetrapod diversification in Euramerica. Geology 38(12), 1079–1082.

Saloman, E. B. (2006). Wavelengths, energy level classifications, and energy levels for the spectrum of neutral mercury. Journal of physical and chemical reference data 35(4), 1519–1548.

Sanborn, M., Telmer, K. (2003). The spatial resolution of LA-ICP-MS line scans across heterogeneous materials such as fish otoliths and zoned minerals. Journal of Analytical Atomic Spectrometry 18(10), 1231–1237.

Sanchez-Villagra, M. R. (2010). Developmental palaeontology in synapsids: the fossil record of ontogeny in mammals and their closest relatives. Proceedings of the Royal Society B: Biological Sciences 277(1685), 1139–1147.

Sander, P. M. (1987). Taphonomy of the Lower Permian Geraldine bonebed in Archer County, Texas. Palaeogeography, Palaeoclimatology, Palaeoecology 61, 221–236.

Sander, P. M. (1989). Early Permian depositional environments and pond bonebeds in central Archer County, Texas. Palaeogeography, Palaeoclimatology, Palaeoecology 69, 1–21.

Saunders, A., Reichow, M. (2009). The Siberian Traps and the End-Permian mass extinction: a critical review. Chinese Science Bulletin 54(1), 20–37.

Schindler, T. (2007). Geologie, Stratigraphie und Genese des permokarbonischen Saar-Nahe-Beckens (p. 4–37). In: Schindler, T .and Heidtke, U. H. J. (eds), Kohlesümpfe, Seen und Halbwüsten. Pollichia Sonderveröffentlichungen 10, Bad Dürkheim.

Schluessel, V., Bennett, M. B., Bleckmann, H., Blomberg, S., Collin, S. P. (2008). Morphometric and ultrastructural comparison of the olfactory system in elasmobranchs: the significance of structure–function relationships based on phylogeny and ecology. Journal of Morphology 269(11), 1365–1386.

Schmitt, A. D. (2016). Earth-surface Ca isotopic fractionations (p. 145–172). In Gussone, N., Schmitt, A. D., Heuser, A., Wombacher, F., Dietzel, M., Tipper, E., Schiller, M. (eds) Calcium Stable Isotope Geochemistry. Springer, Berlin, Heidelberg.

Schoch, R. R., Voigt, S. (2019). A dvinosaurian temnospondyl from the Carboniferous-Permian boundary of Germany sheds light on dvinosaurian phylogeny and distribution. Journal of Vertebrate Paleontology 39(1), e1577874.

Schoeninger, M. J., Hallin, K., Reeser, H., Valley, J. W., Fournelle, J. (2003). Isotopic alteration of mammalian tooth enamel. International Journal of Osteoarchaeology 13(1-2), 11–19.

Schoeninger, M. J. (2012). The ancestral dinner table. Nature 487(7405), 42–43.

Schubert, B. W., Ungar, P. S., DeSantis, L. R. G. (2010). Carnassial microwear and dietary behaviour in large carnivorans. Journal of Zoology 280(3), 257–263.

Schulz, E., Calandra, I., Kaiser, T. M. (2010). Applying tribology to teeth of hoofed mammals. Scanning 32(4), 162–182.

Schulz, E., Calandra, I., Kaiser, T. M. (2013a). Feeding ecology and chewing mechanics in hoofed mammals: 3D tribology of enamel wear. Wear 300(1–2), 169–179.

Schulz, E., Piotrowski, V., Clauss, M., Mau, M., Merceron, G., Kaiser, T. M. (2013b). Dietary abrasiveness is associated with variability of microwear and dental surface texture in rabbits. PLoS ONE 8(2), e56167.

Schulz-Kornas, E., Stuhlträger, J., Clauss, M., Wittig, R. M., Kupczik, K. (2019). Dust affects chewing efficiency and tooth wear in forest dwelling Western chimpanzees (*Pan troglodytes verus*). American journal of physical anthropology 169(1), 66–77.

Schweitzer, M. H., Wittmeyer, J. L., Horner, J. R., Toporski, J. K. (2005). Soft-tissue vessels and cellular preservation in *Tyrannosaurus rex*. Science 307(5717), 1952–1955.

Scott, J. R. (2012). Dental microwear texture analysis of extant African Bovidae. Mammalia 76(2), 157–174.

Scott, J. R., Godfrey, L. R., Jungers, W. L., Scott, R. S., Simons, E. L., Teaford, M. F., Ungar, P. S. Walker, A. (2009). Dental microwear texture analysis of two families of subfossil lemurs from Madagascar. Journal of Human Evolution 56(4), 405–416.

Scott, R. S., Ungar, P. S., Bergstrom, T. S., Brown, C. A., Grine, F. E., Teaford, M. F., Walker, A. (2005). Dental microwear texture analysis shows within-species diet variability in fossil hominins. Nature 436(7051), 693–695.

Scott, R. S., Ungar, P. S., Bergstrom, T. S., Brown, C. A., Childs, B. E., Teaford, M. F., Walker, A. (2006). Dental microwear texture analysis: technical considerations. Journal of Human Evolution 51(4), 339–349.

Scott, T. M. (1988). The lithostratigraphy of the Hawthorn Group (Miocene) of Florida. Florida Geological Survey, 59, 1–148.

Scott, T. M., MacGill, P. M. (1981). The Hawthorne Formation of Central Florida. Part 1 - Geology of the Hawthorne Formation in Central Florida. Florida Bureau of Geology, Report of Investigations 92, 1–32.

Secor, S. M. (2003). Gastric function and its contribution to the postprandial metabolic response of the Burmese python *Python molurus*. Journal of Experimental Biology 206(10), 1621–1630.

Semprebon, G. M., Rivals, F. (2007). Was grass more prevalent in the pronghorn past? An assessment of the dietary adaptations of Miocene to recent Antilocapridae (Mammalia: Artiodactyla). Palaeogeography, Palaeoclimatology, Palaeoecology 253(3–4), 332–347.

Semprebon, G. M., Godfrey, L. R., Solounias, N., Sutherland, M. R., Jungers, W. L. (2004a). Can low-magnification stereomicroscopy reveal diet? Journal of Human Evolution 47(3), 115–144.

Semprebon, G., Janis, C., Solounias, N. (2004b). The diets of the Dromomerycidae (Mammalia: Artiodactyla) and their response to Miocene vegetational change. Journal of Vertebrate Paleontology 24(2), 427–444.

Servais, T., Owen, A. W., Harper, D. A., Kröger, B., Munnecke, A. (2010). The great ordovician biodiversification event (GOBE): the palaeoecological dimension. Palaeogeography, Palaeoclimatology, Palaeoecology 294 (3–4), 99–119.

Shalev, N., Gavrieli, I., Halicz, L., Sandler, A., Stein, M., Lazar, B. (2017). Enrichment of ^{88}Sr in continental waters due to calcium carbonate precipitation. Earth and Planetary Science Letters 459, 381–393.

Shapiro, S. S., Wilk, M. B. (1965). An analysis of variance test for normality (complete samples). Biometrika 52(3/4), 591–611.

Shelton, C. D., Sander, P. M., Stein, K., Winkelhorst, H. (2013). Long bone histology indicates sympatric species of *Dimetrodon* (Lower Permian, Sphenacodontidae). Earth and Environmental Science Transactions of The Royal Society 103, 1–20.

Shelton, C. D. (2013). A new method to determine volume of bromalites: morphometrics of Lower Permian (Archer City Formation) heteropolar bromalites. Swiss Journal of Palaeontology 132(2), 221–238.

Shelton, C. D. (2015). Origins of Endothermy in the mammalian lineage. Dissertation, Universitäts und Landesbibliothek Bonn, Germany.

Shen, S. Z., Ramezani, J., Chen, J., Cao, C. Q., Erwin, D. H., Zhang, H., Xiang, L., Schoepfer, S. D., Henderson, C., M., Zhend, Q.-F., Bowring, S. A., Wang, Y., Li, X.-H., Wang, X.-D., Yuan, D.-X., Zhang, Y.-C., Mu, L., Wang, J, Wu, Y.-S. (2019). A sudden end-Permian mass extinction in South China. GSA Bulletin 131(1-2), 205–223.

Shimada, K. (2005). Types of tooth sets in the fossil record of sharks, and comments on reconstructing dentitions of extinct sharks. Journal of Fossil Research 38(2), 141–145.

Shishkin, M. A., Rubidge, B. S. (2000). A relict rhinesuchid (Amphibia: Temnospondyli) from the Lower Triassic of South Africa. Palaeontology 43(4), 653–670.

Sigogneau-Russell, D., Sun, A. L. (1981). A brief review of Chinese synapsids. Geobios 14(2), 275–279.

Sillen, A., Lee-Thorp, J. A. (1994). Trace element and isotopic aspects of predator-prey relationships in terrestrial foodwebs. Palaeogeography, Palaeoclimatology, Palaeoecology 107(3–4), 243–255.

Sillen, A., Hall, G., Armstrong, R. (1995). Strontium calcium ratios (Sr/Ca) and strontium isotopic ratios ($^{87}Sr/^{86}Sr$) of *Australopithecus robustus* and *Homo* sp. from Swartkrans. Journal of Human Evolution 28(3), 277–285.

Simon, R. V., Sidor, C. A., Angielczyk, K. D., Smith, R. M. (2010). First record of a tapinocephalid (Therapsida: Dinocephalia) from the Ruhuhu Formation (Songea Group) of southern Tanzania. Journal of Vertebrate Paleontology 30(4), 1289–1293.

Simpfendorfer, C. A., Goodreid, A. B., McAuley, R. B. (2001). Size, sex and geographic variation in the diet of the tiger shark, *Galeocerdo cuvier*, from Western Australian waters. Environmental Biology of Fishes 61(1), 37–46.

Skinner, J. D., Chimimba, C. T. (2005). The mammals of the southern African sub-region (pp. 814). Cambridge, New York, Melbourne, Madrid, Cape Town, Singapore, Sao Paulo, Cambridge University Press.

Skulan, J., DePaolo, D. J. (1999). Calcium isotope fractionation between soft and mineralized tissues as a monitor of calcium use in vertebrates. Proceedings of the National Academy of Sciences 96(24), 13709–13713.

Skulan, J., DePaolo, D. J., Owens, T. L. (1997). Biological control of calcium isotopic abundances in the global calcium cycle. Geochimica et Cosmochimica Acta 61(12), 2505–2510.

Smith, L. C. (1997). National Audubon society field guide to tropical marine fishes Caribbean, Gulf of Mexico, Florida, Bahamas, Bermuda (pp. 720). New York, Alfred A. Knopf.

Smith, R. M., Ward, P. D. (2001). Pattern of vertebrate extinctions across an event bed at the Permian-Triassic boundary in the Karoo Basin of South Africa. Geology 29(12), 1147–1150.

Snoeck, C., Lee-Thorp, J., Schulting, R., De Jong, J., Debouge, W., Mattielli, N. (2015). Calcined bone provides a reliable substrate for strontium isotope ratios as shown by an enrichment experiment. Rapid communications in mass spectrometry 29(1), 107–114.

Snyder, A. J., LeBlanc, A. R., Jun, C., Bevitt, J. J., Reisz, R. R. (2020). Thecodont tooth attachment and replacement in bolosaurid parareptiles. PeerJ, 8, e9168.

Snyder, S. W., Riggs, S. R. (1993). Geological overview of Lee Creek Mine and vicinity, North Carolina coastal plain: The Compass, Sigma Gamma Epsilon Journal of Earth Sciences 70, 13–35.

Solounias, N., Semprebon, G. (2002). Advances in the reconstruction of ungulate ecomorphology with application to early fossil equids. American Museum Novitates 2002(3366), 1–49.

Solounias, N., Teaford, M., Walker, A. (1988). Interpreting the diet of extinct ruminants: the case of a non-browsing giraffid. Paleobiology 14(3), 287–300.

Solounias, N., Rivals, F., Semprebon, G. M. (2010). Dietary interpretation and paleoecology of herbivores from Pikermi and Samos (late Miocene of Greece). Paleobiology, 36(1), 113–136.

Sommer, C., Schneider, W., Poutiers, J. M. (1996). The living marine resources of Somalia (pp. 376). Rome, Food and Agriculture Organization of the United Nations.

Sommerville, E., Platell, M. E., White, W. T., Jones, A. A., Potter, I. C. (2011). Partitioning of food resources by four abundant, co-occurring elasmobranch species: relationships between diet and both body size and season. Marine and Freshwater Research 62(1), 54–65.

Spindler, F. (2015). The basal Sphenacodontia–systematic revision and evolutionary implications. Dissertation, Technische Universität Bergakademie Freiberg, Germany.

Spindler, F., Werneburg, R., Schneider, J. W., Luthardt, L., Annacker, V., Rößler, R. (2018). First arboreal 'pelycosaurs'(Synapsida: Varanopidae) from the early Permian Chemnitz Fossil Lagerstätte, SE Germany, with a review of varanopid phylogeny. PalZ 92(2), 315–364.

Spindler, F., Voigt, S., Fischer, J. (2020). Edaphosauridae (Synapsida, Eupelycosauria) from Europe and their relationship to North American representatives. PalZ 94(1), 125–153.

Sponheimer, M., Lee-Thorp, J. A. (2003). Using carbon isotope data of fossil bovid communities for palaeoenvironmental reconstruction: research articles: human origins research in South Africa. South African Journal of Science, 99(5), 273–275.

Sponheimer, M., Lee-Thorp, J. A. (2006). Enamel diagenesis at South African Australopith sites: Implications for paleoecological reconstruction with trace elements. Geochimica et Cosmochimica Acta 70(7), 1644–1654.

Sponheimer, M., de Ruiter, D., Lee-Thorp, J., Späth, A. (2005). Sr/Ca and early hominin diets revisited: new data from modern and fossil tooth enamel. Journal of Human Evolution 48(2), 147–156.

Squires, V. R. (2001). Dust and sandstorms: an early warning of impending disaster (p. 15–28). In: Youlin, Y., Squires, V., Qi, L. (eds) Global alarm: Dust and sandstorms from world's drylands, United Nations.

Steemans, P., Le Hérissé, A., Melvin, J., Miller, M. A., Paris, F., Verniers, J., Wellman, C. H. (2009). Origin and radiation of the earliest vascular land plants. Science 324(5925), 353–353.

Steininger, F. F., Berggren, W. A., Kent, D. V., Bernor, R. L., Sen, S., Agusti, J. (1996). Circum-Mediterranean Neogene (Miocene and Pliocene) marine-continental chronologic correlations of European mammal units (p. 7–46). In: R.L. Bernor, V. Fahlbusch, H.W. Mittmann (eds) The Evolution of Western Eurasian Neogene Mammal Faunas. New York, Columbia University Press.

Stiner, M. C., Kuhn, S. L., Weiner, S., Bar-Yosef, O. (1995). Differential burning, recrystallization, and fragmentation of archaeological bone. Journal of archaeological science 22(2), 223–237.

Strasburg, D. W. (1963). The diet and dentition of *Isistius brasiliensis*, with remarks on tooth replacement in other sharks. Copeia 1963(1), 33–40.

Straube, N., Schliewen, U., Kriwet, J. (2008). Dental structure of the Giant lantern shark *Etmopterus baxteri* (Chondrichthyes: Squaliformes) and its taxonomic implications. Environmental Biology of Fishes 82(2), 133–141.

Strother, P. K., Al-Hajri, S., Traverse, A. (1996). New evidence for land plants from the lower Middle Ordovician of Saudi Arabia. Geology 24(1), 55–58.

Stynder, D. D., DeSantis, L. R., Donohue, S. L., Schubert, B. W., Ungar, P. S. (2019). A dental microwear texture analysis of the early Pliocene African ursid *Agriotherium africanum* (Mammalia, Carnivora, Ursidae). Journal of Mammalian Evolution 26(4), 505–515.

Sues, H. D. (2000). Evolution of herbivory in terrestrial vertebrates: perspectives from the fossil record (pp. 268). Cambridge, New York, Melbourne, Madrid, Cape Town, Singapore, Sao Paulo, Cambridge University Press.

Sues, H. D., Boy, J. A. (1988). A procynosuchid cynodont from central Europe. Nature 331(6156), 523–524.

Sues, H. D., Munk, W. (1996). A remarkable assemblage of terrestrial tetrapods from the Zechstein (Upper Permian: Tatarian) near Korbach (northwestern Hesse). PalZ 70(1), 213–223.

Sues, H. D., Reisz, R. R. (1998). Origins and early evolution of herbivory in tetrapods. Trends in Ecology and Evolution 13(4), 141–145.

Suga, S., Taki, Y., Wada, K., Ogawa, M. (1991). Evolution of fluoride and iron concentrations in the enameloid of fish teeth (p. 439–446). In: Suga S., Nakahara H. (eds) Mechanisms and Phylogeny of Mineralization in Biological Systems. Tokyo, Springer.

Sulej, T., Niedźwiedzki, G. (2019). An elephant-sized Late Triassic synapsid with erect limbs. Science 363(6422), 78–80.

Tabor, N. J., Poulsen, C. J. (2008). Palaeoclimate across the Late Pennsylvanian–Early Permian tropical palaeolatitudes: a review of climate indicators, their distribution, and relation to palaeophysiographic climate factors. Palaeogeography, Palaeoclimatology, Palaeoecology 268(3-4), 293–310.

Tabor, N. J., Sidor, C. A., Smith, R. M., Nesbitt, S. J. Angielczyk, K. D. (2017). Paleosols of the Permian-Triassic: proxies for rainfall, climate change and major changes in terrestrial tetrapod diversity. Journal of Vertebrate Paleontology 37(sup1), 240–253.

Tacail, T., Albalat, E., Télouk, P., Balter, V. (2014). A simplified protocol for measurement of Ca isotopes in biological samples. Journal of Analytical Atomic Spectrometry 29(3), 529–535.

Tacail, T., Le Houedec, S., Skulan, J. L. (2020). New frontiers in calcium stable isotope geochemistry: Perspectives in present and past vertebrate biology. Chemical Geology 537, 119471.

Tamburin, E., Elorriaga-Verplancken, F. R., Estupiñan-Montaño, C., Madigan, D. J., Sánchez-González, A., Padilla, M. H., Wcisel, M., Galván-Magaña, F. (2020). New insights into the trophic ecology of young white sharks (*Carcharodon carcharias*) in waters off the Baja California Peninsula, Mexico. Marine Biology 167, 1–14.

Tanabe, K., Hiraishi, J. (1980). Correction of finite slit width effects on Raman line widths. Spectrochimica Acta Part A: Molecular Spectroscopy 36(4), 341–344.

Taniuchi, T., Kuroda, N., Nose, Y. (1983). Age, growth, reproduction and food habits of the star-spotted dogfish *Mustelus manazo* collected from Choshi [Japan]. Bulletin of the Japanese Society of Scientific Fisheries 49, 1325–1334.

Teaford, M. F. (1988). Scanning electron microscope diagnosis of wear patterns versus artifacts on fossil teeth. Scanning Microscop, 2(2), 1167–1175.

Teaford, M. F., Glander, K. E. (1991). Dental microwear in live, wild‐trapped *Alouatta palliata* from Costa Rica. American Journal of Physical Anthropology 85(3), 313–319.

Teaford, M. F., Glander, K. E. (1996). Dental microwear and diet in a wild population of mantled howling monkeys (*Alouatta palliata*) (p. 433–449). In: Norconk, M. A., Rosenberger, A. L., Garber, P. A. (eds) Adaptive radiations of Neotropical primates. Boston, MA, Springer Science.

Teaford, M. F., Oyen, O. J. (1989). In vivo and in vitro turnover in dental microwear. American Journal of Physical Anthropology 80(4), 447–460.

Terrill, D. F., Henderson, C. M., Anderson, J. S. (2020). New application of strontium isotopes reveals evidence of limited migratory behaviour in Late Cretaceous hadrosaurs. Biology letters 16(3), 20190930.

Thenius, E. (1989). Zähne und Gebiss der Säugetiere. Handbuch der Zoologie. Band VIII. Mammalia, Teilband 56 (pp. 523). Berlin, New York, Walter de Gruyter.

Thomas, D. B., Fordyce, R. E., Frew, R. D., Gordon, K. C. (2007). A rapid, non-destructive method of detecting diagenetic alteration in fossil bone using Raman spectroscopy. Journal of Raman Spectroscopy: An International Journal for Original Work in all Aspects of Raman

Spectroscopy, Including Higher Order Processes, and also Brillouin and Rayleigh Scattering 38(12), 1533–1537.

Thomas, D. B., McGoverin, C. M., Fordyce, R. E., Frew, R. D., Gordon, K. C. (2011). Raman spectroscopy of fossil bioapatite—a proxy for diagenetic alteration of the oxygen isotope composition. Palaeogeography, Palaeoclimatology, Palaeoecology 310(1–2), 62–70.

Tobien, H. (1983). Bemerkungen zur Taphonomie der spättertiären Säugerfauna aus den Dinotheriensanden Rheinhessens (Bundesrepublik Deutschland). Weltenburger Akademie, Erwin Rutte-Festschrift, 191–200.

Tomescu, A. M. F., Rothwell, G. W. (2006). Wetlands before tracheophytes: Thalloid terrestrial communities of the Early Silurian Passage Creek biota (Virginia). Special Papers-Geological Society of America 399, 41.

Tricas, T. C., McCosker, J. E. (1984). Predatory behavior of the white shark *(Carcharodon carcharias*), with notes on its biology. Proceedings of the California Academy of Sciences 43, 221–238.

Trueman, C. N., Tuross, N. (2002). Trace elements in recent and fossil bone apatite. Reviews in mineralogy and geochemistry 48(1), 489–521.

Trueman, C. N., Privat, K., Field, J. (2008). Why do crystallinity values fail to predict the extent of diagenetic alteration of bone mineral? Palaeogeography, Palaeoclimatology, Palaeoecology 266(3–4), 160–167.

Trust, B. A., Fry, B. (1992). Stable sulphur isotopes in plants: a review. Plant, Cell Environment 15(9), 1105–1110.

Tsuji, L. A. (2011). Evolution, morphology and paleobiology of the pareiasauria and their relatives. Dissertation, Humboldt-Universität zu Berlin, Germany.

Tsuji, L. A. (2013). Anatomy, cranial ontogeny and phylogenetic relationships of the pareiasaur *Deltavjatia rossicus* from the Late Permian of central Russia. Earth and Environmental Science Transactions of the Royal Society of Edinburgh 104(2), 81–122.

Turcotte, C. M., Green, D. J., Kupczik, K., McFarlin, S., Schulz-Kornas, E. (2020). Elevated activity levels do not influence extrinsic fiber attachment morphology on the surface of muscle-attachment sites. Journal of Anatomy 236(5), 827–839.

Turner-Walker, G. (2012). Early bioerosion in skeletal tissues: persistence through deep time. Neues Jahrbuch für Geologie und Paläontologie-Abhandlungen 265(2), 165–183.

Tütken, T. (2003). Die Bedeutung der Knochenfrühdiagenese für die Erhaltungsfähigkeit in vivo erworbener Element-und Isotopenzusammensetzungen in fossilen Knochen Diddertation, Universität Tübingen.

Tütken, T., Vennemann, T. W. (2011). Fossil bones and teeth: preservation or alteration of biogenic compositions? Palaeogeography, Palaeoclimatology, Palaeoecology 310, 1–8.

Tütken, T., Vennemann, T. W., Pfretzschner, H. U. (2008). Early diagenesis of bone and tooth apatite in fluvial and marine settings: constraints from combined oxygen isotope, nitrogen and REE analysis. Palaeogeography, Palaeoclimatology, Palaeoecology 266(3–4), 254–268.

Uhl, D., Jasper, A. (2016). New data on the macroflora of the basal Rotliegend group (Remigiusberg Formation; Gzhelian) in the Saar-Nahe Basin (SW-Germany). Fossil Imprint 72(3–4), 239–250.

Ungar, P. S. (1995). A semiautomated image analysis procedure for the quantification of dental microwear II. Scanning 17(1), 57–59.

Ungar, P. S. (2010). Mammal teeth: origin, evolution, and diversity (pp. 320). Balitmore, Johns Hopkins University Press.

Ungar, P. S., Brown, C. A., Bergstrom, T. S., Walker, A. (2003). Quantification of dental microwear by tandem scanning confocal microscopy and scale-sensitive fractal analyses. Scanning: The Journal of Scanning Microscopies 25(4), 185–193.

Ungar, P. S., Merceron, G., Scott, R. S. (2007). Dental microwear texture analysis of Varswater bovids and early Pliocene paleoenvironments of Langebaanweg, Western Cape Province, South Africa. Journal of Mammalian Evolution 14(3), 163–181.

Ungar, P. S., Grine, F. E., Teaford, M. F. (2008). Dental microwear and diet of the Plio-Pleistocene hominin *Paranthropus boisei*. PLoS ONE 3(4), e2044.

Ungar, P. S., Scott, J. R., Curran, S. C., Dunsworth, H. M., Harcourt-Smith, W. E. H., Lehmann, T., Manthi, F. K., McNulty, K. P. (2012). Early Neogene environments in East Africa: Evidence from dental microwear of tragulids. Palaeogeography, Palaeoclimatology, Palaeoecology 342, 84–96.

Ungar, P. S., Abella, E. F., Burgman, J. H., Lazagabaster, I. A., Scott, J. R., Delezene, L. K., Manthi, F. K., Plavcan, J. M., Ward, C. V. (2020). Dental microwear and Pliocene paleocommunity ecology of bovids, primates, rodents, and suids at Kanapoi. Journal of Human Evolution 140, 102315.

Urbanek, S. (2016). rJava: Low-level R to Java interface. R package version 0.9-8.

Van den Brandt, M. J., Abdala, F., Rubidge, B. S. (2020). Cranial morphology and phylogenetic relationships of the Middle Permian pareiasaur *Embrithosaurus schwarzi* from the Karoo Basin of South Africa. Zoological Journal of the Linnean Society 188(1), 202–241.

Van der Merwe, N. J., Masao, F. T., Bamford, M. K. (2008). Isotopic evidence for contrasting diets of early hominins *Homo habilis* and *Australopithecus boisei* of Tanzania. South African Journal of Science 104(3–4), 153–155.

Varriale, F. J. (2016). Dental microwear reveals mammal-like chewing in the neoceratopsian dinosaur *Leptoceratops gracilis*. PeerJ 4, e2132.

Vaske, L., Lessa, R. P., Gadig, O. B. F. (2009). Feeding habits of the Blue shark (*Prionace glauca*) off the coast of Brazil. Biota Neotropica 9(3).

Vennemann, T. W., Hegner, E., Cliff, G., Benz, G. W. (2001). Isotopic composition of recent shark teeth as a proxy for environmental conditions. Geochimica et Cosmochimica Acta 65(10), 1583–1599.

Vogel, J. C. (1978). Isotopic assessment of the dietary habits of ungulates. South African Journal of Science 74(8), 298.

Voigt, S. (2007). Auf den Spuren der Saurier: Die Tetrapodenfährten aus dem Oberkarbon und Unterperm des Saar− Nahe− Beckens (p. 288–303). In: Schindler, T .and Heidtke, U. H. J. (eds) Kohlesümpfe, Seen und Halbwüsten. Pollichia Sonderveröffentlichungen 10, Bad Dürkheim.

Voigt, S., Fischer, J., Schindler, T., Wuttke, M., Spindler, F., Rinehart, L. (2014). On a potential fossil hotspot for Pennsylvanian-Permian non-aquatic vertebrates in central Europe. Freiberger Forschungshefte C 548(22), 39–44.

Vroon, P. Z., Van Der Wagt, B., Koornneef, J. M., Davies, G. R. (2008). Problems in obtaining precise and accurate Sr isotope analysis from geological materials using laser ablation MC-ICPMS. Analytical and Bioanalytical Chemistry 390(2), 465–476.

Wasserstraßen- und Schifffahrstverwaltung des Bundes. http://www.wsd-west.wsv.de/wasserstrassen/verkehrsweg_rhein/technische_daten/index.html

Walker, P. L. (1976). Wear striations on the incisors of ceropithecid monkeys as an index of diet and habitat preference. American Journal of Physical Anthropology 45(2), 299–307.

Walker, A., Hoeck, H. N., Perez, L. (1978). Microwear of mammalian teeth as an indicator of diet. Science 201(4359), 908–910.

Wang, Y., Cerling, T. E. (1994). A model of fossil tooth and bone diagenesis: implications for paleodiet reconstruction from stable isotopes. Palaeogeography, Palaeoclimatology, Palaeoecology 107, 281–289.

Weber, K., Winkler, D. E., Schulz-Kornas, E., Kaiser, T. M., Tütken, T. (in review). The good, the bad and the ugly–a trash or treasure hunt for reliable enamel surface textures in vertebrates. Palaeogeography, Palaeoclimatology, Palaeoecology, in review.

Weber, M., Wassenburg, J. A., Jochum, K. P., Breitenbach, S. F., Oster, J., Scholz, D. (2017). Sr-isotope analysis of speleothems by LA-MC-ICP-MS: High temporal resolution and fast data acquisition. Chemical Geology 468, 63–74.

Weber, M., Lugli, F., Hattendorf, B., Scholz, D., Mertz-Kraus, R., Guinoiseau, D., Jochum, K. P. (2020). NanoSr–A New Carbonate Microanalytical Reference Material for In Situ Strontium Isotope Analysis. Geostandards and Geoanalytical Research 44(1), 69–83.

Weber, M., Leichliter, J., Lugli, F., Jochum, K. P., Clauss, M. Tütken, T. (2020). Controlled Feeding Experiments of Rodents to Determine Intra-Population $^{87}Sr/^{86}Sr$, $\delta^{88}Sr$ and $\delta^{44}Ca$ Variability of Hard and Soft Tissues. Goldschmidt Abstracts,

Weide, D. M., Sidor, C. A., Angielczyk, K. D., Smith, R. M. (2009). A new record of *Procynosuchus delaharpeae* (Therapsida: Cynodontia) from the upper Permian Usili Formation, Tanzania. Palaeontologia Africana 44, 21–26.

Welch, B. L. (1938). The significance of the difference between two means when the population variances are unequal. Biometrika 29(3/4), 350–362.

Welton, B. J., Farish, R. F. (1993). The collector's guide to fossil sharks and rays from the Cretaceous of Texas (pp. 204). Lewisville, TX.

White, W. T., Last, P. R., Stevens, J. D., Yearsly, G. K. (2006). Economically important sharks and rays of Indonesia (pp. 329). Canberra, Australia, Australian Centre for International Agricultural Research.

White, W. T., Ebert, D. A., Naylor, G. J., Ho, H. C., Clerkin, P., Veríssimo, A. N. A., Cotton, C. F. (2013). Revision of the genus *Centrophorus* (Squaliformes: Centrophoridae): Part 1—Redescription of *Centrophorus granulosus* (Bloch and Schneider), a senior synonym of *C. acus* Garman and *C. niaukang* Teng. Zootaxa 3752(1), 35–72.

Whitenack, L. B., Motta, P. J. (2010). Performance of shark teeth during puncture and draw: implications for the mechanics of cutting. Biological Journal of the Linnean Society 100(2), 271–286.

Whitenack, L. B., Simkins Jr, D. C., Motta, P. J., Hirai, M., Kumar, A. (2010). Young's modulus and hardness of shark tooth biomaterials. Archives of oral biology 55(3), 203–209.

Wickham, H. (2011). The Split-Apply-Combine Strategy for Data Analysis. Journal of Statistical Software 40, 1–29.

Wickham, H. (2016). ggplot2: Elegant Graphics for Data Analysis (pp. 260). New York, Springer-Verlag.

Wilcox, R. R. (2003). Applying contemporary statistical techniques (pp. 608). San Diego, Elsevier Academic Press.

Wilcox, R.R. (2005). Introduction to Robust Estimation and Hypothesis Testing, second edition (pp. 608). Burlington, San Diego, London, Elsevier Academic Press.

Wilcox, R. R. (2012). Introduction to robust estimation and hypothesis testing (pp. 608). Burlington, San Diego, London, Elsevier Academic Press.

Wilcox, R.R., Schönbrodt, F.D. (2010). The WRS Package for Robust Statistics in R. [updated 2010 version 0.12.1; cited 2010 27.04.2011]; Available from: http://r-forge.r-project.org/projects/wrs/.

Wilcoxon, F. (1945). Individual comparisons by ranking methods. Biometrics Bulletin 1, 80–83.

Wilga, C. D., Motta, P. J., Sanford, C. P. (2007). Evolution and ecology of feeding in elasmobranchs. Integrative and Comparative Biology 47(1), 55–69.

Williams, V. S., Barrett, P. M., Purnell, M. A. (2009). Quantitative analysis of dental microwear in hadrosaurid dinosaurs, and the implications for hypotheses of jaw mechanics and feeding. Proceedings of the National Academy of Sciences 106(27), 11194–11199.

Wings, O., Eckert, C. (2018). GOTHA: Museum der Natur, Stiftung Schloss Friedenstein Gotha (p. 249-261). In: Beck, L. A., Joger, U. (eds) Paleontological Collections of Germany, Austria and Switzerland: The History of Life of Fossil Organisms at Museums and Universities. Switzerland, Cham, Springer.

Winkler, D. E., Schulz, E., Calandra, I., Gailer, J. P., Landwehr, C., Kaiser, T. M. (2013). Indications for a dietary change in the extinct Bovid genus Myotragus (Plio-Holocene, Mallorca, Spain). Geobios 46(1–2), 143–150.

Winkler, D. E., Andrianasolo, T. H., Andriamandimbiarisoa, L., Ganzhorn, J. U., Rakotondranary, S. J., Kaiser, T. M., Schulz-Kornas, E. (2016). Tooth wear patterns in black rats (*Rattus rattus*) of Madagascar differ more in relation to human impact than to differences in natural habitats. Ecology and Evolution 6(7), 2205–2215.

Winkler, D. E., Schulz-Kornas, E., Kaiser, T. M., Tütken, T. (2019a). Dental microwear texture reflects dietary tendencies in extant Lepidosauria despite their limited use of oral food processing. Proceedings of the Royal Society B 286(1903), 20190544.

Winkler, D. E., Schulz-Kornas, E., Kaiser, T. M., De Cuyper, A., Clauss, M., Tütken, T. (2019b). Forage silica and water content control dental surface texture in guinea pigs and provide implications for dietary reconstruction. Proceedings of the National Academy of Sciences 116(4), 1325–1330.

Winkler, D. E., Schulz-Kornas, E., Kaiser, T. M., Codron, D., Leichliter, J., Hummel, J., Martin, L. F., Clauss, M., Tütken, T. (2020a). The turnover of dental microwear texture: Testing the" last supper" effect in small mammals in a controlled feeding experiment. Palaeogeography, Palaeoclimatology, Palaeoecology 557, 109930.

Winkler, D. E., Clauss, M., Schulz-Kornas, E., Kaiser, T. M., Codron, D., Leichliter, J., Weber, K., Weber, M., Tütken, T. (2020b). Improving dietary reconstruction using dental microwear

texture analysis combined with stable isotope analysis–from experimental to fossil application. SVP Abstracts.

Winkler, D. E., Tütken, T., Schulz-Kornas, E., Kaiser, T. M., Müller, J., Leichliter, J., Weber, K., Hatt, J.-M., Clauss, M. (2020c). Shape, size, and quantity of ingested external abrasives influence dental microwear texture formation in guinea pigs. Proceedings of the National Academy of Sciences, 117(36), 22264–22273.

Witzmann, F. (2013). The stratigraphically oldest eryopoid temnospondyl from the Permo-Carboniferous Saar-Nahe Basin, Germany. PalZ 87(2), 259–267.

Witzmann, F., Voigt, S. (2015). An Eryops-like interclavicle from the Early Permian of the Saar-Nahe Basin, and a discussion of temnospondyl interclavicle characters. *PalZ 89*(3), 449–458.

Witzmann, F., Sues, H. D., Kammerer, C. F., Fröbisch, J. (2019). A new bystrowianid from the upper Permian of Germany: first record of a Permian chroniosuchian (Tetrapoda) outside Russia and China. Journal of Vertebrate Paleontology, 39(4), e1667366.

Woodburne, M. O. (1987). Cenozoic mammals of North America: geochronology and biostratigraphy (pp. 391). New York, Columbia University Press.

Wright, J. S. (2001). “Desert” loess versus “glacial” loess: quartz silt formation, source areas and sediment pathways in the formation of loess deposits. Geomorphology 36(3–4), 231–256.

Wroe, S., Huber, D. R., Lowry, M., McHenry, C., Moreno, K., Clausen, P., Ferrara, T. L., Cunningham, E., Dean, M. N., Summers, A. P. (2008). Three-dimensional computer analysis of white shark jaw mechanics: how hard can a great white bite? Journal of Zoology 276(4), 336–342.

Yamaguchi, A., Taniuchi, T. (2000). Food variations and ontogenetic dietary shift of the starspotteddogfish *Mustelus manazo* at five locations in Japan and Taiwan. Fisheries Science 66(6), 1039–1048.

Yuen, K. K. (1974). The two-sample trimmed t for unequal population variances. Biometrika 61(1), 165–170.

Zanden, M. J. V., Rasmussen, J. B. (2001). Variation in $\delta^{15}N$ and $\delta^{13}C$ trophic fractionation: implications for aquatic food web studies. Limnology and oceanography 46(8), 2061–2066.

Zazzo, A., Lécuyer, C., Mariotti, A. (2004a). Experimentally-controlled carbon and oxygen isotope exchange between bioapatites and water under inorganic and microbially-mediated conditions. Geochimica et Cosmochimica Acta 68(1), 1–12.

Zazzo, A., Lécuyer, C., Sheppard, S. M., Grandjean, P., Mariotti, A. (2004b). Diagenesis and the reconstruction of paleoenvironments: a method to restore original $\delta^{18}O$ values of carbonate and phosphate from fossil tooth enamel. Geochimica et Cosmochimica Acta 68(10), 2245–2258.

Zeeh, S., Becker, F. (2005). Diagenetische Prozesse im Umfeld permischer Spalten der Korbacher Bucht (N-Hessen), Zechstein 1. Zeitschrift der Deutschen Geologischen Gesellschaft 155(2-4), 115–136.

Zeeh, S., Becker, F., Heggemann, H. (2000). Dedolomitization by meteoric fluids: the Korbach fissure of the Hessian Zechstein basin, Germany. Journal of Geochemical Exploration 69, 173–176.

Žigaitė, Ž., Whitehouse, M. (2014). Stable oxygen isotopes of dental biomineral: differentiation at the intra-and inter-tissue level of modern shark teeth. Gff 136(1), 337–340.